

DYNAMIC ANALYSES OF SUSPENSION BRIDGE  
STRUCTURES AND SOME RELATED TOPICS

Thesis by  
Ahmed Mansour Abdel-Ghaffar

In Partial Fulfillment of the Requirements  
for the Degree of  
Doctor of Philosophy

California Institute of Technology  
Pasadena, California

1976

(Submitted May 24, 1976)

## ACKNOWLEDGEMENT

The author wishes to express sincere gratitude to his advisor, Professor G. W. Housner, for encouragement and constructive criticism in the preparation of this thesis. He is also grateful to Professor M. D. Trifunac and H. L. Wong for their collaboration on the soil-bridge interaction chapter. The interesting discussions and various suggestions given by Professors T.K. Caughey and W.D. Iwan and by Dr. K.K. Gupta of the Jet Propulsion Laboratory are also greatly appreciated.

The author further extends thanks to Mr. James Gates of the California Department of Transportation, Division of Highways, for the helpful information he provided concerning the San Pedro-Terminal Island Suspension Bridge; to Mr. Daniel C. Butler, San Pedro Bridge Manager, for the time and effort he contributed to the making of the field measurements; to Mr. P.D. Spanos, Mr. M. A. Haroun and Mr. R. Relles for their assistance in the field tests; and to Mr. D. A. Foutch for his help in the data analysis.

Much appreciation is expressed to the California Institute of Technology and to the National Science Foundation for financial support during the course of this work. The partial support of this investigation by the U. S. Geological Survey is also acknowledged.

Finally, the author dedicates this thesis to his wife, Cathleen, and to his parents.

## ABSTRACT

The thesis is divided into two parts. The first part develops a method of dynamic analysis for vertical, torsional and lateral free vibrations of suspension bridges, based on linearized theory and the finite-element approach. The method involves two distinct steps: (1) specification of the potential and kinetic energies of the vibrating members of the continuous structure, leading to derivation of the equations of motion by Hamilton's Principle, (2) use of the finite-element technique to: (a) discretize the structure into equivalent systems of finite elements, (b) select the displacement model most closely approximating the real case, (c) derive element and assemblage stiffness and inertia properties, and finally (d) form the matrix equations of motion and the resulting eigenvalue problems. The stiffness and inertia properties are evaluated by expressing the potential and kinetic energies of the element (or the assemblage) in terms of nodal displacements. Detailed numerical examples are presented to illustrate the applicability and effectiveness of the analysis and to investigate the dynamic characteristics of suspension bridges with widely different properties. This method eliminates the need to solve transcendental frequency equations, simplifies the determination of the energy stored in different members of the bridge, and represents a simple, fast and accurate tool for calculating the natural frequencies and modes of vibration by means of a digital computer.

The method is illustrated by calculating the modes and frequencies of a bridge and comparing them with the measured frequencies.

The second part contains two studies on the effect of differential motions of two foundations upon the response of the superstructure of a bridge. The first study deals with the dynamic response of a "long beam" model of a bridge to both steady-state and random excitations applied at the supports. The second study develops a method to analyze the dynamic soil-bridge interaction of a simple bridge model erected on an elastic half-space, and the input motion is in the form of incident plane SH-waves. The dynamic response of the bridge and the effect of the radiative damping in the half-space on the interaction of the bridge are also studied.

## TABLE OF CONTENTS

| <u>Part</u> | <u>Chapter</u> | <u>Title</u>   | <u>Page</u> |
|-------------|----------------|--|-------------|
| A           |                | FREE VIBRATIONS OF SUSPENSION BRIDGES                                    | 1           |
|             |                | General Introduction   | 1           |
|             | I              | FREE VERTICAL VIBRATIONS OF SUSPENSION BRIDGES                           | 8           |
|             |                | I-1. Introduction  | 8           |
|             |                | I-2. Preliminary Considerations and<br>Fundamental Assumptions           | 17          |
|             |                | I-2-1. Elucidation of the structural<br>members of suspension bridges    | 17          |
|             |                | I-2-2. Coordinate systems  | 21          |
|             |                | I-2-3. Fundamental assumptions   | 22          |
|             |                | I-3. Analysis of Suspension Bridges Having<br>Negligible Tower Stiffness | 28          |
|             |                | I-3-1. Potential energy of the cables                                    | 29          |
|             |                | I-3-2. Potential energy of the suspended<br>structure                    | 37          |
|             |                | I-3-3. Kinetic energy of the vertically<br>vibrating suspension bridge   | 41          |
|             |                | I-3-4. Variational formulation of the<br>equations of motion             | 42          |
|             |                | I-4. A Finite Element Approach to Vertical<br>Vibrations                 | 52          |
|             |                | I-4-1. Idealization of the structure and<br>the displacement model       | 54          |
|             |                | I-4-2. Evaluation of structural-property<br>matrices                     | 58          |
|             |                | I-4-3. Evaluation of inertia-property<br>matrices                        | 67          |
|             |                | I-4-4. Variational formulation of the matrix<br>equations of motion      | 69          |
|             |                | I-4-5. Illustrative numerical examples                                   | 73          |
|             |                | I-5. Effect of Tower Stiffness Upon Free<br>Vertical Vibration           | 97          |
|             |                | I-5-1. Correction for strain energy of the<br>cables                     | 98          |
|             |                | I-5-2. Potential energy absorbed by the<br>towers                        | 103         |
|             |                | I-5-3. Equations of motion for the towers                                | 104         |
|             |                | I-6. Finite Element Approach for the Overall<br>Problem                  | 108         |
|             |                | I-6-1. Modification of structural-property<br>matrices                   | 108         |
|             |                | I-6-2. Modification of the matrix equations<br>of motion                 | 111         |

| <u>Part</u> | <u>Chapter</u> | <u>Title</u>   | <u>Page</u> |
|-------------|----------------|--|-------------|
|             |                | I-6-3. Illustrative numerical example                                      | 115         |
|             | I-7.           | Appendices   | 121         |
|             | I-a.           | Cable Profiles of Suspension<br>Bridges and their Associated<br>Properties | 121         |
|             | I-b.           | The Cable Equation (Compatibility<br>Equation)                             | 130         |
|             | I-c.           | An Alternative Approach to the<br>Inextensibility Condition                | 134         |
|             | I-d.           | Effect of Shear Deformation and<br>Rotary Inertia                          | 136         |
|             |                | REFERENCES OF CHAPTER I  | 142         |
| II          |                | FREE TORSIONAL VIBRATIONS OF<br>SUSPENSION BRIDGES                         | 145         |
|             | II-1.          | Introduction   | 145         |
|             | II-2.          | Preliminary Considerations and<br>Fundamental Assumptions                  | 150         |
|             | II-2-1.        | Types of suspended structures  | 150         |
|             | II-2-2.        | Coordinate systems   | 152         |
|             | II-2-3.        | Simplified assumptions   | 154         |
|             | II-3.          | Analysis of Suspension Bridges Having<br>Negligible Tower Stiffness        | 158         |
|             | II-3-1.        | Potential energy of the<br>suspended structure                             | 159         |
|             |                | a. strain energy of the chords<br>(or flanges)                             | 168         |
|             |                | b. strain energy of the web<br>systems                                     | 170         |
|             | II-3-2.        | Potential energy of the cables   | 173         |
|             | II-3-3.        | Kinetic energy of the torsionally<br>vibrating suspension bridge           | 176         |
|             | II-3-4.        | Variational formulation of the<br>equations of motion                      | 178         |
|             | II-4.          | A Finite Element Approach to Torsional<br>Vibrations                       | 187         |
|             | II-4-1.        | Idealization of the structure and<br>the displacement model                | 187         |
|             | II-4-2.        | Evaluation of structural-property<br>matrices                              | 188         |
|             | II-4-3.        | Evaluation of the inertia-<br>property matrix                              | 195         |

| <u>Part</u> <u>Chapter</u> | <u>Title</u>   | <u>Page</u> |
|----------------------------|--|-------------|
|                            | II-4-4. Variational formulation of the matrix equation of motion         | 197         |
|                            | II-4-5. Numerical example  | 199         |
| II-5.                      | Effect of Torsional Rigidity of the Towers Upon Free Torsional Vibration | 212         |
|                            | II-5-1. Correction for strain energy of the cables                       | 212         |
|                            | II-5-2. Potential energy absorbed by the towers                          | 216         |
| II-6.                      | Finite Element Approach to Include the Effect of the Towers              | 219         |
|                            | II-6-1. Modification of structural-property matrices                     | 220         |
|                            | II-6-2. Modification of the matrix equation of motion                    | 222         |
|                            | II-6-3. Numerical example  | 223         |
| II-7.                      | Appendices   | 226         |
|                            | II-a. Shear Resistance Coefficients $\mu_v$ and $\mu_h$                  | 226         |
|                            | II-b. Longitudinal Warping Displacement                                  | 229         |
|                            | II-c. The Warping Constant   | 230         |
|                            | II-d. Solutions of the Differential Equations of Motion                  | 232         |
|                            | REFERENCES OF CHAPTER II   | 238         |
| III                        | FREE LATERAL VIBRATIONS OF SUSPENSION BRIDGES                            | 240         |
|                            | III-1. Introduction  | 240         |
|                            | III-2. Preliminary Considerations and Fundamental Assumptions            | 244         |
|                            | III-2-1. Coordinate systems and vibrational-displacements                | 244         |
|                            | III-2-2. Basis for analysis  | 246         |
|                            | III-3. Derivation of the Equations of Motion                             | 249         |
|                            | III-3-1. Potential energy of the cables                                  | 249         |
|                            | III-3-2. Potential energy of the suspended structure                     | 254         |
|                            | III-3-3. Kinetic energy of the laterally vibrating suspension bridge     | 256         |
|                            | III-3-4. Variational formulation of the equations of motion              | 257         |

| <u>Part</u> | <u>Chapter</u> | <u>Title</u>  | <u>Page</u> |
|-------------|----------------|---|-------------|
|             | III-4.         | A Finite Element Approach to Lateral Vibrations   | 267         |
|             | III-4-1.       | Idealization of the structure and the displacement models   | 267         |
|             | III-4-2.       | Evaluation of structural-property matrices  | 271         |
|             | III-4-3.       | Evaluation of inertia-property matrices   | 280         |
|             | III-4-4.       | Variational formulation of the matrix equations of motion   | 283         |
|             | III-4-5.       | Numerical example   | 285         |
|             | III-5.         | Appendices  | 300         |
|             | III-a.         | An Approximate Solution for the Equations of Motion   | 300         |
|             |                | REFERENCES OF CHAPTER III   | 304         |
| IV          |                | VIBRATION STUDIES AND TESTS OF THE SAN PEDRO-TERMINAL ISLAND SUSPENSION BRIDGE                                  | 305         |
|             | IV-1.          | Introduction  | 305         |
|             | IV-2.          | Description of the Bridge   | 313         |
|             | IV-3.          | Dynamic Characteristics of the Bridge   | 321         |
|             | IV-4.          | Measuring the Natural Frequencies of the Bridge   | 330         |
|             | IV-4-1.        | Description of the measuring equipment  | 330         |
|             | IV-4-2.        | Measuring procedures  | 323         |
|             | IV-4-3.        | Data analysis   | 338         |
|             | IV-5.          | Comparison Between the Computed and the Measured Frequencies  | 343         |
|             | IV-6.          | Summary and Conclusions   | 357         |
|             |                | REFERENCES OF CHAPTER IV  | 358         |
|             |                | Summary and Conclusions of Part A   | 360         |
| B           |                | EFFECT OF DIFFERENTIAL MOTIONS OF TWO (OR MORE) FOUNDATIONS UPON THE RESPONSE OF THE SUPERSTRUCTURE OF A BRIDGE | 363         |
|             |                | General Introduction  | 363         |

| <u>Part</u> <u>Chapter</u> | <u>Title</u>   | <u>Page</u> |
|----------------------------|--|-------------|
| V                          | DYNAMIC RESPONSE OF A LONG BEAM<br>MODEL OF A BRIDGE STRUCTURE SUBJECT<br>TO TWO END EXCITATIONS | 365         |
|                            | V-1. Introduction  | 365         |
|                            | V-2. Steady-State Vibration Analysis   | 369         |
|                            | V-2-1. Undamped natural frequencies<br>and mode shapes   | 369         |
|                            | V-2-2. Equation of motion of damped<br>shear beam  | 370         |
|                            | V-2-3. Steady-state solution   | 370         |
|                            | V-2-4. Dynamic response of the beam<br>(Numerical results)                                       | 374         |
|                            | V-2-5. Energy consideration  | 379         |
|                            | V-3. Random Vibration Analysis   | 386         |
|                            | V-3-1. Equation of motion  | 386         |
|                            | V-3-2. Dynamic response under random<br>displacements  | 388         |
|                            | V-3-3. Dynamic response under random<br>accelerations  | 394         |
|                            | V-4. Conclusions   | 400         |
|                            | V-5. Appendices  | 401         |
|                            | V-a. Expressions for $J_n(\omega, t; \alpha, \beta)$ and<br>$J_n(\omega, t; 1, 1)$               | 401         |
|                            | V-b. Expression for $I(\omega, t)$   |             |
|                            | REFERENCES OF CHAPTER V  | 405         |
| VI                         | ANTIPLANE DYNAMIC SOIL-BRIDGE<br>INTERACTION FOR INCIDENT PLANE<br>SH-WAVES                      | 406         |
|                            | VI-1. Introduction   | 406         |
|                            | VI-2. The Model, the Excitation and the<br>Exact Solution  | 410         |
|                            | VI-2-1. The coordinate systems   | 410         |
|                            | VI-2-2. Motion of the soil   | 412         |
|                            | VI-2-3. Forces generated by the soil<br>and compliance functions                                 | 414         |
|                            | VI-3. Dynamic Analysis of the Bridge   | 417         |
|                            | VI-3-1. Motion of the bridge   | 417         |
|                            | VI-3-2. Forces exerted by the bridge   | 418         |
|                            | VI-4. Dynamic Soil-Bridge-Soil Interaction   | 420         |
|                            | VI-5. Interpretation of the Interaction  | 425         |

| <u>Part</u> | <u>Chapter</u> | <u>Title</u>             | <u>Page</u> |
|-------------|----------------|--------------------------|-------------|
|             | VI-6.          | Response of the Bridge   | 443         |
|             | VI-7.          | Conclusions              | 447         |
|             |                | REFERENCES OF CHAPTER VI | 449         |

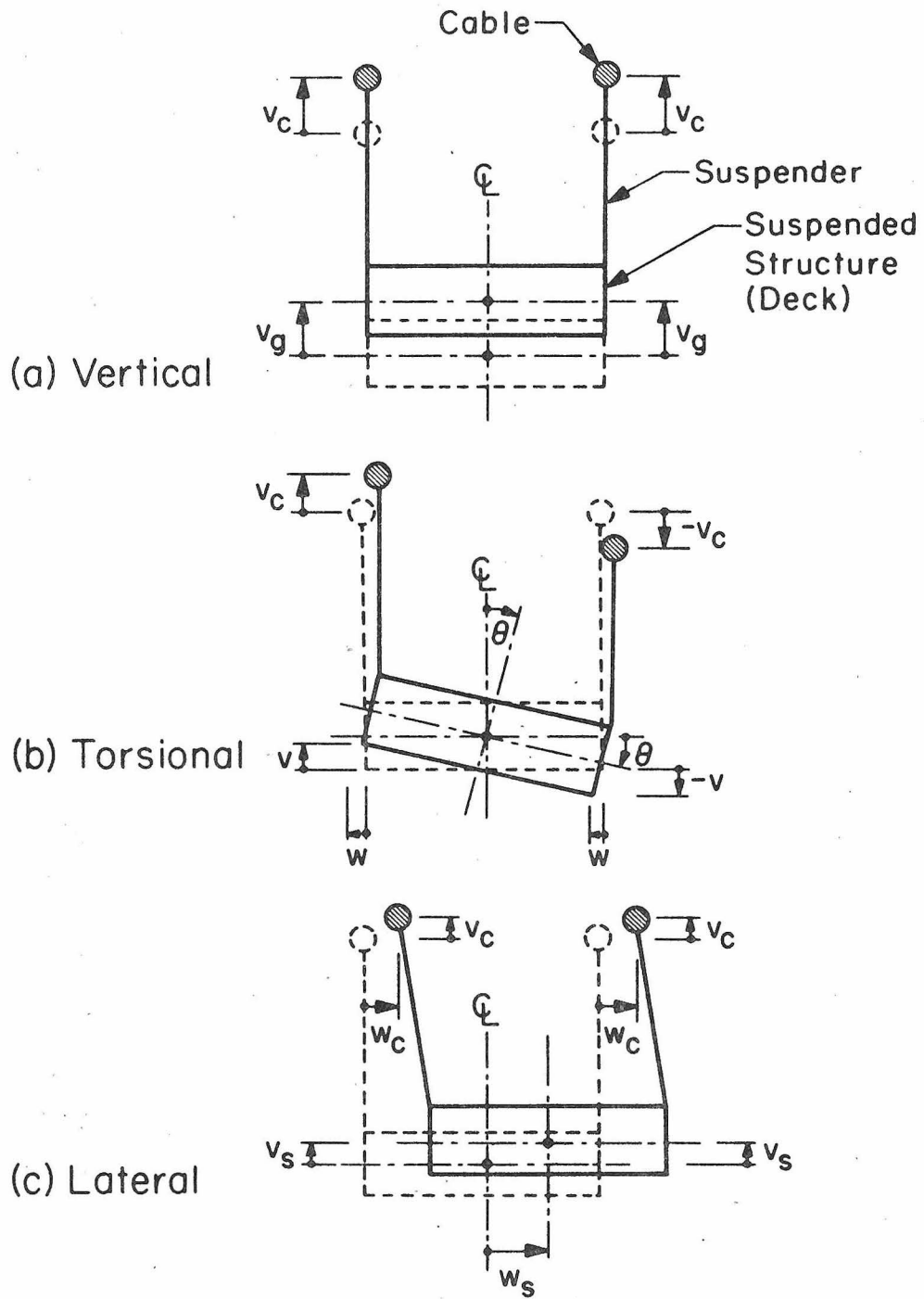
PART A

FREE VIBRATIONS OF SUSPENSION BRIDGES

General Introduction

Throughout the history of suspension bridges, their tendency to vibrate under different dynamic loads has been a matter of concern which, in modern times, has led to several investigations into their vibrational properties. As a prerequisite to the further investigation of aerodynamic stability, traffic impact, soil-structure interaction and earthquake resistant design of suspension bridges, it is necessary to know certain dynamic characteristics such as the natural frequencies and the possible modes of motion during vibration.

The natural, free vibrational modes of a suspension bridge may be classified as vertical, torsional and lateral, as shown in Fig. A-1. In pure vertical modes of vibration, all points on a given cross section of the bridge move the same amount in only the vertical direction, and they remain in phase (see Fig. A-1-a). In pure torsional modes, each cross section of the bridge rotates about an axis which is parallel to the longitudinal axis of the bridge and which is in the same vertical plane as the centerline of the bridge. Corresponding points on opposite sides of the centerline of the roadway attain equal displacements, but in opposite directions, as shown in Fig. A-1-b. In pure lateral motion, each cross section swings in a pendular fashion in its own vertical plane, and, therefore, there is



### TYPES OF VIBRATIONAL MOTION IN SUSPENSION BRIDGES

Fig. A-1

upward movement of the cables and of the suspended structure incidental to their lateral movements, as shown in Fig. A-1-c.

Problems in the dynamic analysis of the free vertical vibration of suspension bridges have been investigated by many specialists during the past few decades; the fundamental equations expressing this type of free vibration were well understood many decades ago. Much of the development which made these equations and their solutions versatile in application, however, has taken place in the wake of the collapse of the Tacoma Narrows Bridge in 1940. However, there have been few investigations into, and relatively little work published on, the dynamic analysis of either torsional or lateral vibration. Generally, in all past studies of the different types of vibration, investigators have started with certain more or less valid assumptions, have made a series of approximations in varying degrees, and have attempted to develop equations and formulas that would predict with fair precision the performance of suspension bridges in free vibration. The relative value of these equations and formulas lies in their reliability for such prediction and, also, in their agreement with results obtained from experiments with models and with full-scale structures. In this regard, most of the complex formulas developed so far are not adequate beyond the first few modes; this is either due to the type of assumptions involved or to the type of solution techniques adopted.

Current investigations have implied that the problem of the dynamic analysis of suspension bridges cannot be solved effectively

by analytical methods, but that the evolution of both the digital computer and various associated numerical techniques of analysis have significantly enhanced solution capability. Thus, in spite of the recognition of the problem and intermittent attempts at its solution, the state-of-the-art of the study of suspension bridges' free vibration is, still, not satisfactory.

The following study, in which the modern digital computer and the finite element method of analysis play a central role, develops methods to analyze the dynamic problems of suspension bridges. The finite element method is very useful in that it provides a unified approach to discretization which can be applied to complex structures such as suspension bridges; the digital computer makes it possible to routinely solve the resulting equations of motion, which may involve even hundreds of degrees of freedom. The methods of analysis developed here are designed to present general theories and their applications in order to determine the dynamic characteristics, namely the natural frequencies, the modes of vibration, and the energy storage capacity, of the different members of a suspension bridge. In order to simplify the presentation, coupling among vertical, torsional and lateral motions is neglected, and some conventional assumptions are used.

In general, it is believed that the theoretical treatments presented yield practical solutions with reasonable accuracy and increase understanding of the general characteristics of vertical, torsional and lateral vibrations of suspension bridges. Furthermore,

the formulation of the problem provides a basis for future theoretical study in two directions: analysis of geometric-nonlinear free vibrations and of earthquake-resistant design.

This first part of the thesis is divided into four chapters, and each chapter is further divided into several sections and sub-sections. Each chapter, and many of the sections, have individual introductions which give brief accounts of the historical development of the particular subject under investigation. The historical information has been collected from many sources; in some cases the original works have been referred to, as in others, where source material is difficult to obtain, the reader is directed to treatises which list references. Many references have been included so that the reader may easily obtain a more complete discussion of the various phases of the total subject.

The first chapter contains analyses of the free vertical vibration of a broad class of suspension bridges. In the first section, a detailed introduction is presented, and in the second section preliminary considerations and fundamental assumptions are given. The third section discusses the different expressions for energy in the vertically vibrating system and the derivation of the equations of motion by means of Hamilton's Principle. In the fourth section, topics which receive attention are: the finite element formulation, the solutions obtained, and detailed numerical examples which examine the effect of the extensibility of the cables and the continuity of the suspended structure. In the analyses in the third and the fourth sections, it is assumed

either that the cables rest on nests of rollers at the tower tops or that the towers are of rocker type with pin-bearings at their bases. Thereafter, in the fifth and the sixth sections, it is assumed that the saddles are fixed at the tower tops, and therefore, the towers offer a certain bending resistance to any horizontal displacement at their tops. Also, the in-plane free horizontal vibration of the towers has been considered. The fifth section contains the energy expressions modified due to the rigidity of the tower, and it also includes the derivation of the equation of motion for the towers. The sixth section concerns the finite element solutions of the overall problem (which includes the suspended structures, the cables and the towers). A numerical example, to illustrate the tower effect, is presented.

The second chapter is concerned with analyses of free torsionally vibrating suspension bridges. Two advancements are made in this chapter. Firstly, a detailed treatment of a generalized theory of free torsional vibration for a wide class of suspension bridges having double lateral systems is developed, taking into account the warping of the cross section of the bridge deck and the effect of torsional rigidity of the towers. Secondly, a method of dynamic analysis based on a finite element approach is developed to determine vibrational properties in torsion. Almost the same procedures which were followed in the vertical vibration chapter are followed in this chapter on torsional vibration.

The third chapter contains analyses of the free lateral vibration of suspension bridges. The upward movements of the cables and of

the suspended structure, incidental to their lateral movements, are taken into consideration. The first and second sections contain some theoretical preliminaries and fundamental concepts. The third section contains the different expressions for energy in the laterally vibrating suspension bridge and the derivation of the equations of motion which couple the vibrational movements of the cables with those of the suspended structure. The fourth section is concerned with the finite element formulation, the solutions, and a numerical example which illustrates and augments the analyses of this chapter.

In the last chapter of this part of the thesis, vibration studies and experiments with the Vincent Thomas suspension bridge (between San Pedro and Terminal Island, California) are presented to illustrate the applicability and the effectiveness of the analyses under consideration as well as to investigate the dynamic characteristics of a real bridge. To further prove the validity and reliability of these analyses, a rigorous comparison with previous results obtained by other investigators has been made. In addition, the computed frequencies of this bridge have been compared with the measured frequencies, and the results of simple experiments conducted on the bridge are presented.

## CHAPTER I

### FREE VERTICAL VIBRATIONS OF SUSPENSION BRIDGES

#### I-1. Introduction

The Tacoma Narrows Bridge disaster in 1940 profoundly influenced suspension bridge research by sharply focusing attention on the related dynamic problems. Prior to that time, the gradual development of suspension bridge theory, which took place during the nineteenth century and the first half of the twentieth century, had led to the construction of progressively more economical and more slender structures, such as the Tacoma Narrows Bridge. Early warnings of suspension bridge failures caused by vibration during high winds then culminated in the warning signs of the major disaster that befell Moisseiff's Tacoma Bridge. It was a slender bridge of 2800 ft. span that showed a marked tendency to vibrate in the wind, both in flexure (vertically) and torsion, soon after construction, and finally, after a life of only a few months, it collapsed as a result of excessive vibrations in a transverse wind of approximately 40 m. p. h.

This disaster so shocked the engineering world that major efforts were made to understand the nature of the dynamic problem of suspension bridges and to learn how to counter it. In accordance with this, several investigations into the vibrational properties of suspension bridges were conducted, and, as a result, it was found

that severe vibrations can be largely caused not only by wind but also by various dynamic loads, such as moving vehicles and earthquakes.

One approach to this dynamic problem used aerodynamic theories and the research methods of aeronautics. The most extensive studies using this approach are the model investigations of Farquharson [8], von Kármán [6], Frazer [10], Scruton [10], Steinman [14] and Selberg [16], and the theoretical work of Bleich [9], and others. Thus, the aerodynamic stability of suspension bridges has been of central interest for bridge designers and scientists and has been the subject of numerous treatises, while there have been comparatively few investigations into their response to other dynamic loads or into their general dynamic characteristics.

However, in the last decade, Hirai and Ito [21] did lead an investigation into the practicability of railway suspension bridges. They studied their response to moving vehicles, theoretically and experimentally, and they provided information enabling the creation of an impact specification for a long-span railway suspension bridge. The live load intensity on a bridge of this type is, of course, large compared with that in a highway bridge, and thus the dynamic effects in the former are generally much more remarkable. Although significant in the area of railway bridges, their research did not address the general problem of traffic loads.

Design of a major suspension bridge for a region where severe earthquakes may be expected is a problem which has also received little study; even though it is a much more demanding problem than the design of a typical multi-story building frame. Modern building codes have now been developed to the point where the basic earthquake requirements to be imposed on a "standard" building are specified adequately, and intelligent consideration of these requirements will lead to the design of a safe and economical structure. A large suspension bridge, however, is a vastly different structure than a typical frame building. The fundamental period of vibration of the suspension bridge may be many times as great as the longest period of a building (in which the first mode is primary), and it may be necessary to include a relatively large number of modes of vibration in order to obtain a reasonable representation of the total response.

Knowledge of the natural frequencies and possible modes of vibration of a suspension bridge is necessary to investigate the response to aerodynamic forces, live loads and earthquake loads. The earliest relevant investigations of natural frequencies and modes, concerned the vibrations of a heavy, isolated suspension cable in a vertical plane. The first known theoretical treatments of this problem were by Poisson [28] in 1820, and by Rohrs [1] in 1851. The latter examined the symmetrical modes of a nearly horizontal cable which was assumed to be inextensible and produced results for the first two natural modes. The same problem was

examined more generally by Routh [2] in 1868, at which time he gave an exact solution for the symmetrical vertical vibrations (and associated longitudinal motion) of a heterogeneous cable which hung in a cycloid. Like Rohrs, he also assumed that the cable was inextensible. He showed that the result for a cycloidal cable could be reduced to Rohrs' solution for the uniform cable, when the ratio of sag to span was small. Routh also obtained an exact solution for the antisymmetric, vertical vibrations (and associated longitudinal motion) of the cycloidal cable.

At this point the subject appears to have been laid to rest until the aerodynamic failure of the Tacoma Bridge which, as explained previously, initiated a comprehensive investigation of the problem of dynamic vibrations of suspension bridges. In 1941, Rannie [6] and von Kármán [5, 6] derived results for an inextensible, three-span cable. In 1945, Vincent [15, 18] extended Rannie's and von Kármán's analyses to allow for the effects of cable elasticity in the calculation of the symmetric vertical motion of the three-span cable. However, he did not explore the nature of the solution so obtained and, therefore, he appears to have been unaware of the substantial effect which the inclusion of cable elasticity can have.

From 1941 to 1943, Steinman [14] derived a number of simplified formulas for computing the frequencies and the modes of both vertical and torsional vibrations of suspension bridges. They have been independently checked for validity and accuracy by investigators using more complex formulas. Steinman's formulas appear to be the simplest and most practical to date, but some of

the more involved modes predicted by these formulas have not been found in other solutions.

A semi-empirical theory for the natural frequencies of the first in-plane (vertical) modes of a uniform suspended cable was put forward by Pugsley [13] in 1949. He demonstrated the applicability of his results by conducting experiments on cables in which the ratio of sag to span ranged from 1:10 up to approximately 1:4.

Later, various analytical studies were made to develop formulas for computing the frequencies and modes of vertical as well as torsional vibrations of suspension bridges with and without recognition of the extensibility of the cable. Formulas for most of these cases and for other cases as well were developed by Bleich [9]. He analyzed free vibration by the so-called exact method (i. e., by solution of the fourth order linearized differential equations of motion), and he applied this method to various examples. An approximate method, based on the Rayleigh-Ritz approach and representing the deformation of the structure by Fourier series was also developed by Bleich, though this method can be applied usefully only to the first few modes because of the complexity and the redundancy of suspension bridges.

In 1952, Pugsley [11] discussed the stiffness of a heavy inextensible cable in terms of work done by the cable against gravity when the cable is loaded; he also examined the relationship between this energy treatment and the conventional "linearized deflection theory" in common use. The latter is often presented in a form that

appears to imply that the gravity stiffness of a cable is negligible; this has proved to be misleading and results from neglect of a term in the expression for zero extension.

Until the sixties, it was believed that the best formulas for computing the frequencies and the modes of suspension bridge vibrations were those developed at the University of Washington by Smith and Vincent [15]. These formulas were derived from the differential equation of motion in bending (vertical vibration); unfortunately, the misleading condition of inextensibility of the cable, which Pugsley has critically examined, was used in some of these formulas.

As mentioned before, recent studies have implied that the problem of the dynamic analysis of suspension bridges cannot be solved effectively by analytical methods, but that the evolution of both the digital computer and various associated numerical techniques of analysis have significantly enhanced solution capability. Therefore, with the advance made in the computer, it has become possible to solve even extremely complex cases.

The first use of a digital computer in analyzing this problem achieved significant results. This first trial was made by Clough [17], as a consultant in earthquake engineering, in an unpublished report, "Seismic analysis of the main piers for the Tagus River Bridge." The earthquake behavior of the Tagus River Bridge (in Lisbon, Portugal) was studied in the late fifties and early sixties by Housner, Converse [17] and Clough. The vibrational analysis of this bridge

was based on a lumped mass system, which was interconnected by elements having shearing and bending stiffness representative of the actual structure. Rotational stiffness of the foundation material was considered also.

In the early 1960's, Konishi, Yamada and Takaoka [19, 20] started an extensive research study to investigate the dynamics of suspension bridges and their earthquake resistant design. They simulated a three-span suspension bridge, structurally comprised of systems of masses and springs, and using linearized theory, calculated the periods and modes of free vertical vibration. In this study, the vibration of the towers was considered as well as the vibration of the suspended structure and the cables.

In the late 1960's, Tezcan and Cherry [23] undertook similar research concerned with the earthquake analysis of suspension bridges, in which the effect of large deflections was taken into account. Their study dealt with an iteration scheme for the nonlinear static analysis of suspension bridges by means of tangent stiffness matrices. The concept of these matrices was then introduced in the frequency equation governing the free vibration of the system. The bridge was idealized as a three-dimensional lumped mass system and was subjected to three orthogonal components of earthquake ground motion producing horizontal, vertical and torsional vibrations. As the first nonlinear analysis of a vibrating suspension bridge, this study provided a foundation for further nonlinear suspension bridge research.

The following study develops a method of analyzing the dynamics of suspension bridges by means of a digital computer. This method is designed to determine the dynamic characteristics, namely the natural frequencies, the modes of vertical vibration, and the energy storage capacities, of the different members of the structure. This method is based on the so-called "linearized deflection theory" and a finite element approach. The method incorporates certain special simplifying features, and it involves two distinct steps which are summarized as follows:

1. Specification of the different potential and kinetic energies of the vertically vibrating members of the real continuous structure and then derivation of the equations of motion, and
2. Use of the finite element procedures to: a) discretize the structure into equivalent systems of finite elements, b) select the displacement model most closely approximating the real case, c) derive element and assemblage stiffness and inertia properties, and finally d) form the matrix equations of motion and the resulting eigenvalue problems.

The evaluation of the stiffness and inertia properties of the idealized structural element and assemblage is based on the expression of the potential and kinetic energies of the element (or the assemblage) in terms of nodal displacements. This determines expressions for the stiffness and mass matrices. Hamilton's principle is then used to derive the matrix equations of motion. This finite-element technique furnishes a system with finite degrees

of freedom upon which matrix algebra operations can be performed. It has proved convenient to separate the investigation of the symmetric modes from that of the antisymmetric modes.

Finally, detailed numerical examples are presented to illustrate the applicability and the effectiveness of the analysis and to investigate the dynamic characteristics of a broad class of suspension bridges with widely different properties. In these examples, the effect of cable extensibility, tower stiffness, and suspended structure continuity are examined and some useful comparisons are drawn.

## I-2. Preliminary Considerations and Fundamental Assumptions

The following section is intended to briefly delineate the essential structural members of suspension bridges and their functions and to discuss advantages of the suspension bridge over other bridge types. An outline of the coordinate systems used in the following analysis is also presented. Finally, this section contains the fundamental assumptions involved in the subsequent analysis.

### I-2-1. Elucidation of the structural members of suspension bridges

Suspension bridges consist essentially of cables, suspenders, towers, anchorages, and a suspended structure or bridge deck. The two cables are the principle carrying members and are fixed at their ends to anchor blocks which resist the cable pull. The cables are generally continuous over saddles at the tops of the towers; these saddles are either bolted to the tops of the towers or are equipped with rollers as shown in Fig. I-2-b. In modern suspension bridges the ratio of the cable sag to the span length ranges generally between  $1/8$  and  $1/11$ .

The tower is usually composed of two parts: the substructure or pier, and the tower proper extending above the roadway and supporting the cables. The pier does not involve any special features differentiating it from ordinary bridge piers. The tower is composed of a column or tower leg for each suspension system. For lateral stability, the tower legs are braced by means of cross-girders and cross-bracings. The tower leg may be fixed to the pier or may be

of rocker type with a pin-bearing at the base. Rocker towers afford the most economical and scientific design for bridges of longer span; however, they must be secured against overturning during construction.

The suspended structure consists of two stiffening trusses (or girders) and one or two lateral wind bracings to counter transverse wind pressure and lateral forces from moving loads, and to carry these forces to the piers. Stiffening trusses (or girders) are usually added to reduce and control the vertical movements due to heavy live loads and any other dynamic loads. When the required depth of a stiffening structure of the plate girder type exceeds practical or economical limitations, an open truss type can provide a solution. The two stiffening structures are located in the same planes as the suspenders and cables; they are hung from the suspenders which are attached to the suspension cables. Besides carrying the floor, they act vertically as stiffening trusses (or girders) and horizontally as chords of the lateral bracing system. The stiffening structures in each span are restrained at their ends by the towers so as to prevent horizontal movement of the bridge deck.

The stiffening girder (or truss) is usually very shallow in comparison with its length, (and the same is usually true of the lateral bracing). In practical terms, a three-span suspension bridge may incorporate three different types of stiffening structures in connection with the general problem under consideration:

1. The stiffening structures might be continuous over all three spans with suspenders throughout those spans. And, although it is extremely unusual, they might actually be continuous over two of the spans and non-continuous over the third span.
2. As a second major alternative, the stiffening structures might be continuous over all three spans, but with no suspenders in the side spans. In this case, the stiffening structures in the side spans would probably be much shorter than the full length of the side spans.
3. Finally, the stiffening structures might be of the two-hinged type; it is widely used and is probably the most efficient. Also, it is more economical than the continuous type. In this case, the hinges are located in the towers where they are least objectionable. Actually, the stiffening structures might be a three-hinged type, but this is little used because it lacks rigidity and has other disadvantages arising from the hinge at mid-span.

Suspension bridges are, in general, very flexible as compared with other types of bridge structures, the amplitudes being many times as great. It should be noted also that the rigidity of each member of a suspension bridge is markedly different from the rigidity of each of the other members. Furthermore, interaction occurs among members of the bridge from one end of the cable to the other, so that consideration of one member involves study of all

of the members. The stresses in some members of the structure — like the towers, cables and anchorages — are due largely to dead loads, while the stresses in other members — such as the stiffening girders (or trusses) and lateral bracings — are due entirely to live loads, winds, changes of temperature and possibly earthquakes.

Economic utilization of construction materials demands that, as far as possible, the predominant stresses in any structure should be those for which the material is best adapted. Because steel is a very economic material, especially when used in a condition of tensile stress, the suspension bridge type, which undergoes primarily tension rather than compression, provides a superior design for long spans. To summarize, the superior economy of suspension bridges as long-span structures is fundamentally due to the following: a) the very direct stress paths from the point of loading to the point of support, b) the predominance of tensile stress, and c) the highly increased ultimate resistance of steel in the form of cable wire.

Furthermore, for heavy railway bridges, the suspension bridge is more economical than any other type for spans exceeding about 1500 ft. And, as the live load becomes lighter in proportion to the dead load, the suspension bridge becomes increasingly more economical in comparison with other types. Based on a study of existing bridges, Thul [22] has compared the center span length to the total length of three-span continuous girder bridges, of cable-stayed bridges, and of suspension bridges. His results are summarized in the following table:

---

| Bridge type span comparison          | Center Span   | $\left(\frac{\text{Center span}}{\text{Total span}}\right)\%$ |
|--------------------------------------|---------------|---|
| Three-span continuous girder bridges | up to 700 ft. | 30%-50%   |
| Cable-stayed bridges                 | 500-1200 ft.  | 50%-60%   |
| Suspension bridges                   | 1000-4000 ft. | 60%-70%   |

---

This table indicates that suspension bridges have a lower economic limit of approximately 1000 ft., with a ratio of center span to total span of approximately 60%.

In addition to the economic advantages, the suspension bridge has several other points of superiority. It is light, aesthetic, and graceful; it easily provides a roadway at low elevation, and it has a low center of wind pressure. It is also easily constructed, using materials that are easily transported. There is little danger of failure during erection, and after completion, it is the safest structure known to bridge engineers. In other structures, the failure of a single truss or girder member may precipitate a collapse; in a suspension bridge, the rest of the structure will be unaffected.

#### I-2-2. Coordinate systems

The following coordinate systems are used for the typical three-span suspension bridge shown in Fig. I-1. These coordinate systems have been chosen because they are appropriate for a wide class of suspension bridges, including a single suspended span as well as multiple suspended spans, either continuous or hinged.

Obviously, any number of spans may be considered.

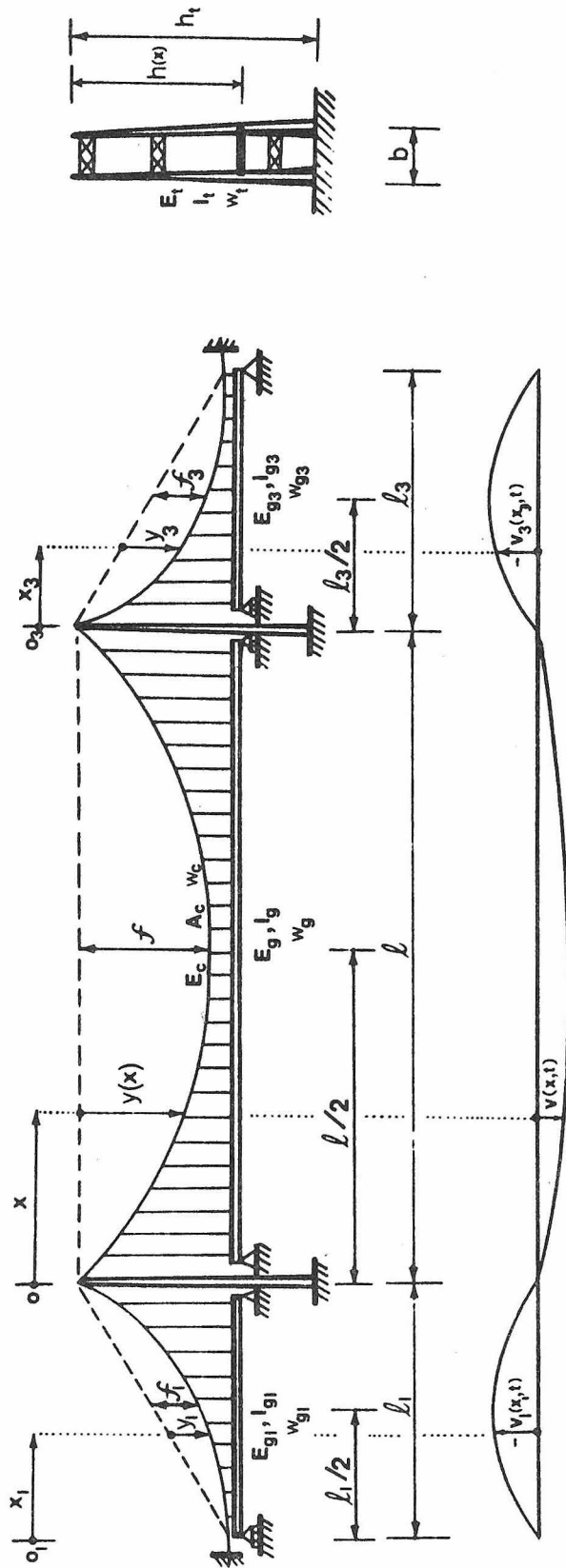
1. For the cable, the  $x_i$ -axis of the  $i^{\text{th}}$  span ( $i=1, 2, 3$ ) is defined as the horizontal line starting from the vertical plane passing through the left support of each span as shown in Fig. I-1, while the ordinate  $y_i$  of the  $i^{\text{th}}$  span is measured downward from the closing chord of each span, i. e., the straight line connecting the extremities of the cable in the  $i^{\text{th}}$  span. (Note: in Fig. I-1, the subscript  $i$  has been left out for convenience)
2. For the stiffening girders (or trusses), the  $x_i$ -axis of the  $i^{\text{th}}$  span ( $i=1, 2, 3$ ) is defined along the centerline of the span with the origin located at the left support of that  $i^{\text{th}}$  span.
3. For the towers, the  $x'$ -axis is taken to be the centerline of the tower column or leg with the top of the column (or leg) being the origin, as shown in Fig. I-2-b.

### I-2-3. Fundamental assumptions

In a consideration of the different factors affecting the dynamic analysis of a suspension bridge, the following general assumptions and approximations are made:

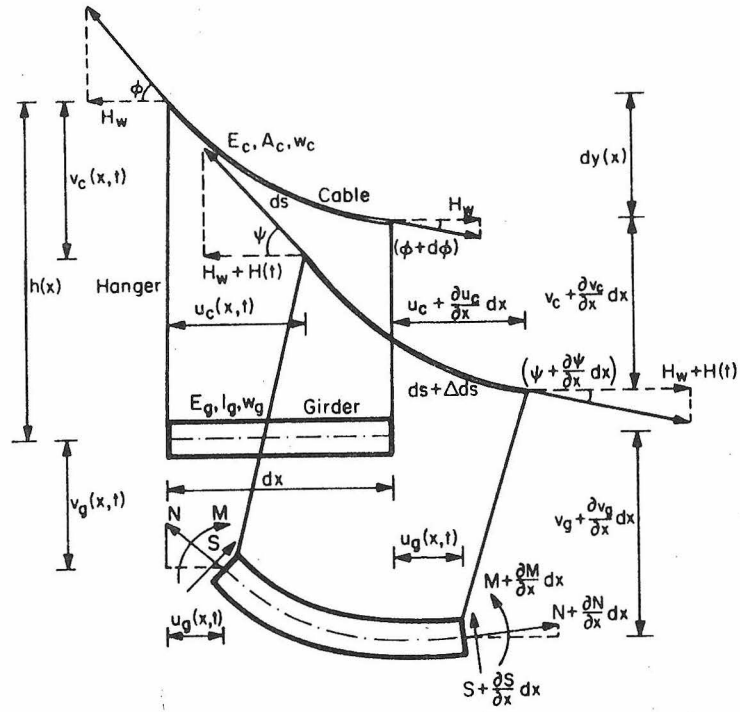
1. All stresses in the bridge remain within the limits of proportionality and thus follow Hooke's law.
2. The initial dead load is carried by the cable without causing stress in the stiffening girder (or truss).

This condition is generally desirable since it simplifies construction. However, if the bridge is erected in such a manner

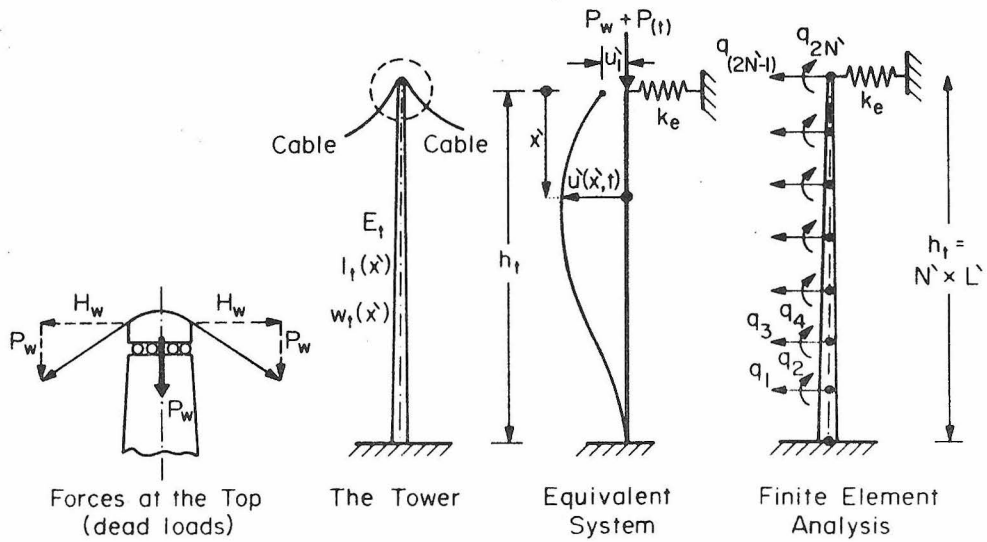


**THE SUSPENSION BRIDGE, THE PROPERTIES AND THE COORDINATE SYSTEMS**

Fig. I-1 A typical three-span suspension bridge with hinged-stiffening girders (or trusses).



(a) ELEMENT IN ORIGINAL & DEFLECTED POSITION



(b) DEFINITION DIAGRAM FOR THE TOWER

Fig. I-2

that the dead load does cause certain stresses in the stiffening structure, this may be compensated for, in the dynamic problem, by taking into consideration all the initial stresses involved.

3. The cable is assumed to be of a uniform cross section and of a parabolic profile under dead load. The assumption of a parabolic profile requires that the ratio of the sag to the span be kept relatively small; in other words, the cable slopes are, and remain, small. For example, the analyses to be presented are valid provided that the ratio of sag to span is 1:8 or less, so that the weight of the cable may be assumed to be uniformly distributed along the span rather than along the length of the cable (see Appendix I-a).
4. The cables are assumed to be perfectly flexible. In consideration of the small moment of inertia of the cable as compared with that of the stiffening structure, this assumption is obviously close to being exact for the purpose of determining horizontal cable tension and the stresses in the stiffening structure. The flexural stiffness of the cables was thoroughly investigated, and it was found that the bending stresses in the cables could be neglected.
5. The vibrational suspender forces, instead of being treated as concentrated forces, are considered as distributed loads in the same manner as if the distance between the suspenders were very small, the suspenders thus forming a continuous sheet or wall without shearing resistance.

6. The suspenders or hangers are considered inextensible and are assumed to remain vertical during the vibration of the bridge; therefore, the vertical vibrational displacement of the cable,  $v_c(x_i, t)$ ,  $i = 1, 2, 3$ , and that of the stiffening girder (or truss),  $v_{gi}(x_i, t)$ ,  $i = 1, 2, 3$ , are assumed to be identical (see Fig. I-2-a); i. e.,

$$v_c(x_i, t) \equiv v_{gi}(x_i, t) = v_i(x_i, t) \quad , \quad i = 1, 2, 3, \quad (1.1)$$

where  $v_i(x_i, t)$  represents the generalized vertical displacement of the vibrating system. Consideration of the effect of the suspender elongation results in a negligible gain in accuracy (Johnson, Bryan and Turneaure [26] ) at the expense of a notable complication of the analyses, and it is therefore not to be recommended. Steinman [3] estimates the contribution of the deformation of the suspenders to be only a fraction of one per cent. Selberg [16] indicates that the change of inclination of the hangers is greatest near the center of a symmetrical stiffening structure. On the other hand, he finds that the influence of the hangers' deviation from the vertical upon the vibration of the bridge is negligible even for a slender stiffening structure.

7. To stay within the linear theory, small vibrational displacements from the position of the static equilibrium have been assumed; i. e., in the following analysis, attention will be restricted to small vibrations in the vertical plane.

8. The additional horizontal component,  $H(t)$ , of cable tension caused by the inertia forces is small in comparison with  $H_w$ , the initial horizontal component of cable tension due to dead loads, i. e.,

$$H_w + H(t) \simeq H_w \quad . \quad (1.2)$$

Similarly, the additional axial force  $P(t)$  due to inertia forces at the top of the tower is small compared with that due to dead loads,  $P_w$ , i. e.,

$$P_w + P(t) \simeq P_w \quad . \quad (1.3)$$

In studying free vertical vibration, it has been assumed that there are no live loads on the vibrating bridge, vibration damping of the structure is neglected, and the total mass of the bridge deck is assumed to be concentrated along the centerline of the stiffening girders (or trusses). Furthermore, the initial curvature of the stiffening structure is considered small in comparison with the cable curvature, and therefore it can be neglected.

Other assumptions will be discussed as they are encountered in the development of the analysis.

I-3. Analysis of Suspension Bridges Having Negligible Tower Stiffness

In order to lay a foundation from which later work is herein developed, the differential equations of motion of a typical three-span suspension bridge and their associated boundary conditions will be derived by means of Hamilton's Principle. Application of this variational principle requires a knowledge of the different expressions of energy of the vibrating bridge structure (which will also be very useful later on). In addition, the use of Hamilton's Principle has the advantage of furnishing, automatically, the correct number of boundary conditions and their correct expressions. There is no necessity to solve the differential equations of motion nor the resulting transcendental frequency equations, since they have both received considerable attention from other investigators.

In the following analyses, the horizontal components of cable tension,  $H_w$  and  $H(t)$  due to dead loads and inertia forces respectively, are assumed to be the same on both sides of the tower in all spans of the cable. (There is no tower resistance to displacement at the top.) This presupposes that the tower cable saddles are free to move horizontally either upon roller nests under the saddles or via rocker tower bases. The former construction, however, is now considered obsolete.

I-3-1. Potential energy of the cables

As a result of small, free vibrations about the position of static equilibrium, the horizontal component of cable tension,  $H_w$  will change to  $[H_w + H(t)]$ , and the differential length of the cable  $ds_i$ , in the  $i^{\text{th}}$  span will increase to  $(ds_i + \Delta ds_i)$ , as shown in Fig. I-2-a. (Note: The subscript  $i$  has been left out of Fig. I-2-a for convenience.)

Now, the potential energy of this cable element,  $ds_i$ , can be expressed as

$$dV_c(x_i, t) = \left\{ [H_w + \frac{1}{2}H(t)] \frac{ds_i}{dx_i} \right\} \cdot \Delta ds_i - \dot{w}_i^* v_c dx_i, \quad i=1, 2, 3 \quad (1.4)$$

where  $\Delta ds_i$  is the cable stretch of the differential length  $ds_i$ ,  $\dot{w}_i^*$  is the dead weight of the cable ( $w_c$ ) per unit length of the  $i^{\text{th}}$  span plus the dead load of the stiffening girder or truss ( $w_{gi}$ ) per unit length of that  $i^{\text{th}}$  span, and  $v_c$  the vertical vibrational displacement of the cable. The first term in Eq. 1.4 is the strain energy stored in the element  $ds_i$  and is equal to the average force  $[H_w + \frac{1}{2}H(t)] \frac{ds_i}{dx_i}$  times the cable stretch  $\Delta ds_i$ . The factor  $\frac{1}{2}$  is needed due to the fact that  $H(t)$  increases from zero to its maximum value  $H(t)$ ;  $\frac{ds_i}{dx_i}$  is the cosine of the angle of inclination,  $\phi_i$ , as shown in Fig. I-2-a. The second term represents the gravity energy, i. e., the potential energy loss due to the lowered position of the dead load.

It is seen from the geometry of displacement (Fig. I-2-a) that, in static equilibrium, the element of length  $ds_i$  of the cable can be given by

$$ds_i^2 = dx_i^2 + dy_i^2, \quad i = 1, 2, 3. \quad (1.5)$$

When the cable is displaced (in-plane), its length increases to  $(ds_i + \Delta ds_i)$ ,  $dx_i$  increases to  $dx_i + \frac{\partial u_c}{\partial x_i} dx_i$  where  $u_c$  is the horizontal movement of the element, and  $dy_i$  becomes  $dy_i + \frac{\partial v_c}{\partial x_i} dx_i$ . Then, for the vibrational displaced position,

$$(ds_i + \Delta ds_i)^2 = \left( dx_i + \frac{\partial u_c}{\partial x_i} dx_i \right)^2 + \left( dy_i + \frac{\partial v_c}{\partial x_i} dx_i \right)^2, \quad i = 1, 2, 3,$$

or

$$2ds_i \Delta ds_i + (\Delta ds_i)^2 = 2dx_i \frac{\partial u_c}{\partial x_i} dx_i + \left( \frac{\partial u_c}{\partial x_i} \right)^2 dx_i^2 + 2dy_i \frac{\partial v_c}{\partial x_i} dx_i + \left( \frac{\partial v_c}{\partial x_i} \right)^2 dx_i^2, \quad i = 1, 2, 3.$$

In general,  $u_c(x_i, t)$  is small in comparison with  $v_c(x_i, t)$ ; therefore, the increment in the length of the cable element  $\Delta ds_i$ , correct to the second order of small quantities, is

$$\Delta ds_i \approx \frac{\partial u_c}{\partial x_i} \frac{dx_i}{ds_i} dx_i + \frac{\partial v_c}{\partial x_i} \frac{dy_i}{ds_i} dx_i + \frac{1}{2} \left( \frac{\partial v_c}{\partial x_i} \right)^2 \frac{dx_i}{ds_i} dx_i, \quad i = 1, 2, 3. \quad (1.6)$$

Integrating Eq. 1.4 over all spans and substituting Eq. 1.6, the potential energy  $V_c(t)$  of the cable may be written as

$$\begin{aligned}
 v_c(t) = \sum_{i=1}^3 \left\{ \left[ H_w + \frac{1}{2} H(t) \right] \left[ \int_0^{l_i} \frac{\partial u_c}{\partial x_i} dx_i + \int_0^{l_i} \left( \frac{\partial v_c}{\partial x_i} \right) \left( \frac{dy_i}{dx_i} \right) dx_i \right. \right. \\
 \left. \left. + \frac{1}{2} \int_0^{l_i} \left( \frac{\partial v_c}{\partial x_i} \right)^2 dx_i \right] - \int_0^{l_i} \tilde{w}_i^* v_c dx_i \right\}, \quad (1.7)
 \end{aligned}$$

where  $l_i$  is the length of the  $i^{\text{th}}$  span.

Integration of the second term (in the second set of brackets) by parts gives

$$\begin{aligned}
 \int_0^{l_i} \left( \frac{\partial v_c}{\partial x_i} \right) \left( \frac{dy_i}{dx_i} \right) dx_i &= \frac{dy_i}{dx_i} v_c \Big|_0^{l_i} - \int_0^{l_i} \frac{d^2 y_i}{dx_i^2} v_c dx_i \\
 &= - \int_0^{l_i} \frac{d^2 y_i}{dx_i^2} v_c dx_i, \quad i = 1, 2, 3. \quad (1.8)
 \end{aligned}$$

providing that  $\left( \frac{dy_i}{dx_i} \right)$  and  $\left( \frac{\partial v_c}{\partial x_i} \right)$  can be treated as continuous functions of  $x_i$  and that  $v_c(x_i, t)$  vanishes at the ends  $x_i = 0$  and  $x_i = l_i$ .

Appendix I-a gives the parabolic profile of a hanging uniform cable of the  $i^{\text{th}}$  span having a load uniformly distributed along the horizontal span. It also gives the other cable profiles. The parabolic profile is expressed as

$$y_i(x_i) = \frac{\tilde{w}_i^* l_i^2}{2H_w} \left[ \frac{x_i}{l_i} - \left( \frac{x_i}{l_i} \right)^2 \right], \quad i = 1, 2, 3. \quad (1.9)$$

The cable deflection at mid-span  $\left( x_i = \frac{l_i}{2} \right)$  is the sag,  $f_i$ , and the

horizontal component of cable tension is

$$H_w = \frac{\overset{*}{w}_i \ell_i^2}{8f_i} \quad . \quad (1.10)$$

With the aid of Eq. 1.10, Eq. 1.9 is more conveniently written as

$$y_i(x_i) = 4f_i \left[ \frac{x_i}{\ell_i} - \left( \frac{x_i}{\ell_i} \right)^2 \right] \quad , \quad i = 1, 2, 3 \quad . \quad (1.11)$$

Eqs. 1.9 and 1.11 give

$$\frac{d^2 y_i}{dx_i^2} = - \frac{\overset{*}{w}_i}{H_w} = - \frac{8f_i}{\ell_i^2} \quad , \quad i = 1, 2, 3 \quad . \quad (1.12)$$

Now, Eq. 1.8, with the aid of Eq. 1.10, becomes

$$\int_0^{\ell_i} \left( \frac{\partial v_c}{\partial x_i} \right) \left( \frac{dy_i}{dx_i} \right) dx_i = \frac{\overset{*}{w}_i}{H_w} \int_0^{\ell_i} v_c dx_i \quad , \quad i = 1, 2, 3 \quad . \quad (1.8')$$

Using the result of Eq. 1.8', the potential energy  $V_c(t)$  of the cable (Eq. 1.7) may be written as

$$\begin{aligned} V_c(t) = \sum_{i=1}^3 \left\{ \left[ H_w + \frac{1}{2} H(t) \right] \cdot u_c \int_{x_i=0}^{x_i=\ell_i} + \frac{1}{2} H_w \int_0^{\ell_i} \left( \frac{\partial v_c}{\partial x_i} \right)^2 dx_i \right. \\ \left. + \frac{1}{2} H(t) \left[ \int_0^{\ell_i} \left( \frac{\partial v_c}{\partial x_i} \right) \left( \frac{dy_i}{dx_i} \right) dx_i + \frac{1}{2} \int_0^{\ell_i} \left( \frac{\partial v_c}{\partial x_i} \right)^2 dx_i \right] \right\} \quad . \quad (1.13) \end{aligned}$$

The assumption that there are no movements of the tower tops or of the anchorages makes it possible to reduce the potential energy,  $V_c(t)$ , of the cable (Eq. 1.13) to

$$\begin{aligned}
 V_c(t) = \frac{1}{2} \sum_{i=1}^3 \left\{ H_w \int_0^{\ell_i} \left( \frac{\partial v_c}{\partial x_i} \right)^2 dx_i + H(t) \left[ \int_0^{\ell_i} \left( \frac{\partial v_c}{\partial x_i} \right) \left( \frac{dy_i}{dx_i} \right) dx_i \right. \right. \\
 \left. \left. + \frac{1}{2} \int_0^{\ell_i} \left( \frac{\partial v_c}{\partial x_i} \right)^2 dx_i \right] \right\} .
 \end{aligned}
 \tag{1.14}$$

In order to put Eq. 1.14 in a more convenient form, reference can be made to the cable equation which relates the stretching of the cable element to the geometric displacements which it undergoes. A derivation of this general cable equation can be found in Appendix I-b. In the present context, the equation reads

$$\frac{H(t)L_{ei}}{E_c A_c} = \int_0^{\ell_i} \left( \frac{\partial v_c}{\partial x_i} \right) \left( \frac{dy_i}{dx_i} \right) dx_i + \frac{1}{2} \int_0^{\ell_i} \left( \frac{\partial v_c}{\partial x_i} \right)^2 dx_i \pm \epsilon_t \Delta T_i L_{ti} \quad , \quad i = 1, 2, 3 .
 \tag{1.15}$$

where  $E_c$  is modulus of elasticity of the cable material,  $A_c$  is the effective cross-sectional area of the cable,  $\epsilon_t$  is the coefficient of thermal expansion,  $\Delta T_i$  is the incremental change in temperature in the  $i^{\text{th}}$  span (it is assumed uniform along the  $i^{\text{th}}$  span) and  $L_{ei}$  and  $L_{ti}$  are virtual lengths of the cable in the  $i^{\text{th}}$  span; they are defined by

$$L_{ei} = \int_0^{\ell_i} \left( \frac{ds_i}{dx_i} \right)^3 dx_i \quad \text{and} \quad L_{ti} = \int_0^{\ell_i} \left( \frac{ds_i}{dx_i} \right)^2 dx_i \quad , \quad i = 1, 2, 3 .
 \tag{1.16}$$

The cable equation of compatibility (Eq. 1.15) can be written for the whole cable, i. e., for a suspended cable hanging between two rigid anchorages and passing over vertical towers, by summation over the

three spans, as

$$\frac{H(t)L_E}{E_c A_c} = \sum_{i=1}^3 \left[ \int_0^{\ell_i} \left( \frac{\partial v_c}{\partial x_i} \right) \left( \frac{dy_i}{dx_i} \right) dx_i + \frac{1}{2} \int_0^{\ell_i} \left( \frac{\partial v_c}{\partial x_i} \right)^2 dx_i \pm \epsilon_t \Delta T_i L_{ti} \right], \quad (1.17)$$

where  $L_E = \sum_{i=1}^3 L_{ei}$  for the entire length of the cable.

Substituting Eq. 1.17 into Eq. 1.14, and assuming that the thermal effect is of minor importance and may consequently be neglected, then the potential energy of the cable is

$$V_c(t) = \frac{1}{2} \sum_{i=1}^3 \left[ H_w \int_0^{\ell_i} \left( \frac{\partial v_c}{\partial x_i} \right)^2 dx_i \right] + \frac{1}{2} \left[ \frac{H^2(t) \cdot L_E}{E_c A_c} \right]. \quad (1.18)$$

It will be recognized that the second term of Eq. 1.18, which includes the area, the virtual length and the modulus of elasticity of the cable, expresses that part of potential energy stored elastically in the cable, i. e., the strain energy stored in the cable. The first term contains the constant  $H_w$  and the expression for the change in length of the cable, and actually represents the potential energy resulting from the elevation of the center of gravity of the entire structure while the cable is momentarily distorted under the influence of the inertia forces. These two terms of the potential energy expression, Eq. 1.18, were adopted by both Vincent [15] and Bleich [9], though on different grounds.

To further clarify the two terms of the preceding potential energy expression (Eq. 1.18) via a physical interpretation, and to

examine the relations between the energy treatment and the conventional, commonly used "linearized deflection theory," one must consider the strain energy and the strainless or gravitational energy separately.

The strain energy stored in the cable due to the change in tension associated with  $H(t)$  is designated by  $V_{ce}(t)$ . At any point in the cable, this change of tension is  $H(t) \frac{ds_i}{dx_i}$ , so that the strain energy amounts to:

$$V_{ce}(t) = \sum_{i=1}^3 \int_0^{\ell_i} \frac{\left[ H(t) \frac{ds_i}{dx_i} \right]^2}{2E_c A_c} ds_i = \sum_{i=1}^3 \int_0^{\ell_i} \frac{H^2(t)}{2E_c A_c} \left( \frac{ds_i}{dx_i} \right)^2 dx_i ,$$

which, upon using the virtual length definition of Eq. 1.16, will give

$$V_{ce}(t) = \frac{1}{2} \left[ \frac{H^2(t) \cdot L_E}{E_c A_c} \right] , \quad (1.19)$$

which is exactly the second term of Eq. 1.18.

Now, to clarify the first term of Eq. 1.18, assume an inextensible cable, and consider the change in potential energy of the system arising from movement within the gravity field. Due to the vibrational displacement  $V_c$ , each element of weight  $w_i^* dx_i$  of the bridge will lose potential energy equal to  $w_i^* V_c dx_i$ . Thus the total change of potential energy arising from gravity will be

$$V_{cg}(t) = - \sum_{i=1}^3 \int_0^{\ell_i} w_i^* V_c dx_i . \quad (1.20)$$

But, for an inextensible cable, the elastic extension of the cable due to vibration,  $\frac{H(t) \cdot L_E}{E_c A_c}$ , given by Eq. 1.17, is zero, and therefore Eq. 1.17, with the aid of Eq. 1.8', is reduced to the inextensibility condition:

$$-\sum_{i=1}^3 \int_0^{\ell_i} w_i^* v_c dx_i = \frac{H_w}{2} \sum_{i=1}^3 \int_0^{\ell_i} \left( \frac{\partial v_c}{\partial x_i} \right)^2 dx_i \quad (1.21)$$

Thus incorporating the inextensibility condition (Eq. 1.21), the change in potential energy arising from gravity can be written as

$$V_{cg}(t) = \frac{1}{2} \sum_{i=1}^3 \left[ H_w \int_0^{\ell_i} \left( \frac{\partial v_c}{\partial x_i} \right)^2 dx_i \right], \quad (1.22)$$

which is identical to the first term of the equation for the potential energy of the cable, Eq. 1.18. There is thus an effective gravity stiffness associated with the vibration of the cable of the suspension bridge. This emphasis on gravity stiffness brings to the fore a type of stiffness that is not generally familiar but which helps to present the problem of the dynamics of suspension bridges in clear physical terms, in a way that brings out the nature of the nonlinearity present.

It is worthwhile to indicate that the so-called "Linearized Deflection Theory of Suspension Bridges" in common use, is often presented in a form that appears to imply that the gravity stiffness of the cable is negligible; this is obviously misleading and results from neglect of the higher order term in the cable equation, Eq. 1.17, when it is used to obtain the expression for zero extension. This first

approximation, which corresponds to the condition of inextensibility and which has been used very commonly, is expressed by the relation

$$\sum_{i=1}^3 \int_0^{\ell_i} v_c dx_i = 0 \quad . \quad (1.23)$$

Now Eq. 1.23 suggests that the change in potential energy arising from gravity, Eqs. 1.20, 1.21 and 1.22, approximates zero for the inextensible cable.

It is seen by comparing Eqs. 1.21 and 1.23, that the conventional approach treats the integral in Eq. 1.23 as approximating zero, as though the gravity stiffness of the cable, given by Eqs. 1.20 and 1.22, were negligible and as though the cable were in a state of neutral equilibrium! This is obviously paradoxical. Actually, Pugsley [11] was the first one to examine more critically the use of the expression for an extensible cable (Eq. 1.21), when he studied the nonlinear response of a simple cable to a static concentrated load by using an energy approach. More discussion and alternative viewpoints on the inextensibility condition of the cable can be found in Appendix I-c.

### I-3-2. Potential energy of the suspended structure

The potential energy stored in the stiffening girders (or trusses) is in the form of strain energy due to the effects of bending moments, shearing forces and normal forces (see Fig. I-2-a).

The total vertical vibrational displacements,  $v_{gi}(x_i, t)$  or  $v_i(x_i, t)$ , of the  $i^{\text{th}}$  stiffening structure at a point  $x_i$ , consists of two parts, one caused by bending and one by shear, so the slope of

the deflection curve at the point  $x_i$  can be written as

$$\frac{\partial v_i(x_i, t)}{\partial x_i} = \eta_i(x_i, t) + \beta_i(x_i, t) \quad , \quad i = 1, 2, 3 \quad , \quad (1.24)$$

where  $\eta_i(x_i, t)$  is the slope of the deflection curve when the shearing force is neglected (i. e. , it is rotation due to bending) and  $\beta_i(x_i, t)$  is the angle of shear at the neutral axis in the same cross section. As usual, the linear deflection and the angular deflection are assumed small.

From the elementary flexural theory, the relation between the bending moment and the bending deformation is derived as

$$M_i(x_i, t) = E_{gi} I_{gi}(x_i) \frac{\partial \eta_i(x_i, t)}{\partial x_i} \quad , \quad i = 1, 2, 3 \quad , \quad (1.25)$$

where  $E_{gi}$  is the modulus of elasticity of the stiffening structure in the  $i^{\text{th}}$  span and  $I_{gi}(x_i)$  is the area moment of inertia of the stiffening girder (or truss) about its horizontal axis in the  $i^{\text{th}}$  span.

It is worthwhile to note that, in the case of a stiffening truss

$$I_{gi}(x_i) = 2A_i(x_i) \frac{d_i^2}{4} = A_i(x_i) \frac{d_i^2}{2} \quad , \quad i = 1, 2, 3 \quad , \quad (1.26)$$

where  $A_i(x_i)$  is the area of one chord at section  $x_i$  in the  $i^{\text{th}}$  span and  $d_i$  is the depth of the vertical truss in the  $i^{\text{th}}$  span.

The relation between the shearing force and shearing deformation is given by

$$S_i(x_i, t) = G_{gi} \mu_{vi}(x_i) \beta_i(x_i, t) \quad , \quad i = 1, 2, 3 \quad , \quad (1.27)$$

where  $G_{gi}$  is the shear modulus of the  $i^{\text{th}}$  stiffening structure and  $\mu_{vi}(x_i)$  is the shear resistance coefficient of the vertical web plate (or diagonal and vertical truss members). The value of the shear resistance coefficient depends on the effective cross-sectional area of the web plate (stiffening girder); in the case of a truss,  $\mu_{vi}$  depends on the equivalent solid web section, i. e., on the sectional area of the diagonal and vertical members in the truss panel. In the latter case it also depends on the type of truss system used. The shear resistance coefficients for the different types of trusses which are commonly used as stiffening trusses can be found in Chapter II. Because of shear alone, the element undergoes distortion but no rotation.

Now the potential energy due to vertical displacement can be expressed by

$$\begin{aligned}
 V_{gv}(t) &= \frac{1}{2} \sum_{i=1}^3 \int_0^{\ell_i} M_i(x_i, t) \frac{\partial \eta_i(x_i, t)}{\partial x_i} dx_i + \frac{1}{2} \sum_{i=1}^3 \int_0^{\ell_i} S_i(x_i, t) \beta_i(x_i, t) dx_i, \\
 &= \frac{1}{2} \sum_{i=1}^3 \int_0^{\ell_i} E_{gi} I_{gi}(x_i) \left( \frac{\partial \eta_i(x_i, t)}{\partial x_i} \right)^2 dx_i + \frac{1}{2} \sum_{i=1}^3 \int_0^{\ell_i} G_{gi} \mu_{vi}(x_i) \beta_i^2(x_i, t) dx_i.
 \end{aligned} \tag{1.28}$$

It is important to note that the first term of this equation represents the strain energy stored in the flanges (or chords) of the stiffening structure, while the second term represents the strain energy stored in the web system of the stiffening structure as a result of transverse shear deformation. The inclusion of shear flexibility in

the dynamical beam problem is known as the Timoshenko beam theory, in contrast to the Bernoulli-Euler theory, in which there is no transverse shear deformation.

The strain energy of the Timoshenko beam, Eq. 1.28, may be rewritten, conveniently, as

$$V_{gv}(t) = \frac{1}{2} \sum_{i=1}^3 \int_0^{\ell_i} E_{gi} I_{gi} \left( \frac{\partial \eta_i}{\partial x_i} \right)^2 dx_i + \frac{1}{2} \sum_{i=1}^3 \int_0^{\ell_i} G_{gi} \mu_{vi} \left( \frac{\partial v_i}{\partial x_i} - \eta_i \right)^2 dx_i . \quad (1.29)$$

Using Bernoulli-Euler theory, Eq. 1.24 reduces to

$$\frac{\partial v_i}{\partial x_i} = \eta_i , \quad i = 1, 2, 3 , \quad (1.30)$$

and it follows from Eq. 1.25 that

$$M_i = E_{gi} I_{gi} \frac{\partial^2 v_i}{\partial x_i^2} , \quad i = 1, 2, 3 , \quad (1.31)$$

The strain energy of the Bernoulli-Euler beam can now be written as

$$\tilde{V}_{gv}(t) = \frac{1}{2} \sum_{i=1}^3 \int_0^{\ell_i} E_{gi} I_{gi} \left( \frac{\partial^2 v_i}{\partial x_i^2} \right)^2 dx_i . \quad (1.32)$$

In general, the shear deformation effect plays an important role in the vibration of higher frequencies when a vibrating beam is subdivided by nodal cross sections into comparatively short portions. In other words, for the purpose of taking into account the effects of the cross-sectional dimensions on the frequencies, shear deformation

must be considered. When the cross-sectional dimensions of the beam are small in comparison with its length, Bernoulli-Euler theory can be used with acceptable accuracy.

The expression for the potential (or strain) energy of the stiffening structure, deforming longitudinally, is

$$V_{ge}(t) = \frac{1}{2} \sum_{i=1}^3 \int_0^{\ell_i} E_{gi} A_{gi}(x_i) \left( \frac{\partial u_{gi}(x_i, t)}{\partial x_i} \right)^2 dx_i, \quad (1.33)$$

where  $u_{gi}(x_i, t)$  is the longitudinal displacement of the  $i^{\text{th}}$  span and  $A_{gi}(x_i)$  is the cross-sectional area. In general, the longitudinal vibrational displacement  $u_{gi}(x_i, t)$  is very small as compared with the vertical displacement  $v_{gi}(x_i, t)$ .

The following analysis will consider only the vertical vibrational displacements of the structure.

### I-3-3. Kinetic energy of the vertically vibrating suspension bridge

In the Timoshenko beam theory, the kinetic energy of the vertically vibrating bridge is due to translation and rotation and is expressed as

$$T_v(t) = \frac{1}{2} \sum_{i=1}^3 \int_0^{\ell_i} m_i^*(x_i) \left( \frac{\partial v_i(x_i, t)}{\partial t} \right)^2 dx_i + \frac{1}{2} \sum_{i=1}^3 \int_0^{\ell_i} J_{gi}(x_i) \left( \frac{\partial \eta_i(x_i, t)}{\partial t} \right)^2 dx_i, \quad (1.34)$$

where  $m_i^*(x_i)$  is the mass of the bridge (i. e., cables and stiffening structures) per unit length of the  $i^{\text{th}}$  span, and  $J_{gi}(x_i)$  is the mass

moment of inertia per unit length of the  $i^{\text{th}}$  stiffening structure about the neutral axis which passes through the center of the girder (or truss). But  $J_{gi}(x_i)$  is related to  $I_{gi}(x_i)$  by

$$J_{gi}(x_i) = \rho_{gi} I_{gi}(x_i) = \frac{m_{gi}(x_i)}{A_{gi}(x_i)} I_{gi}(x_i) = r_i^2(x_i) m_{gi}(x_i) \quad , \quad i = 1, 2, 3 \quad , \quad (1.35)$$

where  $\rho_{gi}$  is the mass density of the  $i^{\text{th}}$  stiffening structure,  $m_{gi}(x_i)$  is the mass per unit length of the  $i^{\text{th}}$  stiffening structure and  $r_i(x_i)$  is the radius of gyration about the neutral axis.

When the cross-sectional dimensions are small compared with the length of span, the rotary inertia effects represented by the second integral in the kinetic energy expression, Eq. 1.34, can be neglected. Therefore, the kinetic energy expression of the vibrating bridge reduces to

$$\tilde{T}_V(t) = \frac{1}{2} \sum_{i=1}^3 \int_0^{\ell_i} m_i^*(x_i) \left( \frac{\partial v_i(x_i, t)}{\partial t} \right)^2 dx_i \quad . \quad (1.36)$$

The kinetic energy due to longitudinal deformations will not be considered since only vertical vibrational deformations are assumed.

#### I-3-4. Variational formulation of the equations of motion

##### a. Derivation of the general equations of motion

For convenience and simplicity, the differential equations of motion will be derived by Hamilton's principle, without taking into account the effects of shear deformations and rotary inertia. However,

Appendix I-e contains the derivation of the governing equations of motion including the effect of transverse shear deformations and rotary inertia.

Hamilton's principle is given by the integral form

$$\int_{t_1}^{t_2} \delta(T-V) dt = 0 \quad , \quad (1.37)$$

where  $T$  is the total kinetic energy of the vertically vibrating birdge,  $V$  is the total potential energy of the system, including both the strain energy and the potential energy of any conservative forces, and  $\delta$  is a variational operator taken during the indicated time interval.

The variation of kinetic energy,  $\tilde{T}_V(t)$ , has the form

$$\delta \tilde{T}_V(t) = \sum_{i=1}^3 \int_0^{\ell_i} m_i^*(x_i) \frac{\partial v_i}{\partial t} \delta \left( \frac{\partial v_i}{\partial t} \right) dx_i = \sum_{i=1}^3 \int_0^{\ell_i} m_i^*(x_i) \frac{\partial v_i}{\partial t} \frac{\partial}{\partial t} (\delta v_i) dx_i \quad ;$$

therefore,

$$\begin{aligned}
 \int_{t_1}^{t_2} \delta \tilde{T}_v(t) dt &= \int_{t_1}^{t_2} \sum_{i=1}^3 \left[ \int_0^{\ell_i} m_i^*(x_i) \frac{\partial v_i}{\partial t} \frac{\partial}{\partial t} (\delta v_i) dx_i \right] dt \\
 &= \sum_{i=1}^3 \int_0^{\ell_i} \left[ \int_{t_1}^{t_2} m_i^*(x_i) \frac{\partial v_i}{\partial t} \frac{\partial}{\partial t} (\delta v_i) dt \right] dx_i \\
 &= \sum_{i=1}^3 \int_0^{\ell_i} \left[ m_i^*(x_i) \frac{\partial v_i}{\partial t} \delta v_i \Big|_{t_1}^{t_2} - \int_{t_1}^{t_2} \frac{\partial}{\partial t} \left( m_i^*(x_i) \frac{\partial v_i}{\partial t} \right) \frac{\partial}{\partial t} (\delta v_i) dt \right] dx_i \\
 &= - \sum_{i=1}^3 \int_{t_1}^{t_2} \int_0^{\ell_i} m_i^*(x_i) \frac{\partial^2 v_i}{\partial t^2} \delta v_i dx_i dt \quad , \tag{1.38}
 \end{aligned}$$

Note that the order of integration with respect to  $x_i$  and  $t$  is interchangeable, and the variation and differentiation operators are commutative, so the integration can be performed by parts. Also, by definition,  $\delta v_i(x_i, t)$  is zero at  $t = t_1$  and  $t = t_2$ .

The total potential energy,  $\tilde{V}(t)$ , of the vertically vibrating bridge can be expressed, from Eq. 1.14, after substituting  $v_i$  for  $v_c$ , and from Eq. 1.32, as

$$\begin{aligned}
 \tilde{V}(t) = V_c(t) + \tilde{V}_{gv}(t) &= \frac{1}{2} \sum_{i=1}^3 \left\{ H_w \int_0^{\ell_i} \left( \frac{\partial v_i}{\partial x_i} \right)^2 dx_i \right. \\
 &\quad + H(t) \left[ \int_0^{\ell_i} \left( \frac{\partial v_i}{\partial x_i} \right) \left( \frac{dy_i}{dx_i} \right) dx_i + \frac{1}{2} \int_0^{\ell_i} \left( \frac{\partial v_i}{\partial x_i} \right)^2 dx_i \right] \\
 &\quad \left. + \int_0^{\ell_i} E_{gi} I_{gi} \left( \frac{\partial^2 v_i}{\partial x_i^2} \right)^2 dx_i \right\} \quad , \tag{1.39}
 \end{aligned}$$

and therefore, the variation of the total potential energy may be written as

$$\begin{aligned}
 \delta \tilde{V}(t) &= \sum_{i=1}^3 \left\{ H_w \int_0^{\ell_i} \frac{\partial v_i}{\partial x_i} \delta \left( \frac{\partial v_i}{\partial x_i} \right) dx_i + H(t) \left[ \int_0^{\ell_i} \left( \frac{dy_i}{dx_i} \right) \delta \left( \frac{\partial v_i}{\partial x_i} \right) dx_i + \int_0^{\ell_i} \left( \frac{\partial v_i}{\partial x_i} \right) \delta \left( \frac{\partial v_i}{\partial x_i} \right) dx_i \right] \right. \\
 &\quad \left. + \int_0^{\ell_i} E_{gi} I_{gi} \frac{\partial^2 v_i}{\partial x_i^2} \delta \left( \frac{\partial^2 v_i}{\partial x_i^2} \right) dx_i \right\} , \\
 &= \sum_{i=1}^3 \left\{ H_w \int_0^{\ell_i} \frac{\partial v_i}{\partial x_i} \frac{\partial}{\partial x_i} (\delta v_i) dx_i \right. \\
 &\quad \left. + H(t) \left[ \int_0^{\ell_i} \left( \frac{dy_i}{dx_i} \right) \frac{\partial}{\partial x_i} (\delta v_i) dx_i + \int_0^{\ell_i} \left( \frac{\partial v_i}{\partial x_i} \right) \frac{\partial}{\partial x_i} (\delta v_i) dx_i \right] \right. \\
 &\quad \left. + \int_0^{\ell_i} E_{gi} I_{gi} \frac{\partial^2 v_i}{\partial x_i^2} \frac{\partial}{\partial x_i^2} (\delta v_i) dx_i \right\} ,
 \end{aligned}$$

then integrating by parts, if it is necessary, yields

$$\begin{aligned}
 \delta \tilde{V}(t) &= \sum_{i=1}^3 \left\{ H_w \frac{\partial v_i}{\partial x_i} \delta v_i \Big|_0^{\ell_i} - \int_0^{\ell_i} \left( \frac{\partial}{\partial x_i} \left( H_w \frac{\partial v_i}{\partial x_i} \right) \right) \delta v_i dx_i \right. \\
 &\quad \left. + H(t) \left[ \frac{dy_i}{dx_i} \delta v_i \Big|_0^{\ell_i} - \int_0^{\ell_i} \frac{d^2 y_i}{dx_i^2} \delta v_i dx_i + \frac{\partial v_i}{\partial x_i} \delta v_i \Big|_0^{\ell_i} - \int_0^{\ell_i} \frac{\partial^2 v_i}{\partial x_i^2} \delta v_i dx_i \right] \right. \\
 &\quad \left. + E_{gi} I_{gi} \frac{\partial^2 v_i}{\partial x_i^2} \frac{\partial}{\partial x_i} (\delta v_i) \Big|_0^{\ell_i} - \frac{\partial}{\partial x_i} \left( E_{gi} I_{gi} \frac{\partial^2 v_i}{\partial x_i^2} \right) \delta v_i \Big|_0^{\ell_i} \right. \\
 &\quad \left. + \int_0^{\ell_i} \frac{\partial^2}{\partial x_i^2} \left( E_{gi} I_{gi} \frac{\partial^2 v_i}{\partial x_i^2} \right) \delta v_i dx_i \right\} ,
 \end{aligned}$$

$$\begin{aligned}
 \therefore \delta \tilde{V}(t) = & \sum_{i=1}^3 \left\{ \left[ \left( H_w + H(t) \right) \frac{\partial v_i}{\partial x_i} + H(t) \frac{dy_i}{dx_i} - \frac{\partial}{\partial x_i} \left( E_{gi} I_{gi} \frac{\partial^2 v_i}{\partial x_i^2} \right) \right] \delta v_i \right|_0^{\ell_i} \\
 & + E_{gi} I_{gi} \frac{\partial^2 v_i}{\partial x_i^2} \frac{\partial}{\partial x_i} (\delta v_i) \Big|_0^{\ell_i} \\
 & - \int_0^{\ell_i} \left[ \left( H_w + H(t) \right) \frac{\partial^2 v_i}{\partial x_i^2} + H(t) \frac{d^2 y_i}{dx_i^2} - \frac{\partial^2}{\partial x_i^2} \left( E_{gi} I_{gi} \frac{\partial^2 v_i}{\partial x_i^2} \right) \delta v_i dx_i \right] \Big\} .
 \end{aligned} \tag{1.40}$$

Introducing Eqs. 1.38 and 1.40 into Eq. 1.37 after using Eq. 1.12, gives

$$\begin{aligned}
 - \sum_{i=1}^3 \int_{t_1}^{t_2} \left\{ \int_0^{\ell_i} \left[ m_i^*(x_i) \frac{\partial^2 v_i}{\partial t^2} + \frac{\partial^2}{\partial x_i^2} \left( E_{gi} I_{gi}(x_i) \frac{\partial^2 v_i}{\partial x_i^2} \right) - \left( H_w + H(t) \right) \frac{\partial^2 v_i}{\partial x_i^2} \right. \right. \\
 \left. \left. + H(t) \frac{w_i^*}{H_w} \right] \delta v_i dx_i - E_{gi} I_{gi} \frac{\partial^2 v_i}{\partial x_i^2} \delta \left( \frac{\partial v_i}{\partial x_i} \right) \Big|_0^{\ell_i} \right. \\
 \left. + \left[ \frac{\partial}{\partial x_i} \left( E_{gi} I_{gi} \frac{\partial^2 v_i}{\partial x_i^2} \right) - \left( H_w + H(t) \right) \frac{\partial v_i}{\partial x_i} - H(t) \frac{dy_i}{dx_i} \right] \delta v_i \Big|_0^{\ell_i} \right\} dt = 0
 \end{aligned} \tag{1.41}$$

The integral must vanish for any arbitrary values of  $\delta v_i$  and  $\delta \left( \frac{\partial v_i}{\partial x_i} \right)$ , so these variations can be set equal to zero at  $x_i = 0$  and  $x_i = \ell_i$ ,  $i = 1, 2, 3$  and different from zero throughout the domains  $0 < x_i < \ell_i$ ,  $i = 1, 2, 3$ . Therefore, one must have

$$m_i^*(x_i) \frac{\partial^2 v_i}{\partial t^2} + \frac{\partial^2}{\partial x_i^2} \left( E_{gi} I_{gi}(x_i) \frac{\partial^2 v_i}{\partial x_i^2} \right) - \left( H_w + H(t) \right) \frac{\partial^2 v_i}{\partial x_i^2} + \frac{w_i^*}{H_w} H(t) = 0 , \tag{1.42}$$

$i = 1, 2, 3 ,$

where

$$H(t) = \frac{E_c A_c}{L_E} \sum_{i=1}^3 \left[ \int_0^{\ell_i} \left( \frac{\partial v_i}{\partial x_i} \right) \left( \frac{dy_i}{dx_i} \right) dx_i + \frac{1}{2} \int_0^{\ell_i} \left( \frac{\partial v_i}{\partial x_i} \right)^2 dx_i \right] . \quad (1.43)$$

Eqs. 1.42 and 1.43 are the basic differential and integral equations expressing the vertical vibration of suspension bridges. The symbol of summation in Eq. 1.43 is applied when the bridge has suspended side spans. Eqs. 1.42 and 1.43 are the well-known equations in the theory of suspension bridges.

Furthermore, because of the arbitrary nature of the variation, in considering Eq. 1.41, one can write

$$E_{gi} I_{gi} \frac{\partial^2 v_i}{\partial x_i^2} \delta \left( \frac{\partial v_i}{\partial x_i} \right) \Big|_0^{\ell_i} = 0 , \quad i = 1, 2, 3 , \quad (1.44)$$

and

$$\left[ \frac{\partial}{\partial x_i} \left( E_{gi} I_{gi} \frac{\partial^2 v_i}{\partial x_i^2} \right) - \left( H_w + H(t) \right) \frac{\partial v_i}{\partial x_i} - H(t) \frac{dy_i}{dx_i} \right] \delta v_i \Big|_0^{\ell_i} = 0 , \quad i = 1, 2, 3 , \quad (1.45)$$

which take into account the possibility that either

$$E_{gi} I_{gi} \frac{\partial^2 v_i}{\partial x_i^2} = 0 \quad \text{or} \quad \frac{\partial v_i}{\partial x_i} = 0 \quad \text{at} \quad x_i = 0 , \quad x_i = \ell_i , \quad i = 1, 2, 3 , \quad (1.46)$$

and that

$$\left[ \frac{\partial}{\partial x_i} \left( E_{gi} I_{gi} \frac{\partial^2 v_i}{\partial x_i^2} \right) - \left( H_w + H(t) \right) \frac{\partial v_i}{\partial x_i} - H(t) \frac{dy_i}{dx_i} \right] = 0 \quad (1.47)$$

$$\text{or} \quad v_i = 0 \quad \text{at} \quad x_i = 0 , \quad x_i = \ell_i , \quad i = 1, 2, 3 .$$

Eqs. 1.46 and 1.47 represent the boundary conditions associated with the equations of motion for vertically vibrating suspension bridges. The first part of Eq. 1.46 implies that the bending moment at each end vanishes, as in a bridge which has a stiffening structure with a free end or a simply supported end (hinged end). The second part of Eq. 1.46 indicates that the slope of the deflection curve vanishes at each end, such as when the ends of the stiffening structure are fixed (built-in ends). The first part of Eq. 1.47 requires that the vibrational resisting shear, which is developed by the vibration of the stiffening structure at the ends of each span, be equal to the vibrational shear which is developed by cable forces. The second part of Eq. 1.47 means that the vibrational displacement is zero at each end. Hence, both the natural and geometrical boundary conditions of the problem are presented.

Thus, Hamilton's principle has furnished the fundamental differential equation of vertical vibration corresponding to the defined energy, and it furnished conveniently all the most meaningful boundary conditions.

The differential equations including the effects of shear deformations and rotary inertia, derived in Appendix I-d, are:

$$\begin{aligned}
 & m_i^* \frac{\partial^2 v_i}{\partial t^2} + \frac{\partial^2}{\partial x_i^2} \left( E_{gi} I_{gi} \frac{\partial^2 v_i}{\partial x_i^2} \right) - m_{gi} r_i^2 \left( 1 + \frac{E_{gi} I_{gi}}{G_{gi} \mu_{vi} r_i^2} \right) \frac{\partial^4 v_i}{\partial x_i^2 \partial t^2} \\
 & + \frac{m_{gi} r_i^2}{G_{gi} \mu_{vi}} \frac{\partial^4 v_i}{\partial t^4} - (H_w + H(t)) \frac{\partial^2 v_i}{\partial x_i^2} + \frac{w_i^*}{H_w} H(t) = 0 \quad , \quad i = 1, 2, 3 ,
 \end{aligned}
 \tag{1.48}$$

where the effect of rotary inertia is represented by the term

$$m_{gi} r_i^2 \frac{\partial^4 v_i}{\partial x_i^2 \partial t^2} , \text{ while the effect of the shearing deformations is}$$

represented by the terms  $\left( m_{gi} \frac{E_{gi} I_{gi}}{G_{gi} \mu_{vi}} \frac{\partial^4 v_i}{\partial x_i^2 \partial t^2} + \frac{m_{gi}^2 r_i^2}{G_{gi} \mu_{vi}} \frac{\partial^4 v_i}{\partial t^4} \right) .$

b. Conventional linearized theory

The equations of motion, the cable equation and the boundary conditions which were derived above, have nonlinear terms:

- i. the term  $H(t) \frac{\partial^2 v_i}{\partial x_i^2}$  (Eqs. 1.42 and 1.48) ,
- ii. the term  $H(t) \frac{\partial v_i}{\partial x_i}$  (Eq. 1.47) , and
- iii. the term  $\frac{1}{2} \int_0^l \left( \frac{\partial v_i}{\partial x_i} \right)^2 dx_i$  (Eq. 1.43) .

Two useful simplifications are possible as aids in linearizing the problem:

1. It has been assumed that the horizontal component of cable tension  $H(t)$  due to inertia loads is small compared with the initial tension  $H_w$  . In this case, Eqs. 1.42, 1.47 and 1.48 can be simplified by the omission of  $H(t)$  , to read:

$$m_i^*(x_i) \frac{\partial^2 v_i}{\partial t^2} + \frac{\partial^2}{\partial x_i^2} \left( E_{gi} I_{gi}(x_i) \frac{\partial^2 v_i}{\partial x_i^2} \right) - H_w \frac{\partial^2 v_i}{\partial x_i^2} + \frac{w_i^*}{H_w} H(t) = 0 , \quad i = 1, 2, 3 ,$$

(1.49)

$$\left[ \frac{\partial}{\partial x_i} \left( E_{gi} I_{gi} \frac{\partial^2 v_i}{\partial x_i^2} \right) - H_w \frac{\partial v_i}{\partial x_i} - H(t) \frac{dy_i}{dx_i} \right] = 0 \text{ at } x_i = 0, \text{ at } x_i = \ell_i, \quad (1.50)$$

$i = 1, 2, 3,$

and

$$\begin{aligned} m_i^* \frac{\partial^2 v_i}{\partial t^2} + \frac{\partial^2}{\partial x_i^2} \left( E_{gi} I_{gi} \frac{\partial^2 v_i}{\partial x_i^2} \right) - m_{gi} r_i^2 \left( 1 + \frac{E_{gi} I_{gi}}{G_{gi} \mu_{vi} r_i^2} \right) \frac{\partial^4 v_i}{\partial x_i^2 \partial t^2} \\ + \frac{m_{gi}^2 r_i^2}{G_{gi} \mu_{vi}} \frac{\partial^4 v_i}{\partial t^4} - H_w \frac{\partial^2 v_i}{\partial x_i^2} + \frac{w_i^*}{H_w} H(t) = 0, \quad i = 1, 2, 3, \end{aligned} \quad (1.51)$$

2. Since small vibrational displacements have been assumed, the nonlinear, second order term in the cable equation (Eq. 1.43) may be neglected, and the cable equation is reduced to

$$\tilde{H}(t) = \frac{E_c A_c}{L_E} \sum_{i=1}^3 \left[ \int_0^{\ell_i} \left( \frac{\partial v_i}{\partial x_i} \right) \left( \frac{dy_i}{dx_i} \right) dx_i \right], \quad (1.52-a)$$

or (by using Eq. 1.8')

$$\tilde{H}(t) = \frac{E_c A_c}{L_E} \sum_{i=1}^3 \left[ \frac{w_i^*}{H_w} \int_0^{\ell_i} v_i dx_i \right]. \quad (1.52-b)$$

The basic equations of motion (Eq. 1.49 or Eq. 1.51) thus become linear differential equations. These equations have been studied at some length by Steinman [14] and by Bleich [9]. The former concentrated on study of bridges having an inextensible cable. Bleich's work on this problem, using the full equations of motion (Eq. 1.49), allowed for the elastic extensibility of the cable

and led to expressions for the frequency equations that are much more complicated and that, therefore, could not be solved explicitly.

Another way of treating the linearized problem is by means of energy relations, using trigonometrical series for the approximate representation of the modes of vertical vibration. This series method was, as in so many structural problems, first applied by Timoshenko. Then the application of the Rayleigh-Ritz method in dynamics leads to a system of linear, homogeneous equations determining the natural frequencies. Bleich [9] used this approximate technique for the determination of the first three modes of vertical vibration (and their natural frequencies) of suspension bridges with hinged and continuous three-span stiffening structures.

#### I-4. A Finite Element Approach to Vertical Vibrations

The finite element method, an effective and commonly used discretization procedure, provides a convenient and reliable idealization of the structure under consideration and is particularly effective in a digital-computer analysis.

The first step in the finite-element idealization of the structure involves dividing the suspension bridge into an appropriate number of segments, or elements. Their size is arbitrary; they may all be of the same size or may all be different. Then, a set of nodal points is selected along the boundaries of these elements. The displacements of these nodal points are taken as the degrees of freedom (generalized coordinates) of the system.

The deflection of the complete structure can now be expressed in terms of these generalized coordinates by means of an appropriate set of assumed displacement functions. In this case, however, the displacement functions are called interpolation functions because they define the shape of the displacement curve between the specified nodal displacements. Furthermore, as the displacements associated with any degree of freedom are non-zero over only the neighboring finite elements, the mass and stiffness matrices will be very sparse, and the degrees of freedom can be ordered so as to arrange the matrices in banded form, leading to great reductions in the computational effort and the computer storage required for analysis. However, as is discussed later, there is a case where evaluation of the interaction among all elements is necessary in order to formulate the elastic stiffness matrix, and this necessitates a full matrix.

The evaluation of the stiffness matrices for the finite elements involves expressing the potential (or strain) energy of the element or the assemblage in terms of nodal displacements, which leads to an expression for the stiffness matrices in terms of the finite element interpolation functions and various other structural properties.

Except for satisfying the appropriate continuity conditions at inter-element boundaries, considerable freedom exists in selecting the interpolation functions. The computational effort required in determining the element stiffness matrices, and the accuracy with which the element represents the stress and deformation state in the structure, depends on the interpolation functions, i. e., on the order of the polynomial if interpolating polynomials are being used.

The element consistent mass matrix can be determined in a manner similar to the formulation of the stiffness matrix. Basically, the kinetic energy of the element is expressed in terms of the nodal velocities, leading to an expression for the mass matrix in terms of the mass density and interpolation functions (which were used in determining the stiffness matrix).

In this section, the underlying principles of structural idealization for suspension bridge structures are discussed. Also, stiffness and inertia properties are developed for the elements and for the entire assembled suspension bridge, using the different energy expressions developed for suspension bridges in the previous section. Finally, Hamilton's Principle is used to derive the equations of motion, from which the natural frequencies and modes of vibration are obtained.

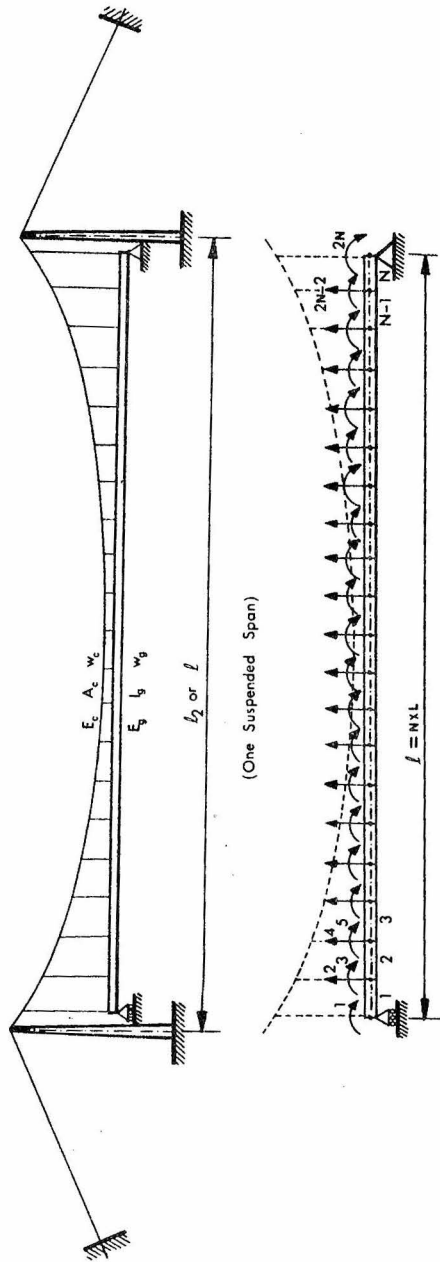
This formulation has the advantage of dealing only with purely scalar energy quantities. Several numerical examples are included to illustrate the effectiveness and the applicability of the analysis under consideration, and to investigate the dynamic characteristics of suspension bridges.

I-4-1. Idealization of the structure and the displacement model

By the finite element approach, the suspension bridge structure is assumed to be divided into a system of discrete elements which are interconnected only at a finite number of nodal points. It has been assumed previously, in Sec. I-2, that the suspenders are inextensible and remain vertical during vibration, and that consequently the vibrational displacements of both the cable and the stiffening structure are identical; these assumptions lead to the following:

1. The element consists of cable and girder (or truss) elements connected by two or more rigid suspenders, as shown in Fig. I-3-b.
2. The elements are connected to each other at common cross sections or interfaces; this defines the cable nodes as well as the stiffening girder (or truss) nodes.
3. Since the displacements of each stiffening structure node must equal the displacements of the corresponding cable node (joined by a single suspender), it is appropriate to define only the nodes on the centerline of the stiffening structure, as shown in Fig. I-3-a.

FINITE ELEMENT ANALYSIS OF SUSPENSION BRIDGES  
FREE VERTICAL VIBRATIONS



(a) Translation and Rotation Coordinates

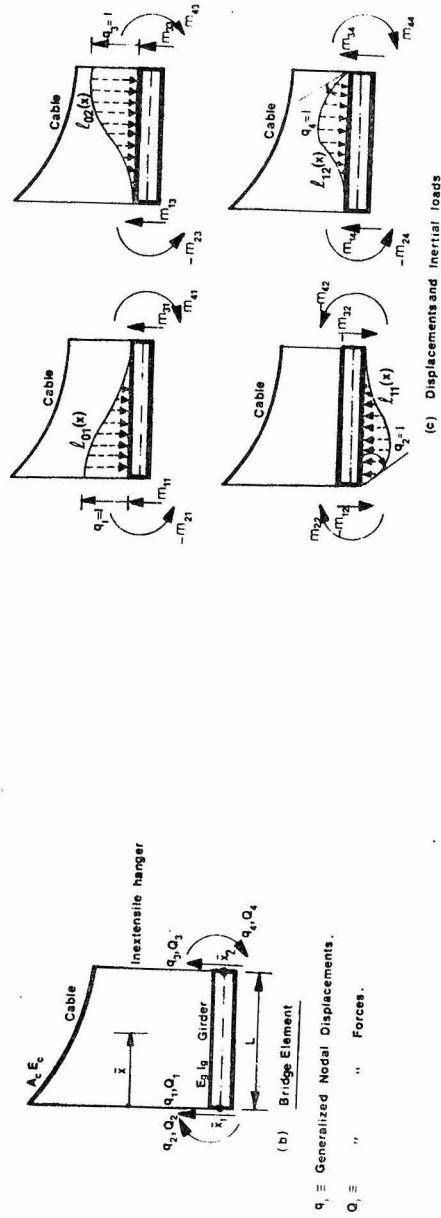


Fig. I-3. Finite-element definition diagram.

The two nodal points by which this type of element can be assembled into the suspended bridge structure are located at its ends. Obviously any number of elements may be chosen in establishing the idealized system, depending on the accuracy desired. If only vertical plane displacements are considered, there are two nodal degrees of freedom at each node: vertical translation and rotation. The interpolation functions associated with the two degrees of freedom of the nodal point, which produce vertical displacements, could be any arbitrary shapes which satisfy nodal and internal continuity requirements, but they are generally assumed to be the shapes which develop in a uniform beam subjected to these nodal displacements. These are cubic Hermitian polynomials which are sketched in Fig. I-3-c, and may be expressed as:

$$\left. \begin{aligned} l_{01}(\bar{x}) &= 1 - 3 \frac{\bar{x}^2}{L^3} + 2 \frac{\bar{x}^3}{L^3} , \\ l_{02}(\bar{x}) &= 3 \frac{\bar{x}^2}{L^2} - 2 \frac{\bar{x}^3}{L^3} , \\ l_{11}(\bar{x}) &= \bar{x} - 2 \frac{\bar{x}^2}{L} + \frac{\bar{x}^3}{L^2} , \\ l_{12}(\bar{x}) &= -\frac{\bar{x}^2}{L} + \frac{\bar{x}^3}{L^2} , \end{aligned} \right\} \quad (1.53)$$

where  $L$  is the length of an element in the suspended structure.

With these four interpolation functions, the deflection shape  $v_e(\bar{x}, t)$ , of the element can now be expressed in terms of its nodal displacements as:

$$v_e(\bar{x}, t) = l_{01}(\bar{x})q_1(t) + l_{11}(\bar{x})q_2(t) + l_{02}(\bar{x})q_3(t) + l_{12}(\bar{x})q_4(t) , \quad (1.54)$$

where  $e$  is the subscript indicating "element," and  $q_i(t)$ ,  $i = 1, 2, 3, 4$  are the nodal displacements for the element. (See Fig. I-3-b.)

Eq. 1.54 can be written in a matrix form as

$$v_e(\bar{x}, t) = \{f(\bar{x})\}_e^T \{q(t)\}_e , \quad (1.55)$$

in which  $\{f(\bar{x})\}_e^T$  represents the transpose of  $\{f(\bar{x})\}_e$ ; it is the vector of the polynomials

$$\{f(\bar{x})\}_e^T = \left[ l_{01}(\bar{x}), l_{11}(\bar{x}), l_{02}(\bar{x}), l_{12}(\bar{x}) \right] , \quad (1.56)$$

and  $\{q(t)\}$  is the vector of nodal displacement for the element.

By introducing the normalized coordinates

$$\xi_1(\bar{x}) = \left( 1 - \frac{\bar{x}}{L} \right) \quad \text{and} \quad \xi_2(\bar{x}) = \left( \frac{\bar{x}}{L} \right) , \quad (1.57)$$

any point  $\bar{x}$  in the element  $[0, L]$  can be referred to in terms of the "coordinate functions,"  $\xi_1(\bar{x})$  and  $\xi_2(\bar{x})$ , as new coordinates.

Therefore, Eq. 1.55 can be written as

$$v_e(\xi_1, \xi_2; t) = \left[ \xi_1^2(3 - 2\xi_1), -L\xi_1^2\xi_2, \xi_2^2(3 - 2\xi_2), L\xi_1\xi_2^2 \right] \{q(t)\} . \quad (1.58)$$

Finally, integration of the polynomial terms in the normalized coordinates is conveniently expressed by the formula

$$\int_0^L \xi_1^n \xi_2^m d\bar{x} = \frac{n! m!}{(n+m+1)!} L , \quad (1.59)$$

where  $n!$  is the factorial product  $n(n-1)(n-2) \dots (1)$ , and  $0!$  is defined as unity. Also, differentiation with respect to  $\bar{x}$  is given by the formula

$$\frac{d}{d\bar{x}} \left( \quad \right) = \sum_{i=1}^2 \frac{\partial \xi_i}{\partial \bar{x}} \cdot \frac{\partial}{\partial \xi_i} \left( \quad \right) = \frac{1}{L} \left[ \frac{\partial}{\partial \xi_2} \left( \quad \right) - \frac{\partial}{\partial \xi_1} \left( \quad \right) \right]. \quad (1.60)$$

#### I-4-2. Evaluation of structural-property matrices

In practice, the finite element approach frequently provides the most convenient means for evaluating the elastic or stiffness properties of the complete structure. These properties are found by evaluating the properties of the individual finite elements and superposing them appropriately. Thus the problem of defining the stiffness properties of the structure is reduced basically to evaluating the stiffness of a typical element.

##### a. Elastic stiffness matrix of the stiffening girder (or truss)

The strain energy of the stiffening structure due to bending only (Bernoulli-Euler beam), Eq. 1.32, may be expressed (with the aid of the displacement model, Eq. 1.58), as

$$\tilde{V}_{gv}(t) = \frac{1}{2} \sum_{i=1}^3 \left[ \sum_{e=1}^{N_i} \int_0^L E_{ge} I_{ge}(\bar{x}) \left( \{f''\}_e^T \{q\}_e \right)^T \left( \{f''\}_e \{q\}_e \right) d\bar{x} \right], \quad (1.61)$$

where  $N_i$  is the total number of elements used to present the  $i^{\text{th}}$  bridge span, and  $E_{ge} I_{ge}$  is the flexural rigidity of the element; it is assumed uniform over the entire element. The integrations involved

in Eq. 1.61 are performed for the individual elements before the summation inherent in the assembly process is carried out. Here,  $\{f''\}_e$  is the vector of the curvature model; this vector can be accomplished by using Eqs. 1.58 and 1.59. The resulting curvature model vector is

$$\{f''\}_e^T = \{f''(\xi_1, \xi_2)\}_e^T = \frac{1}{L^2} \left[ (6-12\xi_1), L(4\xi_1-2\xi_2), (6-12\xi_2), L(2\xi_1-4\xi_2) \right]. \quad (1.62)$$

Eq. 1.61 may be expressed conveniently in terms of the stiffness matrix, as

$$\tilde{V}_{gv}(t) = \frac{1}{2} \sum_{e=1}^N \{q\}_e^T [\tilde{k}_{ge}]_e \{q\}_e, \quad (1.63)$$

with the understanding that  $N = \sum_{i=1}^3 N_i$  is the total number of elements used to present the entire assembled structure, and

$$[\tilde{k}_{ge}]_e = \int_0^L E_{ge} I_{ge} \{f''\}_e \{f''\}_e^T d\bar{x}, \quad (1.64)$$

is the element elastic stiffness matrix of the stiffening girder (or truss). The subscript  $ge$  indicates "girder elastic," while the subscript  $e$  alone indicates "element." The integration involved in the evaluation of  $[\tilde{k}_{ge}]_e$  can be accomplished by using Eq. 1.62 and the integration property (Eq. 1.59) of the interpolation function. The resulting stiffness matrix is

$$[\tilde{k}_{ge}]_e = \frac{E_{ge} I_{ge}}{L^3} \begin{bmatrix} 12 & -6L & -12 & -6L \\ -6L & 4L^2 & 6L & 2L^2 \\ -12 & 6L & 12 & 6L \\ -6L & 2L^2 & 6L & 4L^2 \end{bmatrix} \quad (1.65)$$

It should be noted that these stiffness coefficients are the exact values for a uniform beam without shear deformation because the interpolation functions used in Eq. 1.53 are the true shapes for this case. For an analysis of the effect of shear deformations on a beam element, refer to Ref. [27]; this consideration of shear deformation naturally leads to rather complicated expressions for the interpolation functions, and consequently the formulation of the elastic stiffness matrix is complex and is therefore not presented here. The matrix itself reads:

$$[k_{ge}]_e = \frac{E_{ge} I_{ge}}{L^3 (1+\Phi)} \begin{bmatrix} 12 & -6L & -12 & -6L \\ -6L & (4+\Phi)L^2 & 6L & (2-\Phi)L^2 \\ -12 & 6L & 12 & 6L \\ -6L & (2-\Phi)L^2 & 6L & (4+\Phi)L^2 \end{bmatrix}, \quad (1.66)$$

where

$$\Phi = \left( \frac{12E_{ge} I_{ge}}{G_{ge\mu} L^2} \right), \quad (1.67)$$

in which  $G_{ge\mu}$  is the shear rigidity of the element.

As mentioned earlier, the process of constructing the equations for the assemblage from the equations for the individual elements is

routine. Nodal compatibility is used as the basis for this process. Because the displacements are matched at the nodes, the stiffnesses are added at these locations; therefore, the assemblage stiffness matrix and the nodal displacements can be written as follows

$$[\tilde{K}_{GE}] = \sum_{e=1}^N [\tilde{k}_{ge}]_e \text{ or } [K_{GE}] = \sum_{e=1}^N [k_{ge}]_e , \quad (1.68)$$

and

$$\{r\} = \sum_{e=1}^N \{q\}_e . \quad (1.69)$$

Now, the total strain energy of the assemblage due to the contribution from the stiffening girders (or trusses) can be written as

$$\tilde{V}_{gv}(t) = \frac{1}{2} \{r\}^T [\tilde{K}_{GE}] \{r\} \text{ or } V_{gv}(t) = \frac{1}{2} \{r\}^T [K_{GE}] \{r\} . \quad (1.70)$$

Finally, when it is noted that the strain energy stored in a stable structure during distortion must always be positive, it is evident that

$$\frac{1}{2} \{r\}^T [\tilde{K}_{GE}] \{r\} > 0 \text{ or } \frac{1}{2} \{r\}^T [K_{GE}] \{r\} > 0 .$$

Matrices which satisfy this condition, where  $\{r\}$  is any arbitrary nonzero vector, are said to be positive definite; positive definite matrices (and consequently stiffness matrices) are nonsingular and can be inverted. The stiffness matrix is also symmetric and banded.

b. Consistent gravity-stiffness matrix of the cable

From the strainless or gravitational energy expression of the cable (Eq. 1.22), it has been found that this energy depends not only on the change in the shape of the cable but also on the initial internal stress, represented by the constant  $H_w$ . A similar situation exists in the buckling problems. In these problems, the geometric-stiffness property represents the tendency toward buckling induced in a structure by axially directed load components; thus it depends not only on the configuration of the structure but also on its condition of loading.

The finite-element concept can be used to obtain a higher-order approximation of gravity stiffness by using Hermitian interpolation functions (Eq. 1.53) in deriving the gravity-stiffness coefficients; the result is called the consistent gravity-stiffness matrix. Thus the consistent gravity-stiffness matrix represents rotational as well as translational degrees of freedom.

Now, the gravitational energy of the cable  $V_{cg}(t)$  (Eq. 1.22) and the displacement model (Eq. 1.58), give

$$V_{cg}(t) = \frac{1}{2} \sum_{e=1}^N \left[ \int_0^L H_w (\{f'\}_e^T \{q\})^T (\{f'\}_e^T \{q\}_e) d\bar{x} \right], \quad (1.71)$$

where  $\{f'\}_e$  is the vector of the slope of the model displacement and is expressed by

$$\{f'\}_e^T = \frac{1}{L} \left[ 6\xi_1(\xi_1 - 1), L\xi_1(2\xi_2 - \xi_1), 6\xi_2(1 - \xi_2), L\xi_2(2\xi_1 - \xi_2) \right] \quad (1.72)$$

Eq. 1.71 may be expressed conveniently in terms of the consistent gravity-stiffness matrix, as follows

$$V_{cg}(t) = \frac{1}{2} \sum_{e=1}^N \{q\}_e^T [k_{cg}]_e \{q\}_e \quad , \quad (1.73)$$

in which

$$[k_{cg}]_e = H_w \int_0^L \{f'\}_e \{f'\}_e^T d\bar{x} \quad , \quad (1.74)$$

in the element consistent gravity-stiffness matrix. In the double subscript  $cg$ ,  $c$  indicates "cable" and  $g$  indicates "gravity."

Substituting Eq. 1.72 into Eq. 1.74, and using the integration property (Eq. 1.59) in the resulting matrix, the element consistent gravity-stiffness matrix can be obtained as

$$[k_{cg}]_e = \frac{H_w}{30L} \begin{bmatrix} 36 & -3L & -36 & -3L \\ -3L & 4L^2 & 3L & -L^2 \\ -36 & 3L & 36 & 3L \\ -3L & -L^2 & 3L & 4L^2 \end{bmatrix} \quad . \quad (1.75)$$

The assemblage gravity-stiffness matrix can be obtained by merely adding the element stiffness coefficients appropriately and by taking the boundary conditions into consideration, it is expressed as

$$[K_{CG}] = \sum_{e=1}^N [k_{cg}]_e \quad ,$$

which has a similar configuration (positions of the non-zero terms) as the elastic stiffness matrix  $[K_{GE}]$ .

Now, the potential energy expression (due to gravity) of the assemblage may be given as

$$V_{cg}(t) = \frac{1}{2} \{r\}^T [K_{CG}] \{r\} , \quad (1.76)$$

in which  $[K_{CG}]$  is a positive definite, symmetric and banded matrix.

c. Elastic stiffness matrix of the cable

Using the linearized cable equation (Eq. 1.52-b), the strain energy of the cable due to the additional cable tension caused by vibration (Eq. 1.19) may be written as

$$\tilde{V}_{ce}(t) = \frac{1}{2} \frac{\tilde{H}^2(t) L_E}{E_c A_c} = \frac{1}{2} \frac{L_E}{E_c A_c} \left[ \frac{E_c A_c}{L_E} \sum_{i=1}^3 \frac{\tilde{w}_i^*}{H_w} \int_0^L v_i(x_i, t) dx_i \right]^2 \quad (1.77)$$

With the aid of the displacement model (Eq. 1.58), the energy expression (Eq. 1.77) becomes

$$\tilde{V}_{ce}(t) = \frac{1}{2} \left( \frac{E_c A_c}{L_E} \right) \sum_{i=1}^3 \left[ \sum_{e=1}^{N_i} \frac{\tilde{w}_i^*}{H_w} \int_0^L \{f\}_e^T \{q\}_e d\bar{x} \right]^T \left[ \sum_{e=1}^{N_i} \frac{\tilde{w}_i^*}{H_w} \int_0^L \{f\}_e^T \{q\}_e d\bar{x} \right] , \quad (1.78)$$

and upon using the assemblage nodal displacement  $\{r\}$  in Eq. 1.78, it can be obtained

$$\tilde{V}_{ce}(t) = \frac{1}{2} \left( \frac{E_c A_c}{L_E} \right) \{r\}^T \left[ \sum_{i=1}^3 \left( \sum_{e=1}^{N_i} \frac{\tilde{w}_i^*}{H_w} \int_0^L \{f\}_e^T d\bar{x} \right)^T \left( \sum_{e=1}^{N_i} \frac{\tilde{w}_i^*}{H_w} \int_0^L \{f\}_e^T d\bar{x} \right) \right] \{r\} . \quad (1.79)$$

Now, define the vector  $\{\hat{f}\}_e$  as the integral

$$\{\hat{f}\}_e^T = \int_0^L \{f\}_e^T d\bar{x} = \left[ \frac{L}{2}, -\frac{L^2}{12}, \frac{L}{2}, \frac{L^2}{12} \right] , \quad (1.80)$$

and

$$\{\hat{f}\}_{N_i} = \sum_{e=1}^{N_i} \{f\}_e \quad ; \quad (1.81)$$

then Eq. 1.79 becomes

$$\tilde{V}_{ce}(t) = \frac{1}{2} \{r\}^T \left[ \frac{E_c A_c}{L_E} \left( \sum_{i=1}^3 \frac{\bar{w}_i^*}{H_w} \{\hat{f}\}_{N_i} \right) \left( \sum_{i=1}^3 \frac{\bar{w}_i^*}{H_w} \{\hat{f}\}_{N_i}^T \right) \right] \{r\}, \quad (1.82)$$

or equivalently

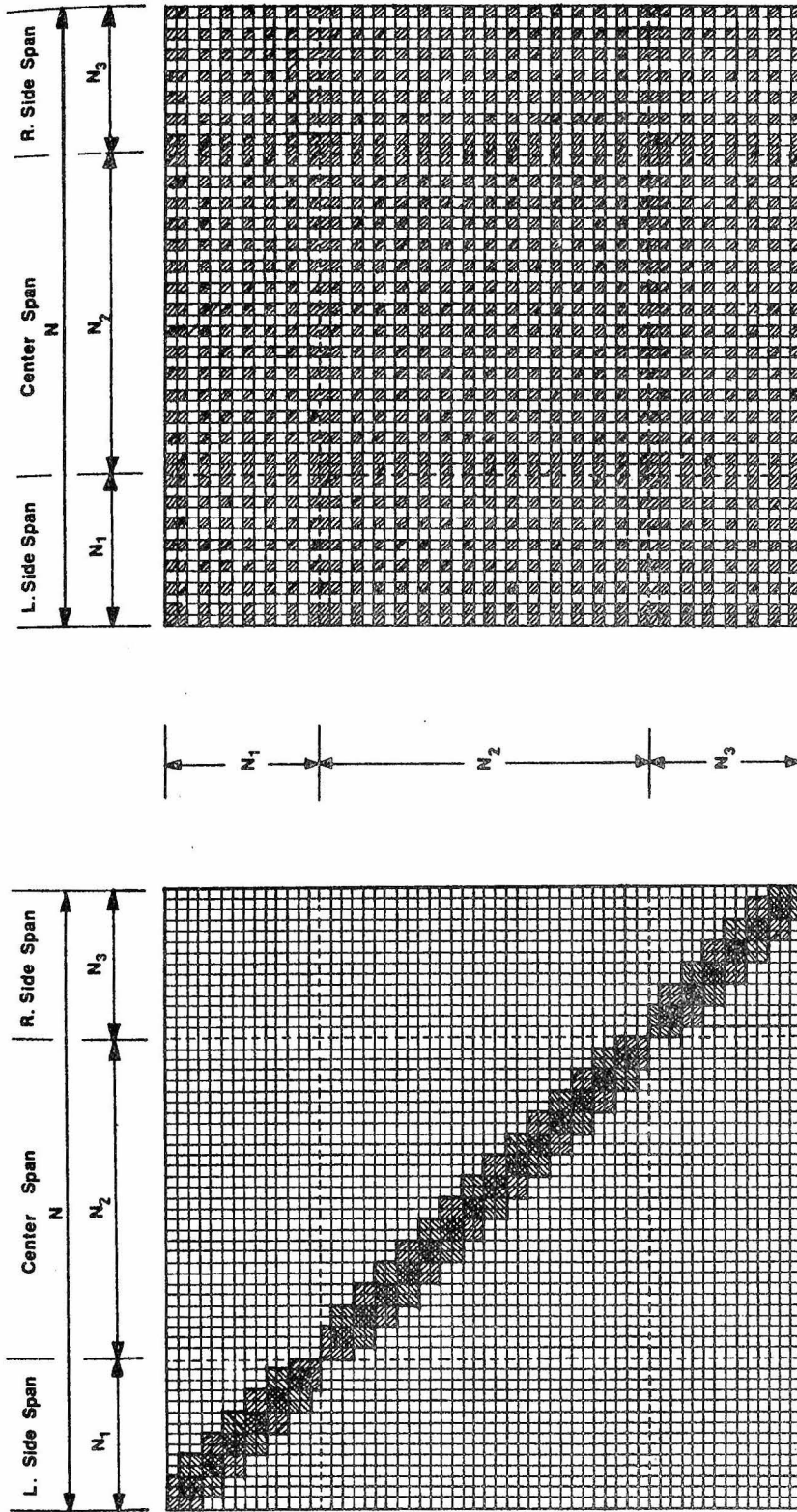
$$\tilde{V}_{ce}(t) = \frac{1}{2} \{r\}^T [K_{CE}] \{r\} \quad , \quad (1.83)$$

in which  $[K_{CE}]$  is the assemblage elastic stiffness matrix of the cable; it can be defined as

$$[K_{CE}] = \frac{E_c A_c}{L_E} \left[ \left( \sum_{i=1}^3 \frac{\bar{w}_i^*}{H_w} \{\hat{f}\}_{N_i} \right) \left( \sum_{i=1}^3 \frac{\bar{w}_i^*}{H_w} \{\hat{f}\}_{N_i}^T \right) \right] \quad . \quad (1.84)$$

This matrix is symmetric and is a partially complete matrix (i. e., not banded); the arrays are well distributed over the matrix. A general form for such a matrix and for the banded stiffness matrices  $[K_{GE}]$  and  $[K_{CG}]$  is shown schematically in Fig. I-4; only the hatched blocks are non-zero arrays. These matrices are the assemblage matrices for the special case of a suspension bridge with hinged stiffening structures.

AN EXAMPLE: (SUSPENSION BRIDGE WITH THREE SPANS [HINGED])



General Form of Banded Coefficient Matrices  $[M]$ ,  $[K_{GE}]$  &  $[K_{CE}]$ .

General Form of Full Coefficient Matrix  $[K_{CE}]$ .

Fig. I-4. Schematics of the form of the stiffness and inertia matrices (banded and full).

I-4-3. Evaluation of inertia-property matrices

Making use of the finite-element concept, it is possible to evaluate mass influence coefficients for each element of the bridge by a procedure similar to the analyses of element stiffness matrices. The degrees of freedom of the element are the translation and rotation at each end, and it is assumed that the displacements within the element are defined by the same interpolation functions used in deriving the element stiffnesses; the result is called the consistent-mass matrix.

Consistent-mass matrix

When interpolation displacement models are used, Eq. 1.58 can be inserted into the expression for translational kinetic energy (Eq. 1.36) to obtain,

$$\tilde{T}_V(t) = \frac{1}{2} \sum_{i=1}^3 \left[ \sum_{e=1}^{N_i} m_e^* \int_0^L (\{f\}_e^T \{\dot{q}\}_e)^T (\{f\}_e^T \{\dot{q}\}_e) d\bar{x} \right], \quad (1.85)$$

where  $m_e^*$  is the mass of the bridge element per unit length.

Eq. 1.85 can also be written as

$$\tilde{T}_V(t) = \frac{1}{2} \sum_{i=1}^3 \left( \sum_{e=1}^{N_i} \{\dot{q}\}_e^T [\tilde{m}]_e \{\dot{q}\}_e \right), \quad (1.86)$$

where  $[\tilde{m}]_e$  is the consistent mass matrix of the element which is defined as

$$[\tilde{m}]_e = m_e^* \int_0^L \{f\}_e \{f\}_e^T d\bar{x} . \quad (1.87)$$

The integration involved in the evaluation of  $[\tilde{m}_e]$  can be accomplished by using Eqs. 1.58 and 1.59. The resulting consistent-mass matrix is

$$[\tilde{m}]_e = \frac{m_e^* L}{420} \begin{bmatrix} 156 & -22L & 54 & 13L \\ -22L & 4L^2 & -13L & -3L^2 \\ 54 & -13L & 156 & 22L \\ 13L & -3L^2 & 22L & 4L^2 \end{bmatrix} \quad (1.88)$$

The physical meaning of the different coefficients of this matrix is shown in Fig. I-3-c. The mass matrix of the complete element assemblage can be developed by exactly the same type of superposition procedure as that described for development of the assemblage stiffness matrix. The resulting mass matrix will have the same general configuration (that is, arrangement of non-zero terms) as the stiffness matrices  $[K_{GE}]$  and  $[K_{CG}]$ . The assemblage consistent-mass matrix is

$$[\tilde{M}] = \sum_{e=1}^N [\tilde{m}]_e \quad , \quad (1.89)$$

and, therefore, the translational kinetic energy can be written as

$$\tilde{T}_V(t) = \frac{1}{2} \{\dot{r}\}^T [\tilde{M}] \{\dot{r}\} \quad . \quad (1.90)$$

The evaluation of the consistent-mass matrix, when the effects of both shear deformation and rotary inertia are accounted for, is very involved (see Ref. 27). However, if the kinetic energy due to translation and rotation is considered and the shear deformation is

neglected the resulting consistent-mass matrix takes the form

$$[m]_e = \frac{\dot{m}_e^* L}{420} \begin{bmatrix} 156 & -22L & 54 & 13L \\ -22L & 4L^2 & -13L & -3L^2 \\ 54 & -13L & 156 & 22L \\ 13L & -3L^2 & 22L & 4L^2 \end{bmatrix} + \frac{m_{ge} r_e^2}{30L} \begin{bmatrix} 36 & 3L & -36 & 3L \\ 3L & 4L^2 & -3L & -L^2 \\ -36 & -3L & 36 & -3L \\ 3L & -L^2 & -3L & 4L^2 \end{bmatrix}, \quad (1.91)$$

where  $m_{ge}$  is the mass of the stiffening girder (or truss) element per unit length and  $r_e$  is the radius of gyration of the element cross section. The first term in Eq. 1.91 represents the translational inertia of the element, i. e., the mass matrix  $[\tilde{m}]_e$ , while the second term represents the rotatory inertia. A derivation of the general consistent-mass matrix can be found in Ref. 27.

#### I-4-4. Variational formulation of the matrix equations of motion

To establish the matrix equations of motion, one can make use of the scalar energy quantities, already obtained, in a variational form. The most generally applicable variational concept is Hamilton's Principle (Eq. 1.37), which leads directly to the equation of motion.

Now, inserting Eqs. 1.70, 1.76, 1.83 and 1.90 into Hamilton's Principle (Eq. 1.37), one can obtain for the assemblage

$$\delta \int_{t_1}^{t_2} \frac{1}{2} \left( \{\dot{r}\}^T [\tilde{M}] \{\dot{r}\} - \{r\}^T [\tilde{K}_{GE}] \{r\} - \{r\}^T [K_{CG}] \{r\} - \{r\}^T [K_{CE}] \{r\} \right) dt = 0 .$$

Applying the variational operator yields

$$\int_{t_1}^{t_2} \left( \{\delta \dot{r}\}^T [\tilde{M}] \{\dot{r}\} - \{\delta r\}^T \left[ [\tilde{K}_{GE}] + [K_{CG}] + [K_{CE}] \right] \{r\} \right) dt = 0 \quad (1.92)$$

Integration of the first term by parts with respect to time gives

$$\int_{t_1}^{t_2} \{\delta \dot{r}\}^T [\tilde{M}] \{\dot{r}\} dt = \left( \{\delta r\}^T [\tilde{M}] \{\dot{r}\} \right) \Big|_{t_1}^{t_2} - \int_{t_1}^{t_2} \{\delta r\}^T [\tilde{M}] \{\ddot{r}\} dt \quad (1.93)$$

Again, according to Hamilton's Principle, the tentative displacement configuration must satisfy given conditions at time  $t_1$  and  $t_2$ . Hence,  $\{\delta r(t_1)\} = \{\delta r(t_2)\} = \{0\}$ , so the first term on the right hand side of Eq. 1.93 vanishes. Substituting the remaining term into Eq. 1.92 gives

$$\int_{t_1}^{t_2} \{\delta r\}^T \left[ [\tilde{M}] \{\ddot{r}\} + \left( [\tilde{K}_{GE}] + [K_{CG}] + [K_{CE}] \right) \{r\} \right] dt = 0 \quad .$$

Since the variations of the nodal displacement,  $\{\delta r\}$ , are arbitrary, the expression in brackets must vanish. Therefore, the matrix equation of motion for the assemblage can be obtained in the form

$$[\tilde{M}] \{\ddot{r}\} + \left( [\tilde{K}_{GE}] + [K_{CG}] + [K_{CE}] \right) \{r\} = \{0\} \quad , \quad (1.94)$$

where the tilde indicates that in this matrix equation of motion neither the shear deformation effect nor the rotatory inertia effect has been considered. However, if these secondary effects are taken into account,

Eq. 1.94 becomes

$$[M]\{\ddot{r}\} + \left( [K_{GE}] + [K_{CG}] + [K_{CE}] \right) \{r\} = \{0\} , \quad (1.95)$$

with  $[M] = \sum_{e=1}^N [m]_e$  ;  $[m]_e$  is given by Eq. 1.91 and  $[K_{GE}]$  is given by Eq. 1.68.

Eq. 1.94 (or Eq. 1.95) is the governing matrix equation of the vertical vibration of suspension bridges. There are two separate parts of the problem, i. e. , two independent eigenvalue problems, which must be considered. They are:

1. The symmetric eigenvalue problem having the symmetric modes of vertical vibration, which include additional cable tension, and in which there are an even number of internal nodes along the spans. Here,  $H(t)$  is not zero and accordingly, the stiffness matrix  $[K_{CE}]$  is not a zero matrix.
2. The antisymmetric eigenvalue problem having the antisymmetric modes of vertical vibration, which cause no additional cable tension, and in which there are an odd number of internal nodes along the spans. Here  $H(t)$  is zero, and accordingly the stiffness matrix  $[K_{CE}]$  is a null matrix.

Thus, for the symmetric modes:

$$[K_S] = [K_{GE}] + [K_{CG}] + [K_{CE}] , \quad (1.96)$$

and for the antisymmetric modes:

$$[K_{AS}] = [K_{GE}] + [K_{CG}] . \quad (1.97)$$

Then the matrix equations for the free, vertical-undamped symmetric and antisymmetric vibrations of the suspension bridge structure are, respectively:

$$[M]\{\ddot{r}_S\} + [K_S]\{r_S\} = \{0\} , \quad (1.98-a)$$

and

$$[M]\{\ddot{r}_{AS}\} + [K_{AS}]\{r_{AS}\} = \{0\} . \quad (1.98-b)$$

By writing the solutions of Eq. 1.98 in the familiar form

$$\{r_S(t)\} = \{r_S^*\}e^{i\omega t} \quad , \quad \{r_{AS}(t)\} = \{r_{AS}^*\}e^{i\omega t} \quad ; \quad i = \sqrt{-1} \quad (1.99)$$

and substituting Eq. 1.99 into Eq. 1.98 (leaving out the common factor  $e^{i\omega t}$ ), the following equations are obtained

$$(-\omega^2 [M] + [K_S])\{r_S^*\} = \{0\} \quad , \quad (1.100-a)$$

$$(-\omega^2 [M] + [K_{AS}])\{r_{AS}^*\} = \{0\} \quad , \quad (1.100-b)$$

where  $\{r_S^*\}$  and  $\{r_{AS}^*\}$  are the vectors of the displacement amplitudes (which do not change with time) of both symmetric and antisymmetric vibrations, respectively, and  $\omega$  is the natural circular frequency.

Now it can be shown by Cramer's rule that the solutions of these two sets of simultaneous equations (Eqs. 1.100-a and b) are of the form

$$\{r_S^*\} = \frac{\{0\}}{\| [K_S] - \omega^2 [M] \|} \quad , \quad (1.101-a)$$

$$\{r_{AS}^*\} = \frac{\{0\}}{\| [K_{AS}] - \omega^2 [M] \|} \quad . \quad (1.101-b)$$

Hence a nontrivial solution for each problem is possible only when the denominator determinant vanishes. In other words, non-zero amplitude free vibrations are possible only when

$$\| [K_S] - \omega^2 [M] \| = 0 \quad , \quad (1.102-a)$$

and

$$\| [K_{AS}] - \omega^2 [M] \| = 0 \quad . \quad (1.102-b)$$

Eqs. 1.102-a and b are called the frequency equations of the symmetric and antisymmetric vertical vibrations, respectively. Expanding each determinant will give an algebraic equation of the  $N^{\text{th}}$  degree in the frequency parameter  $\omega^2$  for a system having  $N$  degrees of freedom.

Because of the positive definitiveness of  $[M]$ ,  $[K_S]$  and  $[K_{AS}]$ , the roots  $\omega_1^2, \omega_2^2, \dots, \omega_N^2$  (eigenvalues) of each problem are real and positive quantities; Eqs. 1.100-a and b provide non-zero solution vectors  $\{r_S^*\}$  and  $\{r_{AS}^*\}$  (eigenvectors) for each root  $\omega^2$  of the symmetric and antisymmetric problems, respectively.

#### I-4-5. Illustrative numerical examples

Three examples of suspension bridges with widely different properties are presented to demonstrate the applicability of the analysis developed herein, and to cover the dynamic characteristics of these suspension bridges. In these examples, the free vertical vibrations of suspension bridges are analyzed. The natural frequencies and modes of vibration of the system are computed, and the distribution of the energy stored in the various members of the structure is

also determined. A knowledge of the energy of vibration of a given mode of vibration of a suspension bridge is essential if any study of the damping and exciting forces is to be made. Furthermore, if the motions and resisting actions of the various members of the structure are kept clearly in mind, it will not be difficult to anticipate which are likely to have a significant effect on a given mode.

Also, the influence of both the extensibility of the cable and the continuity of the stiffening girders (trusses) upon the vertical vibration frequencies and modes is considered in these examples.

Lastly, the computation of the eigenvalues  $\omega_i^2$  and the eigenvectors  $\{r_i^*\}$ ,  $i = 1, 2, \dots, N$ , for both the symmetric and the anti-symmetric vibrations, is worked out through a Householder-QR-Inverse Iteration Solution subroutine. A double precision version is available from the Caltech computer (IBM 370/158 system) program library and is written for the solution of the problem in the standard form  $([A] - \lambda[I])\{x\} = \{0\}$ , where  $[A]$  is a real matrix,  $\lambda$  is the eigenvalue,  $[I]$  is the unity matrix and  $\{x\}$  is the eigenvector. Consequently, Eqs. 1.100-a and b must be converted to the standard form by premultiplying each by the matrix  $[M]^{-1}$ . Thus, a matrix inversion subroutine is also needed and the final forms of the eigenvalue and eigenvector problems for both symmetric and antisymmetric vibration, will be

$$([M]^{-1}[K_S] - \omega^2[I])\{r_S^*\} = \{0\} \quad , \quad (1.103-a)$$

and

$$([M]^{-1}[K_{AS}] - \omega^2[I])\{r_{AS}^*\} = \{0\} \quad . \quad (1.103-b)$$

Finally, for simplicity of presentation, the effects of shear deformation and rotatory inertia will be neglected (in all examples), but if required, they can be accounted for without difficulty.

Example 1. (One suspended span)

The suspension bridge shown in Fig. I-3-a, having one suspended span, has the following properties:

a) stiffening girder (or truss)

$$\begin{aligned} l_2 = l = 2800 \text{ ft.} & , & I_{g2} = I_g = 128400 \text{ ft.}^2 \text{ in.}^2 \\ w_2^* = w^* = 2.85 \text{ Kip/ft.} & , & E_{g2} = E_g = 29600 \text{ Kip/in.}^2 \end{aligned}$$

b) cable

$$\begin{aligned} f_2 = f = 232 \text{ ft.} & , & A_c = 1.915 \text{ in.}^2 \\ H_w = 120040 \text{ Kips.} & , & E_c = 26000 \text{ Kip/in.}^2 \\ L_E = L_{e2} = 4000 \text{ ft.} & & \end{aligned}$$

The number of elements ( $N_2 = N$ ) was taken to be 20 elements; therefore, the number of expected modes is  $(N - 1)$  (i. e., 19 modes are expected), and the length of each element  $L$  is 140 ft.

The two eigenvalue problems (Eqs. 1.103-a and b) have been solved by the Caltech digital computer (IBM 370/158) system). The computed natural periods and frequencies, for different cases, are presented in Table I.1, and the mode-shapes of both translational and rotational displacements are shown in Fig. I-5.

Bleich [3] calculated the first two symmetric modes for the same bridge by solving the frequency equation (involving trigonometric and

TABLE I-1

a. Natural Frequencies and Periods of the Symmetric Modes  
 Effect of the Extensibility of the Cable  
 (One Suspended Span)

| Mode Order | Extensible Cable     |               | Inextensible Cable   |               |
|------------|----------------------|---------------|----------------------|---------------|
|            | Frequency (rad/sec.) | Period (sec.) | Frequency (rad/sec.) | Period (sec.) |
| 1          | 1.397460             | 4.496146      | 0.481302             | 13.054559     |
| 2          | 2.704650             | 2.323105      | 2.653828             | 2.367593      |
| 3          | 6.847194             | 0.917629      | 6.841255             | 0.918426      |
| 4          | 13.118742            | 0.478947      | 13.116910            | 0.479014      |
| 5          | 21.510308            | 0.292101      | 21.509355            | 0.292114      |
| 6          | 32.068751            | 0.195929      | 32.068340            | 0.195931      |
| 7          | 44.883375            | 0.139989      | 44.883155            | 0.139990      |
| 8          | 60.088212            | 0.104566      | 60.881410            | 0.104566      |
| 9          | 77.848210            | 0.080711      | 77.848260            | 0.080711      |
| 10         | 97.978733            | 0.064128      | 97.978832            | 0.064128      |

b. Natural Frequencies and Periods of the Antisymmetric Modes  
 Comparison Between the Finite Element Method and Exact Solution  
 (One Suspended Span)

| Mode Order | Finite Element Method |               | Exact Solution<br>(Using Eq. 1.104) |               |
|------------|-----------------------|---------------|-------------------------------------|---------------|
|            | Frequency (rad/sec.)  | Period (sec.) | Frequency (rad/sec.)                | Period (sec.) |
| 1          | 1.333049              | 4.749018      | 1.331842                            | 4.717666      |
| 2          | 4.487016              | 1.400304      | 4.490103                            | 1.399341      |
| 3          | 9.716318              | 0.646663      | 9.713860                            | 0.646827      |
| 4          | 17.046238             | 0.368597      | 17.020489                           | 0.369154      |
| 5          | 26.513585             | 0.236980      | 26.412797                           | 0.237884      |
| 6          | 38.186522             | 0.164539      | 37.891516                           | 0.165820      |
| 7          | 52.176271             | 0.120423      | 49.739350                           | 0.126322      |
| 8          | 68.640026             | 0.091538      | 67.139526                           | 0.093584      |
| 9          | 87.697946             | 0.071646      | 82.281857                           | 0.076362      |

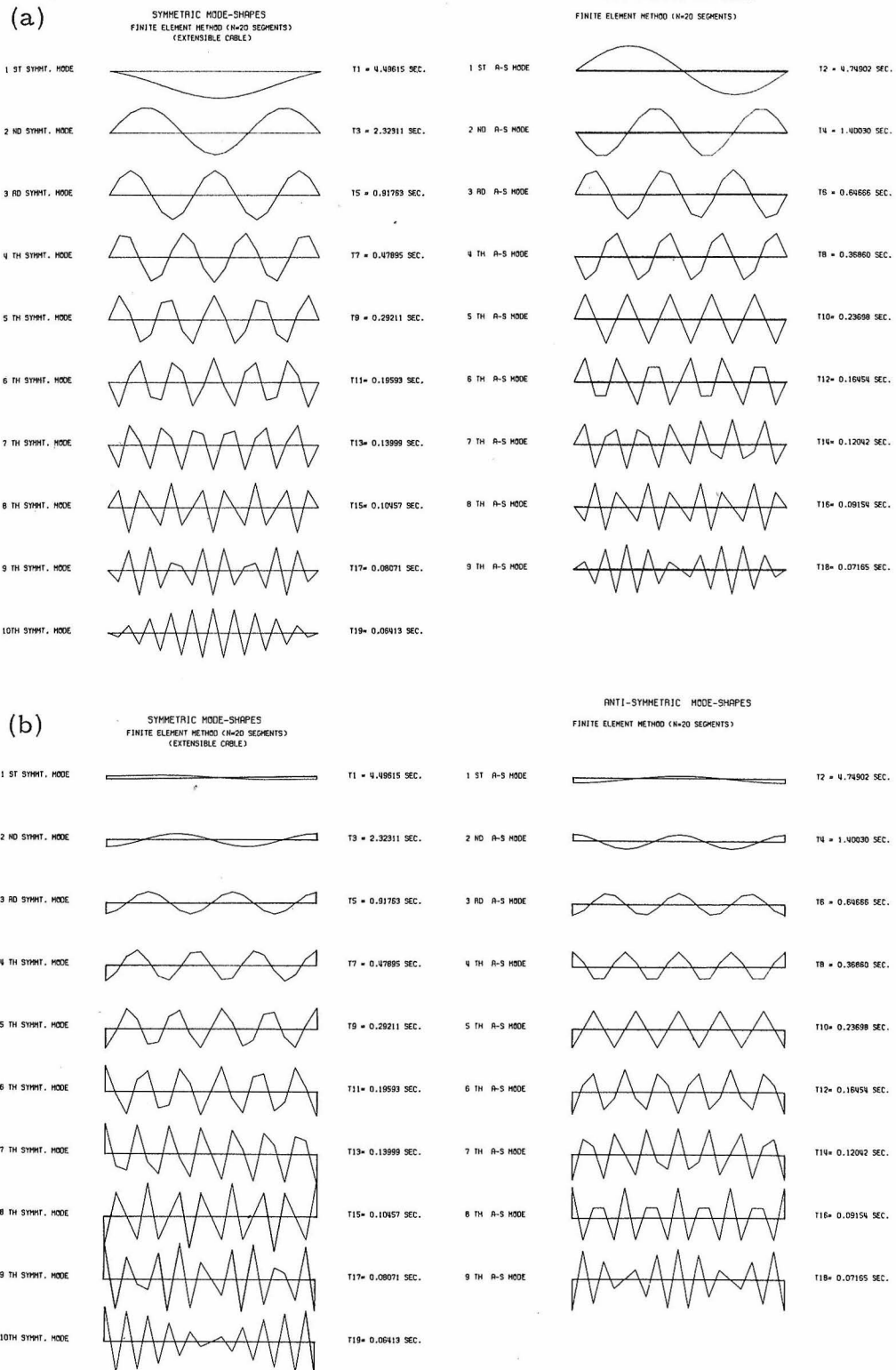


Fig. I-5. Symmetric and antisymmetric modes of vertical vibration of a one-span suspension bridge; (a) translation, (b) rotation.

hyperbolic functions) resulting from the linearized equation of motion (Eq. 1.49) and the linearized cable equation (Eq. 1.52); he used a process of trial and error, and he found that:

$$\omega_1 = 1.400 \text{ rad/sec.} \quad \text{and} \quad \omega_2 = 2.696 \text{ rad/sec.},$$

Then, using the approximate energy method (Rayleigh-Ritz), he arrived at

$$\omega_1 = 1.402 \text{ rad/sec.} \quad \text{and} \quad \omega_2 = 2.705 \text{ rad/sec.}$$

The method of analysis under investigation gives

$$\omega_1 = 1.3975 \text{ rad/sec.} \quad \text{and} \quad \omega_2 = 2.7046 \text{ rad/sec.},$$

in addition to the higher frequencies.

For the antisymmetric case, the frequency equation resulting from the linearized equation of motion (Eq. 1.49 with  $H(t) = 0$ ) has a simple form:

$$\omega_n = \frac{2n\pi}{l^2} \sqrt{\frac{g}{w} \left( H_w + \frac{4n^2 \pi^2 E I g}{l^2} \right)}, \quad n = 1, 2, 3, \dots \quad (1.104)$$

It is easy, now, to compare the results obtained by the method of analysis under study and the results obtained by the frequency expression (Eq. 1.104). Table I-1-b. and Figs. I-6 and I-7-a indicate a very close agreement between the two solutions. The degree of accuracy increases as the mode order decreases (i. e, in the higher modes the finite element solution represents an upper bound to the exact solution).

To demonstrate the influence of the extensibility of the cable, calculations of frequencies and modes with cable extensibility and without are shown in Table I-1-a and in Fig. I-8. Inextensibility of

the cable is mathematically expressed by the equation  $E_c A_c \sim \infty$  (i. e.,  $\frac{H(t)L_E}{E_c A_c} = 0$ ); therefore, the second term of Eq. 1.18, expressing the strain energy of the cable, equals zero, and accordingly, the stiffness matrix  $[K_{CE}]$  in Eq. 1.94 equals the null matrix. In this context the stiffness of the cable is seen to arise largely from its own weight and from the dead load upon it, and as indicated before, the interaction between the cables and the stiffening girders (or trusses) is regarded as the interplay of the gravity stiffness (essentially nonlinear) of the cable and the elastic stiffness (linear) of the stiffening structure.

Inspection of Table I-1-a and Fig. I-8 shows that the effect of cable stretch on the frequencies is limited to only the first few modes. This suggests that the actual extension of the cable in the higher modes is quite small and that consequently  $H(t)$  is also small. Fig. I-7-b also shows the magnitude of the cable tension  $H(t)$  which decreases rapidly as the number of modes of vibration increases. On the other hand, Fig. I-8 shows that extension of the cable permits a mode (the fundamental mode) that is quite different from that which results with an inextensible cable.

In Fig. I-9, the various energies accumulated in the cables, the stiffening structure and the system as a whole have been considered at each of the symmetric and antisymmetric modes. In this figure, the normalized factor is designated by the total energy of the particular mode. The relative contribution of the strain energy of the cable to the total energy storage capacity of the structure is greatest

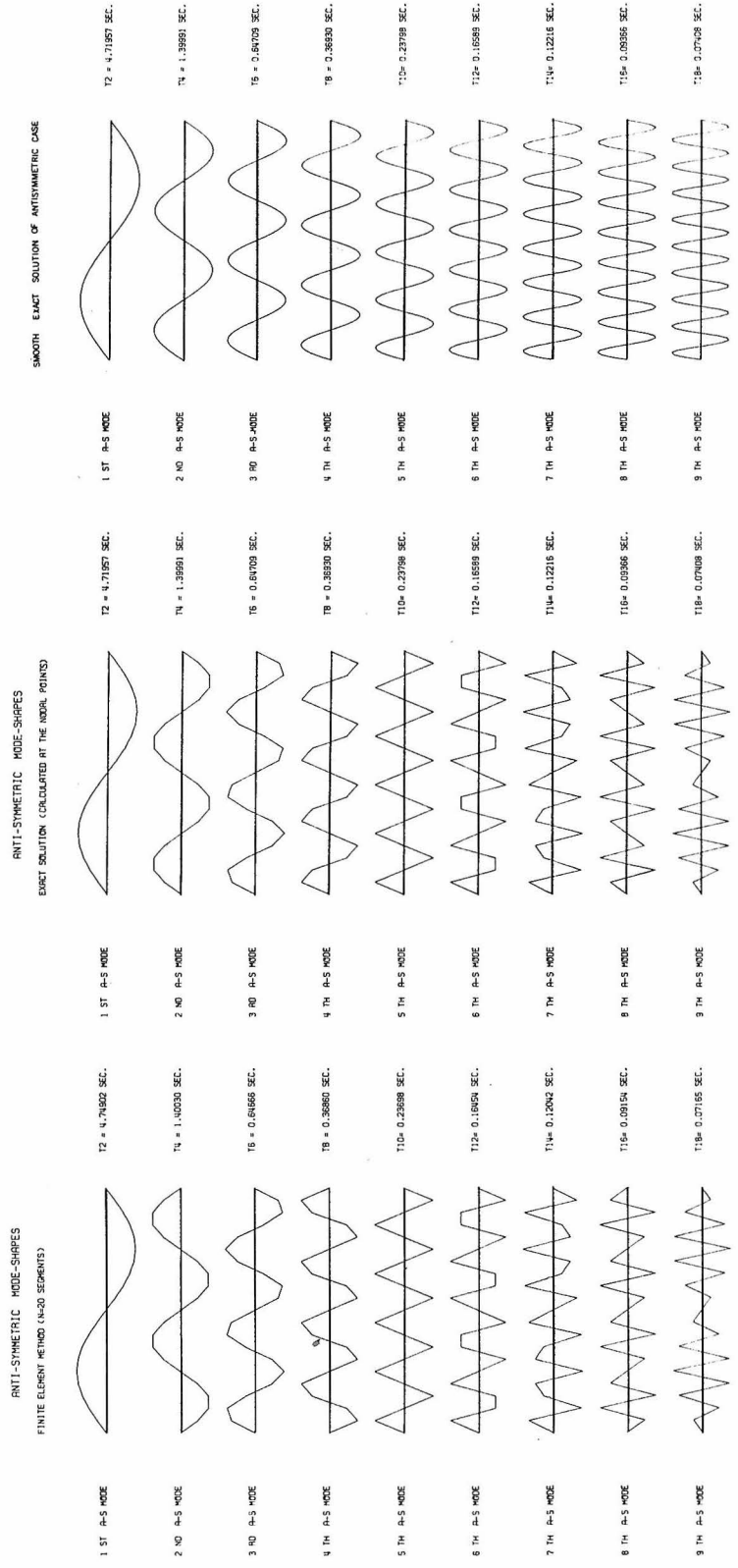


Fig. I-6. Comparison between the mode-shapes from the finite-element approach and those from the exact solution (antisymmetric modes of vibration).

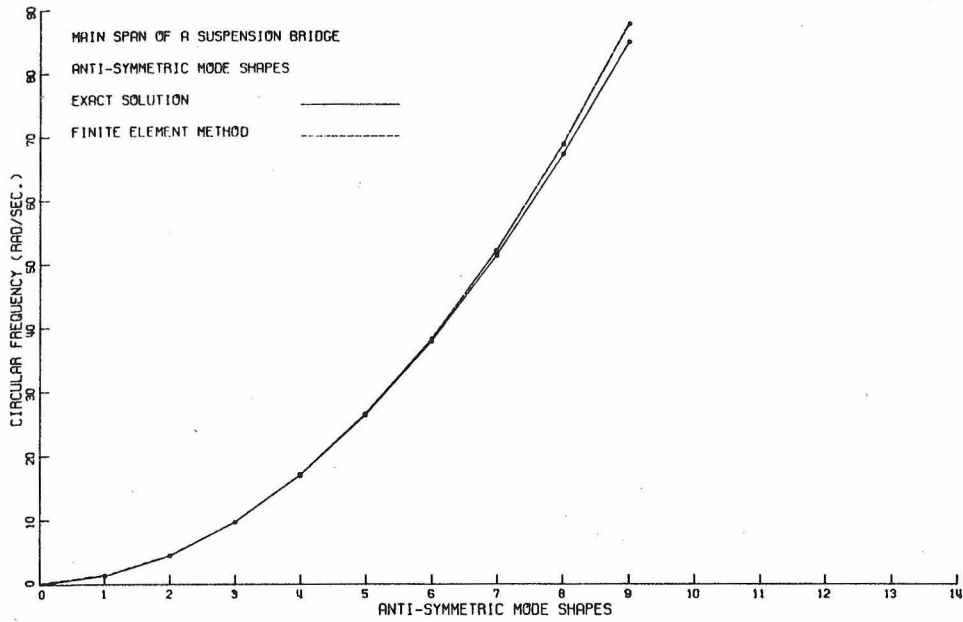


Fig. I-7-a. Comparison between frequencies from the finite-element approach and those from the exact solution (antisymmetric modes).

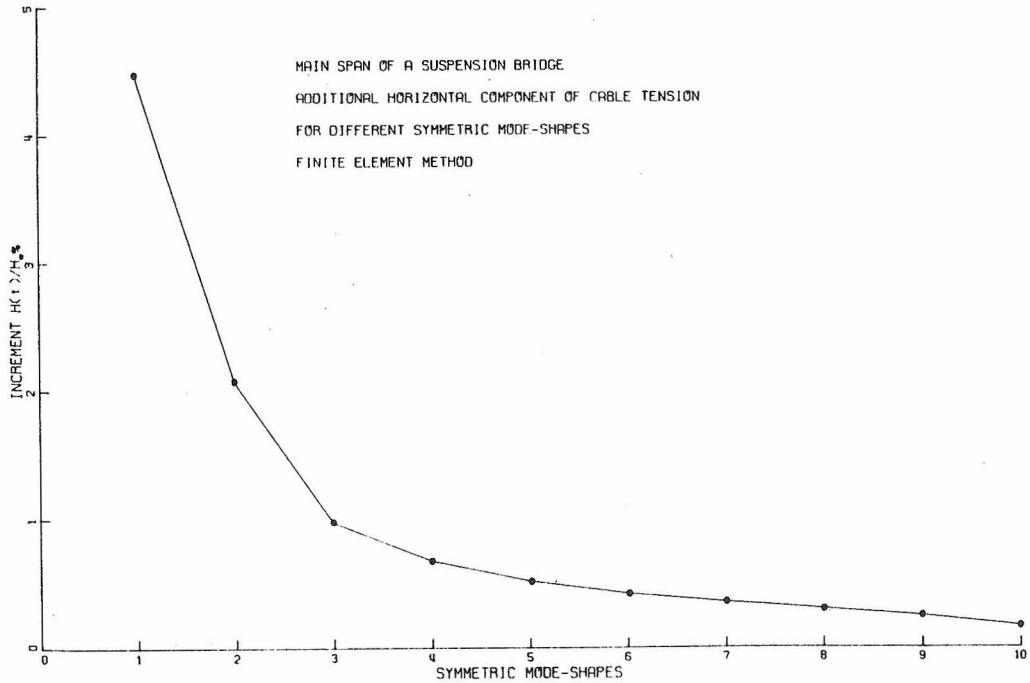


Fig. I-7-b. Magnitude of the horizontal component of additional cable tension,  $H(t)$  for various symmetric modes.

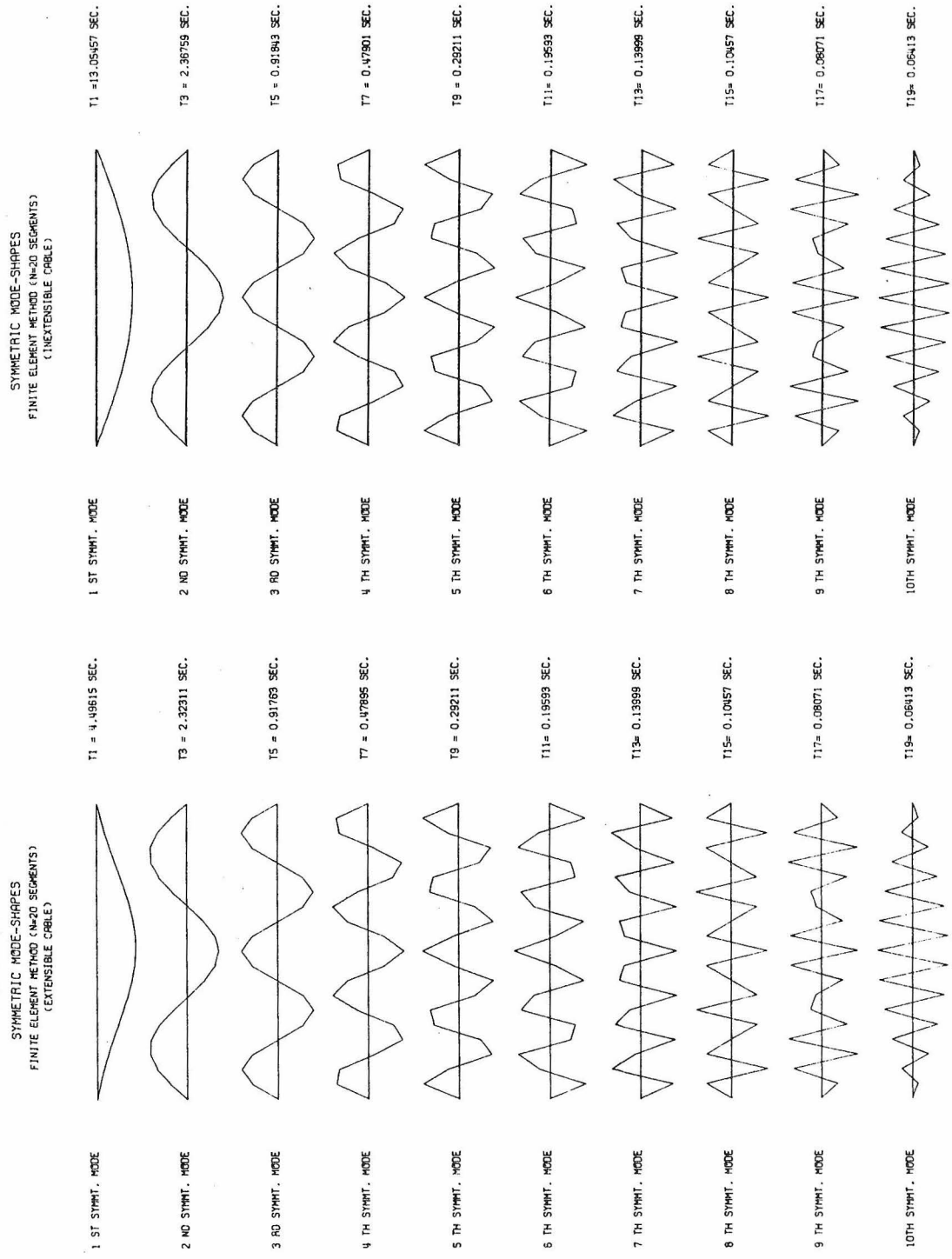


Fig. I-8. The effect of extensibility of the cable on symmetric modes of vertical vibration.

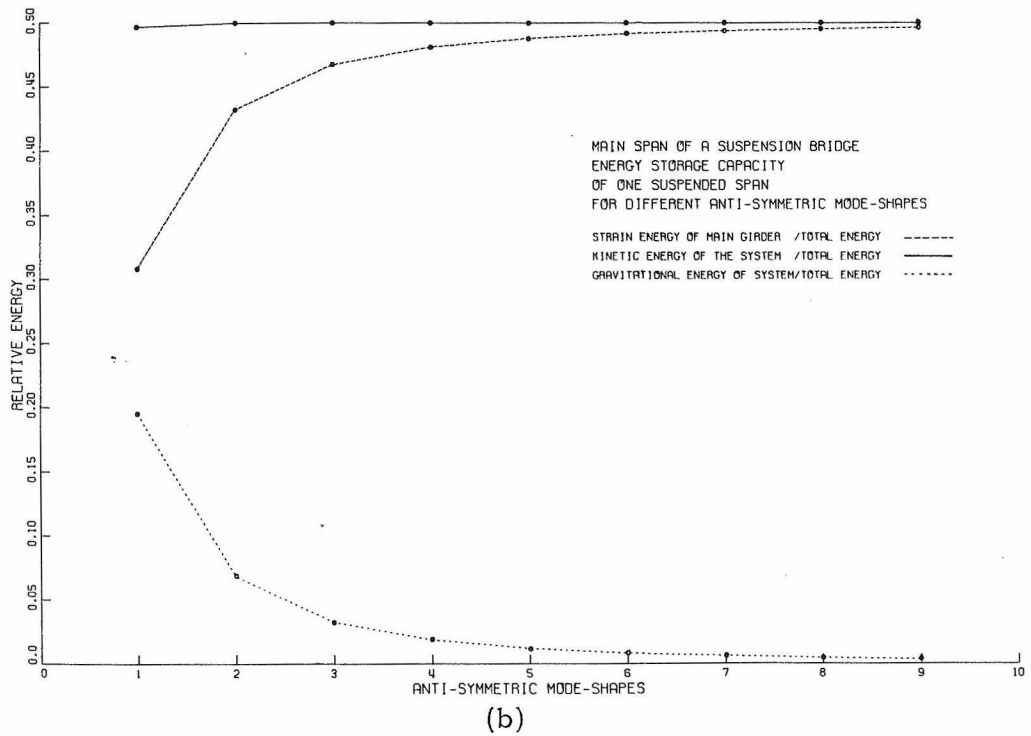
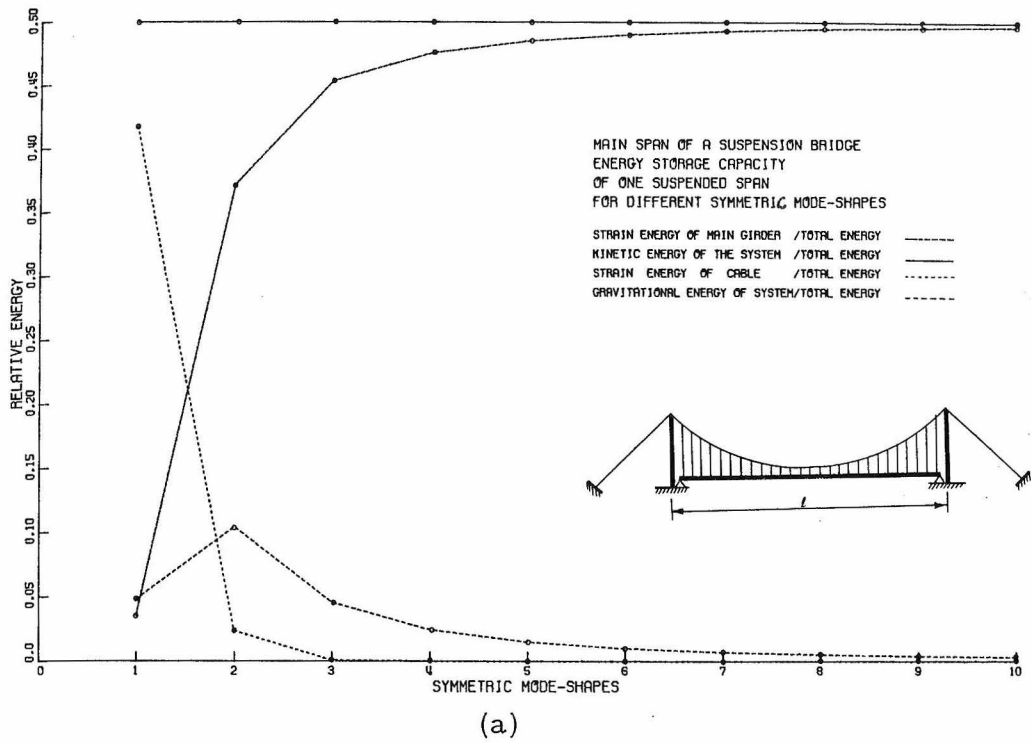


Fig. I-9. Relative energy storage capacity for:  
(a) symmetric modes and (b) antisymmetric modes.

in the first two symmetric modes, while the relative contribution of the strain energy of the stiffening girder (or truss) builds until it governs almost all of the potential energy of the structure. Therefore, the stiffening structures have a significant role in determining the modes and frequencies of the higher modes of vibration; these higher modes with their shorter waves involve sharper curvature in the stiffening girder and, therefore, greater bending moment. Furthermore, they reflect accordingly the influence of the stiffening girders' stiffness to a greater degree than do the lower modes.

Generally, the results obtained by using this analysis satisfy the principle of conservation of energy so that for each mode the total potential energy is equal to the total kinetic energy.

Example 2. (Three suspended spans with hinged stiffening structures)

The properties and dimensions of the second suspension bridge are:

- a) stiffening girders (or trusses)

- side spans

$$l_1 = l_3 = 1100 \text{ ft.}$$

$$E_{g1} = E_{g3} = 29600 \text{ Kip/in.}^2$$

$$I_{g1} = I_{g3} = 128400 \text{ ft.}^2 \text{ in.}^2$$

$$\bar{w}_1^* = \bar{w}_3^* = 2.85 \text{ Kip/ft.}$$

- b) cable

$$f_2 = f = 232 \text{ ft.}$$

$$E_c = 26000 \text{ Kip/in.}^2$$

$$A_c = 191.5 \text{ in.}^2$$

$$H_w = 12040 \text{ Kips.}$$

$$L_E = \sum_{i=1}^3 L_{ei} = 6080 \text{ ft.}$$

The number of elements in each side span,  $N_1 = N_3$ , was taken to be 11 elements, providing 10 modes per side span. Each element has a length  $L = 140$  ft.; the number of elements in the center span  $N_2$ , was taken to be 28 elements of the same length, giving 27 possible modes.

Table I-2 shows the computed natural periods and frequencies of vertical vibration for the symmetric and antisymmetric cases respectively, while Fig. I-10 shows the modes of vibration.

Again, to illustrate the effectiveness of the analysis under consideration, a comparison between the obtained results and Bleich's [3] results has been made. Bleich's frequency equation (resulting from the linearized equation of motion, Eq. 1.49, and the linearized cable equation, Eq. 1.52) for the symmetric modes gives:

$\omega_1 = 1.051$  rad/sec. as compared with  $\omega_1 = 1.05144$  rad/sec. from the method under consideration. Bleich's approximate method (Rayleigh-Ritz method) gives:  $\omega_1 = 1.055$  rad/sec.,  $\omega_2 = 2.255$  rad/sec. and  $\omega_3 = 2.699$  rad/sec. as compared with  $\omega_1 = 1.055$  rad/sec.,  $\omega_2 = 2.254$  rad/sec. and  $\omega_3 = 2.698$  rad/sec., for the first three symmetric modes.

As seen from Fig. I-10, in the lowest three modes the center span and side spans vibrate together, but in the higher modes the center and side spans vibrate separately. This illustrates the role played by the cable during the first few modes of vibration where the cable creates an interaction between the side spans and the center span.

Natural Frequencies and Periods of the Symmetric and the Antisymmetric Modes  
(Three Suspended Spans)

Comparison Between a Hinged-Span Type and a Continuous-Span Type of Suspension Bridge

| Mode Order | Hinged-Span Type Bridge       |                 |                               |                 | Continuous-Span Type Bridge   |                 |                               |                 |
|------------|-------------------------------|-----------------|-------------------------------|-----------------|-------------------------------|-----------------|-------------------------------|-----------------|
|            | Symmetric Modes               |                 | Antisymmetric Modes           |                 | Symmetric Modes               |                 | Antisymmetric Modes           |                 |
|            | Frequency $\omega$ (rad/sec.) | Period T (sec.) |
| 1          | 1.051440                      | 5.975742        | 1.331846                      | 4.717653        | 1.054853                      | 5.956453        | 1.491775                      | 4.211885        |
| 2          | 2.253794                      | 2.787825        | 1.991611                      | 3.154826        | 2.360502                      | 2.661800        | 2.503552                      | 2.509708        |
| 3          | 2.698388                      | 2.328495        | 4.490219                      | 1.399305        | 3.368425                      | 1.865319        | 4.978025                      | 1.262184        |
| 4          | 6.845525                      | 0.917853        | 7.082068                      | 0.887196        | 6.942432                      | 0.905041        | 7.854399                      | 0.799957        |
| 5          | 7.081548                      | 0.887262        | 9.715157                      | 0.646740        | 8.518772                      | 0.737569        | 10.670907                     | 0.588815        |
| 6          | 13.110450                     | 0.479250        | 15.542407                     | 0.404261        | 13.748498                     | 0.457009        | 16.182179                     | 0.388278        |
| 7          | 15.545494                     | 0.404180        | 17.027741                     | 0.368997        | 17.051554                     | 0.368482        | 18.788934                     | 0.334409        |
| 8          | 21.470666                     | 0.292640        | 26.440227                     | 0.237637        | 22.640142                     | 0.277524        | 26.803445                     | 0.234417        |
| 9          | 27.400472                     | 0.229310        | 27.400628                     | 0.229308        | 28.861987                     | 0.217648        | 30.068428                     | 0.208963        |
| 10         | 31.939672                     | 0.196720        | 37.972421                     | 0.165467        | 33.788252                     | 0.185958        | 39.165616                     | 0.160426        |
| 11         | 42.697810                     | 0.147155        | 42.697481                     | 0.147156        | 43.553837                     | 0.144262        | 45.099992                     | 0.139317        |
| 12         | 44.543138                     | 0.141058        | 51.657665                     | 0.121631        | 47.633907                     | 0.131906        | 53.575460                     | 0.117277        |
| 13         | 59.322982                     | 0.105915        | 61.510254                     | 0.102149        | 60.093162                     | 0.104557        | 63.578542                     | 0.098826        |
| 14         | 61.510178                     | 0.102149        | 67.547730                     | 0.093018        | 65.300898                     | 0.096219        | 70.405329                     | 0.089243        |
| 15         | 76.341798                     | 0.028303        | 83.968661                     | 0.074828        | 78.181530                     | 0.080367        | 84.835540                     | 0.074063        |
| 16         | 83.968654                     | 0.074828        | 85.716961                     | 0.073302        | 87.232719                     | 0.072028        | 90.420063                     | 0.069489        |
| 17         | 95.686260                     | 0.065664        | 106.264475                    | 0.059128        | 98.463274                     | 0.063812        | 107.576656                    | 0.058407        |
| 18         | 110.265029                    | 0.056983        | 110.265077                    | 0.056983        | 112.875895                    | 0.055665        | 115.147794                    | 0.054566        |
| 19         | 117.467120                    | 0.053489        | 129.309984                    | 0.048590        | 121.509346                    | 0.051709        | 131.905527                    | 0.047634        |
| 20         | 140.643155                    | 0.044675        | 140.643158                    | 0.044675        | 141.256744                    | 0.044481        | 144.725414                    | 0.043415        |
| 21         | 141.806416                    | 0.044308        | 154.961806                    | 0.040547        | 148.432639                    | 0.042330        | 158.634755                    | 0.039608        |

TABLE I-2

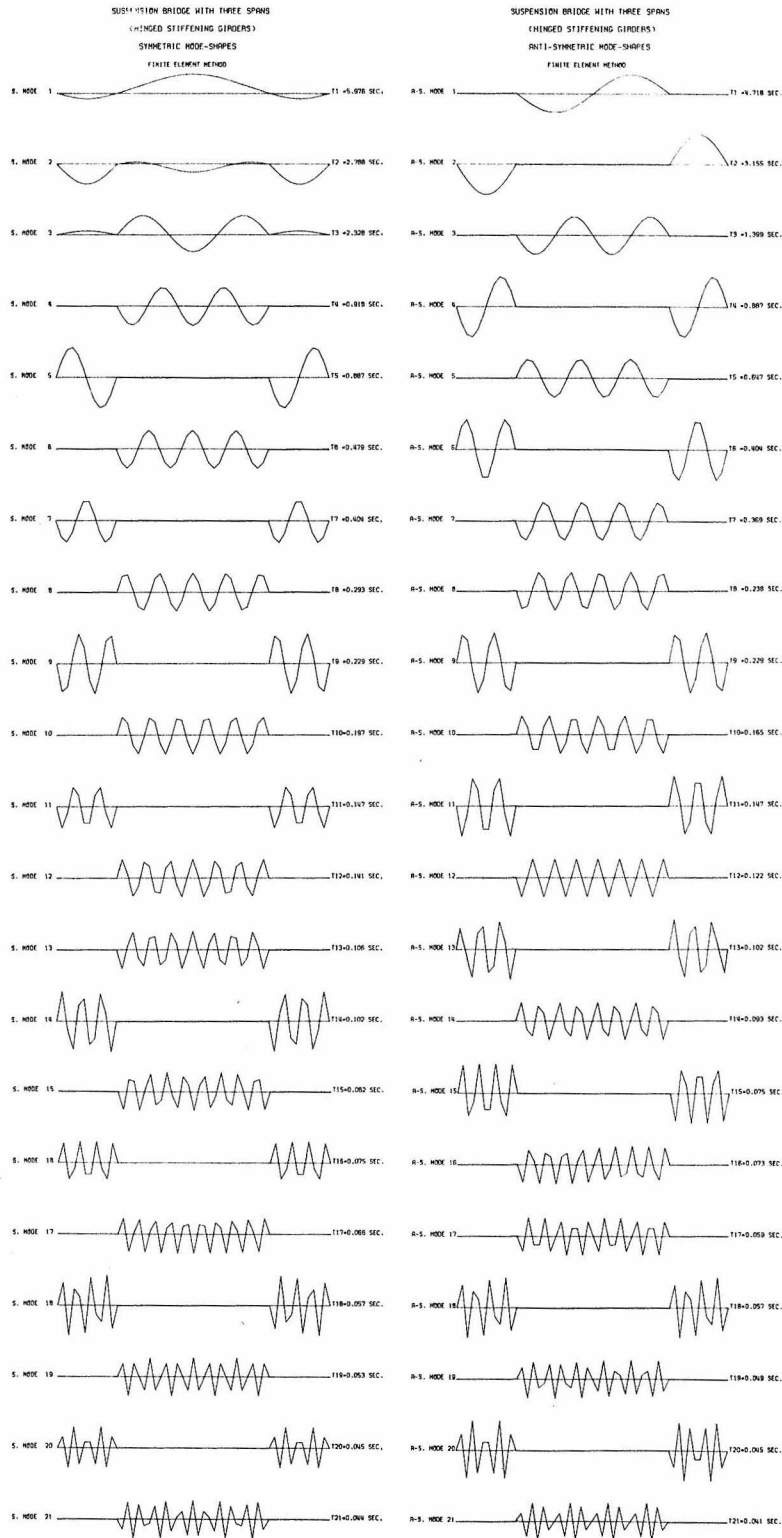


Fig. I-10. Mode-shapes of the symmetric and the antisymmetric vertical vibration (Example 2).

The antisymmetric deflections of the cable and the stiffening structures cause no additional cable tension  $H(t)$  because the downward movement on one side of the centerline of the center span tends to increase the cable length, while at the same time the upward movement on the other side of the center span tends to reduce cable length, and the effects balance each other. In consequence of the lack of additional cable tension,  $H(t)$ , there is no interaction between the center span and the side spans; i. e., two types of independent vibration are possible. Both types of vibration may occur at one time, and any mode of one type may be combined with any mode of the other.

The distribution of the energies stored in the various members of the structure, for both the symmetric and antisymmetric cases, is demonstrated by Fig. I-11. From this Figure the significance of the relative contributions of the cable and the stiffening structures to the total energy storage capacity of the bridge structure can easily be extracted. The lower modes reflect the influence of the strain and strainless (gravitational) energies of the cable, while the higher modes with their relatively shorter waves involve sharper curvature in the stiffening girder (or truss) and, therefore, involve greater bending moments. Furthermore, they reflect accordingly the influence of the stiffening girder to a greater degree than do the lower modes. It is worthwhile to note that in the antisymmetric modes, all of the cable energy storage is of this strainless, i. e., gravitational energy type.

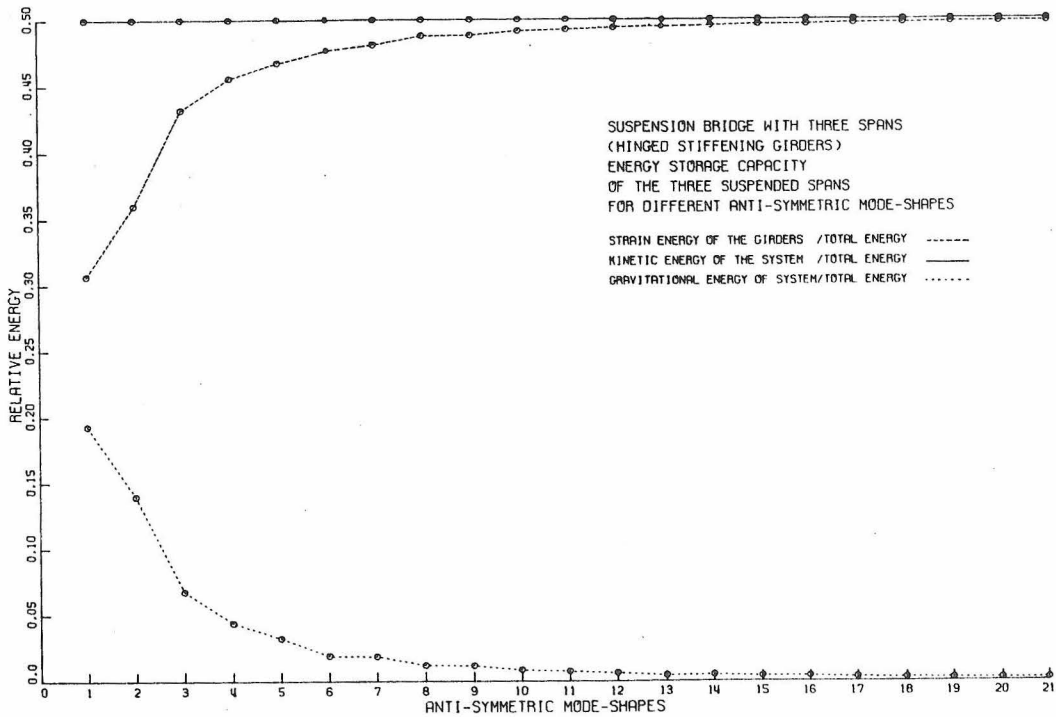
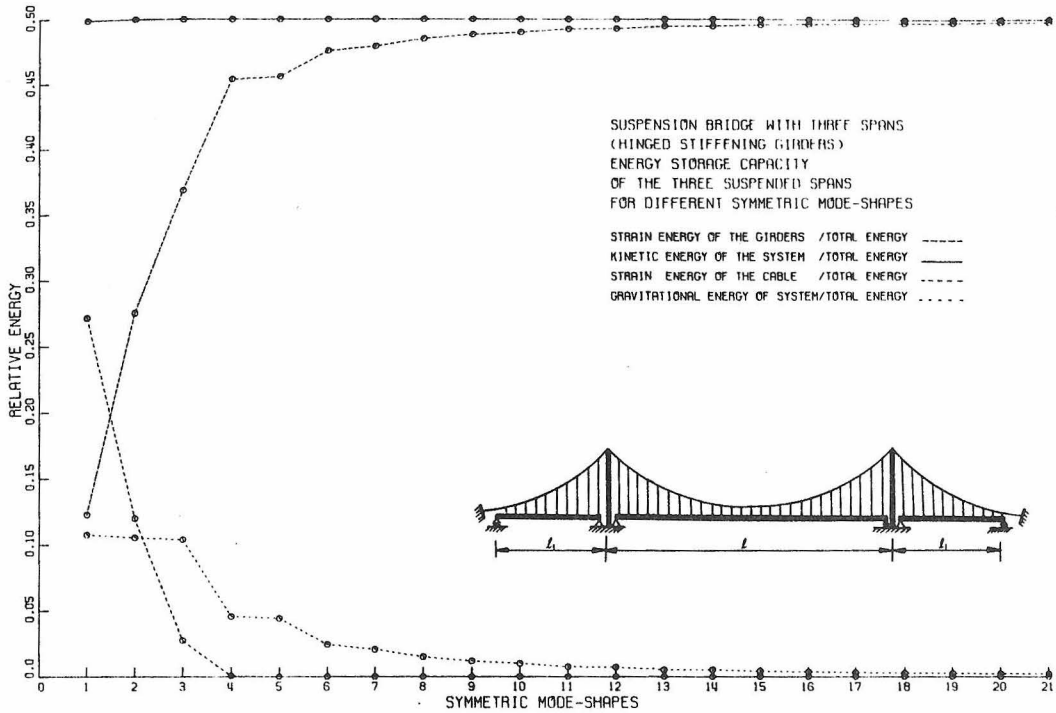


Fig. I-11. Relative energy storage capacity for the hinged-span suspension bridge (Example 2) .

Table I-3 illustrates the effect of the inextensibility of the cable upon the frequencies of free vertical vibration for the symmetric modes, while Fig. I-12 shows a comparison between the modes of vibration for the extensible cable and those for the inextensible cable. It is seen that the role played by the extensibility of the cable is confined to only the first few modes where the interaction between side and center spans exists. In the first mode, the inextensibility effect increases the fundamental period to two times its value when the cable is extensible, and for the second and third modes the magnifications are about 13% and 2%, respectively. This, again, demonstrates the significant contribution at these modes from the elastic strain energy of the cable.

Another effect of inextensibility is seen in the independent vibration of both the center and side spans. It is desirable to re-examine more critically, the use of the expression for an inextensible cable (Eq. 1.23). This inextensibility expression, which is a result of the conventional deflection theory, requires that the algebraic sum of the areas between the deflection curve and the line of static equilibrium be zero. But it has already been shown, by considering a higher order term in the cable equation (Eq. 1.17), that the form of this conventional expression for inextensibility appears to imply that the gravity stiffness of the cable is negligible. This is seen to be misleading, because were this gravity stiffness negligible, there would be no potential energy contribution from the cable at all, and the only energy contribution would be from the stiffening girders. This is

Effect of the Flexural Rigidity of the Towers and the Extensibility of the Cables  
Upon the Frequencies of the Free Vertical Vibration of a Three-Span Suspension  
Bridge with Hinged Stiffening Girders (Symmetric Mode-Shapes)

| Mode Order | No Consideration of Towers (Extensible Cables) |                 | Effect of Tower Elasticity    |                 | Inextensible Cables           |                 |
|------------|--|-----------------|-------------------------------|-----------------|-------------------------------|-----------------|
|            | Frequency $\omega$ (rad/sec.)                  | Period T (sec.) | Frequency $\omega$ (rad/sec.) | Period T (sec.) | Frequency $\omega$ (rad/sec.) | Period T (sec.) |
| 1          | 1.051439                                       | 5.975791        | 1.064820                      | 5.900697        | 0.489181                      | 12.844279       |
| 2          | 2.253794                                       | 2.787825        | 2.255588                      | 2.785608        | 1.991610                      | 3.154826        |
| 3          | 2.698388                                       | 2.328495        | 2.698381                      | 2.328501        | 2.655838                      | 2.365800        |
| 4          | 6.845524                                       | 0.917852        | 6.845535                      | 0.917851        | 6.842445                      | 0.918266        |
| 5          | 7.081548                                       | 0.887261        | 7.081553                      | 0.887260        | 7.082067                      | 0.887196        |
| 6          | 13.110450                                      | 0.479250        | 13.110453                     | 0.479250        | 13.109816                     | 0.479273        |
| 7          | 15.545494                                      | 0.404180        | 15.545535                     | 0.404179        | 15.542406                     | 0.404260        |
| 8          | 21.470666                                      | 0.292640        | 21.470667                     | 0.292640        | 21.470514                     | 0.292642        |
| 9          | 27.400477                                      | 0.229309        | 27.400477                     | 0.229309        | 27.400628                     | 0.229308        |
| 10         | 31.939672                                      | 0.196720        | 31.939672                     | 0.196720        | 31.939653                     | 0.196720        |
| 11         | 42.697810                                      | 0.147154        | 42.697815                     | 0.147154        | 42.697480                     | 0.147155        |
| 12         | 44.543138                                      | 0.141058        | 44.543138                     | 0.141058        | 44.543161                     | 0.141058        |
| 13         | 59.322981                                      | 0.105914        | 59.322981                     | 0.105914        | 59.323018                     | 0.105914        |
| 14         | 61.510177                                      | 0.102148        | 61.503568                     | 0.102148        | 61.510254                     | 0.102148        |
| 15         | 76.341797                                      | 0.082303        | 76.341797                     | 0.082303        | 76.341836                     | 0.082303        |
| 16         | 83.968653                                      | 0.074827        | 83.968655                     | 0.074827        | 83.968600                     | 0.074827        |
| 17         | 95.686259                                      | 0.065664        | 95.686259                     | 0.065664        | 95.686298                     | 0.065664        |
| 18         | 110.265029                                     | 0.054982        | 110.265028                    | 0.054982        | 110.265077                    | 0.054982        |
| 19         | 117.467101                                     | 0.053488        | 117.471018                    | 0.053488        | 117.467138                    | 0.053488        |
| 20         | 140.643155                                     | 0.044674        | 140.643155                    | 0.044674        | 140.643158                    | 0.044674        |
| 21         | 141.806415                                     | 0.044308        | 141.806415                    | 0.044308        | 141.806450                    | 0.044308        |

TABLE I-3

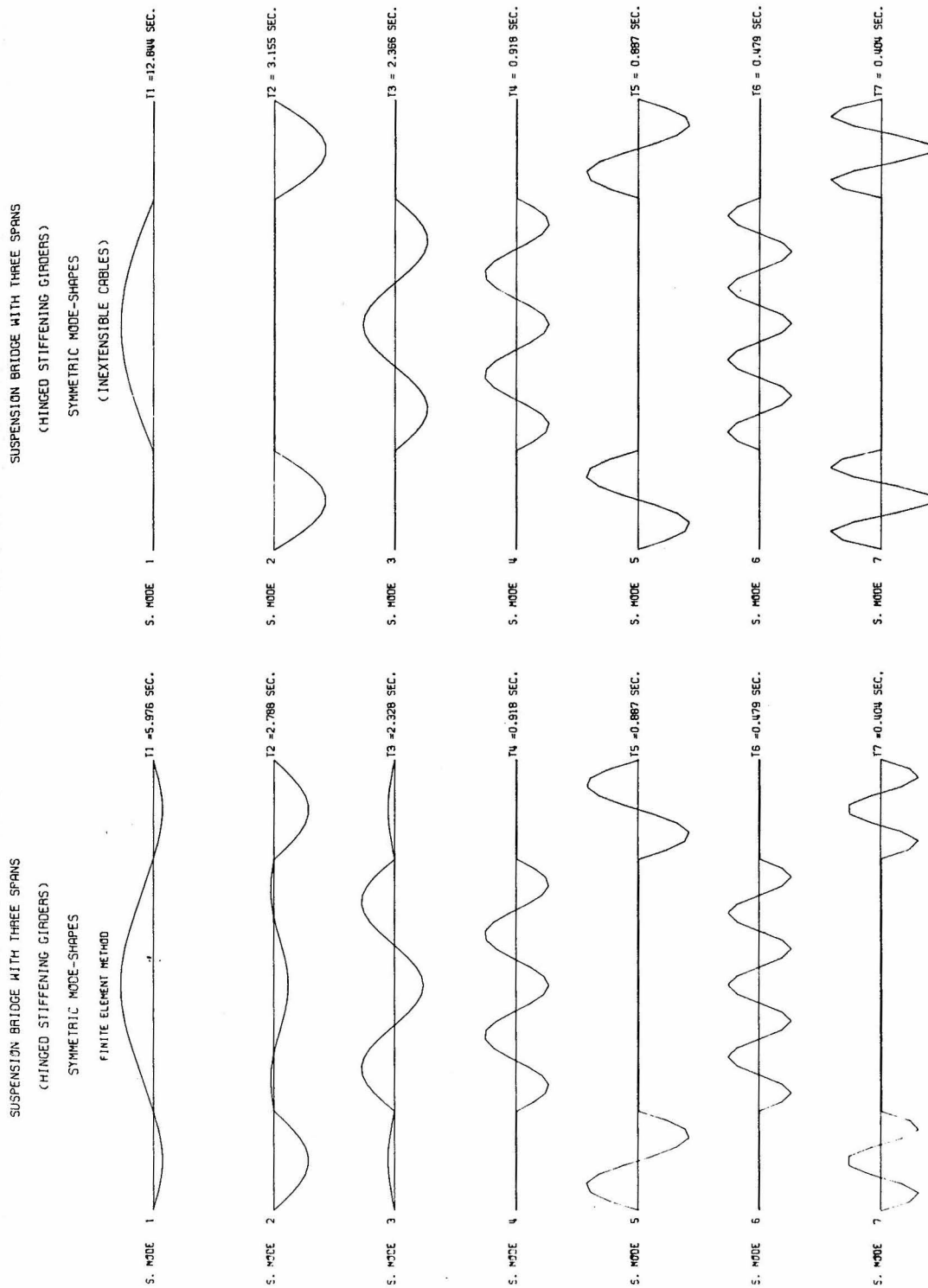


Fig. I-12. Comparison between modes of symmetric vibration for the extensible cable and those for the inextensible cable (Example 2).

certainly contradictory and violates the fundamental assumptions which say that the cable and the stiffening structure have the same vibrational displacement.

Thus, the relation between the inextensibility condition and the gravity stiffness, heretofore virtually ignored, must be considered, and therefore the general problem of the dynamics of suspension bridges still involves the interaction of the two major members (the suspension cables and the stiffening structures), regardless of the extensibility of the cable.

Example 3. (Three suspended spans with a continuous stiffening structure)

The properties and dimensions of Example 2 have also been used to compute the frequencies and modes of vibration of a suspension bridge having continuous stiffening girders (or trusses). The computed natural periods and frequencies are presented in Table I-2, and the mode-shapes are shown in Fig. I-13.

In order to judge the effect of continuity upon the frequencies of both the symmetric and antisymmetric modes, the frequencies of the suspension bridge with hinged stiffening structures (Example 2) are shown in the same table. This table suggests that the adoption of continuous stiffening structures in suspension bridges offers the advantage of increased stiffness in comparison with the hinged stiffening structures normally used in suspension bridges. This increased stiffness has the tendency to increase the value of the frequencies, as seen from Table I-2. No remarkable long span suspension bridge

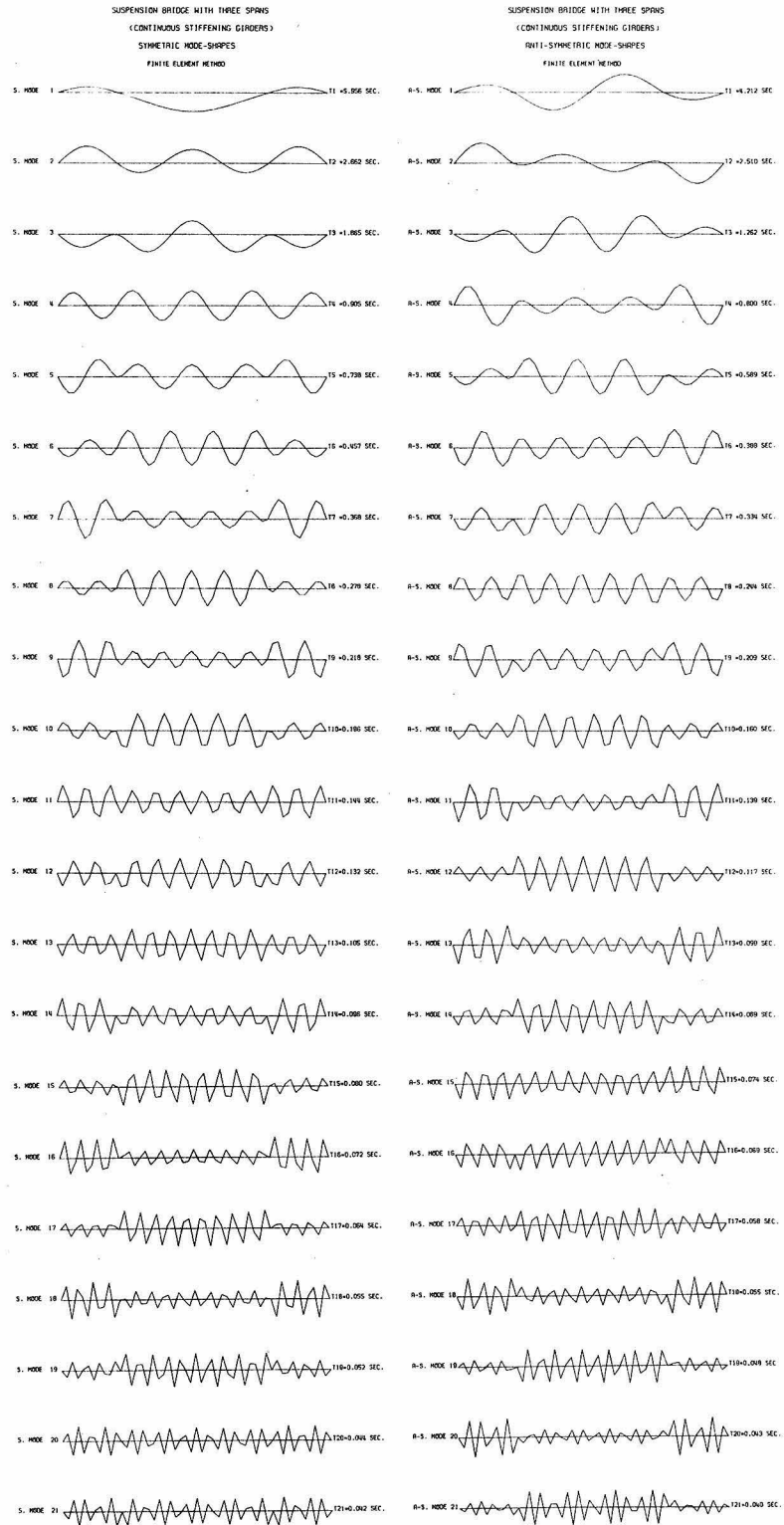


Fig. I-13. Mode shapes of a suspension bridge with continuous stiffening structures (Example 3).

having continuous stiffening structures has been acknowledged in the literature. However, the effect of a continuous stiffening structure on the dynamic characteristics of a suspension bridge is an important question in a comprehensive study of the dynamics of suspension bridges.

Inspection of Table I-2 reveals that the effect of continuity of the stiffening structure upon the frequencies of the symmetric modes is very small, while the effect upon the frequencies of the anti-symmetric modes is considerable.

As a comparison, the approximate energy-method (Rayleigh-Ritz method) gives  $\omega_1 = 1.060$  rad/sec. for the first symmetric mode and  $\omega_1 = 1.495$  rad/sec. for the first antisymmetric mode, as compared with  $\omega_1 = 1.0549$  rad/sec. for the first symmetric mode and  $\omega_1 = 1.4918$  rad/sec. for the first antisymmetric mode, from the analysis under consideration.

Again, it is desirable to compute the amount of potential energy stored elastically in the stiffening structure and in the cable separately from that due to the change of elevation of the structure, at different modes, in order to anticipate which are likely to have a significant effect on a given mode. Also, because the damping action differs in the various members of the bridge, the total energy lost per cycle depends upon the distribution of the potential energy. Fig. I-14 shows the distribution of the energy storage capacity in the various members of the structure for both symmetric and antisymmetric modes of vibration. The relative distribution of the energies is seen to have the same trend as in a suspension bridge having hinged stiffening structures.

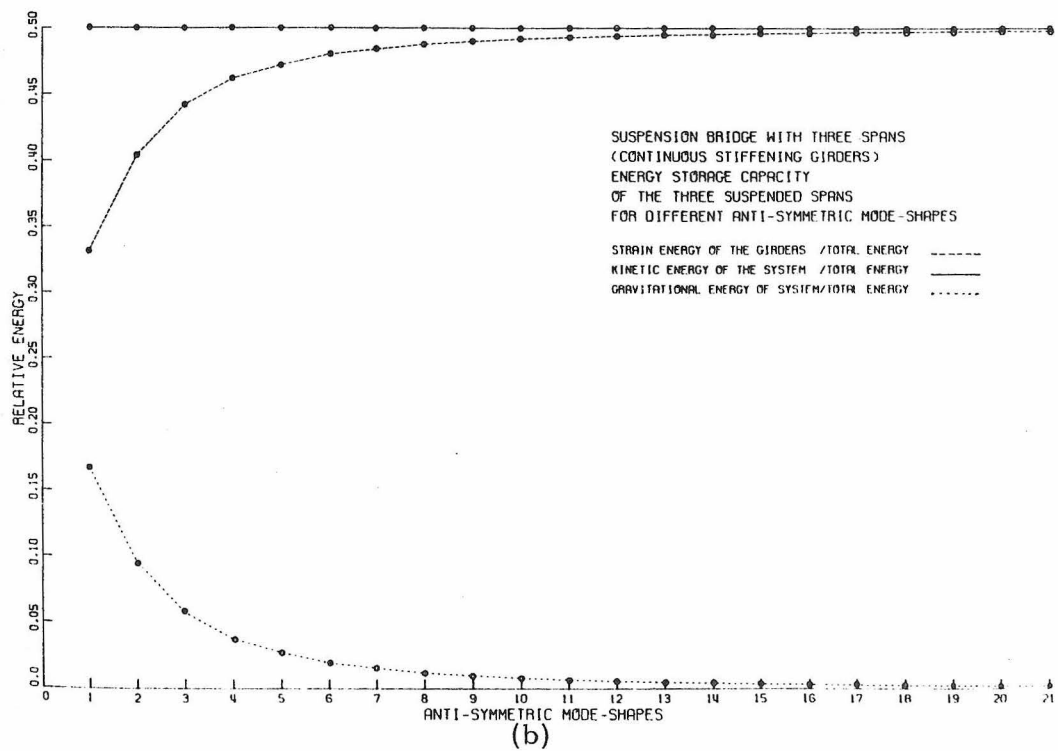
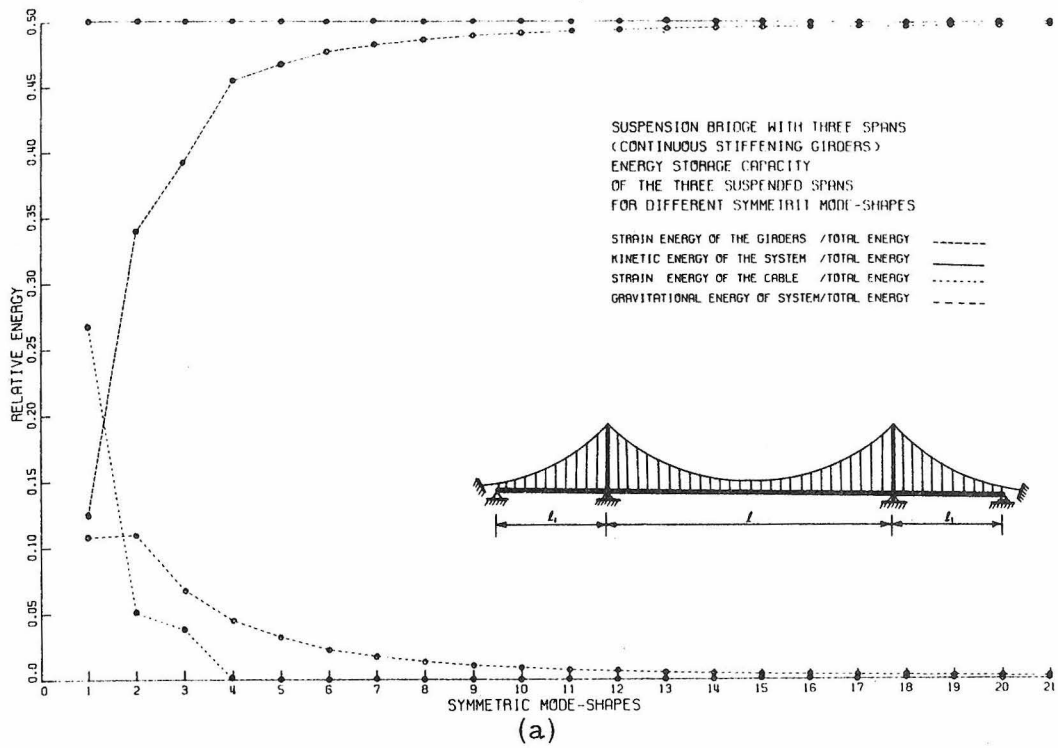


Fig. I-14. Relative energy storage capacity for the continuous-span suspension bridge (Example 3).

I-5. Effect of Tower Stiffness Upon Free Vertical Vibrations

In the preceding analysis, it was assumed that the tower cable saddles were free to move horizontally either upon roller nests under the saddles or by means of rockers at the bases of the towers. However, the construction of hinged tower bases is often found impractical especially in larger bridges, and so fixed tower bases are often resorted to. Fixed saddles provide one of the simplest and safest constructions, but the friction forces accompanying this design are so high that the tower tops move in unison with the adjacent cables.

A consequence of the fixed tower-base or fixed saddle is that the horizontal movement of the top of the tower is accompanied by a horizontal component of the force between the cable and the tower. Thus the horizontal force in the side spans will differ from that in the center span, but usually by only small amounts if the towers are well-designed. A modification of the analysis for this complication will be made. Furthermore, the vibration of the entire tower should be considered as the tower is an important member of the suspension bridge.

In general this section will include analysis of the following:

1. The effect of the elasticity of towers on the free vertical vibration of suspension bridges.
2. The in-plane free horizontal vibration of the towers, i. e., their vibration in the longitudinal direction of the bridge.

I-5-1. Correction for strain energy of the cables

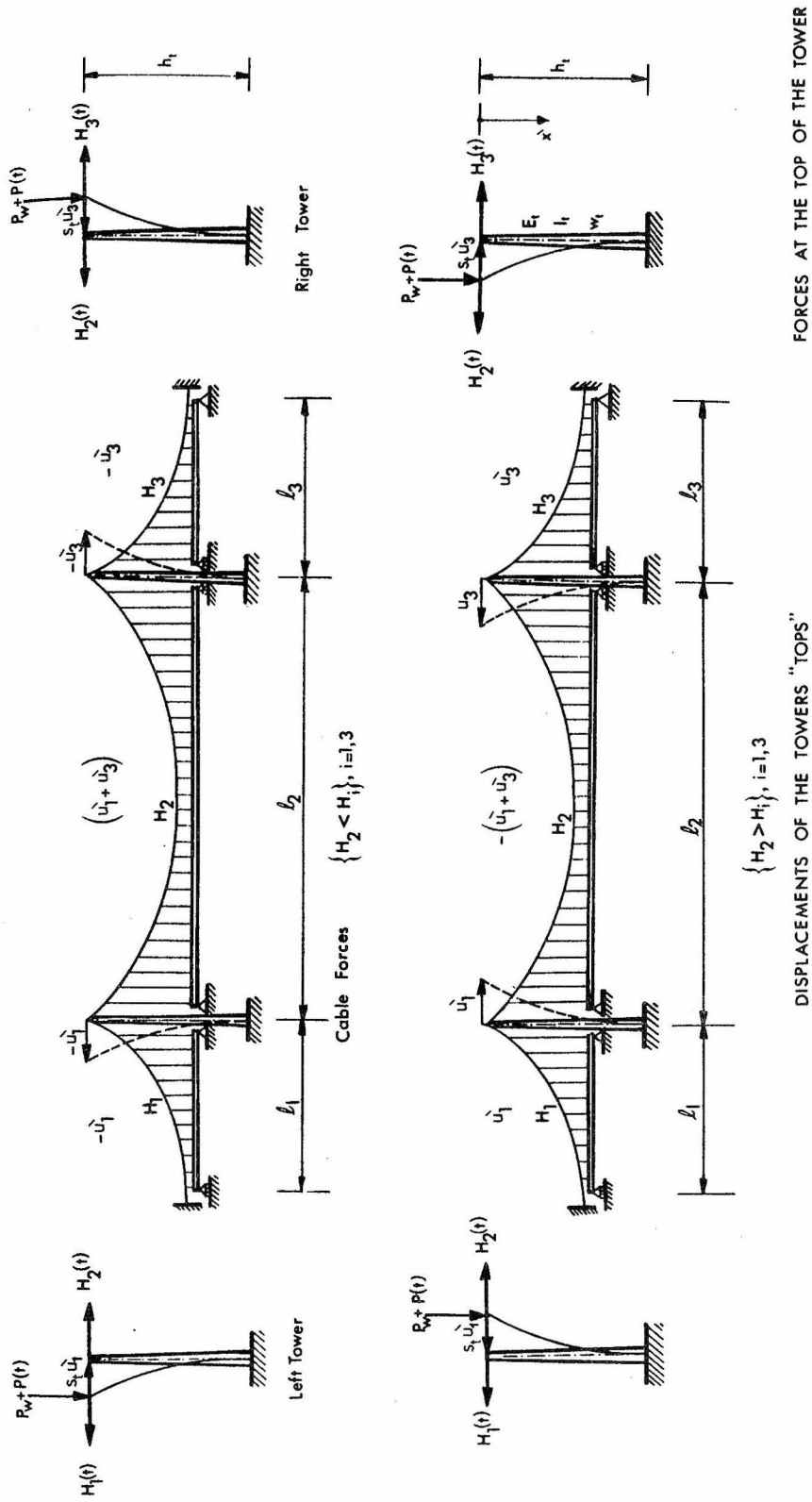
In the entire preceding analysis, it was assumed that the horizontal component of cable tension,  $H(t)$  was the same on both sides of the tower. However, this is not true if the tower resists displacement at the top. If, for example, it is deflected toward the side span as shown in the upper half of Fig. I-15, the increase in tension in that span,  $H_1(t)$  or  $H_3(t)$ , must equal the sum of the center span increase,  $H_2(t)$ , and the elastic resistance of the tower. This tower resistance can be expressed as the product of the tower top movement,  $u'_1(t)$  or  $u'_3(t)$ , and the elastic resistance of the tower,  $s_{t1}$  or  $s_{t3}$ . The displacements and forces at the top of the towers are shown in Fig. I-15, with their sign conventions. When the top of each tower moves toward or away from the center of the bridge the cable tension component  $H_i(t)$ ,  $i = 1, 3$  acts on the  $i^{\text{th}}$  span, and the tension component  $H_2(t)$  acts on the center span.

Given this new situation, the strain energy of the cable, Eq. 1.19, should be modified; the linearized part of Eq. 1.19 can be written as follows

$$\dot{V}_{ce}^*(t) = \frac{1}{2} \left[ \sum_{i=1}^3 H_i(t) \int_0^{l_i} \left( \frac{dy_i}{dx_i} \right) \left( \frac{\partial v_i}{\partial x_i} \right) dx_i \right] , \quad (1.105)$$

or by using Eq. 1.8'

$$\dot{V}_{ce}^*(t) = \frac{1}{2} \left[ \sum_{i=1}^3 H_i(t) \frac{\dot{w}_i^*}{H_w} \int_0^{l_i} v_i dx_i \right] . \quad (1.106)$$



EFFECT OF THE ELASTICITY OF TOWERS ON VERTICAL VIBRATIONS

Fig. I-15

Upon recalling the linearized cable equation (from Appendix I-b),

i. e. ,

$$\frac{H_i(t)L_{ei}}{E_c A_c} = u_c(x_i, t) \int_{x_i=0}^{x_i=l_i} + \int_0^{l_i} \left( \frac{dy_i}{dx_i} \right) \left( \frac{\partial v_i}{\partial x_i} \right) dx_i, \quad i = 1, 2, 3, \quad (1.107)$$

and noting that:

$$u_c(x_1, t) \Big|_0^{l_1} = u_c(l_1, t) - u_c(0, t) = u'_1(t),$$

$$u_c(x_2, t) \Big|_0^{l_2} = u_c(l_2, t) - u_c(0, t) = -(u'_1(t) + u'_3(t)), \quad (1.108)$$

and

$$u_c(x_3, t) \Big|_0^{l_3} = u_c(l_3, t) - u_c(0, t) = -u'_3(t),$$

where the assumption of fixed anchorages has been made, then the modified linearized cable equations, applied successively to the side and center spans, become

$$u'_i(t) = \frac{H_i(t)L_{ei}}{E_c A_c} - \int_0^{l_i} \left( \frac{dy_i}{dx_i} \right) \left( \frac{\partial v_i}{\partial x_i} \right) dx_i, \quad i = 1, 3, \quad (1.109)$$

and

$$-(u'_1(t) + u'_3(t)) = \frac{H_2(t)L_{e2}}{E_c A_c} - \int_0^{l_2} \left( \frac{dy_2}{dx_2} \right) \left( \frac{\partial v_2}{\partial x_2} \right) dx_2. \quad (1.110)$$

For symmetric suspension bridges, the two towers are identical and, except for the sign, the displacements  $u'_1(t)$  and  $u'_3(t)$  at the top of the left and right towers, respectively, must be the same. There-

fore, the linearized cable equation for the entire bridge can be written by summing Eqs. 1.109 and 1.110 to give

$$\sum_{i=1}^3 \frac{H_i(t)L_{ei}}{E_c A_c} - \sum_{i=1}^3 \int_0^{\ell_i} \left( \frac{dy_i}{dx_i} \right) \left( \frac{\partial v_i}{\partial x_i} \right) dx_i = 0 . \quad (1.111)$$

Considering the equilibrium of the horizontal forces at the top of the towers, the following is obtained:

$$\left| H_2(t) - H_1(t) \right| = s_{ti} u_i'(t) , \quad i = 1, 3 , \quad (1.112)$$

where  $s_{ti}$ ,  $i = 1, 3$  characterizes the elastic resistance of the  $i^{\text{th}}$  tower; this resistance is the force required to deflect the  $i^{\text{th}}$  tower by unit deflection, and it can be expressed, for uniform  $I_{ti}$ , as

$$s_{ti} \approx \frac{3E_{ti}I_{ti}}{h_{ti}^3} , \quad i = 1, 3 , \quad (1.113)$$

where  $E_{ti}$  is the modulus of elasticity of the  $i^{\text{th}}$  tower material,  $I_{ti}$  is the average value of the moment of inertia of the  $i^{\text{th}}$  tower leg about a horizontal axis perpendicular to the longitudinal axis of the bridge, and  $h_{ti}$  is the height of the  $i^{\text{th}}$  tower leg.

The next step to be taken is to express  $H_i(t)$ ,  $i = 1, 2, 3$  in terms of the displacement  $v_i$ ,  $i = 1, 2, 3$ . For this purpose, the displacements of the tops  $u_1'(t)$  and  $u_3'(t)$  have been eliminated from Eqs. 1.109 and 1.110, and Eq. 1.111 has been used to give

$$H_i(t) = \frac{(E_c A_c)^2}{(E_c A_c L_E + L_{e2} L_{ei} s_{ti})} \left[ \sum_{j=1}^3 \int_0^{\ell_j} \left( \frac{dy_j}{dx_j} \right) \left( \frac{\partial v_j}{\partial x_j} \right) dx_j + \frac{L_{e2} s_{ti}}{E_c A_c} \int_0^{\ell_i} \left( \frac{dy_i}{dx_i} \right) \left( \frac{\partial v_i}{\partial x_i} \right) dx_i \right],$$

$i = 1, 3 . \quad (1.114)$

When the coefficients  $c_{1i}$  and  $c_{2i}$ ,  $i = 1, 3$  are defined as

$$c_{1i} = \frac{(E_c A_c)^2}{(E_c A_c L_E + L_{e2} L_{ei} s_{ti})} \quad \text{and} \quad c_{2i} = \frac{L_{e2} s_{ti}}{E_c A_c}, \quad i = 1, 3 ,$$

$(1.115)$

Eq. 1.114, can be written as

$$H_i(t) = c_{1i} \left[ \sum_{j=1}^3 \int_0^{\ell_j} \left( \frac{dy_j}{dx_j} \right) \left( \frac{\partial v_j}{\partial x_j} \right) dx_j + c_{2i} \int_0^{\ell_i} \left( \frac{dy_i}{dx_i} \right) \left( \frac{\partial v_i}{\partial x_i} \right) dx_i \right], \quad i = 1, 3 .$$

$(1.116)$

Substitution of Eq. 1.116 into Eq. 1.111, yields

$$H_\gamma(t) = c_{1i} \left[ \left( 1 + c_{2i} \frac{L_{ei}}{L_{e2}} \right) \sum_{j=1}^3 \int_0^{\ell_j} \left( \frac{dy_j}{dx_j} \right) \left( \frac{\partial v_j}{\partial x_j} \right) dx_j - 2c_{2i} \frac{L_{ei}}{L_{e2}} \int_0^{\ell_i} \left( \frac{dy_i}{dx_i} \right) \left( \frac{\partial v_i}{\partial x_i} \right) dx_i \right],$$

$i = 1 \text{ or } 3 . \quad (1.117)$

Therefore the modified strain energy of the cable, Eq. 1.106, with the aid of Eqs. 1.116, 1.117 and 1.8', may be written as

$$\begin{aligned} \dot{V}_{ce}^*(t) = & \frac{1}{2} \left\{ \sum_{i=1, 3}^3 \frac{\dot{w}_i^*}{H_w} \left[ c_{1i} \sum_{j=1}^3 \frac{\dot{w}_j^*}{H_w} \int_0^{\ell_j} v_j dx_j + c_{1i} c_{2i} \frac{\dot{w}_i^*}{H_w} \int_0^{\ell_i} v_i dx_i \right] \left[ \int_0^{\ell_i} v_i dx_i \right] \right. \\ & \left. + \frac{\dot{w}_2^*}{H_w} \left[ c_{1i} \left( 1 + c_{2i} \frac{L_{ei}}{L_{e2}} \right) \sum_{j=1}^3 \frac{\dot{w}_j^*}{H_w} \int_0^{\ell_j} v_j dx_j - 2c_{1i} c_{2i} \frac{\dot{w}_i^*}{H_w} \int_0^{\ell_i} v_i dx_i \right] \left[ \int_0^{\ell_2} v_2 dx_2 \right] \right\}, \end{aligned}$$

$(1.118)$

where the index  $i$ , indicated between the second set of brackets, is either 1 or 3 .

I-5-2. Potential energy absorbed by the towers

Now, the strain energy due to the bending of the two towers is given by

$$V_{tb}(t) = \frac{1}{2} \sum_{i=1,3}^3 \int_0^{h_{ti}} \frac{M_{x'_i}^2}{E_{ti} I_{ti}} dx'_i, \quad (1.119)$$

where  $M_{x'_i}$  is the bending moment of the tower leg at the point  $x'_i$ ,  $i = 1, 3$  caused by the horizontal force  $|H_2(t) - H_1(t)|$ ,  $i = 1, 3$  and is expressed by

$$M_{x'_i} = |H_2(t) - H_1(t)| \cdot x'_i, \quad i = 1, 3. \quad (1.120)$$

Substitution of this expression into Eq. 1.119 and then integration, yields

$$V_{tb}(t) = \frac{1}{2} \sum_{i=1,3}^3 \left( \frac{|H_2(t) - H_1(t)|^2 \cdot h_{ti}^2}{3E_{ti} I_{ti}} \right). \quad (1.121)$$

From Eqs. 1.116 and 1.117 the force  $|H_2(t) - H_1(t)|$  can be obtained as

$$|H_2(t) - H_1(t)| = s_{ti} \left[ \frac{L_{ei}}{L_E} \left( \sum_{j=1}^3 \int_0^{\ell_j} \left( \frac{dy_j}{dx_j} \right) \left( \frac{\partial v_j}{\partial x_j} \right) dx_j \right) - \int_0^{\ell_i} \left( \frac{dy_i}{dx_i} \right) \left( \frac{\partial v_i}{\partial x_i} \right) dx_i \right], \quad i=1, 3. \quad (1.122)$$

Therefore, the strain energy absorbed by the two tower legs, Eq. 1.119, can be written, with the aid of Eqs. 1.122 and 1.8', as

$$V_{tb}(t) = \frac{1}{2} \sum_{i=1, 3}^3 \left\{ \frac{h_{ti}^2 s_{ti}^2}{3E_{ti} I_{ti}} \left[ \frac{L_{ei}}{L_E} \left( \sum_{j=1}^3 \frac{\bar{w}_j^*}{H_w} \int_0^{\ell_j} v_j dx_j \right) - \frac{\bar{w}_i^*}{H_w} \int_0^{\ell_i} v_i dx_i \right]^2 \right\} . \quad (1.123)$$

Because of the complexity of the resulting equations, it is not desirable to derive the differential equations of motion which include the effect of tower rigidity. Instead, the solutions will be obtained by the finite element approach.

### I-5-3. Equations of motion for the towers

In order to derive the differential equations of motion, each tower of the suspension bridge is now replaced by the equivalent system shown in Fig. I-2-b, where the elastic constraint by the cables at the top of the tower is simulated by a spring of stiffness  $k_{ei}$ ,  $i = 1, 3$  (see Refs. 19 and 20). It has been assumed that the centerline of the tower is allowed only horizontal motion in the longitudinal direction of the bridge, and the axial and horizontal forces acting on the top of the tower have been taken into consideration.

The bending-strain energy in the towers may be written as

$$V_{te}(t) = \frac{1}{2} \sum_{i=1, 3}^3 \int_0^{h_{ti}} E_{ti} I_{ti}(x'_i) \left( \frac{\partial^2 u'(x'_i, t)}{\partial x'_i{}^2} \right)^2 dx'_i , \quad (1.124)$$

where the index  $i$  implies the left ( $i=1$ ) and the right ( $i=3$ ) towers.

In Fig. I-2-b this index has been omitted for simplicity.

In order to calculate the potential energy of the tower due to the static and dynamic reactions of the cable, the relative displacement

$\Delta h_{ti}$  ,  $i = 1, 3$  caused by the vertical loads during bending must first be determined. With this in mind, consider an element  $ds'$  of the tower leg in its deflected shape; the infinitesimal relative displacement over the element of the tower leg is

$$ds' - dx' = \frac{(ds')^2 - (dx')^2}{ds' + dx'} \approx \frac{\left(\frac{\partial u'}{\partial x'}\right)^2 (dx')^2}{2dx'} = \frac{1}{2} \left(\frac{\partial u'}{\partial x'}\right)^2 dx' ; \quad (1.125)$$

therefore,

$$\Delta h_{ti} = \int_0^{h_{ti}} (ds'_i - dx'_i) = \frac{1}{2} \int_0^{h_{ti}} \left(\frac{\partial u'_i}{\partial x'_i}\right)^2 dx'_i , \quad i = 1, 3 . \quad (1.126)$$

During this displacement, the load  $P_w$  remains constant, while the load  $P(t)$  increases gradually. Therefore, the potential energy of the two loads in the deflected position is:

$$\begin{aligned} V_{ta}(t) &= - \sum_{i=1,3}^3 \left( P_w + \frac{1}{2} P(t) \right) \cdot \Delta h_{ti} , \quad i = 1, 3 , \\ &= - \sum_{i=1,3}^3 \left( P_w + \frac{1}{2} P(t) \right) \int_0^{h_{ti}} \frac{1}{2} \left(\frac{\partial u'_i}{\partial x'_i}\right)^2 dx'_i , \quad i = 1, 3 , \\ &\approx - \frac{1}{2} \sum_{i=1,3}^3 P_w \int_0^{h_{ti}} \left(\frac{\partial u'_i}{\partial x'_i}\right)^2 dx'_i , \quad i = 1, 3 . \end{aligned} \quad (1.127)$$

In deriving this relation, assumption no. 8 (Eq. 1.3) of the fundamental assumptions mentioned in section I-2-3, has been used.

The potential energy stored in the equivalent spring is

$$V_{es}(t) = \frac{1}{2} \sum_{i=1,3}^3 k_{ei} u_i'^2(t) , \quad (1.128)$$

where  $k_{ei}$ ,  $i = 1, 3$  is the stiffness of the equivalent spring at each tower top. Konishi and Yamada [19, 20] have estimated the value of the spring stiffness,  $k_{ei}$ , to be

$$k_{ei} \approx \frac{E_c A_c}{L_{e2}} + \frac{E_c A_c}{L_{ei}} , \quad i = 1, 3 . \quad (1.129)$$

Now, the total potential energy in the towers,  $V_t(t)$ , is

$$V_t(t) = V_{te}(t) + V_{ta} + V_{es}(t) . \quad (1.130)$$

The kinetic energy for the tower legs can be expressed as

$$T_t(t) = \frac{1}{2} \sum_{i=1,3}^3 \int_0^{h_{ti}} m_{ti}(x'_i) \left( \frac{\partial u_i'(x'_i, t)}{\partial t} \right)^2 dx'_i , \quad (1.131)$$

where  $m_{ti}(x'_i)$  is the mass per unit length of the  $i^{\text{th}}$  tower leg.

Application of Hamilton's Principle, Eq. 1.37, as before, enables derivation of the equation of motion of the  $i^{\text{th}}$  tower leg in the form:

$$m_{ti}(x'_i) \frac{\partial^2 u_i'}{\partial t^2} + \frac{\partial^2}{\partial x_i'^2} \left( E_{ti} I_{ti}(x'_i) \frac{\partial^2 u_i'}{\partial x_i'^2} \right) + P_w \frac{\partial^2 u_i'}{\partial x_i'^2} = 0 , \quad i = 1, 3, \quad (1.132)$$

and the associated boundary conditions are

$$\frac{\partial}{\partial x'_i} \left( E_{ti} I_{ti}(x'_i) \frac{\partial^2 u'_i}{\partial x'^2_i} \right) + P_w \frac{\partial u'_i}{\partial x'_i} = k_{ei} u'_i, \quad i = 1, 3, \quad (1.133)$$

and

$$E_{ti} I_{ti}(x'_i) \frac{\partial^2 u'_i}{\partial x'^2_i} \cdot \frac{\partial}{\partial x'_i} (\delta u'_i) = 0, \quad i = 1, 3. \quad (1.134)$$

I-6. Finite Element Approach for the Overall Problem

This section contains the finite element solutions for the overall problem, i. e., for the suspended structure, the cables and the towers. Therefore, the stiffness and inertia characteristics of the entire assembled suspension bridge structure must be determined.

I-6-1. Modification of structural-property matrices

a. The modified elastic stiffness matrix of the cable

With the aid of the displacement model, Eq. 1.58, the modified energy expression, Eq. 1.118, becomes

$$\begin{aligned} \dot{V}_{ce}^*(t) = \frac{1}{2} \left\{ \sum_{i=1,3}^3 \frac{\dot{w}_i^* c_{1i}}{H_w} \left[ \sum_{j=1}^3 \left( \sum_{e=1}^{N_j} \frac{\dot{w}_i^*}{H_w} \int_0^L \{f\}_e^T \{q\}_e d\bar{x} \right) \right. \right. \\ + c_{2i} \sum_{e=1}^{N_i} \frac{\dot{w}_i^*}{H_w} \int_0^L \{f\}_e^T \{q\}_e d\bar{x} \left. \right]^T \left[ \sum_{e=1}^{N_i} \int_0^L \{f\}_e^T \{q\}_e d\bar{x} \right] \\ + \frac{\dot{w}_i^* c_{1i}}{H_w} \left[ \left( 1 + c_{2i} \frac{L_{ei}}{L_{e2}} \right) \sum_{j=1}^3 \left( \sum_{e=1}^{N_j} \frac{\dot{w}_j^*}{H_w} \int_0^L \{f\}_e^T \{q\}_e d\bar{x} \right) \right. \\ \left. - 2c_{2i} \frac{L_{ei}}{L_{e2}} \sum_{e=1}^{N_i} \frac{\dot{w}_i^*}{H_w} \int_0^L \{f\}_e^T \{q\}_e d\bar{x} \right]^T \left[ \sum_{e=1}^{N_2} \int_0^L \{f\}_e^T \{q\}_e d\bar{x} \right] \left. \right\} . \end{aligned}$$

Using the integral of Eq. 1.80 and the definition of Eq. 1.81 in this modified energy expression leads to

$$\begin{aligned}
 \dot{V}_{ce}^*(t) = & \frac{1}{2} \{r\}^T \left[ \sum_{i=1,3}^3 c_{1i} \frac{\dot{w}_i^*}{H_w} \left( \sum_{j=1}^3 \frac{\dot{w}_j^*}{H_w} \{\hat{f}\}_{N_j} + c_{2i} \frac{\dot{w}_i^*}{H_w} \{\hat{f}\}_{N_i} \right) \left( \{\hat{f}\}_{N_i}^T \right) \right. \\
 & + c_{1i} \frac{\dot{w}_2^*}{H_w} \left( \left( 1 + c_{2i} \frac{L_{ei}}{L_{e2}} \right) \sum_{j=1}^3 \frac{\dot{w}_j^*}{H_w} \{\hat{f}\}_{N_j} \right. \\
 & \left. \left. - 2c_{2i} \frac{L_{ei}}{L_{e2}} \frac{\dot{w}_i^*}{H_w} \{\hat{f}\}_{N_i} \right) \left( \{\hat{f}\}_{N_2}^T \right) \right] \{r\} \quad , \quad (1.135)
 \end{aligned}$$

or equivalently

$$\dot{V}_{ce}^*(t) = \frac{1}{2} \{r\}^T [\dot{K}_{CE}^*] \{r\} \quad , \quad (1.136)$$

where  $[\dot{K}_{CE}^*]$  is the modified assemblage elastic stiffness matrix of the cable; it can be defined as

$$\begin{aligned}
 [\dot{K}_{CE}^*] = & \left[ \sum_{i=1,3}^3 c_{1i} \frac{\dot{w}_i^*}{H_w} \left( \sum_{j=1}^3 \frac{\dot{w}_j^*}{H_w} \{\hat{f}\}_{N_j} + c_{2i} \frac{\dot{w}_i^*}{H_w} \{\hat{f}\}_{N_i} \right) \left( \{\hat{f}\}_{N_i}^T \right) \right. \\
 & + c_{1i} \frac{\dot{w}_2^*}{H_w} \left( \left( 1 + c_{2i} \frac{L_{ei}}{L_{e2}} \right) \sum_{j=1}^3 \frac{\dot{w}_j^*}{H_w} \{\hat{f}\}_{N_j} \right. \\
 & \left. \left. - 2c_{2i} \frac{L_{ei}}{L_{e2}} \frac{\dot{w}_i^*}{H_w} \{\hat{f}\}_{N_i} \right) \left( \{\hat{f}\}_{N_2}^T \right) \right] \quad , \quad (1.137)
 \end{aligned}$$

where, again, the index  $i$ , indicated between the second set of parentheses, is either 1 or 3.

b. The elastic stiffness matrix of the towers  
corresponding to bending of the towers by the  
cable forces

The strain energy absorbed by the two towers, Eq. 1.123, due to their elastic resistance to the movement of their tops, can be expressed in a matrix form by using the displacement model, Eq. 1.158, as follows

$$V_{tb}(t) = \frac{1}{2} \left\{ \sum_{i=1,3}^3 \frac{(h_{ti} s_{ti})^2}{3E_{ti} I_{ti}} \left[ \frac{L_{ei}}{L_E} \sum_{j=1}^3 \left( \sum_{e=1}^{N_j} \frac{\bar{w}_j^*}{H_w} \int_0^L \{f\}_e^T \{q\}_e d\bar{x} \right) - \sum_{e=1}^{N_i} \frac{\bar{w}_i^*}{H_w} \int_0^L \{f\}_e^T \{q\}_e d\bar{x} \right]^2 \right\} .$$

Expanding, and using Eqs. 1.80 and 1.81, this expression becomes

$$V_{tb}(t) = \frac{1}{2} \{r\}^T \left[ \sum_{i=1,3}^3 \frac{(h_{ti} s_{ti})^2}{3E_{ti} I_{ti}} \left( \frac{L_{ei}}{L_E} \sum_{j=1}^3 \frac{\bar{w}_j^*}{H_w} \{\hat{f}\}_{N_j} - \frac{\bar{w}_i^*}{H_w} \{\hat{f}\}_{N_i} \right) \left( \frac{L_{ei}}{L_E} \sum_{j=1}^3 \frac{\bar{w}_j^*}{H_w} \{\hat{f}\}_{N_j} - \frac{\bar{w}_i^*}{H_w} \{\hat{f}\}_{N_i} \right)^T \right] \{r\} , \quad (1.138)$$

or equivalently

$$V_{tb}(t) = \frac{1}{2} \{r\}^T [K_{TB}] \{r\} , \quad (1.139)$$

where  $[K_{TB}]$  is the bending stiffness matrix of the towers; it is defined in Eq. 1.138.

So far, the stiffness and mass matrices have been of order  $N \times N$ , where  $N$  is the number of degrees of freedom of the suspended structure and the cable, i. e., the number of unknown nodal displacements. The vector of nodal displacement for the assemblage  $\{r\}$ , is of order  $N \times 1$ . Even the bending stiffness matrix of the tower is of order  $N \times N$ , since it is expressed in terms of the nodal displacements of the suspended structure and the cable.

I-6-2. Modification of the matrix equations of motion

To formulate the overall problem, the stiffness and inertia matrices of the towers must be determined. For this, the towers are divided into small elements as shown in Fig. I-2-b. The top element of the tower must include the equivalent spring which simulates the influence of the restraint of the tower by the main cable.

The element elastic stiffness matrix due to flexural rigidity for the elements of the tower is the same as that for the elements of the stiffening structure, Eq. 1.65, excepting the matrix for the uppermost element which includes the spring effect; the latter is in the form

$$[k_{te}]_{ei} = \frac{E_{te} I_{te}}{L'^3} \begin{bmatrix} 12 & -6L' & -12 & -6L' \\ -6L' & 4L'^2 & 6L' & 2L'^2 \\ -12 & 6L' & 12+k_{ei} & 6L' \\ -6L' & 2L'^2 & 6L' & 4L'^2 \end{bmatrix},$$

$$i = 1, 3, \quad (1.140)$$

where  $E_{te} I_{te}$  is the flexural rigidity of the individual element; it is assumed that  $I_{te}$  is constant along the element.  $L'$  is the element length.

The assemblage bending-stiffness matrix for the two towers is thus

$$[K_{TE}] = \sum_{i=1,3}^3 \left( \sum_{e=1}^{N'_i} [k_{te}]_{ei} \right) . \quad (1.141)$$

Here,  $N'_i$  is the total number of elements in the  $i^{\text{th}}$  tower leg.

The nodal displacements can now be written as

$$\{r_t\} = \sum_{e=1}^{N'} \{q_t\}_e \quad \text{with} \quad N' = \sum_{i=1,3}^3 N'_i . \quad (1.142)$$

The element geometric-stiffness matrix due to the compressive load  $P_w$  then takes the form

$$[k_{tg}]_e = \frac{-P_w}{30L'} \begin{bmatrix} 36 & -3L' & -36 & -3L' \\ -3L' & 4L'^2 & 3L' & -L'^2 \\ -36 & 3L' & 36 & 3L' \\ -3L' & -L'^2 & 3L' & 4L'^2 \end{bmatrix} . \quad (1.143)$$

The assemblage geometric-stiffness matrix for the two towers is

$$[K_{TG}] = \sum_{i=1,3}^3 \left( \sum_{e=1}^{N'_i} [k_{tg}]_e \right) . \quad (1.144)$$

The consistent-mass matrix for the element of the tower can be written as

$$[m_t]_e = \frac{m_{te} L'}{420} \begin{bmatrix} 156 & -22L' & 54 & 13L' \\ -22L' & 4L'^2 & -13L' & -3L'^2 \\ 54 & -13L' & 156 & 22L' \\ 13L' & -3L'^2 & 22L' & 4L'^2 \end{bmatrix}, \quad (1.145)$$

where  $m_{te}$  is the element distributed mass per unit length.

The assemblage consistent mass matrix for the two towers is

$$[M_T] = \sum_{i=1,3}^3 \left( \sum_{e=1}^{N'_i} [m_t]_e \right).$$

Now, the nodal displacements, that is, the unknowns for the entire assemblage, may be written in the following partitioned form

$$\{\hat{r}\} = \begin{Bmatrix} \{r\} \\ \{r_t\} \end{Bmatrix}, \quad (1.146)$$

where the subvector  $\{r\}$  is of the order  $N \times 1$ , while the subvector  $\{r_t\}$  is of order  $N'_1 \times 1$ ; therefore, the order of  $\{\hat{r}\}$  is  $(N+N') \times 1$ .

To form the overall stiffness and inertia matrices more conveniently for both the suspended structures and the cables on one hand, and the two towers on the other hand, one can write each matrix in a partitioned form. Two examples, one for the suspended structure and the cable and the other for the towers, are presented as follows

$$[\hat{K}_{GE}] = \begin{bmatrix} [K_{GE}] & [0] \\ [0] & [0] \end{bmatrix}_{(N+N') \times (N+N')}, \quad (1.147)$$

and

$$[\hat{K}_{TE}] = \begin{bmatrix} [0] & [0] \\ [0] & [K_{TE}] \end{bmatrix} \quad (N+N') \times (N+N') \quad (1.148)$$

Now, performing the same variational procedure as before, the assemblage (overall) matrix equations of motion for symmetric vibrations may be written as

$$\begin{aligned} ([\hat{M}] + [\hat{M}_T])\{\ddot{\hat{r}}\} + ([\hat{K}_{GE}] + [\hat{K}_{CG}] + [\hat{K}_{CE}^*] + [\hat{K}_{TB}] + [\hat{K}_{TE}] + [\hat{K}_{TG}])\{\hat{r}\} \\ = \{0\} \quad , \end{aligned} \quad (1.149)$$

or more conveniently

$$[\hat{M}_S]\{\ddot{\hat{r}}_S\} + [\hat{K}_S]\{\hat{r}_S\} = \{0\} \quad , \quad (1.150)$$

where  $[\hat{K}_S]$  is a symmetric, full, positive definite matrix, of order  $(N+N') \times (N+N')$ ; it is defined through Eq. 1.149. Eq. 1.149 (or 1.150) is subjected to the constraint

$$q_{(2N'-1)_i} = u'_i(t) = \frac{H_i(t)L_{ei}}{E_c A_c} - \frac{\bar{w}_i^*}{H_w} \int_0^{\ell_i} v_i dx_i \quad , \quad i = 1, 3 \quad , \quad (1.151)$$

which can be written, by the aid of Eqs. 1.116, 1.158, as

$$\begin{aligned} q_{(2N'-1)_i} = u'_i(t) = \left( c_{1i} \frac{L_{ei}}{E_c A_c} \left[ \sum_{j=1}^3 \frac{\bar{w}_j^*}{H_w} \{\hat{f}\}_{N_j}^T \{r\} + c_{2i} \frac{\bar{w}_i^*}{H_w} \{\hat{f}\}_{N_i}^T \{r\} \right] \right. \\ \left. - \frac{\bar{w}_i^*}{H_w} \{\hat{f}\}_{N_i}^T \{r\} \right) \quad , \quad i = 1, 3 \quad , \quad (1.152) \end{aligned}$$

this is actually the relation between the nodal displacement,  $q_{(2N'-1)}$ , at the top of the tower and the nodal displacements  $\{r\}$  of the

suspended structure.

For the antisymmetric vibrations

$$[\hat{K}_{CE}^*] = [0] \quad \text{and} \quad [\hat{K}_{TB}] = [0] , \quad (1.153)$$

and the equation of motion (1.150) reduces to

$$\left( [\hat{M}] + [\hat{M}_T] \right) \{\ddot{\hat{r}}\} + \left( [\hat{K}_{GE}] + [\hat{K}_{CG}] + [\hat{K}_{TE}] + [\hat{K}_{TG}] \right) \{\hat{r}\} = \{0\} , \quad (1.154)$$

or

$$[\hat{M}_S] \{\ddot{\hat{r}}_{AS}\} + [\hat{K}_{AS}] \{\hat{r}_{AS}\} = \{0\} , \quad (1.155)$$

where  $[\hat{K}_{AS}]$  is a symmetric, banded, positive definite matrix of order  $(N+N') \times (N+N')$ ; it is defined through Eq. 1.154.

The formulation of the eigenvalue problem, for both the symmetric and the antisymmetric vibrations, follows similar procedures to those which were used in section I-4.

The following computation illustrates the application of the previous analysis to the overall problem.

### I-6-3. Illustrative numerical example

To clarify the effect of the flexural rigidity of the towers upon the dynamic characteristics of suspension bridges and to show the different modes of vibration of the towers, a numerical example has been worked out for the suspension bridge in Example 2. Additional information about the towers follows:

$$I_{t1} = I_{t3} = 20,000 \text{ ft.}^2 \text{ in.}^2$$

$$w_{t1} = w_{t3} = 4.0 \text{ Kip/ft.}$$

$$h_{t1} = h_{t3} = 400 \text{ ft.}$$

$$P_w = 10,000 \text{ Kips.}$$

$$E_{t1} = E_{t3} = 29,600 \text{ Kip/in.}^2$$

The frequencies and modes of vibration have been computed for the symmetric case of the overall problem. The number of elements in each tower leg ( $N'_i$ ,  $i=1,3$ ), was taken to be 10 elements and therefore the length of each element  $L'$  is equal to 42 ft.

The frequencies of vibration and the mainly vibrating members corresponding to each frequency, are shown in Table I-4. While Table I-3 shows that the effect of the flexural rigidity of the towers upon the frequencies of the vertically vibrating stiffening structure is comparatively small and is limited to only the first few frequencies.

The vibrational modes of the system, shown in Fig. I-16, can be separated into two groups. In one group, the displacements of the stiffening structures are predominant, and in the other group, the displacements of the towers are predominant. Therefore, investigation of the energy accumulated in the different members of the suspension bridge, may require separation of the energies into two groups. Fig. I-17-a represents the energy storage capacity of the cables and the stiffening structures as one group, including that part of the potential energy absorbed by the towers during vibration of the suspended structures. The minor (or secondary) role the towers play in the energy storage capacity of vertically vibrating bridge is indicated by the dotted line near the horizontal axis. The correction in the strain energy of the cable (Eq. 1.118) can be shown

TABLE I-4

Natural Periods and Frequencies of Vertical Vibration  
 The Overall Problem  
 (Symmetric Mode Shapes)

| Mode Order | Frequency $\omega$ (rad/sec) | Period T (sec.) | Frequency f (cps) | Member of Dominant Vibration |
|------------|------------------------------|-----------------|-------------------|------------------------------|
| 1          | 1.064821                     | 5.900698        | 0.169471          | center and side spans        |
| 2          | 2.255588                     | 2.785608        | 0.358988          | center and side spans        |
| 3          | 2.698381                     | 2.328502        | 0.429461          | center and side spans        |
| 4          | 5.477865                     | 1.147013        | 0.871830          | towers                       |
| 5          | 6.845536                     | 0.917851        | 1.089501          | center span                  |
| 6          | 7.081554                     | 0.887261        | 1.127064          | side spans                   |
| 7          | 13.110453                    | 0.479250        | 2.086594          | center span                  |
| 8          | 15.545536                    | 0.404179        | 2.474151          | side spans                   |
| 9          | 17.733480                    | 0.354312        | 2.822371          | towers                       |
| 10         | 21.470668                    | 0.292640        | 3.417168          | center span                  |
| 11         | 27.400477                    | 0.229309        | 4.360928          | side spans                   |
| 12         | 31.939673                    | 0.196720        | 5.083367          | center span                  |
| 13         | 33.794722                    | 0.185922        | 5.378600          | towers                       |
| 14         | 42.697815                    | 0.147155        | 6.795556          | side spans                   |
| 15         | 44.543139                    | 0.141058        | 7.089282          | center span                  |
| 16         | 53.246513                    | 0.118002        | 8.474433          | towers                       |
| 17         | 59.322982                    | 0.105915        | 9.441533          | center span                  |
| 18         | 76.341798                    | 0.082303        | 12.150225         | center span                  |
| 19         | 81.392639                    | 0.077196        | 12.954039         | towers                       |
| 20         | 83.968655                    | 0.074828        | 13.363981         | side spans                   |
| 21         | 95.686260                    | 0.065664        | 15.229045         | center span                  |
| 22         | 117.471018                   | 0.053489        | 18.695433         | center span                  |
| 23         | 119.085201                   | 0.052762        | 18.953034         | towers                       |
| 24         | 140.643156                   | 0.044675        | 22.383884         | side spans                   |
| 25         | 141.806416                   | 0.044308        | 22.569288         | center span                  |
| 26         | 165.742317                   | 0.037909        | 26.378960         | towers                       |
| 27         | 168.755532                   | 0.037232        | 26.858616         | center span                  |
| 28         | 197.325764                   | 0.031842        | 31.405063         | center span                  |

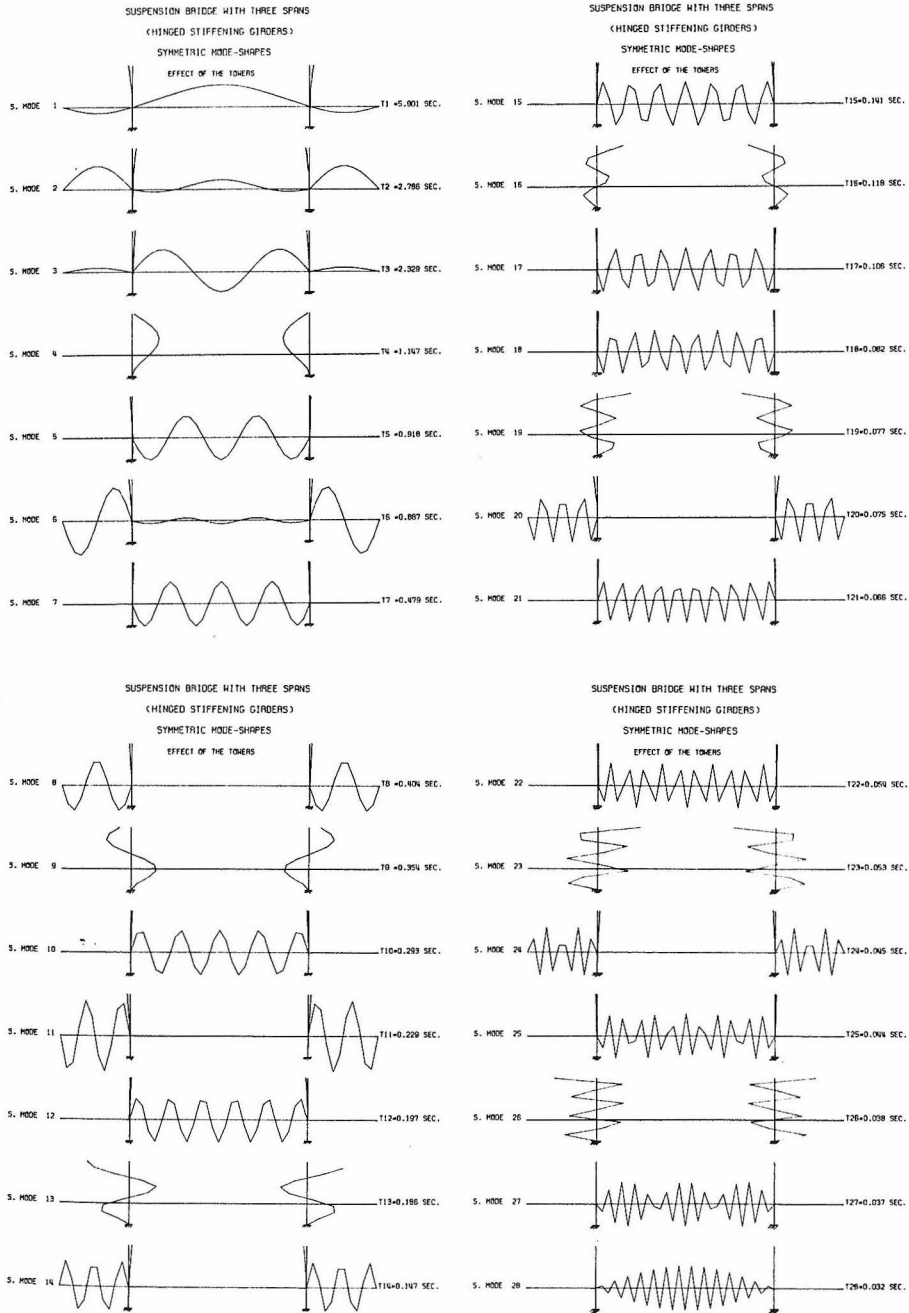
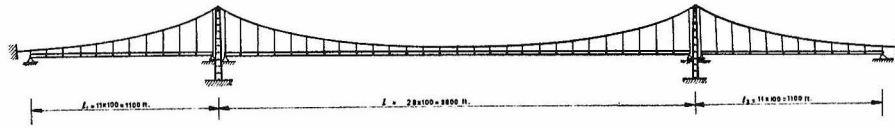


Fig. I-16. Symmetric mode-shapes of a three-span suspension bridge (including the towers).

by a comparison between Fig. I-11-a and Fig. I-17-a; actually it is very small. Fig. I-17-b shows the energy storage capacity of the towers at different modes, as the other group (when the main vibrating elements are the towers). The very small contribution of the negative potential energy of the axial force,  $P_w$ , due to cable reaction is an interesting phenomena. Actually, the drop of the relative kinetic energy in the first two modes is caused by that negative potential energy.

As is seen, there is no situation in which the towers and the suspended structures vibrate simultaneously in a common mode; however, the towers vibrate opposite to each other so when their vibration is significant, the stiffening structure vibration will increase.

It is important to note that in all the previous numerical examples the mode shapes obtained by the finite element method are distorted in the higher modes because they are determined by connecting the displacements at the various nodal points, and these nodal points, of course, do not describe all points on the curve; in the lower modes, each loop is described by more nodal points, enabling a smoother curve.

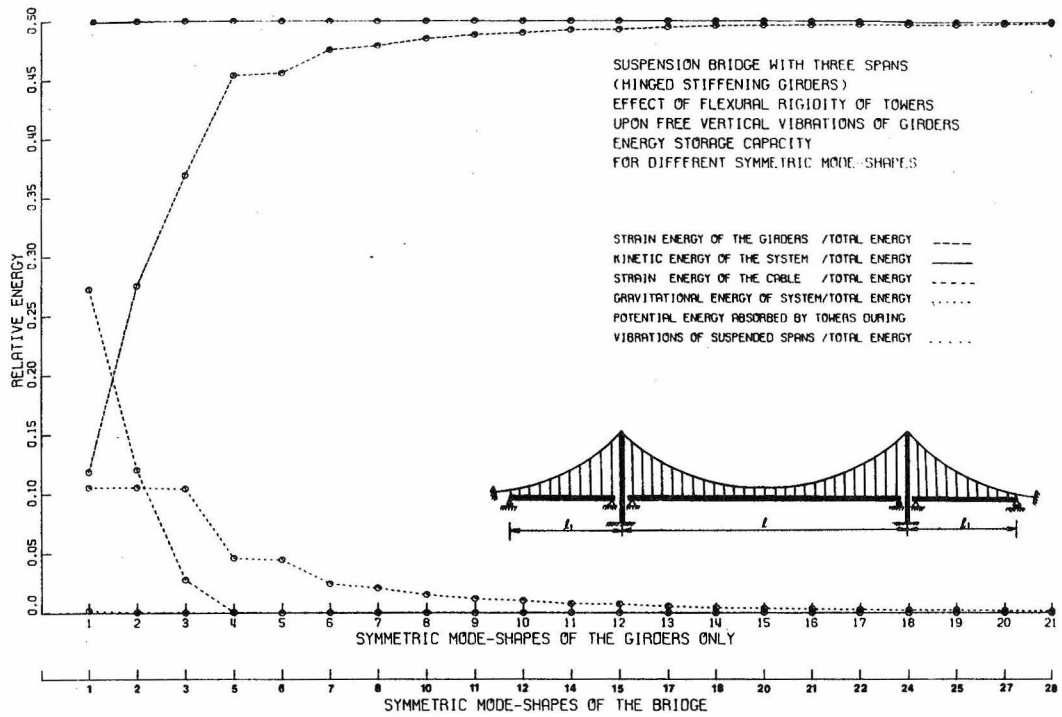


Fig. I-17-a. Relative energy storage capacity for the suspended structures and the cables.

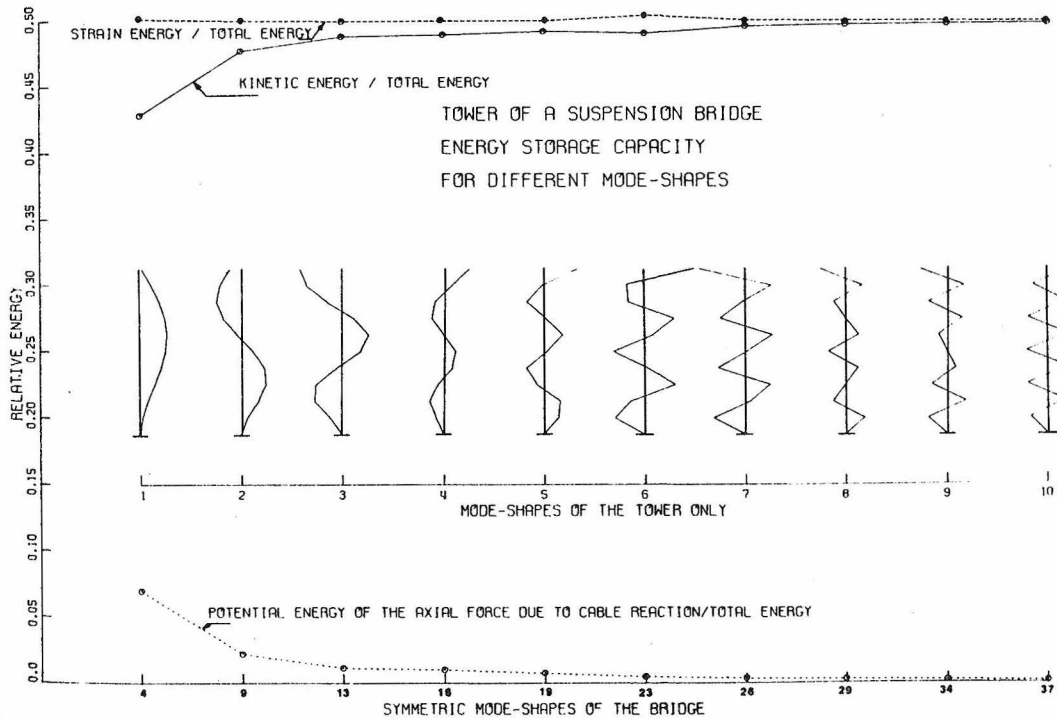


Fig. I-17-b. Relative energy storage capacity for the towers.

I-7. Appendices

Appendix I-a

Cable Profiles of Suspension Bridges and their Associated Properties

A single flexible cable suspended between two fixed points is the simplest suspension bridge. The initial problem in such a case is to determine the form adopted by the cable when it is loaded solely by its own weight, and to find the tension in the cable at any point along its length. The solution of this problem provides a starting point for a consideration of the effects upon a suspended cable of extraneous applied forces, such as the dead weight of the stiffening structures of a practical suspension bridge. This appendix is devoted to the initial problem of determining the different cable profiles of suspension bridges and their associated properties, as well as discovering the most usable profile.

1. The Common Catenary

The curve in which a perfectly flexible uniform cable hangs when freely suspended between two fixed points is called a catenary. "Perfectly flexible" means that the cable resists applied load by developing direct stresses only. It follows, therefore, that at any cross section the resultant cable force is tangential to the cable profile at that point and acts through the centroid of the cross section. "Uniform" indicates that the weight per unit length,  $w$ , of the cable is constant. This defines the classical problem of the common

catenary which was first solved by James Bernoulli, in 1691; the earliest published solution was by David Gregory in 1697.

Consider a cable hanging symmetrically between two fixed points at the same level, as shown in Fig. I-a-i. Let 0 be the origin for the ordinates  $x$  and  $y$ . If the cable is treated as inextensible, the vertical equilibrium of the element of the cable shown in Fig. I-a-ii requires that

$$\frac{d}{ds} \left( T \frac{dy}{ds} \right) = -\bar{w}, \quad (\text{I-a-1})$$

where  $T$  is the tension in the cable,  $\bar{w}$  is the weight of the cable per unit length of the cable curve and  $\frac{dy}{ds}$  is the sine of the angle of inclination, i. e.,  $\sin\phi$ .

The horizontal component of cable tension,  $H_w$ , is constant since there are no acting longitudinal components of load.

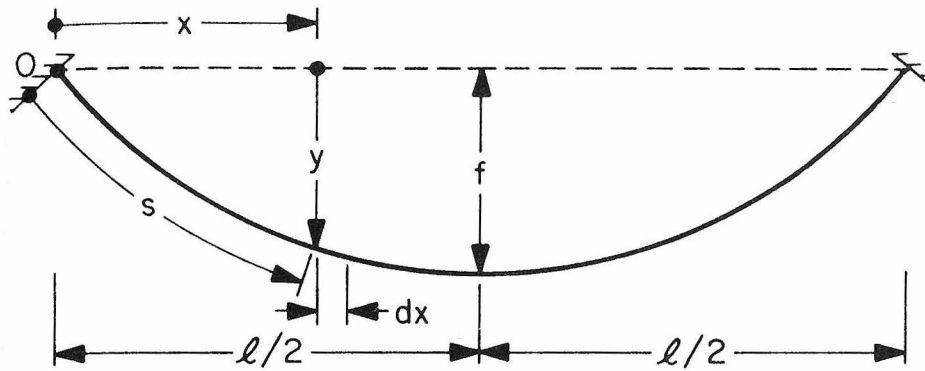
$$H_w = T \frac{dx}{ds} = \text{constant}, \quad (\text{I-a-2})$$

where  $\frac{dx}{ds} = \cos\phi$ . Consequently, Eq. I-a-1 is reduced to

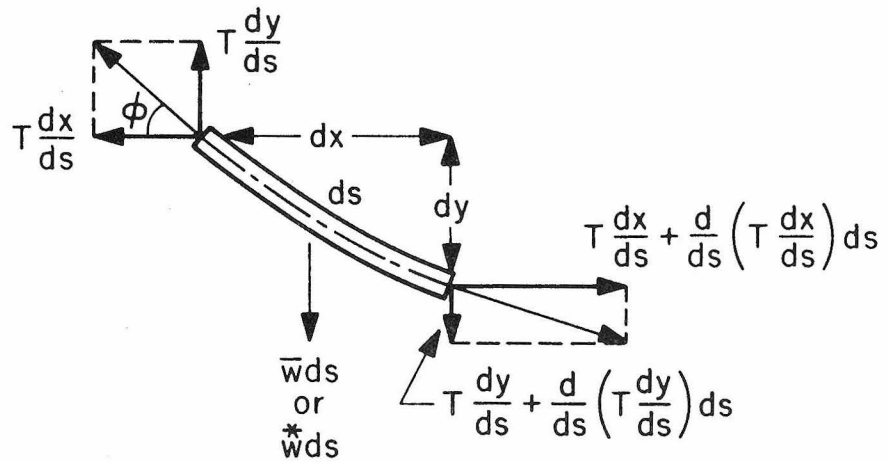
$$\begin{aligned} H_w \frac{d^2y}{dx^2} &= -\bar{w} \frac{ds}{dx}, \\ \text{or} \quad H_w \frac{d^2y}{dx^2} &= -\bar{w} \left[ 1 + \left( \frac{dy}{dx} \right)^2 \right]^{\frac{1}{2}}. \end{aligned} \quad (\text{I-a-3})$$

Since  $\bar{w}$  is constant, the solution of Eq. I-a-3 gives the Catenary. Integration of Eq. I-a-3 yields

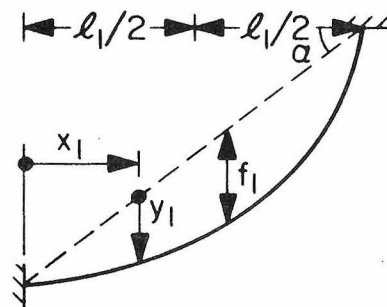
$$\sinh^{-1} \frac{dy}{dx} = -\frac{\bar{w}}{H_w} x + c_1,$$



i-Definition Diagram



ii-Equilibrium of an Element



iii-Cable Profile in a Side Span

Fig. I-a

where  $c_1$  is a constant of integration. But at  $x = \frac{\ell}{2}$ ,  $\frac{dy}{dx} = 0$ , so that  $c_1 = \frac{\bar{w}}{H_w} \frac{\ell}{2}$  and

$$\sinh^{-1} \frac{dy}{dx} = \frac{\bar{w}}{H_w} \left( \frac{\ell}{2} - x \right). \quad (\text{I-a-4})$$

Integration again, the following can be obtained

$$y = -\frac{H_w}{\bar{w}} \cosh \left[ \frac{\bar{w}}{H_w} \left( \frac{\ell}{2} - x \right) \right] + c_2,$$

where  $c_2$  is another constant of integration. The cable deflection at mid-span ( $x = \frac{\ell}{2}$ ) is the sag,  $f$ , and therefore  $c_2 = f + 1$  and

$$y = \frac{H_w}{\bar{w}} \left\{ 1 - \cosh \left[ \frac{\bar{w}}{H_w} \left( \frac{\ell}{2} - x \right) \right] \right\} + f. \quad (\text{I-a-5})$$

This gives the shape of the curve adopted by the cable. When required, the length of the catenary is given by

$$s = \int_0^{\ell} \left[ 1 + \left( \frac{dy}{dx} \right)^2 \right]^{\frac{1}{2}} dx. \quad (\text{I-a-6})$$

Substituting  $\frac{dy}{dx}$ , obtained from Eq. I-a-5, in Eq. I-a-6 and integrating yields

$$s = 2 \frac{H_w}{\bar{w}} \sinh \left( \frac{\bar{w}\ell}{2H_w} \right). \quad (\text{I-a-7})$$

The tension at any point in the cable is given by Eq. I-a-2 or

$$T = H_w \frac{ds}{dy} = H_w \left[ 1 + \left( \frac{dy}{dx} \right)^2 \right]^{\frac{1}{2}}. \quad (\text{I-a-8})$$

Substituting the value  $\frac{dy}{dx}$  derived from Eq. I-a-5, Eq. I-a-8 is reduced to

$$T = H_w \cosh \left[ \frac{\bar{w}}{H_w} \left( \frac{\ell}{2} - x \right) \right]. \quad (\text{I-a-9})$$

This tension will be maximum at the ends of the span, where  $x = 0$  or  $x = \ell$ , yielding

$$T_{\max} = H_w \cosh \left( \frac{\bar{w}\ell}{2H_w} \right). \quad (\text{I-a-10})$$

All the above results depend upon a knowledge of the parameter  $\frac{\bar{w}}{H_w}$  for their usefulness.

## 2. The Parabolic Cable

In many practical suspension bridges the total dead weight of the bridge, instead of being distributed as though uniform along the cables, is distributed more uniformly across the span. Of more practical importance than the common catenary, therefore, is the case of a cable suspended between two points and so loaded (or with a weight per unit length such) that the load per unit of span,  $\ell$ , rather than the curve, is constant. Remarkably enough, although the catenary was understood at the end of the seventeenth century, this related yet simpler problem was not solved until one hundred years later. In 1794, a suspension bridge was proposed across the Neva, near Leningrad, and it was as a result of considering this proposed bridge that Nicholas Fuss published his solution that year.

Now, consider the cable, as before, to be perfectly flexible and inextensible. The vertical load on the element,  $ds$ , of the cable will be  $w^* ds$  (instead of  $\bar{w} ds$  which was for the common

catenary). Again, the equilibrium of this element of the cable gives

$$T \frac{dx}{ds} = H_w = \text{constant} \quad , \quad (\text{I-a-11})$$

and

$$\frac{d}{ds} \left( T \frac{dy}{ds} \right) = - w^* \quad . \quad (\text{I-a-12})$$

Furthermore, Eqs. I-a-11 and I-a-12 give

$$H_w \frac{d^2 y}{dx^2} = - w^* \frac{ds}{dx} \quad . \quad (\text{I-a-13})$$

When  $w^* \frac{ds}{dx}$  is constant, the profile of the cable is a parabola (which is the essence of the discovery made by Fuss).

However, for flat-sag cables of constant weight per unit length, the slope of the cable profile is everywhere small and, therefore

$$ds \simeq dx \quad .$$

The differential equation of the equilibrium curve is then accurately specified as

$$H_w \frac{d^2 y}{dx^2} = - w^* \quad . \quad (\text{I-a-14})$$

The solution of this differential equation, for the coordinate system shown in Fig. I-a-i, is the parabola

$$y = \frac{w^* l^2}{2H_w} \left[ \frac{x}{l} - \left( \frac{x}{l} \right)^2 \right] \quad . \quad (\text{I-a-15})$$

The cable deflection at mid-span  $\left( x = \frac{l}{2} \right)$  is the sag,  $f$ , and the horizontal component of cable tension is

$$H_w = \frac{w\ell^2}{8f} \quad . \quad (\text{I-a-16})$$

The tension at any point in the cable is given by Eq. I-a-8, and its value is

$$T = H_w \left[ 1 + \frac{w^2 \ell^2}{4H_w^2} \left( 1 - 2\left(\frac{x}{\ell}\right) \right)^2 \right]^{\frac{1}{2}} \quad (\text{I-a-17})$$

The maximum tension in the cable, occurring at either support, will be

$$T_{\max} = \sqrt{H_w^2 + \left(\frac{1}{2}w\ell\right)^2} \quad . \quad (\text{I-a-18})$$

With the aid of Eq. I-a-16, Eq. I-a-15 is more conveniently written as

$$y = \frac{4f}{\ell^2} x(\ell - x) \quad . \quad (\text{I-a-19})$$

It is worthwhile to note that this equation is also valid for the parabolic cable shown in Fig. I-a-iii.

The length of the parabolic cable is given in general by Eq. I-a-6, and in this particular case the total length is therefore

$$s = \int_0^{\ell} \left[ 1 + \left\{ \frac{4f}{\ell} \left( 1 - 2\left(\frac{x}{\ell}\right) \right) \right\}^2 \right]^{\frac{1}{2}} dx \quad . \quad (\text{I-a-20})$$

It is convenient, and sufficiently accurate, to expand the integrand of Eq. I-a-20 in a binomial series and then to carry out the integration term by term. If this is done, it is found that

$$s = \ell \left[ 1 + \frac{8}{3} \left(\frac{f}{\ell}\right)^2 - \frac{32}{5} \left(\frac{f}{\ell}\right)^4 + \dots \right] \quad , \quad (\text{I-a-21})$$

and for small  $\frac{f}{l}$  ratios, it is sufficient to adopt

$$s \simeq l \left[ 1 + \frac{8}{3} \left( \frac{f}{l} \right)^2 \right] ,$$

for most practical purposes.

Similarly, in the more general case when the two ends are not on the same level, as shown in Fig. I-a-iii, this formula for  $s$  still holds provided that both  $y_1$  and the sag  $f_1$  are measured from the closing chord joined the two end supports.

### 3. Some Other Cases

In the case of the common catenary,  $\bar{w}$  was constant measured along the cable; in the case of the parabolic cable,  $\bar{w}^*$  was constant measured along the span (horizontal) of the cable. In addition, there is the heterogeneous cable in which  $w$  is a variable, whether measured along the cable or the span. Shortly after solving the catenary problem, Bernoulli proceeded to solve this more general problem, inquiring into the law of the variation of  $w$  associated with various possible geometrical forms for the cable. The main result from this kind of approach concludes that  $w$  measured along the cable must vary so that  $w \frac{ds}{dx}$ , corresponding to  $\bar{w}^*$  measured along the span, is a constant. A further result of interest is that when  $w \left( \frac{ds}{dx} \right)^3$  is constant, the curve is cycloid. Another example of a possible cable profile is the catenary of uniform strength developed by Gilbert in 1826, in which the cable's cross sectional area is proportional to the tension acting upon it. But this approach limits

the spans of suspension bridge cables, which should be set by considerations other than mathematical limits.

#### 4. Comparison of Cable Profiles

The cables of suspension bridges are commonly constructed with a uniform cross-sectional area, and thus, if allowed to hang freely, they would adopt the form of the common catenary given by Eq. I-a-5. But in practice they are often constructed at the site on a temporary platform, and the roadway is hung from them by vertical suspension rods so that when all is complete, and the structure is bearing its own weight, the form of the cables is more nearly parabolic. The aim of this erection procedure is to ensure that the dead weight of the whole bridge (roughly uniform measured along the span) be carried wholly by the cables and suspension rod without causing bending actions in any stiffening structures.

Thus practical interest naturally settles upon the parabolic rather than the catenary profile of cable, but there is another reason for this. The profiles of the two curves are very similar in terms of their ratios of span to sag which fall in the range common in suspension bridges (usually 8:1 or more). And since the cable profiles are alike, the loads in the cable and in any subsidiary structure of the real bridge will also be similar. In these circumstances it is natural to adopt the parabolic profile, with its greater simplicity and familiarity, as the standard one for suspension bridges, and this has become the general custom.

Appendix I-b

The Cable Equation (Compatibility Equation)

The cable equation provides a compatibility or closure condition relating the changes which occur in the cable tension to the changes in cable geometry when the cable is displaced (in-plane) from its original equilibrium position.

It is seen from the geometry of displacement (Fig. I-2-a), that for the static position of equilibrium, the element of length  $ds_i$  in the  $i^{\text{th}}$  span of the cable can be given by

$$ds_i^2 = dx_i^2 + dy_i^2 \quad , \quad i = 1, 2, 3 .$$

When the cable is displaced (in-plane) due to vibration, its length increases to  $ds_i + \Delta ds_i$  ,  $dx_i$  increases to  $dx_i + \frac{\partial u_c}{\partial x_i} dx_i$  where  $u_c$  is the vibrational horizontal movement of the element, and  $dy_i$  becomes  $dy_i + \frac{\partial v_c}{\partial x_i} dx_i$  where  $v_c$  is the vibrational vertical movement of the element. Then for the vibrationally displaced position

$$\left(ds_i + \Delta ds_i\right)^2 = \left(dx_i + \frac{\partial u_c}{\partial x_i} dx_i\right)^2 + \left(dy_i + \frac{\partial v_c}{\partial x_i} dx_i\right)^2 \quad ,$$

or

$$2ds_i \Delta ds_i + (\Delta ds_i)^2 = 2dx_i \frac{\partial u_c}{\partial x_i} dx_i + \left(\frac{\partial u_c}{\partial x_i}\right)^2 dx_i^2 + 2dy_i \frac{\partial v_c}{\partial x_i} dx_i + \left(\frac{\partial v_c}{\partial x_i}\right)^2 dx_i^2 .$$

In general  $u_c(x_i, t)$  is small in comparison with  $v_c(x_i, t)$  ; therefore the increment in the length of the cable element  $\Delta ds_i$  , correct to the second order of small quantities, is

$$\Delta ds_i \simeq \frac{\partial u_c}{\partial x_i} \frac{dx_i}{ds_i} dx_i + \frac{\partial v_c}{\partial x_i} \frac{dy_i}{ds_i} dx_i + \frac{1}{2} \left( \frac{\partial v_c}{\partial x_i} \right)^2 \frac{dx_i}{ds_i} dx_i, \quad i = 1, 2, 3.$$

Hooke's Law, applied to the element, requires that

$$\frac{H(t)}{E_c A_c} \frac{ds_i}{dx_i} = \frac{\Delta ds_i}{ds_i}, \quad i = 1, 2, 3,$$

where  $H(t) \frac{ds_i}{dx_i}$  is the increment in tension exerted on the element,  $E_c$  is the modulus of elasticity of the cable material and  $A_c$  is the effective cross-sectional area of the cable. Consequently, the cable equation for the element reads

$$\frac{H(t)}{E_c A_c} \left( \frac{ds_i}{dx_i} \right)^3 = \frac{\partial u_c}{\partial x_i} + \frac{\partial v_c}{\partial x_i} \frac{dy_i}{dx_i} + \frac{1}{2} \left( \frac{\partial v_c}{\partial x_i} \right)^2, \quad i = 1, 2, 3.$$

The effect of a change in temperature can readily be accommodated, and the cable element equation then is

$$\frac{H(t)}{E_c A_c} \left( \frac{ds_i}{dx_i} \right)^3 = \frac{\partial u_c}{\partial x_i} + \frac{\partial v_c}{\partial x_i} \frac{dy_i}{dx_i} + \frac{1}{2} \left( \frac{\partial v_c}{\partial x_i} \right)^2 \pm \epsilon_t \Delta T_i \left( \frac{ds_i}{dx_i} \right)^2, \quad i = 1, 2, 3,$$

where  $\epsilon_t$  is the coefficient of thermal expansion and  $\Delta T_i$  is the incremental change in temperature in the  $i^{\text{th}}$  span.

The above cable equation may be integrated, for each span, to give

$$\frac{H(t)L_{ei}}{E_c A_c} = u_c(x_i, t) \Big|_{x_i=0}^{x_i=l_i} + \int_0^{l_i} \left( \frac{\partial v_c}{\partial x_i} \right) \left( \frac{dy_i}{dx_i} \right) dx_i + \frac{1}{2} \int_0^{l_i} \left( \frac{\partial v_c}{\partial x_i} \right)^2 dx_i \pm \epsilon_t \Delta T_i L_{ti},$$

$i = 1, 2, 3,$

where  $L_{ei}$  and  $L_{ti}$  are virtual lengths of the cable in the  $i^{\text{th}}$  span which are defined by

$$L_{ei} = \int_0^{\ell_i} \left( \frac{ds_i}{dx_i} \right)^3 dx_i \quad \text{and} \quad L_{ti} = \int_0^{\ell_i} \left( \frac{ds_i}{dx_i} \right)^2 dx_i, \quad i = 1, 2, 3,$$

and it has been assumed that  $\Delta T_i$  is uniform along the  $i^{\text{th}}$  span.

In the case of a suspended cable, hanging between rigid supports, the above cable equation reduces to

$$\frac{H(t)L_{ei}}{E_c A_c} = \int_0^{\ell_i} \left( \frac{\partial v}{\partial x_i} \right) \left( \frac{dy_i}{dx_i} \right) dx_i + \frac{1}{2} \int_0^{\ell_i} \left( \frac{\partial v}{\partial x_i} \right)^2 dx_i \pm \epsilon_t \Delta T_i L_{ti}, \quad i = 1, 2, 3.$$

Finally, to evaluate  $L_{ei}$ , the expression for  $y_i$  is:

$$y_i = 4 \frac{f_i}{\ell_i^2} x_i (\ell_i - x_i), \quad i = 1, 2, 3,$$

$$\therefore \frac{dy_i}{dx_i} = 4 \frac{f_i}{\ell_i} - 8 f_i \frac{x_i}{\ell_i^2},$$

but

$$\left( \frac{ds_i}{dx_i} \right)^3 = \left[ 1 + \left( \frac{dy_i}{dx_i} \right)^2 \right]^{3/2},$$

expansion of the series  $\left( \frac{ds_i}{dx_i} \right)^3$  yields

$$\left( \frac{ds_i}{dx_i} \right)^3 = 1 + \frac{3}{2} \left( \frac{dy_i}{dx_i} \right)^2 + \frac{3}{8} \left( \frac{dy_i}{dx_i} \right)^4 + \dots$$

Hence

$$\begin{aligned}
 \int_0^{\ell_i} \left( \frac{ds_i}{dx_i} \right)^3 dx_i &= \ell_i + \frac{3}{2} \int_0^{\ell_i} \left( \frac{dy_i}{dx_i} \right)^2 dx_i + \frac{3}{8} \int_0^{\ell_i} \left( \frac{dy_i}{dx_i} \right)^4 dx_i + \dots \\
 &= \ell_i + \frac{3}{2} \int_0^{\ell_i} \left( 4 \frac{f_i}{\ell_i} - 8 \frac{f_i}{\ell_i^2} x_i \right)^2 dx_i + \frac{3}{8} \int_0^{\ell_i} \left( 4 \frac{f_i}{\ell_i} - 8 \frac{f_i}{\ell_i^2} x_i \right)^4 dx_i + \dots \\
 &= \ell_i + \frac{3}{2} \left( 16 \frac{f_i^2}{\ell_i} - \frac{32 f_i^2}{\ell_i} + \frac{64}{3} \frac{f_i^2}{\ell_i} \right) + 0 \left( \frac{f_i}{\ell_i} \right)^4 + \dots \\
 &= \ell_i + \frac{3}{2} \left( \frac{16}{3} \frac{f_i^2}{\ell_i} \right) + 0 \left( \frac{f_i}{\ell_i} \right)^4 + \dots ,
 \end{aligned}$$

therefore the virtual length  $L_{ei}$  is defined by

$$L_{ei} \simeq \ell_i \left[ 1 + 8 \left( \frac{f_i}{\ell_i} \right)^2 \right] .$$

Similarly, for  $L_{ti}$ , one can write

$$L_{ti} \simeq \ell_i \left[ 1 + \frac{16}{3} \left( \frac{f_i}{\ell_i} \right)^2 \right] .$$

Appendix I-c

An Alternative Approach to the Inextensibility Condition

To re-examine more critically the use of the expression (Eq. 1.23) (Eq. 1.23) for an inextensible cable. In the presentations given by von Kármán, Boit and Rannie [5, 6] it is noted that the initial total length of the cable is given by

$$s = \sum_{i=1}^3 \left\{ \int_0^{\ell_i} \left[ 1 + \left( \frac{dy_i}{dx_i} \right)^2 \right]^{\frac{1}{2}} dx_i \right\}, \quad (\text{I-c-1})$$

and hence, by replacing  $y_i$  with  $(y_i + v_c(x_i, t))$  and expanding in a Taylor series, the variation  $\Delta s$ , for the entire length, is found to be

$$\Delta s = \sum_{i=1}^3 \left\{ \int_0^{\ell_i} \left( \frac{\left( \frac{dy_i}{dx_i} \right) \left( \frac{\partial v_c}{\partial x_i} \right)}{\left[ 1 + \left( \frac{dy_i}{dx_i} \right)^2 \right]^{\frac{1}{2}}} \right) dx_i \right\}, \quad (\text{I-c-2})$$

neglecting higher terms in  $v_c$ . Hence, by integrating by parts, noting that  $v_c = 0$  at the two limits of the integral, and by neglecting the departure from unity of the denominator of Eq. I-c-2, it is found that

$$\Delta s = - \sum_{i=1}^3 \left\{ \int_0^{\ell_i} v_c \frac{d^2 y_i}{dx_i^2} dx_i \right\} = \sum_{i=1}^3 \left\{ \frac{w_i^*}{H_w} \int_0^{\ell_i} v_c dx_i \right\}, \quad (\text{I-c-3})$$

where  $\frac{d^2 y_i}{dx_i^2} = - \frac{w_i^*}{H_w}$  (see Appendix I-a, Eq. I-a-14).

Eq. 1.23 is identical to Eq. I-c-3 when  $\Delta s$  is zero.

From a review of the approximations made in this argument, it is apparent that the paradox noted has been unaffected by the replacement of  $\left[1 + \left(\frac{dy_i}{dx_i}\right)^2\right]^{\frac{1}{2}}$  in Eq. I-c-2 with unity; the explanation must lie, at least in part, in the neglect of higher-terms in the Taylor series for  $s$ . If further term is included then

$$\Delta s = \sum_{i=1}^3 \left\{ \int_0^{l_i} \left(\frac{dy_i}{dx_i}\right) \left(\frac{\partial v_c}{\partial x_i}\right) dx_i + \frac{1}{2} \int_0^{l_i} \left(\frac{\partial v_c}{\partial x_i}\right)^2 dx_i \right\} . \quad (\text{I-c-4})$$

The second term here is, of course, the same as the change in length, due to  $v_c$ , of a straight member from  $x_i = 0$  to  $x_i = l_i$ .

Again, the substitution of  $\left(\frac{w_i^*}{H_w} \int_0^{l_i} v_c dx_i\right)$  for the first of

these two integrals in Eq. I-c-4 depends upon a process of integration by parts which is strictly legitimate only when  $\left(\frac{dy_i}{dx_i}\right)$  and  $\left(\frac{\partial v_c}{\partial x_i}\right)$  are continuous functions of  $x_i$  between the limits  $x_i = 0$  and  $x_i = l_i$ .

Thus, for an inextensible cable, the further equation

$$-\sum_{i=1}^3 \left\{ \frac{w_i^*}{H_w} \int_0^{l_i} v_c dx_i - \frac{1}{2} \int_0^{l_i} \left(\frac{\partial v_c}{\partial x_i}\right)^2 dx_i \right\} = 0 ,$$

or

$$\sum_{i=1}^3 w_i^* \int_0^{l_i} v_c dx_i = \frac{1}{2} \sum_{i=1}^3 H_w \int_0^{l_i} \left(\frac{\partial v_c}{\partial x_i}\right)^2 dx_i , \quad (\text{I-c-5})$$

is the inextensibility condition for the cable.

Appendix I-d

Effect of Shear Deformation and Rotary Inertia

The governing equations of motion for the vertical vibration of suspension bridges, including adjustments for the effect of transverse shear deformations and rotary inertia, will be derived by Hamilton's Principle.

The kinetic energy is due to translation and rotation (Eq. 1.34) and is expressed by

$$T(t) = \frac{1}{2} \sum_{i=1}^3 \int_0^{\ell_i} m_i^* \left( \frac{\partial v_i}{\partial t} \right)^2 dx_i + \frac{1}{2} \sum_{i=1}^3 \int_0^{\ell_i} J_{gi} \left( \frac{\partial \eta_i}{\partial t} \right)^2 dx_i ,$$

where  $m_i^*$  is the mass of the bridge per unit length of the  $i^{\text{th}}$  span,  $J_{gi}$  is the mass moment of inertia per unit length of the  $i^{\text{th}}$  stiffening structure about the neutral axis,  $v_i$  is the total vibrational displacement and  $\eta_i$  is the angle of rotation due to bending, i. e. ,

$$\frac{\partial v_i}{\partial x_i} = \eta_i + \beta_i , \quad i = 1, 2, 3 ,$$

with  $\beta_i$  as the angle of distortion due to shear. But  $J_{gi}$  is related to  $I_{gi}$  (the moment of inertia of the  $i^{\text{th}}$  stiffening structure) by

$$J_{gi} = \rho_{gi} I_{gi} = \frac{m_{gi}}{A_{gi}} I_{gi} = r_i^2 m_{gi} ,$$

where  $\rho_{gi}$  is the mass density of the  $i^{\text{th}}$  stiffening structure,  $m_{gi}$  is the mass per unit length of the  $i^{\text{th}}$  stiffening structure and  $r_i$  is the radius of gyration about the neutral axis.

Furthermore, the variation of  $T(t)$  can be written as

$$\delta T(t) = \sum_{i=1}^3 \int_0^{\ell_i} \dot{m}_i^* \frac{\partial v_i}{\partial t} \delta \left( \frac{\partial v_i}{\partial t} \right) dx_i + \sum_{i=1}^3 \int_0^{\ell_i} r_i^2 m_{gi} \frac{\partial \eta_i}{\partial t} \delta \left( \frac{\partial \eta_i}{\partial t} \right) dx_i .$$

The potential energy of the stiffening structure (Eq. 1.29) is

$$V_{gv}(t) = \frac{1}{2} \sum_{i=1}^3 \int_0^{\ell_i} E_{gi} I_{gi} \left( \frac{\partial \eta_i}{\partial x_i} \right)^2 dx_i + \frac{1}{2} \sum_{i=1}^3 \int_0^{\ell_i} G_{gi} \mu_{vi} \left( \frac{\partial v_i}{\partial x_i} - \eta_i \right)^2 dx_i ,$$

where  $E_{gi} I_{gi}$  and  $G_{gi} \mu_{vi}$  are the flexural and shear rigidities, respectively, of the  $i^{\text{th}}$  stiffening structure. Hence the variation of the potential energy,  $V_{gv}$ , has the form

$$\begin{aligned} \delta V_{gv}(t) = & \sum_{i=1}^3 \int_0^{\ell_i} E_{gi} I_{gi} \frac{\partial \eta_i}{\partial x_i} \delta \left( \frac{\partial \eta_i}{\partial x_i} \right) dx_i \\ & + \sum_{i=1}^3 \int_0^{\ell_i} G_{gi} \mu_{vi} \left( \frac{\partial v_i}{\partial x_i} - \eta_i \right) \delta \left( \frac{\partial v_i}{\partial x_i} - \eta_i \right) dx_i . \end{aligned}$$

It is convenient to consider only these two energies  $T(t)$  and  $V_{gv}(t)$  since the potential energy of the cable,  $V_c(t)$ , has been dealt with before.

Introducing  $\delta T(t)$  and  $\delta V_{gv}(t)$  in the variational principle leads to

$$\begin{aligned}
 \int_{t_1}^{t_2} \delta(T - V_{gv}) dt &= \sum_{i=1}^3 \left\{ \int_{t_1}^{t_2} \left[ \int_0^{\ell_i} m_i^* \frac{\partial v_i}{\partial t} \delta\left(\frac{\partial v_i}{\partial t}\right) dx_i + \int_0^{\ell_i} r_i^2 m_{gi} \frac{\partial \eta_i}{\partial t} \delta\left(\frac{\partial \eta_i}{\partial t}\right) dx_i \right. \right. \\
 &\quad \left. \left. - \int_0^{\ell_i} E_{gi} I_{gi} \frac{\partial \eta_i}{\partial x_i} \delta\left(\frac{\partial \eta_i}{\partial x_i}\right) dx_i \right. \right. \\
 &\quad \left. \left. - \int_0^{\ell_i} G_{gi} \mu_{vi} \left(\frac{\partial v_i}{\partial x_i} - \eta_i\right) \delta\left(\frac{\partial v_i}{\partial x_i} - \eta_i\right) dx_i \right] dt \right\} = 0 .
 \end{aligned}$$

The order of integrations with respect to  $x_i$  and  $t$  is interchangeable and the variation and differentiation operators are commutative, so one can perform the following integrations by parts:

$$\begin{aligned}
 \int_{t_1}^{t_2} m_i^* \frac{\partial v_i}{\partial t} \delta\left(\frac{\partial v_i}{\partial t}\right) dt &= \int_{t_1}^{t_2} m_i^* \frac{\partial v_i}{\partial t} \frac{\partial}{\partial t} (\delta v_i) dt \\
 &= m_i^* \frac{\partial v_i}{\partial t} \delta v_i \Big|_{t_1}^{t_2} - \int_{t_1}^{t_2} \frac{\partial}{\partial t} \left( m_i^* \frac{\partial v_i}{\partial t} \right) \delta v_i dt \\
 &= - \int_{t_1}^{t_2} m_i^* \frac{\partial^2 v_i}{\partial t^2} \delta v_i dt ,
 \end{aligned}$$

because  $\delta v_i$  vanishes at  $t = t_1$  and  $t = t_2$ . In a similar fashion one can obtain

$$\int_{t_1}^{t_2} r_i^2 m_{gi} \frac{\partial \eta_i}{\partial t} \delta\left(\frac{\partial \eta_i}{\partial t}\right) dt = - \int_{t_1}^{t_2} r_i^2 m_{gi} \frac{\partial^2 \eta_i}{\partial t^2} \delta \eta_i dt .$$

On the other hand, integration over the spatial variable yields

$$\int_0^{\ell_i} E_{gi} I_{gi} \frac{\partial \eta_i}{\partial x_i} \delta \left( \frac{\partial \eta_i}{\partial x_i} \right) dx_i = \int_0^{\ell_i} E_{gi} I_{gi} \frac{\partial \eta_i}{\partial x_i} \frac{\partial}{\partial x_i} (\delta \eta_i) dx_i$$

$$= \left( E_{gi} I_{gi} \frac{\partial \eta_i}{\partial x_i} \right) \delta \eta_i \Big|_0^{\ell_i} - \int_0^{\ell_i} \frac{\partial}{\partial x_i} \left( E_{gi} I_{gi} \frac{\partial \eta_i}{\partial x_i} \right) \delta \eta_i dx_i,$$

$$\int_0^{\ell_i} G_{gi} \mu_{vi} \left( \frac{\partial v_i}{\partial x_i} - \eta_i \right) \delta \left( \frac{\partial v_i}{\partial x_i} - \eta_i \right) dx_i = \int_0^{\ell_i} G_{gi} \mu_{vi} \left( \frac{\partial v_i}{\partial x_i} - \eta_i \right) \frac{\partial}{\partial x_i} (\delta v_i) dx_i$$

$$- \int_0^{\ell_i} G_{gi} \mu_{vi} \left( \frac{\partial v_i}{\partial x_i} - \eta_i \right) \delta \eta_i dx_i$$

$$= \left[ G_{gi} \mu_{vi} \left( \frac{\partial v_i}{\partial x_i} - \eta_i \right) \right] \delta v_i \Big|_0^{\ell_i}$$

$$- \int_0^{\ell_i} \frac{\partial}{\partial x_i} \left[ G_{gi} \mu_{vi} \left( \frac{\partial v_i}{\partial x_i} - \eta_i \right) \right] \delta v_i dx_i$$

$$- \int_0^{\ell_i} G_{gi} \mu_{vi} \left( \frac{\partial v_i}{\partial x_i} - \eta_i \right) \delta \eta_i dx_i.$$

Using the above expression in the variational principle produces

$$\delta I = \sum_{i=1}^3 \int_{t_1}^{t_2} \left\{ - \int_0^{\ell_i} m_i^* \frac{\partial^2 v_i}{\partial t^2} \delta v_i dx_i - \int_0^{\ell_i} r_i^2 m_{gi} \frac{\partial^2 \eta_i}{\partial t^2} \delta \eta_i dx_i - \left( E_{gi} I_{gi} \frac{\partial \eta_i}{\partial x_i} \right) \delta \eta_i \Big|_0^{\ell_i} \right.$$

$$\left. + \int_0^{\ell_i} \frac{\partial}{\partial x_i} \left( E_{gi} I_{gi} \frac{\partial \eta_i}{\partial x_i} \right) \delta \eta_i dx_i - \left[ G_{gi} \mu_{vi} \left( \frac{\partial v_i}{\partial x_i} - \eta_i \right) \right] \delta v_i \Big|_0^{\ell_i} \right.$$

$$\begin{aligned}
 & + \int_0^{\ell_i} \frac{\partial}{\partial x_i} \left[ G_{gi} \mu_{vi} \left( \frac{\partial v_i}{\partial x_i} - \eta_i \right) \right] \delta v_i dx_i \\
 & + \int_0^{\ell_i} G_{gi} \mu_{vi} \left( \frac{\partial v_i}{\partial x_i} - \eta_i \right) \delta \eta_i dx_i \Big\} dt \quad , \\
 = & \sum_{i=1}^3 \int_{t_1}^{t_2} \left[ \int_0^{\ell_i} \left\{ \frac{\partial}{\partial x_i} \left[ G_{gi} \mu_{vi} \left( \frac{\partial v_i}{\partial x_i} - \eta_i \right) \right] - m_i^* \frac{\partial^2 v_i}{\partial t^2} \right\} \delta v_i dx_i \right. \\
 & + \int_0^{\ell_i} \left\{ \left[ \frac{\partial}{\partial x_i} \left( E_{gi} I_{gi} \frac{\partial \eta_i}{\partial x_i} \right) + G_{gi} \mu_{vi} \left( \frac{\partial v_i}{\partial x_i} - \eta_i \right) \right] - r_i^2 m_{gi} \frac{\partial^2 \eta_i}{\partial t^2} \right\} \delta \eta_i dx_i \\
 & \left. - \left( E_{gi} I_{gi} \frac{\partial \eta_i}{\partial x_i} \right) \delta \eta_i \Big|_0^{\ell_i} - \left[ G_{gi} \mu_{vi} \left( \frac{\partial v_i}{\partial x_i} - \eta_i \right) \right] \delta \eta_i \Big|_0^{\ell_i} \right] dt \quad .
 \end{aligned}$$

The virtual displacements  $\delta \eta_i$  and  $\delta v_i$  are arbitrary and independent, so they can be taken equal to zero at  $x_i = 0$  and  $x_i = \ell_i$  and arbitrary for  $0 < x_i < \ell_i$ ; therefore, after including the variation of the cable's potential energy from Eq. 1.40, one must have

$$\frac{\partial}{\partial x_i} \left[ G_{gi} \mu_{vi} \left( \frac{\partial v_i}{\partial x_i} - \eta_i \right) \right] - m_i^* \frac{\partial^2 v_i}{\partial t^2} + (H_w + H(t)) \frac{\partial^2 v_i}{\partial x_i^2} - \frac{w_i^*}{H_w} H(t) = 0 \quad ,$$

$i = 1, 2, 3 \quad ,$

$$\frac{\partial}{\partial x_i} \left( E_{gi} I_{gi} \frac{\partial \eta_i}{\partial x_i} \right) + G_{gi} \mu_{vi} \left( \frac{\partial v_i}{\partial x_i} - \eta_i \right) - r_i^2 m_{gi} \frac{\partial^2 \eta_i}{\partial t^2} = 0 \quad , \quad i = 1, 2, 3 \quad ,$$

throughout the domain. In addition, one can write

$$\left( E_{gi} I_{gi} \frac{\partial \eta_i}{\partial x_i} \right) \delta \eta_i \Big|_0^{\ell_i} = 0, \quad i = 1, 2, 3,$$

$$\left[ G_{gi} \mu_{vi} \left( \frac{\partial v_i}{\partial x_i} - \eta_i \right) + (H_w + H(t)) \frac{\partial v_i}{\partial x_i} + H(t) \frac{dy_i}{dx_i} \right] \delta v_i \Big|_0^{\ell_i} = 0, \quad i = 1, 2, 3.$$

Eliminating  $\eta_i$  from the two resulting equations of motion, a more complete differential equation for the vertically vibrating suspension bridge can be obtained as follows:

$$\begin{aligned} m_i^* \frac{\partial^2 v_i}{\partial t^2} + \frac{\partial^2}{\partial x_i^2} \left( E_{gi} I_{gi} \frac{\partial^2 v_i}{\partial x_i^2} \right) - m_{gi} r_i^2 \left( 1 + \frac{E_{gi} I_{gi}}{G_{gi} \mu_{vi} r_i^2} \right) \frac{\partial^4 v_i}{\partial x_i^2 \partial t^2} \\ + \frac{m_{gi}^2 r_i^2}{G_{gi} \mu_{vi}} \frac{\partial^4 v_i}{\partial t^4} - (H_w + H(t)) \frac{\partial^2 v_i}{\partial x_i^2} + \frac{w_i^*}{H_w} H(t) = 0, \quad i = 1, 2, 3. \end{aligned}$$

In this manner, the effect of rotary inertia is represented by

$$\left( m_{gi} r_i^2 \frac{\partial^4 v_i}{\partial x_i^2 \partial t^2} \right), \text{ while the effect of shearing deformations is}$$

represented by

$$\left( m_{gi} \frac{E_{gi} I_{gi}}{G_{gi} \mu_{vi}} \frac{\partial^4 v_i}{\partial x_i^2 \partial t^2} + \frac{m_{gi}^2 r_i^2}{G_{gi} \mu_{vi}} \frac{\partial^4 v_i}{\partial t^4} \right).$$

REFERENCES OF CHAPTER I

1. Rohrs, J. H., "On the Oscillations of a Suspension Chain," Transactions Cambridge Philosophical Society, Vol. IX, Part III, December 1851.
2. Routh, E. J., Analytical Statics, Cambridge, Vol. I, Chapter X, 1891.
3. Steinman, D. B., A Practical Treatise on Suspension Bridges, John Wiley & Sons, Inc., New York, 1922.
4. Timoshenko, S., "The Stiffness of Suspension Bridges," Transactions American Society of Civil Engineers, Vol. 94, 1930.
5. von Kármán, T. and Biot, M. A., Mathematical Methods in Engineering, McGraw-Hill, 1940.
6. Rannie, W. D., The Failure of the Tacoma Narrows Bridge, Board of Engineers, Amman, O. H., von Kármán, T., Woodruff, G., Federal Works Agency, March 28, 1941.
7. Timoshenko, S., "Theory of Suspension Bridges," Journal of the Franklin Institute, Vol. 235, No. 3, pp. 213-238, March, 1943. (Note: Part II of this paper appears in Vol. 235, No. 4, pp. 327-349, April, 1943.)
8. Farquharson, V., "Aerodynamic Stability of Suspension Bridges," Bulletin No. 116, Part I-IV, University of Washington Eng. Exp. Stat., 1949.
9. Bleich, F., McCullough, C. B., Rosecrans, R. and Vincent, G. S., The Mathematical Theory of Vibration in Suspension Bridges, U. S. Bureau of Public Roads, Government Printing Office, Washington 25, D. C., 1950.
10. Frazer, R. A. and Scruton, C., "A Summarized Account of the Severn Aerodynamic Investigations," Report N. P. L. /Aero/222, Nat. Phys. Lab., 1952.
11. Pugsley, A. G., "The Gravity Stiffness of a Suspension Bridge Cable," Quarterly Journal of Mechanics and Applied Mathematics, Vol. V, Part 4, 1952, pp. 385-394.
12. Saxon, D. S., Cahn, A. S., "Modes of Vibration of a Suspended Cable," Quarterly Journal of Mechanics and Applied Mathematics, Vol. VI, Part 3, 1953, pp. 273-285.

13. Pugsley, A. G., The Theory of Suspension Bridges, Edward Arnold, London, 1957.
14. Steinman, D. B., "Modes and Natural Frequencies of Suspension Bridge Oscillations," A. S. C. E., pp. 148-173, September, 1959.
15. Smith, F. C. and Vincent, G. S., "Aerodynamic Stability of Suspension Bridges with Special Reference to the Tacoma Narrow Bridge, Part II. Mathematical Analysis," University of Washington, Engineering Experiment Station Bulletin No. 116, Part II.
16. Selberg, A., Oscillation and Aerodynamic Stability of Suspension Bridges, ACTA Polytechnica Scandinavia, Civil Engineering and Building Construction Series, CI 13, 1961, pp. 308-377.
17. Housner, G. W., Converse, F. J. and Clough, R. W., Seismic Analysis of the Main Piers for the Tagus River Bridge, Lisbon, Portugal. Unpublished Report, Tudor Engineering Company, San Francisco, California, June, 1961.
18. Vincent, G. S., "A Summary of Laboratory and Field Studies in the United States on Wind Effects on Suspension Bridges," Proceedings of Conference on Wind Effects on Buildings and Structures, Teddington, England, H. M. O. S., 1965, Vol. II, pp. 488-515. (Also see a discussion, Transactions A. S. C. E. 1945, Vol. 110, pp. 512-522.)
19. Konishi, I. and Yamada, Y., "Studies on the Earthquake Resistant Design of Suspension Bridge Tower and Pier Systems," Proceedings of 4th WCEE, Vol. 1, B-4, pp. 107-118, 1969.
20. Konishi, I., Yamada, Y., and Takaoka, N., "Earthquake Response and Earthquake Resistant Design of Long Span Suspension Bridges," Proceedings of 3rd WCEE, Vol. III, IV-312, 1965.
21. Hirai, A. and Ito, M., "Dynamic Effects Produced by Trains Upon Suspension Bridges," Proceedings of the International Symposium on Suspension Bridges, Lisbon, 1966.
22. Thul, H., "Cable Stayed Bridges in Germany," Proceedings of the Conference on Structural Steelwork, held at the Institution of Civil Engineers, September 1966, The British Constructional Steelwork Association, Ltd., London, England, pp. 69-81.
23. Tezcan, S. S. and Cherry, S., "Earthquake Analysis of Suspension Bridges," Proceedings of the 4th World Conference on Earthquake Engineering, Santiago, Chile, January, 1969, Vol. II-A3, pp. 125-140.

24. Desai, C. S. and Abel, J. F., Introduction to the Finite Element Method, Van Nostrand Reinhold Company, 1972.
25. Martin, H. C. and Carey, G. F., Introduction to the Finite Element Analysis, McGraw-Hill Book Company, 1973.
26. Johnson, J. B., Bryan, C. W. and Turneaure, F. E., The Theory and Practice of Modern Framed Structures, 2nd. Vol., Ninth Edition, New York, John Wiley & Sons, 1911, p. 276, and succeeding editions.
27. Przemieniecki, J. S., Theory of Matrix Structural Analysis, McGraw-Hill Book Company, 1968.
28. Routh, E. J., Advanced Dynamics of Rigid Bodies, Sixth Edition, Dover, 1955, p. 278, Chapter XIII, and, in particular, pp. 410-412.

## CHAPTER II

### FREE TORSIONAL VIBRATIONS OF SUSPENSION BRIDGES

#### II-1. Introduction

Torsional vibration of a suspension bridge may be produced by: a) unsymmetrical live loads such as a traffic load on only one side of the bridge roadway, b) unsymmetrical dead loads created during erection, c) aerodynamic forces which tend to twist the roadway of the bridge about a longitudinal axis, and d) earthquake ground motion perpendicular to the longitudinal centerline of the bridge and transmitted through the piers, foundations, and anchorages to the bridge deck and cables. Each of these loading conditions produces vibrational torque of the bridge deck about the longitudinal axis of the bridge together with opposed-phase vertical vibration of the two cables.

As mentioned in Chapter I, the analysis of vertical, flexural vibrations of suspension bridges has a long history and is well established. However, torsional analyses have been much less frequently made; there have been few investigations into, and relatively little work published on, the torsional vibrations of suspension bridges. For example, few analytical studies have been made to develop formulas for computing the natural frequencies and mode shapes, and most of those which have been developed are not precise either due to the assumptions involved or due to the type of

solution techniques adopted. Standard treatises such as those by Steinman [13], Smith, Vincent [11] and Bleich [3] call attention to the undeveloped state of torsional analyses, and recent investigations such as those of Selberg [9] and Irvine [5, 6] imply that the problem of the torsional vibration of suspension bridges needs to be treated more effectively by either analytical or approximate methods. Thus, in spite of the recognition of the problem and intermittent attempts at its solution, the state-of-the art of free torsional vibration of suspension bridges is, still, not satisfactory. Nonetheless, in order to achieve a complete picture of the problem, a brief review of the literature (in English) seems appropriate.

In 1941, in connection with the spectacular failure of the Tacoma Narrows bridge, Rannie [8] presented an approximate analysis of the free torsional vibrations of a three-span bridge which lacked a lower lateral wind-bracing system; in his study, the torsional stiffness of the deck was ignored, but the flexural rigidity of the stiffening trusses in the vertical planes was considered, and the cables were assumed inextensible.

In 1948, Smith and Vincent [11] extended Rannie's analytical approach by including the extensibility of the cables. They found that the simplified approach of Rannie did not agree well with the observed torsional frequencies for the Tacoma Narrows bridge and for its model. Accordingly, they also modified the analysis to take into account the torsional rigidity of the suspended structure. They assumed a linear relation between the angle of twist and the torque induced in the

suspended structure. The torque was represented by a couple consisting of two equal and opposite forces acting vertically on the two stiffening structures; then, when this additional force was added to the equation of vertical vibration, with modified inertia load, the torsional equation of motion was obtained. However, Smith and Vincent recognized that in an actual bridge, in order to attain any substantial torsional rigidity, both top and bottom lateral bracing systems must be used, so that the entire deck system would act like a rectangular tube.

In 1950, in a comprehensive work on the theory of vibrations of suspension bridges, Bleich [3], et al., studied the torsional vibration of a suspension bridge having a uniform four-truss box deck with heavy chord members at the corners. In this structure, bending deformations resulted from the longitudinal strains in the chord members, and shear deformations resulted from strains in the bracing members. They assumed that the torque, due to the inertia forces, produced in each of the four trusses a bending moment and a torsional shearing force, both acting in the plane of the truss. They further assumed that the longitudinal stresses in each chord were as a result of the bending of the vertical as well as the horizontal truss in which this chord participated. These longitudinal stresses were later corrected by Steinman [13]. Bleich did not obtain the differential equation of motion in its most general form, but used an approximate method of solution involving a Fourier series to evaluate the first few torsional frequencies and modes of motion. This was the first attempt to deal

with the torsional vibration of a bridge having a box-shaped deck system.

Later, in 1957, Sih [10] presented a brief paper analyzing static torsion in box truss suspension bridges. In his paper, equations were derived to determine the stresses in the stiffening trusses due to torsion considering cable interaction, and for the first time, the effect of warping was considered. Warping involves the longitudinal movement of points on a cross section (sometimes it is known as bending-torsion).

In 1959, Steinman [13] published a paper in which he presented simplified formulas for the calculation of the natural frequencies and modes of torsional vibration of suspension bridges. Some of these formulas were derived by Steinman in 1941-1943 and were subsequently modified (to include box-shaped decks) and tested for simplicity and practical usefulness. In his study, he essentially adopted Bleich's approach. He considered the bending moment contributions of the vertical and the horizontal trusses to be equal; however, Steinman concluded that when Bleich added the two contributions, he created a duplication, identical chords being counted in both the horizontal and vertical trusses.

A recent and extensive treatment of torsional vibration is the one by Selberg [9]. In 1961, he deduced the fundamental equations of motion of a torsionally vibrating suspension bridge, including warping effects. He made a significant modification by adopting both Bleich's approach and Steinman's approximate method of analysis, in

a very careful and precise way. In fact his work was the first to provide major refinement of the previous approaches and was also the first to treat the problem of torsional vibration of suspension bridges in as general a manner as possible.

In 1974, Irvine [5, 6] made a detailed analysis of the response of the boxgirder, single-span suspension bridge to static torsional loading, and he later developed a linear theory for the free torsional vibration of this type of bridge. He considered the deck to be a thin-walled box-girder of elliptical cross section and assumed there would be no warping associated with torsion.

In the following analysis, two further advances in the analysis of torsional vibrations of suspension bridges have been made:

1. A theory of free torsional vibration for a wide class of suspension bridges, having double lateral systems, is developed taking into account the warping of the cross section. Certain simplifying assumptions are made, and Hamilton's Principle is used to derive the equations of motion and the associated boundary conditions. Solutions of the differential equations are obtained.
2. A method of dynamic analysis based on the finite element approach is developed for calculating the natural frequencies and modes of free torsional vibration.

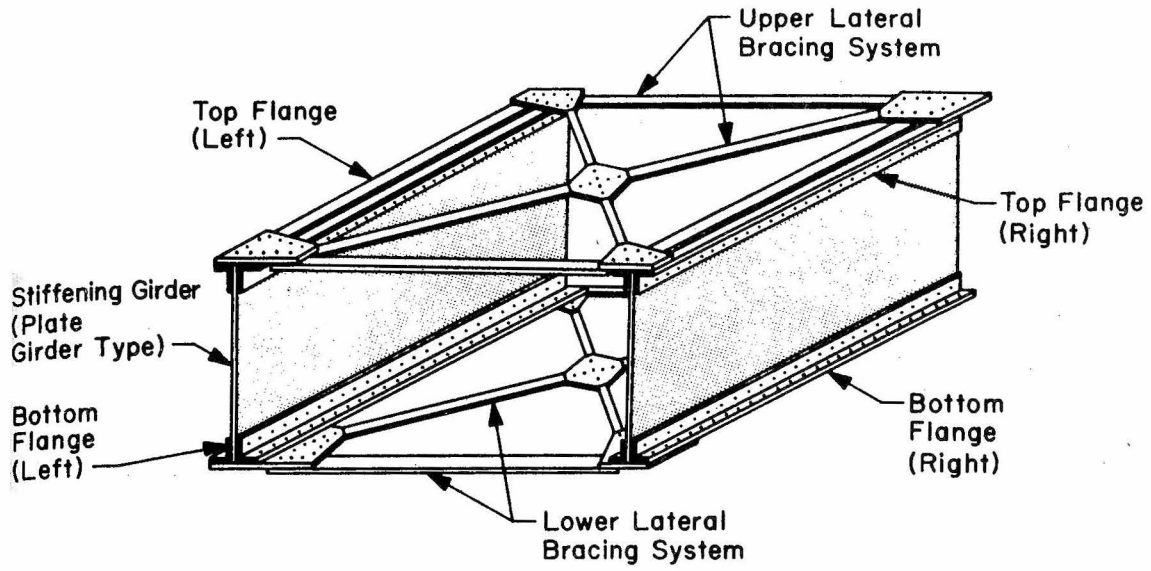
In addition to the theoretical analysis, some approximate equations and formulas are derived which help to clarify the torsional behavior of suspension bridges. Finally, a numerical example is presented.

## II-2. Preliminary Considerations and Fundamental Assumptions

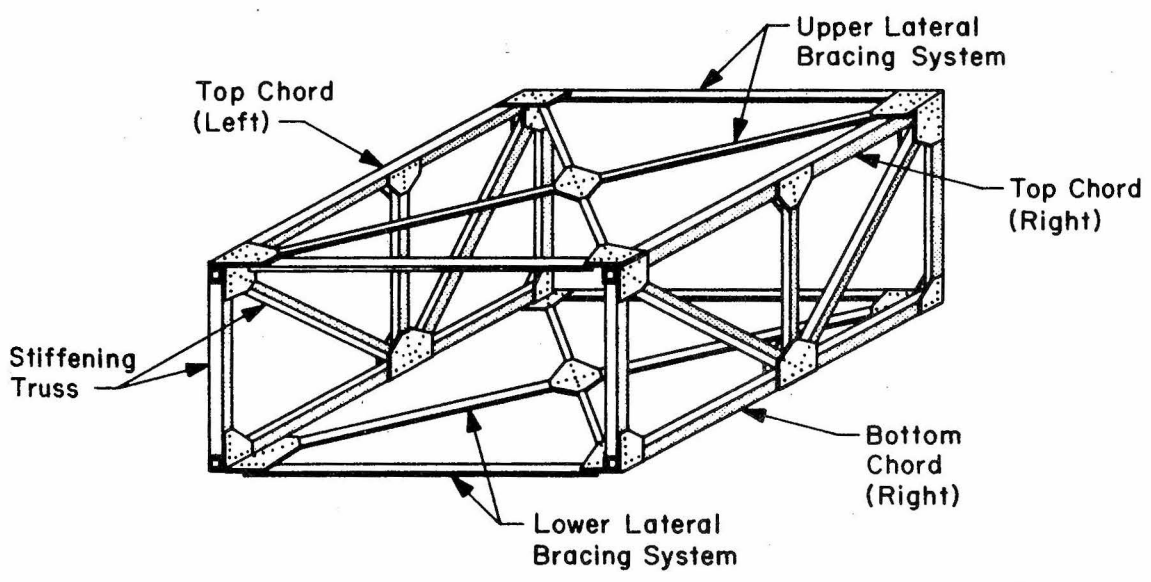
The main aim of this section is to present a brief description of the different types of suspended structures (or bridge decks) commonly used in modern long-span suspension bridges. These suspended structures have a very significant role in resisting torsional vibrations. The section is also intended to outline the coordinate systems used, and it contains the simplifying assumptions involved in the subsequent analysis.

### II-2-1. Types of suspended structures and their torsional resistance

The old type of suspended structure (bridge deck), consisting of two stiffening girders (or trusses) and a single lateral wind bracing system below the floor stringers, had so small a torsional rigidity that its effect on torsional vibrations could be disregarded [2, 8, 11, 13]. The only restoring forces provided by the deck came from the bending resistance of the stiffening girders (or trusses). Accordingly, the principal torsional modes in this case are identical to the corresponding vertical modes, except that the two sides of the deck and the two cables each move in opposite directions, i. e.,  $180^\circ$  out of phase. Certain differences between the frequencies of these two comparable modes — flexural and torsional — arise, however, from the different inertial conditions involved. In the flexural mode, the vertical motion of the deck is uniform across any one cross-section; in the torsional mode, one side is rising when the other is going down, and the mid-point of the deck remains stationary.



(a) Stiffening Plate - Girder Type



(b) Stiffening Truss Type

DIFFERENT TYPES OF STIFFENING GIRDERS

Fig. II-1

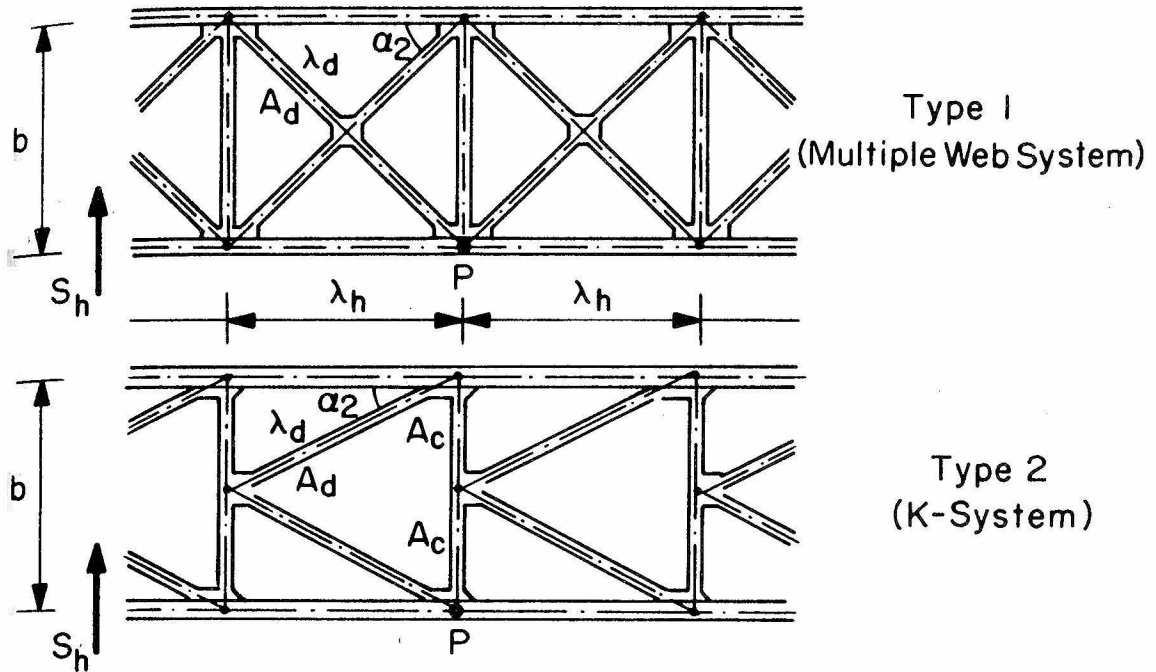
Modern long-span suspension bridges frequently have decks which are comprised of two lateral wind-bracing trusses provided in the horizontal planes of the top and bottom chords (or flanges) of the stiffening trusses (or girders). This four-walled bridge deck represents a rectangular tube of high torsional rigidity which has a significant effect on torsional vibrations.

Fig. II-1 shows two examples of the rectangular deck: one with stiffening plate-girders and the other with stiffening trusses. Two lateral bracing systems, of truss type, are in the plane of the top chord and the plane of the bottom chord. Fig. II-2 shows commonly used types of stiffening trusses and lateral bracing systems.

#### II-2-2. Coordinate systems

In this chapter, the dead load ordinate of the cable, measured from the closing line to the cable of the  $i^{\text{th}}$  span, is defined as  $y_c(x_i)$  to avoid confusion with the  $y_i$ -axis of the deck cross section shown in Fig. II-3. (Note: In this figure, the subscript  $i$  has been left out for convenience.) The  $x_i$ -axis of the  $i^{\text{th}}$  span coincides with the longitudinal axis of the bridge (i. e., the axis of rotation); this is the axis along which there is no movement. The coordinate origin for the deck is located at the left support of each span, while for the cable it is located at the left support of the cable whether it is an anchorage or a tower top. Beside the  $x_i$ ,  $y_i$  and  $z_i$  coordinate system of the deck in the  $i^{\text{th}}$  span, an additional coordinate system  $J_i$  for the  $i^{\text{th}}$  span is established along the perimeter of the section of the suspended

(a) Lateral Bracing System (Commonly Used)



(b) Stiffening Girder (Truss Type)

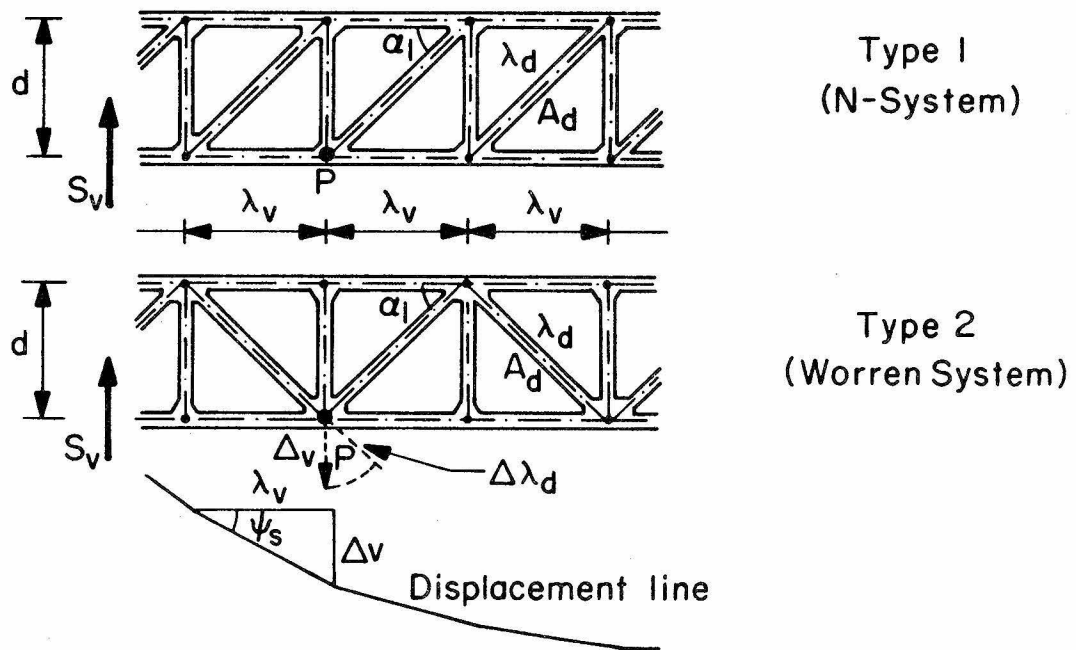


Fig. II-2. Different types of trusses commonly used for (a) lateral bracings and (b) stiffening structures.

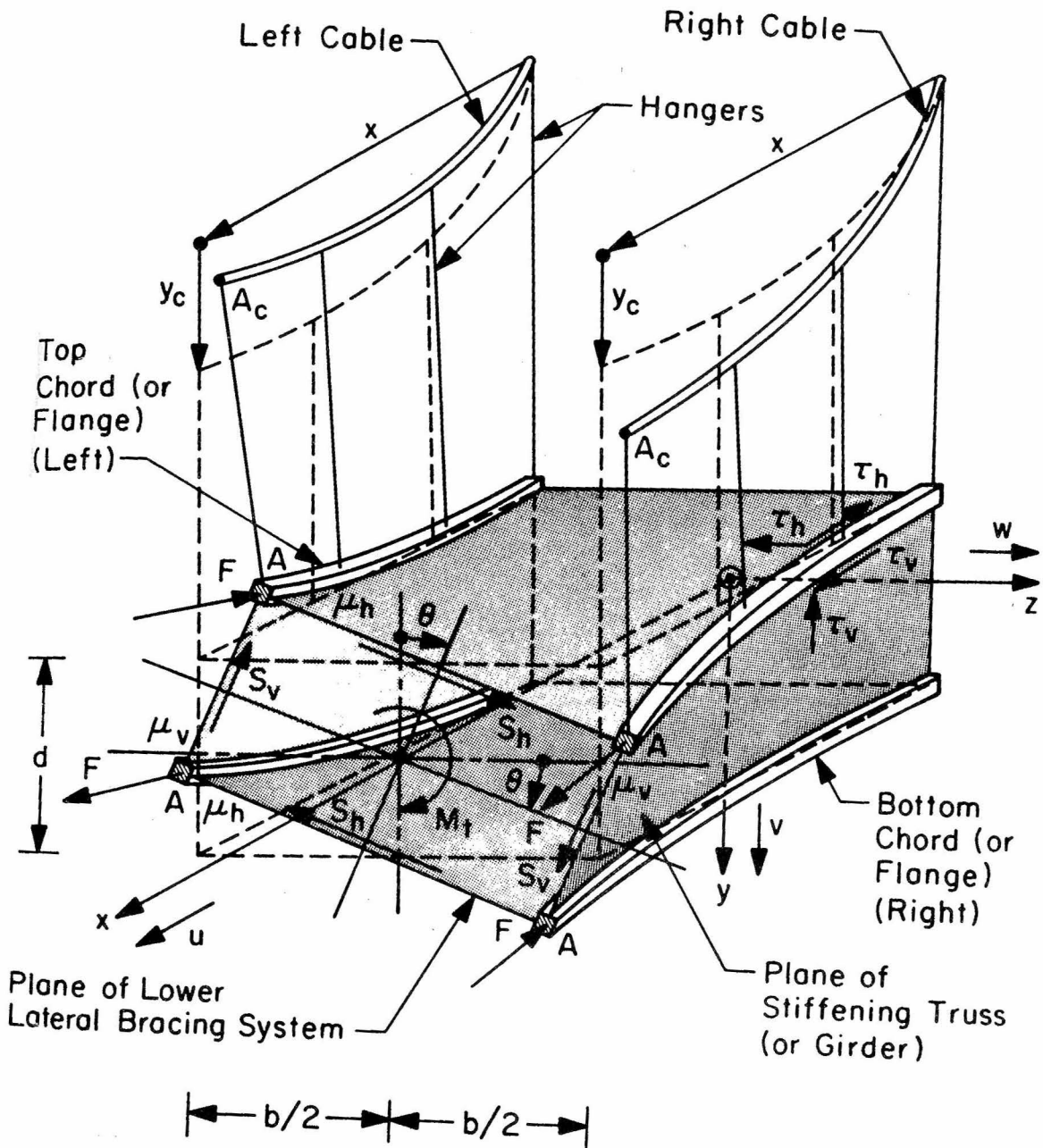
structure as shown in Fig. II-4. This peripheral coordinate  $\phi_i$  is measured clockwise along the centerline of the cross-section walls.

### II-2-3. Simplifying assumptions

When a rectangular bridge deck, having one or more cross sections constrained against warping, is vibrating torsionally, a complex distribution of longitudinal stresses is developed that cannot be evaluated using elementary theories of stress analysis. The assumption that plane sections remain plane during deformation is no longer valid, and applications of Saint-Venant's Principle may lead to serious error. The well-known example of the twist of a cantilever I-beam that is built-in at one end illustrates the nature of the problem.

Finding an exact solution of the problem of free torsional vibration of a suspension bridge having a rectangular deck structure is not possible. Certain simplifying assumptions must be introduced in addition to the fundamental assumptions adopted in the analysis of vertical vibration (Chapter I). Not only is it assumed that the hangers are vertical and inextensible, the cables parabolic, and only small deformations allowed, but also the following simplifying assumptions are introduced:

1. The cross section of the bridge deck is assumed to be symmetric about the center of the section. This cross section consists of four horizontal chords (or flanges), and four shear web systems (either diagonal and vertical truss members or web



TORSIONALLY VIBRATING SUSPENSION BRIDGE  
DEFINITION DIAGRAM

Fig. II-3

plates). The two chords (or flanges) of each stiffening truss (or girder) in the  $i^{\text{th}}$  span have the same effective cross-sectional area  $A_i$ ,  $i = 1, 2, 3$ , and the web members of the top and bottom bracing systems are also the same. Accordingly,  $y_i$  and  $z_i$ ,  $i = 1, 2, 3$ , are axes of symmetry of the four-walled structure shown in Fig. II-3.

2. The four horizontal chords (or flanges) transmit axial forces only, and the axial stresses in each chord (or flange) are distributed uniformly over its cross-sectional area  $A_i$ ,  $i = 1, 2, 3$ .
3. The web systems of the vertical walls (either plates or trusses) and the horizontal walls (usually trusses) transmit pure shear (there is no tension or compression in the horizontal or vertical directions). Also, the shear stress is constant through the web system. Thus, the shear stresses are in the web systems only, while the direct stresses are in the corner chords (or flanges).
4. The original shape of every cross-section is unaltered during vibrational deformation. Thus, the geometric dimensions of every plane normal to the bridge's longitudinal axis remain unchanged, although the section may undergo out-of-plane deformation (warping). Also, the peripheral bending in the walls of the section is negligible.

In view of the last assumption regarding rotation and out-of-plane deformation of the cross-section, it follows that the vibrational angle of twist,  $\theta_i$ ,  $i = 1, 2, 3$ , of a cross section in the  $i^{\text{th}}$  span and the  $y_i$ ,  $z_i$  components of the vibrational displacements  $v_i$  and  $w_i$  are

functions only of  $x_i$  and of time  $t$ , while the longitudinal vibrational displacement  $u_i$  is a function of  $\phi_i$ ,  $x_i$  and time  $t$ .

Other assumptions will be discussed as they are encountered in the development of the analysis.

### II-3. Analysis of Suspension Bridges Having Negligible Tower

#### Stiffness

The following analysis assumes either that the cable rests on nests of rollers at the tower top (i. e. , with a movable saddle) or that the tower is of the rocker type with a pin-bearing at the base. In both cases, the horizontal components of cable tension,  $H_w$  (due to dead load) and  $H(t)$  (due to inertia load), are the same on both sides of the tower since there is no tower resistance to displacement at the top. The equations of motion of the torsionally vibrating suspension bridge and the associated boundary conditions will be derived by means of Hamilton's Principle:

$$\int_{t_1}^{t_2} \delta(T-V) dt = 0 \quad , \quad (2.1)$$

where  $T$  is the total kinetic energy of the torsionally vibrating bridge,  $V$  is the total potential energy of the system, including both the strain energy and the potential energy of any conservative forces, and  $\delta$  is the variational operator taken during the indicated time interval.

The kinetic energy  $T$  consists of two parts: the kinetic energy  $T_c$  of the two cables vibrating in their vertical planes,  $180^\circ$  out of phase, and the kinetic energy  $T_s$  due to the rotation of the entire cross section of the suspended structure. Similarly, the potential energy of vibration  $V$  consists of two parts: the potential energy  $V_c$  of the vibrating cables and the potential energy  $V_s$  of the elastic deformation of the torsionally vibrating suspended structure.

II-3-1. Potential energy of the suspended structure

Based on the previous simplifying assumptions in Section II-2, the elastic potential energy  $V_s$ , i. e., the strain energy stored in the deck, can be divided into two parts:  $V_{sc}$  the strain energy due to the direct longitudinal stresses in the corner chords (or flanges) and  $V_{sd}$  the strain energy due to the shearing of the web system of both the stiffening trusses (or girders) and the lateral bracings.

The total strain energy  $V_s$  of the suspended structure is computed by summing the strain energy of each of the individual components of the cross section. Thus,  $V_s$  is given by

$$V_s(t) = \frac{1}{2} \sum_{i=1}^3 \left[ \iiint_V (4\sigma_i \epsilon_i + 2\gamma_{vi} \tau_{vi} + 2\gamma_{hi} \tau_{hi}) dV \right], \quad (2.2)$$

where  $\sigma_i$  and  $\epsilon_i$  are the direct longitudinal strain and stress due to a non-constant rate of twist measured at the cross section of each of the four corner chords (or flanges) in the  $i^{\text{th}}$  span;  $\tau_{vi}$  and  $\gamma_{vi}$  are the torsional shear stress and strain in the web system of the two vertical walls (stiffening trusses or girders) in the  $i^{\text{th}}$  span, and finally,  $\tau_{hi}$  and  $\gamma_{hi}$  are the shear stress and strain in the web system of the two horizontal walls (lateral bracings) in the  $i^{\text{th}}$  span. The summations extend over all three spans. In general, the shear stress and strain in the four walls depend on the effective cross-sectional area of the web plate for a plate girder type. In the case of a truss they depend on the equivalent solid web section, i. e., on the sectional area of the diagonal members or of the truss panel members.

The first term in Eq. 2.2, as indicated above, is the portion of the strain energy  $V_{sc}$  stored in the four chords (or flanges), i. e., the strain energy associated with warping, while the second and third terms are the portions of the strain energy  $V_{sd}$  stored in the web system of the two vertical and the two horizontal walls, respectively.

In order to further evaluate  $V_s$ , a knowledge of direct and shearing stresses resulting from torsional vibration, in terms of the vibrational angle of twist,  $\theta_i$ ,  $i = 1, 2, 3$ , must be specified.

### 1. Stress-Strain Relationships

From a consideration of the deformation of an element of length  $dx_i$  in both the vertical and horizontal web systems, illustrated in Fig. II-4, the vibrational shear strain due to the warping displacement  $u_i$  and the twist  $\theta_i$  about point 0 in the vertical system of the cross-section in the  $i^{\text{th}}$  span may be expressed as

$$\gamma_{vi} = \frac{\tau_{vi}}{G_i} = \frac{\partial v_i}{\partial x_i} + \frac{\partial u_i}{\partial \theta_i} \quad , \quad i = 1, 2, 3 \quad . \quad (2.3)$$

Here  $G_i$  is the shear modulus of the  $i^{\text{th}}$  span,  $v_i$  is the vertical vibrational displacement of the vertical system and  $u_i$  is the vibrational axial displacement of the corner chords (or flanges) in the  $i^{\text{th}}$  span. This axial displacement is the same (excepting the sign) for each of the chords in any given cross-section. From Fig. II-4-a, for the vertical system, it can be seen that

$$v_i(x_i, t) = \frac{b_i}{2} \theta_i(x_i, t) \quad , \quad i = 1, 2, 3 \quad , \quad (2.4)$$

where  $b_i$  is the width of the deck in the  $i^{\text{th}}$  span.

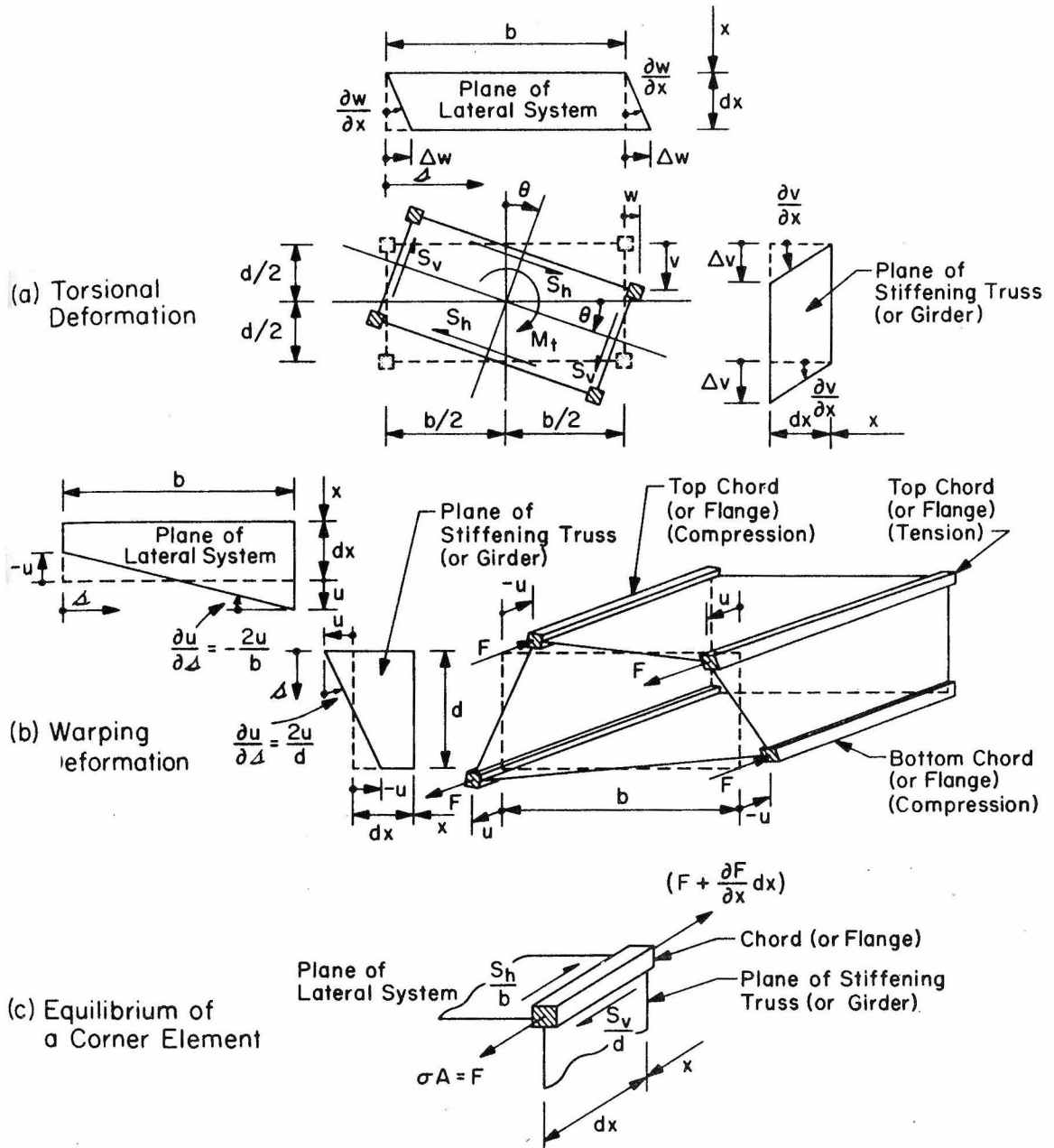


Fig. II-4

The shear strain due to warping displacement  $u_i$  in the vertical system is given by

$$\frac{\partial u_i}{\partial \phi_i} = \frac{2u_i}{d_i} \quad , \quad i = 1, 2, 3 \quad , \quad (2.5)$$

where  $d_i$  is the depth of the deck in the  $i^{\text{th}}$  span.

The vertical vibrational shear force  $S_{vi}$  is equal to the product of the shear stiffness and the shear strain; i. e.,

$$S_{vi}(x_i, t) = G_i \mu_{vi} \gamma_{vi}(x_i, t) \quad , \quad i = 1, 2, 3 \quad , \quad (2.6)$$

where  $\mu_{vi}$  is the shear resistance coefficient of the vertical web system and  $G_i \mu_{vi}$  is the shear stiffness of the wall. The value of the shear resistance coefficient depends on the effective cross-sectional area of the web plate (plate girder type). In the case of a truss,  $\mu_{vi}$  depends on the equivalent solid web section, i. e., on the sectional area of the diagonal member or members in a truss panel. In the latter case  $\mu_{vi}$  also depends on the type of truss system used. Appendix II-a demonstrates the shear resistance coefficient for the different types of trusses commonly used in stiffening trusses and in lateral bracing systems. These types are shown in Fig. II-2.

Substitution of Eqs. 2.4, 2.5 and 2.6 into Eq. 2.3 yields

$$\gamma_{vi} = \frac{S_{vi}}{G_i \mu_{vi}} = \frac{b_i}{2} \frac{\partial \theta_i}{\partial x_i} + \frac{2u_i}{d_i} \quad , \quad i = 1, 2, 3 \quad . \quad (2.7)$$

Similarly, the vibrational shear strain in the lateral system is given by

$$\gamma_{hi} = \frac{\tau_{hi}}{G_i} = \frac{\partial w_i}{\partial x_i} + \frac{\partial u_i}{\partial \phi_i} \quad , \quad i = 1, 2, 3 . \quad (2.8)$$

Here  $w_i$  is the horizontal vibrational displacement of the lateral system, and can be expressed as

$$w_i(x_i, t) = \frac{d_i}{2} \theta_i(x_i, t) \quad , \quad i = 1, 2, 3 . \quad (2.9)$$

From Fig. II-4-b, the shear strain due to warping displacement  $u_i$  in the horizontal wall can be written as

$$\frac{\partial u_i}{\partial \phi_i} = - \frac{2u_i}{b_i} \quad , \quad i = 1, 2, 3 . \quad (2.10)$$

The horizontal vibrational shear force  $S_{hi}$  can be expressed as

$$S_{hi}(x_i, t) = G_i \mu_{hi} \gamma_{hi}(x_i, t) \quad , \quad i = 1, 2, 3 , \quad (2.11)$$

with  $\mu_{hi}$  being the shear resistance coefficient of the horizontal web system.

Substitution of Eqs. 2.9, 2.10 and 2.11 into Eq. 2.8, yields

$$\gamma_{hi} = \frac{S_{hi}}{G_i \mu_{hi}} = \frac{d_i}{2} \frac{\partial \theta_i}{\partial x_i} - \frac{2u_i}{b_i} \quad , \quad i = 1, 2, 3 . \quad (2.12)$$

Now, the direct axial strain  $\epsilon_i$  and stress  $\sigma_i$  due to warping in the corner chords (or flanges) of the  $i^{\text{th}}$  span are

$$\epsilon_i = \frac{\partial u_i}{\partial x_i} \quad , \quad \sigma_i = E_i \epsilon_i = E_i \frac{\partial u_i}{\partial x_i} \quad , \quad i = 1, 2, 3 , \quad (2.13)$$

where  $E_i$  is the modulus of elasticity of the deck in the  $i^{\text{th}}$  span.

The axial force  $F_i$  acting at each chord (or flange) of the  $i^{\text{th}}$  span as shown in Fig. II-3, is given by

$$F_i = E_i A_i \frac{\partial u_i}{\partial x_i} \quad , \quad i = 1, 2, 3 \quad , \quad (2.14)$$

where  $A_i$  is the equivalent cross-sectional area of the corner chord (or flange).

Since the total axial force in the deck structure must equal zero at any section, the following relation must hold

$$\iint_A \sigma_i A_i dA = 0 \quad \forall \text{ } i^{\text{th}} \text{ span} \quad , \quad (2.15)$$

where  $A$  is the entire cross-sectional area.

## 2. Equilibrium Relationships

At a section of the  $i^{\text{th}}$  span there are two shear forces  $S_{vi}$  that form a couple, and two shear forces  $S_{hi}$  that form another couple, and there are four chord forces  $F_i$ . The two couples have a resulting twisting moment  $M_{ti}$ .

From consideration of the equilibrium of an element of length  $dx_i$ , located at the corner chord (or flange) as illustrated in Fig. II-5-c, it can be seen that

$$\frac{\partial F_i}{\partial x_i} = \frac{S_{vi}}{d_i} - \frac{S_{hi}}{b_i} \quad , \quad i = 1, 2, 3 \quad , \quad (2.16)$$

and the equilibrium of the torsional moment gives

$$M_{ti} = S_{vi} \cdot b_i + S_{hi} \cdot d_i \quad , \quad i = 1, 2, 3 \quad . \quad (2.17)$$

Eqs. 2.16 and 2.17 express the two equilibrium relationships for the various vibrational forces.

The next step is to express the forces  $F_i$ ,  $S_{vi}$  and  $S_{hi}$ , and accordingly  $M_{ti}$ , in terms of the vibrational angle of twist  $\theta_i$ .

### 3. Force-displacement Relationships

Multiplying Eq. 2.7 by  $d_i$  and Eq. 2.12 by  $b_i$  and then adding yields:

$$b_i d_i \frac{\partial \theta_i}{\partial x_i} = \frac{d_i}{\mu_{vi} G_i} S_{vi} + \frac{b_i}{\mu_{hi} G_i} S_{hi} \quad , \quad i = 1, 2, 3 . \quad (2.18)$$

Substitution of Eq. 2.18 into Eq. 2.16 then gives

$$\frac{\partial F_i}{\partial x_i} = \frac{b_i}{d_i} \mu_{vi} G_i \frac{\partial \theta_i}{\partial x_i} - \left( \frac{b_i^2 \mu_{vi} + d_i^2 \mu_{hi}}{b_i d_i \mu_{vi} \mu_{hi}} \right) \frac{\mu_{vi}}{d_i} S_{hi} \quad , \quad i = 1, 2, 3 , \quad (2.19)$$

or

$$\frac{\partial F_i}{\partial x_i} = - \frac{d_i}{b_i} \mu_{hi} G_i \frac{\partial \theta_i}{\partial x_i} + \left( \frac{b_i^2 \mu_{vi} + d_i^2 \mu_{hi}}{b_i d_i \mu_{vi} \mu_{hi}} \right) \frac{\mu_{vi}}{d_i} S_{vi} \quad , \quad i = 1, 2, 3 . \quad (2.20)$$

Introducing the coefficient  $\beta_i$  as

$$\beta_i = \frac{b_i d_i \mu_{vi} \mu_{hi}}{b_i^2 \mu_{vi} + d_i^2 \mu_{hi}} \quad , \quad i = 1, 2, 3 , \quad (2.21)$$

into Eqs. 2.19 and 2.20 gives the following

$$\frac{\partial F_i}{\partial x_i} = \frac{b_i}{d_i} \mu_{vi} G_i \frac{\partial \theta_i}{\partial x_i} - \frac{\mu_{vi}}{\beta_i d_i} S_{hi} \quad , \quad i = 1, 2, 3 , \quad (2.19')$$

and

$$\frac{\partial F_i}{\partial x_i} = \frac{-d_i}{b_i} \mu_{hi} G_i \frac{\partial \theta_i}{\partial x_i} + \frac{\mu_{hi}}{\beta_i b_i} S_{vi} \quad , \quad i = 1, 2, 3 . \quad (2.20')$$

Differentiating Eq. 2.7 twice and Eq. 2.14 once (w.r.t.  $x_i$ ), combining the two equations, and then substituting Eq. 2.20' in the resulting equation obtains:

$$S_{vi} = G_i \beta_i d_i \frac{\partial \theta_i}{\partial x_i} - E_i A_i \frac{b_i d_i \beta_i}{2\mu_{hi}} \left( \frac{b_i}{2} \frac{\partial^3 \theta_i}{\partial x_i^3} - \frac{1}{\mu_{vi} G_i} \frac{\partial^2 S_{vi}}{\partial x_i^2} \right), \quad i = 1, 2, 3. \quad (2.22)$$

A similar expression for  $S_{hi}$  can be obtained by using the same procedure; it can be written as

$$S_{hi} = G_i \beta_i b_i \frac{\partial \theta_i}{\partial x_i} - E_i A_i \frac{b_i d_i \beta_i}{2\mu_{vi}} \left( \frac{d_i}{2} \frac{\partial^3 \theta_i}{\partial x_i^3} - \frac{1}{\mu_{vi} G_i} \frac{\partial^2 S_{hi}}{\partial x_i^2} \right), \quad i = 1, 2, 3. \quad (2.23)$$

Differentiating Eqs. 2.22 and 2.23 twice and substituting the resulting expressions for the last term in each equation results in a final expression for the torsional shearing forces, given in terms of  $\theta_i$ .

$$S_{vi} = G_i \beta_i d_i \frac{\partial \theta_i}{\partial x_i} - E_i A_i \frac{b_i d_i \beta_i}{2\mu_{vi}} \left( \frac{b_i}{2} - \frac{\beta_i b_i}{\mu_{vi}} \right) \frac{\partial^3 \theta_i}{\partial x_i^3} - \frac{1}{G_i \mu_{vi}} \left( E_i A_i \frac{b_i d_i \beta_i}{2\mu_{hi}} \right)^2 \left( \frac{b_i}{2} - \frac{\beta_i d_i}{\mu_{vi}} \right) \frac{\partial^5 \theta_i}{\partial x_i^5} + \dots \quad i = 1, 2, 3. \quad (2.24)$$

$$S_{hi} = G_i \beta_i b_i \frac{\partial \theta_i}{\partial x_i} - E_i A_i \frac{b_i d_i \beta_i}{2\mu_{vi}} \left( \frac{d_i}{2} - \frac{\beta_i b_i}{\mu_{vi}} \right) \frac{\partial^3 \theta_i}{\partial x_i^3} - \frac{1}{G_i \mu_{hi}} \left( E_i A_i \frac{b_i d_i \beta_i}{2\mu_{vi}} \right)^2 \left( \frac{d_i}{2} - \frac{\beta_i b_i}{\mu_{hi}} \right) \frac{\partial^5 \theta_i}{\partial x_i^5} + \dots \quad i = 1, 2, 3. \quad (2.25)$$

The Saint-Venant shear forces are now given by the first term of both Eqs. 2.24 and 2.25; i. e., they are proportional to the rate of twist.

Neglect of terms of higher derivatives than 3 is identical to the usual neglect of shear deformation of beams. Consequently,

$$S_{vi} = G_i \beta_i d_i \frac{\partial \theta_i}{\partial x_i} - E_i A_i \frac{b_i d_i \beta_i}{2\mu_{hi}} \left( \frac{b_i}{2} - \frac{\beta_i d_i}{\mu_{vi}} \right) \frac{\partial^3 \theta_i}{\partial x_i^3}, \quad i = 1, 2, 3. \quad (2.24')$$

$$S_{hi} = G_i \beta_i b_i \frac{\partial \theta_i}{\partial x_i} - E_i A_i \frac{b_i d_i \beta_i}{2\mu_{vi}} \left( \frac{d_i}{2} - \frac{\beta_i b_i}{\mu_{hi}} \right) \frac{\partial^3 \theta_i}{\partial x_i^3}, \quad i = 1, 2, 3. \quad (2.25')$$

Introducing expressions 2.24' and 2.25' into Eq. 2.17,  $M_{ti}$  can be written as

$$M_{ti} = 2G_i \beta_i b_i d_i \frac{\partial \theta_i}{\partial x_i} - E_i \frac{A_i b_i d_i \beta_i}{2} \left[ \frac{b_i}{\mu_{hi}} \left( \frac{b_i}{2} - \frac{\beta_i d_i}{\mu_{vi}} \right) + \frac{d_i}{\mu_{vi}} \left( \frac{d_i}{2} - \frac{\beta_i b_i}{\mu_{hi}} \right) \right] \frac{\partial^3 \theta_i}{\partial x_i^3},$$

$$i = 1, 2, 3. \quad (2.26)$$

The warping displacement  $u_i$  of the cross-section in the  $i^{\text{th}}$  span is given by

$$u_i = \frac{d_i}{2} \left( \frac{1}{\mu_{vi} G_i} S_{vi} - \frac{b_i}{2} \frac{\partial \theta_i}{\partial x_i} \right), \quad i = 1, 2, 3, \quad (2.7')$$

or

$$u_i = \frac{b_i}{2} \left( \frac{1}{\mu_{hi} G_i} S_{hi} - \frac{d_i}{2} \frac{\partial \theta_i}{\partial x_i} \right), \quad i = 1, 2, 3. \quad (2.12')$$

Using the expressions for  $S_{vi}$  and  $S_{hi}$  (Eqs. 2.24' and 2.25'), Eqs. 2.7' and 2.12' can be expressed in terms of  $\theta_i$  as follows:

$$u_i = \frac{d_i}{2} \left( \frac{\beta_i d_i}{\mu_{vi}} - \frac{b_i}{2} \right) \frac{\partial \theta_i}{\partial x_i} + E_i \frac{A_i b_i d_i^2 \beta_i}{4\mu_{vi} \mu_{hi} G_i} \left( \frac{\beta_i d_i}{\mu_{vi}} - \frac{b_i}{2} \right) \frac{\partial^3 \theta_i}{\partial x_i^3}, \quad i = 1, 2, 3, \quad (2.27)$$

or

$$u_i = \frac{b_i}{2} \left( \frac{d_i}{2} - \frac{\beta_i b_i}{\mu_{hi}} \right) \frac{\partial \theta_i}{\partial x_i} + E_i \frac{A_i b_i^2 d_i \beta_i}{4\mu_{vi} \mu_{hi} G_i} \left( \frac{d_i}{2} - \frac{\beta_i b_i}{\mu_{hi}} \right) \frac{\partial^3 \theta_i}{\partial x_i^3}, \quad i = 1, 2, 3. \quad (2.28)$$

Appendix II-b gives a proof showing that expressions 2.27 and 2.28, for the longitudinal warping displacement, are identical.

The axial force  $F_i$  can now be obtained by substituting Eq. 2.27 or 2.28 into Eq. 2.14 to get

$$F_i = E_i A_i \frac{d_i}{2} \left( \frac{\beta_i b_i}{\mu_{vi}} - \frac{b_i}{2} \right) \frac{\partial^2 \theta_i}{\partial x_i^2} + (E_i A_i)^2 \frac{b_i d_i^2 \beta_i}{4\mu_{vi} \mu_{hi} G_i} \left( \frac{\beta_i d_i}{\mu_{vi}} - \frac{b_i}{2} \right) \frac{\partial^4 \theta_i}{\partial x_i^4},$$

$i = 1, 2, 3, \quad (2.29)$

or

$$F_i = E_i A_i \frac{b_i}{2} \left( \frac{d_i}{2} - \frac{\beta_i d_i}{\mu_{hi}} \right) \frac{\partial^2 \theta_i}{\partial x_i^2} + (E_i A_i)^2 \frac{b_i^2 d_i \beta_i}{4\mu_{vi} \mu_{hi} G_i} \left( \frac{d_i}{2} - \frac{\beta_i b_i}{\mu_{hi}} \right) \frac{\partial^4 \theta_i}{\partial x_i^4},$$

$i = 1, 2, 3, \quad (2.30)$

Now, all displacements, strains, stresses and forces are expressed in terms of the vibrational angle of twist  $\theta_i$ .

Neglecting the high derivative terms in the above expressions for  $u_i$ , leaves

$$u_i \approx \frac{d_i}{2} \left( \frac{\beta_i d_i}{\mu_{vi}} - \frac{b_i}{2} \right) \frac{\partial \theta_i}{\partial x_i} = \bar{u}_i \frac{\partial \theta_i}{\partial x_i}, \quad i = 1, 2, 3, \quad (2.31)$$

or

$$u_i \approx \frac{b_i}{2} \left( \frac{d_i}{2} - \frac{\beta_i b_i}{\mu_{hi}} \right) \frac{\partial \theta_i}{\partial x_i} = \bar{u}_i \frac{\partial \theta_i}{\partial x_i}, \quad i = 1, 2, 3, \quad (2.32)$$

where  $\bar{u}_i$  is now the warping per unit rate of twist of the  $i^{\text{th}}$  span.

#### a. Strain energy of the chords (or flanges)

The strain energy  $V_{sc}$  stored in the corner chords (or flanges) of the cross section, due to direct (torsion-bending) stresses, may be

expressed as:

$$V_{sc}(t) = \frac{1}{2} \sum_{i=1}^3 \left[ \iiint_V 4 \sigma_i \epsilon_i dV \right] = \frac{1}{2} \sum_{i=1}^3 \left[ \int_0^{\ell_i} 4 E_i A_i \epsilon_i^2 dx_i \right], \quad (2.33)$$

using the linear stress-strain law (Hookean elasticity).

Using Eqs. 2.13, 2.31 and 2.32, the direct strain  $\epsilon_i$  and stress  $\sigma_i$  due to a non-uniform rate of twist become

$$\epsilon_i = \bar{u}_i \frac{\partial^2 \theta_i}{\partial x_i^2}, \quad \sigma_i = E_i \bar{u}_i \frac{\partial^2 \theta_i}{\partial x_i^2}, \quad i = 1, 2, 3. \quad (2.34)$$

Therefore, the strain energy associated with warping can be written, with the aid of Eqs. 2.31 through 2.34, as

$$V_{sc}(t) = \frac{1}{2} \sum_{i=1}^3 \left\{ \int_0^{\ell_i} 2 E_i A_i \left[ \frac{d_i}{2} \left( \frac{\beta_i d_i}{\mu_{vi}} - \frac{b_i}{2} \right) \frac{\partial^2 \theta_i}{\partial x_i^2} \right]^2 dx_i + \int_0^{\ell_i} 2 E_i A_i \left[ \frac{b_i}{2} \left( \frac{d_i}{2} - \frac{\beta_i b_i}{\mu_{hi}} \right) \frac{\partial^2 \theta_i}{\partial x_i^2} \right]^2 dx_i \right\},$$

or

$$V_{sc}(t) = \frac{1}{2} \sum_{i=1}^3 \left\{ \int_0^{\ell_i} E_i \left[ A_i \frac{d_i^2}{2} \left( \frac{\beta_i d_i}{\mu_{vi}} - \frac{b_i}{2} \right)^2 + A_i \frac{b_i^2}{2} \left( \frac{d_i}{2} - \frac{\beta_i b_i}{\mu_{hi}} \right)^2 \right] \left( \frac{\partial^2 \theta_i}{\partial x_i^2} \right)^2 dx_i \right\}, \quad (2.35)$$

or equivalently

$$V_{sc}(t) = \frac{1}{2} \sum_{i=1}^3 \left[ \int_0^{\ell_i} E_i \Gamma_i \left( \frac{\partial^2 \theta_i}{\partial x_i^2} \right)^2 dx_i \right], \quad (2.36)$$

where  $\Gamma_i$  is the warping constant of the cross section in the  $i^{\text{th}}$  span (sometimes called the torsion-bending constant); it is expressed by

$$\Gamma_i = A_i \frac{d_i^2}{2} \left( \frac{\beta_i d_i}{\mu_{vi}} - \frac{b_i}{2} \right)^2 + A_i \frac{b_i^2}{2} \left( \frac{d_i}{2} - \frac{\beta_i b_i}{\mu_{hi}} \right)^2, \quad i = 1, 2, 3. \quad (2.37)$$

The warping constant has units of length to the sixth power. The product,  $E_i \Gamma_i$ , in Eq. 2.36 is called the warping rigidity of the cross section in the  $i^{\text{th}}$  span. The expression for the warping constant,  $\Gamma_i$ , (Eq. 2.37) is the same as the coefficient of

$E_i \frac{\partial^3 \theta_i}{\partial x_i^3}$  in the second term of the vibrational torsional moment

(Eq. 2.26). Appendix II-c contains a proof of this equality.

#### b. Strain energy of the web systems

The strain energy  $V_{sd}$  stored in the web system of both the vertical and the horizontal walls of the cross section, using a linear stress-strain law, is given by

$$V_{sd}(t) = \frac{1}{2} \sum_{i=1}^3 \left[ \iiint_V (2 \gamma_{vi} \tau_{vi} + 2 \gamma_{hi} \tau_{hi}) dV \right],$$

or

$$V_{sd}(t) = \frac{1}{2} \sum_{i=1}^3 \left[ 2 \int_0^{\ell} \left( \mu_{vi} \frac{\tau_{vi}^2}{G_i} + \mu_{hi} \frac{\tau_{hi}^2}{G_i} \right) dx_i \right]. \quad (2.38)$$

Using Eqs. 2.24' and 2.25' and noting that

$$\tau_{vi} = \frac{S_{vi}}{\mu_{vi}} \quad \text{and} \quad \tau_{hi} = \frac{S_{hi}}{\mu_{hi}} \quad , \quad (2.39)$$

then Eq. 2.38 can be written as:

$$V_{sd}(t) = \frac{1}{2} \sum_{i=1}^3 \left\{ \int_0^{\ell_i} 2 \frac{\mu_{vi}}{G_i} \left[ \frac{G_i \beta_i d_i}{\mu_{vi}} \frac{\partial \theta_i}{\partial x_i} - E_i A_i \frac{b_i d_i \beta_i}{2 \mu_{vi} \mu_{hi}} \left( \frac{b_i}{2} - \frac{\beta_i d_i}{\mu_{vi}} \right) \frac{\partial^3 \theta_i}{\partial x_i^3} \right]^2 dx_i \right. \\ \left. + \int_0^{\ell_i} 2 \frac{\mu_{hi}}{G_i} \left[ \frac{G_i \beta_i b_i}{\mu_{hi}} \frac{\partial \theta_i}{\partial x_i} - E_i A_i \frac{b_i d_i \beta_i}{2 \mu_{vi} \mu_{hi}} \left( \frac{d_i}{2} - \frac{\beta_i b_i}{\mu_{hi}} \right) \frac{\partial^3 \theta_i}{\partial x_i^3} \right]^2 dx_i \right\} . \quad (2.40)$$

Neglecting terms with higher derivatives than the first is identical to assuming that these shear stresses due to twisting are equal to those in St. Venant's theory of torsion. Therefore, the strain energy, in accordance with St. Venant's theory of uniform torsion, will take the form

$$V_{sd}(t) = \frac{1}{2} \sum_{i=1}^3 \left\{ \int_0^{\ell_i} 2 G_i \beta_i^2 \left[ \frac{d_i^2}{\mu_{vi}} + \frac{b_i^2}{\mu_{hi}} \right] \left( \frac{\partial \theta_i}{\partial x_i} \right)^2 dx_i \right\} . \quad (2.41)$$

Recalling the definition of the coefficient  $\beta_i$  (Eq. 2.21), the strain energy expression (Eq. 2.41) becomes

$$V_{sd}(t) = \frac{1}{2} \sum_{i=1}^3 \left[ 2 \int_0^{\ell_i} G_i \beta_i b_i d_i \left( \frac{\partial \theta_i}{\partial x_i} \right)^2 dx_i \right] . \quad (2.42)$$

Defining the torsion constant  $J_i$  as

$$J_i = 2 \beta_i b_i d_i \quad , \quad (2.43)$$

then Eq. 2.42 can be written in a more convenient form as

$$V_{sd}(t) = \frac{1}{2} \sum_{i=1}^3 \left[ \int_0^{\ell_i} G_i J_i \left( \frac{\partial \theta_i}{\partial x_i} \right)^2 dx_i \right] \quad (2.44)$$

Here,  $G_i J_i$  represents the torsional rigidity of the cross section in the  $i^{\text{th}}$  span.

The torsional strain energy can also be examined within the framework of St. Venant's theory of uniform torsion which gives an alternative way to derive Eq. 2.44. The shear stresses due to twisting are assumed to be the same as in St. Venant's theory and the resultant of these shear stresses is a torque which is expressed by the first term of Eq. 2.26; i. e.,

$$M_{ti} \simeq 2 G_i \beta_i b_i d_i \frac{\partial \theta_i}{\partial x_i} \quad \text{or} \quad \tilde{M}_{ti} = G_i J_i \frac{\partial \theta_i}{\partial x_i}, \quad i = 1, 2, 3. \quad (2.45)$$

The strain energy for an element of the bridge deck of length  $dx_i$  is necessarily equal to the work done on the element by the torque  $\tilde{M}_{ti}$ . Therefore,  $V_{sd}$  for the entire bridge deck is

$$V_{sd}(t) = \frac{1}{2} \sum_{i=1}^3 \left[ \int_0^{\ell_i} \tilde{M}_{ti} \frac{\partial \theta_i}{\partial x_i} dx_i \right] = \frac{1}{2} \sum_{i=1}^3 \left[ \int_0^{\ell_i} G_i J_i \left( \frac{\partial \theta_i}{\partial x_i} \right)^2 dx_i \right], \quad (2.44')$$

which is exactly the same expression obtained previously (Eq. 2.44).

Returning to the derivation of the total strain energy stored in the torsionally vibrating suspended structure, Eqs. 2.36 and 2.44 are summed to give:

$$V_s(t) = \frac{1}{2} \sum_{i=1}^3 \left[ \int_0^{\ell_i} E_i \Gamma_i \left( \frac{\partial^2 \theta_i}{\partial x_i^2} \right)^2 dx_i + \int_0^{\ell_i} G_i J_i \left( \frac{\partial \theta_i}{\partial x_i} \right)^2 dx_i \right] . \quad (2.46)$$

It is worthwhile noting that in the St. Venant type of torsion the torque is constant along the beam and the sections of the beam are permitted to warp freely. When the warping is restricted by physical constraints at the ends of the beam, normal stresses arise in addition to the shear stresses, and they contribute an additional resistance to twisting. This same effect is caused by variations in the applied torque along the beam such as a torque caused by inertia forces resulting from vibration. The warping effect is completely absent from beams of circular cross section whose normal sections remain plane during torsion, but it is very important in box-shaped cross sections.

### II-3-2. Potential energy of the cables

In torsional vibration, corresponding points on the two cables move equal distances in opposite directions. For small torsional amplitudes the movement of any point is essentially vertical and the variation of amplitude along the cable is the same as for the corresponding pure vertical vibrational modes. Thus, the two cables vibrate in their vertical planes in opposite phase with antisymmetric vertical movements of  $\pm v_i$ ,  $i = 1, 2, 3$ . The downward movement of the cable tends to increase its length by bending the cable more sharply while at the same time the upward movement tends to reduce its length by straightening the cable. The total potential energy,  $V_c$ , of the two

vibrating cables is composed of the potential energy of the depressed cable,  $V_c^d$ , and the potential energy of the elevated cable,  $V_c^e$ .

If  $H_w \left( \frac{ds_i}{dx_i} \right)$  is the tension of the cable under dead load at a point along the  $i^{\text{th}}$  span, and  $\pm H(t) \left( \frac{ds_i}{dx_i} \right)$  are the vibrational increments in cable tension for the depressed and elevated cables, respectively, then the potential energies  $V_c^d$  and  $V_c^e$  stored in cable length  $dx_i$ , are

$$dV_c^d(x_i, t) = \left\{ \left[ H_w + \frac{1}{2} H(t) \right] \frac{ds_i}{dx_i} \right\} \cdot \Delta d^d s_i - \overset{*}{w}_i v_i dx_i, \quad i = 1, 2, 3, \quad (2.47)$$

and

$$dV_c^e(x_i, t) = \left\{ \left[ H_w - \frac{1}{2} H(t) \right] \frac{ds_i}{dx_i} \right\} \cdot \Delta d^e s_i + \overset{*}{w}_i v_i dx_i, \quad i = 1, 2, 3; \quad (2.48)$$

$H_w$  is the horizontal component of cable tension owing to dead load,  $H(t)$  is the vibrational increment in the horizontal component of cable tension,  $\overset{*}{w}_i$  is the total dead weight of the bridge per unit length per cable, and  $\Delta d^d s_i$  and  $\Delta d^e s_i$  are the vibrational increments in the length of the depressed and elevated cables, respectively. Using the results of the analysis given previously in Chapter I which deals with vertical vibration, the potential energy  $V_c^d$  stored in the depressed cable can be given in the form

$$V_c^d(t) = \frac{1}{2} \sum_{i=1}^3 \left\{ H_w \int_0^{\ell_i} \left( \frac{\partial v_i}{\partial x_i} \right)^2 dx_i + H(t) \left[ \int_0^{\ell_i} \left( \frac{dy_c}{dx_i} \right) \left( \frac{\partial v_i}{\partial x_i} \right) dx_i + \frac{1}{2} \int_0^{\ell_i} \left( \frac{\partial v_i}{\partial x_i} \right)^2 dx_i \right] \right\}, \quad (2.49)$$

where  $\frac{dy_c}{dx_i}$  is the dead load slope in the  $i^{\text{th}}$  span of the cables.

The relationship between  $H(t)$  and  $v_i(x_i, t)$  is expressed by the cable equation which relates the elastic stretching of the cable to the vertical vibrational displacement, as follows:

$$\frac{H(t)L_E}{E_c A_c} = \sum_{i=1}^3 \left[ \int_0^{\ell_i} \left( \frac{dy_c}{dx_i} \right) \left( \frac{\partial v_i}{\partial x_i} \right) dx_i + \frac{1}{2} \int_0^{\ell_i} \left( \frac{\partial v_i}{\partial x_i} \right)^2 dx_i \right] . \quad (2.50)$$

Here,  $E_c$  is the modulus of elasticity of the cable,  $A_c$  is the area of one cable cross section and  $L_E$  is a virtual length of the cable defined by

$$L_E = \sum_{i=1}^3 L_{ei} = \sum_{i=1}^3 \int_0^{\ell_i} \left( \frac{ds_i}{dx_i} \right)^3 dx_i .$$

After substitution of  $-v_i$  and  $-H(t)$  for  $v_i$  and  $H(t)$ , respectively, in Eq. 2.49, an expression for the potential energy of the elevated cable  $V_c^e$  is obtained as

$$V_c^e(t) = \frac{1}{2} \sum_{i=1}^3 \left\{ H_w \int_0^{\ell_i} \left( \frac{\partial v_i}{\partial x_i} \right)^2 dx_i - H(t) \left[ - \int_0^{\ell_i} \left( \frac{dy_c}{dx_i} \right) \left( \frac{\partial v_i}{\partial x_i} \right) dx_i + \frac{1}{2} \int_0^{\ell_i} \left( \frac{\partial v_i}{\partial x_i} \right)^2 dx_i \right] \right\} . \quad (2.51)$$

The total potential energy,  $V_c$  stored in the two cables of the torsionally vibrating suspension bridge, is obtained by the sum of  $V_c^d$  and  $V_c^e$  and is given by

$$V_c(t) = \frac{1}{2} \sum_{i=1}^3 \left\{ 2 H_w \int_0^{\ell_i} \left( \frac{\partial v_i}{\partial x_i} \right)^2 dx_i + 2 H(t) \left[ \int_0^{\ell_i} \left( \frac{dy_c}{dx_i} \right) \left( \frac{\partial v_i}{\partial x_i} \right) dx_i \right] \right\} . \quad (2.52)$$

By noting that  $v_i = \frac{b_i}{2} \theta_i$ , Eq. 2.52 can be rewritten in terms

of  $\theta_i$  , as

$$V_c(t) = \frac{1}{2} \sum_{i=1}^3 \left\{ \frac{H_w b_i^2}{2} \int_0^{\ell_i} \left( \frac{\partial \theta_i}{\partial x_i} \right)^2 dx_i + H(t) b_i \left[ \int_0^{\ell_i} \left( \frac{dy_c}{dx_i} \right) \left( \frac{\partial \theta_i}{\partial x_i} \right) dx_i \right] \right\} . \quad (2.53)$$

It will be noticed that the term  $\frac{H(t)}{2} \int_0^{\ell_i} \left( \frac{\partial \theta_i}{\partial x_i} \right)^2 dx_i$  , has been canceled. Also, it will be recognized that the first term of Eq. 2.53 represents the strainless or gravitational energy while the second term, after neglecting the second order term which appears in the cable equation (Eq. 2.50), represents the strain energy stored in the two cables.

The contributions to the potential energy of the system from the hangers are neglected since they are usually too small to be important [9].

### II-3-3. Kinetic energy of the torsionally vibrating suspension bridge

The expression for the kinetic energy of the torsionally vibrating suspension bridge may also be divided into two parts: one part represents the vibration of the bridge deck,  $T_s$  , and the other part represents the vibration of the two cables,  $T_c$  .

The kinetic energy,  $T_s$  , of the suspended structure (or the deck), for the entire bridge may be expressed by:

$$T_s(t) = \frac{1}{2} \sum_{i=1}^3 \left[ \int_0^{\ell_i} I_{pi} \left( \frac{\partial \theta_i}{\partial t} \right)^2 dx_i \right] , \quad (2.54)$$

where  $I_{pi}$  is the mass polar moment of inertia per unit length of the cross section of the  $i^{\text{th}}$  span. It is equal to  $m_{si}r_{si}^2$ ,  $m_{si}$  being the mass of the  $i^{\text{th}}$  suspended structure per unit length and  $r_{si}$  being the radius of gyration of the cross section.

The two cables, having the weight  $w_c$  per unit length of the span and vibrating with antisymmetric vertical displacements  $\pm v_i$ ,  $i = 1, 2, 3$ , have kinetic energy expressed by

$$T_c(t) = \frac{1}{2} \sum_{i=1}^3 \left[ \frac{w_c}{g} \int_0^{\ell_i} \left( \frac{\partial v_i}{\partial t} \right)^2 dx_i \right], \quad (2.55)$$

but since  $v_i = \frac{b_i}{2} \theta_i$ , the kinetic energy  $T_c$  becomes

$$T_c(t) = \frac{1}{2} \sum_{i=1}^3 \left[ \frac{w_c}{g} \frac{b_i^2}{4} \int_0^{\ell_i} \left( \frac{\partial \theta_i}{\partial t} \right)^2 dx_i \right], \quad (2.56)$$

$g$  being the acceleration of gravity.

The total kinetic energy of the structure is then given by

$$T(t) = T_s(t) + T_c(t) = \frac{1}{2} \sum_{i=1}^3 \left[ \int_0^{\ell_i} \left( I_{pi} + \frac{w_c}{g} \frac{b_i^2}{4} \right) \left( \frac{\partial \theta_i}{\partial t} \right)^2 dx_i \right]. \quad (2.57)$$

The total kinetic energy may also be written in the form

$$T(t) = \frac{1}{2} \sum_{i=1}^3 \left[ \int_0^{\ell_i} I_{mi} \left( \frac{\partial \theta_i}{\partial t} \right)^2 dx_i \right], \quad (2.58)$$

where

$$I_{mi} = \left( I_{pi} + \frac{w_c}{g} \frac{b_i^2}{4} \right), \quad i = 1, 2, 3, \quad (2.59)$$

and  $I_{mi}$  is the equivalent mass polar moment of inertia of the bridge cross section in the  $i^{\text{th}}$  span (including the contribution of the two cables) per unit length.

#### II-3-4. Variational formulation of the equations of motion

The variation of the total kinetic energy can be expressed as

$$\begin{aligned} \int_{t_1}^{t_2} \delta T(t) dt &= \sum_{i=1}^3 \int_0^{\ell_i} \left[ I_{mi} \frac{\partial \theta_i}{\partial t} \delta \theta_i \Big|_{t_1}^{t_2} - \int_{t_1}^{t_2} \frac{\partial}{\partial t} \left( I_{mi} \frac{\partial \theta_i}{\partial t} \right) \delta \theta_i dt \right] dx_i \\ &= - \sum_{i=1}^3 \left[ \int_{t_1}^{t_2} \int_0^{\ell_i} I_{mi} \frac{\partial^2 \theta_i}{\partial t^2} \delta \theta_i dx_i dt \right], \end{aligned} \quad (2.60)$$

since, by definition,  $\delta \theta_i$  is zero at  $t=t_1$  and  $t=t_2$ .

The total potential energy of the torsionally vibrating suspension bridge can also be expressed, from Eqs. 2.46 and 2.53, as

$$\begin{aligned} V(t) &= \frac{1}{2} \sum_{i=1}^3 \left\{ \left[ \int_0^{\ell_i} E_i \Gamma_i \left( \frac{\partial^2 \theta_i}{\partial x_i^2} \right)^2 dx_i + \int_0^{\ell_i} G_i \Gamma_i \left( \frac{\partial \theta_i}{\partial x_i} \right)^2 dx_i \right] \right. \\ &\quad \left. + \left[ \frac{H_w b_i^2}{2} \int_0^{\ell_i} \left( \frac{\partial \theta_i}{\partial x_i} \right)^2 dx_i + H(t) b_i \int_0^{\ell_i} \left( \frac{dy_c}{dx_i} \right) \left( \frac{\partial \theta_i}{\partial x_i} \right) dx_i \right] \right\}. \end{aligned} \quad (2.61)$$

The expression in the first set of brackets represents the potential energy stored in the suspended structure, while that in the second set of brackets represents the potential energy stored in the two cables.

Performing the variation with respect to  $\theta_i$ , of Eq. 2.61, and integrating (by parts, where necessary), the following equation is obtained

$$\begin{aligned} \delta V(t) = & \sum_{i=1}^3 \left\{ E_i \Gamma_i \frac{\partial^2 \theta_i}{\partial x_i^2} \delta \left( \frac{\partial \theta_i}{\partial x_i} \right) \Big|_0^{\ell_i} \right. \\ & + \left[ - \frac{\partial}{\partial x_i} \left( E_i \Gamma_i \frac{\partial^2 \theta_i}{\partial x_i^2} \right) + \left( G_i J_i + \frac{H_w b_i^2}{2} \right) \frac{\partial \theta_i}{\partial x_i} + H(t) b_i \left( \frac{dy_c}{dx_i} \right) \right] \delta \theta_i \Big|_0^{\ell_i} \\ & + \int_0^{\ell_i} \left[ \frac{\partial^2}{\partial x_i^2} \left( E_i \Gamma_i \frac{\partial^2 \theta_i}{\partial x_i^2} \right) - \frac{\partial}{\partial x_i} \left( G_i J_i \frac{\partial \theta_i}{\partial x_i} \right) - \frac{\partial}{\partial x_i} \left( \frac{H_w b_i^2}{2} \frac{\partial \theta_i}{\partial x_i} \right) \right. \\ & \left. - H(t) b_i \left( \frac{d^2 y_c}{dx_i^2} \right) \right] \delta \theta_i dx_i \left. \right\} . \end{aligned} \quad (2.62)$$

Noting that  $\frac{d^2 y_c}{dx_i^2} = - \frac{w_i^*}{H_w}$  where  $w_i^*$  is the dead weight (per

cable) per unit length, and introducing Eqs. 2.60 and 2.62 into

Hamilton's Principle (Eq. 2.1) the following is obtained:

$$\begin{aligned}
 & - \sum_{i=1}^3 \int_{t_1}^{t_2} \left\{ \int_0^{\ell_i} \left[ I_{mi} \frac{\partial^2 \theta_i}{\partial t^2} + \frac{\partial^2}{\partial x_i^2} \left( E_i \Gamma_i \frac{\partial^2 \theta_i}{\partial x_i^2} \right) - \frac{\partial}{\partial x_i} \left( G_i J_i \frac{\partial \theta_i}{\partial x_i} \right) - \frac{\partial}{\partial x_i} \left( \frac{H_w b_i^2}{2} \frac{\partial \theta_i}{\partial x_i} \right) \right. \right. \\
 & \quad \left. \left. + H(t) \frac{w_i^* b_i}{H_w} \right] \delta \theta_i dx_i - E_i \Gamma_i \frac{\partial^2 \theta_i}{\partial x_i^2} \delta \left( \frac{\partial \theta_i}{\partial x_i} \right) \Big|_0^{\ell_i} + \left[ \frac{\partial}{\partial x_i} \left( E_i \Gamma_i \frac{\partial^2 \theta_i}{\partial x_i^2} \right) \right. \right. \\
 & \quad \left. \left. - G_i J_i \frac{\partial \theta_i}{\partial x_i} - \frac{H_w b_i^2}{2} \frac{\partial \theta_i}{\partial x_i} - H(t) b_i \left( \frac{dy_c}{dx_i} \right) \right] \delta \theta_i \Big|_0^{\ell_i} \right\} dt = 0 \quad (2.63)
 \end{aligned}$$

Because the integral must vanish for any arbitrary values of  $\delta \theta_i$  and  $\delta \left( \frac{\partial \theta_i}{\partial x_i} \right)$ , these variations can be set equal to zero at  $x_i = 0$  and  $x_i = \ell_i$ ,  $i = 1, 2, 3$ , and equal to values other than zero throughout the domain  $0 < x_i < \ell_i$ . It follows then that the differential equation governing the torsional vibration of the  $i^{\text{th}}$  span in the suspension bridge is

$$\begin{aligned}
 & I_{mi}(x_i) \frac{\partial^2 \theta_i}{\partial t^2} + \frac{\partial^2}{\partial x_i^2} \left( E_i \Gamma_i \frac{\partial^2 \theta_i}{\partial x_i^2} \right) - \frac{\partial}{\partial x_i} \left( G_i J_i \frac{\partial \theta_i}{\partial x_i} \right) - \frac{\partial}{\partial x_i} \left( \frac{H_w b_i^2}{2} \frac{\partial \theta_i}{\partial x_i} \right) \\
 & \quad + H(t) \frac{w_i^* b_i}{H_w} = 0 \quad , \quad i = 1, 2, 3 \quad , \quad (2.64)
 \end{aligned}$$

where

$$H(t) = \frac{A_c E_c}{L_E} \sum_{i=1}^3 \left[ \frac{w_i^* b_i}{2H_w} \int_0^{\ell_i} \theta_i dx_i + \frac{b_i^2}{8} \int_0^{\ell_i} \left( \frac{\partial \theta_i}{\partial x_i} \right)^2 dx_i \right] \quad (2.65)$$

Equations 2.64 and 2.65 are the basic differential and integral equations of the torsional vibration of suspension bridges.

In addition, because of the arbitrary nature of the variation, the last bracketed term and the term preceding it in Eq. 2.63, vanish, and thus the following conditions are obtained:

$$E_i \Gamma_i \frac{\partial^2 \theta_i}{\partial x_i^2} \delta \left( \frac{\partial \theta_i}{\partial x_i} \right) \Big|_0^{\ell_i} = 0, \quad i = 1, 2, 3, \quad (2.66)$$

and

$$\left[ \frac{\partial}{\partial x_i} \left( E_i \Gamma_i \frac{\partial^2 \theta_i}{\partial x_i^2} \right) - G_i J_i \frac{\partial \theta_i}{\partial x_i} - \frac{H_w b_i^2}{2} \frac{\partial \theta_i}{\partial x_i} - H(t) b_i \left( \frac{dy_c}{dx_i} \right) \right] \cdot \delta \theta_i \Big|_0^{\ell_i} = 0, \quad i = 1, 2, 3, \quad (2.67)$$

which take into account the possibility that either

$$E_i \Gamma_i \frac{\partial^2 \theta_i}{\partial x_i^2} = 0 \quad \text{or} \quad \frac{\partial \theta_i}{\partial x_i} = 0 \quad \text{at} \quad x_i = 0, \quad x_i = \ell_i, \quad i = 1, 2, 3, \quad (2.68)$$

and that

$$\frac{\partial}{\partial x_i} \left( E_i \Gamma_i \frac{\partial^2 \theta_i}{\partial x_i^2} \right) - G_i J_i \frac{\partial \theta_i}{\partial x_i} - \frac{H_w b_i^2}{2} \frac{\partial \theta_i}{\partial x_i} - H(t) b_i \left( \frac{dy_c}{dx_i} \right) = 0$$

or  $\theta_i = 0$  at  $x_i = 0, \quad x_i = \ell_i, \quad i = 1, 2, 3. \quad (2.69)$

Equations 2.68 and 2.69 represent the boundary conditions associated with the differential equations of motion for torsionally vibrating suspension bridges. The first part of Eq. 2.68 requires that the direct stress vanish at each end, as in a bridge which has a deck with a free end or a simply supported end (which are free of normal stress). The second part of Eq. 2.68 requires that the warping

be zero at each end of the structure, such as when the ends of the deck are fixed so that the built-in section can neither twist nor warp. The first part of Eq. 2.69 requires that the vibrational resisting torque  $M_{ti}$  which is developed by the vibration of the deck at the ends of each span be equal to the vibrational torque  $M_{tc}$  which is caused by the vertical shear forces in the depressed and elevated cables at the ends of each span.  $M_{ti}$  is expressed by:

$$M_{ti}(x_i, t) = G_i J_i \frac{\partial \theta_i}{\partial x_i} - \frac{\partial}{\partial x_i} \left( E_i \Gamma_i \frac{\partial^2 \theta_i}{\partial x_i^2} \right), \quad i = 1, 2, 3, \quad (2.70)$$

and  $M_{tc}$  by:

$$M_{tc}(x_i, t) = \frac{H_w b_i^2}{2} \left( \frac{\partial \theta_i}{\partial x_i} \right) + H(t) b_i \left( \frac{dy_c}{dx_i} \right), \quad i = 1, 2, 3. \quad (2.71)$$

The second part of Eq. 2.69 requires that there be no twist at the ends, such as when there are fixed or simply supported ends.

Hence, both the natural and geometric boundary conditions of the problem are presented. The above results are general and provide an accurate formulation of the problem which will be useful for analytical study and for understanding the general characteristics of the vibrations.

Three useful simplifications are possible for the general theory. In the first, the equations are linearized, in the second (see Appendix II-d) the solutions are obtained for a simplified case, and, finally in the third, the equations are verified. These three cases are discussed below.

### 1. Linearization

The problem is linearized by neglecting all second-order terms which appear only in the cable equation. This requires that the term

$\frac{b_i^2}{2} \int_0^{\ell_i} \left( \frac{\partial \theta_i}{\partial x_i} \right)^2 dx_i$  be removed from Eq. 2.65. Consequently, the cable

equation reduces to

$$H(t) = \frac{A_c E_c}{L_E} \sum_{i=1}^3 \left[ \frac{w_i^* b_i}{2H_w} \int_0^{\ell_i} \theta_i dx_i \right]. \quad (2.65')$$

### 2. Solutions

The chief aim of this chapter is to derive the equations of motion in a general form and to outline the procedure for determining the frequencies and modes of torsional motion by a finite element approach. But since solutions of the torsional equations of motion are not well known, they have been derived in order to present a complete theory of the free torsional vibrations of suspension bridges. However, because the solutions are lengthy, they have not been included here but are presented in Appendix II-d.

The solutions of the linearized differential equations of motion are given for a three span symmetric suspension bridge in which the stiffening trusses (or girders) of each span are simply supported, with the cables held on top of the towers by roller supports. It is assumed that the mass of the bridge and its elastic properties are uniform along each span. Both mode shapes and natural frequencies for the symmetric and antisymmetric modes are obtained.

### 3. Verification

In what follows, the reliability and validity of the equations of motion and their associated boundary conditions will be examined by considering the dynamic equilibrium of an element  $dx_i$  of the suspension bridge. Fig. II-5 shows a free body diagram for the bridge element  $dx_i$ . The total vibrational torque,  $M_{Ti}$ , acting at the cross section is equal to the vibrational torque,  $M_{ti}$ , developed by the deck plus the vibrational torque,  $M_{tc}$ , caused by the vertical shear forces in the depressed and elevated cables. As seen from Fig. II-5,

$[H_w + H(t)] \frac{\partial}{\partial x_i} (y_c + v_i)$  and  $[H_w - H(t)] \frac{\partial}{\partial x_i} (y_c - v_i)$  are the vertical shear forces in the depressed and elevated cables, respectively. Thus, the vibrational torque,  $M_{tc}$ , at the cross section is

$$M_{tc}(x_i, t) = \frac{b_i}{2} [H_w + H(t)] \frac{\partial}{\partial x_i} (y_c + v_i) - \frac{b_i}{2} [H_w - H(t)] \frac{\partial}{\partial x_i} (y_c - v_i) ,$$

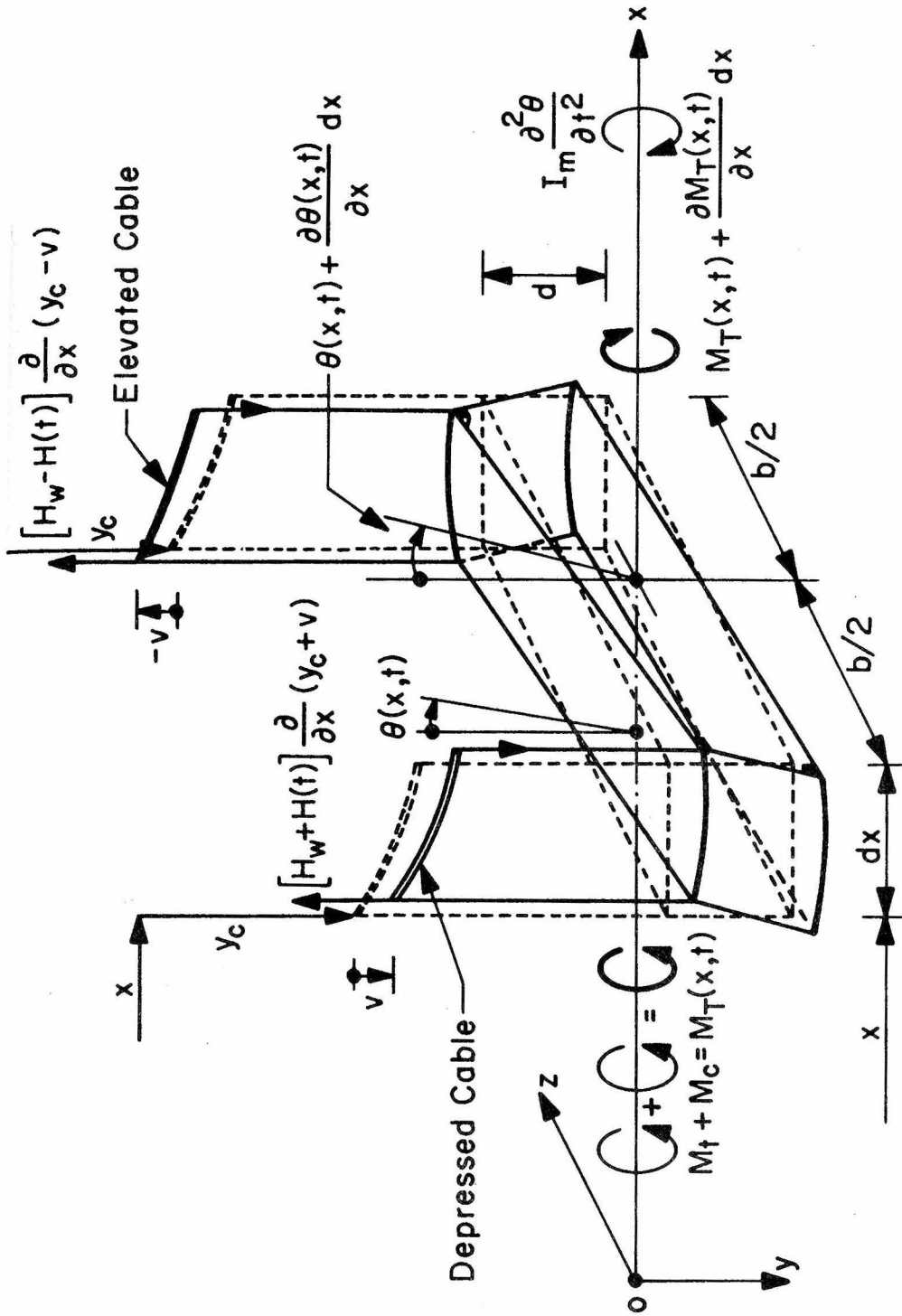
$$i = 1, 2, 3 . \quad (2.72)$$

After substituting  $v_i = \frac{b_i}{2} \theta_i$ , Eq. 2.27 reduces to

$$M_{tc}(x_i, t) = \frac{H_w b_i^2}{2} \frac{\partial \theta_i}{\partial x_i} + H(t) b_i \frac{dy_c}{dx_i} , \quad i = 1, 2, 3 , \quad (2.73)$$

It may be noted that Eq. 2.73 is in exactly the same form as the equation for  $M_{tc}$  obtained from the interpretation of the boundary conditions (Eq. 2.71), and also that the nonlinear terms  $\pm H(t) \frac{b_i}{2} \frac{\partial v_i}{\partial x_i}$  have canceled each other out.

The torque  $M_{ti}$ , which the deck would develop if the cables were absent, is



FREE-BODY DIAGRAM OF A DIFFERENTIAL SEGMENT OF THE BRIDGE

Fig. II-5

$$M_{ti}(x_i, t) = G_i J_i \frac{\partial \theta_i}{\partial x_i} - \frac{\partial}{\partial x_i} \left( E_i \Gamma_i \frac{\partial^2 \theta_i}{\partial x_i^2} \right), \quad i = 1, 2, 3. \quad (2.70')$$

The total torque  $M_{Ti}$  is then given by

$$M_{Ti} = M_{ti} + M_{tc} = G_i J_i \frac{\partial \theta_i}{\partial x_i} - \frac{\partial}{\partial x_i} \left( E_i \Gamma_i \frac{\partial^2 \theta_i}{\partial x_i^2} \right) + \frac{H_w b_i^2}{2} \frac{\partial \theta_i}{\partial x_i} + H(t) b_i \frac{dy_c}{dx_i}, \quad i = 1, 2, 3. \quad (2.74)$$

The equations of the torsional motion can readily be derived by considering the equilibrium of forces acting on the differential segment of the bridge shown in Fig. II-5.

$$\left[ M_{Ti}(x_i, t) + \frac{\partial M_{Ti}(x_i, t)}{\partial x_i} \right] - M_{Ti}(x_i, t) = I_{mi}(x_i) \frac{\partial^2 \theta_i(x_i, t)}{\partial t^2}, \quad i = 1, 2, 3, \quad (2.75)$$

which reduces to

$$\frac{\partial M_{Ti}(x_i, t)}{\partial x_i} = I_{mi}(x_i) \frac{\partial^2 \theta_i(x_i, t)}{\partial t^2}, \quad i = 1, 2, 3. \quad (2.76)$$

In view of Eqs. 2.74 and 2.76 and the relation  $\frac{d^2 y_c}{dx_i^2} = -\frac{w_i^*}{H_w}$ , Eq. 2.76 becomes

$$\frac{\partial}{\partial x_i} \left( G_i J_i \frac{\partial \theta_i}{\partial x_i} \right) - \frac{\partial^2}{\partial x_i^2} \left( E_i \Gamma_i \frac{\partial^2 \theta_i}{\partial x_i^2} \right) + \frac{H_w b_i^2}{2} \frac{\partial^2 \theta_i}{\partial x_i^2} - H(t) \frac{b_i w_i^*}{H_w} = I_{mi} \frac{\partial^2 \theta_i}{\partial t^2}, \quad i = 1, 2, 3, \quad (2.64')$$

which is in precisely the same form as Eq. 2.64, derived by using scalar quantities in a variational form.

II-4. A Finite Element Approach to Torsional Vibrations

I-4-1. Idealization of the structure and the displacement model

The finite-element concept, described in Chapter I, will be used to express the dynamic characteristics of the torsionally vibrating suspension bridge. This approach to the analysis of structural continua frequently provides a convenient and reliable idealization of the system, and it also provides the most convenient means for evaluating structural and inertia properties; it is particularly effective in a digital-computer analysis. In this approach, the bridge is assumed to be divided into the same system of discrete elements which was used in the analysis of vertical vibration; these elements are interconnected only at a finite number of nodal points where both rotations and translations are presented as basic nodal degrees of freedom. Since  $v_i(x_i, t) = \frac{b_i}{2} \theta_i(x_i, t)$ , the vibrational angle of twist  $\theta_i$  can be expressed in terms of the cubic Hermitian polynomials used in Chapter I. Thus

$$\theta_e(\xi_1, \xi_2) = \frac{2}{b_e} v_e(\xi_1, \xi_2) = \frac{2}{b_e} \{f(\xi_1, \xi_2)\}_e^T \{q(t)\}_e$$

$e = 1, 2, \dots, N, \quad (2.77)$

where  $N$  is the total number of elements and  $e$  is an index denoting an element;  $(\xi_1, \xi_2)$  are the normalized coordinates. The vector of interpolating functions  $\{f(\xi_1, \xi_2)\}$  is given by

$$\{f(\xi_1, \xi_2)\}^T = [\xi_1^2(3 - 2\xi_1), -L\xi_1^2\xi_2, \xi_2^2(3 - 2\xi_2), L\xi_1\xi_2^2], \quad (2.78)$$

where  $L$  is the length of an individual element, and  $\{q(t)\}$  is the

vector of nodal displacements.

The structural and inertia properties of the complete structure can now be found by evaluating the properties of the individual finite elements and superposing them appropriately. However, as mentioned in Chapter I, there is a case where evaluation of the interaction between all elements is necessary to formulate the elastic stiffness matrix of the cable.

#### II-4-2. Evaluation of structural-property matrices

##### a. Elastic-stiffness matrix of the chords (or flanges)

The strain energy associated with warping (torsion-bending) which is stored in the four chords (or flanges), Eq. 2.36, may be expressed conveniently in terms of the stiffness matrix (with the aid of the displacement model, Eq. 2.77), as follows:

$$V_{sc}(t) = \frac{1}{2} \sum_{i=1}^3 \left[ \sum_{e=1}^{N_i} \frac{4}{b_e^2} \int_0^L E_e \Gamma_e \left( \{f''\}_e^T \{q\}_e \right)^T \left( \{f''\}_e^T \{q\}_e \right) d\bar{x} \right]. \quad (2.79)$$

Here,  $N_i$  is the total number of elements used to present the  $i^{\text{th}}$  span,  $\bar{x}$  is the horizontal axis of the individual element (note:  $\xi_1 = 1 - \frac{\bar{x}}{L}$  and  $\xi_2 = \frac{\bar{x}}{L}$ ), and  $E_e \Gamma_e$  is the warping rigidity for the element; and is assumed uniform over the entire element.

Eq. 2.79 can be written in a more convenient form as

$$V_{sc}(t) = \frac{1}{2} \sum_{e=1}^N \{q\}_e^T [k_{sc}]_e \{q\}_e, \quad (2.80)$$

where

$N = \sum_{i=1}^3 N_i$  is the total number of elements used to present the entire assembled structure, and

$$[k_{sc}]_e = \frac{4E_e \Gamma_e}{b_e^2} \int_0^L \{f''\}_e \{f''\}_e^T d\bar{x} , \quad (2.81)$$

is the element elastic stiffness matrix associated with warping.

The integration involved in the evaluation of  $[k_{sc}]_e$  can be accomplished as described in Chapter I. The resulting stiffness matrix is

$$[k_{sc}]_e = \frac{4E_e \Gamma_e}{b_e^2 L^3} \begin{bmatrix} 12 & -6L & -12 & -6L \\ -6L & 4L^2 & 6L & 2L^2 \\ -12 & 6L & 12 & 6L \\ -6L & 2L^2 & 6L & 4L^2 \end{bmatrix} . \quad (2.82)$$

The assemblage stiffness matrix and the assemblage nodal displacements are respectively

$$[K_{SC}] = \sum_{e=1}^N [k_{sc}]_e , \quad (2.83)$$

and

$$\{r\} = \sum_{e=1}^N \{q\}_e . \quad (2.84)$$

Now, the total strain energy of the assemblage associated with warping and stored in the chords (or flanges) of the suspended structure may be expressed by

$$V_{sc}(t) = \frac{1}{2} \{r\}^T [K_{SC}] \{r\} , \quad (2.85)$$

Finally, when it is noted that the strain energy stored in a stable structure during any distortion must always be positive, it is evident that

$$\frac{1}{2} \{r\}^T [K_{SC}] \{r\} > 0 \quad . \quad (2.86)$$

Matrices which satisfy this condition, where  $\{r\}$  is any arbitrary non-zero vector, are said to be positive definite. Positive definite matrices, and consequently the stiffness matrices, are nonsingular and can be inverted.

b. Elastic-stiffness matrix of the web system

The strain energy associated with the torsional shear which is stored in the web system of both the vertical and the lateral walls of the bridge deck (Eq. 2.44), can now be expressed conveniently, in terms of the stiffness matrix, as

$$V_{sd}(t) = \frac{1}{2} \sum_{i=1}^3 \left[ \sum_{e=1}^{N_i} \frac{4}{b_e^2} \int_0^L G_e J_e \left( \{f'\}_e^T \{q\}_e \right)^T \left( \{f'\}_e^T \{q\}_e \right) d\bar{x} \right] , \quad (2.87)$$

where  $G_e J_e$  is the torsional rigidity of an element. Simplifying this equation,  $V_{sd}$  can be expressed as

$$V_{sd}(t) = \frac{1}{2} \sum_{e=1}^N \{q\}_e^T [k_{sd}] \{q\}_e \quad , \quad (2.88)$$

where

$$[k_{sd}]_e = \frac{4}{b_e^2} \int_0^L G_e J_e \left( \{f'\}_e \{f'\}_e^T \right) d\bar{x} \quad , \quad (2.89)$$

is the element stiffness matrix associated with St. Venant's uniform torsion. For the special case of a uniform deck segment, the stiffness matrix resulting from Eq. 2.89, when the interpolation functions of Eq. 2.78 are used, may be expressed by

$$[k_{sd}]_e = \frac{2 G_e J_e}{15 b_e^2} \begin{bmatrix} 36 & -3L & -36 & -3L \\ -3L & 4L^2 & 3L & -L^2 \\ -36 & 3L & 36 & 3L \\ -3L & -L^2 & 3L & 4L^2 \end{bmatrix} \quad (2.90)$$

Finally, the assemblage stiffness matrix is

$$[K_{SD}] = \sum_{e=1}^N [k_{sd}]_e \quad , \quad (2.91)$$

and the total strain energy of the assemblage stored in the web system is given by

$$V_{sd}(t) = \frac{1}{2} \{r\}^T [K_{SD}] \{r\} \quad , \quad (2.92)$$

where  $[K_{SD}]$  is a positive definite matrix if one assumes that the boundary conditions have already been incorporated.

c. Gravity-stiffness matrix of the cables

The first term of Eq. 2.53 represents the strainless or gravitational energy of the two cables. The strainless energy,  $V_{cg}(t)$  is given by

$$V_{cg}(t) = \frac{1}{2} \sum_{i=1}^3 \left[ \frac{H_w b_i^2}{2} \int_0^{\ell} \left( \frac{\partial \theta_i}{\partial x_i} \right)^2 dx_i \right] \quad . \quad (2.93)$$

Using the displacement model of Eq. 2.77,  $V_{cg}$  can be expressed in terms of the gravity stiffness matrix to obtain

$$V_{cg}(t) = \frac{1}{2} \sum_{e=1}^N \left[ 2H_w \int_0^L (\{f'\}_e^T \{q\}_e)^T (\{f'\}_e^T \{q\}_e) d\bar{x} \right], \quad (2.94)$$

or equivalently

$$V_{cg}(t) = \frac{1}{2} \sum_{e=1}^N \{q\}_e^T [k_{cg}]_e \{q\}_e, \quad (2.95)$$

where

$$[k_{cg}]_e = 2H_w \int_0^L \{f'\}_e \{f'\}_e^T d\bar{x}, \quad (2.96)$$

is the element gravity-stiffness matrix of the cable; it may also be expressed as

$$[k_{cg}]_e = \frac{H_w}{15L} \begin{bmatrix} 36 & -3L & -36 & -3L \\ -3L & 4L^2 & 3L & -L^2 \\ -36 & 3L & 36 & 3L \\ -3L & -L^2 & 3L & 4L^2 \end{bmatrix} \quad (2.97)$$

Finally, the assemblage gravity stiffness matrix is

$$[K_{CG}] = \sum_{e=1}^N [k_{cg}]_e, \quad (2.98)$$

and the assemblage's potential energy due to gravity (or change of geometry) which is stored in the two cables is given by

$$V_{cg}(t) = \frac{1}{2} \{r\}^T [K_{CG}] \{r\}, \quad (2.99)$$

in which  $[K_{CG}]$  is a positive definite matrix.

d. Elastic-stiffness matrix of the cables

From the second term of Eq. 2.53, the elastic potential energy of the two cables is

$$V_{ce}(t) = \frac{1}{2} \sum_{i=1}^3 \left\{ H(t) b_i \left[ \int_0^{\ell_i} \left( \frac{dy_c}{dx_i} \right) \left( \frac{\partial \theta_i}{\partial x_i} \right) dx_i \right] \right\}, \quad (2.100)$$

where

$$H(t) = \frac{A_c E_c}{L_E} \sum_{i=1}^3 \left[ \frac{w_i^* b_i}{2 H_w} \int_0^{\ell_i} \theta_i dx_i + \frac{b_i^2}{8} \int_0^{\ell_i} \left( \frac{\partial \theta_i}{\partial x_i} \right)^2 dx_i \right]. \quad (2.65')$$

Integrating Eq. 2.100 by parts yields

$$V_{ce}(t) = \frac{1}{2} \sum_{i=1}^3 \left\{ H(t) b_i \left[ \left( \frac{dy_c}{dx_i} \right) \theta_i \Big|_0^{\ell_i} - \int_0^{\ell_i} \left( \frac{d^2 y_c}{dx_i^2} \right) \theta_i dx_i \right] \right\}, \quad (2.101)$$

providing that  $\left( \frac{dy_c}{dx_i} \right)$  and  $\left( \frac{\partial \theta_i}{\partial x_i} \right)$  can be treated as continuous functions of  $x_i$ . Furthermore, because  $\theta_i$  vanishes at the ends where  $x_i = 0$

and  $x_i = \ell_i$ , and because  $\frac{d^2 y_c}{dx_i^2} = -\frac{w_i^*}{H_w}$ , Eq. 2.101 may be reduced to

$$V_{ce}(t) = \frac{1}{2} \sum_{i=1}^3 \left\{ H(t) \left[ \frac{b_i w_i^*}{H_w} \int_0^{\ell_i} \theta_i dx_i \right] \right\}. \quad (2.102)$$

Substitution of Eq. 2.65' into Eq. 2.102, obtains

$$V_{ce}(t) = \frac{1}{2} \sum_{i=1}^3 \left\{ \frac{A_c E_c}{2 L_E} \left[ \left( \frac{b_i w_i^*}{H_w} \int_0^{\ell_i} \theta_i dx_i \right)^2 + \left( \frac{b_i w_i^*}{H_w} \int_0^{\ell_i} \theta_i dx_i \right) \left( \frac{b_i^2}{4} \int_0^{\ell_i} \left( \frac{\partial \theta_i}{\partial x_i} \right)^2 dx_i \right) \right] \right\} \quad (2.103)$$

It may be noted that the first term in Eq. 2.103 represents the linear strain energy, while the second term is the contribution from the nonlinear component of horizontal tension  $H(t)$ .

Now, using the linear part of the strain energy expression (from Eq. 2.103) and the displacement model expression (Eq. 2.77), one obtains

$$V_{ce}(t) \approx \frac{1}{2} \left( \frac{2A_c E_c}{L_E} \right) \sum_{i=1}^3 \left[ \sum_{e=1}^{N_i} \frac{w_e}{H_w} \int_0^L \{f\}_e^T \{q\}_e d\bar{x} \right]^T \left[ \sum_{e=1}^{N_i} \frac{w_e}{H_w} \int_0^L \{f\}_e^T \{q\}_e d\bar{x} \right]. \quad (2.104)$$

Use of the assemblage nodal displacement  $\{r\}$  in Eq. 2.104 yields

$$V_{ce}(t) \approx \frac{1}{2} \left( \frac{2A_c E_c}{L_E} \right) \{r\}^T \left[ \sum_{i=1}^3 \left( \sum_{e=1}^{N_i} \frac{w_e}{H_w} \int_0^L \{f\}_e^T d\bar{x} \right)^T \left( \sum_{e=1}^{N_i} \frac{w_e}{H_w} \int_0^L \{f\}_e^T d\bar{x} \right) \right] \{r\}, \quad (2.105)$$

where  $w_e$  is the total dead weight of the bridge element per unit length for each cable.

As before, in Chapter I, if the vector  $\{\hat{f}\}_e$  is defined as

$$\{\hat{f}\}_e^T = \int_0^L \{f\}_e^T d\bar{x} = \left[ \frac{L}{2}, -\frac{L^2}{12}, \frac{L}{2}, \frac{L^2}{12} \right],$$

and

$$\{\hat{f}\}_{N_i} = \sum_{e=1}^{N_i} \{\hat{f}\}_e, \quad (2.106)$$

then Eq. 2.105 becomes

$$V_{ce}(t) \approx \frac{1}{2} \{r\}^T \left[ \frac{2A_c E_c}{L_E} \left( \sum_{i=1}^3 \frac{w_e}{H_w} \{\hat{f}\}_{N_i} \right) \left( \sum_{i=1}^3 \frac{w_e}{H_w} \{\hat{f}\}_{N_i}^T \right) \right] \{r\} \quad , \quad (2.107)$$

or more conveniently

$$V_{ce}(t) \approx \frac{1}{2} \{r\}^T [K_{CE}] \{r\} \quad , \quad (2.108)$$

where  $[K_{CE}]$  is the assemblage elastic stiffness matrix of the cable defined by

$$[K_{CE}] = \frac{2A_c E_c}{L_E} \left( \sum_{i=1}^3 \frac{w_e}{H_w} \{\hat{f}\}_{N_i} \right) \left( \sum_{i=1}^3 \frac{w_e}{H_w} \{\hat{f}\}_{N_i}^T \right) \quad . \quad (2.109)$$

This matrix is symmetric and is a partially complete matrix (not banded); i. e., the arrays are well distributed over the entire matrix. Thus an interaction exists not only between adjacent elements but also among all elements of the structure.

#### II-4-3. Evaluation of the inertia-property matrix

##### Generalized consistent-mass matrix

The kinetic energy expression (Eq. 2.58), with the aid of the displacement model (Eq. 2.77), gives:

$$T(t) = \frac{1}{2} \sum_{i=1}^3 \left[ \sum_{e=1}^{N_i} I_{me} \frac{4}{b_e^2} \int_0^L \left( \{f\}_e^T \{\dot{q}\}_e \right)^T \left( \{f\}_e^T \{\dot{q}\}_e \right) d\bar{x} \right] \quad , \quad (2.110)$$

where  $I_{me}$  is the equivalent mass polar moment of inertia of the cross

section of an element in the  $i^{\text{th}}$  span per unit length (including the contribution of the two cables). In this case  $I_{me}$  is assumed uniform across the individual element.

Eq. 2.110 may also be written in the form:

$$T(t) = \frac{1}{2} \sum_{i=1}^3 \left[ \sum_{e=1}^{N_i} \{\dot{q}\}_e^T [I_{\theta}]_e \{\dot{q}\}_e \right], \quad (2.111)$$

where  $[I_{\theta}]_e$  is the generalized consistent-mass matrix of the bridge element and is defined by

$$[I_{\theta}]_e = \frac{4I_{me}}{b_e^2} \int_0^L \{f\}_e \{f\}_e^T d\bar{x} \quad (2.112)$$

Upon carrying out the necessary vector multiplications and integrations, this matrix becomes

$$[I_{\theta}]_e = \frac{I_{me} L}{105 b_e^2} \begin{bmatrix} 156 & -22L & 54 & 13L \\ -22L & 4L^2 & -13L & -3L^2 \\ 54 & -13L & 156 & 22L \\ 13L & -3L^2 & 22L & 4L^2 \end{bmatrix} \quad (2.113)$$

When the mass coefficients of the elements of the bridge have been evaluated, the mass matrix of the complete element assemblage can be developed by using the same superposition procedure as that described in developing the deck stiffness matrices from the element stiffnesses. Thus the assemblage generalized consistent-mass matrix

$$[I_{\Theta}] = \sum_{i=1}^3 \left( \sum_{e=1}^{N_i} [I_{\theta}]_e \right) \quad . \quad (2.114)$$

This resulting mass matrix has the same configuration, that is, the same arrangement of nonzero terms, as the deck stiffness matrices.

The total kinetic energy of the system can now be written as

$$T(t) = \frac{1}{2} \{\dot{r}\}^T [I_{\Theta}] \{\dot{r}\} \quad . \quad (2.115)$$

#### II-4-4. Variational formulation of the matrix equation of motion

Inserting the different energy expressions, Eqs. 2.85, 2.92, 2.99, 2.108 and 2.115, into Hamilton's Principle, Eq. 2.1, and then applying the variational operator and integrating by parts obtains the following

$$\int_{t_1}^{t_2} \{\delta r\}^T \left[ [I_{\Theta}] \{\ddot{r}\} + \left( [K_{SC}] + [K_{SD}] + [K_{CG}] + [K_{CE}] \right) \{r\} \right] dt = 0 \quad .$$

Due to the arbitrary nature of the variations in nodal displacement,  $\{\delta r\}$ , the expression in brackets must vanish. Therefore the equations of motion for the assemblage can be obtained in the form

$$[I_{\Theta}] \{\ddot{r}\} + \left( [K_{SC}] + [K_{SD}] + [K_{CG}] + [K_{CE}] \right) \{r\} = \{0\} \quad . \quad (2.116)$$

These are the governing differential equations of the problem. As in the vertical vibration analysis, there are two separate parts of the problem which must be considered. They are:

1. The symmetric modes of vibration in which there are an even number of internal nodes along the center span. Here  $H(t)$  is not zero, and accordingly the stiffness matrix  $[K_{CE}]$  is not a zero matrix.
  2. The antisymmetric modes of vibration which result in an odd number of nodes along the center span. Here  $H(t)$  is zero, and accordingly the stiffness matrix  $[K_{CE}]$  is a null matrix.
- Thus, for the symmetric modes:

$$[K_S] = [K_{SC}] + [K_{SD}] + [K_{CG}] + [K_{CE}] \quad , \quad (2.117)$$

and for the antisymmetric modes:

$$[K_{AS}] = [K_{SC}] + [K_{SD}] + [K_{CG}] \quad . \quad (2.118)$$

Then, the matrix equations for the free undamped symmetric and antisymmetric vibrations of the suspension bridge structure are, respectively:

$$[I_{\Theta}] \{\ddot{r}_S\} + [K_S] \{r_S\} = \{0\} \quad , \quad (2.119-a)$$

and

$$[I_{\Theta}] \{\ddot{r}_{AS}\} + [K_{AS}] \{r_{AS}\} = \{0\} \quad . \quad (2.119-b)$$

By writing the solutions of Eq. 2.119 in the familiar form

$$\{r_S(t)\} = \{r_S^*\} e^{i\omega t} \quad , \quad \{r_{AS}(t)\} = \{r_{AS}^*\} e^{i\omega t} \quad , \quad i = \sqrt{-1} \quad . \quad (2.120)$$

and substituting Eq. 2.120 in Eqs. 2.119 (omitting the common factor  $e^{i\omega t}$ ), the following equations are obtained

$$\left(-\omega^2 [I_{\Theta}] + [K_S]\right) \{r_S^*\} = \{0\} , \quad (2.121-a)$$

and

$$\left(-\omega^2 [I_{\Theta}] + [K_{AS}]\right) \{r_{AS}^*\} = \{0\} , \quad (2.121-b)$$

where  $\{r_S^*\}$  and  $\{r_{AS}^*\}$  are the vectors of the displacement amplitudes (which do not change with time) of both symmetric and antisymmetric vibrations, respectively, and  $\omega$  is the circular frequency.

Then Eqs. 2.121-a and b admit non-trivial solutions if, as is well known,

$$\left\| -\omega^2 [I_{\Theta}] + [K_S] \right\| = 0 , \quad (2.122-a)$$

$$\left\| -\omega^2 [I_{\Theta}] + [K_{AS}] \right\| = 0 . \quad (2.122-b)$$

Eqs. 2.122-a and b are called the frequency equations of the symmetric and antisymmetric vibrations, respectively. Expanding each determinant will give an algebraic equation of the  $N^{\text{th}}$  degree in the frequency parameter  $\omega^2$  for a system having  $N$  degrees of freedom.

Because of the positive definitiveness of  $[I_{\Theta}]$ ,  $[K_S]$  and  $[K_{AS}]$ , the roots  $\omega_1^2$ ,  $\omega_2^2$ , ...,  $\omega_N^2$  (eigenvalues) of each problem are real and positive quantities; Eqs. 1.121-a and b provide non-zero solution vectors  $\{r_S^*\}_i$  and  $\{r_{AS}^*\}_i$  (eigenvectors) for each root  $\omega_i^2$  of the symmetric and antisymmetric problems, respectively.

#### II-4-5. Numerical example

The numerical example is based on computations for the Vincent-Thomas suspension bridge located between San Pedro and Terminal

Island in Los Angeles County, California. An extensive study of this particular bridge, including a complete description, vibration studies and test measurements of the structure, will be presented in Chapter IV; however, the geometry of the bridge and an outline of the structural properties necessary for a torsional vibration study are given by the data below.

Although the frictional resistance between the cables and the saddles of this specific bridge prevents the cables from sliding through the saddles, movement of the tower tops will not be taken into consideration until the subsequent section.

|   |                                      |
|---|--------------------------------------|
| Center span $l_2 = 1,500$ ft.   | Side spans $l_1 = l_3 = 506.5$ ft.   |
| Cable sag $f_2 = 150$ ft.   | $f_1 = f_3 = 17.103$ ft.             |
| Width (center to center of cables)  | $b = 59.17$ ft.                      |
| Depth of stiffening truss (assumed distance between the two lateral systems)  | $d = 15$ ft.                         |
| Dead load on suspended structure (both trusses)                               | $w_s = 6.15$ Kips/ft.                |
| Dead load on cables (both cables)   | $w_c = 0.85$ Kips/ft.                |
| Total dead load of bridge   | $2\bar{w}^* = 7.2$ Kips/ft.          |
| Cable force   | $H_w = 6,750$ Kips/cable.            |
| Cross-sectional area of one cable   | $A_c = 121$ in. <sup>2</sup>         |
| Cross-sectional area of one chord of side span (assumed invariable)           | $A_1 = A_3 = 55.56$ in. <sup>2</sup> |
| Cross-sectional area of one chord of center span (assumed invariable)         | $A_2 = 53.78$ in. <sup>2</sup>       |
| Cross-sectional area of the diagonals of the stiffening truss (average value) | $A_d = 16.9$ in. <sup>2</sup>        |

|   |                             |
|---|-----------------------------|
| Cross-sectional area of the diagonals of the lateral bracings (average value) | $A_d = 16.58 \text{ in.}^2$ |
| Radius of gyration of the cross section                                       | $r_s = 20.3 \text{ ft.}$    |
| Shear modulus of the stiffening truss   | $G = 11,600 \text{ Ksi}$    |
| Modulus of elasticity of the stiffening truss                                 | $E = 29,000 \text{ Ksi}$    |
| Modulus of elasticity of the cable  | $E_c = 27,000 \text{ Ksi}$  |
| Virtual length of the cable   | $L_E = 3,460 \text{ ft.}$   |

The number of elements in the side span,  $N_1 = N_3$ , was taken to be 11 elements; the number of elements in the center span  $N_2$ , was taken to be 28 elements

The computation of the eigenvalues  $\omega_i^2$  and the eigenvectors  $\{r_i^*\}$ , for both the symmetric and the antisymmetric vibrations, is worked out through a Householder method subroutine. A double precision version is available from the Caltech computer program library and is written for the solution of the problem in the standard form  $([A] - \lambda[I])\{x\} = \{0\}$  where  $[A]$  is a real matrix,  $\lambda$  is the eigenvalue,  $[I]$  is the unity matrix and  $\{x\}$  is the eigenvector. Consequently, equations 2.121-a and b must be converted to the standard form by premultiplying each of them by the matrix  $[I_\Theta]^{-1}$ . Thus, a matrix inversion subroutine is also needed, and the final forms of the eigenvalue and eigenvector problem, for both symmetric and antisymmetric vibrations, will be

$$\left( [I_\Theta]^{-1} [K_S] - \omega^2 [I] \right) \{r_S^*\} = \{0\} \quad , \quad (2.121'-a)$$

and

$$\left( [I_\Theta]^{-1} [K_{AS}] - \omega^2 [I] \right) \{r_{AS}^*\} = \{0\} \quad . \quad (2.121'-b)$$

The two eigenvalue problems have been solved on the Caltech digital computer (IBM 370/158 system); some of the computed natural frequencies and periods of symmetric and antisymmetric vibrations are shown in Tables II-1 and II-2 respectively, while Figs. II-6 and II-7 show the modes of torsional vibration for both cases.

To check the effectiveness and reliability of the method of analysis under consideration, a comparison between these results and some previous results is also presented. The first few modes of torsional motion were predicted and the corresponding natural frequencies of the bridge were computed by the Bridge Department of the State of California using the approximate energy method; they were also recorded in a report by Ernest G. Wiles [16]. The following table summarizes this comparison.

|    | Torsional Modes of Vibration | Natural Frequencies cps (Wiles' Report) | Natural Frequencies cps (Tables II-1 & II-2) |
|----|------------------------------|---|--|
| 1. | <u>Symmetric Modes</u>       |   |  |
|    | first                        | 0.46 cps                                | 0.449419 cps                                 |
|    | second                       | 0.66 cps                                | 0.943311 cps                                 |
|    | third                        | 0.95 cps                                | 0.949762 cps                                 |
| 2. | <u>Antisymmetric Modes</u>   |   |  |
|    | first                        | 0.59 cps                                | 0.595927 cps                                 |
|    | second                       | 1.33 cps                                | 0.944303 cps                                 |

Fig. II-8 shows the modes of torsional vibration given in Wiles' report.

From this comparison between Wiles' (predicted) modes (Fig. II-8) and the computed modes (Fig. II-6 and II-7) and from the preceding table, the following observations may be made.

1. The frequency of the first predicted mode (of both symmetric and antisymmetric vibrations) is in very close agreement with that of the computed one, as is the mode shape. This may be explained by the simple configuration of this fundamental mode in both the symmetric and antisymmetric cases.
2. The frequency of the second predicted symmetric mode deviates considerably from the computed one and the mode shapes also disagree. This predicted mode, as shown in Fig. II-8, has the same number of internal nodes along the center span as the third mode of Fig. II-6. However, the positions of these nodes in the two cases are not identical. The computed second mode in Fig. II-6 shows dominant vibration of the side spans with only a slight contribution from the center span.
3. The frequency of the third predicted symmetric mode seems close to the computed one, but at the same time the two mode shapes differ. In the predicted one, this bimodal shape has no nodes along the center span while the computed one has two nodes.
4. The frequency of the second predicted antisymmetric mode agrees with the computed frequency of the third computed mode (in which  $f_3 = 1.36665$  cps), and the two mode shapes are identical. It would seem that the predictions for the antisymmetric case were confined to the center span, because,

apparently, no prediction was made for the second computed mode where the motion of the side spans is dominant.

The distribution of the energy storage capacity in various members of the structure, for both the symmetric and the anti-symmetric cases, is demonstrated in Fig. II-9. From this figure, one can easily extract the most significant dynamic characteristics of the relative contributions of the deck structure and the cables to the total energy storage capacity of the bridge structure at the different modes. The following points are of some interest in this regard:

1. The relative contribution of the strain energy accumulated in the chords builds until, in the high modes, it governs almost all of the potential energy of the structure.
2. For the symmetric case, the strain energy accumulated in the web systems peaks in the second and third modes and then decays, while for the antisymmetric case it begins very high (being significant even in the first mode) and then decays at almost the same rate as for the symmetric case.
3. The relative contribution of the strain energy of the cable to the total energy storage capacity is greatest in the second and fourth symmetric modes, while it is almost zero in the third mode where the positive areas of the deflection curve are canceled by the negative areas. (Note: The additional cable tension  $H(t)$  is proportional to the algebraic sum of the areas under the deflection curve.)

Again, from the symmetric modes of vibration it is easy to recognize that any kind of symmetric-torsional vibration, in particular in the first few modes, causes interaction between the center span and the side spans.

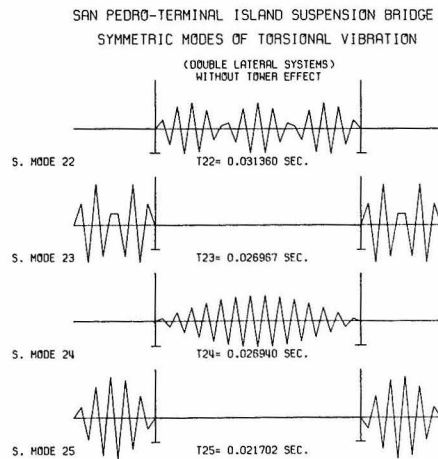
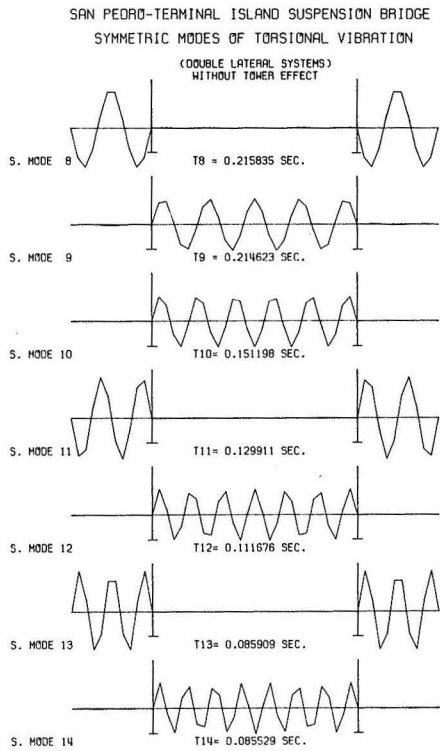
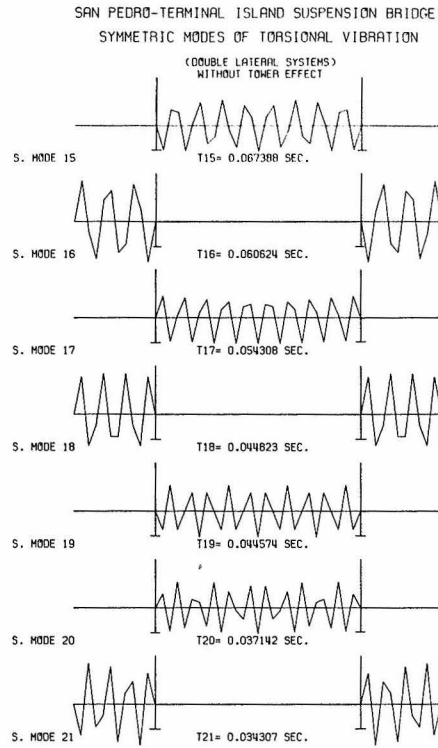
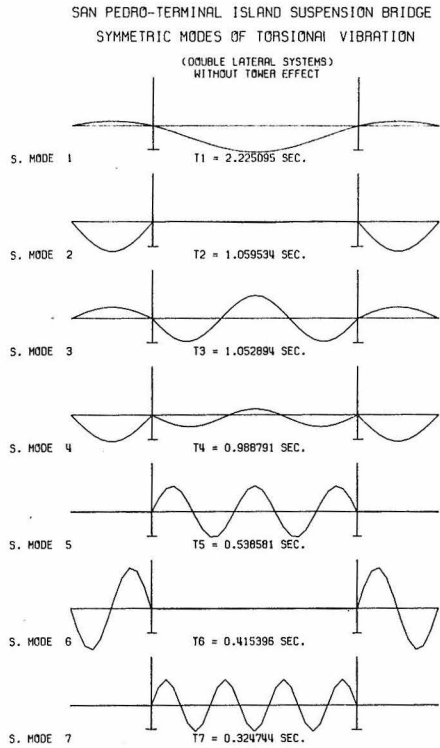


Fig. II-6. Symmetric modes of torsional vibration of the San Pedro-Terminal Island suspension bridge.

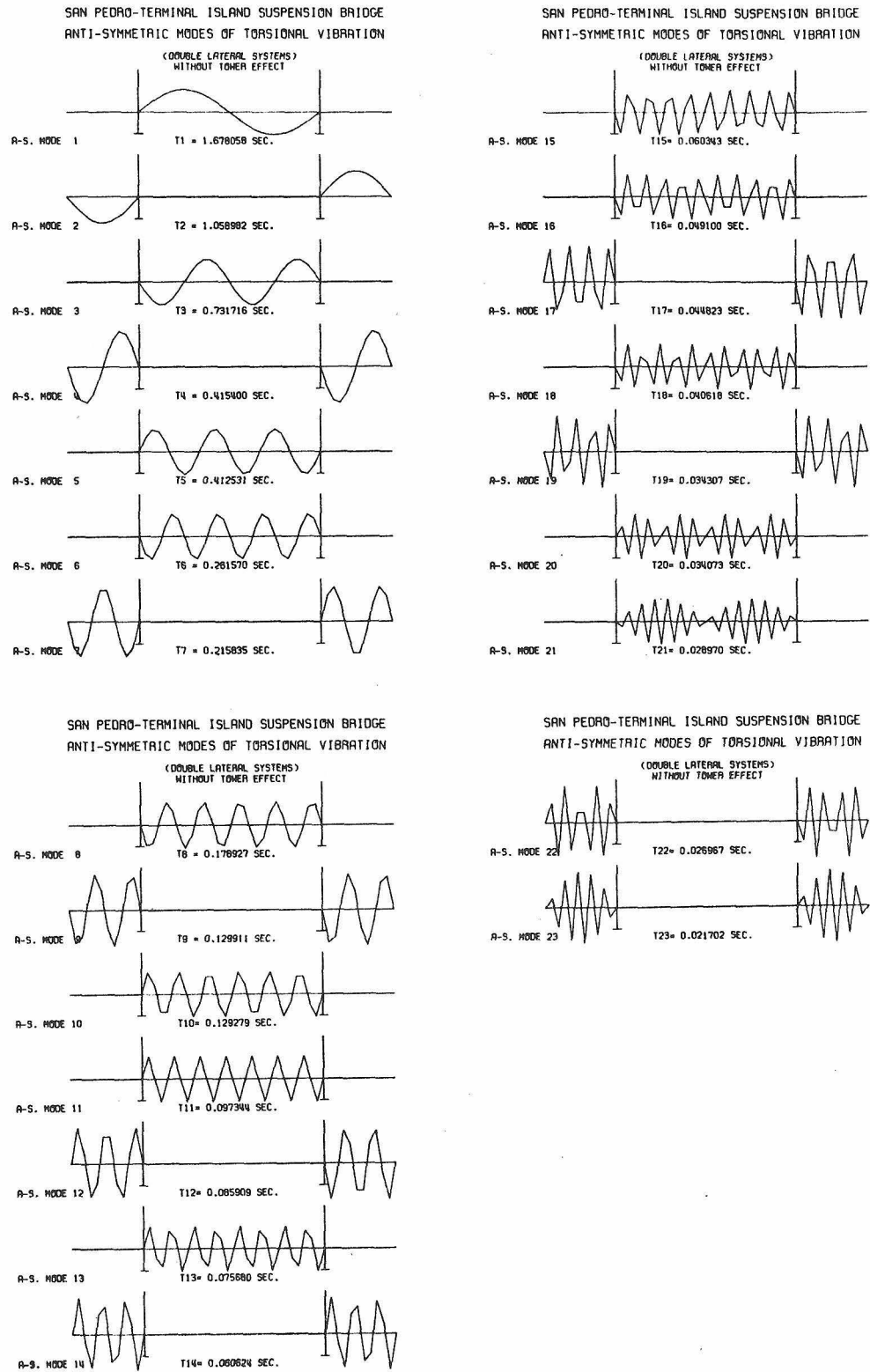
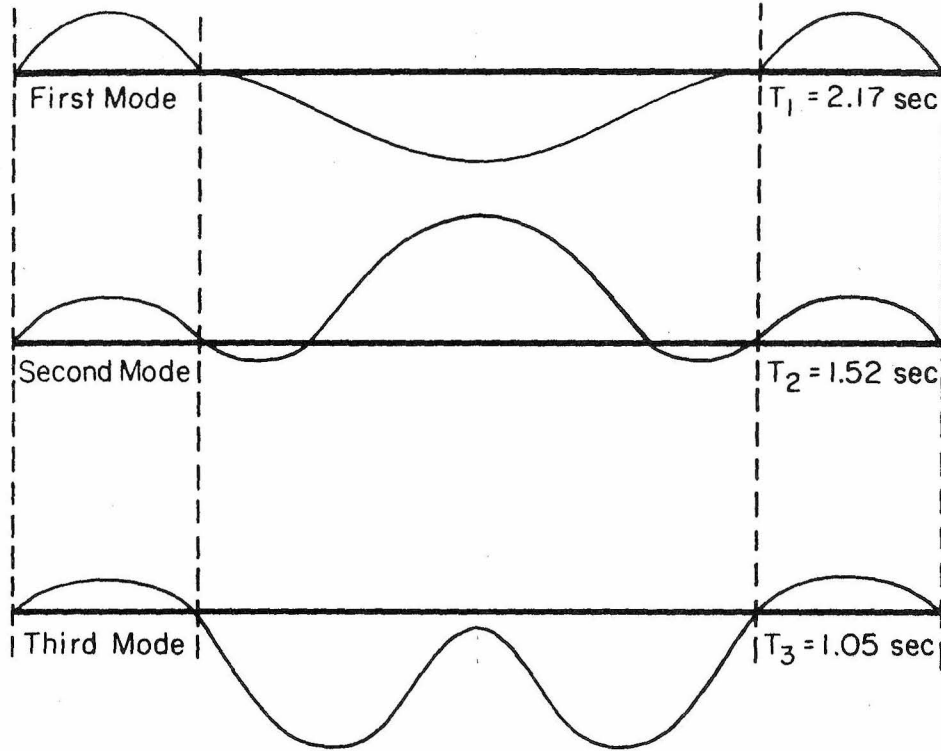
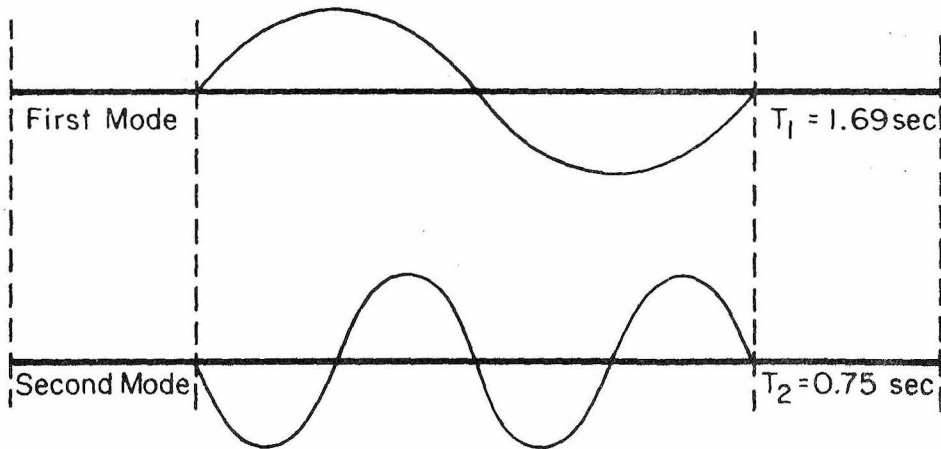


Fig. II-7. Antisymmetric modes of torsional vibration of the San Pedro-Terminal Island suspension bridge.

SYMMETRIC TORSIONAL MODES



ANTI-SYMMETRIC TORSIONAL MODES



PREDICTED TORSIONAL MODES OF THE SAN PEDRO BRIDGE  
(State of California Bridge Department Report)

Fig. II-8

San Pedro-Terminal Island Suspension Bridge  
 Natural Periods and Frequencies of Torsional Vibration  
 (Symmetric Modes)

| Mode Order | Frequency $\omega$<br>rad/sec. | Period T<br>sec. | Frequency f<br>c. p. s. | Member of Dominant Vibration |
|------------|--------------------------------|------------------|-------------------------|------------------------------|
| 1          | 2. 823782                      | 2. 225095        | 0. 449419               | center & side spans          |
| 2          | 5. 930141                      | 1. 059534        | 0. 943311               | side spans                   |
| 3          | 5. 967536                      | 1. 052894        | 0. 949763               | center & side spans          |
| 4          | 6. 354410                      | 0. 988791        | 1. 011336               | center & side spans          |
| 5          | 11. 666183                     | 0. 538581        | 1. 856731               | center span                  |
| 6          | 15. 125776                     | 0. 415396        | 2. 407342               | side spans                   |
| 7          | 19. 348123                     | 0. 324744        | 3. 079349               | center span                  |
| 8          | 29. 111019                     | 0. 215835        | 4. 633163               | side spans                   |
| 9          | 29. 275387                     | 0. 214623        | 4. 659323               | center span                  |
| 10         | 41. 556141                     | 0. 151198        | 6. 613865               | center span                  |
| 11         | 48. 365446                     | 0. 129911        | 7. 697600               | side spans                   |
| 12         | 56. 262482                     | 0. 111676        | 8. 954452               | center span                  |
| 13         | 73. 137340                     | 0. 085909        | 11. 640170              | side spans                   |
| 14         | 73. 462733                     | 0. 085529        | 11. 691957              | center span                  |
| 15         | 93. 238806                     | 0. 067388        | 14. 839417              | center span                  |
| 16         | 103. 641937                    | 0. 060624        | 16. 495127              | side spans                   |
| 17         | 115. 694949                    | 0. 054308        | 18. 413423              | center span                  |
| 18         | 140. 176745                    | 0. 044823        | 22. 309821              | side spans                   |
| 19         | 140. 959612                    | 0. 044574        | 22. 434419              | center span                  |
| 20         | 169. 168520                    | 0. 037142        | 26. 924006              | center span                  |
| 21         | 183. 143410                    | 0. 034307        | 29. 148179              | side spans                   |
| 22         | 200. 359700                    | 0. 031360        | 31. 888237              | center span                  |
| 23         | 232. 994136                    | 0. 026967        | 37. 082168              | side spans                   |
| 24         | 233. 230948                    | 0. 069398        | 37. 119858              | center span                  |
| 25         | 289. 521374                    | 0. 021702        | 46. 078758              | side spans                   |

TABLE II-1

San Pedro-Terminal Island Suspension Bridge  
 Natural Periods and Frequencies of Torsional Vibration  
 (Antisymmetric Modes)

| Mode Order | Frequency $\omega$<br>rad/sec. | Period T<br>sec. | Frequency f<br>c. p. s. | Member of Dominant Vibration |
|------------|--------------------------------|------------------|-------------------------|------------------------------|
| 1          | 3.744319                       | 1.678058         | 0.595927                | center span                  |
| 2          | 5.933231                       | 1.058982         | 0.944303                | side spans                   |
| 3          | 8.586919                       | 0.731716         | 1.366651                | center span                  |
| 4          | 15.125776                      | 0.415396         | 2.407342                | side spans                   |
| 5          | 15.230816                      | 0.412531         | 2.424060                | center span                  |
| 6          | 24.021056                      | 0.261570         | 3.823070                | center span                  |
| 7          | 29.111019                      | 0.215835         | 4.633163                | side spans                   |
| 8          | 35.115879                      | 0.178927         | 5.588866                | center span                  |
| 9          | 48.365446                      | 0.129911         | 7.697597                | side spans                   |
| 10         | 48.601623                      | 0.129279         | 7.735189                | center span                  |
| 11         | 64.545984                      | 0.097344         | 10.272812               | center span                  |
| 12         | 73.137340                      | 0.085909         | 11.640169               | side spans                   |
| 13         | 83.022736                      | 0.075680         | 13.213479               | center span                  |
| 14         | 103.641937                     | 0.060624         | 16.495127               | side spans                   |
| 15         | 104.124277                     | 0.060343         | 16.571893               | center span                  |
| 16         | 127.967338                     | 0.049100         | 20.366634               | center span                  |
| 17         | 140.176750                     | 0.044823         | 22.309822               | side spans                   |
| 18         | 154.688453                     | 0.040618         | 24.619432               | center span                  |
| 19         | 183.143410                     | 0.034307         | 29.148179               | side spans                   |
| 20         | 184.402944                     | 0.034073         | 29.348640               | center span                  |
| 21         | 216.889104                     | 0.028970         | 34.518973               | center span                  |
| 22         | 232.994136                     | 0.026967         | 37.082168               | side spans                   |
| 23         | 289.521374                     | 0.021702         | 46.078758               | side spans                   |

TABLE II-2

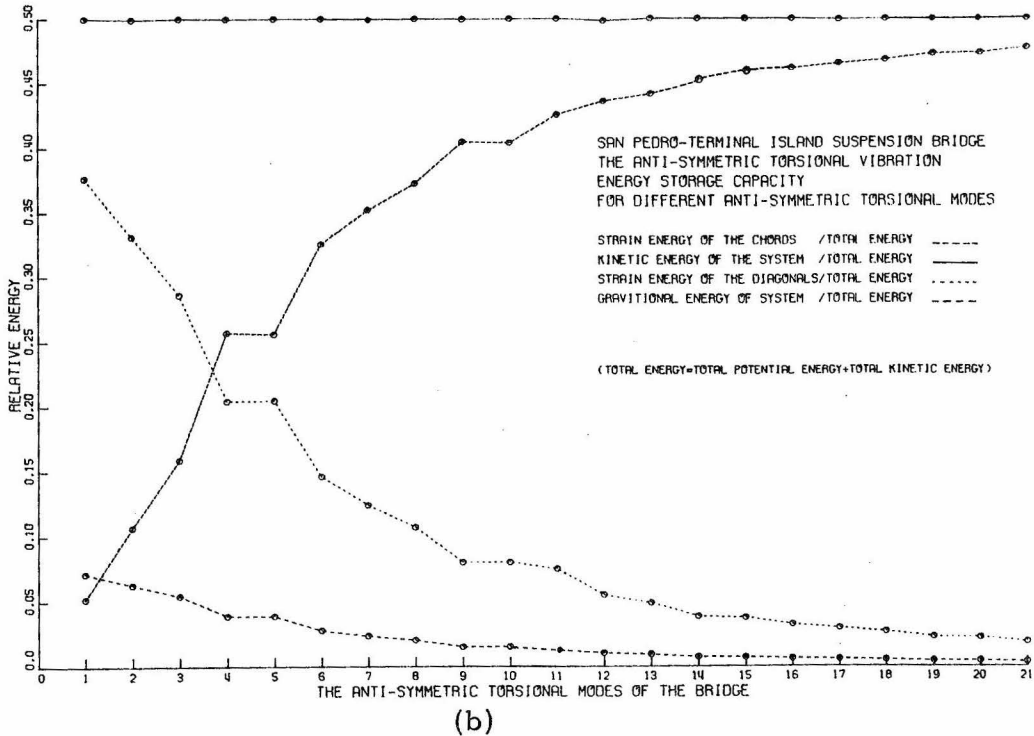
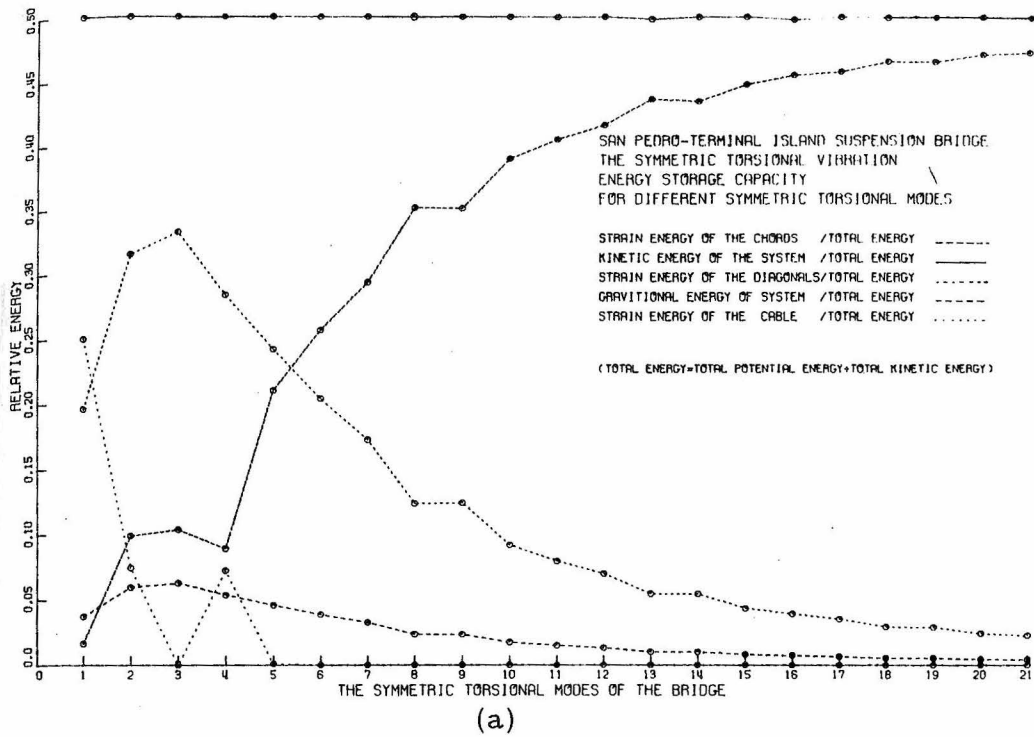


Fig. II-9. Relative energy storage capacity for the San Pedro-Terminal Island suspension bridge (torsional vibration).

II-5. Effect of Torsional Rigidity of the Towers Upon Free Torsional Vibration

In the preceding analysis, it was assumed that the cables either rested on nests of rollers at the tower tops (i. e., on movable saddles) or that the towers were of a rocker type with pin-bearings at the bases. On the whole, however, fixed saddles provide one of the simplest and safest constructions, but the friction forces accompanying the design are so high that the tower tops move in unison with the cables. This results in increments, different in each span, in the horizontal component of cable tension. Furthermore, the towers offer a certain bending and torsional resistance to any horizontal displacement of the top. The effect of this tower resistance upon the dynamic characteristics of a suspension bridge, and the correction for the potential energy stored in the cables, will be considered in this part of the study of torsional vibration.

II-5-1. Correction for strain energy of the cables

To compensate for the fact that the cable tensions due to inertia forces are different in the side spans and the center span, modification of the strain energy of the cables is introduced, for both cables, through the equation

$$\dot{V}_{ce}^* (t) = \frac{1}{2} \left[ \sum_{i=1}^3 H_i(t) b_i \int_0^{\ell_i} \left( \frac{dy_c}{dx_i} \right) \left( \frac{\partial \theta_i}{\partial x_i} \right) dx_i \right], \quad (2.123)$$

where  $H_i(t)$  is the vibrational horizontal component of cable tension in the  $i^{\text{th}}$  span. As in Fig. II-10, if both columns of the two towers

are deflected toward the center span in the vertical plane of the depressed cable, the increment in the horizontal component of cable tension in the center span,  $H_2(t)$ , must equal the sum of the increments in the side spans,  $H_i(t)$ ,  $i = 1, 3$  plus the tower resistance  $R_i$ ,  $i = 1, 3$ . This tower resistance can be expressed as the product of the tower-top movement,  $u'_i(t)$ ,  $i = 1, 3$ , and the elastic resistance  $S_{Ti}$ ,  $i = 1, 3$ .

Recalling the linearized cable equation (Appendix I-b), assuming fixed anchorages, and applying this cable equation successively to the side and center spans, yields

$$u'_i(t) = \frac{H_i(t)L_{ei}}{E_c A_c} - \frac{b_i}{2} \int_0^{\ell_i} \left( \frac{dy_c}{dx_i} \right) \left( \frac{\partial \theta_i}{\partial x_i} \right) dx_i, \quad i = 1, 3, \quad (2.124-a)$$

and

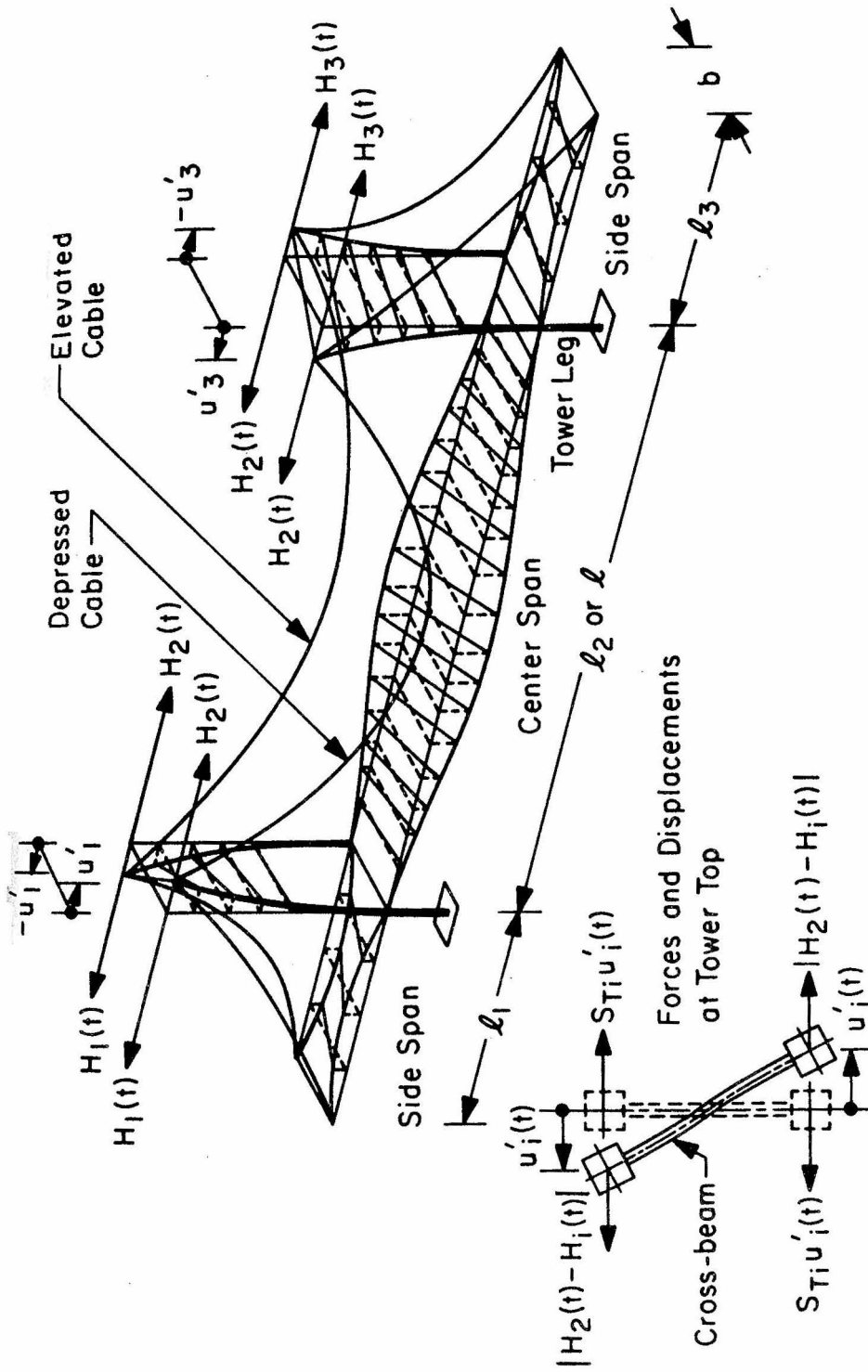
$$-(u'_1(t) + u'_3(t)) = \frac{H_2(t)L_{e2}}{E_c A_c} - \frac{b_2}{2} \int_0^{\ell_2} \left( \frac{dy_c}{dx_2} \right) \left( \frac{\partial \theta_2}{\partial x_2} \right) dx_2. \quad (2.124-b)$$

Therefore, the linearized cable equation for the entire bridge can be written by summing Eqs. 2.124-a and b to give

$$\sum_{i=1}^3 \frac{H_i(t)L_{ei}}{E_c A_c} - \sum_{i=1}^3 \frac{b_i}{2} \int_0^{\ell_i} \left( \frac{dy_c}{dx_i} \right) \left( \frac{\partial \theta_i}{\partial x_i} \right) dx_i = 0. \quad (2.125)$$

Now, from the equilibrium of the horizontal forces at the top of each tower column, the following is obtained

$$\left| H_2(t) - H_i(t) \right| = S_{Ti} u'_i(t), \quad i = 1, 3, \quad (2.126)$$



EFFECT OF TORSIONAL RIGIDITY OF TOWERS UPON FREE  
TORSIONAL VIBRATIONS OF SUSPENSION BRIDGES

Fig. II-10

where  $S_{Ti}$  characterizes the elastic resistance of the tower; it is equal to the force required to deflect the leg (or column) of the  $i^{\text{th}}$  tower by a unit displacement when the other leg is also deflected by a unit displacement in the opposite direction by an equal force. The evaluation of  $S_{Ti}$  is very involved [11] and is best done through the use of the digital computer or through model studies.

Now, to express the horizontal components of cable tension  $H_i(t)$ ,  $i = 1, 2, 3$ , in terms of the vibrational angle of twist,  $\theta_i$ ,  $i = 1, 2, 3$ , the top displacements  $u_1'(t)$  and  $u_3'(t)$  have been eliminated from Eqs. 2.124-a and b, and Eqs. 2.125 and 2.126 have been used, to give

$$H_i(t) = \beta_i \left[ \sum_{j=1}^3 \frac{b_j}{2} \int_0^{\ell_j} \left( \frac{dy_c}{dx_j} \right) \left( \frac{\partial \theta_j}{\partial x_j} \right) dx_j + \alpha_i \frac{b_i}{2} \int_0^{\ell_i} \left( \frac{dy_c}{dx_i} \right) \left( \frac{\partial \theta_i}{\partial x_i} \right) dx_i \right], \quad i = 1, 3, \quad (2.127)$$

where  $\beta_i$  and  $\alpha_i$  are coefficients defined as follows:

$$\beta_i = \frac{(E_c A_c)^2}{(E_c A_c L_E + L_{e2} L_{ei} S_{Ti})} \quad \text{and} \quad \alpha_i = \frac{L_{e2} S_{Ti}}{E_c A_c}, \quad i = 1, 3. \quad (2.128)$$

Substituting Eq. 2.127 into Eq. 2.125 yields:

$$H_2(t) = \beta_i \left[ \left( 1 + \alpha_i \frac{L_{ei}}{L_{e2}} \right) \sum_{j=1}^3 \frac{b_j}{2} \int_0^{\ell_j} \left( \frac{dy_c}{dx_j} \right) \left( \frac{\partial \theta_j}{\partial x_j} \right) dx_j - 2 \alpha_i \frac{L_{ei}}{L_{e2}} \frac{b_i}{2} \int_0^{\ell_i} \left( \frac{dy_c}{dx_i} \right) \left( \frac{\partial \theta_i}{\partial x_i} \right) dx_i \right], \quad i = 1 \text{ or } 3. \quad (2.129)$$

Finally, substituting Eqs. 2.127 and 2.129 into Eq. 2.123 obtains the modified strain energy  $\dot{V}_{ce}^*$  stored in the two cables:

$$\begin{aligned}
 \dot{V}_{ce}^*(t) = & \frac{1}{2} \left\{ \sum_{i=1,3}^3 2\beta_i \left[ \sum_{j=1}^3 \frac{b_j}{2} \int_0^{\ell_j} \left( \frac{dy_c}{dx_j} \right) \left( \frac{\partial \theta_i}{\partial x_j} \right) dx_j \right. \right. \\
 & + \alpha_i \frac{b_i}{2} \int_0^{\ell_i} \left( \frac{dy_c}{dx_i} \right) \left( \frac{\partial \theta_i}{\partial x_i} \right) dx_i \left. \right] \left[ \frac{b_i}{2} \int_0^{\ell_i} \left( \frac{dy_c}{dx_i} \right) \left( \frac{\partial \theta_i}{\partial x_i} \right) dx_i \right] \\
 & + \sum_{i=1,3}^3 \beta_i \left[ \left( 1 + \alpha_i \frac{L_{ei}}{L_{e2}} \right) \sum_{j=1}^3 \frac{b_j}{2} \int_0^{\ell_j} \left( \frac{dy_c}{dx_j} \right) \left( \frac{\partial \theta_i}{\partial x_j} \right) dx_j \right. \\
 & \left. \left. - 2\alpha_i \frac{L_{ei}}{L_{e2}} \frac{b_i}{2} \int_0^{\ell_i} \left( \frac{dy_c}{dx_i} \right) \left( \frac{\partial \theta_i}{\partial x_i} \right) dx_i \right] \left[ \frac{b_2}{2} \int_0^{\ell_2} \left( \frac{dy_c}{dx_2} \right) \left( \frac{\partial \theta_2}{\partial x_2} \right) dx_2 \right] \right\} . \tag{2.130}
 \end{aligned}$$

II-5-2. Potential energy absorbed by the towers

In the vertical vibration analysis presented in Chapter I, the tower stiffness primarily involves the flexural rigidity of the tower legs (or columns). Under torsional vibrations the situation is quite different; resistance to the antisymmetric movement of each leg of a tower can involve flexure and torsion of the leg, and most importantly, flexure of the portal beams (or cross-bracings) between the tower columns. For instance, for the symmetric vibration, the tops of the tower legs undergo horizontal displacement  $u_i'(t)$ ,  $i = 1, 3$ , as illustrated by Fig. I-10 (for the fundamental mode). Since the two legs are connected by relatively stiff horizontal struts, such a displacement is possible only when the tower top rotates about a vertical axis. Thus the two legs are bent and twisted, and the struts are deformed as indicated in Fig. I-10.

The torsional analysis of suspension bridge towers will not be treated here; only the potential energy stored in the towers due to unbalanced top forces will be considered. However, an analytical procedure for torsional analysis of suspension bridge towers can be found in a paper by Baron and Arioto [17].

The potential energy accumulated in one half of a twisted tower acted upon by the top load  $\left| H_2(t) - H_1(t) \right|$ ,  $i = 1, 3$ , is equal to the work done by this top load when the point of application is displaced by a distance  $u'_i(t)$ ,  $i = 1, 3$ . Therefore, the total potential energy,  $V_{te}$ , stored in the two towers, with their four columns supporting the two cables, is

$$V_{te}(t) = 2 \sum_{i=1, 3}^3 \left[ \frac{1}{2} \left| H_2(t) - H_1(t) \right| \cdot u'_i(t) \right], \quad (2.131)$$

where the top load  $\left| H_2(t) - H_1(t) \right|$  is obtained from Eqs. 2.127 and 2.129. For example, for the depressed cable where  $H_2(t) > H_1(t)$ ,  $i = 1, 3$ , the top load takes the form

$$\begin{aligned} [H_2(t) - H_1(t)] = \beta_i \alpha_i \left[ \frac{L_{ei}}{L_{e2}} \sum_{j=1}^3 \frac{b_j}{2} \int_0^{\ell_j} \left( \frac{dy_c}{dx_j} \right) \left( \frac{\partial \theta_j}{\partial x_j} \right) dx_j \right. \\ \left. - \left( 2 \frac{L_{ei}}{L_{e2}} + 1 \right) \frac{b_i}{2} \int_0^{\ell_i} \left( \frac{dy_c}{dx_i} \right) \left( \frac{\partial \theta_i}{\partial x_i} \right) dx_i \right], \quad i = 1, 3. \end{aligned} \quad (2.132)$$

With the aid of Eq. 2.126, Eq. 2.131 can be written in the form

$$V_{te}(t) = \frac{1}{2} \sum_{i=1,3}^3 2 \left[ \frac{|H_2(t) - H_i(t)|^2}{S_{Ti}} \right] , \quad (2.133)$$

and using Eq. 2.132,  $V_{te}$  becomes

$$V_{te}(t) = \frac{1}{2} \left\{ \sum_{i=1,3}^3 2 \frac{\beta_i \alpha_i}{S_{Ti}} \left[ \frac{L_{ei}}{L_{e2}} \sum_{j=1}^3 \frac{b_j}{2} \int_0^{\ell_j} \left( \frac{dy_c}{dx_j} \right) \left( \frac{\partial \theta_j}{\partial x_j} \right) dx_j \right. \right. \\ \left. \left. - \left( 2 \frac{L_{ei}}{L_{e2}} + 1 \right) \frac{b_i}{2} \int_0^{\ell_i} \left( \frac{dy_c}{dx_i} \right) \left( \frac{\partial \theta_i}{\partial x_i} \right) dx_i \right]^2 \right\} . \quad (2.134)$$

The complexity of the resulting differential equations of motion, when this alteration of the potential energy (Eq. 2.130 and 2.134) is added, is so great that it is difficult to deduce any information from them. Accordingly, the analysis will proceed directly to the finite element approach.

II-6. Finite Element Approach to Include the Effect of the Towers

Noting that  $\frac{d^2 y_c}{dx_i^2} = -\frac{\bar{w}_i^*}{H_w}$  (for the parabolic cable), and that

$$\int_0^{\ell_i} \left( \frac{dy_c}{dx_i} \right) \left( \frac{\partial \theta_i}{\partial x_i} \right) dx_i = \frac{dy_c}{dx_i} \theta_i \Big|_0^{\ell_i} - \int_0^{\ell_i} \frac{d^2 y_c}{dx_i^2} \theta_i dx_i = \frac{\bar{w}_i^*}{H_w} \int_0^{\ell_i} \theta_i dx_i \quad ,$$

the energy expressions (Eqs. 2.130 and 2.134) take the following forms

$$\begin{aligned} \bar{V}_{ce}(t) = \frac{1}{2} \left\{ \sum_{i=1,3}^3 \beta_i \left[ \sum_{j=1}^3 \frac{\bar{w}_j^* b_j}{H_w} \int_0^{\ell_j} \theta_j dx_j + \frac{\alpha_i \bar{w}_i^* b_i}{H_w} \int_0^{\ell_i} \theta_i dx_i \right] \left[ \frac{b_i \bar{w}_i^*}{2H_w} \int_0^{\ell_i} \theta_i dx_i \right] \right. \\ \left. + \sum_{i=1,3}^3 \beta_i \left[ \left( 1 + \alpha_i \frac{L_{ei}}{L_{e2}} \right) \sum_{j=1}^3 \frac{b_j \bar{w}_j^*}{2H_w} \int_0^{\ell_j} \theta_j dx_j \right. \right. \\ \left. \left. - \alpha_i \frac{L_{ei}}{L_{e2}} \frac{\bar{w}_i^* b_i}{H_w} \int_0^{\ell_i} \theta_i dx_i \right] \left[ \frac{\bar{w}_2^* b_2}{2H_w} \int_0^{\ell_2} \theta_2 dx_2 \right] \right\} \quad , \quad (2.135) \end{aligned}$$

and

$$\begin{aligned} V_{te}(t) = \frac{1}{2} \left\{ \sum_{i=1,3}^3 2 \frac{\beta_i L_{e2}}{E_c A_c} \left[ \frac{L_{ei}}{L_{e2}} \sum_{j=1}^3 \frac{\bar{w}_j^* b_j}{2H_w} \int_0^{\ell_j} \theta_j dx_j \right. \right. \\ \left. \left. - \left( 2 \frac{L_{ei}}{L_{e2}} + 1 \right) \frac{\bar{w}_i^* b_i}{2H_w} \int_0^{\ell_i} \theta_i dx_i \right]^2 \right\} \quad . \quad (2.136) \end{aligned}$$

II-6-1. Modification of structural-property matrices

a. The modified elastic-stiffness matrix of the cable

With the aid of the displacement model, Eq. 2.77, the modified strain energy, Eq. 2.135, becomes

$$\begin{aligned}
 \dot{V}_{ce}^*(t) = & \frac{1}{2} \left\{ \sum_{i=1,3}^3 \beta_i \left[ \sum_{j=1}^3 \frac{\dot{w}_j b_j}{H_w} \left( \sum_{e=1}^{N_j} \int_0^L \{f\}_e^T \{q\}_e d\bar{x} \right) \right. \right. \\
 & + \left. \left. \frac{\alpha_i \dot{w}_i b_i}{H_w} \left( \sum_{e=1}^{N_i} \int_0^L \{f\}_e^T \{q\}_e d\bar{x} \right) \right]^T \left[ \frac{\dot{w}_i b_i}{2H_w} \left( \sum_{e=1}^{N_i} \int_0^L \{f\}_e^T \{q\}_e d\bar{x} \right) \right] \right. \\
 & + \sum_{i=1,3}^3 \beta_i \left[ \left( 1 + \alpha_i \frac{L_{ei}}{L_{e2}} \right) \sum_{j=1}^3 \frac{\dot{w}_j b_j}{2H_w} \left( \sum_{e=1}^{N_j} \int_0^L \{f\}_e^T \{q\}_e d\bar{x} \right) \right. \\
 & \left. \left. - \alpha_i \frac{L_{ei}}{L_{e2}} \frac{\dot{w}_i b_i}{H_w} \left( \sum_{e=1}^{N_i} \int_0^L \{f\}_e^T \{q\}_e d\bar{x} \right) \right]^T \left[ \frac{\dot{w}_2 b_2}{2H_w} \left( \sum_{e=1}^{N_2} \int_0^L \{f\}_e^T \{q\}_e d\bar{x} \right) \right] \right\}. \quad (2.137)
 \end{aligned}$$

Using the integral and the definition of Eq. 2.106 in this modified energy expression yields

$$\begin{aligned}
 \dot{V}_{ce}^*(t) = & \frac{1}{2} \{r\}^T \left[ \sum_{i=1,3}^3 \beta_i \left( \sum_{j=1}^3 \frac{\dot{w}_j b_j}{H_w} \{f\}_{N_j} + \frac{\alpha_i \dot{w}_i b_i}{H_w} \{f\}_{N_i} \right) \left( \frac{\dot{w}_i b_i}{2H_w} \{f\}_{N_i} \right)^T \right. \\
 & + \sum_{i=1,3}^3 \beta_i \left( \left( 1 + \alpha_i \frac{L_{ei}}{L_{e2}} \right) \sum_{j=1}^3 \frac{\dot{w}_j b_j}{2H_w} \{f\}_{N_j} \right. \\
 & \left. \left. - \alpha_i \frac{L_{ei}}{L_{e2}} \frac{\dot{w}_i b_i}{H_w} \{f\}_{N_i} \right) \left( \frac{\dot{w}_2 b_2}{2H_w} \{f\}_{N_2} \right)^T \right] \{r\}, \quad (2.138)
 \end{aligned}$$

or equivalently

$$\dot{V}_{ce}^*(t) = \frac{1}{2} \{r\}^T [K_{CE}^*] \{r\} \quad , \quad (2.139)$$

where  $[K_{CE}^*]$  is the modified assemblage elastic stiffness matrix of the two cables; it is defined by the matrix resulting from vectorial multiplication of the quantities between brackets in Eq. 2.138.

b. The elastic-stiffness matrix resulting from the contribution of the towers

The portion of the potential energy absorbed by the structure and stored in the towers (Eq. 2.134) can now be expressed in a matrix form by using the displacement model of Eq. 2.78, as follows

$$V_{te}(t) = \frac{1}{2} \left\{ \sum_{i=1,3}^3 2 \frac{\beta_i L_{e2}}{E_c A_c} \left[ \frac{L_{ei}}{L_{e2}} \sum_{j=1}^3 \frac{w_{jbi}^*}{2H_w} \left( \sum_{e=1}^{N_j} \int_0^L \{f\}_e^T \{q\} d\bar{x} \right) - \left( 2 \frac{L_{ei}}{L_{e2}} + 1 \right) \frac{w_{ibi}^*}{2H_w} \left( \sum_{e=1}^{N_i} \int_0^L \{f\}_e^T \{q\}_e d\bar{x} \right) \right]^2 \right\} \quad . \quad (2.140)$$

Expanding and using Eq. 2.106, it becomes

$$V_{te}(t) = \frac{1}{2} \{r\}^T \left[ \sum_{i=1,3}^3 2 \frac{\beta_i L_{e2}}{E_c A_c} \left( \frac{L_{ei}}{L_{e2}} \sum_{j=1}^3 \frac{w_{jbi}^*}{2H_w} \{\hat{f}\}_{N_j} - \left( 2 \frac{L_{ei}}{L_{e2}} + 1 \right) \frac{w_{ibi}^*}{2H_w} \{\hat{f}\}_{N_i} \right) \left( \frac{L_{ei}}{L_{e2}} \sum_{j=1}^3 \frac{w_{jbi}^*}{2H_w} \{\hat{f}\}_{N_j} - \left( 2 \frac{L_{ei}}{L_{e2}} + 1 \right) \frac{w_{ibi}^*}{2H_w} \{\hat{f}\}_{N_i} \right)^T \right] \{r\} \quad , \quad (2.141)$$

or equivalently

$$V_{te}(t) = \frac{1}{2} \{r\}^T [K_{TE}] \{r\} \quad , \quad (2.142)$$

where  $[K_{TE}]$  is the elastic stiffness matrix of the tower and is defined by the matrix between two brackets in Eq. 2.141.

#### II-6-2. Modification of the matrix equation of motion

The assemblage equation of motion for symmetric vibration may now be written as

$$[I_{\Theta}] \{\ddot{r}\} + \left( [K_{SC}] + [K_{SD}] + [K_{CG}] + [K_{CE}^*] + [K_{TE}] \right) \{r\} = \{0\} \quad , \quad (2.143)$$

or more conveniently as

$$[I_{\Theta}] \{\ddot{r}\} + [K_S^*] \{r\} = \{0\} \quad , \quad (2.144)$$

where the symmetric matrix  $[K_S^*]$  is defined through Eq. 2.143, it is a full, real and positive definite matrix of order  $N \times N$   $\left( N = \sum_{i=1}^3 N_i \right)$ .

It is important to note that, in the case of antisymmetric vibration where the center of the cable is not tied to the stiffening girder (or truss), the inertia forces do not produce any stresses in the cables, and no interaction occurs between the center span and the side spans. Hence, the tower remains at rest.

The solutions of Eq. 2.144 can be obtained in the same manner as before. The following computation shows an application of the above analysis, taking into account the effect of the torsional rigidity of the towers upon the free torsional vibration of the suspension bridge.

### II-6-3. Numerical example

To illustrate the effect of the torsional rigidity of cantilever towers upon the dynamic characteristics of suspension bridges, a numerical example has been worked out for the San Pedro-Terminal Island Suspension Bridge. The elastic resistance of the tower,  $S_{Ti}$ ,  $i = 1, 3$ , has been computed by applying Castigliano's second theorem; it is found to be

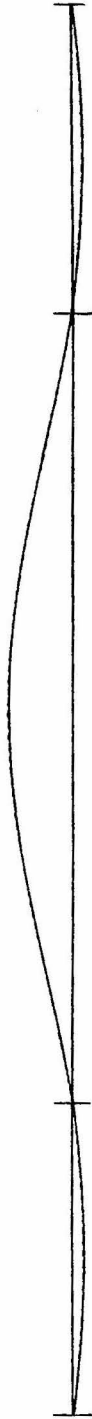
$$S_{T1} = S_{T3} = 235.4323 \text{ Kips/ft.}$$

The eigenvalue problem resulting from the equations of motion (Eq. 2.144), was solved by the Caltech digital computer. Some of the computed natural frequencies of symmetric vibration are shown in Table II-3. Inspection of this table shows that the effect of the torsional rigidity of the towers upon the frequencies of the torsionally vibrating bridge is comparatively small and is limited to only the first few frequencies. Fig. II-11 shows the effect of the torsional rigidity of the towers on the first four mode shapes. The first, third and fourth modes show very slight alteration due to tower effect, but the second mode shows a significant alteration, particularly of the center span amplitudes. Without this tower effect, the second mode has very small amplitudes in the center span; however, when the tower rigidity is taken into consideration, the simultaneous movement of the tower tops toward the center span and the corresponding upward motion of the side spans are reflected in increased center span amplitudes.

SAN PEDRO-TERMINAL ISLAND SUSPENSION BRIDGE

SYMMETRIC MODES OF TORSIONAL VIBRATION

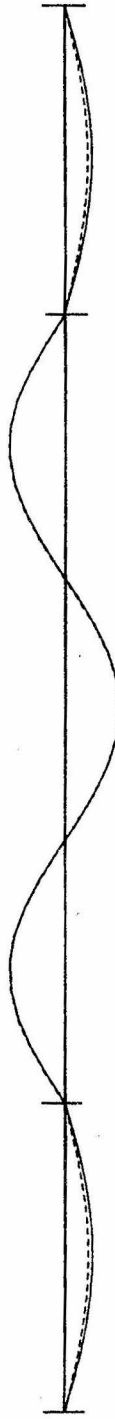
EFFECT OF TORSIONAL RIGIDITY OF TOWERS UPON FREE TORSIONAL VIBRATION OF THE BRIDGE  
(DOUBLE LATERAL SYSTEMS)



FIRST SYMMETRIC MODE — (WITHOUT TOWERS)  $T_1=2.22509544$  SEC. .... (WITH TOWERS)  $T_1=2.19086948$  SEC.



SECOND SYMMETRIC MODE — (WITHOUT TOWERS)  $T_2=1.05953397$  SEC. .... (WITH TOWERS)  $T_2=1.05259694$  SEC.



THIRD SYMMETRIC MODE — (WITHOUT TOWERS)  $T_3=1.05289433$  SEC. .... (WITH TOWERS)  $T_3=1.05181217$  SEC.



FOURTH SYMMETRIC MODE — (WITHOUT TOWERS)  $T_4=0.98879133$  SEC. .... (WITH TOWERS)  $T_4=0.98814557$  SEC.

Fig. II-11

SAN PEDRO-TERMINAL ISLAND SUSPENSION BRIDGE

SYMMETRIC MODES OF TORSIONAL VIBRATION

EFFECT OF TORSIONAL RIGIDITY OF TOWERS UPON FREE TORSIONAL VIBRATION OF THE BRIDGE

(DOUBLE LATERAL SYSTEMS)



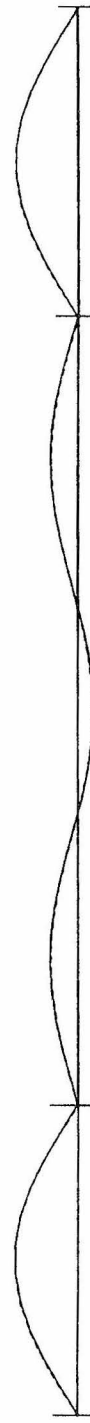
FIRST SYMMETRIC MODE — (WITHOUT TOWERS)  $T_1=2.22509544$  SEC. ----- (WITH TOWERS)  $T_1=2.19086948$  SEC.



SECOND SYMMETRIC MODE — (WITHOUT TOWERS)  $T_2=1.05953397$  SEC. ----- (WITH TOWERS)  $T_2=1.05259694$  SEC.



THIRD SYMMETRIC MODE — (WITHOUT TOWERS)  $T_3=1.05289433$  SEC. ----- (WITH TOWERS)  $T_3=1.05191217$  SEC.



FOURTH SYMMETRIC MODE — (WITHOUT TOWERS)  $T_4=0.98879133$  SEC. ----- (WITH TOWERS)  $T_4=0.98814557$  SEC.

Fig. II-11

TABLE II-3

Effect of the Torsional Rigidity of the Towers  
Upon the Frequencies of the Free Torsional  
Vibration of the San Pedro-Terminal Island Suspension Bridge  
(Symmetric Mode-Shapes)

| Mode Order | No Consideration of Towers<br>(Frequency $\omega$ rad/sec.) | Effect of Tower Elasticity<br>(Frequency $\omega$ rad/sec.) |
|------------|---|---|
| 1          | 2.823782  | 2.867896  |
| 2          | 5.930141  | 5.969224  |
| 3          | 5.967536  | 5.973676  |
| 4          | 6.354410  | 6.358562  |
| 5          | 11.666183   | 11.666594   |
| 6          | 15.125776   | 15.125776   |
| 7          | 19.348123   | 19.348246   |
| 8          | 29.111019   | 29.111410   |
| 9          | 29.275387   | 29.275433   |
| 10         | 41.556141   | 41.556164   |
| 11         | 48.365446   | 48.365446   |
| 12         | 56.262482   | 56.262494   |
| 13         | 73.137340   | 73.137421   |
| 14         | 73.462733   | 73.462740   |
| 15         | 93.238806   | 93.238810   |
| 16         | 103.641937  | 103.641937  |
| 17         | 115.694949  | 115.694952  |
| 18         | 140.176745  | 140.176766  |
| 19         | 140.959612  | 140.959614  |
| 20         | 169.168520  | 169.168521  |
| 21         | 183.143402  | 183.143410  |
| 22         | 200.359700  | 200.359700  |
| 23         | 232.994136  | 232.994143  |
| 24         | 233.230948  | 233.230948  |
| 25         | 289.521374  | 289.521374  |

II-7. Appendices

Appendix II-a

Shear Resistance Coefficients  $\mu_v$  and  $\mu_h$

To determine the value of the shear resistance coefficients  $\mu_v$  and  $\mu_h$  for different types of trusses used in both the stiffening trusses and the lateral bracing systems, shown in Fig. II-2, consider, for convenience, a panel of vertical stiffening truss shown in Fig. II-2 as type 2 (Warren System). This truss is subject to vertical shear force  $S_v$  (with negligible warping). The vertical displacement of the panel at point p due to the elongation  $\Delta\lambda_d$  of the diagonal which is stressed by the force  $S_v/\sin\alpha_1$  and which has the cross-sectional area  $A_d$  is given by

$$\Delta v = \frac{\Delta\lambda_d}{\sin\alpha_1} = \frac{S_v\lambda_d}{EA_d} \frac{1}{\sin^2\alpha_1} = \frac{S_v d}{EA_d} \frac{1}{\sin^3\alpha_1}, \quad (\text{II-a-1})$$

where  $\lambda_d$  is the length of the diagonal,  $\alpha_1$  is the angle of inclination from the horizontal of the diagonal and  $E$  is the modulus of elasticity of the truss material. (Note: In the above equation, the relation  $\lambda_d = d/\sin\alpha_1$  is used where  $d$  is the depth of the truss.)

By considering the displacement line shown in Fig. II-2, it is possible to write

$$\tan\psi_s = \frac{\Delta v}{\lambda_v} = \frac{S_v}{EA_d} \frac{d}{\lambda_v} \frac{1}{\sin^3\alpha_1}; \quad (\text{II-a-2})$$

here  $\lambda_v$  is the panel length. But because  $(d/\lambda_v) = \tan \alpha_1$ , Eq. II-a-2 can be written as

$$\tan \psi_s = \frac{S_v}{G} \frac{G}{EA_d} \frac{1}{\sin^2 \alpha_1 \cos \alpha_1} = \frac{S_v}{G\mu_v}, \quad (\text{II-a-3})$$

where  $G$  is the shear modulus of the truss.

Thus, the shear resistance coefficient,  $\mu_v$ , for this truss is given by

$$\mu_v = \frac{E}{G} A_d \sin^2 \alpha_1 \cos \alpha_1. \quad (\text{II-a-4})$$

Replacing the broken displacement line with a continuous curve,  $\tan \psi_s$  may be replaced at any point of the curve by  $\frac{\partial v}{\partial x}$ ; therefore Eq. II-a-3 becomes

$$\frac{\partial v}{\partial x} = \frac{S_v}{G\mu_v}. \quad (\text{II-a-5})$$

Following the same procedure, the shear resistance coefficients  $\mu_v$  and  $\mu_h$  can easily be obtained for the different patterns of trusses shown in Fig. II-2.

For type 1 of the lateral bracing systems, known as the multiple web system, the force in each diagonal is equal to  $\frac{1}{2}(S_h/\sin \alpha_2)$ , which gives

$$\mu_h = 2 \frac{E}{G} A_d \sin^2 \alpha_2 \cos \alpha_2. \quad (\text{II-a-6})$$

For type 1 of the stiffening trusses, known as the N-system, the vertical displacement of the panel at point P due to the elongation  $\Delta\lambda_d$  of the diagonal and the elongation  $\Delta d$  of the vertical member is given by

$$\Delta v = \frac{\Delta \lambda_d}{\sin \alpha_1} + \Delta d = \frac{S_v d}{EA_d} \frac{1}{\sin^3 \alpha_1} + \frac{S_v d}{EA_v} \quad , \quad (\text{II-a-7})$$

which gives

$$\mu_v = \frac{E}{G} \left( \frac{A_d A_v \sin^2 \alpha_1 \cos \alpha_1}{A_v + A_d \sin^3 \alpha_1} \right) \quad . \quad (\text{II-a-8})$$

From which it can be seen that there is a contribution from the vertical members of that particular system.

Finally, for type 2 of the lateral bracing systems, known as the K-system, the shear resistance coefficient  $\mu_h$  is given by

$$\mu_h = \frac{E}{G} \left( \frac{2A_d A_v \sin^2 \alpha_2 \cos \alpha_2}{A_v + A_d \sin^3 \alpha_2} \right) \quad . \quad (\text{II-a-9})$$

Now, if the stiffening structure is a plate-girder type, then

Eq. II-a-5 can be written as

$$\frac{\partial v}{\partial x} = \frac{S_v}{Gdt} \quad , \quad (\text{II-a-10})$$

which gives  $\mu_v = dt$  ;  $t$  is the thickness of the plate.

Appendix II-b

Longitudinal Warping Displacement

To prove the equivalence of the two expressions for the longitudinal warping displacement,  $u$ , equate the coefficients of similar terms in Eqs. 2.27 and 2.28, as follows

a) coefficients of  $\frac{\partial \theta}{\partial x}$  :

$$\frac{d}{2} \left( \frac{\beta d}{\mu_v} - \frac{b}{2} \right) = \frac{b}{2} \left( \frac{d}{2} - \frac{\beta b}{\mu_h} \right),$$

$$\therefore \beta \left( \frac{d^2}{\mu_v} + \frac{b^2}{\mu_h} \right) = bd \quad ,$$

$$\text{i. e.} \quad \beta = \frac{bd\mu_v\mu_h}{d^2\mu_h + b^2\mu_v} \quad .$$

This is consistent with the definition of the coefficient  $\beta$  defined before by Eq. 2.21

b) coefficient of  $\frac{\partial^3 \theta}{\partial x^3}$  :

$$\frac{bd^2EA\beta}{4\mu_h\mu_vG} \left( \frac{\beta d}{\mu_v} - \frac{b}{2} \right) = \frac{b^2dEA\beta}{4\mu_h\mu_vG} \left( \frac{d}{2} - \frac{\beta b}{\mu_h} \right) \quad ,$$

or

$$\beta \left( \frac{d^2}{\mu_v} + \frac{b^2}{\mu_h} \right) = bd \quad ,$$

giving

$$\beta = \frac{bd\mu_v\mu_h}{d^2\mu_h + b^2\mu_v} \quad .$$

Thus the two expressions for the warping displacement  $u$  are identical.

Appendix II-c

The Warping Constant

The coefficient of  $E_i \frac{\partial^3 \theta_i}{\partial x_i^3}$  in the second term of the expression

for the vibrational torsional moment,  $M_{ti}$ , (Eq. 2.25), is given as

$$\frac{A_i b_i^2 d_i \beta_i}{2 \mu_{hi}} \left( \frac{b_i}{2} - \frac{\beta_i d_i}{\mu_{hi}} \right) + \frac{A_i b_i d_i^2 \beta_i}{2 \mu_{vi}} \left( \frac{d_i}{2} - \frac{\beta_i d_i}{\mu_{vi}} \right), \quad i = 1, 2, 3. \quad (\text{II-c-1})$$

Expanding and rearranging obtains

$$\frac{A_i \beta_i b_i d_i}{4} \left( \frac{b_i^2}{\mu_{hi}} + \frac{d_i^2}{\mu_{vi}} \right) - \frac{A_i \beta_i^2 b_i^2 d_i^2}{\mu_{hi} \mu_{vi}}, \quad i = 1, 2, 3. \quad (\text{II-c-2})$$

Now, upon recalling the definition of the coefficient  $\beta_i$  (Eq. 2.20),

Eq. II-c-2 becomes

$$\frac{A_i b_i^2 d_i^2}{4} - \frac{A_i \beta_i^2 b_i^2 d_i^2}{\mu_{hi} \mu_{vi}},$$

or

$$\frac{A_i b_i^2 d_i^2}{4 \mu_{hi} \mu_{vi}} \left[ \mu_{vi} \mu_{hi} - 4 \beta_i^2 \right], \quad (\text{II-c-3})$$

The warping constant  $\Gamma_i$  resulting from the expression for the strain energy of the chords  $V_{sc}$  and defined by Eq. 2.37, can be rewritten as

$$\Gamma_i = A_i \frac{d_i^2}{2} \left( \frac{\beta_i d_i}{\mu_{vi}} - \frac{b_i}{2} \right)^2 + A_i \frac{b_i^2}{2} \left( \frac{d_i}{2} - \frac{\beta_i b_i}{\mu_{hi}} \right)^2. \quad (\text{II-c-4})$$

Expand and rearrange the terms to get

$$\Gamma_i = \frac{A_i b_i^2 d_i^2}{4} - \frac{A_i \beta_i b_i d_i}{2} \left( \frac{d_i^2}{\mu_{vi}} + \frac{b_i^2}{\mu_{hi}} \right) + \frac{A_i \beta_i^2}{2} \left( \frac{d_i^4}{\mu_{vi}^2} + \frac{b_i^4}{\mu_{hi}^2} \right) . \quad (\text{II-c-5})$$

Again, using the definition of the coefficient  $\beta_i$  from Eq. 2.20,

Eq. II-c-5 takes the form

$$\Gamma_i = \frac{A_i b_i^2 d_i^2}{4} - \frac{A_i \beta_i b_i d_i}{2} \left( \frac{d_i^2}{\mu_{vi}} + \frac{b_i^2}{\mu_{hi}} \right) + \frac{A_i \beta_i^2}{2} \left( \frac{d_i^4}{\mu_{vi}^2} + \frac{b_i^4}{\mu_{hi}^2} \right) - A_i \beta_i^2 \frac{b_i^2 d_i^2}{\mu_{vi} \mu_{hi}} ,$$

$$\therefore \Gamma_i = - \frac{A_i \beta_i b_i d_i}{2} \left( \frac{d_i^2}{\mu_{vi}} + \frac{b_i^2}{\mu_{hi}} \right) + \frac{A_i \beta_i^2}{2} \left( \frac{d_i^4}{\mu_{vi}^2} + \frac{b_i^4}{\mu_{hi}^2} \right) - A_i \beta_i^2 \frac{b_i^2 d_i^2}{\mu_{vi} \mu_{hi}} ,$$

and finally,

$$\Gamma_i = \frac{A_i b_i^2 d_i^2}{4 \mu_{vi} \mu_{hi}} \left( \mu_{vi} \mu_{hi} - 4 \beta_i^2 \right) , \quad (\text{II-c-6})$$

which is identical to Eq. II-c-3. Therefore, the vibrational

torsional moment  $M_{ti}$  can be written, with the aid of Eq. 2.45, as

$$M_{ti} = G_i J_i \frac{\partial \theta_i}{\partial x_i} - E_i \Gamma_i \frac{\partial^3 \theta_i}{\partial x_i^3} , \quad i = 1, 2, 3 . \quad (\text{II-c-7})$$

Thus, the total vibrational twisting moment developed in the deck cross section may be expressed as the sum of two parts – a moment results solely from torsional shearing stresses, it is related to the angle of twist  $\theta_i$  by the relation of the first term of Eq. II-c-7, and a warping torque results from the stresses produced by restrained warping.

Appendix II-d

Solutions of the Differential Equations of Motion

If it is assumed that the mass of the bridge as well as its elastic properties are uniform along the  $i^{\text{th}}$  span, the equations of motion become

$$I_{mj} \frac{\partial^2 \theta_j}{\partial t^2} + E_j \Gamma_j \frac{\partial^4 \theta_j}{\partial x_j^4} - \left( G_j J_j + H_w \frac{b_j^2}{2} \right) \frac{\partial^2 \theta_j}{\partial x_j^2} + H(t) \frac{w_j b_j}{H_w} = 0, \quad j = 1, 2, 3, \quad (\text{II-d-1})$$

with  $H(t)$  as

$$H(t) = \frac{A_c E_c}{L_E} \sum_{j=1}^3 \left[ \frac{w_j b_j}{2H_w} \int_0^{\ell_j} \theta_j dx_j + \frac{b_j^2}{8} \int_0^{\ell_j} \left( \frac{\partial \theta_j}{\partial x_j} \right)^2 dx_j \right]. \quad (\text{II-d-2})$$

It may be further assumed that

$$\theta_j(x_j, t) = \tilde{\theta}_j(x_j) e^{i\omega t}, \quad H(t) = \tilde{H} e^{i\omega t}, \quad j = 1, 2, 3, \quad (\text{II-d-3})$$

in which  $i = \sqrt{-1}$  and  $\omega$  is the natural circular frequency of torsional vibration. Substituting Eq. II-d-3 into Eq. II-d-1, yields the equations of motion in the form

$$-\omega^2 I_{mj} \tilde{\theta}_j + E_j \Gamma_j \frac{d^4 \tilde{\theta}_j}{dx_j^4} - \left( G_j J_j + H_w \frac{b_j^2}{2} \right) \frac{d^2 \tilde{\theta}_j}{dx_j^2} + \frac{w_j b_j}{H_w} \tilde{H} = 0, \quad j = 1, 2, 3. \quad (\text{II-d-4})$$

Because  $\tilde{H}$  is independent of  $x_j$  and may be treated as a constant, Eq. II-d-4 represents linear, ordinary differential equations of the fourth order with constant coefficients. The general solutions of Eq. (IV-4) are nonhomogeneous differential equations and are expressed as

$$\tilde{\theta}_j(x_j) = C_1 \sinh \lambda_j x_j + C_2 \cosh \lambda_j x_j + C_3 \sin \mu_j x_j + C_4 \cos \mu_j x_j + \frac{w_j b_j \tilde{H}}{\omega^2 H_w I_{mj}},$$

$$j = 1, 2, 3, \quad (\text{II-d-5})$$

where

$$\lambda_j = \frac{\Phi_j}{\ell_j} \sqrt{\frac{Z_j + 1}{2}}, \quad \mu_j = \frac{\Phi_j}{\ell_j} \sqrt{\frac{Z_j - 1}{2}}, \quad \Phi_j = \ell_j \sqrt{\frac{(G_j J_j + H_w \frac{b_j^2}{2})}{E_j I_j}}$$

and

$$Z_j = \sqrt{1 + \frac{4 I_{mj} \ell_j^2 \omega^2}{\Phi_j^2 (G_j J_j + H_w \frac{b_j^2}{2})}} \quad j = 1, 2, 3, \quad (\text{II-d-6})$$

$C_1$ ,  $C_2$ ,  $C_3$  and  $C_4$  are arbitrary constants and are determined in conformity with the boundary conditions of the vibrating structure; i. e., the boundary conditions at the supports of the  $j^{\text{th}}$  stiffening girder (or truss). The first four terms of Eq. II-d-5 represent the general solutions of the homogeneous equations ( $\tilde{H} = 0$ ), while the last term of the same equation represents the particular solutions of the complete differential equations.

The cable equation, Eq. II-d-2, which relates the elastic and geometric compatibility of the cable, is expressed, to the first order of small quantities, as:

$$\tilde{H} = \frac{A_c E_c}{L_E} \sum_{j=1}^3 \left[ \frac{w_j b_j}{2 H_w} \int_0^{\ell_j} \tilde{\theta}_j(x_j) dx_j \right]. \quad (\text{II-d-7})$$

It is convenient to separate the investigation of the symmetric modes from that of the antisymmetric modes; i. e., the problem can be divided into two parts:

1. The symmetric modes of vibration in which there are an even number of internal nodes along the center span. Here  $\tilde{H}$  is not zero.
2. The antisymmetric modes of vibration which result in an odd number of internal nodes along the center span. Here  $\tilde{H}$  is zero.

Symmetric Modes of Torsional Vibration

When the bridge is a three-span, symmetric type in which the stiffening structures of each span are simply supported by cables held on top of the towers by roller supports, the boundary conditions are:

$$\begin{array}{l}
 \text{for } x_j = 0 : \quad \tilde{\theta}_j = 0 ; \text{ and } E_j \Gamma_j \frac{d^2 \theta_j}{dx_j^2} = 0 \\
 \text{and} \\
 \text{for } x_j = l_j : \quad \tilde{\theta}_j = 0 ; \text{ and } E_j \Gamma_j \frac{d^2 \theta_j}{dx_j^2} = 0
 \end{array}
 \left. \vphantom{\begin{array}{l} \text{for } x_j = 0 : \\ \text{and} \\ \text{for } x_j = l_j : \end{array}} \right\} j = 1, 2, 3 ,$$

(II-d-8)

expressing the fact that the angle of twist and the normal stress are zero at the supports of each span. Therefore, modes of the symmetric vibration become

$$\begin{aligned} \tilde{\theta}_i(x_i) = \frac{\tilde{w}_i^* b_i \tilde{H}}{2 \omega^2 I_{mi} Z_i H_w} & \left\{ 2 Z_i + (Z_i - 1) \left[ \tanh \frac{\Phi_i \sqrt{Z_i + 1}}{2 \sqrt{2}} \sinh \frac{\Phi_i \sqrt{Z_i + 1}}{\sqrt{2}} \cdot \frac{x_i}{l_i} \right. \right. \\ & - \left. \left. \cosh \frac{\Phi_i \sqrt{Z_i + 1}}{\sqrt{2}} \cdot \frac{x_i}{l_i} \right] - (Z_i + 1) \left[ \tan \frac{\Phi_i \sqrt{Z_i - 1}}{2 \sqrt{2}} \sin \frac{\Phi_i \sqrt{Z_i - 1}}{\sqrt{2}} \cdot \frac{x_i}{l_i} \right. \right. \\ & \left. \left. + \cos \frac{\Phi_i \sqrt{Z_i - 1}}{\sqrt{2}} \cdot \frac{x_i}{l_i} \right] \right\} \quad i = 1, 3, \text{ i. e., for side spans,} \end{aligned} \quad (\text{II-d-9})$$

and

$$\begin{aligned} \tilde{\theta}_2(x_2) = \frac{\tilde{w}_2^* b_2 \tilde{H}}{2 \omega^2 I_{m2} Z_2 H_w} & \left\{ 2 Z_2 - (Z_2 - 1) \operatorname{sech} \frac{\Phi_2 \sqrt{Z_2 + 1}}{2 \sqrt{2}} \cosh \frac{\Phi_2 \sqrt{Z_2 + 1}}{\sqrt{2}} \cdot \frac{x_2}{l_2} \right. \\ & \left. - (Z_2 + 1) \sec \frac{\Phi_2 \sqrt{Z_2 - 1}}{2 \sqrt{2}} \cos \frac{\Phi_2 \sqrt{Z_2 - 1}}{\sqrt{2}} \cdot \frac{x_2}{l_2} \right\}, \end{aligned} \quad (\text{II-d-10})$$

for the center span.

Finally, substituting Eqs. II-d-10 and II-d-9 in Eq. II-d-7 in order to obtain the frequency equation, the following characteristics equation is obtained

$$\begin{aligned} \frac{L_E}{E_c A_c} = \sum_{i=1}^3 & \left\{ \left( \frac{\tilde{w}_i^* b_i}{H_w} \right)^2 \cdot \frac{\sqrt{2} l_i^2}{\left( G_i J_i + H_w \frac{b_i^2}{2} \right)} \cdot \frac{1}{\Phi_i^3 Z_i (Z_i - 1)} \left[ \sqrt{2} Z_i \Phi_i \right. \right. \\ & \left. \left. - \frac{Z_i + 1}{\sqrt{Z_i - 1}} \tan \left( \frac{\Phi_i \sqrt{Z_i - 1}}{2 \sqrt{2}} \right) - \frac{Z_i - 1}{\sqrt{Z_i + 1}} \tanh \left( \frac{\Phi_i \sqrt{Z_i + 1}}{2 \sqrt{2}} \right) \right] \right\}. \end{aligned} \quad (\text{II-d-11})$$

Antisymmetric Modes of Torsional Vibration

An antisymmetric vibrational deflection of the cable and of the stiffening girder causes no additional cable tension  $\tilde{H}$ . Therefore, there is no interaction between the center span and the side spans. For this reason, two types of independent vibration in a three-span bridge are possible.

The boundary conditions for the center span are:

$$\left. \begin{aligned} \text{for } x_2 = 0 : \quad & \tilde{\theta}_2 = 0; \quad \text{and} \quad E_2 \Gamma_2 \frac{d^2 \tilde{\theta}_2}{dx_2^2} = 0, \\ \text{and} \\ \text{for } x_2 = \frac{l_2}{2} : \quad & \tilde{\theta}_2 = 0; \quad \text{and} \quad E_2 \Gamma_2 \frac{d^2 \tilde{\theta}_2}{dx_2^2} = 0 \end{aligned} \right\} \text{ (II-d-12)}$$

The second part of Eq. II-d-12 indicates that the center of the span remains at rest and that an inflexion point of the deflection curve does exist.

After dropping the last term, depending on  $\tilde{H}$  in Eq. II-d-5, and using Eq. II-d-12, the frequency equation is derived in the form

$$\sin\left(\frac{\mu_2 l_2}{2}\right) = 0 \quad , \quad \text{(II-d-13)}$$

from which may be derived

$$\mu_2 l_2 = 2 n \pi \quad (n = 1, 2, 3, \dots) \quad .$$

The characteristic value  $Z_2$  is obtained from the second equation of (II-d-6)

$$Z_2 = \frac{2\mu_2^2 \ell_2^2}{\Phi_2^2} + 1 = 1 + \frac{8n^2 \pi^2}{\Phi_2^2}$$

Substituting this in the last equation (II-d-6), the natural circular frequency for the center span is determined:

$$\omega_{2n} = \frac{2n\pi}{\ell_2} \sqrt{\frac{1}{I_{m2}} \left[ \left( G_2 J_2 + H_w \frac{b_2^2}{2} \right) + \frac{4n^2 \pi^2 E_2 I_2}{\ell_2^2} \right]} \quad n = 1, 2, 3, \dots \quad (\text{II-d-14})$$

The antisymmetric modes are given by

$$\tilde{\theta}_{2n}(x_2) = C_{3n} \sin \frac{2n\pi x_2}{\ell_2}, \quad n = 1, 2, 3, \dots \quad (\text{II-d-15})$$

In a similar way, the frequency equation for any side span is found to be  $\sin \mu_i \ell_i = 0$ ,  $i = 1, 3$ . Therefore,

$$\tilde{\theta}_{in}(x_i) = C_{in} \sin \frac{n\pi x_i}{\ell_i}, \quad i = 1, 3, \quad n = 1, 2, 3, \dots \quad (\text{II-d-16})$$

and the natural circular frequency is determined by

$$\omega_{in} = \frac{n\pi}{\ell_i} \sqrt{\frac{1}{I_{mi}} \left[ \left( G_i J_i + H_w \frac{b_i^2}{2} \right) + \frac{n^2 \pi^2 E_i I_i}{\ell_i^2} \right]}, \quad i = 1, 3, \quad n = 1, 2, 3, \dots \quad (\text{II-d-17})$$

REFERENCES OF CHAPTER II

1. Argyris, J.H. and Kelsey, S., Energy Theorems and Structural Analysis, Butterworths, London, 1960, pp. 11, 36-43.
2. Bleich, F. and Bleich, H., "Bending, Torsion and Buckling of Bars Composed of Thin Walls," International Association of Bridge and Structural Engineering, Second Congress, Berlin-Munich, Oct. 1936, V3, pp. 871-894.
3. Bleich, F., McCullough, C. B., Rosecrans, R. and Vincent, G. S., The Mathematical Theory of Vibration in Suspension Bridges, U. S. Government Printing Office, 1950, pp. 135-186.
4. Green, W. L. and Gill, S. S., "Torsion of a Constrained Rectangular Box Section," Aircraft Engineering, Vol. XXVI, 1954, pp. 34-40.
5. Irvine, H.M., "Torsional Analysis of Boxgirder Suspension Bridges," Journal of the Structural Division, A. S. C. E., ST4, April 1974, pp. 789-812.
6. Irvine, H.M., "Torsional Vibrations in Boxgirder Suspension Bridges," Earthquake Engineering and Structural Dynamics, Vol. 3, 1974, pp. 203-214.
7. Kollbrunner, C. F. and Basler, Torsion, Springer-Verlag, Berlin, 1966 (in German), pp. 19-22, 156-158.
8. Rannie, W. D., The Failure of the Tacoma Narrows Bridge, Board of Engineers, O. H. Amman, T. von Kármán, G. B. Woodruff, Federal Works Agency, Appendix VI, March 28, 1941.
9. Selberg, A., Oscillation and Aerodynamic Stability of Suspension Bridges, Acta Polytechnica Scandinavia, 1961, pp. 308-377.
10. Sih, Nan-sze, "Torsion Analysis for Suspension Bridges," Journal of the Structural Division, A. S. C. E., Vol. 83, No. ST6, Proc. Paper 1431, Nov. 1957, pp. 1-8.
11. Smith, F. and Vincent G. S., The Aerodynamic Stability of Suspension Bridges with Special Reference to the Tacoma Narrows Bridge, Bull. No. 116, Part II, "Mathematical Analysis," Univ. of Washington Engineering Experiment Station (1949-1954).
12. Steinman, D. B., A Practical Treatise on Suspension Bridges, John Wiley & Sons, Inc., New York, 1922, pp. 69-118.

13. Steinman, D. B., "Modes and Natural Frequencies of Suspension Bridge Oscillations," Journal of the Franklin Institute, Philadelphia, U. S. A., Sept. 1959, pp. 148-174.
14. Washizu, K., Variational Methods in Elasticity and Plasticity, Pergamon Press Ltd., 2nd edition, 1975, pp. 303-305.
15. Williams, D., Theory of Aircraft Structures, Edward Arnold Ltd., London, 1960, pp. 235-241.
16. Wiles, E.G., "Report of Aerodynamic Studies on Proposed San Pedro-Terminal Island Suspension Bridge, California," Bridge Research Branch, Division of Physical Research, Bureau of Public Roads, U. S. Department of Commerce, 1960.
17. Baron, F. and Arioto, A., "Torsional Analysis of Suspension Bridge Towers," Journal of the Structural Division, A. S. C. E., ST1, Jan. 1960, pp. 143-169.

## CHAPTER III

### FREE LATERAL VIBRATIONS OF SUSPENSION BRIDGES

#### III-1. Introduction

The great span length of suspension bridges makes their static and dynamic behavior under the action of lateral forces an important engineering problem. The most significant lateral forces are due to wind and to earthquakes. In the literature, little can be found on the subject of lateral vibrations in suspension bridges, although many studies deal extensively with the subject of vertical vibrations (as seen in Chapter I). There have been few publications in recent decades dealing with the lateral rigidity of suspension bridges under wind loading, but there have been at least three investigations [6, 7, 8] on lateral vibrations and earthquake resistant design of these structures.

Lateral forces such as horizontal wind pressures, when acting on a suspension bridge, are sustained by the cables and the suspended structure, which transmit the resulting reactions to the towers and abutments or piers. The hangers, which connect the stiffening structure to the cables, cause the two loaded systems to interact so that the deformation of one system exerts an influence on the other. For instance, compared with the suspended structure, the cables

themselves offer only a small exposed area to wind pressure, but part of the forces which act on the suspended structure are transmitted through the inclined hangers to the cables. The magnitude of the transmitted forces depends on the respective stiffnesses of the two systems and on the ratio of the wind forces acting on them.

Methods of analysis of suspension bridges subject to lateral wind forces acting as static loads were derived by Moisseiff, et al. [1], Silverman [3], Erzen, et al. [5], and Selberg [2]. In these studies, the lateral bending of a suspension bridge is examined, considering the combined influence of the suspended structure and the cables by distributing the wind load between the two systems. In general, these investigations showed clearly how the cables, hangers, and suspended structures participate and cooperate in resisting lateral forces. Also, the numerical results obtained in these investigations revealed previously unknown characteristics of the static behavior of suspension bridges, and formed a good starting point for the study of the dynamic behavior of these structures.

The first attempt at investigation of the free lateral vibration of suspension bridges was made by Silverman [3] in 1957. He proposed a formula, based on a Fourier series solution, for calculating the natural frequencies, but some of his assumptions about the coupling between the cables and the suspended structure are questionable. In 1958, Selberg [4] found that Silverman's analysis gave an incorrect equation of motion. Selberg corrected the equation of motion to include

the interaction between the cables and the suspended structure and, using a Fourier series solution, obtained formulas for the natural frequencies.

In the early 1960's, Ito, Hirai, Okumura and Narita [6, 7, 9] undertook an extensive investigation of the lateral rigidity of a suspension bridge subjected to static lateral loads and to foundation-motion. In their publications, they discuss the free lateral vibration of the bridge and its bending deformations due to lateral loads, both theoretically and experimentally. They applied an approximate method of analysis (the Ritz-method) to the equations of motion already derived by Selberg [4], and thus obtained frequency equations. Then, they developed these equations to include the effect of the upward deflection of the cables and the suspended structure which accompanies the lateral movement. Their analysis is an improvement over that of Selberg, but they were careful to point out that further improvements were required.

Despite the foregoing efforts, an entirely satisfactory vibration problem has not yet been derived. It would appear that the most promising direction of research on this problem would be to utilize the capabilities of the digital computer. The first use of a digital computer in approaching this problem, by Konishi and Yamada [8], achieved significant results. Their vibrational analysis was based on a lumped-mass and spring system representing a one-span suspension bridge. Natural periods and mode shapes were obtained, and it was found that some of their modes did not agree with those predicted by the approximate methods of Selberg [4] and Ito, et al. [7].

In the following study, methods of analysis are developed employing a digital computer and the finite-element technique. The objective of the study is to determine a sufficient number of natural frequencies and mode-shapes to enable an accurate analysis to be made for practical purposes. The problem is linearized by restricting the amplitudes of vibration to be small. Free lateral vibrations are investigated using the same procedures employed in the analyses of vertical and torsional vibrations. The governing differential equations of motion of the cable and of the suspended structure are derived first, using Hamilton's Principle. These equations include the effect of upward deflections associated with lateral movements; that is, the pendulum action of the cable and suspended structure is taken into account. The study uses a matrix discrete method based on a finite-element idealization, as in Chapters I and II. A numerical example is presented as verification of the analysis. This method appears to be the simplest and most practical thus far developed for calculating the natural frequencies and mode shapes required for a satisfactory analysis of a laterally vibrating suspension bridge.

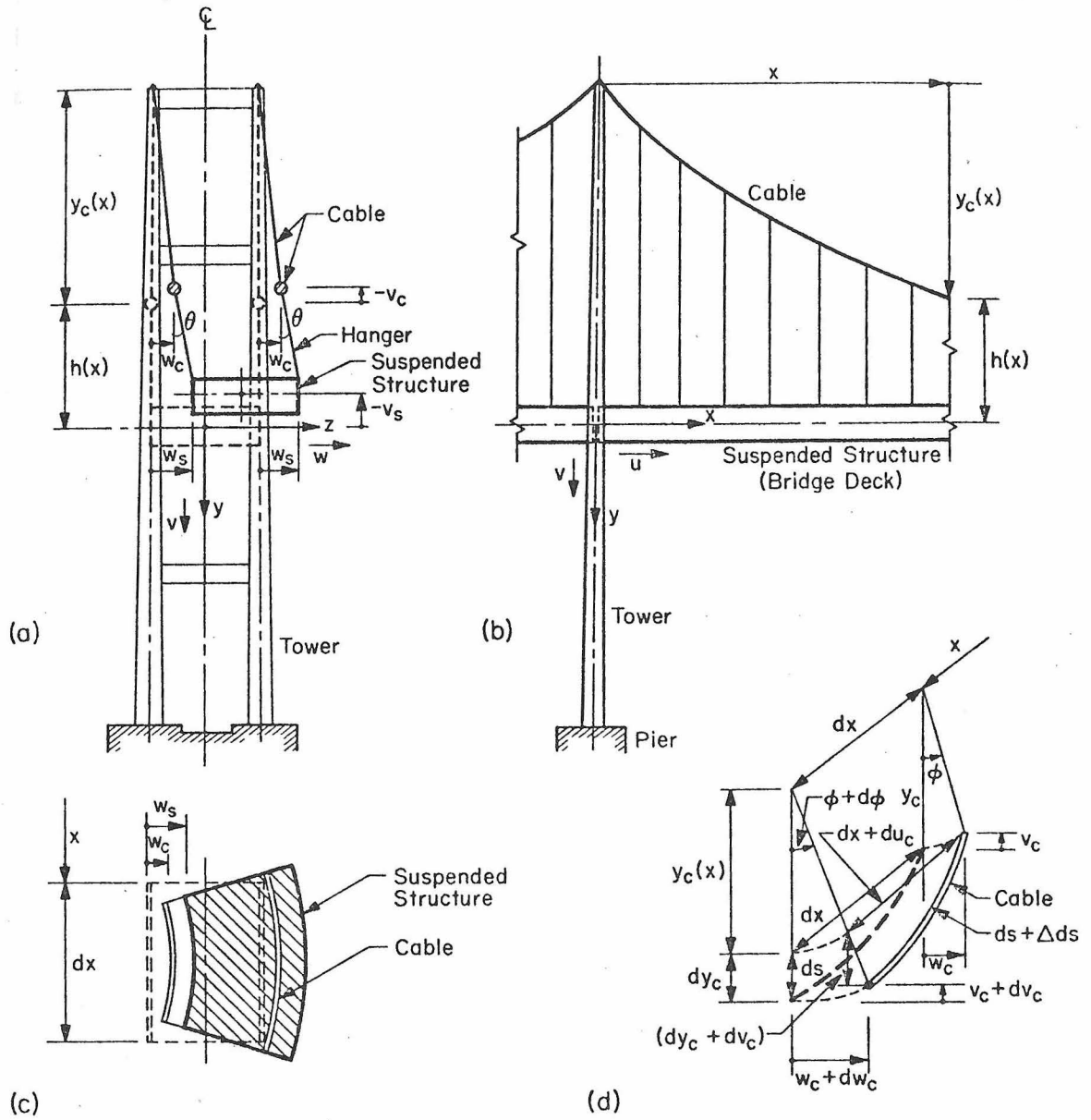
### III-2. Preliminary Considerations and Fundamental Assumptions

The following section contains a description of the coordinate systems used in this analysis and of the different vibrational-displacements describing the motion of the cable and the suspended structure. In addition, a discussion of the simplifying assumptions involved in the analysis is presented.

#### III-2-1. Coordinate systems and vibrational-displacements

For the suspended structure system, the  $x_i$ -axis,  $i = 1, 2, 3$ , of the  $i^{\text{th}}$  span coincides with the equilibrium position of the longitudinal axis of the bridge deck with the origin located at the left support of each span; the  $y_i$ -axis,  $i = 1, 2, 3$  is vertical and the  $z_i$ -axis is horizontal, as shown in Fig. III-1-a. For the cable system, the cables' dead-load ordinate,  $y_c(x_i)$ , is measured downwards from the closing chord-line to the cable of the  $i^{\text{th}}$  span. The origin for this cable system is located at the left support of each cable span whether it is an anchorage or a tower top.

The vibrational displacements of the suspended structure are measured from the  $x_i$ - $y_i$  plane and the  $x_i$ - $z_i$  plane. The cable's vibrational-displacements are measured vertically and horizontally from the static position of the cable itself, as shown in Fig. III-1. The coordinates of vibrational-displacements of the suspended structure are  $u_s(x_i, t)$ ,  $v_s(x_i, t)$  and  $w_s(x_i, t)$  in the  $x_i$ ,  $y_i$  and  $z_i$  directions, respectively, and the coordinates of displacement of the cable are  $u_c(x_i, t)$ ,  $v_c(x_i, t)$  and  $w_c(x_i, t)$  in the  $x_i$ ,  $y_c$  and  $z_i$



LATERALLY VIBRATING SUSPENSION BRIDGE  
DEFINITION DIAGRAMS

Fig. III-1

directions, as shown in Fig. III-1. (Note: Again, the subscript  $i$  has been left out of this figure for convenience.)

III-2-2. Basis for analysis

The following simplifications are introduced in the analysis.

1. Small vibrations about the position of equilibrium are assumed; i. e., the amplitudes of vibration about the static equilibrium configuration are taken to be sufficiently small so that the stiffness of the structure may be taken to be constant during the motion.

As a corollary to the above, the increment of horizontal component of cable tension,  $H(t)$ , due to lateral vibration is small in comparison with the initial dead-load horizontal component of cable tension  $H_w$ .

2. In this theoretical analysis, the ends of the cables are taken to be immovable. Actually, the tops of the towers on a real bridge will move in response to changing forces, and this properly should be taken into account in the specification of the end conditions; but for purposes of exposition, the tower tops are taken to be immovable. In the finite element analysis, the deformations of the towers can be taken into account; in fact, the deformations of the towers may have a significant effect on the natural periods of vibration and the mode shapes.

3. The coupling between lateral, torsional and vertical motions should be taken into consideration when a suspension bridge is transversely vibrating. However, as this coupling leads to very intricate calculations and has significant influence only for non-small displacements, it is not considered here.
4. In addition to the above assumptions, it has also been assumed, in studying free lateral vibration, that vibration damping of the structure may be neglected, the suspenders (or hangers) are inextensible, the cables are parabolic, and the mass of the cables is separate from that of the suspended structure.

There are upward vibrational-displacements of the cables and the suspended structure incidental to their lateral movements. A pendulum action occurs which may be defined in terms of the coupling between these upward and transverse motions. For small vibrations (assumption 1) the upward movements can be found as follows.

By considering Fig. III-1-a, the upward displacements  $v_c$  and  $v_s$  of the cables and the suspended structure, respectively, may be expressed as

$$v_c(x_i, t) = y_c(x_i)[1 - \cos\phi_i] \quad , \quad i = 1, 2, 3 \quad , \quad (3.1)$$

and

$$v_s(x_i, t) = y_c(x_i)[1 - \cos\phi_i] + h(x_i)[1 - \cos\theta_i] \quad , \quad i = 1, 2, 3 \quad , \quad (3.2)$$

where  $\phi_i$  is the angle of rotation of the cable plane (at section  $x_i$ ) with respect to the vertical plane passing through tower top and  $\theta_i$  is the angle of rotation of the suspended structure with respect to the

vertical plane passing through the deflected position of the cable at section  $x_i$  (see Fig. III-1-a and III-1-d).

Since  $w_c$  and  $w_s$  are very small quantities compared with  $y_c$  and  $h$ , one can write

$$\varphi_i(x_i, t) \simeq \left[ \frac{w_c(x_i, t)}{y_c(x_i)} \right], \quad i = 1, 2, 3, \quad (3.3)$$

and

$$\theta_i(x_i, t) \simeq \left[ \frac{w_s(x_i, t) - w_c(x_i, t)}{h(x_i)} \right], \quad i = 1, 2, 3. \quad (3.4)$$

Expanding Eqs. 3.1 and 3.2, and using Eqs. 3.3 and 3.4, one obtains

$$v_c \simeq y_c \left[ 1 - 1 + \frac{\varphi_i^2}{2!} - \frac{\varphi_i^4}{4!} + \dots \right], \quad i = 1, 2, 3$$

or

$$v_c \simeq y_c \left[ \frac{w_c^2}{2y_c^2} \right] = \frac{w_c^2}{2y_c}; \quad (3.5)$$

and

$$v_s \simeq y_c \left[ 1 - 1 + \frac{\varphi_i^2}{2!} - \frac{\varphi_i^4}{4!} + \dots \right] + h \left[ 1 - 1 + \frac{\theta_i^2}{2!} - \frac{\theta_i^4}{4!} + \dots \right],$$

$i = 1, 2, 3$

or

$$v_s \simeq y_c \left[ \frac{w_c^2}{2y_c^2} \right] + h \left[ \frac{(w_s - w_c)^2}{2h^2} \right] = \frac{w_c^2}{2y_c} + \frac{(w_s - w_c)^2}{2h}. \quad (3.6)$$

### III-3. Derivation of the Equations of Motion

In this section, the governing differential equations of lateral vibration of the cable and suspended structure systems are derived in a very general form by using Hamilton's variational principle. The resulting equations are linearized and reduced to a standard form through use of the previously stated simplifying assumptions.

#### III-3-1. Potential energy of the cables

The potential energy of the laterally vibrating cable,  $V_c(t)$ , is comprised of two parts: the strain energy,  $V_{ce}(t)$ , of the cable, and the gravitational potential energy,  $V_{cg}(t)$ . Thus, the total potential energy of the cable is expressed as:

$$V_c(t) = V_{ce}(t) + V_{cg}(t) \quad . \quad (3.7)$$

The expression for the strain energy,  $V_{ce}(t)$ , will be derived by considering the inertia forces and the corresponding small vibrational-deformations. The inertia forces change the horizontal component of cable tension  $H_w$  to  $H_w \pm H(t)$ , where  $H(t)$  is the horizontal-component of cable tension caused by the vibration. As illustrated in Fig. III-1-d, the horizontal displacement of the cable is accompanied by a vertical displacement. The length of the cable element  $ds_i$ , in the  $i^{\text{th}}$  span,  $i = 1, 2, 3$ , under dead load is  $ds_i^2 = dx_i^2 + dy_c^2$ ,  $dx_i$  and  $dy_c$  being the projections in the horizontal and vertical directions, respectively. As a result of small, free lateral-vibration about the position of static equilibrium, the length of the cable element will become  $ds_i + \Delta ds_i$  in the laterally

displaced-position with projections  $dx_i + du_c$  along the  $i^{\text{th}}$  span,  $dy_c + dv_c$  in the vertical direction, and  $dw_c$  in the lateral direction, as shown in Fig. III-1-d. Here  $u_c$  and  $v_c$  are the longitudinal and vertical components of the in-plane motion, respectively, and  $w_c$  is the lateral horizontal component of motion (perpendicular to the vertical plane through the two bearing points of the cable in any span). The components of motion are functions of both position and time. Therefore, one has

$$(ds_i + \Delta ds_i)^2 = (dx_i + du_c)^2 + (dy_c + dv_c)^2 + (dw_c)^2, \quad i = 1, 2, 3, \quad (3.8)$$

and consequently

$$2ds_i \Delta ds_i + (\Delta ds_i)^2 = 2dx_i du_c + 2dy_c dv_c + du_c^2 + dv_c^2 + dw_c^2$$

since  $ds_i^2 = dx_i^2 + dy_c^2$ ; it follows that

$$2ds_i \Delta ds_i + (\Delta ds_i)^2 = \left[ 2 \frac{\partial u_c}{\partial x_i} + 2 \left( \frac{\partial v_c}{\partial x_i} \right) \left( \frac{dy_c}{dx_i} \right) + \left( \frac{\partial v_c}{\partial x_i} \right)^2 + \left( \frac{\partial w_c}{\partial x_i} \right)^2 \right] dx_i^2.$$

Since the analyses are to be valid for cables with sag to span ratios of about 1:8 or less (flat-sag cables), the slope of the cable profile is consistently small; furthermore the longitudinal component of motion  $u_c$  is a small quantity in comparison with  $w_c$  and  $v_c$ .

Consequently,  $\left( \frac{\partial u_c}{\partial x_i} \right)^2$  is a small quantity of higher order, and so the differential extension,  $\Delta ds_i$ , in the length of the cable element, correct to the second order of small quantities, is

$$\Delta ds_i \approx \frac{\partial u_c}{\partial x_i} \frac{dx_i}{ds_i} dx_i + \frac{\partial v_c}{\partial x_i} \frac{dy_c}{ds_i} dx_i + \frac{1}{2} \left( \frac{\partial v_c}{\partial x_i} \right)^2 \frac{dx_i}{ds_i} dx_i + \frac{1}{2} \left( \frac{\partial w_c}{\partial x_i} \right)^2 \frac{dx_i}{ds_i} dx_i, \quad i = 1, 2, 3. \quad (3.9)$$

The strain energy of the cable element,  $ds_i$ , in the  $i^{\text{th}}$  span, can be expressed as

$$dV_{ce}(t) = \left\{ \left[ H_w + \frac{1}{2} H(t) \right] \frac{ds_i}{dx_i} \right\} \cdot \Delta ds_i, \quad i = 1, 2, 3. \quad (3.10)$$

In this equation, the factor  $\frac{1}{2}$  is needed due to the fact that  $H(t)$  increases from zero to its maximum value  $H(t)$ .

Substituting the expression for the cable stretch  $\Delta ds_i$  (Eq. 3.9) into Eq. 3.10 and then integrating over all spans, the strain energy,  $V_{ce}(t)$ , of the two cables may be written as

$$V_{ce}(t) = \sum_{i=1}^3 \left\{ 2 \left[ H_w + \frac{1}{2} H(t) \right] \left[ \int_0^{\ell_i} \frac{\partial u_c}{\partial x_i} dx_i + \int_0^{\ell_i} \left( \frac{\partial v_c}{\partial x_i} \right) \left( \frac{dy_c}{dx_i} \right) dx_i + \frac{1}{2} \int_0^{\ell_i} \left( \frac{\partial v_c}{\partial x_i} \right)^2 dx_i + \frac{1}{2} \int_0^{\ell_i} \left( \frac{\partial w_c}{\partial x_i} \right)^2 dx_i \right] \right\}, \quad (3.11)$$

where  $\ell_i$  is the length of the  $i^{\text{th}}$  span. This energy expression can be written more conveniently as

$$V_{ce}(t) = \sum_{i=1}^3 \left\{ 2 \left[ H_w + \frac{1}{2} H(t) \right] \left[ u_c \Big|_0^{\ell_i} + \int_0^{\ell_i} \left( \frac{\partial v_c}{\partial x_i} \right) \left( \frac{dy_c}{dx_i} \right) + \frac{1}{2} \int_0^{\ell_i} \left( \frac{\partial v_c}{\partial x_i} \right)^2 dx_i + \frac{1}{2} \int_0^{\ell_i} \left( \frac{\partial w_c}{\partial x_i} \right)^2 dx_i \right] \right\}.$$

The assumption that there are no movements of the tower tops or of the anchorages makes it possible to reduce this energy expression to

$$V_{ce}(t) = \sum_{i=1}^3 \left\{ 2 \left[ H_w + \frac{1}{2} H(t) \right] \left[ \int_0^{\ell_i} \left( \frac{\partial v_c}{\partial x_i} \right) \left( \frac{dy_c}{dx_i} \right) dx_i + \frac{1}{2} \int_0^{\ell_i} \left( \frac{\partial v_c}{\partial x_i} \right)^2 dx_i + \frac{1}{2} \int_0^{\ell_i} \left( \frac{\partial w_c}{\partial x_i} \right)^2 dx_i \right] \right\} . \quad (3.12)$$

Now, the cable equation, which relates the stretching of the cable element to the geometric displacements which it undergoes, can be modified to include the lateral vibrational-displacement  $w_c$  as follows: (See Appendix I-b.)

$$\frac{H(t)L_{ei}}{E_c A_c} = \frac{1}{2} \int_0^{\ell_i} \left( \frac{\partial w_c}{\partial x_i} \right)^2 dx_i + \int_0^{\ell_i} \left( \frac{\partial v_c}{\partial x_i} \right) \left( \frac{dy_c}{dx_i} \right) dx_i + \frac{1}{2} \int_0^{\ell_i} \left( \frac{\partial v_c}{\partial x_i} \right)^2 dx_i , \quad i = 1, 2, 3 , \quad (3.13)$$

where  $E_c$  is the modulus of elasticity of the cable,  $A_c$  is the area of the cable, and  $L_{ei}$  is the virtual length of the cable which is defined

by  $L_{ei} = \int_0^{\ell_i} \left( \frac{ds_i}{dx_i} \right)^3 dx_i$  . (An evaluation of the virtual length can also

be found in Appendix I-b.) This cable equation can be written for the entire cable, in the three spans, as

$$\frac{H(t)L_E}{E_c A_c} = \sum_{i=1}^3 \left[ \frac{1}{2} \int_0^{\ell_i} \left( \frac{\partial w_c}{\partial x_i} \right)^2 dx_i + \int_0^{\ell_i} \left( \frac{\partial v_c}{\partial x_i} \right) \left( \frac{dy_c}{dx_i} \right) dx_i + \frac{1}{2} \int_0^{\ell_i} \left( \frac{\partial v_c}{\partial x_i} \right)^2 dx_i \right] , \quad (3.14)$$

where  $L_E = \sum_{i=1}^3 L_{ei}$  for the entire length of the cable.

Substituting Eq. 3.14 into Eq. 3.12, the strain energy of the cable becomes

$$V_{ce}(t) = 2 \left[ \frac{H_w H(t) L_E}{E_c A_c} \right] + 2 \left[ \frac{H^2(t) L_E}{2E_c A_c} \right] \quad (3.15)$$

Attention is drawn to the fact that if the dead-load cable tension were to remain constant during vibration with a horizontal component  $H_w$ , and if  $H(t)$  were due only to the inertia load, then the first term of Eq. 3.15 would be the dead-load work stored in the cable while the second term would be the energy of vibration stored in the cable. However, the dead-load cable tension changes because of the altered cable curve, and  $H(t)$  represents the combined effect of this change in dead-load stress plus the inertia load stress.

The expression for gravitational energy,  $V_{cg}(t)$ , of the two cables due to the upward deflection,  $v_c$ , incidental to their lateral movement  $w_s$ , can be written (in view of the preceding analysis) as

$$V_{cg}(t) = \sum_{i=1}^3 \int_0^{\ell_i} \bar{w}_c^* v_c(x_i, t) dx_i \quad (3.16)$$

where  $\bar{w}_c^*$  is the dead weight of the two cables per unit length of the span.

Using the approximate relation between  $v_c$  and  $w_c$  (Eq. 3.5), Eq. 3.16 can be expressed as

$$V_{cg}(t) = \sum_{i=1}^3 \int_0^{\ell_i} w_c^* \left( \frac{w_c^2(x_i, t)}{2y_c(x_i)} \right) dx_i \quad (3.17)$$

Now, (after substituting Eqs. 3.15 and 3.17 into Eq. 3.7) the expression for the total potential energy of the cable is

$$V_c(t) = 2 \left[ \frac{H_w H(t) L E}{E_c A_c} \right] + 2 \left[ \frac{H^2(t) L E}{2 E_c A_c} \right] + \sum_{i=1}^3 \int_0^{\ell_i} w_c^* \left( \frac{w_c^2}{2y_c} \right) dx_i \quad (3.7')$$

### III-3-2. Potential energy of the suspended structure

The potential energy of the laterally vibrating suspended structure,  $V_s(t)$ , also consists of two parts: the elastic potential energy (i. e., the strain energy),  $V_{se}(t)$ , due to the effects of bending moments, shearing forces and normal forces, and the gravitational potential energy,  $V_{sg}(t)$ , due to upward movement; i. e.,

$$V_s(t) = V_{se}(t) + V_{sg}(t) \quad (3.18)$$

Neglecting the effects of shear and longitudinal deformations, the strain energy stored in the suspended structure due to bending can be written as

$$V_{se}(t) = \frac{1}{2} \sum_{i=1}^3 \int_0^{\ell_i} E_{si} I_{si} \left( \frac{\partial^2 w_s(x_i, t)}{\partial x_i^2} \right)^2 dx_i \quad (3.19)$$

where  $E_{si}$  is the modulus of elasticity of the suspended structure in the  $i^{\text{th}}$  span, and  $I_{si}$  is the area moment of inertia of the suspended structure about its vertical axis,  $y_i$ , in the  $i^{\text{th}}$  span. This moment

of inertia includes the contribution from the two stiffening girders (or trusses) as well as the contribution from the lateral bracing systems. The suspended structure displacement,  $w_c$ , is measured from the vertical plane through the longitudinal centerline of the span.

The gravitational energy,  $V_{sg}(t)$ , of the suspended structure due to the upward displacement  $v_s$  is

$$V_{sg}(t) = \sum_{i=1}^3 \int_0^{\ell_i} w_{si}^* v_s(x_i, t) dx_i, \quad (3.20)$$

where  $w_{si}^*$  is the dead weight of the suspended structure per unit length of the  $i^{\text{th}}$  span.

By the aid of Eq. 3.6, this gravitational energy becomes

$$V_{sg}(t) = \sum_{i=1}^3 \int_0^{\ell_i} w_{si}^* \left[ \frac{w_c^2(x_i, t)}{2y_c(x_i)} + \frac{(w_s(x_i, t) - w_c(x_i, t))^2}{2h(x_i)} \right] dx_i, \quad (3.21)$$

where  $h(x_i)$  is the length of a hanger in the  $i^{\text{th}}$  span at section  $x_i$ .

It should be noted that Eq. 3.21 contains a coupling between the vibrational-displacements of the cable and those of the suspended structure systems.

Now, the equation for the total potential energy of the suspended structure (Eq. 3.18), becomes

$$V_s(t) = \frac{1}{2} \sum_{i=1}^3 \left[ \int_0^{\ell_i} E_{si} I_{si} \left( \frac{\partial^2 w_c}{\partial x_i^2} \right)^2 dx_i + \int_0^{\ell_i} w_{si}^* \left[ \frac{w_c^2}{y_c} + \frac{(w_s - w_c)^2}{h} \right] dx_i \right]. \quad (3.18')$$

III-3-3. Kinetic energy of the laterally vibrating suspension bridge

The kinetic energies caused by the lateral vibrational displacements  $w_c$  and  $w_s$ , of the two cables and of the suspended structure, respectively, are expressed as

$$T_c(t) = \frac{1}{2} \sum_{i=1}^3 \int_0^{\ell_i} m_c^* \left( \frac{\partial w_c(x_i, t)}{\partial t} \right)^2 dx_i, \quad (3.22)$$

and

$$T_s(t) = \frac{1}{2} \sum_{i=1}^3 \int_0^{\ell_i} m_{si}^* \left( \frac{\partial w_s(x_i, t)}{\partial t} \right)^2 dx_i, \quad (3.23)$$

where  $m_c^* = \frac{w_c^*}{g}$  is the mass of the two cables per unit length of the span, and  $m_{si}^* = \frac{w_{si}^*}{g}$  is the mass of the suspended structure per unit length of the  $i^{\text{th}}$  span;  $g$  is the acceleration due to gravity.

The kinetic energies caused by the incidental vertical movements,  $v_c$  and  $v_s$ , of the cables and the suspended structure, respectively, are given by

$$\tilde{T}_c(t) = \frac{1}{2} \sum_{i=1}^3 \int_0^{\ell_i} m_c^* \left( \frac{\partial v_c(x_i, t)}{\partial t} \right)^2 dx_i, \quad (3.24)$$

and

$$\tilde{T}_s(t) = \frac{1}{2} \sum_{i=1}^3 \int_0^{\ell_i} m_{si}^* \left( \frac{\partial v_s(x_i, t)}{\partial t} \right)^2 dx_i. \quad (3.25)$$

Using the relation between the lateral and vertical movements

of the bridge (Eqs. 3.5 and 3.6), Eqs. 3.24 and 3.25 become

$$\tilde{T}_c(t) = \frac{1}{2} \sum_{i=1}^3 \int_0^{\ell_i} m_c^* \left[ \frac{\partial}{\partial t} \left( \frac{w_c^2}{2y_c} \right) \right]^2 dx_i, \quad (3.26)$$

and

$$\tilde{T}_s(t) = \frac{1}{2} \sum_{i=1}^3 \int_0^{\ell_i} m_{si}^* \left[ \frac{\partial}{\partial t} \left( \frac{w_c^2}{2y_c} + \frac{(w_s - w_c)^2}{2h} \right) \right]^2 dx_i. \quad (3.27)$$

### III-3-4. Variational formulation of the equations of motion

#### a. Derivation of the general equations of motion

When applying Hamilton's Principle to derive the differential equations in terms of the lateral displacements  $w_c$  and  $w_s$ ,  $T$  and  $V$  must be functions of the dependent variables  $w_c$  and  $w_s$  only. This requires making use of the approximate relations given by Eqs. 3.5 and 3.6 which can be expressed in variational form as

$$\delta v_c = \delta \left( \frac{w_c^2}{2y_c} \right) = \frac{w_c}{y_c} \delta w_c, \quad (3.28)$$

and

$$\delta v_s = \delta \left[ \frac{w_c^2}{2y_c} + \frac{(w_s - w_c)^2}{2h} \right] = \left[ \frac{(w_s - w_c)}{h} \right] \delta w_s + \left[ \frac{w_c}{y_c} - \frac{(w_s - w_c)}{h} \right] \delta w_c. \quad (3.29)$$

The variation to be performed on the kinetic energy is

$$\int_{t_1}^{t_2} \delta T dt = \int_{t_1}^{t_2} \delta (T_c + T_s + \tilde{T}_c + \tilde{T}_s) dt. \quad (3.30)$$

Expanding, performing the variation of each of the terms for the various kinetic energies with respect to  $w_c$  and  $w_s$ , and integrating by parts where necessary, yields

$$\int_{t_1}^{t_2} \delta T_c dt = - \sum_{i=1}^3 \int_{t_1}^{t_2} \int_0^{\ell_i} m_c^* \frac{\partial^2 w_c}{\partial t^2} \delta w_c dx_i dt \quad , \quad (3.30-a)$$

$$\int_{t_1}^{t_2} \delta T_s dt = - \sum_{i=1}^3 \int_{t_1}^{t_2} \int_0^{\ell_i} m_{si}^* \frac{\partial^2 w_s}{\partial t^2} \delta w_s dx_i dt \quad , \quad (3.30-b)$$

$$\begin{aligned} \int_{t_1}^{t_2} \delta \tilde{T}_c dt &= - \sum_{i=1}^3 \int_{t_1}^{t_2} \int_0^{\ell_i} m_c^* \frac{\partial^2 v_c}{\partial t^2} \delta v_c dx_i dt \quad , \\ &= - \sum_{i=1}^3 \int_{t_1}^{t_2} \int_0^{\ell_i} m_c^* \frac{w_c}{y_c} \frac{\partial^2}{\partial t^2} \left[ \frac{w_c^2}{2y_c} \right] \delta w_c dx_i dt \quad , \end{aligned} \quad (3.30-c)$$

and

$$\begin{aligned} \int_{t_1}^{t_2} \delta \tilde{T}_s dt &= - \sum_{i=1}^3 \int_{t_1}^{t_2} \int_0^{\ell_i} m_{si}^* \frac{\partial^2 v_s}{\partial t^2} \delta v_s dx_i dt \quad , \\ &= - \sum_{i=1}^3 \int_{t_1}^{t_2} \int_0^{\ell_i} m_{si}^* \left\{ \left( \frac{w_s - w_c}{h} \right) \frac{\partial^2}{\partial t^2} \left[ \frac{w_c^2}{2y_c} + \frac{(w_s - w_c)^2}{2h} \right] \delta w_s \right. \\ &\quad \left. + \left( \frac{w_c}{y_c} - \frac{(w_s - w_c)}{h} \right) \frac{\partial^2}{\partial t^2} \left[ \frac{w_c^2}{2y_c} + \frac{(w_s - w_c)^2}{2h} \right] \delta w_c \right\} dx_i dt \quad . \end{aligned} \quad (3.30-d)$$

The above equations have incorporated the fact that  $\delta w_c$ ,  $\delta w_s$ ,  $\delta v_c$  and  $\delta v_s$  are zero at  $t = t_1$  and  $t = t_2$ .

The variation to be performed on the potential energy  $V$  is

$$\int_{t_1}^{t_2} \delta V dt = \int_{t_1}^{t_2} \delta (V_{ce} + V_{cg} + V_{se} + V_{sg}) dt \quad (3.31)$$

Proceeding as in the case of the kinetic energy, the variation of the potential energy terms can be obtained.

$$\begin{aligned} \int_{t_1}^{t_2} \delta V_{ce} dt &= \sum_{i=1}^3 \int_{t_1}^{t_2} \left\{ 2[H_w + H(t)] \delta \left[ \frac{1}{2} \int_0^{\ell_i} \left( \frac{\partial w_c}{\partial x_i} \right)^2 dx_i + \int_0^{\ell_i} \left( \frac{\partial v_c}{\partial x_i} \right) \left( \frac{dy_c}{dx_i} \right) dx_i \right. \right. \\ &\quad \left. \left. + \frac{1}{2} \int_0^{\ell_i} \left( \frac{\partial v_c}{\partial x_i} \right)^2 dx_i \right] \right\} dt \quad , \\ &= \sum_{i=1}^3 \int_{t_1}^{t_2} \left\{ 2[H_w + H(t)] \left[ \frac{\partial w_c}{\partial x_i} \delta w_c \Big|_0^{\ell_i} - \int_0^{\ell_i} \frac{\partial^2 w_c}{\partial x_i^2} \delta w_c dx_i + \frac{dy_c}{dx_i} \delta v_c \Big|_0^{\ell_i} \right. \right. \\ &\quad \left. \left. - \int_0^{\ell_i} \frac{d^2 y_c}{dx_i^2} \delta v_c dx_i + \frac{\partial v_c}{\partial x_i} \delta v_c \Big|_0^{\ell_i} - \int_0^{\ell_i} \frac{\partial^2 v_c}{\partial x_i^2} \delta v_c dx_i \right] \right\} dt \quad (3.31-a) \end{aligned}$$

Substituting Eqs. 3.5, 3.6, 3.28 and 3.29 into Eq. 3.31-a, and noting that for the parabolic cable  $\frac{d^2 y_c}{dx_i^2} = -\frac{1}{2} \left( \frac{w_c^* + w_{si}^*}{H_w} \right)$ , gives

$$\begin{aligned} \int_{t_1}^{t_2} \delta V_{ce} dt &= \sum_{i=1}^3 \int_{t_1}^{t_2} \left\{ 2[H_w + H(t)] \left[ - \int_0^{\ell_i} \left\{ \frac{\partial^2 w_c}{\partial x_i^2} - \frac{1}{2} \frac{w_c}{y_c} \left( \frac{w_c^* + w_{si}^*}{H_w} \right) + \frac{w_c}{y_c} \frac{\partial^2}{\partial x_i^2} \left( \frac{w_c^2}{2y_c} \right) \right\} \delta w_c dx_i \right. \right. \\ &\quad \left. \left. + \left\{ \frac{\partial w_c}{\partial x_i} + \frac{w_c}{y_c} \frac{dy_c}{dx_i} + \frac{w_c}{y_c} \frac{\partial}{\partial x_i} \left( \frac{w_c^2}{2y_c} \right) \right\} \delta w_c \Big|_0^{\ell_i} \right] \right\} dt \quad (3.31-a') \end{aligned}$$

For the other terms of the integral of Eq. 3.31, one obtains

$$\int_{t_1}^{t_2} \delta V_{cg} dt = \sum_{i=1}^3 \int_{t_1}^{t_2} \int_0^{\ell_i} \overset{*}{w}_c \delta v_c dx_i dt = \sum_{i=1}^3 \int_{t_1}^{t_2} \int_0^{\ell_i} \overset{*}{w}_c \frac{w_c}{y_c} \delta w_c dx_i dt, \quad (3.31-b)$$

$$\begin{aligned} \int_{t_1}^{t_2} \delta V_{se}(t) = \sum_{i=1}^3 \int_{t_1}^{t_2} \left\{ E_{si} I_{si} \frac{\partial^2 w_s}{\partial x_i^2} \delta \left( \frac{\partial w_s}{\partial x_i} \right) \Big|_0^{\ell_i} - \frac{\partial}{\partial x_i} \left( E_{si} I_{si} \frac{\partial^2 w_s}{\partial x_i^2} \right) \delta w_s \Big|_0^{\ell_i} \right. \\ \left. + \int_0^{\ell_i} \frac{\partial^2}{\partial x_i^2} \left( E_{si} I_{si} \frac{\partial^2 w_s}{\partial x_i^2} \right) \delta w_s dx_i \right\} dt, \quad (3.31-c) \end{aligned}$$

and, finally

$$\begin{aligned} \int_{t_1}^{t_2} \delta V_{sg} dt = \sum_{i=1}^3 \int_{t_1}^{t_2} \int_0^{\ell_i} \overset{*}{w}_{si} \delta v_s dx_i dt \\ = \sum_{i=1}^3 \int_{t_1}^{t_2} \left\{ \int_0^{\ell_i} \left( \overset{*}{w}_{si} \left[ \frac{w_s - w_c}{h} \right] \delta w_s + \overset{*}{w}_{si} \left[ \frac{w_c}{y_c} - \frac{(w_s - w_c)}{h} \right] \delta w_c \right) dx_i \right\} dt. \quad (3.31-d) \end{aligned}$$

Having the foregoing variations of the different energies, Hamilton's Principle, after rearranging terms, gives

$$\begin{aligned} - \sum_{i=1}^3 \int_{t_1}^{t_2} \left\{ \int_0^{\ell_i} \left[ m_c \left( \frac{\partial^2 w_c}{\partial t^2} + \frac{w_c}{y_c} \frac{\partial^2}{\partial t^2} \left( \frac{w_c}{2y_c} \right) \right) \right. \right. \\ \left. \left. + m_{si} \left( \frac{w_c}{y_c} - \frac{(w_s - w_c)}{h} \right) \frac{\partial^2}{\partial t^2} \left( \frac{w_c}{2y_c} + \frac{(w_s - w_c)^2}{2h} \right) \right] \right\} dt \end{aligned}$$

$$\begin{aligned}
 & - 2[H_w + H(t)] \left( \frac{\partial^2 w_c}{\partial x_i^2} - \frac{1}{2} \frac{w_c}{y_c} \left( \frac{w_c^* + w_{si}^*}{H_w} \right) + \frac{w_c}{y_c} \frac{\partial^2}{\partial x_i^2} \left( \frac{w_c^2}{2y_c} \right) \right) \\
 & + \frac{w_c}{y_c} w_c^* + w_{si}^* \left( \frac{w_c}{y_c} - \frac{(w_s - w_c)}{h} \right) \delta w_c dx_i \\
 & + 2[H_w + H(t)] \left[ \frac{\partial w_c}{\partial x_i} + \frac{w_c}{y_c} \frac{dy_c}{dx_i} + \frac{w_c}{y_c} \frac{\partial}{\partial x_i} \left( \frac{w_c^2}{2y_c} \right) \right] \delta w_c \Big|_0^{l_i} \\
 & + \int_0^{l_i} \left[ m_{si}^* \left( \frac{\partial^2 w_c}{\partial t^2} + \frac{(w_s - w_c)}{h} \frac{\partial^2}{\partial t^2} \left( \frac{w_c^2}{2y_c} + \frac{(w_s - w_c)^2}{2h} \right) \right) \right. \\
 & + \frac{\partial^2}{\partial x_i^2} \left( E_{si} I_{si} \frac{\partial^2 w_s}{\partial x_i^2} \right) + w_{si}^* \left( \frac{w_s - w_c}{h} \right) \delta w_s dx_i \\
 & \left. + E_{si} I_{si} \frac{\partial^2 w_s}{\partial x_i^2} \delta \left( \frac{\partial w_s}{\partial x_i} \right) \Big|_0^{l_i} - \frac{\partial}{\partial x_i} \left( E_{si} I_{si} \frac{\partial^2 w_s}{\partial x_i^2} \right) \delta w_s \Big|_0^{l_i} \right] dt = 0
 \end{aligned}
 \tag{3.32}$$

The coefficients of  $\delta w_c$  and  $\delta w_s$  that appear under the integral signs must be equal to zero, and the integral terms must be equal to zero at  $x_i = 0$  and  $x_i = l_i$ . It follows then that the differential equations governing the lateral vibration of the cable and the suspended structure are given by

$$m_c^* \left[ \frac{\partial^2 w_c}{\partial t^2} + \frac{w_c}{y_c} \frac{\partial^2}{\partial t^2} \left( \frac{w_c^2}{2y_c} \right) \right] + m_{si}^* \left[ \left( \frac{w_c}{y_c} - \frac{(w_s - w_c)}{h} \right) \frac{\partial^2}{\partial t^2} \left( \frac{w_c^2}{2y_c} + \frac{(w_s - w_c)^2}{2h} \right) \right]$$

$$\begin{aligned}
 & - 2[H_w + H(t)] \left[ \frac{\partial^2 w_c}{\partial x_i^2} - \frac{1}{2} \frac{w_c}{y_c} \left( \frac{w_c^* + w_{si}^*}{H_w} \right) + \frac{w_c}{y_c} \frac{\partial^2}{\partial x_i^2} \left( \frac{w_c^2}{2y_c} \right) \right] + \frac{w_c}{y_c} w_c^* \\
 & + w_{si}^* \left[ \frac{w_c}{y_c} - \frac{(w_s - w_c)}{h} \right] = 0 \quad , \quad i = 1, 2, 3 , \quad (3.33)
 \end{aligned}$$

and

$$\begin{aligned}
 & m_{si}^* \left[ \frac{\partial^2 w_s}{\partial t^2} + \frac{(w_s - w_c)}{h} \frac{\partial^2}{\partial t^2} \left( \frac{w_c^2}{2y_c} + \frac{(w_s - w_c)^2}{2h} \right) \right] \\
 & + \frac{\partial^2}{\partial x_i^2} \left( E_{si} I_{si} \frac{\partial^2 w_s}{\partial x_i^2} \right) + w_{si}^* \left[ \frac{(w_s - w_c)}{h} \right] = 0 \quad , \quad i = 1, 2, 3 , \quad (3.34)
 \end{aligned}$$

where

$$\begin{aligned}
 H(t) &= \frac{A_c E_c}{L_E} \sum_{i=1}^3 \frac{1}{2} \int_0^{l_i} \left( \frac{\partial w_c}{\partial x_i} \right)^2 dx_i + \int_0^{l_i} \left( \frac{dy_c}{dx_i} \right) \frac{\partial}{\partial x_i} \left( \frac{w_c^2}{2y_c} \right) dx_i \\
 &+ \frac{1}{2} \int_0^{l_i} \left[ \frac{\partial}{\partial x_i} \left( \frac{w_c^2}{2y_c} \right) \right]^2 dx_i \quad . \quad (3.35)
 \end{aligned}$$

Integrating the second term by parts and using the relation

$$\frac{d^2 y_c}{dx_i^2} = - \frac{1}{2} \left( \frac{w_c^* + w_{si}^*}{H_w} \right) \quad \text{gives}$$

$$\begin{aligned}
 H(t) = \frac{A_c E_c}{L E} \sum_{i=1}^3 \left[ \frac{1}{2} \int_0^{\ell_i} \left( \frac{\partial w_c}{\partial x_i} \right)^2 dx_i + \frac{(w_{si}^* + w_c^*)}{2H_w} \int_0^{\ell_i} \left( \frac{w_c^2}{2y_c} \right) dx_i \right. \\
 \left. + \frac{1}{2} \int_0^{\ell_i} \left[ \frac{\partial}{\partial x_i} \left( \frac{w_c^2}{2y_c} \right) \right]^2 dx_i \right] \quad (3.36)
 \end{aligned}$$

The two equations of motion (Eqs. 3.33 and 3.34) describe the coupled vibrational motion of the cables and the suspended structure. These two equations, as well as the cable equation (Eq. 3.35 or Eq. 3.36) contain nonlinear terms.

The boundary conditions specified by Eq. 3.32 are

$$2[H_w + H(t)] \left[ \frac{\partial w_c}{\partial x_i} + \frac{w_c}{y_c} \frac{dy_c}{dx_i} + \frac{w_c}{y_c} \frac{\partial}{\partial x_i} \left( \frac{w_c^2}{2y_c} \right) \right] \delta w_c \Big|_0^{\ell_i} = 0, \quad i = 1, 2, 3, \quad (3.37)$$

$$E_{si} I_{si} \frac{\partial^2 w_s}{\partial x_i^2} \delta \left( \frac{\partial w_s}{\partial x_i} \right) \Big|_0^{\ell_i} = 0, \quad i = 1, 2, 3, \quad (3.38)$$

and

$$\frac{\partial}{\partial x_i} \left( E_{si} I_{si} \frac{\partial^2 w_s}{\partial x_i^2} \right) \delta w_s \Big|_0^{\ell_i} = 0, \quad i = 1, 2, 3; \quad (3.39)$$

these can be satisfied by

$$2[H_w + H(t)] \left[ \frac{\partial w_c}{\partial x_i} + \frac{w_c}{y_c} \frac{dy_c}{dx_i} + \frac{w_c}{y_c} \frac{\partial}{\partial x_i} \left( \frac{w_c^2}{2y_c} \right) \right] = 0 \quad \text{or}$$

$$w_c = 0 \quad \text{at} \quad x_i = 0 \quad \text{and} \quad x_i = \ell_i, \quad i = 1, 2, 3, \quad (3.40)$$

$$E_{si} I_{si} \frac{\partial^2 w_s}{\partial x_i^2} = 0 \quad \text{or} \quad \frac{\partial w_s}{\partial x_i} = 0 \quad \text{at} \quad x_i = 0 \quad \text{and} \quad x_i = \ell_i, \quad i = 1, 2, 3, \quad (3.41)$$

$$\frac{\partial}{\partial x_i} \left( E_{si} I_{si} \frac{\partial^2 w_s}{\partial x_i^2} \right) = 0 \quad \text{or} \quad w_s = 0 \quad \text{at} \quad x_i = 0 \quad \text{and} \quad x_i = \ell_i, \quad i = 1, 2, 3. \quad (3.42)$$

Eqs. 3.40, 3.41 and 3.42 represent the boundary conditions associated with the differential equations 3.33 and 3.34.

The first part of Eq. 3.40 can be rewritten as

$$2[H_w + H(t)] \frac{\partial w_c}{\partial x_i} + 2[H_w + H(t)] \left( \frac{dy_c}{dx_i} + \frac{\partial v_c}{\partial x_i} \right) \cdot \frac{w_c}{y_c}, \quad \text{in which the first}$$

term represents the lateral shear force transmitted by the cables to the tower tops or anchorages due to only the lateral displacement  $w_c$ . The second term represents the transverse component of the shearing force,  $2[H_w + H(t)] \left( \frac{dy_c}{dx_i} + \frac{\partial v_c}{\partial x_i} \right)$ , in the rotated plane of the cable which is produced by the vertical displacement  $v_c$ . Eq. 3.40 requires that either the lateral shearing force or the lateral deflection of the cable be zero at each end of the cable span. As indicated in the simplifying assumptions, the deflection of the cable span is zero at both ends, so its variation is zero, and the geometric boundary condition of Eq. 3.37 is satisfied.

The first part of Eq. 3.41 requires that the bending moment vanish at each end of the suspended structure, while the second part requires that the rotation vanish at each end. Eq. 3.42 requires that either the shearing force or the deflection be zero at each end of the

suspended structure. For a suspended structure hinged at both ends, the bending moment and the deflection are zero at both ends, and Eqs. 3.38 and 3.39 are satisfied. In this case, there is one geometric and one natural boundary condition.

b. Linearization of the equations of motion

When the higher order terms in Eqs. 3.33 and 3.34 are neglected, the linearized forms of the equations are obtained:

$$\begin{aligned} \dot{m}_c \frac{\partial^2 w_c}{\partial t^2} - 2H_w \frac{\partial^2 w_c}{\partial x_i^2} + \frac{w_c}{y_c} (w_c^* + w_{si}^*) + \frac{w_c}{y_c} w_c^* + \frac{w_c}{y_c} w_{si}^* - w_{si}^* \left( \frac{w_s - w_c}{h} \right) = 0, \\ i = 1, 2, 3, \end{aligned} \quad (3.43)$$

or

$$\dot{m}_c \frac{\partial^2 w_c}{\partial t^2} - 2H_w \frac{\partial^2 w_c}{\partial x_i^2} - w_{si}^* \left( \frac{w_s - w_c}{h} \right) + 2(w_c^* + w_{si}^*) \frac{w_c}{y_c} = 0, \quad i = 1, 2, 3, \quad (3.43')$$

for the cable; and

$$\dot{m}_{si} \frac{\partial^2 w_c}{\partial t^2} + \frac{\partial^2}{\partial x_i^2} \left( E_{si} I_{si} \frac{\partial^2 w_s}{\partial x_i^2} \right) + w_{si}^* \left( \frac{w_s - w_c}{h} \right) = 0, \quad i = 1, 2, 3 \quad (3.44)$$

for the suspended structure.

The first term of Eq. 3.43 results from consideration of the kinetic energy caused by the lateral displacement  $w_c$  only (Eq. 3.22). The second and third terms are from the linear strain energy expression of the cable, which is derived from Eq. 3.12 in the form:

$$V_{ce}(t) = \sum_{i=1}^3 2H_w \left[ \int_0^{\ell_i} \left( \frac{\partial w_c}{\partial x_i} \right) \left( \frac{dy_c}{dx_i} \right) dx_i + \frac{1}{2} \int_0^{\ell_i} \left( \frac{\partial w_c}{\partial x_i} \right)^2 dx_i \right]$$

Upon integrating by parts, noting that  $\frac{d^2 y_c}{dx_i^2} = -\frac{1}{2} \left( \frac{w_c^* + w_{si}^*}{H_w} \right)$ , and using Eq. 3.5, this equation becomes

$$\tilde{V}_{ce}(t) = \sum_{i=1}^3 2H_w \left[ \frac{1}{2} \int_0^{\ell_i} \left( \frac{\partial w_c}{\partial x_i} \right)^2 dx_i + \frac{1}{2} \left( \frac{w_c^* + w_{si}^*}{H_w} \right) \int_0^{\ell_i} \left( \frac{w_c}{2y_c} \right)^2 dx_i \right]. \quad (3.12')$$

The fourth term in Eq. 3.43 results from the gravitational energy expression of the cable (Eq. 3.16) due to the upward displacement,  $v_c$ , while the last two terms result from the gravitational energy expression of the suspended structure (Eq. 3.21) due to the upward displacement  $v_s$ .

Comparison of Eqs. 3.34 and 3.44 reveals that the only linearization is due to neglect of the kinetic energy caused by the upward displacement  $v_s$  of the suspended structure.

Finally, Eqs. 3.43' and 3.44 are identical to those derived by Selberg [4], except for the last term of Eq. 3.43', which is a consequence of taking into consideration the upward movements of the structure. No solutions of Eqs. 3.43' and 3.44 in closed form are known. However, Fourier series solutions, and energy approximate methods have been used by Selberg and Ito [7, 6] to determine natural frequencies by assuming sine mode shapes. An approximate solution of these two linear differential equations of motion (Eqs. 3.43' and 3.44), in which the frequency equations are obtained, can be found in Appendix III-a. In this solution, sine mode shapes are assumed, and the orthogonality property of the modes is used.

#### III-4. A Finite Element Approach to Lateral Vibrations

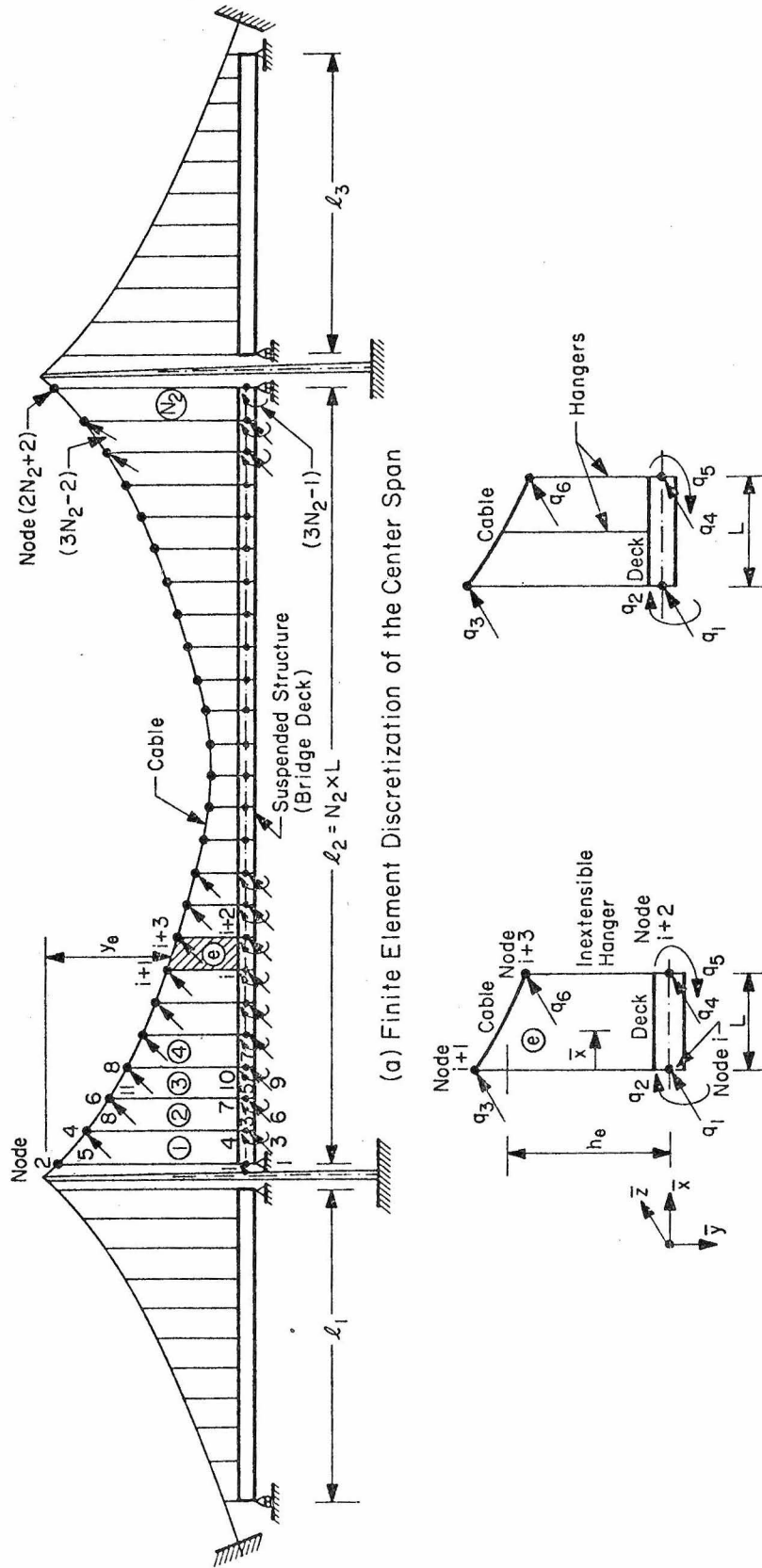
A method of analysis based on the finite element technique is presented in the following section. The method takes into account the characteristics of both the cable and the suspended structure. The cable is idealized by a set of string elements, while the suspended structure is idealized by a set of beam elements. The two sets of elements, connected by rigid hangers, form the bridge elements. The stiffness and inertia properties for each set of elements are derived and assembled to obtain the gross assemblage characteristics. Finally, Hamilton's Principle is used to derive the matrix equations of motion for the entire bridge structure, from which the natural frequencies and modes of vibration are obtained. To illustrate the applicability of the analysis, and to exhibit the dynamic characteristics of lateral vibration, a numerical example is presented.

In deriving the finite-element solutions, the strain energy of vibration stored in the cables due to  $H(t)$  (second part of Eq. 3.15) and the kinetic energy caused by the upward motion of the suspended structure and the cables are both neglected. In addition, the previous assumptions presented in Section III-2-2 are employed.

##### III-4-1. Idealization of the structure and the displacement models

The suspension bridge structure is divided into an appropriate number of elements which are interconnected only at a finite number of nodal points along the cable and the suspended structure, as shown in Fig. III-2-a (for the center span only). Each bridge element

FINITE ELEMENT ANALYSIS OF SUSPENSION BRIDGES  
FREE LATERAL VIBRATIONS



(b) Bridge Element ⑥ with the Generalized Nodal Displacements (c) The Bridge Element Used in the Numerical Example (San Pedro Bridge)

Fig. III-2

consists of a cable subelement and a suspended structure subelement connected by two or more rigid suspenders, as in Figs. III-2-b and c.

Since the lateral vibrational-displacement of each suspended-structure nodal-point is different from the lateral vibrational-displacement of the corresponding cable nodal-point, it is necessary to make a distinction between the two nodes. Thus, each bridge element has four nodal-points, two for the suspended-structure subelement and two for the cable subelement. For the suspended-structure subelement, there are two nodal degrees of freedom at each node: one is the translation of the cross section defined by the node and the other is the rotation of that cross section in the horizontal plane (as shown in Fig. III-1-c). The cable subelement has only one translational degree of freedom at each node. This introduces six degrees of freedom (or nodal displacements) for the bridge element, designated by  $q_j(t)$ ,  $j = 1, 2, 3, 4, 5$  and  $6$ , at the nodes  $i, i+1, i+2$  and  $i+3$ . (In Fig. IV-2, the suspended-structure nodes  $i$  and  $i+2$  are connected to the cable nodes  $i+1$  and  $i+3$ , respectively.)

The interpolation functions associated with the two degrees of freedom of the nodal-point in the suspended-structure subelement are taken to be cubic Hermitian polynomials (used before in Chapters I and II). Consequently, the lateral vibration of the suspended-structure can now be expressed in terms of the bridge-element nodal displacements  $q_j(t)$ ,  $j = 1, 2, 3, 4, 5$  and  $6$ , as

$$w_{se}(\xi_1, \xi_2; t) = \left[ \xi_1^2(3-2\xi_1), -L\xi_1^2\xi_2, 0, \xi_2^2(3-2\xi_2), L\xi_1\xi_2^2, 0 \right]_e \{q(t)\}_e,$$

or

$$w_{se}(\xi_1, \xi_2; t) = \{f_s(\xi_1, \xi_2)\}_e^T \{q(t)\}_e, \quad (3.45)$$

where  $e$  is the subscript indicating "element,"  $L$  is the length of the element, and  $\xi_1$  and  $\xi_2$  are the normalized coordinates defined by

$$\xi_1(\bar{x}) = (1 - \frac{\bar{x}}{L}) \quad \text{and} \quad \xi_2(\bar{x}) = \frac{\bar{x}}{L}. \quad (3.46)$$

$\bar{x}$  is the horizontal axis of the individual element, as shown in Fig. III-2-b.

In Eq. 3.45,  $\{f_s(\xi_1, \xi_2)\}_e^T$  represents the transpose of  $\{f_s(\xi_1, \xi_2)\}_e$ ; it is the vector of the polynomial for the suspended-structure subelement, and  $\{q(t)\}_e$  is the vector of the six nodal-displacements for the bridge element.

The interpolation displacement polynomial associated with the one degree of freedom of the cable nodal-point is taken to be a linear interpolation function, i. e., interpolation where only function values and no function derivatives are prescribed. Thus, the cable lateral vibrational-displacement can be expressed in terms of the six nodal-displacements of the bridge-element, as

$$w_{ce}(\bar{x}; t) = \left[ 0, 0, \hat{l}_1(\bar{x}), 0, 0, \hat{l}_2(\bar{x}) \right]_e \{q(t)\}_e. \quad (3.47)$$

Here,  $\hat{l}_1(\bar{x})$  and  $\hat{l}_2(\bar{x})$  are the linear interpolation functions for the cable-subelement, and are given (on  $[0, L]$ ) as

$$\hat{l}_1(\bar{x}) = \left( 1 - \frac{\bar{x}}{L} \right) \quad \text{and} \quad \hat{l}_2(\bar{x}) = \frac{\bar{x}}{L}. \quad (3.48)$$

By introducing the normalized coordinates  $\xi_1$  and  $\xi_2$  (Eq. 3.46), any point in the cable subelement  $[0, L]$  can be referred to in terms of  $\xi_1$  and  $\xi_2$  as new coordinates. Therefore, Eq. 3.47 becomes

$$w_{ce}(\xi_1, \xi_2; t) = \begin{bmatrix} 0 & 0 & \xi_1 & 0 & 0 & \xi_2 \end{bmatrix}_e \{q(t)\}_e ,$$

or

$$w_{ce}(\xi_1, \xi_2; t) = \{f_c(\xi_1, \xi_2)\}_e^T \{q(t)\}_e , \quad (3.49)$$

where  $\{f_c(\xi_1, \xi_2; t)\}_e$  is the vector of the polynomials of the cable-subelement.

Equations 3.45 and 3.49 furnish the displacement models for the bridge-element.

Each bridge-element has an average suspender length  $h_e$ , and an average dead-load cable ordinate  $y_e$ , as shown in Fig. III-2.

#### III-4-2. Evaluation of structural-property matrices

For the derivation of the various stiffness matrices of the individual bridge element, it is again convenient to treat the suspended-structure subelement and the cable-structure subelement separately. Then by superposing them appropriately, the structural or stiffness properties of the entire element (or assemblage) can be found.

##### a. Elastic-stiffness matrix of the suspended structure

The strain energy of the suspended structure due to bending, Eq. 3.19, may be expressed (with the aid of the displacement model for the suspended-structure subelement, Eq. 3.45), as

$$V_{se}(t) = \frac{1}{2} \sum_{i=1}^3 \left[ \sum_{e=1}^{N_i} \int_0^L E_{se} I_{se} (\{f''_s\}_e^T \{q\}_e)^T (\{f''_s\}_e^T \{q\}_e) d\bar{x} \right]. \quad (3.50)$$

Here,  $N_i$  is the total number of bridge elements used to present the  $i^{\text{th}}$  span;  $E_{se} I_{se}$ , the flexural rigidity for the element, is assumed uniform over the entire element.

Writing Eq. 3.50 in a more convenient form provides the elastic-stiffness matrix for the element, as follows

$$V_{se}(t) = \frac{1}{2} \sum_{e=1}^N \{q\}_e^T [k_{se}]_e \{q\}_e. \quad (3.51)$$

where  $N = \sum_{i=1}^3 N_i$  is the total number of elements used to present the entire assembled structure, and

$$[k_{se}]_e = \int_0^L E_{se} I_{se} \{f''_s\}_e \{f''_s\}_e^T d\bar{x}, \quad (3.52)$$

is the element elastic-stiffness matrix of the suspended-structure sub-element. The integration involved in the evaluation of  $[k_{se}]_e$  can be accomplished as described in Chapter I. The resulting elastic-stiffness

matrix is

$$[k_{se}]_e = \frac{E_{se} I_{se}}{L^3} \begin{bmatrix} 12 & -6L & 0 & -12 & -6L & 0 \\ -6L & 4L^2 & 0 & 6L & 2L^2 & 0 \\ 0 & 0 & 0 & 0 & 0 & 0 \\ -12 & 6L & 0 & 12 & 6L & 0 \\ -6L & 2L^2 & 0 & 6L & 4L^2 & 0 \\ 0 & 0 & 0 & 0 & 0 & 0 \end{bmatrix}. \quad (3.53)$$

Note that zeros are used for the columns and the corresponding rows of the nodal-displacements of the cable subelement, as is expected from the assumptions associated with the individual displacement models of the two systems.

For the complete system, the assemblage elastic-stiffness matrix and the assemblage nodal displacements are, respectively

$$[K_{SE}] = \sum_{e=1}^N [k_{se}]_e , \quad (3.54)$$

and

$$\{r\} = \sum_{e=1}^N \{q\}_e , \quad (3.55)$$

Now, the total strain energy of the assemblage associated with bending and stored in the suspended structure may be expressed by

$$V_{se}(t) = \frac{1}{2} \{r\}^T [K_{SE}] \{r\} . \quad (3.56)$$

The stiffness matrix of the complete system  $[K_{SE}]$  is symmetric, positive-definite and thinly populated (i. e. banded).

b. Gravity-stiffness matrix of the suspended structure

The gravitational energy associated with the upward deflection of the suspended structure (Eq. 3.21) can be written, by using the displacement models for  $w_s$  and  $w_c$  (Eqs. 3.45 and 3.49), as

$$V_{sg}(t) = \frac{1}{2} \sum_{i=1}^3 \left[ \sum_{e=1}^{N_i} \left\{ \int_0^L \frac{w_{se}^*}{y_e} (\{f_c\}_e^T \{q\}_e)^2 d\bar{x} + \int_0^L \frac{w_{se}^*}{h_e} (\{f_s\}_e^T \{q\}_e - \{f_c\}_e^T \{q\}_e)^2 d\bar{x} \right\} \right], \quad (3.57)$$

where  $w_{se}^*$  is the weight of the suspended-structure subelement per unit length, and  $y_e$  and  $h_e$  are the geometric properties defined as before.

It is important to note that the second term of Eq. 3.57 represents the coupled vibrational-motions of the cable and the suspended structure.

Now, define the vector  $\{\Phi\}_e$  as follows

$$\{\Phi\}_e = (\{f_s\}_e - \{f_c\}_e) \quad , \quad (3.58)$$

which in terms of the normalized coordinates, becomes

$$\{\Phi\}_e^T = \left[ \xi_1^2(3-2\xi_1) \quad , \quad -L\xi_1^2\xi_2 \quad , \quad -\xi_1 \quad , \quad \xi_2^2(3-2\xi_1) \quad , \quad L\xi_1\xi_2^2 \quad , \quad -\xi_2 \right]_e \quad . \quad (3.59)$$

Then Eq. 2.57, may be expressed as

$$V_{sg}(t) = \frac{1}{2} \sum_{e=1}^N \left[ \{q\}_e^T \left( \int_0^L \frac{w_{se}^*}{y_e} \{f_c\}_e \{f_c\}_e^T d\bar{x} + \int_0^L \frac{w_{se}^*}{h_e} \{\Phi\}_e \{\Phi\}_e^T d\bar{x} \right) \{q\}_e \right], \quad (3.60)$$

or more conveniently

$$\begin{aligned}
 V_{sg}(t) &= \frac{1}{2} \sum_{e=1}^N \{q\}_e^T \left( [k_{s1}]_e + [k_{s2}]_e \right) \{q\}_e , \\
 &= \frac{1}{2} \sum_{e=1}^N \{q\}_e^T [k_{sg}]_e \{q\}_e , \quad (3.61)
 \end{aligned}$$

where  $[k_{sg}]_e$  is the element gravity-stiffness matrix of the suspended structure; it consists of the sum of two matrices. The first matrix,  $[k_{s1}]_e$ , is due to the contribution from the cable, and is expressed by

$$[k_{s1}]_e = \int_0^L \frac{w_{se}^*}{y_e} \{f_c\}_e \{f_c\}_e^T d\bar{x} ; \quad (3.62)$$

while the second matrix,  $[k_{s2}]_e$ , is due to the coupled motion of the cable and the suspended structure, and is expressed by

$$[k_{s2}]_e = \int_0^L \frac{w_{se}^*}{h_e} \{\Phi\}_e \{\Phi\}_e^T d\bar{x} . \quad (3.63)$$

The integration involved in the evaluation of both matrices,  $[k_{s1}]_e$  and  $[k_{s2}]_e$ , can be accomplished by the integration property (Eq. 1.59) of the interpolation functions in Chapter I. The resulting

matrices are

$$[k_{s1}]_e = \frac{w_{se}^* L}{6 y_c} \begin{bmatrix} 0 & 0 & 0 & 0 & 0 & 0 \\ 0 & 0 & 0 & 0 & 0 & 0 \\ 0 & 0 & 2 & 0 & 0 & 1 \\ 0 & 0 & 0 & 0 & 0 & 0 \\ 0 & 0 & 0 & 0 & 0 & 0 \\ 0 & 0 & 1 & 0 & 0 & 2 \end{bmatrix} , \quad (3.64)$$

$$[k_{s2}]_e = \frac{w_{se}^* L}{420 h_e} \begin{bmatrix} 156 & -22L & -147 & 54 & 13L & -63 \\ -22L & 4L^2 & 21L & -13L & -3L^2 & 14L \\ -147 & 21L & 140 & -63 & -14L & 70 \\ 54 & -13L & -63 & 156 & 22L & -147 \\ 13L & -3L^2 & -14L & 22L & 4L^2 & -21L \\ -63 & 14L & 70 & -147 & -22L & 140 \end{bmatrix} \quad (3.65)$$

Therefore, the resulting gravity-stiffness matrix of the bridge-element (due to the suspended-structure's upward motion) has non-zero coefficients corresponding to the six nodal-displacements for the element; it is

$$[k_{sg}]_e = \frac{w_{se}^* L}{420 h_e} \begin{bmatrix} 156 & -22L & -147 & 54 & 13L & -63 \\ -22L & 4L^2 & 21L & -13L & -3L^2 & 14L \\ -147 & 21L & 140(1+\frac{h_e}{y_e}) & -63 & -14L & 70(1+\frac{h_e}{y_e}) \\ 54 & -13L & -63 & 156 & 22L & -147 \\ 13L & -3L^2 & -14L & 22L & 4L^2 & -21L \\ -63 & 14L & 70(1+\frac{h_e}{y_e}) & -147 & -21L & 140(1+\frac{h_e}{y_e}) \end{bmatrix} \quad (3.66)$$

The assemblage gravity-stiffness matrix can be obtained by merely adding the element stiffness coefficients appropriately; it is expressed as

$$[K_{SG}] = \sum_{e=1}^N [k_{sg}]_e \quad (3.67)$$

Thus, the gravitational energy associated with the upward motion of the suspended structure, for the assemblage, may be given as

$$V_{sg}(t) = \frac{1}{2} \{r\}^T [K_{SG}] \{r\} \quad , \quad (3.68)$$

in which  $[K_{SG}]$  is a symmetric, positive-definite and banded matrix.

c. Elastic-stiffness matrix of the cables

Recalling the expression for the strain energy of the cables, Eq. 3.15, and using Eq. 3.36 (the expression for  $H(t)$ ), yields

$$\begin{aligned} V_{ce}(t) = & \sum_{i=1}^3 2 H_w \left[ \frac{1}{2} \int_0^{\ell_i} \left( \frac{\partial w_c}{\partial x_i} \right)^2 dx_i + \frac{(\overset{*}{w}_{si} + \overset{*}{w}_c)}{2 H_w} \int_0^{\ell_i} \left( \frac{w_c^2}{2 y_c} \right) dx_i + \frac{1}{2} \int_0^{\ell_i} \left[ \frac{\partial}{\partial x_i} \left( \frac{w_c^2}{2 y_c} \right) \right]^2 dx_i \right] \\ & + \sum_{i=1}^3 \frac{E_c A_c}{L_E} \left[ \frac{1}{2} \int_0^{\ell_i} \left( \frac{\partial w_c}{\partial x_i} \right)^2 dx_i + \frac{(\overset{*}{w}_{si} + \overset{*}{w}_c)}{2 H_w} \int_0^{\ell_i} \left( \frac{w_c^2}{2 y_c} \right) dx_i + \frac{1}{2} \int_0^{\ell_i} \left[ \frac{\partial}{\partial x_i} \left( \frac{w_c^2}{2 y_c} \right) \right]^2 dx_i \right] . \end{aligned} \quad (3.69)$$

The second term of this equation, which is the energy of vibration stored in the cables, is a very small quantity of higher order and may be ignored; furthermore, the last term in the first set of brackets is unimportant and may also be neglected. Therefore, the strain energy of the cable reduces to the linear form

$$V_{ce}(t) = \frac{1}{2} \sum_{i=1}^3 \left[ 2 H_w \int_0^{\ell_i} \left( \frac{\partial w_c}{\partial x_i} \right)^2 dx_i \right] + \frac{1}{2} \sum_{i=1}^3 \left[ (\overset{*}{w}_{si} + \overset{*}{w}_c) \int_0^{\ell_i} \left( \frac{w_c^2}{y_c} \right) dx_i \right] . \quad (3.70)$$

With the aid of the displacement model of the cable subelement (Eq. 3.49), the energy expression (Eq. 3.70) becomes

$$V_{ce}(t) = \frac{1}{2} \sum_{i=1}^3 \left[ \sum_{e=1}^{N_i} 2H_w \int_0^L (\{f'_c\}_e^T \{q\}_e)^2 d\bar{x} \right] + \frac{1}{2} \sum_{i=1}^3 \left[ \sum_{e=1}^{N_i} \frac{(w_{se}^* + w_{ce}^*)}{y_e} \int_0^L (\{f_c\}_e^T \{q\}_e)^2 d\bar{x} \right], \quad (3.71)$$

where  $w_{ce}^*$  is the weight of the cable subelement per unit length, and  $\{f'_c\}_e$  is the vector of the slope of the cable model-displacement, expressed by

$$\{f'_c\}_e^T = \frac{1}{L} [0, 0, -1, 0, 0, 1]. \quad (3.72)$$

Eq. 3.71 may be expressed in more convenient terms as

$$V_{ce}(t) = \frac{1}{2} \sum_{e=1}^N \left[ \{q\}_e^T \left( 2H_w \int_0^L \{f'_c\}_e \{f'_c\}_e^T d\bar{x} + \frac{w_{se}^* + w_{ce}^*}{y_e} \int_0^L \{f_c\}_e \{f_c\}_e^T d\bar{x} \right) \{q\}_e \right]. \quad (3.73)$$

or

$$V_{ce}(t) = \frac{1}{2} \sum_{e=1}^N \{q\}_e^T ([k_{c1}]_e + [k_{c2}]_e) \{q\}_e = \frac{1}{2} \sum_{e=1}^N \{q\}_e^T [k_{ce}]_e \{q\}_e, \quad (3.74)$$

where  $[k_{ce}]_e$  is the element elastic-stiffness matrix of the cable; again it consists of the sum of two matrices, and can be evaluated, as before, to give

$$[k_{ce}]_e = \frac{2H_w}{L} \begin{bmatrix} 0 & 0 & 0 & 0 & 0 & 0 \\ 0 & 0 & 0 & 0 & 0 & 0 \\ 0 & 0 & 1 & 0 & 0 & -1 \\ 0 & 0 & 0 & 0 & 0 & 0 \\ 0 & 0 & 0 & 0 & 0 & 0 \\ 0 & 0 & -1 & 0 & 0 & 1 \end{bmatrix} + \frac{(w_{se}^* + w_{ce}^*)}{6y_e} \begin{bmatrix} 0 & 0 & 0 & 0 & 0 & 0 \\ 0 & 0 & 0 & 0 & 0 & 0 \\ 0 & 0 & 2 & 0 & 0 & 1 \\ 0 & 0 & 0 & 0 & 0 & 0 \\ 0 & 0 & 0 & 0 & 0 & 0 \\ 0 & 0 & 1 & 0 & 0 & 2 \end{bmatrix} \quad (3.75)$$

Once more, note that zeros are used for the columns and the corresponding rows of the nodal-displacements of the suspended-structure subelement, as the previous assumptions would indicate.

The assemblage elastic-stiffness matrix of the cables can now be written as

$$[K_{CE}] = \sum_{e=1}^N [k_{ce}]_e \quad (3.76)$$

and consequently, the strain energy expression of the cables is

$$V_{ce}(t) = \frac{1}{2} \{r\}^T [K_{CE}] \{r\} \quad (3.77)$$

#### d. Gravity-stiffness matrix of the cables

The gravitational energy associated with the upward motion of the cables (Eq. 3.17) can be expressed, by using the cable displacement-model (Eq. 3.49), as follows

$$\begin{aligned} V_{cg}(t) &= \frac{1}{2} \sum_{i=1}^3 \left[ \sum_{e=1}^{N_i} \frac{w_{ce}^*}{y_e} \int_0^L (\{f_{ce}\}^T \{q\}_e)^T (\{f_{ce}\}^T \{q\}_e) d\bar{x} \right] , \\ &= \frac{1}{2} \sum_{e=1}^N \{q\}_e^T \left[ \frac{w_{ce}^*}{y_e} \int_0^L \{f_{ce}\} \{f_{ce}\}^T d\bar{x} \right] \{q\}_e , \end{aligned} \quad (3.78)$$

or

$$V_{cg}(t) = \frac{1}{2} \sum_{e=1}^N \{q\}_e^T [k_{cg}]_e \{q\}_e \quad .$$

Here,  $[k_{cg}]_e$  is the element gravity-stiffness matrix of the cables; it can be obtained by using Eqs. 3.62, 3.64 and 3.78 and is given as

$$[k_{cg}]_e = \frac{w_{ce}^* L}{6 y_e} \begin{bmatrix} 0 & 0 & 0 & 0 & 0 & 0 \\ 0 & 0 & 0 & 0 & 0 & 0 \\ 0 & 0 & 2 & 0 & 0 & 1 \\ 0 & 0 & 0 & 0 & 0 & 0 \\ 0 & 0 & 0 & 0 & 0 & 0 \\ 0 & 0 & 1 & 0 & 0 & 2 \end{bmatrix} \quad . \quad (3.79)$$

Superposing appropriately gives the assemblage gravity-stiffness matrix of the cables as

$$[K_{CG}] = \sum_{e=1}^N [k_{cg}]_e \quad , \quad (3.80)$$

and, therefore, the gravitational energy expression of the cables may be written as

$$V_{cg}(t) = \frac{1}{2} \{r\}^T [K_{CG}] \{r\} \quad . \quad (3.81)$$

### III-4-3. Evaluation of inertia-property matrices

In evaluating the mass matrices of the system, the kinetic energy caused by the incidental vertical motion of the laterally

vibrating suspension bridge (Eqs. 3.26 and 3.27) is neglected because the upward deflections  $v_c$  and  $v_s$  are small quantities of higher order than the lateral displacements  $w_c$  and  $w_s$ .

a. Consistent-mass matrix of the suspended structure

The kinetic energy expression (Eq. 3.23) of the suspended structure due to lateral displacement, with the aid of the suspended-structure displacement model (Eq. 3.45), gives

$$T_s(t) = \frac{1}{2} \sum_{i=1}^3 \left[ \sum_{e=1}^{N_i} \bar{m}_{se}^* \int_0^L (\{f_s\}_e^T \{\dot{q}\}_e)^T (\{f_s\}_e^T \{\dot{q}\}_e) d\bar{x} \right], \quad (3.82)$$

where  $\bar{m}_{se}^*$  is the mass of the suspended-structure subelement per unit length. In this case  $\bar{m}_{se}^*$  is assumed uniform along the individual element.

Eq. 3.82 may also be written in the form

$$T_s(t) = \frac{1}{2} \sum_{i=1}^3 \left[ \sum_{e=1}^{N_i} \{\dot{q}\}_e^T [m_s]_e \{\dot{q}\}_e \right], \quad (3.83)$$

where  $[m_s]_e$  is the consistent-mass matrix of the suspended-structure subelement and is defined by

$$[m_s]_e = \bar{m}_{se}^* \int_0^L \{f_s\}_e \{f_s\}_e^T d\bar{x} \quad (3.84)$$

Upon carrying out the necessary vector multiplications and integrations, this matrix becomes

$$[m_s]_e = \frac{m_{se}^* L}{420} \begin{bmatrix} 156 & -22L & 0 & 54 & 13L & 0 \\ -22L & 4L^2 & 0 & -13L & -3L^2 & 0 \\ 0 & 0 & 0 & 0 & 0 & 0 \\ 54 & -13L & 0 & 156 & 22L & 0 \\ 13L & -3L & 0 & 22L & 4L^2 & 0 \\ 0 & 0 & 0 & 0 & 0 & 0 \end{bmatrix} \quad (3.85)$$

Thus, the assemblage consistent-mass matrix of the suspended structure is

$$[M_s] = \sum_{e=1}^N [m_s]_e \quad , \quad (3.86)$$

and, the kinetic energy expression (Eq. 3.83) becomes

$$T_s(t) = \frac{1}{2} \{\dot{r}\}^T [M_s] \{\dot{r}\} \quad . \quad (3.87)$$

b. Mass matrix of the cable

The kinetic energy expression (Eq. 3.22) of the cable due to lateral displacement, can now be expressed conveniently, in terms of the stiffness matrix, as

$$\begin{aligned} T_c(t) &= \frac{1}{2} \sum_{i=1}^3 \left[ \sum_{e=1}^{N_i} m_{ce}^* \int_0^L (\{f_c\}_e^T \{\dot{q}\}_e)^T (\{f_c\}_e^T \{\dot{q}\}_e) d\bar{x} \right] \\ &= \frac{1}{2} \sum_{e=1}^N \{\dot{q}\}_e^T [m_c]_e \{\dot{q}\}_e \end{aligned} \quad (3.88)$$

where

$$[m_c]_e = \dot{m}_{ce}^* \int_0^L \{f_c\}_e \{f_c\}_e^T d\bar{x} \quad (3.89)$$

is the element-mass matrix of the cable structure, and  $\dot{m}_{ce}^*$  is the mass of the cable subelement per unit length.

The element-mass matrix resulting from Eq. 3.89, when the results of Eqs. 3.62 and 3.64 are used, may be expressed by

$$[m_c]_e = \frac{\dot{m}_{ce}^* L}{6} \begin{bmatrix} 0 & 0 & 0 & 0 & 0 & 0 \\ 0 & 0 & 0 & 0 & 0 & 0 \\ 0 & 0 & 2 & 0 & 0 & 1 \\ 0 & 0 & 0 & 0 & 0 & 0 \\ 0 & 0 & 0 & 0 & 0 & 0 \\ 0 & 0 & 1 & 0 & 0 & 2 \end{bmatrix} \quad (3.90)$$

Finally, the assemblage mass matrix of the cables is

$$[M_c] = \sum_{e=1}^N [m_c]_e \quad ,$$

and the kinetic energy of the assemblage is given by

$$T_c(t) = \frac{1}{2} \{\dot{r}\}^T [M_c] \{\dot{r}\} \quad (3.91)$$

#### III-4-4. Variational formulation of the matrix equations of motion

Inserting the different energy expressions, Eqs. 3.56, 3.68, 3.77, 3.81, 3.87 and 3.91 into Hamilton's Principle, and performing

the variations and the integration by parts, one obtains the following

$$\int_{t_1}^{t_2} \{\delta r\}^T \left[ \left( [M_S] + [M_C] \right) \{\ddot{r}\} + \left( [K_{SE}] + [K_{SG}] + [K_{CE}] + [K_{CG}] \right) \{r\} \right] dt = 0 .$$

Due to the arbitrary nature of the variations in nodal displacement,  $\{\delta r\}$ , the expression in square brackets must vanish.

Therefore, the equations of motion for the gross assemblage has the form

$$\left( [M_S] + [M_C] \right) \{\ddot{r}\} + \left( [K_{SE}] + [K_{SG}] + [K_{CE}] + [K_{CG}] \right) \{r\} = \{0\} . \quad (3.92)$$

These are the governing differential equations for the problem of lateral vibrations of suspension bridge structures.

The matrix equations of motion for the free, lateral undamped vibrations of the suspension bridge can be conveniently written as

$$[M] \{\ddot{r}\} + [K] \{r\} = 0 , \quad (3.93)$$

where

$$[M] = [M_S] + [M_C] \quad (3.93-a)$$

and

$$[K] = [K_{SE}] + [K_{SG}] + [K_{CE}] + [K_{CG}] \quad (3.93-b)$$

are the mass and stiffness matrices, respectively, for the complete system; they are positive definite, symmetric, and banded matrices.

Again, by writing the solutions of Eq. 3.93 in the well-known form

$$\{r(t)\} = \{r^*\} e^{i\omega t} , \quad i = \sqrt{-1} , \quad (3.94)$$

the eigenproblem, identical in form to those given in Chapters I and II,

appears as

$$\left( [K] - \omega^2 [M] \right) \{r^*\} = \{0\} \quad . \quad (3.95)$$

Here  $\omega$  is the natural circular frequency of free vibration, and  $\{r^*\}$  is the vector of the displacement amplitudes.

Multiplying throughout by  $[M]^{-1}$ , one has the more standard representation

$$\left( [M]^{-1} [K] - \omega^2 [I] \right) \{r^*\} = \{0\} \quad . \quad (3.96)$$

If the matrices  $[M]$  and  $[K]$  are  $n \times n$  matrices corresponding to  $n$  degrees of freedom, then there will be  $n$  eigenvalues ( $\omega_n^2$ ) and  $n$  corresponding eigenvectors ( $\{r_n^*\}$ ) satisfying Eq. 3.95; the above-mentioned eigenvectors will not necessarily be distinct from one another.

#### III-4-5. Numerical example

A numerical example is presented to demonstrate the effectiveness of the analysis developed in this chapter. In this example, the finite-element results are compared with those obtained by an approximate method of analysis (i. e., one based on deriving the frequency equations). In general, the numerical example is presented not only in order to illustrate the satisfactory agreement of the results but also to delineate some characteristics of the dynamic behavior of laterally vibrating suspension bridges.

Computations using data from the San Pedro-Terminal Island Suspension Bridge provide the basis for this example. Lateral vibrations of the center span cable and suspended structure are

investigated. In this illustrative example, the lateral displacements of the cable segments and the ends of the suspended structure are taken to be zero.

The structural properties used in this example are:

$$I_{s2} = 293,000 \text{ in.}^2 \text{ft.}^2$$

$$E_{s2} = 29,000 \text{ Kip/in.}^2$$

$$H_w = 6,750 \text{ Kips/cable.}$$

$$w_c^* = 1.042 \text{ Kip/ft. per bridge.}$$

$$w_{s2}^* = 6.152 \text{ Kip/ft. per bridge.}$$

The span was subdivided into  $N_2 = 24$  elements, as shown in Figs. III-2-a and b, and the length of each element  $L$  is 62.5 ft. There are  $(2N_2 + 2)$  nodes, starting with node 1 at the left support of the suspended structure and ending with node  $(2N_2 + 2)$  at the top of the right tower. There are  $(3N_2 - 1)$  degrees of freedom for the complete structure, with the numbering system shown in Fig. III-2.

The eigenvalue problem (Eq. 3.95 or 3.96) was solved on the Caltech digital computer (IBM 370/158 system). Some of the computed natural periods and frequencies are presented, for the symmetric and antisymmetric vibrations, in Tables III-1 and III-2, respectively, and the corresponding mode-shapes are shown in Figs. III-3, III-4 and III-5. It can be seen in these figures that:

1. In the lower modes there is a coupled motion between the cables and the suspended structure, while in the higher modes the two systems vibrate in a prescribed manner.

San Pedro-Terminal Island Suspension Bridge  
 Natural Periods and Frequencies of Lateral Vibration  
 (Symmetric Modes of Center Span)

| Mode Order | Frequency $\omega$<br>rad/sec. | Period T<br>sec. | Frequency f<br>c. p. s. | Member of Dominant<br>Vibration |
|------------|--------------------------------|------------------|-------------------------|---------------------------------|
| 1          | 1.086967                       | 5.780476         | 0.172996                | Suspended structure & Cable     |
| 2          | 3.545266                       | 1.773577         | 0.563832                | Suspended structure & Cable     |
| 3          | 5.177737                       | 1.213500         | 0.824062                | Cable                           |
| 4          | 7.568050                       | 0.830225         | 1.204493                | Cable                           |
| 5          | 8.423586                       | 0.745904         | 1.340655                | Suspended structure & Cable     |
| 6          | 10.348652                      | 0.607150         | 1.647039                | Cable                           |
| 7          | 13.355416                      | 0.470460         | 2.125581                | Cable                           |
| 8          | 16.601443                      | 0.378472         | 2.642202                | Cable                           |
| 9          | 20.094666                      | 0.312679         | 3.198166                | Cable                           |
| 10         | 23.182960                      | 0.271026         | 3.689683                | Suspended structure             |
| 11         | 23.807144                      | 0.263920         | 3.789025                | Cable                           |
| 12         | 27.622482                      | 0.227466         | 4.396254                | Cable                           |
| 13         | 31.266521                      | 0.200956         | 4.976221                | Cable                           |
| 14         | 34.260207                      | 0.183396         | 5.452681                | Cable                           |
| 15         | 35.765184                      | 0.175679         | 5.692206                | Cable                           |
| 16         | 45.422362                      | 0.138328         | 7.229193                | Suspended structure             |
| 17         | 75.135126                      | 0.083625         | 11.958127               | Suspended structure             |
| 18         | 112.405055                     | 0.055898         | 17.889820               | Suspended structure             |
| 19         | 157.392528                     | 0.039920         | 25.049799               | Suspended structure             |
| 20         | 210.356996                     | 0.029869         | 33.479356               | Suspended structure             |
| 21         | 271.674485                     | 0.023128         | 43.238337               | Suspended structure             |

TABLE III-1

San Pedro-Terminal Island Suspension Bridge  
 Natural Periods and Frequencies of Lateral Vibration  
 (Antisymmetric Modes of Center Span)

| Mode Order | Frequency $\omega$<br>rad/sec. | Period T<br>sec. | Frequency f<br>c. p. s. | Member of Dominant<br>Vibration |
|------------|--------------------------------|------------------|-------------------------|---------------------------------|
| 1          | 3.550943                       | 1.769441         | 0.565150                | Suspended structure & Cable     |
| 2          | 4.039458                       | 1.555452         | 0.642900                | Suspended structure & Cable     |
| 3          | 6.256057                       | 1.004336         | 0.995682                | Cable                           |
| 4          | 8.926214                       | 0.703903         | 1.420651                | Cable                           |
| 5          | 11.822368                      | 0.531466         | 1.881588                | Cable                           |
| 6          | 14.855277                      | 0.422960         | 2.364291                | Suspended structure & Cable     |
| 7          | 14.948389                      | 0.420325         | 2.379110                | Cable                           |
| 8          | 18.317546                      | 0.343015         | 2.915328                | Cable                           |
| 9          | 21.927925                      | 0.286538         | 3.489938                | Cable                           |
| 10         | 25.714545                      | 0.244343         | 4.092597                | Cable                           |
| 11         | 29.490808                      | 0.213056         | 4.693608                | Cable                           |
| 12         | 32.878375                      | 0.191104         | 5.232756                | Cable                           |
| 13         | 33.371105                      | 0.188282         | 5.311176                | Suspended structure             |
| 14         | 35.296178                      | 0.178013         | 5.617561                | Cable                           |
| 15         | 59.340902                      | 0.105883         | 9.444398                | Suspended structure             |
| 16         | 92.817460                      | 0.067694         | 14.772358               | Suspended structure             |
| 17         | 133.920464                     | 0.046917         | 21.314104               | Suspended structure             |
| 18         | 182.856993                     | 0.034361         | 29.102594               | Suspended structure             |
| 19         | 239.943451                     | 0.026186         | 38.188186               | Suspended structure             |
| 20         | 305.613998                     | 0.020559         | 48.639978               | Suspended structure             |
| 21         | 380.365770                     | 0.016519         | 60.537092               | Suspended structure             |

TABLE III-2

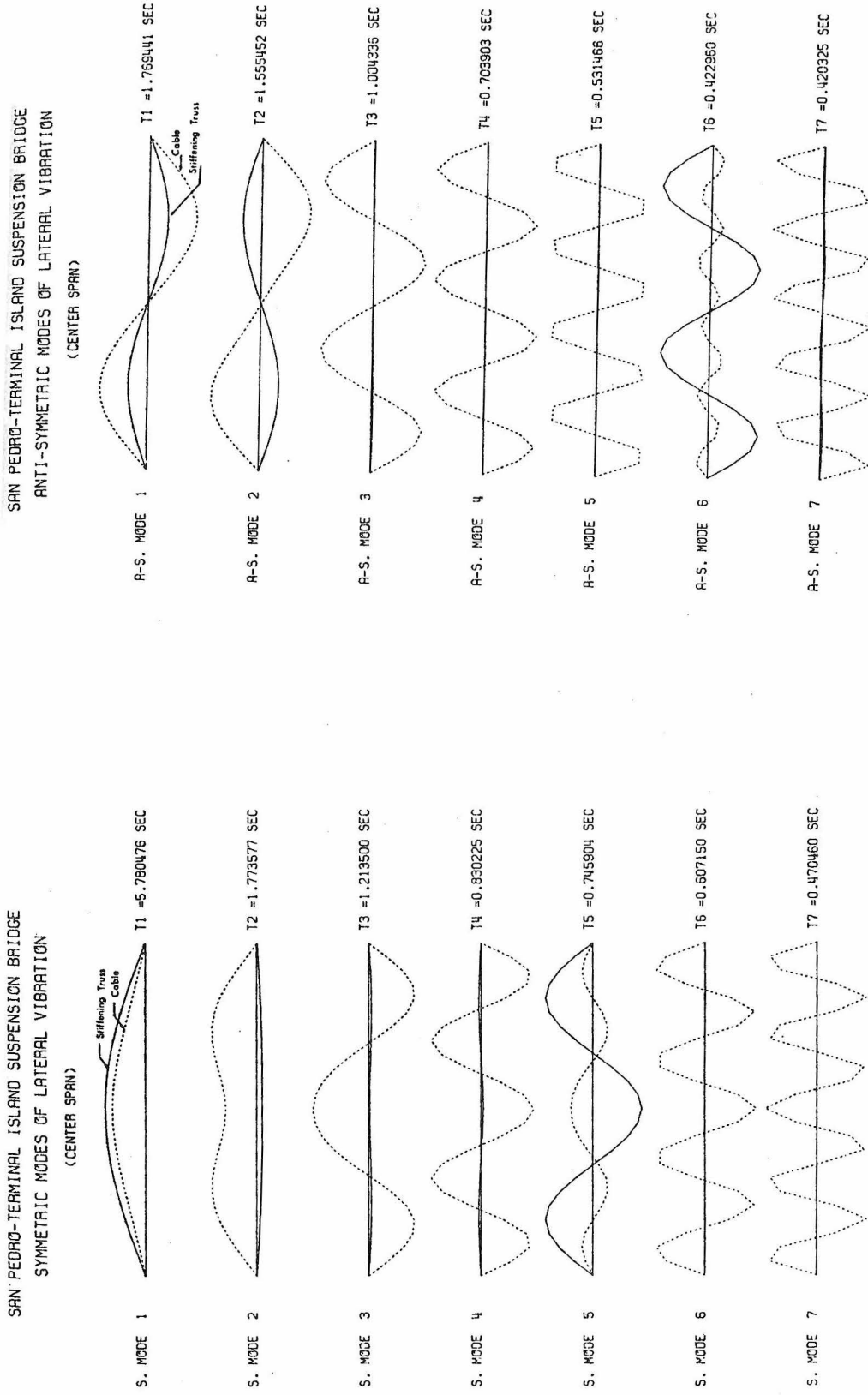


Fig. III-3

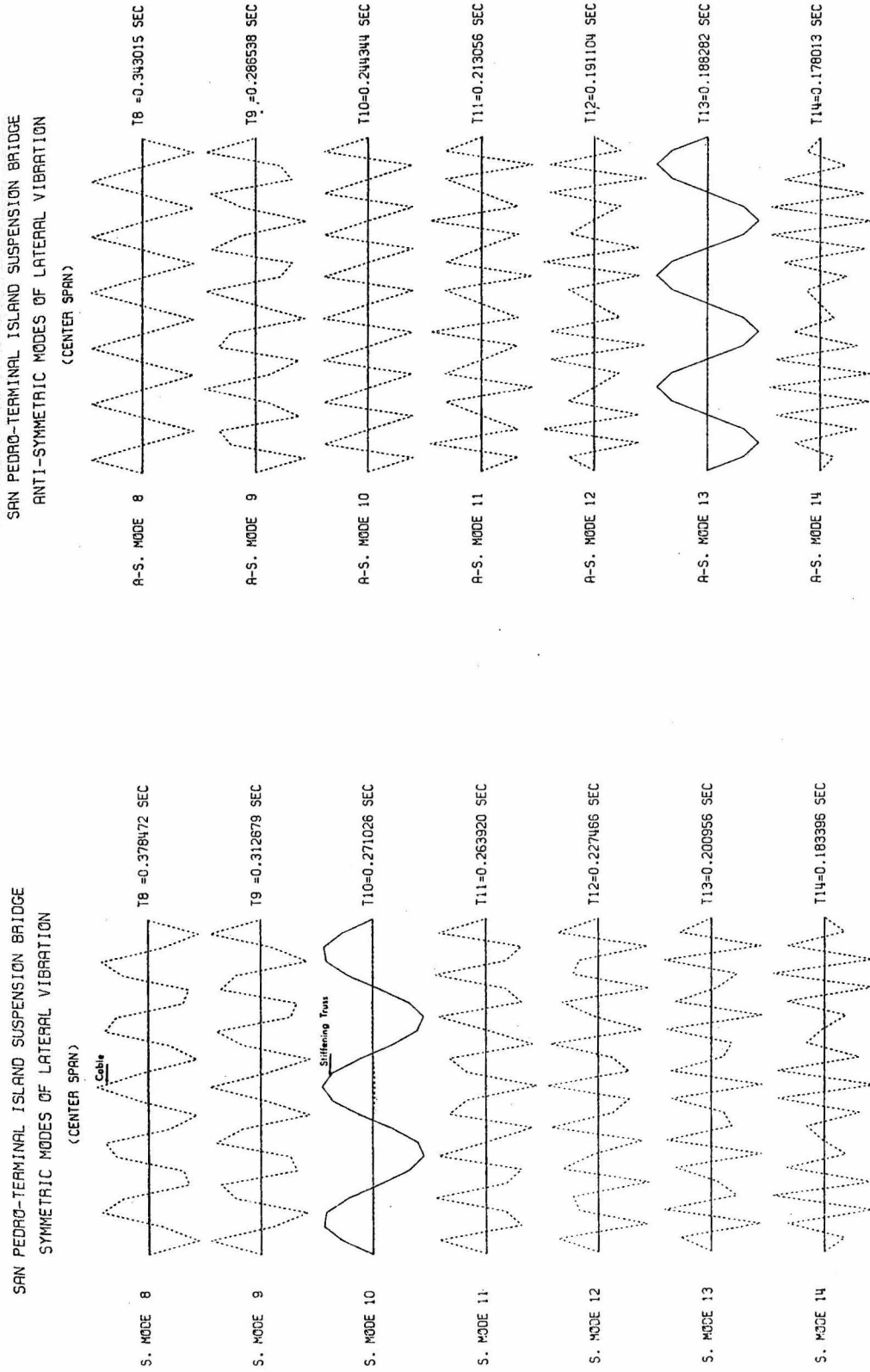


Fig. III-4

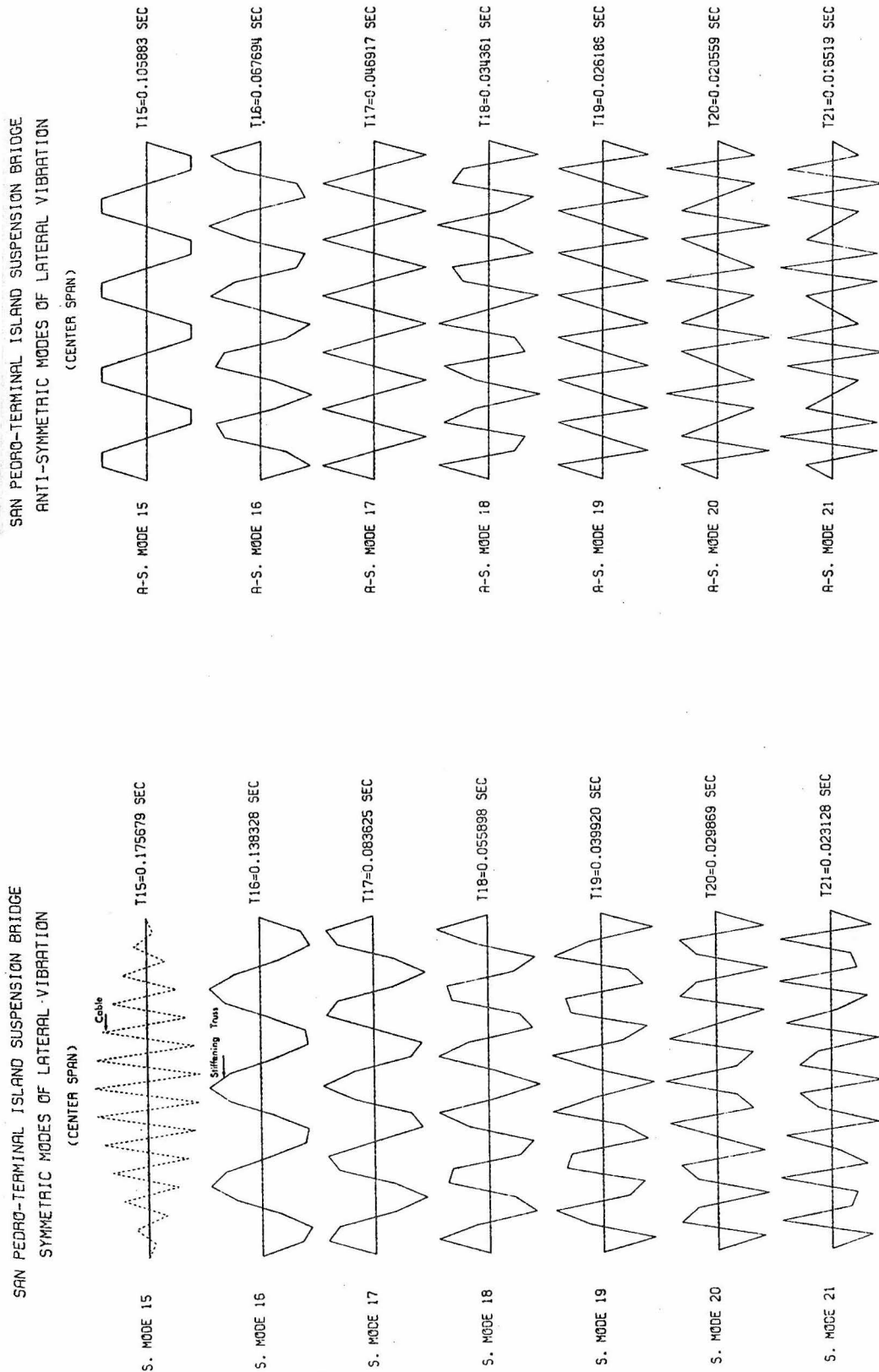


Fig. III-5

2. The first two symmetric (and antisymmetric) modes have a similar configuration except for the fact that in the first mode the cable and the suspended structure are moving in phase, while in the second mode they are moving  $180^{\circ}$  out of phase. Furthermore, the effect of short suspenders at the mid-span is clear in the second mode from the depression or dip in the middle region.
3. In most of the coupled modes (such as the 5<sup>th</sup> symmetric and the 6<sup>th</sup> antisymmetric modes) the nodal points of the cable and those of the suspended structure do not coincide.
4. In the higher modes, where the two systems vibrate in a prescribed manner, the cable frequencies are smaller than those of the suspended structure even when the respective mode configurations are the same; see mode 6 (for the cable) and mode 16 (for the suspended structure).

The distribution of the various energies stored in the cable and in the suspended structure, for both symmetric and antisymmetric vibrations, is illustrated in Figs. III-6 and III-7. As presented in Fig. III-6-a, the relative contribution of the kinetic energy of the suspended structure is greatest in the first mode (about 90% of the total kinetic energy, while the contribution of the cables is about 10%); the opposite is true for the second symmetric mode. Subsequently, the kinetic energy comes entirely from either the cable or from the suspended structure, depending on which is dominant. The potential energy of the complete system in the first mode is 70% strain energy

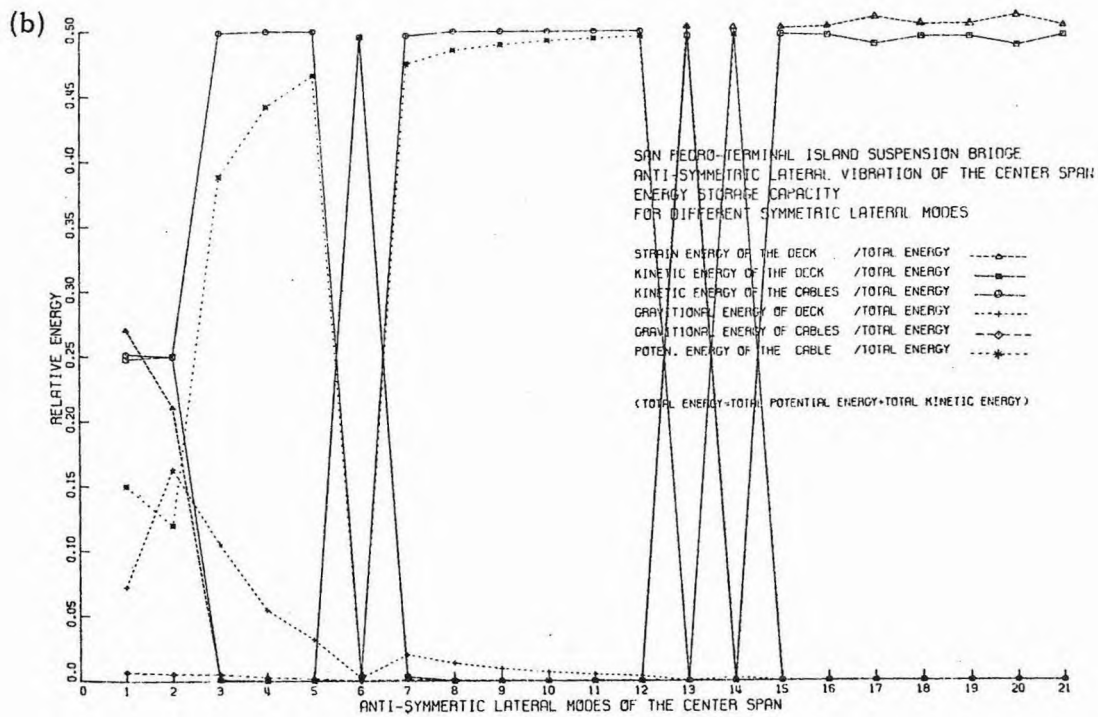
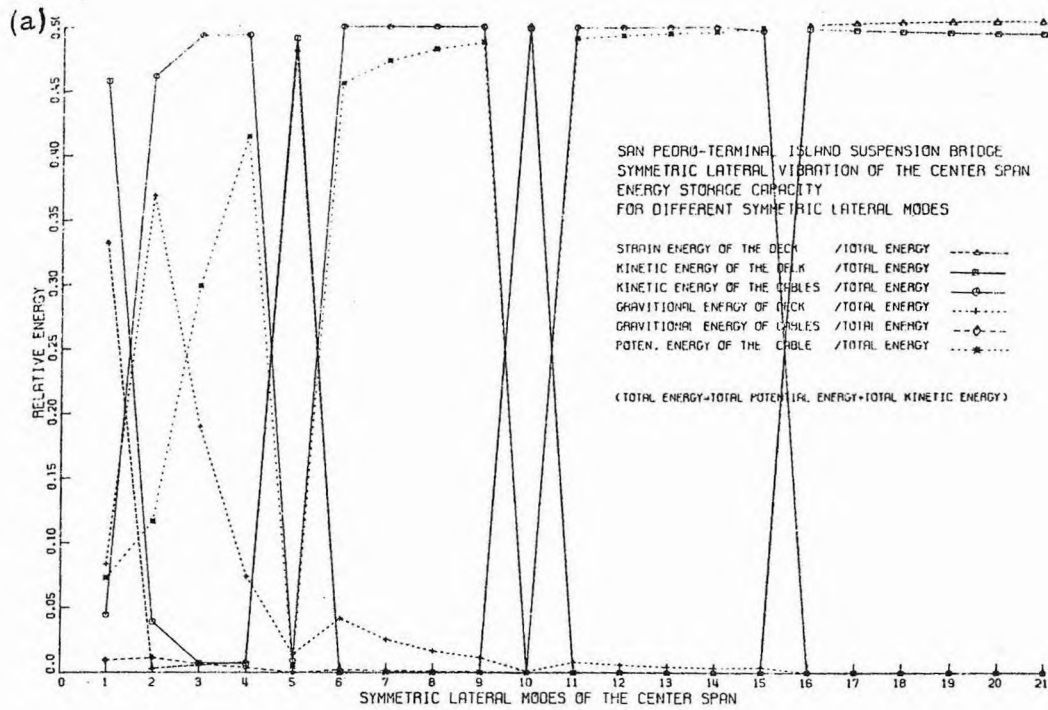


Fig. III-6. Relative energy storage capacity of the cable and suspended structure for the (a) symmetric modes and (b) antisymmetric modes.

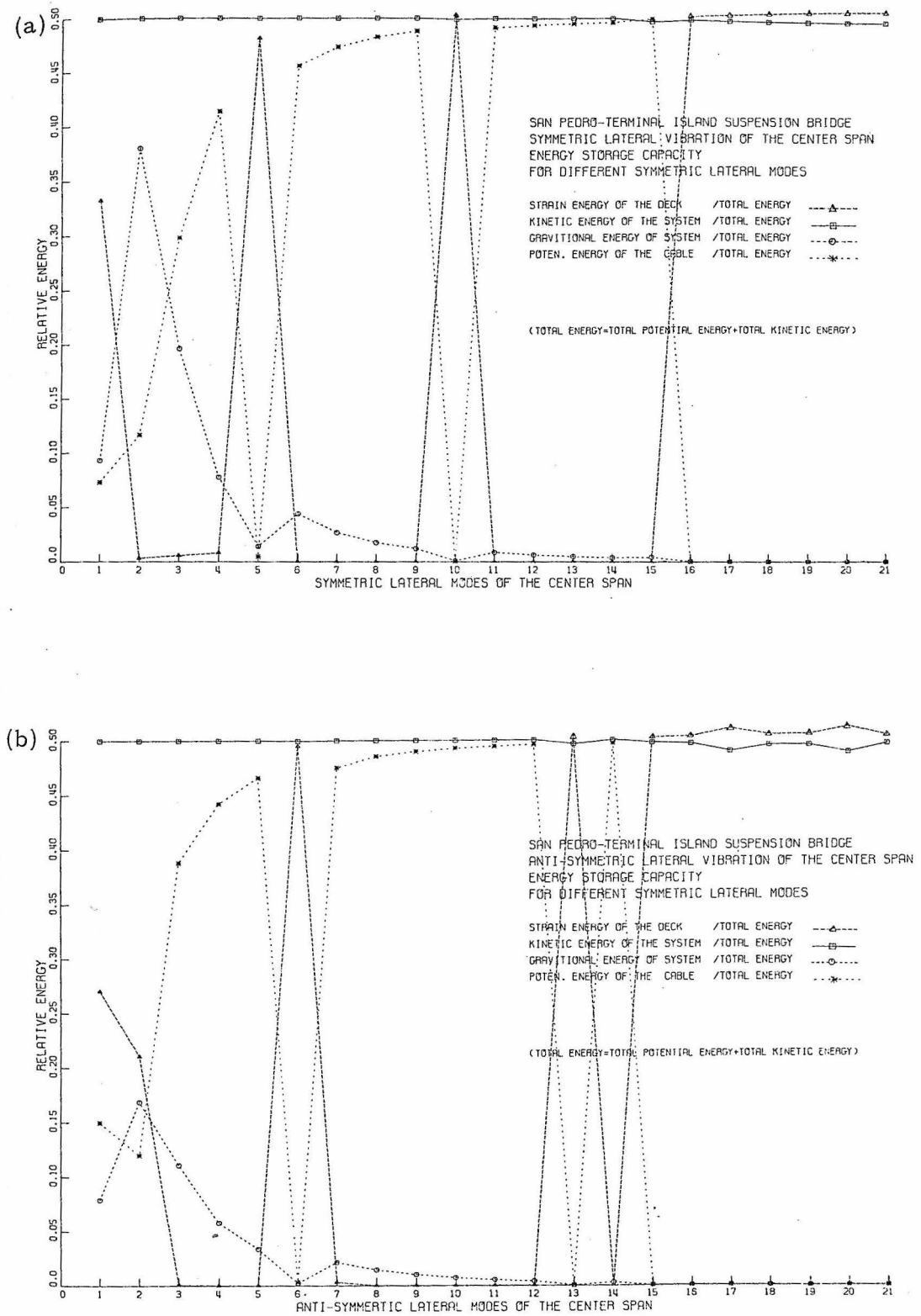


Fig. III-7. Relative energy storage capacity of the system for the (a) symmetric modes and (b) antisymmetric modes.

of the suspended structure, 15% strain energy of the cable and 15% gravitational energy of the suspended structure. The contribution of this gravitational energy is greatest in the second symmetric mode. In Fig. III-6-b, the relative contribution from the kinetic energy of the cable is shown to be the same as that from the kinetic energy of the bridge deck in the first and second antisymmetric modes. In general, the relative contribution from the strain energy (of both the suspended structure and the cable) increases in the higher modes until it provides almost all of the potential energy of the structure; the principle effect of gravitational energy is confined to the first few modes of the suspended structure vibration. Contribution from the gravitational energy of the cable is extremely small throughout.

Now, by considering the two linear differential equations of motion (Eqs. 3.43' and 3.44), by assuming sine mode shapes and by using the orthogonality property of the modes, the frequency equations can be obtained. Appendix III-a contains a detailed derivation of these frequency equations. The roots of each frequency equation (i. e., the natural frequencies) reflect both the in-phase vibration of the cable and suspended structure systems and the vibration when the systems are  $180^{\circ}$  out of phase. The first few frequencies and some of their corresponding modes are shown in Tables III-3 and III-4 and in Fig. III-8. In these tables, a comparison between the finite-element solutions and the approximate results is included. There is a close agreement between the frequencies of the finite-element solution and those of the frequency-equations solution. It will be noted that some

Comparison Between the Frequencies Obtained by the Finite-Element Method and Those Obtained by the Frequency Equations (Symmetric Modes)

| Number of half sine waves $n$ | Roots of the Frequency Equation (App. III-a) |                | Classification of the different symmetric modes and comparison with the finite-element solutions. |            |                          |                     |            |                          |
|-------------------------------|--|----------------|---|------------|--------------------------|---------------------|------------|--------------------------|
|                               | (1) $\omega_n$                               | (2) $\omega_n$ | Motion in Phase   | Mode Order | Finite-Element Solutions | Motion out of Phase | Mode Order | Finite-Element Solutions |
| 1                             | 1.085  | 3.625          | 1.085   | 1          | 1.086967                 | 3.625               | 2          | 3.545266                 |
| 3                             | 5.247  | 8.371          | 5.247   | 3          | 5.177737                 | 8.371               | 5          | 8.423586                 |
| 5                             | 7.540  | 23.169         | 7.540   | 4          | 7.568050                 | 23.169              | 10         | 23.182960                |
| 7                             | 10.039                                       | 45.394         | 10.039  | 6          | 10.348652                | 45.394              | 16         | 45.422362                |
| 9                             | 12.623                                       | 75.033         | 12.623  | 7          | 13.355416                | 75.033              | 17         | 75.135126                |
| 11                            | 15.249                                       | 112.083        | 15.249  | 8          | 16.601443                | 112.083             | 18         | 112.405055               |
| 13                            | 17.899                                       | 156.545        | 17.899  | 9          | 20.094668                | 156.545             | 19         | 157.392528               |
| 15                            | 20.564                                       | 208.416        | 20.564  | 10         | 23.182960                | 208.416             | 20         | 210.356996               |
| 17                            | 23.237                                       | 267.699        | 23.237  | 11         | 23.807144                | 267.699             | 21         | 271.674485               |

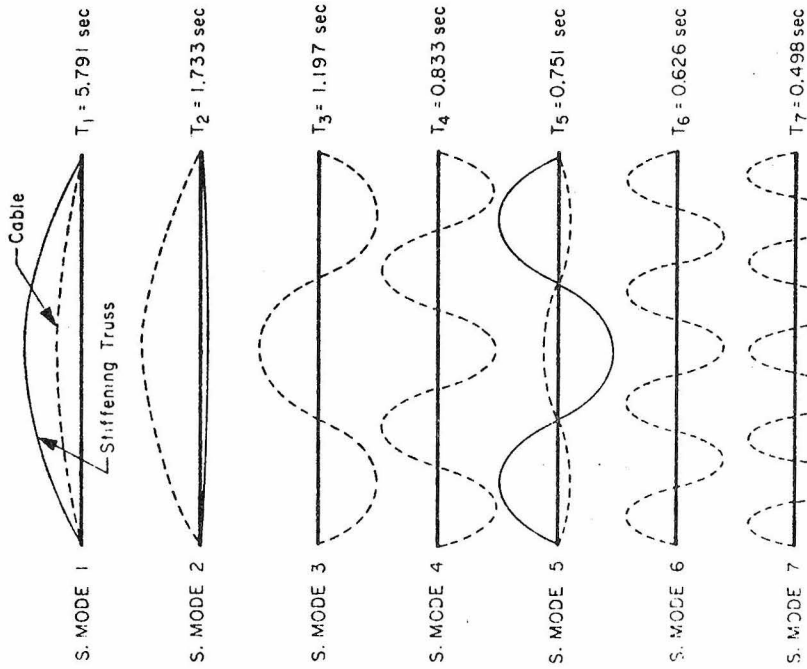
TABLE III-3

Comparison Between the Frequencies Obtained by the Finite-Element Method and Those Obtained by the Frequency Equations  
(Antisymmetric Modes)

| Number of half sine waves $n$ | Roots of the Frequency Equation (App. III-a) |                | Classification of the different antisymmetric modes and comparison with the finite-element solutions. |            |                          |                     |            |                          |
|-------------------------------|--|----------------|---|------------|--------------------------|---------------------|------------|--------------------------|
|                               | (1) $\omega_n$                               | (2) $\omega_n$ | Motion in Phase   | Mode Order | Finite-Element Solutions | Motion out of Phase | Mode Order | Finite-Element Solutions |
| 2                             | 3.708  | 4.351          | 3.708   | 1          | 3.550943                 | 4.351               | 2          | 4.039458                 |
| 4                             | 6.355  | 14.839         | 6.355   | 3          | 6.256057                 | 14.839              | 6          | 14.855277                |
| 6                             | 8.774  | 33.354         | 8.774   | 4          | 8.926214                 | 33.354              | 13         | 33.371105                |
| 8                             | 11.324                                       | 59.287         | 11.324  | 5          | 11.822368                | 59.287              | 15         | 59.340902                |
| 10                            | 13.933                                       | 92.632         | 13.933  | 6          | 14.855277                | 92.632              | 16         | 92.8p7460                |
| 12                            | 16.572                                       | 133.388        | 16.572  | 7          | 14.948389                | 133.388             | 17         | 133.920464               |
| 14                            | 19.230                                       | 181.554        | 19.230  | 8          | 18.317546                | 181.554             | 18         | 182.856993               |
| 16                            | 21.900                                       | 237.131        | 21.900  | 9          | 21.927925                | 237.131             | 19         | 239.943451               |

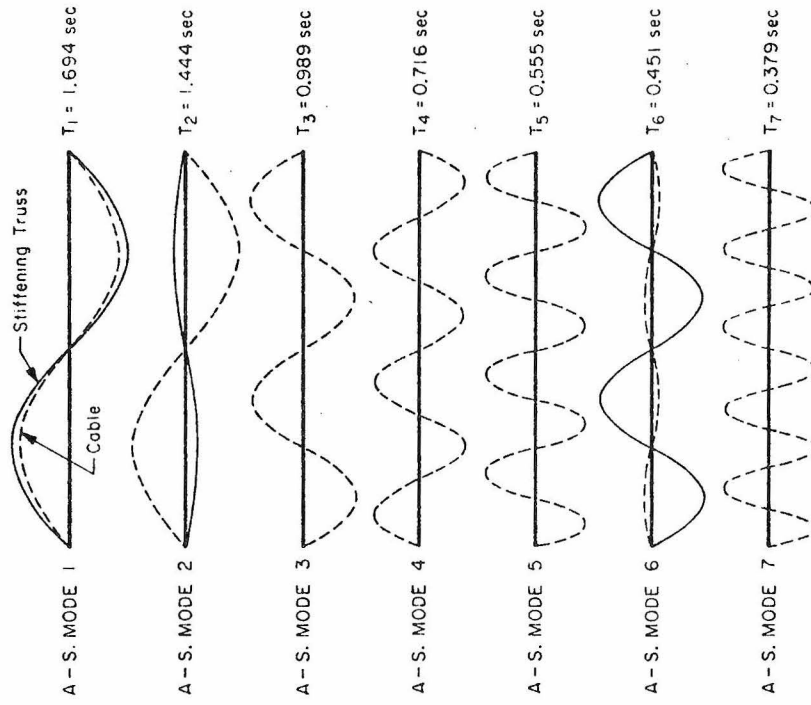
TABLE III-4

SAN PEDRO - TERMINAL ISLAND SUSPENSION BRIDGE  
 SYMMETRIC MODES OF LATERAL VIBRATION  
 (CENTER SPAN)



SYMMETRIC MODES OBTAINED BY AN APPROXIMATE METHOD

SAN PEDRO - TERMINAL ISLAND SUSPENSION BRIDGE  
 ANTI-SYMMETRIC MODES OF LATERAL VIBRATION  
 (CENTER SPAN)



ANTI-SYMMETRIC MODES OBTAINED  
 BY AN APPROXIMATE METHOD

Fig. III-8

of the assumed "sine" mode-shapes do not agree with those of the finite-element solutions; for instance: a) the second assumed "sine" symmetric mode (Fig. III-8) does not show the effect of the short suspenders in the mid-span, b) in the fifth assumed "sine" symmetric mode, the two systems have the same number of nodal points, as was assumed in a prerequisite to deriving the frequency equation (this is also true in the sixth antisymmetric mode), c) the first assumed "sine" antisymmetric mode is completely different from the finite-element solution, and finally d) the coupling between the two systems has disappeared in some modes of the approximate solution.

III-5. Appendices

Appendix III-a

An Approximate Solution for the Equations of Motion

The two linear differential equations of motion (Eqs. 3.43 and 3.44) recalled from section III-3 of this chapter, are

$$\begin{aligned} \dot{m}_c^* \frac{\partial^2 w_c}{\partial t^2} - 2 H_w \frac{\partial^2 w_c}{\partial x_j^2} - \dot{w}_{sj}^* \left( \frac{w_s - w_c}{h(x_j)} \right) + 2 (\dot{w}_{sj}^* + \dot{w}_c^*) \frac{w_c}{y_c(x_j)} = 0, \\ j = 1, 2, 3, \quad \text{(III-a-1)} \end{aligned}$$

and

$$\dot{m}_{sj}^* \frac{\partial^2 w_s}{\partial t^2} + E_{sj} I_{sj} \frac{\partial^4 w_s}{\partial x_j^4} + \dot{w}_{sj}^* \left( \frac{w_s - w_c}{h(x_j)} \right) = 0, \quad j = 1, 2, 3, \quad \text{(III-a-2)}$$

where  $y_c(x_j) = \frac{4 f_j}{\ell_j^2} x_j (\ell_j - x_j)$  and  $h(x_j) = h_T - y_c(x_j)$ ,  $j = 1, 2, 3$ ,

with  $h_T$  being the height of the suspender close to the tower.

These equations cannot be solved in closed form; however, one can approximate their eigenfunctions and find the corresponding eigenvalues.

First, define a normal mode vibration as one in which each system (cable and suspended structure) undergoes harmonic motion of the same frequency. For each motion one can write

$$\left. \begin{aligned} w_c(x_j, t) &= \tilde{w}_c(x_j) e^{i\omega t} \\ w_s(x_j, t) &= \tilde{w}_s(x_j) e^{i\omega t} \end{aligned} \right\} j = 1, 2, 3, \quad \text{(III-a-3)}$$

where  $\omega$  is the natural circular frequency and  $i = \sqrt{-1}$ .

Substituting these into the two differential equations, multiplying the first equation (III-a-1) by  $y_c(x_j) h(x_j)$  and the second equation (III-a-2) by  $h(x_j)$  and rearranging the terms, gives

$$2H_w h(x_j) y_c(x_j) \frac{d^2 \tilde{w}_c}{dx_j^2} - \left[ \tilde{w}_{sj}^* y_c(x_j) + 2 \left( \tilde{w}_c^* + \tilde{w}_{sj}^* \right) h(x_j) \right] \tilde{w}_c + m_c^* \omega^2 h(x_j) y_c(x_j) \tilde{w}_c + \tilde{w}_{sj}^* y_c(x_j) \tilde{w}_s = 0, \quad j = 1, 2, 3 \quad \text{(III-a-4)}$$

and

$$E_{sj} I_{sj} h(x_j) \frac{d^4 \tilde{w}_s}{dx_j^4} + \tilde{w}_{sj}^* \tilde{w}_s - m_{sj}^* \omega^2 h(x_j) \tilde{w}_s - \tilde{w}_{sj}^* \tilde{w}_c = 0, \quad j = 1, 2, 3 \quad \text{(III-a-5)}$$

By letting  $\omega_n$  and  $\omega_m$  be two different eigenvalues with the corresponding eigenfunctions  $\tilde{w}_c^n$ ,  $\tilde{w}_s^n$  and  $\tilde{w}_c^m$ ,  $\tilde{w}_s^m$ , the orthogonality conditions can be derived in the forms

$$\left. \begin{aligned} \int_0^{l_j} h(x_j) y_c(x_j) \tilde{w}_c^n \tilde{w}_c^m dx_j &= 0 \\ \int_0^{l_j} h(x_j) \tilde{w}_s^n \tilde{w}_s^m dx_j &= 0 \end{aligned} \right\} j = 1, 2, 3. \quad \text{(III-a-6)}$$

Define  $\tilde{w}_c$  and  $\tilde{w}_s$  as

$$\left. \begin{aligned} \tilde{w}_c(x_j) &= A_n \sin \frac{n\pi x_j}{l_j} \\ \tilde{w}_s(x_j) &= B_n \sin \frac{n\pi x_j}{l_j} \end{aligned} \right\} j = 1, 2, 3, \quad n = 1, 2, 3, 4, \dots \quad \text{(III-a-7)}$$

Substituting these into the ordinary differential equations (III-a-4 and 5), multiplying each equation by  $\sin \frac{n\pi x_j}{l_j}$  and using the orthogonality conditions (Eq. III-a-6), give

$$\left. \begin{aligned} (a_{11}) A_n + (a_{12}) B_n &= 0 \\ (a_{21}) A_n + (a_{22}) B_n &= 0 \end{aligned} \right\} n = 1, 2, 3, \dots \quad (\text{III-a-8})$$

where the coefficients  $a_{ij}$ ,  $i, j = 1, 2$ , are given by

$$\begin{aligned} a_{11} = & -2 H_w \left( \frac{n\pi}{l_j} \right)^2 \int_0^{l_j} h(x_j) y_c(x_j) \sin^2 \left( \frac{n\pi x_j}{l_j} \right) dx_j - \bar{w}_{sj}^* \int_0^{l_j} y_c(x_j) \sin^2 \left( \frac{n\pi x_j}{l_j} \right) dx_j \\ & + 2 (\bar{w}_c^* + \bar{w}_{sj}^*) \int_0^{l_j} h(x_j) \sin^2 \left( \frac{n\pi x_j}{l_j} \right) dx_j + m_c^* \omega_n^2 \int_0^{l_j} h(x_j) y_c(x_j) \sin^2 \left( \frac{n\pi x_j}{l_j} \right) dx_j \end{aligned}$$

$$a_{12} = \bar{w}_{sj}^* \int_0^{l_j} y_c(x_j) \sin^2 \left( \frac{n\pi x_j}{l_j} \right) dx_j$$

$$a_{21} = - \bar{w}_{sj}^* \int_0^{l_j} \sin^2 \left( \frac{n\pi x_j}{l_j} \right) dx_j = - \bar{w}_{sj}^* \frac{l_j}{2}$$

and

$$\begin{aligned} a_{22} = & E_{sj} I_{sj} \left( \frac{n\pi}{l_j} \right)^4 \int_0^{l_j} h(x_j) \sin^2 \left( \frac{n\pi x_j}{l_j} \right) dx_j + \bar{w}_{sj}^* \frac{l_j}{2} \\ & - m_{sj}^* \omega_n^2 \int_0^{l_j} h(x_j) \sin^2 \left( \frac{n\pi x_j}{l_j} \right) dx_j \end{aligned}$$

These coefficients can be evaluated by direct integrations.

Equation III-a-8 is satisfied for any  $A_n$  and  $B_n$  if the following determinant is zero

$$\begin{vmatrix} a_{11} & a_{12} \\ a_{21} & a_{22} \end{vmatrix} = 0 . \quad \text{(III-a-9)}$$

Letting  $\omega_n^2 = \lambda_n$ , the above determinant leads to the characteristic equation. The two roots of this equation, for each value of  $n$ , reflect both the in-phase vibration of the cable and suspended structure systems and the vibration when the systems are  $180^\circ$  out of phase.

Finally, substituting these natural frequencies into Eq. III-a-8 enables one to find the ratio of the amplitudes  $A_n/B_n$ ,  
 $n = 1, 2, 3, 4, \dots$

REFERENCES OF CHAPTER III

1. Moisseiff, L. S. and Lienhard, F., "Suspension Bridges under the Action of Lateral Forces," Trans. Am. Soc. C.E., Vol. 98, 1933, pp. 1080-1109.
2. Selberg, A., "Calculation of Lateral Truss in Suspension Bridges," International Association for Bridges and Structural Engineering, Zurich, 1943-1944, Vol. 7, pp. 311-325.
3. Silverman, I. K., "The Lateral Rigidity of Suspension Bridges," Proc. Am. Soc. C.E., EM3, Vol. 83, July 1957, pp. 1292-1 to 1292-17.
4. Selberg, A., "Discussion to the Paper by I. K. Silverman - The Lateral Rigidity of Suspension Bridges," Proc. Am. Soc. C.E., EM1, January 1958, pp. 1520-29 to 1520-31.
5. Erzen, C. Z., "Lateral Bending of Suspension Bridges," Separate No. 663, Proceedings Am. Soc. C.E., pp. 1-7.
6. Hirai, A., Okumura, T., Ito, M. and Narita, N., "Lateral Stability of a Suspension Bridge Subjected to Foundation-Motion," Proceedings of the Second World Conference on Earthquake Engineering, Japan, Vol. II, 1960, pp. 931-945.
7. Ito, M., "Lateral Rigidity of a Suspension Bridge," Symposium on Suspension Bridges, Lisbon, Nov. 1966, Paper No. 7, pp. 7.1-7.8.
8. Konishi, I. and Yamada, Y., "Earthquake Response and Earthquake Resistant Design of Long Span Suspension Bridges," Proceedings of the Third World Conference on Earthquake Engineering, New Zealand, Vol. II, 1965, p. IV/K/12.
9. Hirai, A., "Aerodynamic Stability of Suspension Bridges under Wind Action," Proc. Japan Academy, Vol. 31, No. 9, 1955.

CHAPTER IV  
VIBRATION STUDIES AND TESTS OF THE  
SAN PEDRO-TERMINAL ISLAND SUSPENSION BRIDGE

IV-1. Introduction

The need for extensive dynamic tests of full size suspension bridge structures has been apparent for many years. Although the only certain way to determine the parameters of major interest in structural dynamics problems, such as the frequencies, the modes of vibration and the amount of energy dissipated by the structure, is by testing actual structures, very few of these tests have been performed [2, 6, 7, 9, 10]. Knowledge of these properties is essential if one is to understand and interpret with confidence the structural response of suspension bridges to strong earthquake ground motion, to wind excitation and to moving vehicles on the bridge deck. Unfortunately, testing complete or section models does not provide adequate information [1, 4, 8]. Tests of actual suspension bridge structures have rarely been possible due to the difficulty of making the necessary measurements of dynamic structural response, and due to the lack of development of appropriate instrumentation. In most of the previous trials, the field measurements were made on wind excited vibrations, and the motions usually observed were predominately vertical modes, whereas, the

most hazardous wind induced vibrations are predominantly torsional (see Refs. 2, 8). In severe wind induced vibrations, only one of the lower modes is significantly excited, whereas during an earthquake, many modes may contribute to the response and, therefore, measurements made to throw light on wind induced vibrations are usually not adequate for studying earthquake induced vibrations.

Early observations of suspension bridge motions [1, 7], excited by wind or traffic, were inaccurate and incomplete. In tests recorded before special modern instruments were developed and installed, the period of vibration was estimated or was measured approximately by using a pocket watch. Wave forms were noted and remembered according to the impression of the observer. In some instances, amplitudes were estimated by sighting on bridge elements. At other times sightings were taken with a transit which was located on rods attached to the bridge. Using these methods, vibrations sufficient to be of interest were observed [2] on the Golden Gate Bridge. For example, an engineer who was involved in the construction of the bridge, later recorded observations of the bridge motion during two storms, one on February 9, 1938, some eight months after the bridge was opened to traffic, and the other on February 11, 1941. During the first storm, the movements were evidently in a multi-noded vertical mode. No evidence was given which would indicate lateral or torsional vibration. The highest frequency observed, 0.33 to 0.5 c. p. s., corresponds to Vincent's [2] subsequent computations for the six-noded vertical mode. The computed loop length of the six-noded mode averages 600 ft. No

other recorded observations describe movements having a frequency as high or loops as short as these. The movements during the second storm suggest the second symmetric vertical mode which has a computed period of 6.3 seconds.

The failure of the Tacoma Narrows Bridge in 1940 led to a close scrutiny of all evidence of wind-forced vibration of suspension bridges by engineers and scientists concerned with the problem [1, 9]. As a result, a cooperative research project, between the Golden Gate Bridge and Highway District and the Bureau of Public Roads, was created. Under this agreement, instruments for measuring movements of a bridge were developed, and several of them were installed on the Golden Gate Bridge in 1942. Examples of these early instruments are the anemometer and the accelerometer (see Ref. 2). The anemometer was installed on the bridge to record the velocity and direction of the wind vs. time. The accelerometer, also known as the Hall Recorder, had two conical pendulums for measuring the two horizontal components of motion as well as a mass on a helical spring for measuring the velocity component. The spring suspension could be adjusted to record within a considerable range of natural frequencies, permitting the selection of frequencies most favorable to the recording of the expected vibrations. The record was made by a stylus on smoked paper which was fixed to a drum that was revolved in a spiral motion by clockwork. Later this instrument was replaced by new types which were designed to record only vertical vibration.

In the past, most of the data obtained from different records was analyzed in the time domain. When the time scale of the record was

selected, it was thought that one would only need to determine the frequency over a few cycles with sufficient accuracy to obtain the fundamental frequency, or at the most, the first few natural frequencies, in order to correlate the observations with theoretical calculations of the frequencies of vibration. The scale was adequate for these purposes and for identifying pure vertical or pure torsional motion by noting which stations moved in phase and which moved in opposite phase. However, subsequent experimental work [1, 2, 8] and theoretical analysis revealed that a truss-stiffened suspension bridge might be expected to vibrate in coupled vertical and torsional motion at an altered frequency and with a distinctive phase difference in the two motions. Evidence of such motion had existed in the records, but the time scale had been too small to permit the determination of phase differences.

In the late 1960's and early 1970's, work was begun to study the effect of natural winds on suspension bridges. During this time instrumentation was being developed for measuring all components of the wind velocity at several locations along a suspension bridge. The objective was to record the results in such a manner that they could be analyzed by an electronic computer to produce data on the potential of the wind for producing vibration, as well as on its potential for producing static loading over areas of different sizes. In this regard, the California Division of Highways installed instrumentation on most of the state suspension bridges, including the San Pedro Bridge. One of their reports shows that the bridge has a fundamental period of 4.5 seconds in vertical vibration.

In recent years a method for testing structures based on wind- and microtremor-induced vibrations has been developed. Although the method has been in use for almost 40 years by the United States Coast and Geodetic Survey [7] to measure fundamental periods of building structures, it was not until recently that this approach was extended to higher modes (see Refs. 5 and 6) and also to different structures (other than buildings).

Current studies in Earthquake Engineering and Structural Dynamics, utilize the Fourier techniques which represent an important tool for understanding and interpreting the frequency content of various time signals. An ambient vibration test is only one of the examples in which Fourier representations are widely used. Furthermore, with the advance made in sensitive vibration-instruments, digital computers, measuring techniques and data processing and analysis, it has become possible to accurately obtain a wide band of natural frequencies of a structure, to identify the different modes and to study the other dynamic characteristics such as damping and nonlinearity.

In 1971, under a contract with the Department of Transportation, Federal Highway Administration, Bureau of Public Roads, and as a part of their continuing program to improve the methodology for predicting the aeroelastic behavior of suspension bridges, McLamore, Hart and Stubbs [6] experimentally determined the natural frequencies, damping and normal mode shapes of vibration for two American suspension bridges — the Newport Bridge in Rhode Island, and the William Preston Lane Memorial Bridge in Maryland. The bridges'

responses to motion caused by traffic, wind, and other environmental factors were measured using sensitive seismometers. The recorded motions were analyzed using spectral techniques (a fast Fourier transform computer program). The dynamical behavior of both bridges included vertical, lateral and torsional vibrations. The study revealed a total of 20 modes of different vibrational motion in the frequency range 0 Hz-1 Hz. No coupling between torsional and vertical motion was observed.

In 1974 and 1975, as part of a project to conduct extensive repairs to the deck of the Lions' Gate Suspension Bridge (Vancouver, Canada), an aerodynamic investigation was undertaken which included a full-scale aeroelastic model. To obtain some guidance in establishing the dynamic parameters for the model tests and the design calculations, measurements on the existing structure were carried out by Rainer and Selst [10]. In determining the bridge's dynamic properties, they followed exactly the same procedure as did McLamore, et al. [6], discussed above. Ambient vibrations due to vehicular traffic as well as forced vibrations due to a series of simulated impacts applied to the bridge, were recorded. The data was analyzed using the Fourier technique, and modal damping was computed using the log decrement relationship. The measured frequencies ranged from 0 to 1 c. p. s. Two methods were used to calculate the modal properties of the bridge: a continuum model, where the solutions to the differential equations describing the vibration problem were evaluated, and a lumped mass, linear stiffness model, for which eigenmodes were found. Some calculated modes and frequencies were in close agreement with the

measured values, for the vertical and the lowest horizontal modes. However, for the frequencies of the torsional modes, the calculated values showed substantial differences from the measured ones. Also, in many cases, the measured frequencies corresponding to peak amplitudes, lacked corresponding computed frequencies.

It is possible that other experimental work equal to or exceeding the value of the abovementioned studies has been conducted; but no such works are known to this investigator outside the present study.

Much effort has been made by the faculty and the graduate students at the California Institute of Technology to establish a measurement system for the dynamic response of full-scale civil engineering structures. The system adopted for this investigation has been used for many full-scale and reduced-scale studies of the dynamic response of structures such as earth dams and buildings. The technique most often used for the experimental determination of natural frequencies of vibration of large structures involves measurement of the motion excited by wind or traffic by means of sensitive instruments, and then analysis of that motion using Fourier methods.

The present chapter is concerned primarily with experimental dynamic studies which were performed on the Vincent-Thomas Suspension Bridge between San Pedro and Terminal Island, California. The detailed study of the experimental measurements is directed toward three major objectives:

1. To check the accuracy and demonstrate the essential reliability of the dynamic methods of analysis developed in Chapters I through III of this thesis, by correlating the observed motion of the

bridge with its computed frequencies of vibration.

2. To make a field trial of both the vibration instruments and this complex suspension bridge structure.
3. To further the understanding of the dynamic properties of full-scale suspension bridges, and to lay a foundation from which later work can be developed.

The instrumentation used in the experiments is described, and the main features of the structure itself are also presented. The natural frequencies of the modes of vibration of the bridge were accurately determined by measuring wind- and traffic-excited vibrations with a sensitive seismometer mounted at various locations on the bridge. The Fourier amplitude spectrum of the recorded movements was computed and plotted. The measurements revealed a wide band of natural frequencies. In addition, the results for the vertical and torsional natural frequencies were correlated with the computed frequencies. The results of the field measurements agreed very well with the theoretical results which confirms the validity of the assumptions that were made in the previous chapters.

The experience gained in making these measurements will be valuable in planning future, more complete, measurements.

#### IV-2. Description of the Bridge

The Vincent-Thomas Suspension Bridge, shown in Figs. IV-1 and IV-3, was constructed in the early 1960's across the Main Channel of the Los Angeles Harbor from San Pedro to Terminal Island. The bridge was designed by the Bridge Department, Division of Highways, Department of Public Works of the State of California. The bridge superstructure consists of a 1500 ft. suspended center span, two 506.5 ft. suspended side spans, two 151.5 ft. backstay (or approach) spans, a 52 ft. wide roadway and two safety curbs. There are also tower foundations, anchorages, navigation and maintenance equipment, a highway lighting system and other items and details necessary for the proper functioning of the bridge. The approach spans consist of simply supported welded-plate girders, which serve to bring the cable down from the roadway grade to the anchorages below (see Fig. IV-2). There are two 32 ft. splay spans contained within the anchorages which serve to spread the cables into 20 separate parts and thereby distribute the force in the cables throughout a large area of the anchorages. A vertical sag of 150 ft. is provided for the cable at the center of the main span. The supporting towers are vertical, and the suspended portion of the structure, including the backstay and anchor spans, are symmetrical about the center of the main span.

The suspended structure consists of two stiffening trusses, floor beams and a lower wind bracing system of the K-truss type shown in Fig. IV-3. The suspended structure carries a four lane roadway 52 feet wide and curbs and sidewalks 10 inches high and 2 feet, 3-3/8 inches wide (see Fig. IV-4). The cables and the stiffening trusses are 59 feet, 2 inches

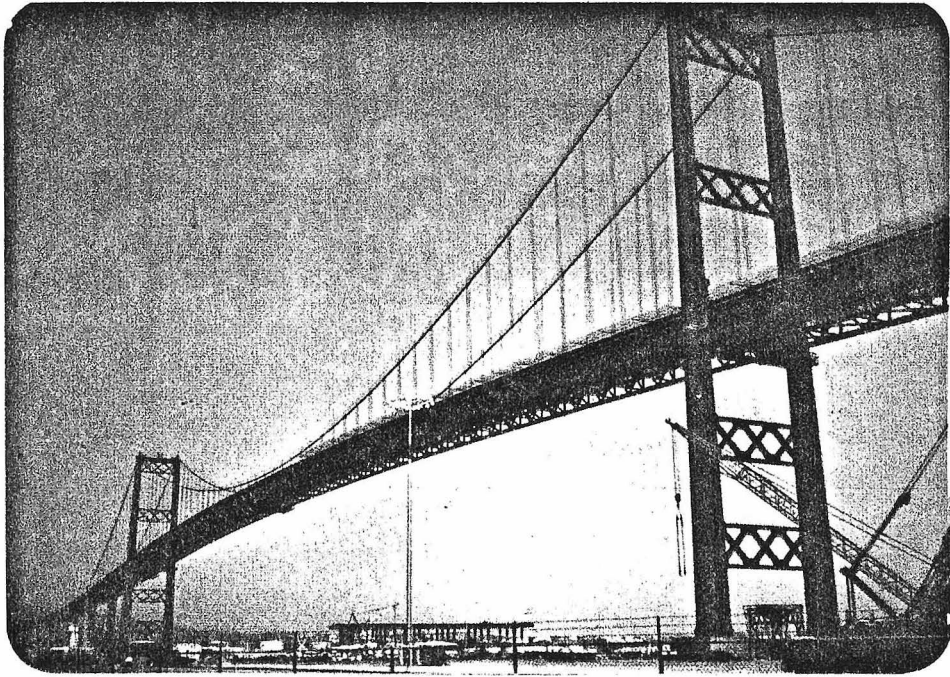


Fig. IV-1. The San Pedro-Terminal Island Suspension Bridge.

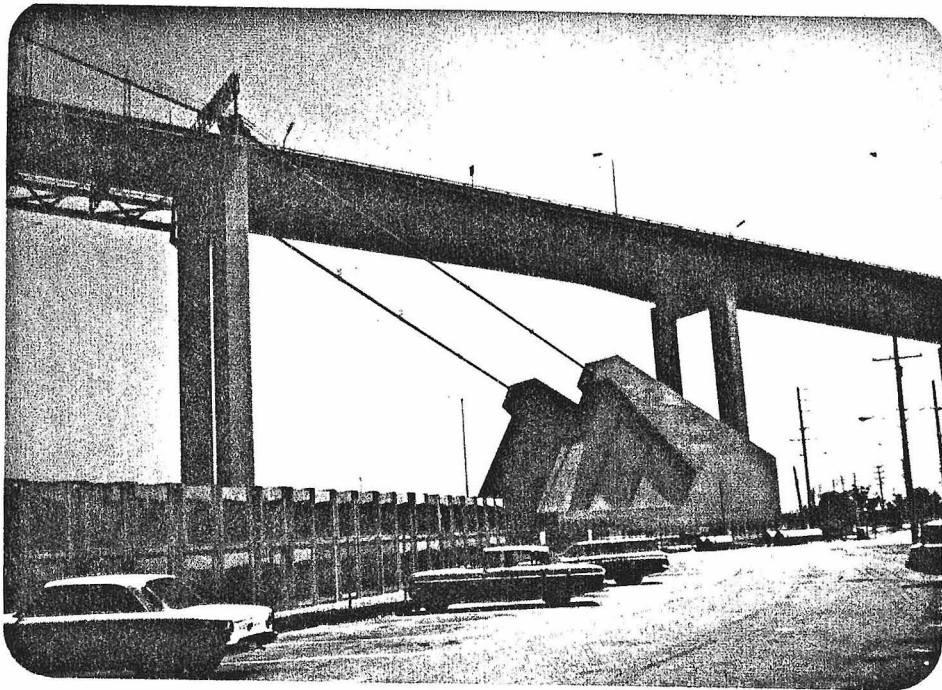
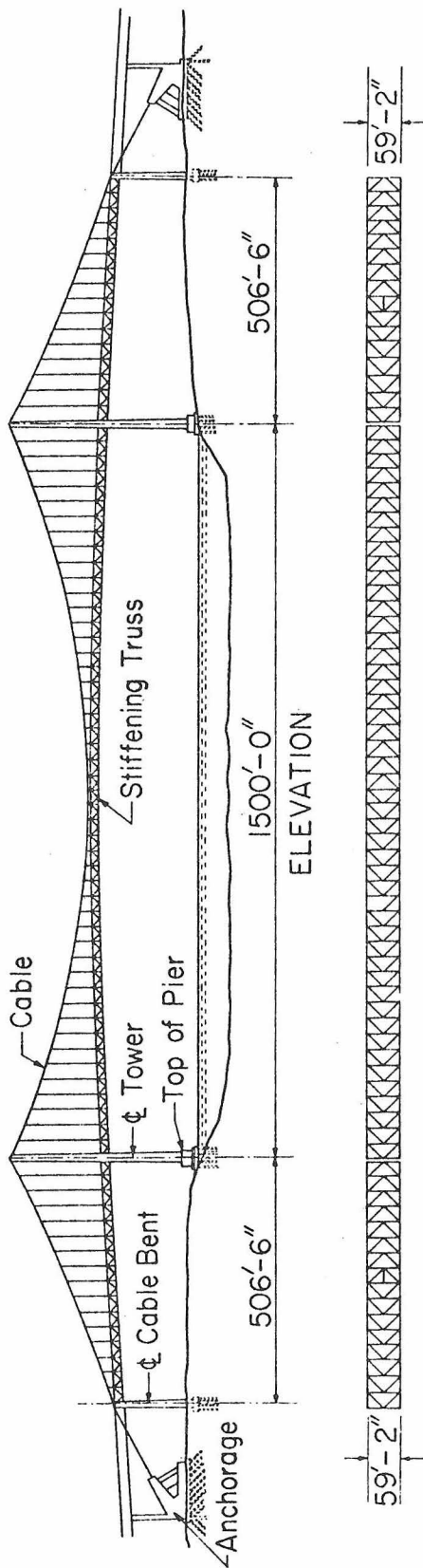


Fig. IV-2. The anchorages and the approach spans.

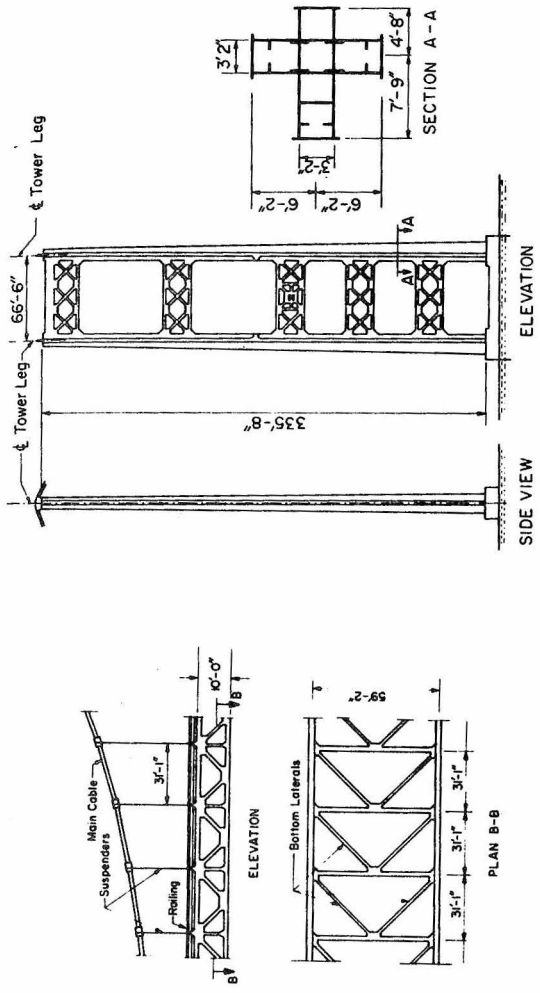


BOTTOM LATERAL SYSTEM  
SAN PEDRO-TERMINAL ISLAND SUSPENSION BRIDGE

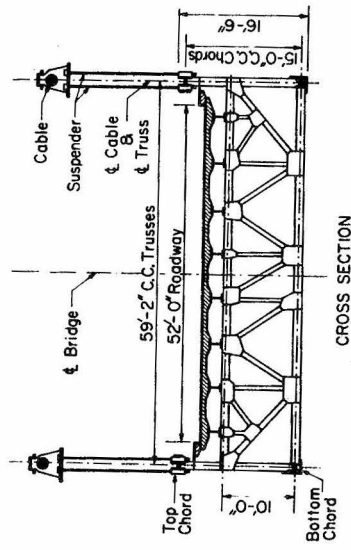
Fig. IV-3

apart from center to center. The stiffening truss, from center to center of the upper and lower chord members, is 15 feet deep. The floor beams are trusses. The top edge of the roadway is 3 feet below the top edge of the stiffening trusses. The bridge was designed with bottom lateral and stringer ties in the trussed floor beam system to develop torsional stiffness. The deck system for the suspended spans consists of transverse rolled girders, which are 7 feet apart center to center, and which are supported by the transverse top chords of the floor truss. Lightweight concrete was utilized for the deck slabs on both the approach and suspended spans. Reinforcement is conventional, consisting of straight and truss transverse bars and of longitudinal top and bottom bars on 12 inch centers.

The San Pedro and Terminal Island towers are supported on steel piles penetrated to an average elevation of -75 feet at the Terminal Island tower and to an average elevation of -135 feet at the San Pedro tower (see Fig. IV-4). The towers are 335 feet high and extend 360 feet above M. H. H. W. The main tower is made up of 3/4 inch steel plate. Each tower leg is anchored to the tower footing by thirty nine 2-1/2 inch (in diameter) and 25 feet long prestressed rods. There is a total of 5,550 Kips of structural steel in the towers and the tower bracings. The tower legs are made up of sections of cruciform design (see Fig. IV-4); they consist of four welded box sections, field bolted with 1 inch diameter high strength bolts. In order for the towers to be vertical under ordinary conditions, the horizontal force in the cables must be equal on each side of the towers.



TOWER



CROSS SECTION

SAN PEDRO-TERMINAL ISLAND SUSPENSION BRIDGE

Fig. IV-4. Some structural details of suspended structure, cross section and tower.

The cable in the suspended spans for this structure consists of 4028 cold drawn, galvanized, 6 gage steel wires providing 121.5 square inches of area including the galvanizing. The ultimate strength of the wire was required to be 225,000 psi providing a theoretical cable strength of 27,337 Kips. The maximum design tension in the cable at the towers was 9,620 Kips. This indicates a design safety factor of about 3. The suspenders are made of small diameter, high strength wires layed up into rope. The cable saddles are centered on the tower legs. This causes the cable to spread at the tower tops where the frictional resistance between the cable and the saddle is sufficient to prevent the cable from slipping through the saddle.

Table IV-1 contains a summary of the structural properties of the San Pedro Suspension Bridge.

TABLE IV-1

Structural Properties of the San Pedro Suspension Bridge

| Parameter                                       | Description                                 | Center Span | Side Span |
|---|---|-------------|-----------|
| Weight<br>(Kip/ft.)                             | <u>Bridge Floor</u>                         |             |           |
|   | Curb, bracket and armour                    | 0.203       |           |
|   | Grating and railing                         | 0.199       |           |
|   | Lightweight concrete                        | 2.592       |           |
|   | Reinforcement steel                         | 0.173       |           |
|   | Stringers and bracings                      | 0.682       |           |
|   | Floor truss, wind shoes and inspection walk | 0.613       |           |
|   | <u>Stiffening Truss</u>                     |             |           |
|   | Top chords                                  | 0.315       |           |
|   | Bottom chords                               | 0.302       |           |
|   | Gusset plates, splices, etc.                | 0.124       |           |
|   | Webs  | 0.142       |           |
|   | Posts                                       | 0.053       |           |
|   | Struts, rivets, bolts, etc.                 | 0.007       |           |
|   | <u>Lateral System</u>                       | 0.159       |           |
| <u>Cable</u>                                    |   |             |           |
| Cables  | 1.025                                       |             |           |
| Suspenders                                      | <u>0.054</u>                                |             |           |
|   | TOTAL DEAD WEIGHT                           | 7.177       |           |
| Modulus of Elasticity<br>(Kip/in <sup>2</sup> ) | Suspended structure                         | 29,000      |           |
|   | Cable                                       | 27,000      |           |
|   | Tower                                       | 30,000      |           |
|   | Shear modulus of suspended structure        | 11,600      |           |
| Areas<br>(in <sup>2</sup> )                     | Cable                                       | 121.50      |           |
|   | One chord of stiffening truss (average)     | 53.78       | 55.56     |
|   | Diagonal in stiffening truss (average)      | 16.90       |           |
|   | Diagonal in lateral system (average)        | 16.58       |           |
| Forces<br>(Kips)                                | Horizontal component of cable tension       | 6,750       |           |

Structural Properties of the San Pedro Suspension Bridge (Continued)

| Parameter   | Description  | Center Span | Side Span |
|---|--|-------------|-----------|
| Moment of Inertia (in. <sup>2</sup> .ft. <sup>2</sup> ) | Vertical moment of inertia of stiffening truss   | 6,050       | 6,250     |
|   | Lateral moment of inertia of chords  | 188,500     |           |
|   | Lateral moment of inertia of slab  | 105,000     |           |
|   | Lateral moment of inertia of stringers   | 290         |           |
|   | Lateral moment of inertia of suspended structure   | 293,800     |           |
| Cable Properties (ft.)                                  | Sag  | 150         | 17.103    |
|   | Virtual length $L_{ei}$ , $i = 1, 2, 3$  | 1,620       | 920       |
|   | Virtual length $L_E$   | 3,460       |           |
| Tower Properties  | Longitudinal stiffness (Kip/ft.) (Force applied at tower top for unit deflection)                  | 26.3330     |           |
|   | Torsional stiffness (Kip/ft.) (Forces applied at tower top; tower legs move in opposite direction) | 235.4323    |           |
|   | Dead weight per leg (Kips)   | 2,700       |           |
|   | Vertical reaction from cable (Kips)  | 6,400       |           |
|   | Area at base (in. <sup>2</sup> )   | 1,022       |           |
|   | Area at top (in. <sup>2</sup> )  | 572         |           |
|   | Height (ft.)   | 335         |           |
|   | Longitudinal moment of inertia (average) (in. <sup>2</sup> .ft. <sup>2</sup> )                     | 10,000      |           |

#### IV-3. Dynamic Characteristics of the Bridge

The computed dynamic characteristics of the torsional and lateral vibrations of the San Pedro Suspension Bridge have been presented in the numerical examples of Chapters II and III. These characteristics included the natural frequencies, the corresponding modes of vibrations, and the distribution of the energies accumulated in the various members of the structure, for both the symmetric and antisymmetric cases. The dynamic characteristics of the vertical vibration of the bridge are presented in this section. The computation of the natural frequencies, modes of vibration, and the energy storage capacity of the various members of the San Pedro Suspension Bridge have been calculated by the method of analysis developed in Chapter I. The procedure for the discretization of the suspended structure into finite elements is the same as that used in the numerical example of the torsional analysis in Chapter II. The number of elements in each tower leg was taken to be 10. The structural properties necessary for the vertical vibration study were taken from Table IV-1.

The eigenvalue problems (Eqs. I-100-a and b) were solved by means of the Caltech digital computer. Some of the computed natural periods and frequencies, and the dominant vibrating portion corresponding to each frequency, are shown in Tables IV-2 and IV-3 for the symmetric and antisymmetric cases, respectively, and the corresponding mode-shapes are shown in Figs. IV-5 and IV-6. By considering these figures, the following observations may be made:

1. As seen before, vibration modes of the bridge structure can be separated into two groups having different characteristics. In one group, the displacements of the stiffening truss are predominant, and in the other group, the displacements of the towers are predominant.
2. Based on (1), investigation of the energy accumulated in the different members of the suspension bridge may require separation of the energies into two groups. Fig. IV-7, represents the energy storage capacity of the cables and the stiffening truss together, while Fig. IV-8 shows the energy storage capacity of the towers for different modes.
3. As seen from Fig. IV-5, in the lowest four modes the center span and side spans vibrate together, while in the higher modes the center and side spans vibrate separately.

Other features can be easily extracted from these figures, as have been shown previously in the various numerical examples of Chapters I and II.

Finally, the modes of vertical motion and their corresponding natural periods, which were computed by the Bridge Department of the State of California, are shown in Fig. IV-9. Despite the omission of certain modes, these results are in close agreement with the frequencies (as well as the modes, if the tower is excluded) of the finite-element solution.

San Pedro-Terminal Island Suspension Bridge  
 Natural Periods and Frequencies of Vertical Vibration  
 (Symmetric Mode Shapes)

| Mode Order | Frequency rad/sec. | Period sec. | Frequency c. p. s. | Member of Dominant Vibration |
|------------|--------------------|-------------|--------------------|------------------------------|
| 1          | 1. 387035          | 4. 529939   | 0. 220754          | center & side spans          |
| 2          | 2. 183996          | 2. 876922   | 0. 347504          | side spans                   |
| 3          | 2. 189078          | 2. 870243   | 0. 348403          | center & side spans          |
| 4          | 2. 882802          | 2. 179541   | 0. 458812          | center & side spans          |
| 5          | 5. 045974          | 1. 245188   | 0. 803092          | center span                  |
| 6          | 6. 213617          | 1. 011196   | 0. 988928          | towers                       |
| 7          | 6. 910050          | 0. 909282   | 1. 099769          | side spans                   |
| 8          | 9. 217459          | 0. 681661   | 1. 467004          | center span                  |
| 9          | 14. 703411         | 0. 427328   | 2. 340121          | side spans                   |
| 10         | 14. 775079         | 0. 425256   | 2. 351527          | center span                  |
| 11         | 19. 741413         | 0. 318274   | 3. 141943          | towers                       |
| 12         | 21. 727994         | 0. 289175   | 3. 458118          | center span                  |
| 13         | 25. 615928         | 0. 245284   | 4. 076902          | side spans                   |
| 14         | 30. 095083         | 0. 208778   | 4. 789781          | center span                  |
| 15         | 37. 227818         | 0. 168777   | 5. 924991          | towers                       |
| 16         | 39. 731885         | 0. 158140   | 6. 323526          | side spans                   |
| 17         | 39. 904389         | 0. 157456   | 6. 350981          | center span                  |
| 18         | 51. 197145         | 0. 122725   | 8. 148279          | center span                  |
| 19         | 57. 146709         | 0. 109949   | 9. 095165          | side spans                   |
| 20         | 58. 881539         | 0. 106709   | 9. 371288          | towers                       |
| 21         | 64. 029888         | 0. 098129   | 10. 190673         | center span                  |
| 22         | 78. 022421         | 0. 080531   | 12. 417654         | side spans                   |
| 23         | 78. 474192         | 0. 080067   | 12. 489556         | center span                  |
| 24         | 90. 517896         | 0. 069414   | 14. 406371         | towers                       |
| 25         | 94. 606147         | 0. 066414   | 15. 057036         | center span                  |
| 26         | 102. 583210        | 0. 061250   | 16. 326625         | side spans                   |
| 27         | 112. 444640        | 0. 055878   | 17. 896120         | center span                  |
| 28         | 131. 085487        | 0. 047932   | 20. 862903         | side spans                   |

TABLE IV-2

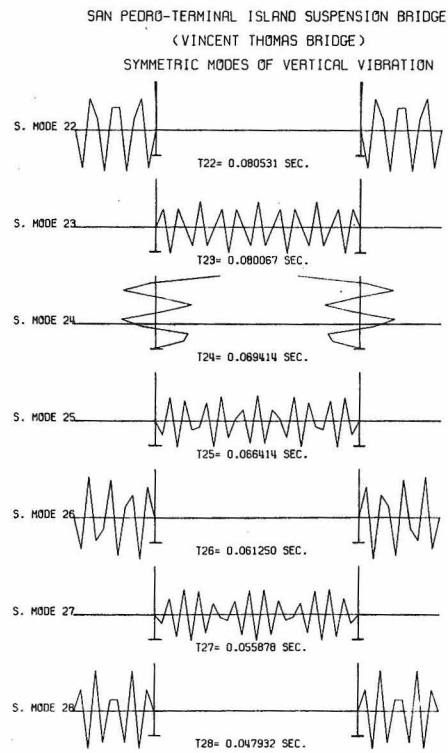
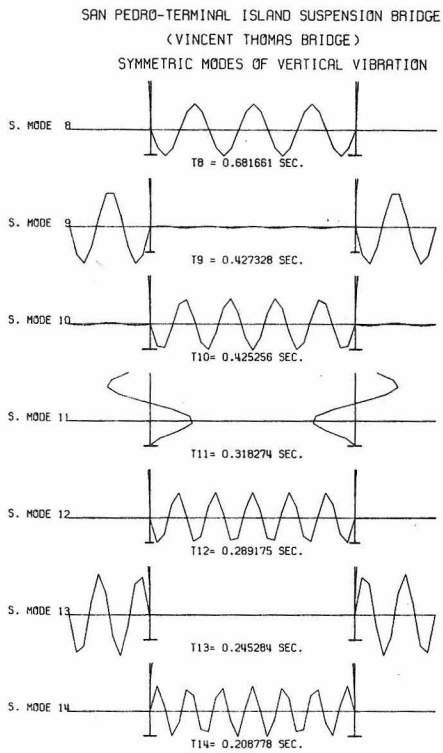
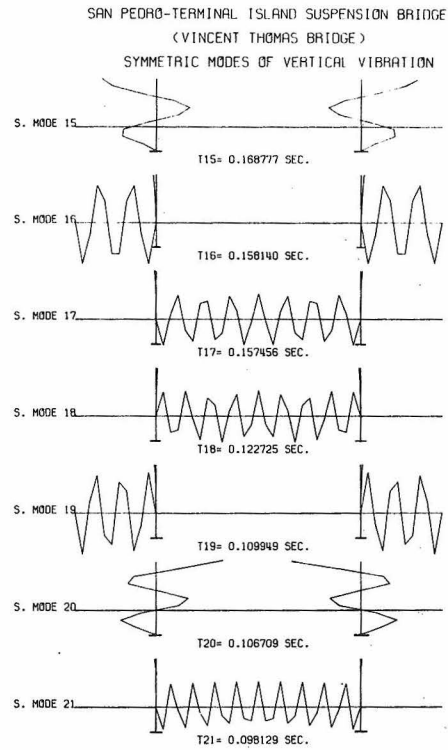
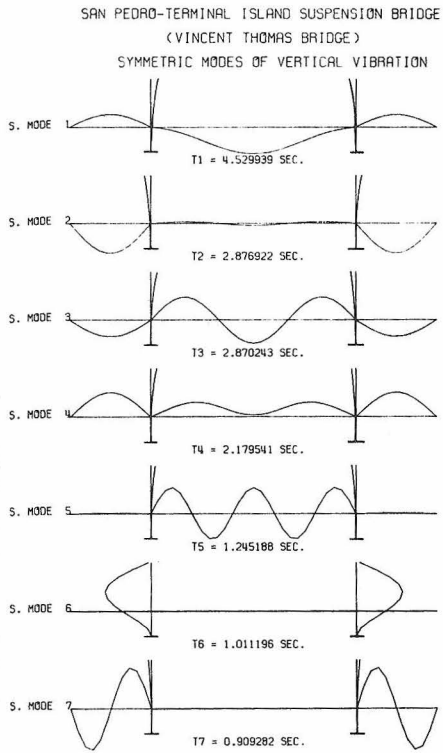


Fig. IV-5. Symmetric modes of vertical vibration of the San Pedro-Terminal Island Suspension Bridge.

San Pedro-Terminal Island Suspension Bridge  
 Natural Periods and Frequencies of Vertical Vibration  
 (Antisymmetric Modes)

| Mode Order | Frequency rad/sec. | Period sec. | Frequency c. p. s. | Member of Dominant Vibration |
|------------|--------------------|-------------|--------------------|------------------------------|
| 1          | 1.237334           | 5.078005    | 0.196928           | center span                  |
| 2          | 2.175632           | 2.887981    | 0.346263           | side spans                   |
| 3          | 3.446829           | 1.822889    | 0.548570           | center span                  |
| 4          | 6.213617           | 1.011196    | 0.988927           | towers                       |
| 5          | 6.919186           | 0.908082    | 1.101223           | side spans                   |
| 6          | 6.951771           | 0.903825    | 1.106409           | center span                  |
| 7          | 11.820628          | 0.531544    | 1.881311           | center span                  |
| 8          | 14.692127          | 0.427657    | 2.338325           | side spans                   |
| 9          | 18.076400          | 0.347591    | 2.876948           | center span                  |
| 10         | 19.741413          | 0.318274    | 3.141943           | towers                       |
| 11         | 22.646759          | 0.277443    | 3.604344           | side spans                   |
| 12         | 25.732931          | 0.244169    | 4.095523           | center span                  |
| 13         | 34.817043          | 0.180462    | 5.541305           | center span                  |
| 14         | 37.227818          | 0.168777    | 5.924991           | towers                       |
| 15         | 40.014998          | 0.157021    | 6.368548           | side spans                   |
| 16         | 45.362089          | 0.138512    | 7.219601           | center span                  |
| 17         | 57.416815          | 0.109431    | 9.138170           | center span                  |
| 18         | 57.658707          | 0.108972    | 9.176668           | side spans                   |
| 19         | 58.881539          | 0.106709    | 9.371288           | towers                       |
| 20         | 71.045632          | 0.088439    | 11.307263          | center span                  |
| 21         | 78.201621          | 0.080346    | 12.446175          | side spans                   |
| 22         | 86.325020          | 0.072785    | 13.739054          | center span                  |
| 23         | 90.517896          | 0.069414    | 14.406371          | towers                       |
| 24         | 102.470430         | 0.061317    | 16.308675          | side spans                   |
| 25         | 103.319071         | 0.060813    | 16.443741          | center span                  |
| 26         | 121.895303         | 0.051546    | 19.400240          | center span                  |
| 27         | 131.906725         | 0.047634    | 20.993607          | side spans                   |
| 28         | 132.680150         | 0.047356    | 21.116702          | towers                       |

TABLE IV-3

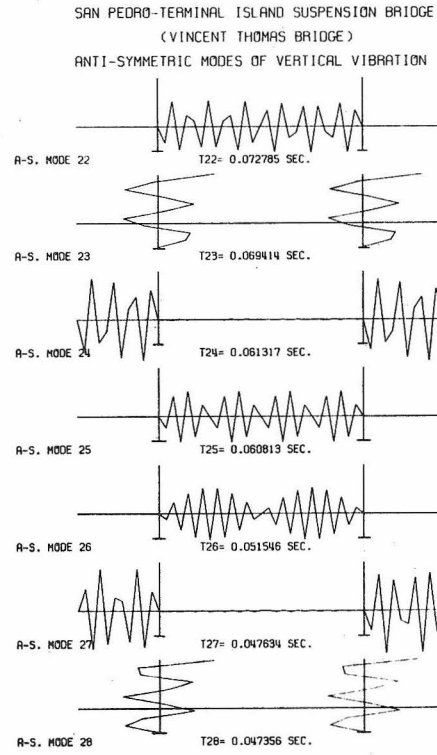
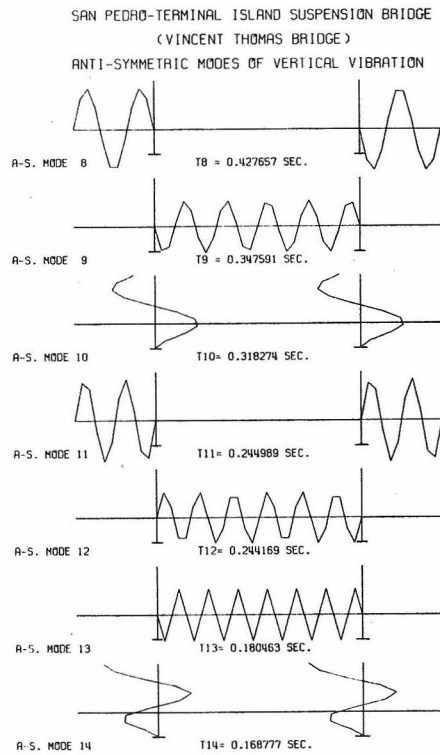
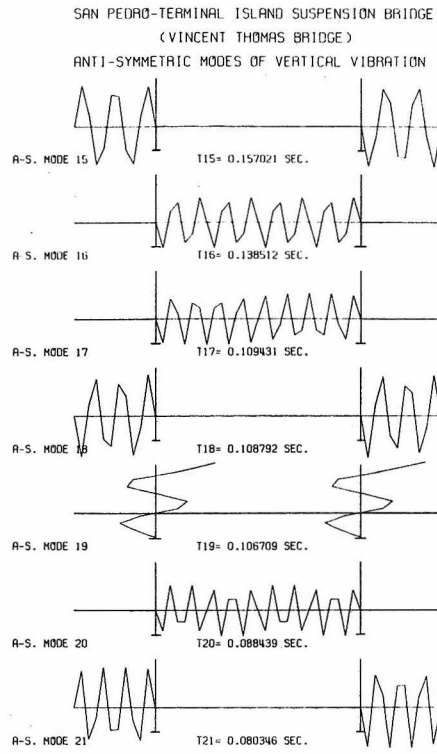
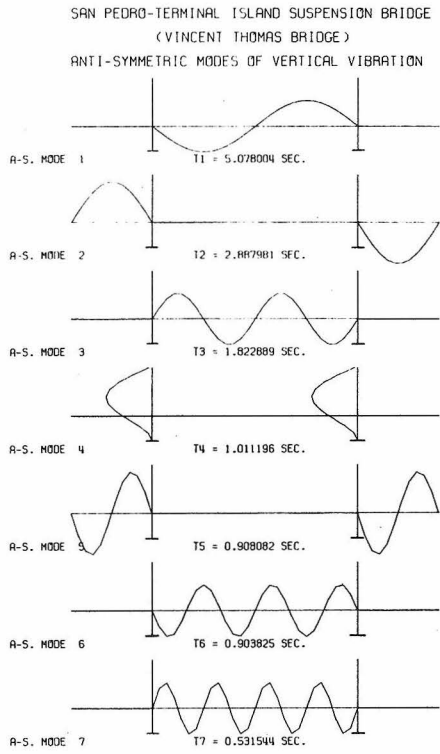
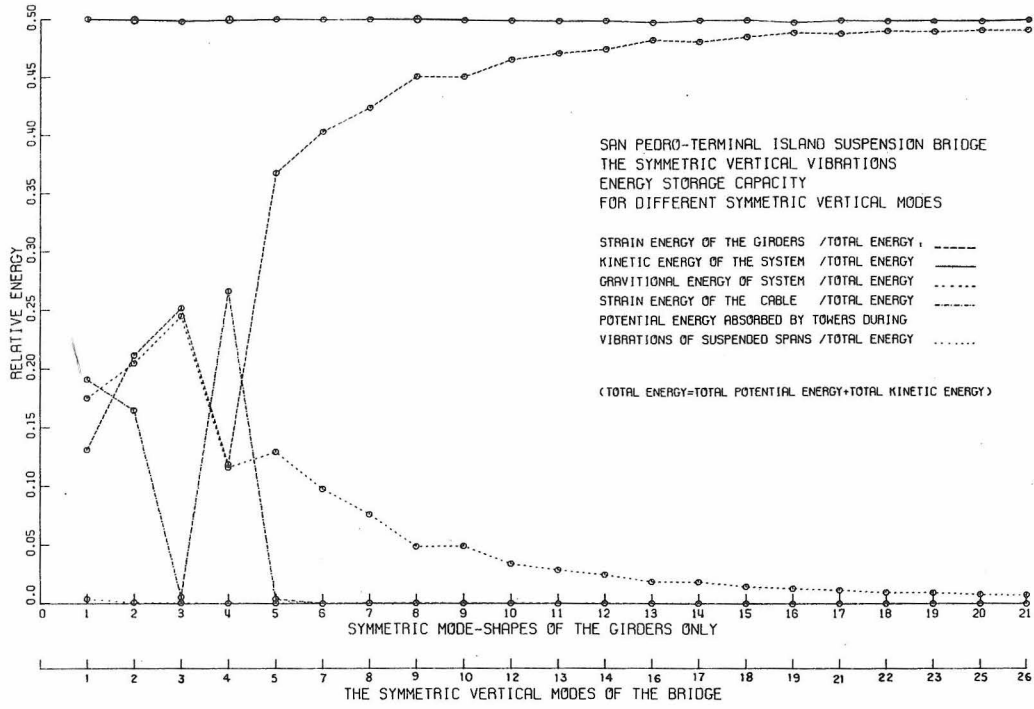
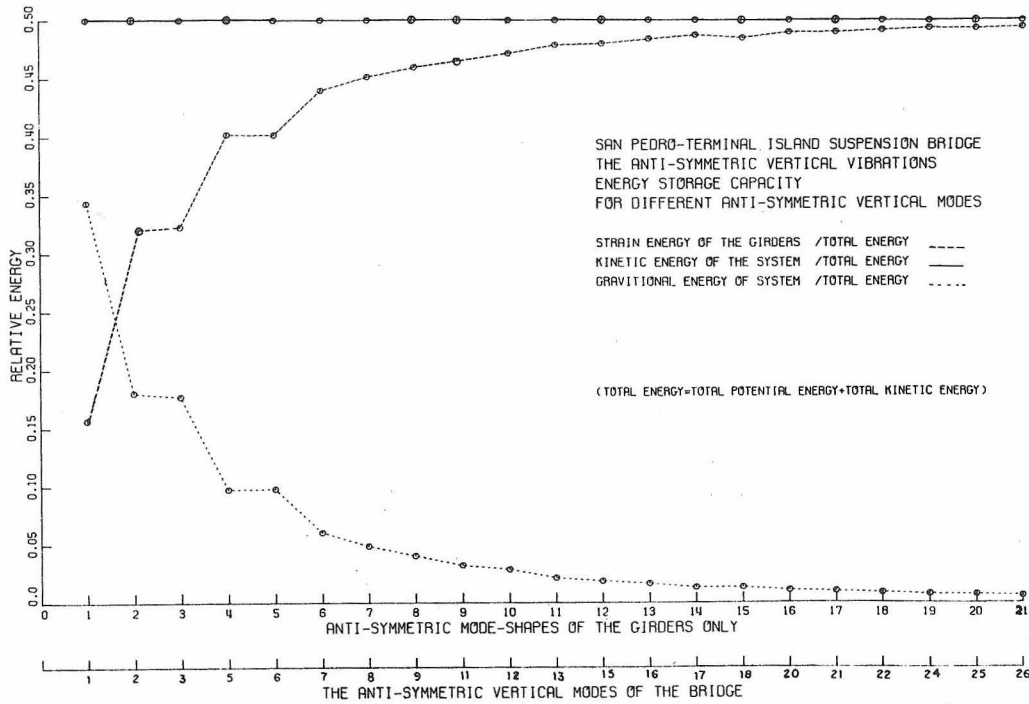


Fig. IV-6. Antisymmetric modes of vertical vibration of the San Pedro-Terminal Island Suspension Bridge.



(a)



(b)

Fig. IV-7

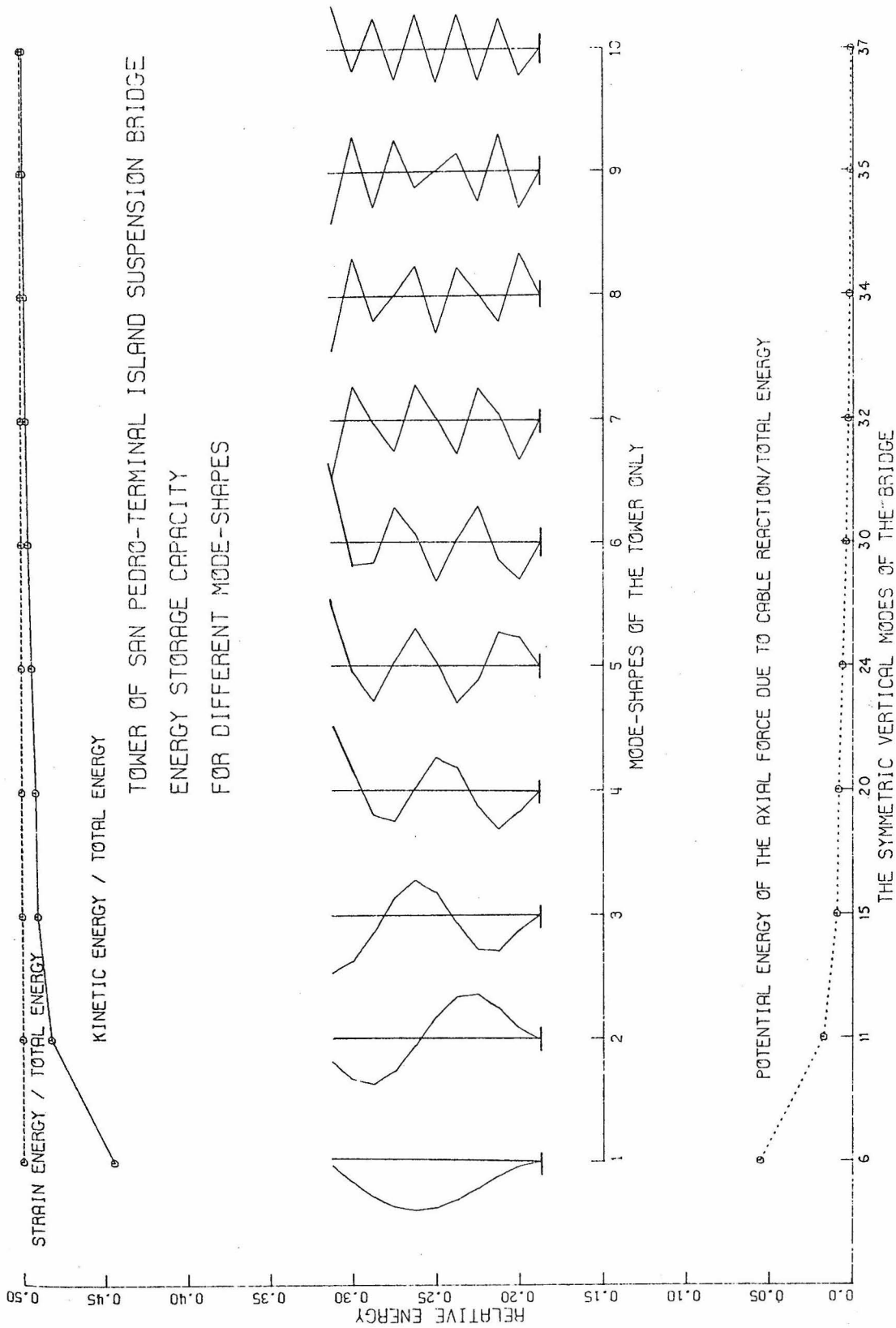
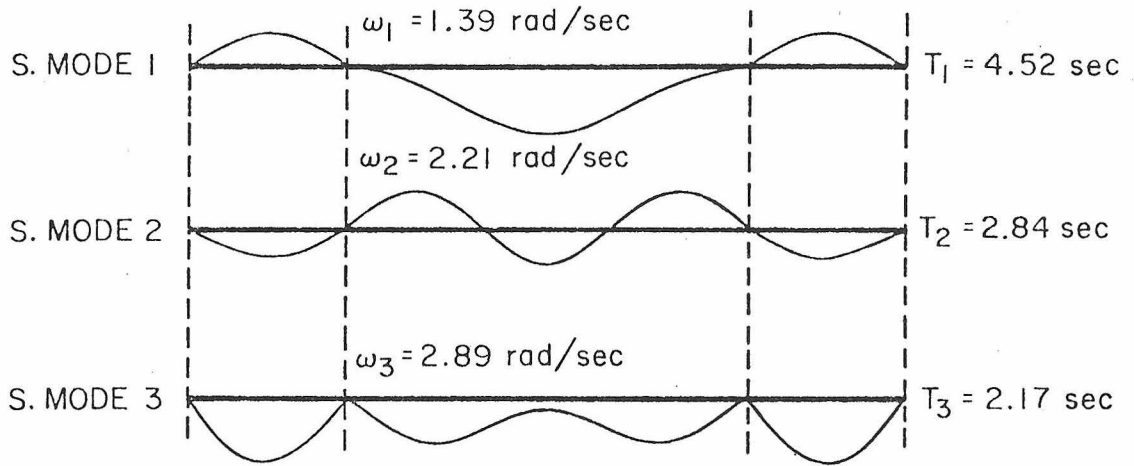
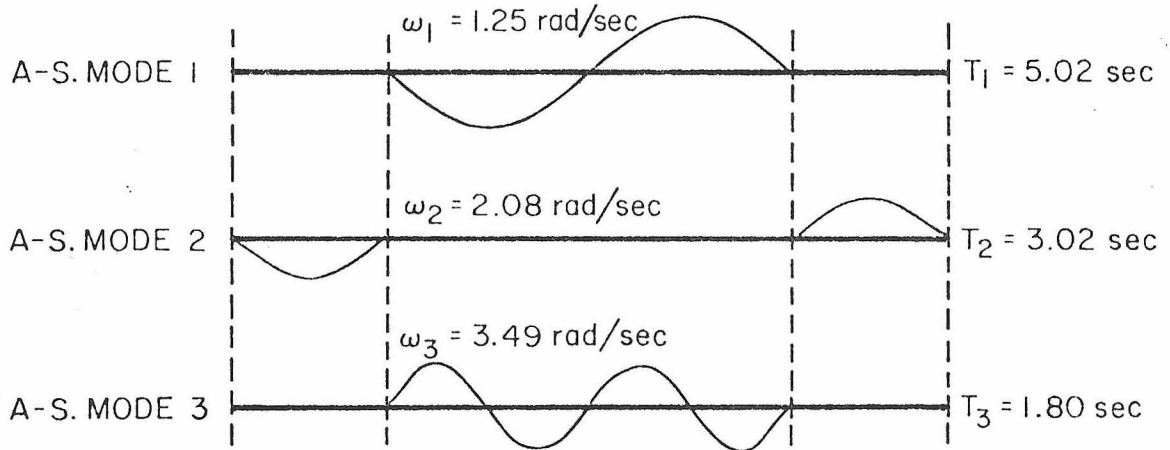


Fig. IV-8

SAN-PEDRO-TERMINAL ISLAND SUSPENSION BRIDGE  
SYMMETRIC MODES OF VERTICAL VIBRATION



ANTI-SYMMETRIC MODES OF VERTICAL VIBRATION



VERTICAL MODES OF VIBRATION COMPUTED BY THE STATE  
OF CALIFORNIA BRIDGE DEPARTMENT

Fig. IV-9

#### IV-4. Measuring the Natural Frequencies of the Bridge

Ambient vibration testing of the San Pedro Suspension Bridge excited by traffic motions is discussed in the following section, with determination of the natural frequencies of possible vertical and torsional modes of vibrations in mind. Information is given also on modern methods of making ambient test measurements based on magnetic tape recording and electronic analog-digital conversion. A complete description of the instruments used in the experiment may be found in Reference [5], but a summary of their salient features is provided here.

##### IV-4-1. Description of the measuring experiment

The measurements of the natural frequencies of the San Pedro Suspension Bridge were carried out with the following instruments.

##### 1. Kinematics (SS-1 Short-Period) Ranger Seismometer

Two seismometers were used at different locations, to measure vertical motions of the bridge. No strong wind occurred during the measurements, and the only significant vibrations recorded were caused by the traffic. The SS-1 Ranger Seismometer is a short-period seismometer usable for portable and fixed station seismological purposes, and is a versatile, sensitive vibration sensor for structural dynamics applications. Mechanically, the Ranger is a "moving coil type" (velocity) transducer, adaptable for either vertical or horizontal operation in the field. Its sensitivity (290 v/m/sec. for 5000 ohm coil), and size make it suitable as a sensor for ambient vibration

measurements of buildings, dams, bridges, foundations, or offshore platforms. The natural period of the seismometer is close to one second. Damping is adjusted by the choice of appropriate resistance in the coil and external circuits. During this experiment, the damping was set at 0.7 of the critical value.

## 2. Earth Sciences SC-1 Signal Conditioner

The signal conditioner is a wide band, low noise amplifier system, designed with filters for use in low level structural vibration and microseismic measurements. Four input channels, each having its own attenuator and adjustable low-pass filter, provide isolated circuitry for a normal, integrated, and/or differentiated output signal (i. e., velocity, displacement, and/or acceleration output using a velocity sensor). All outputs are simultaneously or independently available for recording. The output can be recorded on magnetic tape and/or on a strip-chart recorder. In this experiment, the conditioner was used to amplify and simultaneously control two outputs from the ranger seismometers. The power for this instrument was provided by an A. C. power source in the tower leg.

## 3. Magnetic Tape Recorder (Model 3960 Hewlett-Packard)

The amplified signal, i. e., the voltage proportional to the relative velocity of the seismic mass of the seismometer, is recorded on low noise magnetic tape. It has a separate eight track magnetic tape reel. The electrical output of the recorder can be digitized for computer processing by means of an analog-digital converter.

4. Mark 220 Brush Recorder

To enable immediate visual inspection of the vibrations during each measurement, the signals from both seismometers, via the signal conditioner, were simultaneously recorded on a strip-chart Brush Recorder having two channels. This was necessary to insure that the signal was within the limits of operation of the magnetic tape recorder and the analog-digital computer.

5. Electronic Analog-Digital Converter (Model DDS-1103 Kinometrics)

The DDS-1103 Digital Data Acquisition System is an accurate means of converting analog data from the magnetic tape recorder to digital format on computer compatible digital magnetic tape. At present, it is wired to handle 1 to 8 input channels. The dynamic range of the system is approximately 72 db.

IV-4-2. Measuring procedures

In the past, wind has been the usual source of excitation for suspension bridges. However, traffic excitation [6, 10] of such flexible structures can induce vibrations large enough to yield information about the structural behavior which would be very difficult to obtain in any other way, except during severe winds or strong earthquakes.

The experiments carried out on the San Pedro Suspension Bridge, described in Section IV-2, were performed under traffic excited motion with the principal purpose of finding the natural frequencies of the bridge. Most ambient vibration tests [5, 7] assume that the structure under consideration can be approximated by a damped, linear, discrete

or continuous system. In the experimental study of the bridge vibration, it was assumed that the resulting motions would be expressed as the superposition of modes associated with discrete frequencies. It may be mentioned here that for the measurement of traffic induced vibrations, it is not necessary to calibrate all the seismometers used so that they give the same amplitudes when excited by the same motion. It is also not necessary to know the absolute values of the amplitudes that are recorded, because the frequencies are the only concern; even if the mode shapes are required, the relative amplitudes of the recorded motions is sufficient.

The conditions under which the tests were made were far from ideal, and installing the instruments involved difficult maneuvering. The time schedule for the installation, operation, and recording was very limited by the need to reopen the one closed lane of traffic prior to rush hour, and by other maintenance activities in the area. Only approximately four hours were available for completion of the tests. Additional difficulties were caused by the repainting of the bridge, being done at that time (mid-November, 1975).

The measurements of the bridge frequencies were conducted using the following procedures. The recording instruments, consisting of the Brush Recorder, the signal conditioner and the magnetic tape recorder as shown in Fig. IV-11, were placed on a platform located at the juncture of the tower and the lower wind bracing of the suspended structure. This platform is generally used to provide access to the inspection walk shown in Fig. IV-12. The two seismometers were first placed on the centerline of the lower wind bracing of the center

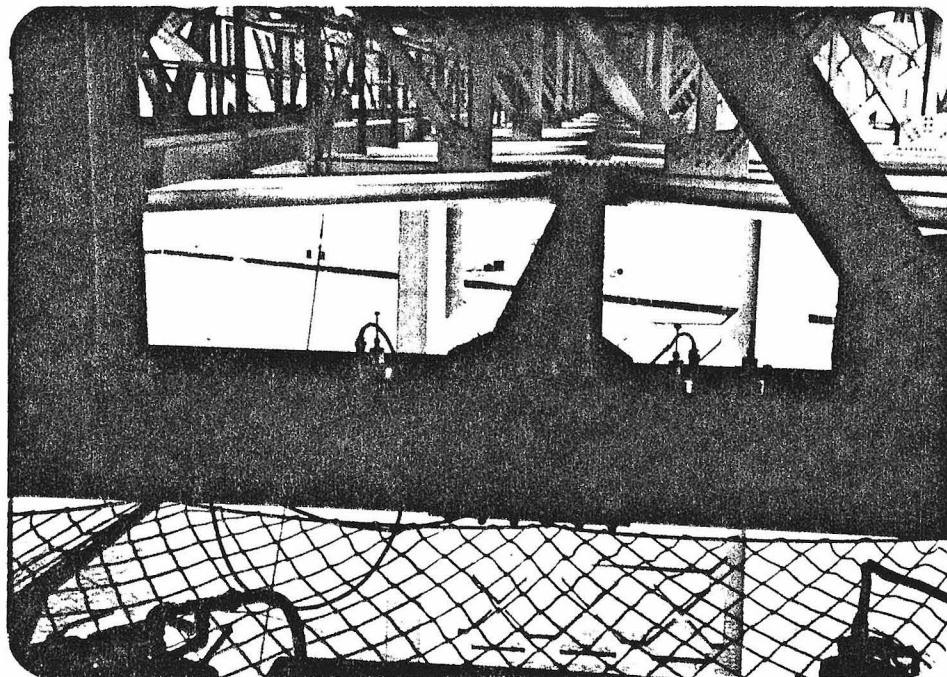


Fig. IV-10. Location of ranger seismometer on the lower wind bracing.

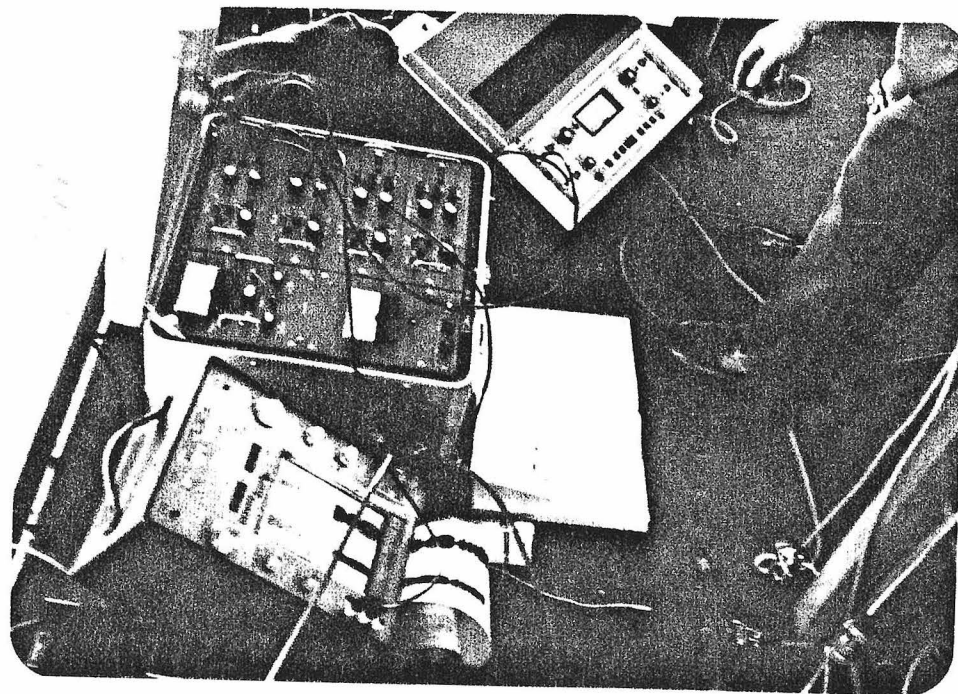
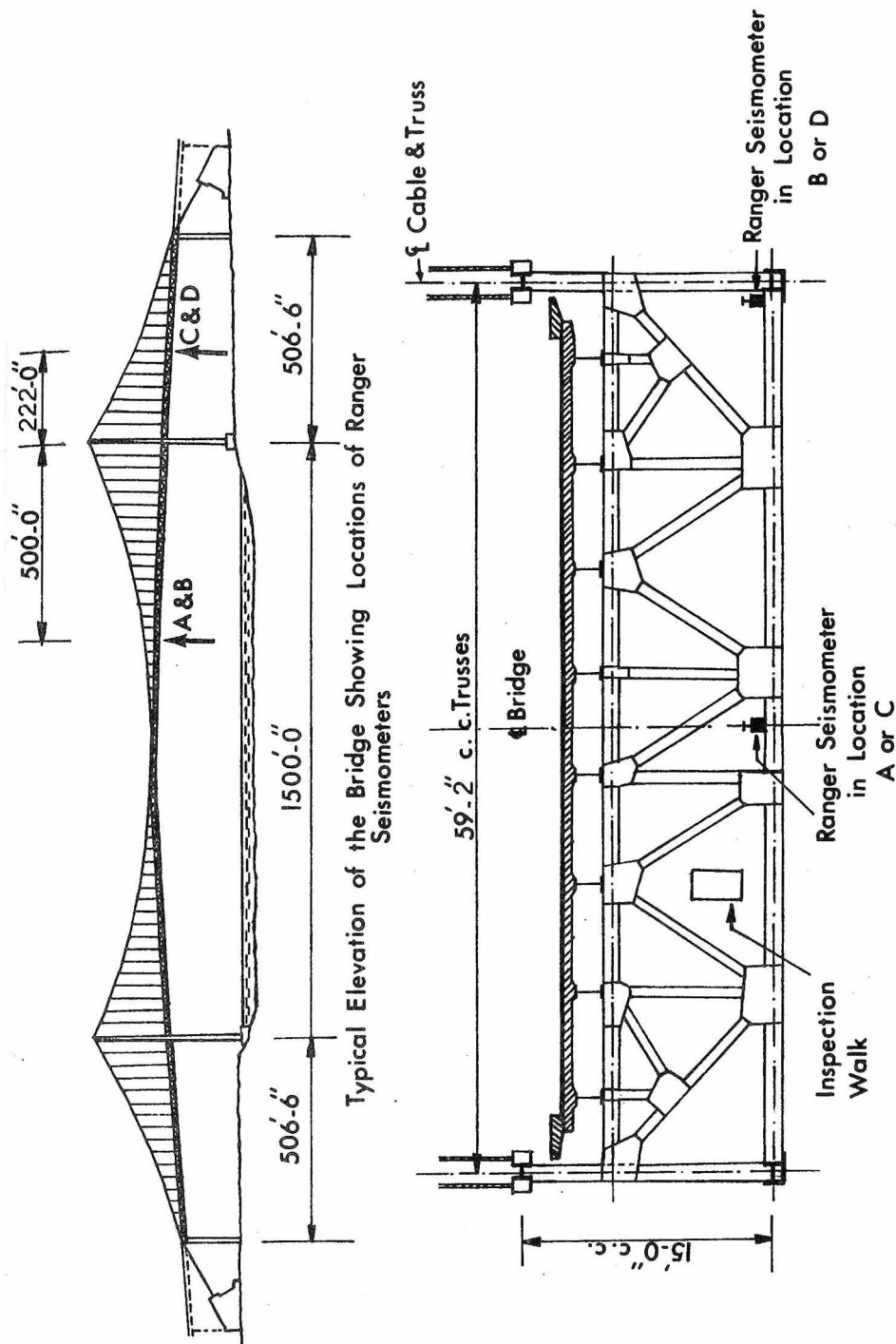


Fig. IV-11. The recording instruments.



Typical Cross Section of the Bridge Showing Locations of Ranger Seismometers

SAN PEDRO-TERMINAL ISLAND SUSPENSION BRIDGE

Fig. IV-12

TABLE IV-4

Sequence of Tests to Determine Natural Frequencies  
of the San Pedro Suspension Bridge

Instrument Locations and Recorded Motions During 8 Tests

| No. | Test | Recorded Motion | Location on the Bridge |                           |        |
|-----|------|-----------------|------------------------|---------------------------|--------|
|     |      |                 | Point                  | Cross Section             | Span   |
| 1   | A-1  | Displacement    | A                      | Center line of the Bridge | Center |
| 2   | A-2  | Velocity        |                        |                           |        |
| 3   | B-1  | Displacement    | B                      | Center line of the Truss  | Center |
| 4   | B-2  | Velocity        |                        |                           |        |
| 5   | C-1  | Displacement    | C                      | Center line of the Bridge | Side   |
| 6   | C-2  | Velocity        |                        |                           |        |
| 7   | D-1  | Displacement    | D                      | Center line of the Truss  | Side   |
| 8   | D-2  | Velocity        |                        |                           |        |

span (i. e., at location A) as shown in Fig. IV-10, and the vertical motion at this location was recorded for about 4 minutes per run. (The recording was begun after several minutes of monitoring the Brush Recorder display during which fine adjustments were made to obtain identical output from the two seismometers.) Then the two seismometers were placed on the centerline of the bottom chord of the stiffening truss (i. e., at location B) in the same cross section of the bridge (see Fig. IV-12). At this location vertical motion was also recorded after all necessary adjustments were made.

These procedures were repeated for the side spans at locations C and D. Fig. IV-12 shows the locations of the Ranger seismometers on both the cross section and the elevation of the bridge; Table IV-4 also shows these locations and the type of the recorded motions during eight tests. It may be mentioned that these particular locations (A, B, C and D) were selected because they provided safety screens which had been installed for use in repainting the bridge. For each location, two simultaneous displacement recordings were made lasting between 2 and 5 minutes in each run; then two simultaneous velocity recordings were made at the same location. Actually, one seismometer would have been adequate for each location, but two recordings were made to verify the results. The seismometers were both connected to the recording instruments by means of various electrical cables which ran along the inspection walk. The recording instruments, as well as the two seismometers, were adjusted at the location, and the various motions of the bridge were displayed on the two-channel Brush

Recorder. All of the instruments functioned satisfactorily throughout the tests.

IV-4-3. Data analysis

The following procedures were used in conducting data processing analysis of the experimental records.

1. The recorded data were converted to digital form on a magnetic tape compatible with the digital computer to be used, and 50 discrete points per second were generated for each analog record.
2. These original records were filtered with a Kronhite analog low-pass filter to remove any aliasing effects in the computed spectrum. Since all frequencies in the records that could be used in comparing the computed and measured frequencies lie well below 20 c. p. s., it was decided to use this limit for the filtering.
3. It was decided that 50 points per second would be appropriate for data processing because this would give a Nyquist frequency of 25 c. p. s., which is well above all the frequencies being considered. A typical record consists of 8192 points ( $2N$  equispaced samples with  $N=4096$  points) or 163.84 seconds. A typical set of records of the first 150 seconds at locations A, C and D is shown in Figs. IV-13, 14, and 15. In these figures, the scale of the vertical axis is proportional to the transducer voltage after the filtration.

4. The Fourier amplitude spectrum for each record of 163.84 seconds was obtained by using the Cooley and Tukey algorithm (the subroutine is available from the Caltech computer program library). This algorithm requires  $2N$  equally spaced data, where  $N = 2^M = 4096$  points, and  $M$  is an integer ( $M = 12$  in this case).

The distribution of the Fourier amplitude spectra versus the distribution of the frequencies (from all 8 tests listed in Table IV-3) was plotted, for up to 10 c. p. s., as shown in Fig. IV-16 through Fig. IV-19. The natural frequencies of vibration were determined by considering the distribution of all peaks in the Fourier spectra for the 8 tests.

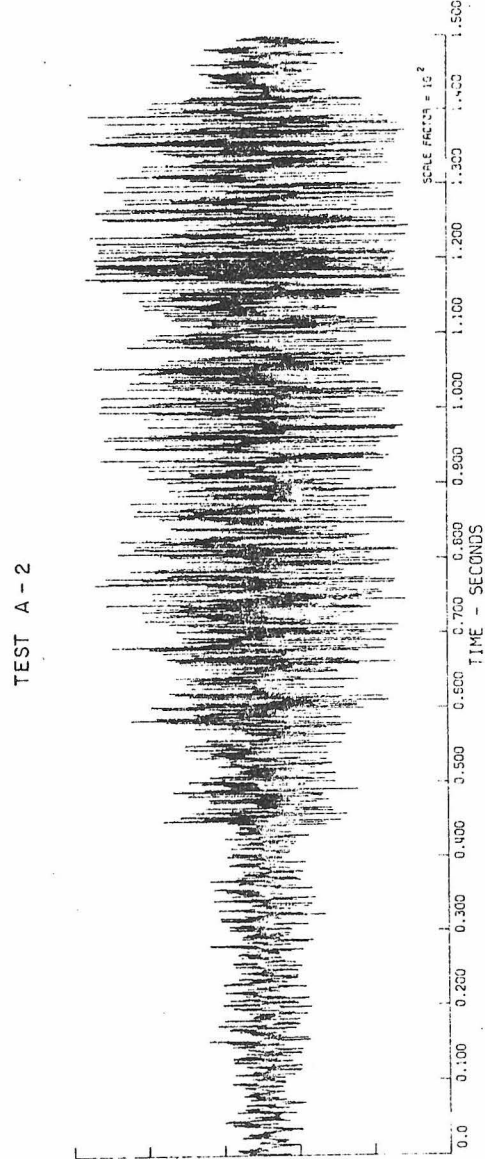
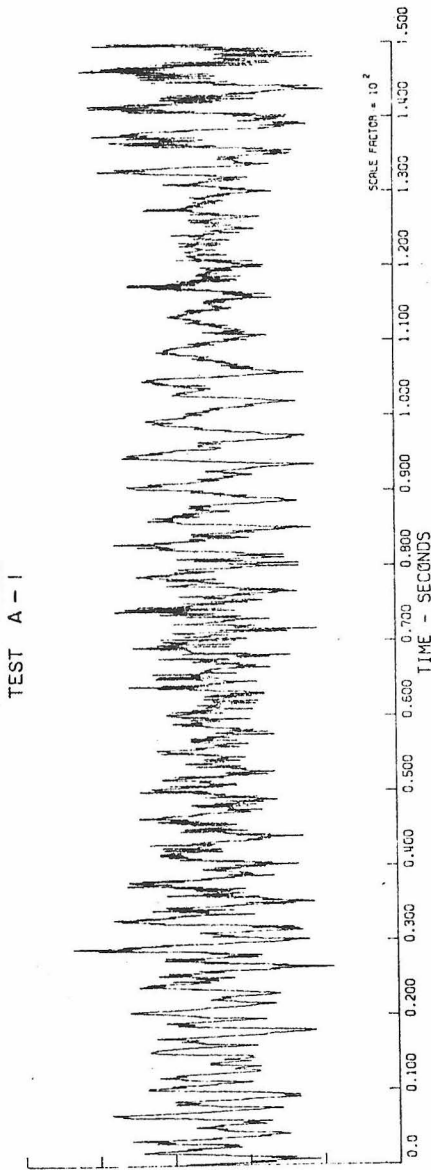
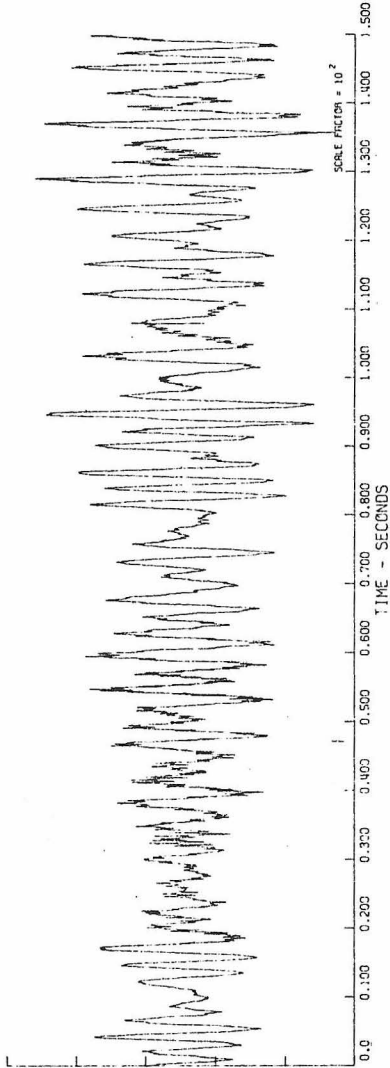


Fig. IV-13. Typical records of 150 seconds at the center line of the bridge (center span): (A-1) displacement record and (A-2) velocity record.

TEST C - 1



TEST C - 2

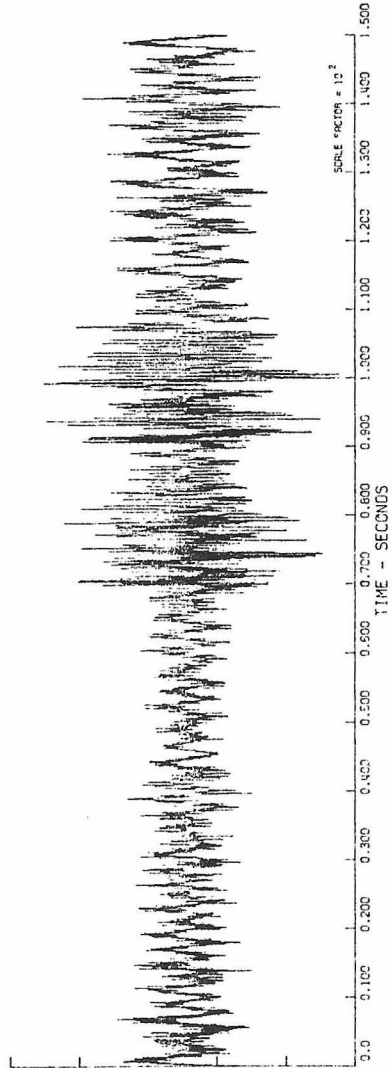


Fig. IV-14. Typical records of 150 seconds at the centerline of the bridge (side span): (C-1) displacement record and (C-2) velocity record.

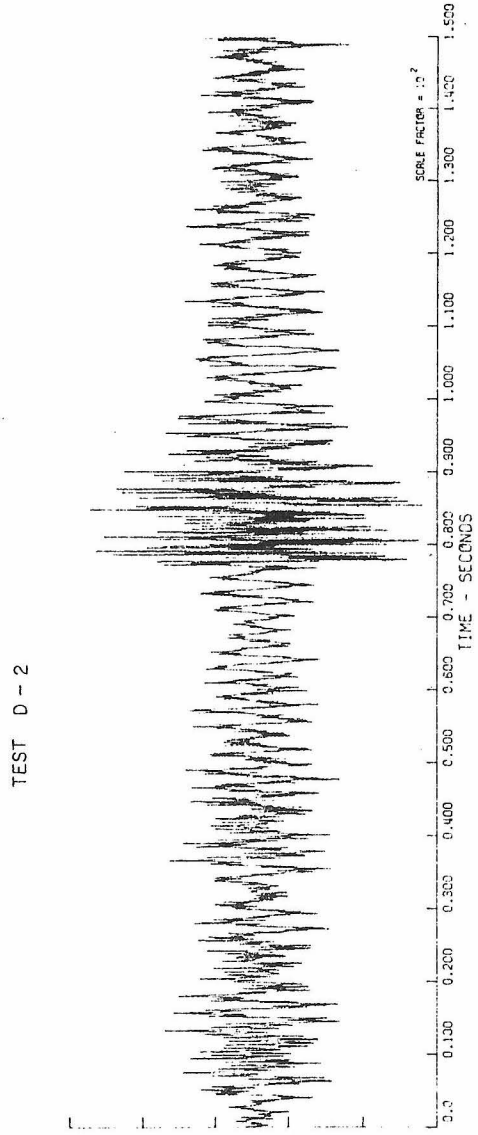
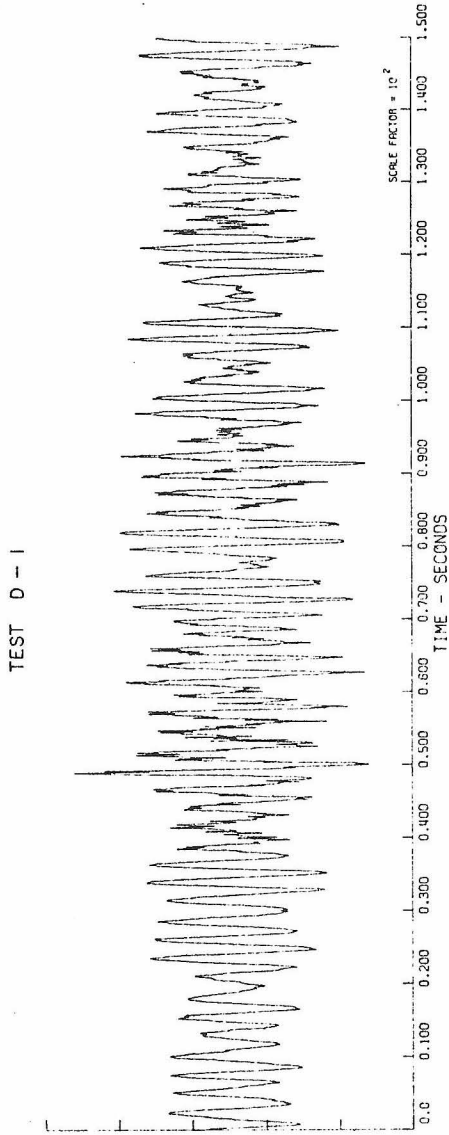


Fig. IV-15. Typical records of 150 seconds at the center of the bottom chord of the side span: (D-1) displacement record and (D-2) velocity record.

#### IV-5. Comparison Between the Computed and the Measured Frequencies

To measure the natural frequencies of the vertical modes of the bridge, the two seismometers were placed near the centerline of the lower wind bracing (Locations A and C). By locating them elsewhere than the center of torsion of the bridge cross section, the vertical motion of that location, which accompanied the torsional vibration of the cross section, was recorded. To obtain more information about the torsional frequencies, the two seismometers were then placed on the center of the bottom chord of the stiffening truss.

Because the possible sites for measurement were limited, it is conceivable that some existing modes were not recorded, if the locations chosen coincided with the nodes of those modes.

The natural frequencies were obtained from the recorded data in two ways.

1. The frequencies corresponding to the spectral peaks of each test were determined and were listed in Tables IV-5 and IV-6 in ascending frequency order (lowest frequency first), along with both the expected vertical and torsional modes for each location and their computed frequencies. To select the frequencies at which the peaks occurred, all of the discrete values of the Fourier amplitude spectrum (the vertical ordinates) were listed opposite their corresponding frequencies (the horizontal values) by using a computer program. The frequencies at which the values peaked were then easily determined.
2. The discrete computed natural frequencies expected for each location (or record) were plotted (and the corresponding numbers

of the modes of vibrations were indicated) on Fourier spectra as seen in Figs. IV-16 through IV-19.

In general, the frequencies corresponding to the peaks in a typical Fourier amplitude spectrum agree closely with the computed values given in Tables IV-5 and IV-6. Actually, the measured frequencies are either the same as or higher than those computed, and the measured and computed frequencies of the first few modes (for instance, from 1 to 6) are almost identical.

For the center span, in Figs. IV-16 and IV-17 and in Table IV-5, there are two peaks corresponding to frequencies of about 0.71 and 4.64 c. p. s. It is possible that these frequencies correspond to the vertical aspect of the lateral modes of frequencies 0.65 and 5.31 c. p. s. (i. e., modes 2 and 13 in Table III-2). In these lateral modes, there is an upward motion incidental to the lateral vibration. It is also possible that the peaks represent the coupling between two different motions, vertical and torsional or lateral and torsional. The analyses in this thesis does not consider the coupled horizontal-torsional motion or vertical-torsional motion because, as indicated previously, the resulting calculations are prohibitively intricate. For the side span, in Figs. IV-18 and IV-19 and in Table IV-6, there are two dominant peaks corresponding to frequencies of about 2.1 and 5.8 c. p. s. These two frequencies do not correlate with any of the computed vertical or torsional natural frequencies of the side spans. It is possible that these frequencies may also correspond to the coupling of different motions.

Figs. IV-20 and IV-21, represent a breakdown of the results presented in Tables IV-5 and IV-6 and also in Figs. IV-16 through IV-19;

the torsional or vertical vibrations, symmetric and antisymmetric are shown individually. Again, the calculated frequencies, joined by the solid line, are in close agreement with the measured frequencies.

It often happens that two vertical modes, two torsional modes or a vertical and a torsional mode are at nearly the same frequency, and the problem of separating the modes may be troublesome.

Examples of these modes having very close frequencies are:

a) for the center span

S-V-2 and S-V-3 , S-V-9 and S-V-10 ,  
S-V-4 and S-V-1 , AS-V-13 and AS-T-1 ,  
AS-V-7 and S-T-5 , AS-V-13 and AS-T-8

b) for the side span

S-V-2 and S-V-3 , S-V-2 , S-V-3 and AS-V-2  
S-V-4 and S-T-1 , S-T-2 and S-T-3 ,  
S-V-7 and S-T-4 , S-V-9 , S-V-10 , AS-V-8, S-T-6 and  
AS-T-4 .

Here "S" and "AS" indicate "symmetric" or "antisymmetric," while "V" and "T" indicate "vertical" or "torsional" vibration.

To identify the different modes of vibration more effectively in future experimental work, the following recommendations are made:

1. Torsional modes of vibration can be recovered by placing two seismometers on the same cross section of the bridge, on the centerline of both stiffening trusses, and simultaneously recording their vertical motions. By then subtracting their outputs, one should recover the torsional motions. Vertical

modes can be isolated similarly by summing the outputs.

2. To obtain more information about torsional modes and, at the same time, to identify the pure lateral modes, two seismometers should be placed in the same cross section, one at each centerline of the top and bottom chords of one stiffening truss to simultaneously record their lateral motions. Summing their outputs will give information about the purely lateral vibration while subtracting their outputs will provide data on purely torsional vibration.

Thus, two seismometers recording vertical motions are needed on the same cross section to distinctly determine both the vertical and the torsional frequencies, while two seismometers recording lateral motions are needed to distinguish torsional and lateral modes of vibrations.

Finally, it may be interesting to note that in Figs. IV-16 through IV-19 the recorded displacements and velocities did not have large spectral amplitudes above approximately 5 c. p. s. ; this gives a limit above which structural motion is practically indistinguishable from other recorded noise. One source of noise causing distortion of the higher modes could be the impact of vehicles crossing expansion and structural joints of the bridge. (This impact was clearly heard and felt while the experiments were being conducted.) The equipment used to repaint the bridge was also a possible source of noise. In general, however, this method of structural testing, based on traffic induced vibrations, can give realistic estimates of the natural frequencies of a wide variety of suspension bridge structures.

From the Earthquake Engineering and Structural Dynamics point of view, the proper location of permanent instrumentation to record strong ground motion, on and in the vicinity of suspension bridges, is an important question. Proper placement will yield information about the response of the bridge, the nature of different modes of vibration and the coupling of those modes. Information indicating the effects of soil-bridge-soil interaction and, possibly, the damping of the structure as well as the phase differences in the motions of the piers and anchorages may also be obtained.

The following are suggestions for appropriate locations of the instruments; it should be noted that these suggestions assume an ideal set of circumstances and, thus, do not consider any economic limitations.

1. A set of three instruments, located on any given cross section of the suspended structure, between the mid-point and the point of support of the span, should be placed on the center span and one of the side spans. Each set would include one instrument on the centerline of the top chord of one of the suspended structures and another instrument on the centerline of the bottom chord. The third instrument would be located on either the top or the bottom chord of the other suspended structure. All of the instruments should be situated so as to record vertical motions, horizontal motions in the longitudinal direction of the bridge, and horizontal motions perpendicular to the bridge. These records would help to identify the different modes of vibrations.

2. Two additional instruments should be used, one located at each pier, in order to correlate the ground motions at the two sites and to evaluate any phase differences. These placements are particularly important in bridges having very long spans.
3. Instruments should be located, also, at each of the supports of the suspended structures on the tower legs; from these locations, information may be obtained to evaluate the effect of the differential motion of the supports on the movements and interaction of the bridge spans, and thus on the mode shapes.
4. To study the soil-structure interaction, an instrument should be located on each of the banks, in line with the piers of the bridge, and below each end of the bridge deck.
5. Finally, although not essential, instruments located at each of the tower tops and at each anchorage would be useful to evaluate the motion of each of those locations.

Comparison Between Computed and Measured Frequencies of the San Pedro Suspension Bridge  
(Center Span Tests)

| Frequencies Corresponding to Peak Values of the Fourier Amplitude Spectrum (c. p. s.) |               |                             |               | Computed Frequencies for Different Modes of Vibration |                    |                 |                     |                 |                          |
|---|---------------|-----------------------------|---------------|---|--------------------|-----------------|---------------------|-----------------|--------------------------|
| Location A<br>(C. L. Bridge)  |               | Location B<br>(C. L. Truss) |               | Average Value   | Vertical Vibration |                 | Torsional Vibration |                 | Expected Asymmetric Mode |
| Rec. Dis-placement  | Rec. Velocity | Rec. Dis-placement          | Rec. Velocity |   | Symmetric Freq.    | Asymmetric Mode | Symmetric Freq.     | Asymmetric Mode |                          |
| 0.2197  | 0.2197        | 0.2197                      | 0.2197        | 0.2197  |                    | 0.1969          | 1                   |                 |                          |
| 0.2319  | 0.2380        | 0.2441                      | 0.2319        | 0.2365  | 1                  |                 |                     | 0.4491          | 1                        |
| 0.4883  | 0.4883        | 0.4883                      | 0.4761        | 0.4852  | 4                  | 0.5486          | 3                   |                 | 0.5939                   |
| 0.5798  | 0.5737        | 0.5859                      | 0.5859        | 0.5814  |                    | ?               |                     | ?               | ?                        |
| --  | 0.6653        | 0.7324                      | 0.7324        | 0.7100  | 5                  |                 |                     |                 |                          |
| 0.8239  | 0.8301        | 0.8301                      | 0.8423        | 0.8316  |                    | 0.8031          |                     |                 | 1.3666                   |
| 1.4343  | 1.4282        | 1.4160                      | --            | 1.4262  | 8                  |                 |                     |                 |                          |
| 1.4465  | 1.4404        | 1.4648                      | 1.4404        | 1.4480  |                    | 1.4670          |                     |                 |                          |
| 1.7700  | 1.7705        | 1.7700                      | 1.7822        | 1.7732  |                    | 1.8813          | 7                   | 1.8567          | 5                        |
| 2.4170  | 2.4292        | --                          | 2.3920        | 2.4129  | 10                 |                 |                     |                 |                          |
| 2.4902  | 2.4962        | 2.5146                      | 2.4902        | 2.4978  |                    |                 |                     |                 |                          |
| 2.5452  | 2.5696        | --                          | --            | 2.5574  |                    |                 |                     |                 |                          |
| 2.8870  | 2.8503        | 2.8687                      | 2.8564        | 2.8656  |                    | 2.8769          | 9                   |                 |                          |
| 3.4310  | 3.3813        | 3.2837                      | 3.2349        | 3.327   |                    |                 |                     | 3.0794          | 7                        |
| --  | 3.5156        | 3.4220                      | --            | 3.4688  |                    |                 |                     |                 |                          |
| 3.5600  | 3.5583        | 3.5513                      | --            | 3.5565  | 12                 |                 |                     |                 |                          |
| 3.6072  | 3.6011        | 3.8218                      | --            | 3.6100  |                    |                 |                     |                 |                          |
| 3.7415  | 3.7903        | --                          | --            | 3.7659  |                    |                 |                     |                 |                          |
| 3.8879  | 3.8818        | --                          | 3.9185        | 3.8961  |                    |                 |                     |                 | 3.8231                   |
| --  | 3.9925        | 3.9587                      | --            | 3.9756  |                    |                 |                     |                 |                          |
| 4.5288  | 4.5471        | 4.2298                      | 4.2481        | 4.3839  |                    | 4.0955          | 12                  |                 |                          |
| 4.6265  | 4.6228        | 4.6319                      | 4.6753        | 4.6391  |                    | ?               |                     | ?               | ?                        |
| 4.8401  | 4.8832        | --                          | 4.8854        | 4.8696  | 14                 |                 |                     |                 |                          |
| 5.4016  | 5.3955        | --                          | 5.2567        | 5.3513  |                    |                 |                     |                 |                          |
| 5.4871  | 5.4932        | 5.4588                      | 5.4563        | 5.4739  |                    |                 |                     |                 |                          |
| 5.7129  | 5.7312        | --                          | --            | 5.7221  |                    | 5.5413          | 13                  |                 | 5.5889                   |

TABLE IV-5

Comparison Between Computed and Measured Frequencies of the San Pedro Suspension Bridge (Side Span Tests)

| Frequencies Corresponding to Peak Values of the Fourier Amplitude Spectrum (c.p.s.) |               |                           |               | Computed Frequencies for Different Modes of Vibration |                 |                              |                 |
|---|---------------|---------------------------|---------------|---|-----------------|------------------------------|-----------------|
| Location C (C. L. Bridge)   |               | Location D (C. L. Bridge) |               | Expected Vertical Vibration                           |                 | Expected Torsional Vibration |                 |
| Rec. Displacement   | Rec. Velocity | Rec. Displacement         | Rec. Velocity | Symmetric Freq.                                       | Asymmetric Mode | Symmetric Freq.              | Asymmetric Mode |
| 0.2319  | 0.2380        | 0.2197                    | 0.2380        | 0.2208  | 1               |                              |                 |
| 0.3784  | 0.3784        | 0.3784                    | 0.3784        | 0.3476  | 2               | 0.3463                       | 2               |
| 0.4883  | 0.4822        | 0.4883                    | 0.4883        | 0.3484  | 3               |                              |                 |
| --  | 0.8118        | 0.7996                    | 0.8057        | 0.4588  | 4               | 0.4494                       | 1               |
| 0.8423  | 0.8423        | 0.9522                    | 0.8789        | 0.8031  | 5               | 0.9433                       | 2               |
| --  | 1.0925        | 1.0254                    | 1.0315        | 0.9498  | 7               | 0.9498                       | 3               |
| 2.0874  | 1.5259        | 2.0632                    | 1.6663        | 1.0113  | 4               | 1.0113                       | 4               |
| 2.3560  | 2.1057        | 2.1118                    | 2.0935        | ?   |                 | ?                            | ?               |
|   | 2.2705        |                           | 2.2583        | 1.1023  | 5               |                              |                 |
| 2.5696  | 2.5146        | 2.4963                    | 2.4292        | 2.3401  | 9               | 2.3383                       | 8               |
| 4.1809  | 4.1321        | --                        | 4.0955        | 2.3515  | 10              |                              |                 |
| --  | 4.2603        | 4.1992                    | 4.1870        | 4.0769  | 13              | 4.0818                       | 11              |
| --  | 4.3579        | --                        | 4.3884        | ?   |                 | ?                            | ?               |
| 5.8105  | 4.6631        | 5.8167                    | 4.6243        | ?   |                 | 4.6332                       | 8               |
| 6.8125  | 5.6580        | --                        | 5.7983        | 6.8745  | 16              | 6.3685                       | 15              |
| --  | 6.8953        | --                        | 6.9158        | 9.0950  | 19              | 7.6976                       | 11              |
|   | 7.6257        | --                        | --            | 9.1767  | 18              |                              |                 |
|   | 9.3556        | --                        | 9.1018        |   |                 |                              |                 |
|   |               |                           | 9.2287        |   |                 |                              |                 |

TABLE IV-6

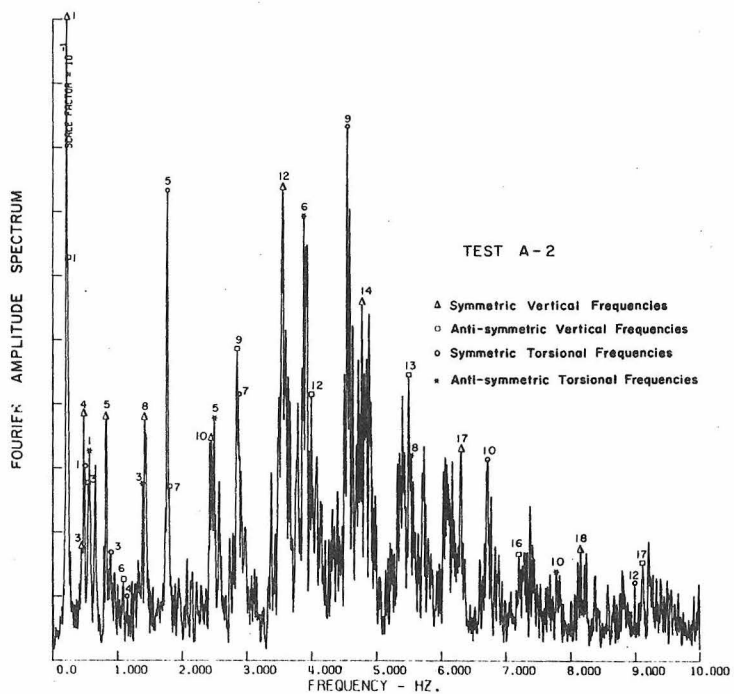
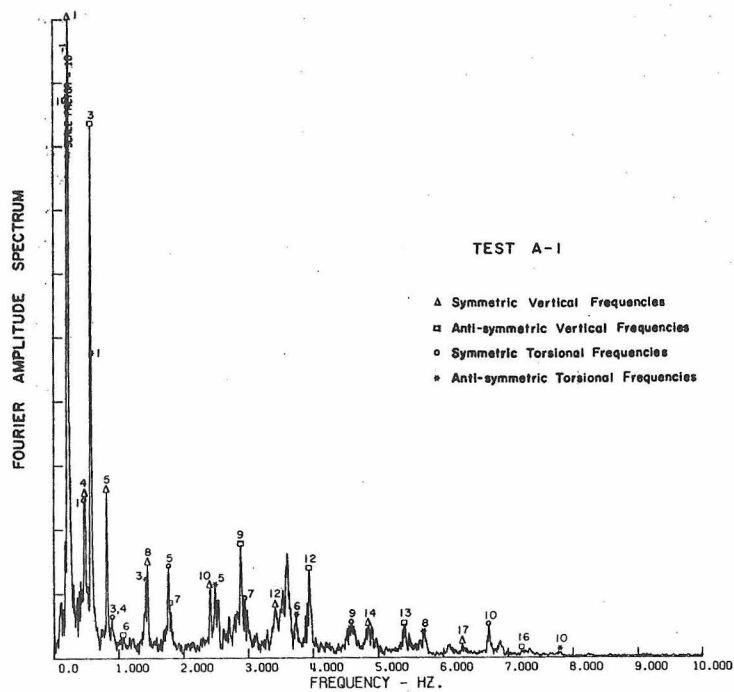


Fig. IV-16. Fourier amplitude spectrum of the (A-1) displacement and (A-2) velocity recorded at location A.

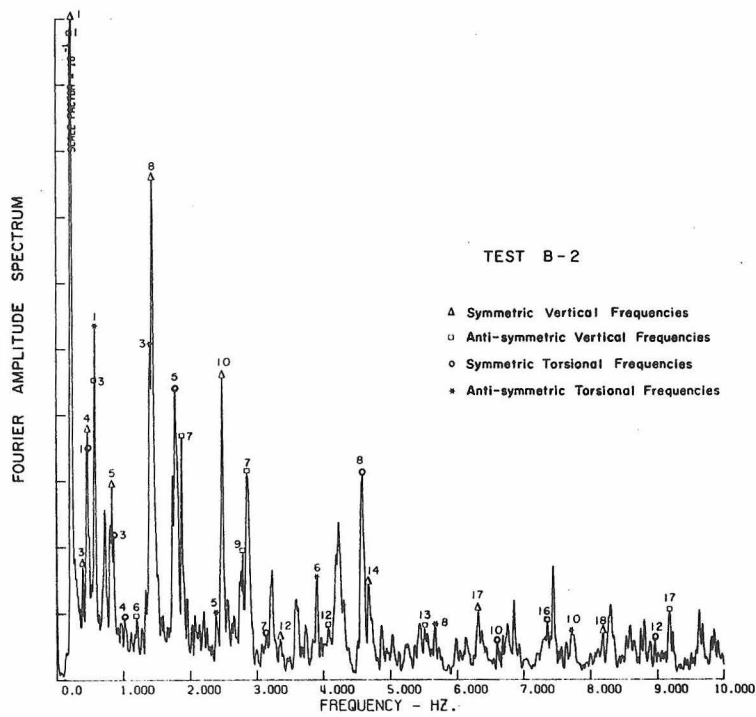
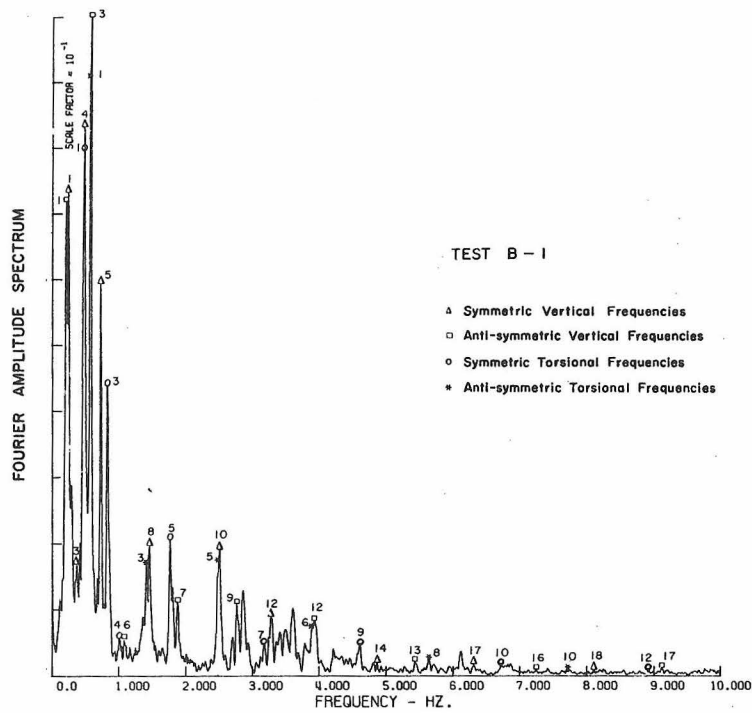


Fig. IV-17. Fourier amplitude spectrum of the (B-1) displacement and (B-2) velocity recorded at location B.

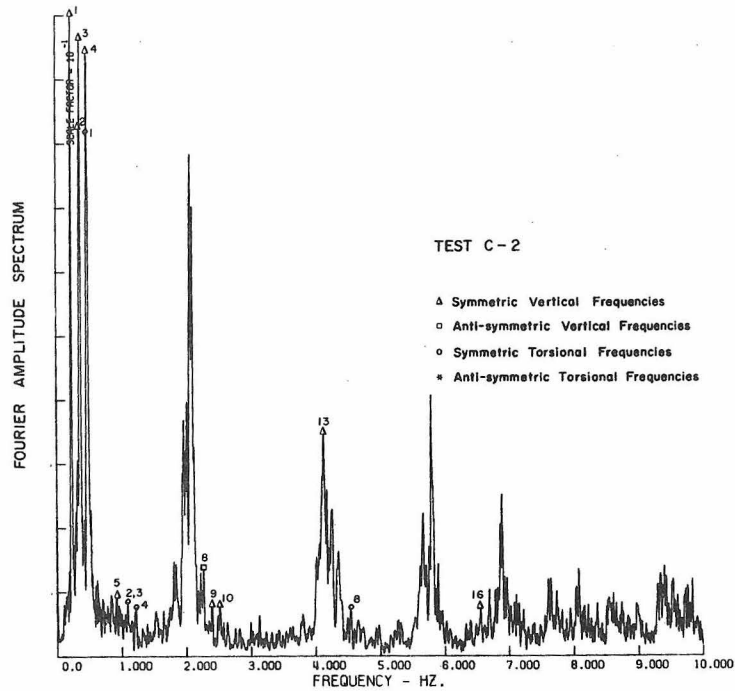
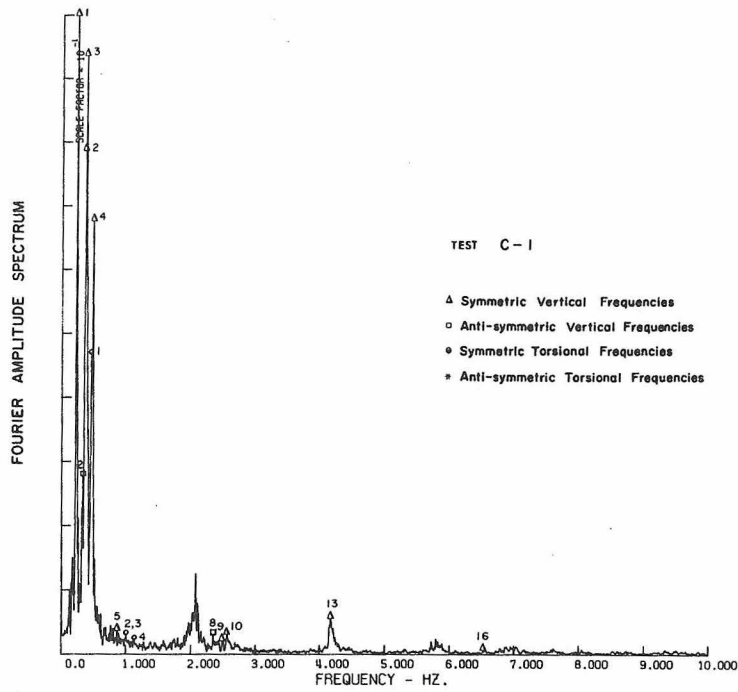


Fig. IV-18. Fourier amplitude spectrum of the (C-1) displacement and (C-2) velocity recorded at location C.

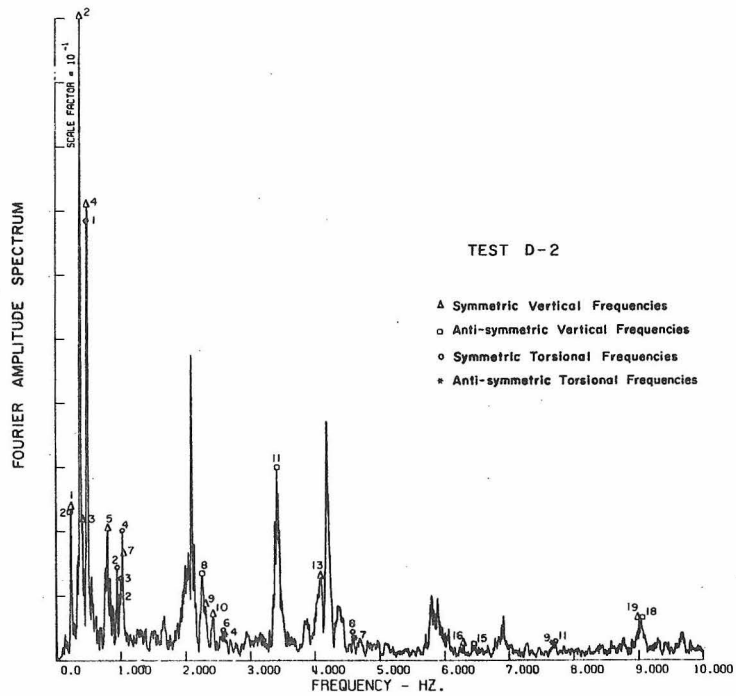
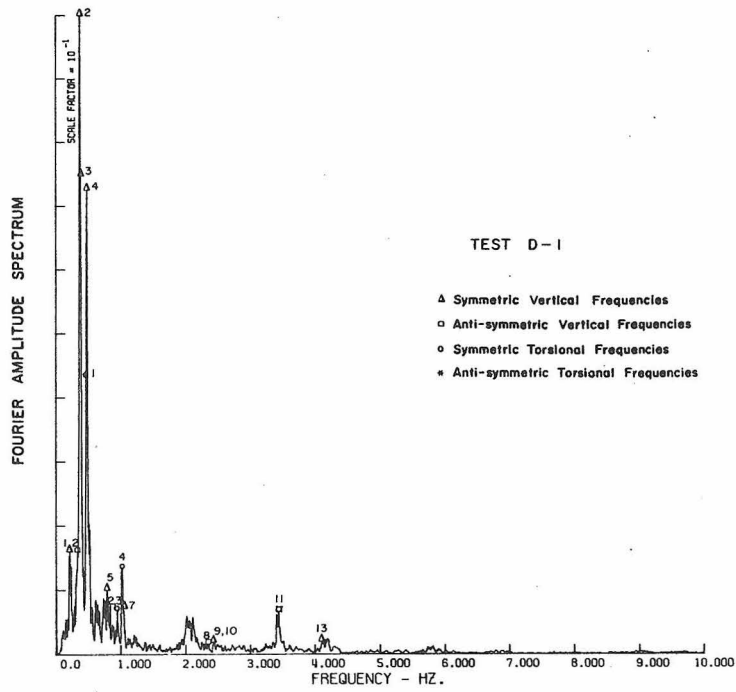


Fig. IV-19. Fourier amplitude spectrum of the (D-1) displacement and (D-2) velocity recorded at location D.

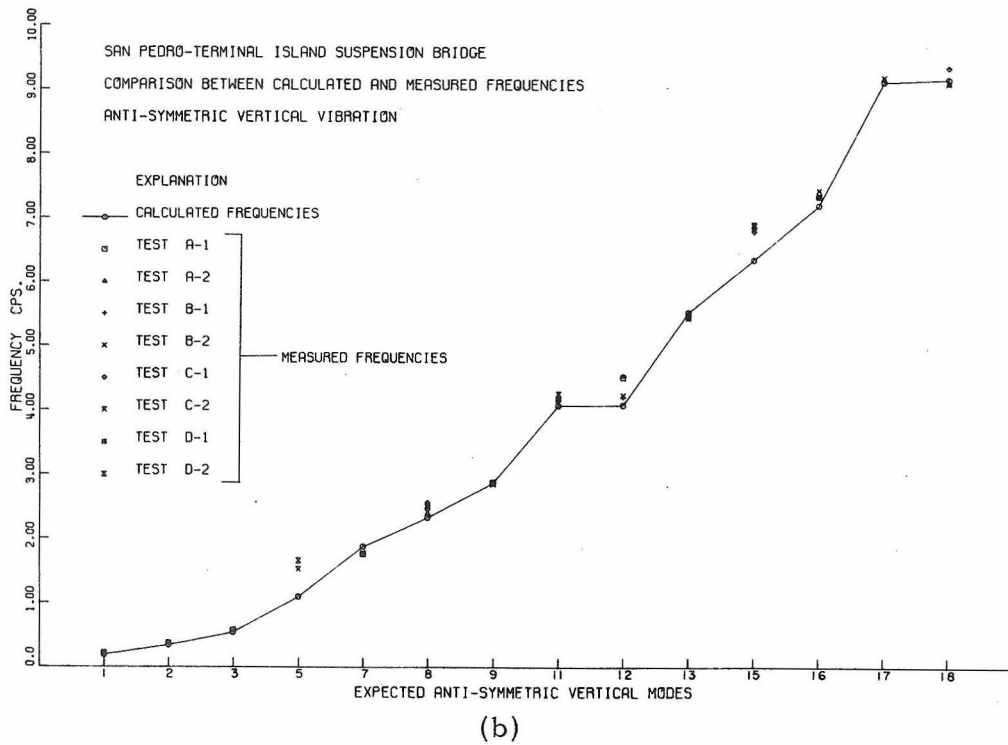
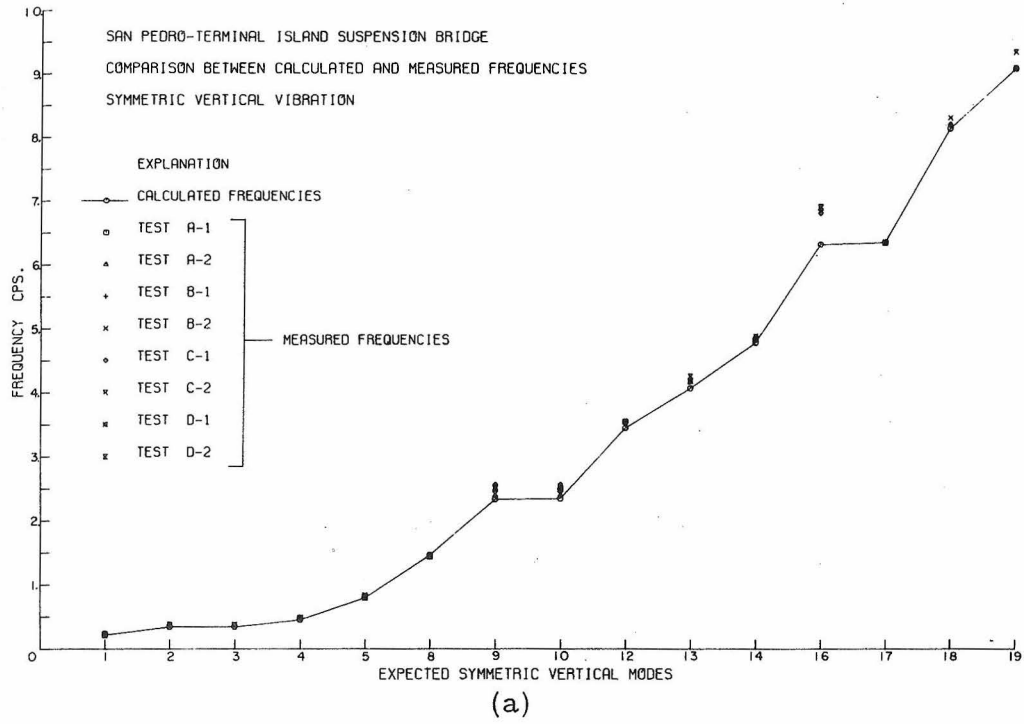
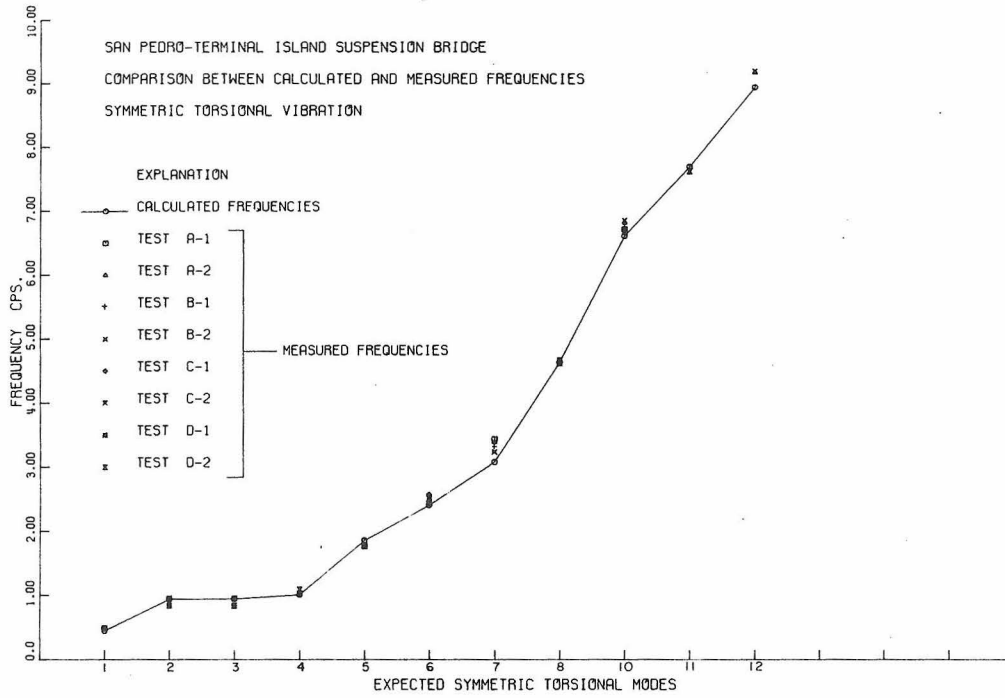
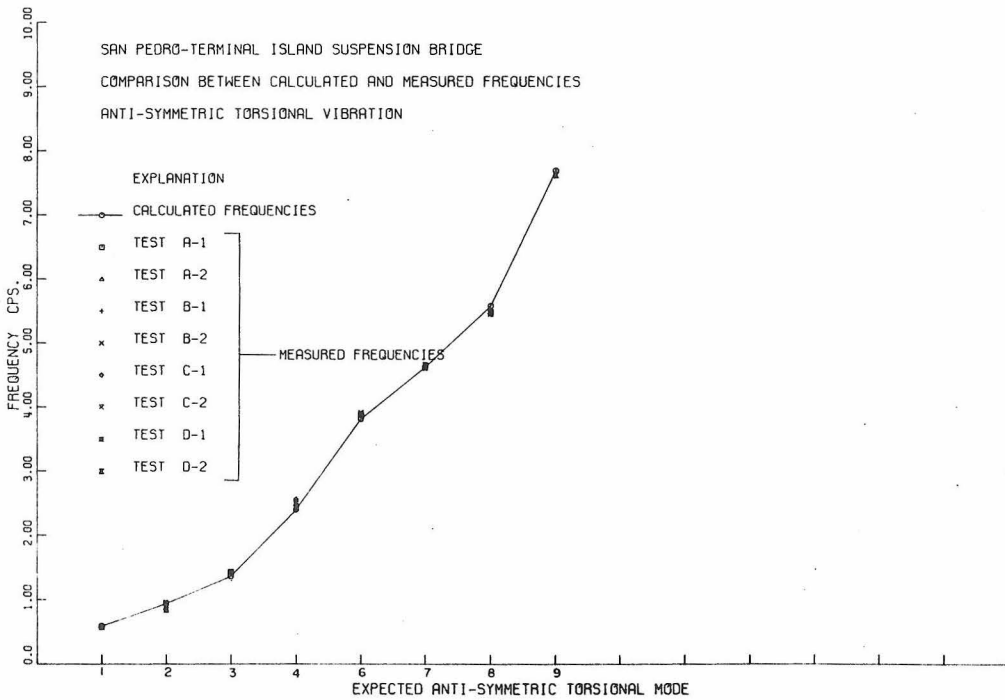


Fig. IV-20. Comparison between calculated and measured frequencies for vertical vibration (a) symmetric and (b) antisymmetric.



(a)



(b)

Fig. IV-21. Comparison between calculated and measured frequencies for torsional vibration (a) symmetric and (b) antisymmetric.

IV-6. Summary and Conclusions

1. The prime objective of this experimental study of the San Pedro Suspension Bridge was to check the reliability of the dynamic methods of analysis developed in Chapters I through III by comparing the measured and computed frequencies.
2. The bridge's response to motion caused mainly by traffic, as well as by wind, and other environmental factors was measured with sensitive seismometers. The recorded motion was analyzed using Fourier techniques and a digital computer.
3. The experimental estimates of the natural frequencies of the bridge revealed many modes of vertical and torsional vibrations in the frequency range 0 c. p. s. - 5 c. p. s.
4. The close spacing of the different modes requires high resolution spectrum analysis and consequently long recording sessions; it also requires proper placement of the seismometers, as indicated.
5. Further recommendations toward obtaining better results are also indicated.
6. The natural frequencies measured showed reasonable agreement with computed values for the vertical and torsional modes of vibrations in the first few modes.

REFERENCES OF CHAPTER IV

1. Vincent, G. S., "A Summary of Laboratory and Field Studies in the United States on Wind Effects on Suspension Bridges." Prepared for the International Conference on Wind Effects on Buildings and Structures, London, England, June 26-28, 1963.
2. Vincent, G. S., "Golden Gate Bridge Vibration Studies," Trans. Am. Soc. of C. E., Vol. 127, 1962, Part II, p. 667.
3. Department of Public Works, "Report of Completion for the Construction of the Superstructure of the Vincent-Thomas Suspension Bridge Between San Pedro and Terminal Island," State of California, Sacramento, File No. VII-LA-167-LA, 61-14SPC2, 1961.
4. Wiles, E. G., "Report of Aerodynamic Studies on Proposed San Pedro-Terminal Island Suspension Bridge, California," Bridge Research Branch, Division of Physical Research, Bureau of Public Roads, U. S. Department of Commerce, 1960.
5. Trifunac, M. D., "Wind and Microtremor Induced Vibrations of a Twenty-Two Story Steel Frame Building," Earthquake Engineering Research Laboratory, California Institute of Technology, Pasadena, California, 1970.
6. McLamore, V. R., Hart, G. C. and Stubbs, I. R., "Ambient Vibration of Two Suspension Bridges," Journal Str. Div., Proc. Am. Soc. of C. E., ST10, October 1971, pp. 2567-2582.
7. Carder, D. S., "Observed Vibrations of Bridges," Bulletin of the Seismological Society of America, Vol. XXVII, p. 267, October 1937.
8. Bleich, F., "Dynamic Instability of Truss-Stiffened Suspension Bridges Under Wind Action," ASCE Transactions, Vol. 114, 1949, p. 1177.
9. Farquharson, F. B., "Aerodynamic Stability of Suspension Bridges with Special Reference to the Tacoma Narrows Bridge, Part IV, Model Investigations which Influenced the Design of the New Tacoma Narrows Bridge," and "Part V, Extended Studies: Logarithmic Decrement, Field Damping, Prototype Predictions, Four Other Bridges," by George S. Vincent, University of Washington Engineering Experiment Station, Bulletin No. 116, Parts IV and V.

10. Rainer, J.H. and Selst, V. A., "Dynamic Properties of Lions' Gate Suspension Bridge," ASCE/EMD Specialty Conference on Dynamic Response of Structures: Instrumentation, Testing Methods and System Identification, University of California, Los Angeles, March 30 and 31, 1976.

### Summary and Conclusions of Part A

This part of the thesis develops a method of dynamic analysis for the free, vertical, torsional and lateral vibrations of suspension bridges. The method is based on the so-called linearized deflection theory, on the finite element approach and on use of the digital computer. It incorporates certain simplifying features and involves two distinct steps:

1. Specification of the different potential and kinetic energies of the vibrating members of the continuous structure, leading to derivation, by Hamilton's Principle, of the differential equations of motion and the associated boundary conditions governing the vertical, torsional and lateral free vibrations. Solutions of the linear differential equations for torsional and lateral free vibrations are obtained; the solutions for vertical vibration have not been derived as they are well known.
2. Use of the finite element technique to:
  - a. discretize the structure into equivalent systems of finite elements,
  - b. select the displacement model most closely approximating the real case,
  - c. derive the element and assemblage stiffness and inertia properties, and finally
  - d. form the matrix equations of motion and the resulting eigenproblems.

The evaluation of the stiffness and inertia properties of the idealized structural element and assemblage is based on the expression of the potential and kinetic energies of the element (or the assemblage) in terms of nodal displacements.

Detailed numerical examples are presented to illustrate the applicability and the effectiveness of the analysis and to investigate the dynamic characteristics of a wide class of suspension bridges with widely different properties. Furthermore, a rigorous comparison with previous results obtained by other investigators has been made.

To further demonstrate the reliability of the analysis, the natural frequencies and mode shapes of vibration of the Vincent-Thomas Suspension Bridge (between San Pedro and Terminal Island, California) have been computed and compared with the measured frequencies of the bridge. The experimental estimates of the natural frequencies revealed many modes of vertical and torsional vibrations in the frequency range 0 c. p. s. -5 c. p. s. The natural frequencies measured showed excellent agreement with the computed values for the vertical and torsional modes of vibration. Further recommendations toward obtaining better results are also indicated.

This method constitutes an advance in the analysis of the dynamics of suspension bridges, in that it eliminates the need to solve transcendental frequency equations, simplifies the accurate computation of both lower and higher modes of vibration, simplifies the determination of the energy stored in different members of the

suspension bridge, and represents from the engineering point of view, a simple, fast and accurate tool for calculating the natural frequencies and modes of vibration by means of a digital computer.

PART B

STUDIES ON THE EFFECT OF DIFFERENTIAL MOTIONS  
OF TWO FOUNDATIONS UPON THE RESPONSE OF  
THE SUPERSTRUCTURE OF A BRIDGE

General Introduction

The effect of differential motions of two (or more) foundations upon the dynamic response of the superstructure of a bridge is a little understood problem which is of considerable interest in earthquake engineering. Although dynamic loadings acting on a bridge structure may result from different sources, including wind or vehicular motions, to the structural engineer one of the most important types of dynamic input is that produced by an earthquake. The definition of an appropriate ground-motion history is the most difficult and uncertain phase of the problem of predicting structural response to earthquakes. A common assumption in the usual treatment of earthquake excitations is that the same motion acts simultaneously at all points of the structure's foundation. If rotation motions are neglected, this assumption is equivalent to considering the foundation soil to be rigid. Such a hypothesis is not consistent with the concept of earthquake wave propagation; however, if the base dimensions of the structure are small relative to the vibration wave length in the soil, the assumption is acceptable. For example, if the velocity of the wave propagation is 6,000 ft/sec., a sinusoidal

wave of 3 Hz frequency will have a length of 2,000 ft. , and a building with a base dimension of 100 ft. will be subjected to essentially the same motions over its entire length. On the other hand, a suspension bridge, which might have a length of several thousand feet, obviously would be subjected to drastically different motions at its two foundations. No direct measurements have been taken of a bridge (or similar structure) at two widely separated foundations during an earthquake; however, it is evident that the motions must vary and their variance could contribute significantly to the dynamic response. Therefore, it is important to develop analytical procedures capable of dealing with multiple support excitation.

In order to lay a foundation from which later work, analyzing the dynamic response of long-span suspension bridges to earthquake ground motions applied at separate points of support, can be developed, two related topics have been studied in this part of the thesis. The first topic, in Chapter V, deals with the dynamic response of a "long beam" model of a bridge span to both steady-state and random excitations applied at the supports; the results involve a large number of modes. The second topic, presented in Chapter VI, develops a method to analyze the dynamic soil-bridge interaction of a simple bridge model erected on an elastic half-space, and the input motion is in the form of incident plane SH-waves. The dynamic response of the girder and the effect of the radiative damping in the half-space on the interaction of the girder are also studied.

It is believed that these preliminary studies provide valuable insight into the structural behavior of suspension bridge structures.

## CHAPTER V

### DYNAMIC RESPONSE OF A LONG BEAM MODEL OF A BRIDGE STRUCTURE SUBJECT TO TWO END EXCITATIONS

#### V-1. Introduction

For long span structures such as suspension bridges, the piers or the abutments of the bridge may be far apart. In such a case, one may have a situation involving ground motion with different characteristics at each point of the bridge structure. For instance, during the 1971 San Fernando earthquake, the motions recorded by instruments located in Millikan library, at one end of the campus of California Institute of Technology, differed greatly from those of the Caltech Athenaeum located at the other end.

The following study deals with the effect of differential motions of two end supports upon the response of the superstructure. The study has been simplified by considering a long shear beam, simply supported at two ends, as shown in Fig. V-1, this beam is subjected to two end excitation,  $f_1(t)$  and  $f_2(t)$ , in the form of ground displacements.

Two cases of excitation have been examined:

1. Harmonic excitations where

$$f_1(t) = A \sin \omega t \quad \text{and} \quad f_2(t) = A \sin(\omega t + \alpha)$$

in which  $A$  is the amplitude of the input motion and  $\alpha$  is the phase difference between the two end excitations, as shown in Fig. V-1-a.

2. Random excitations where

$$f_1(t) = f_2(t) = f(t)$$

in which  $f(t)$  is a random function of time.

For the harmonic excitations, which may differ in phase at the ends, the analysis has been made in the frequency domain by considering the steady state vibrations and calculating the displacement amplitudes at certain points on the beam. The energy content of the system has been presented, and the correlation between the two end excitations has been considered.

For random excitations where  $f_1(t) = f_2(t) = f(t)$ , i. e., where the two ends of the shear beam have the same motion (symmetric mode shapes), the analysis has been made in the time domain; two cases of random motion have been considered: (1) Random motion (or displacement) of the supported ends that might be appropriate for a motion resulting from earthquake acceleration. This random motion was suggested by Shinozuka [1], and is in the form of the integral of a product of an envelope decaying deterministic function times a random function. (2) Random acceleration of the supported ends, which was developed by Tajima [8] from the work of Kanai [9], has been studied. The case where the excitation has a certain duration followed by free vibration has been considered.

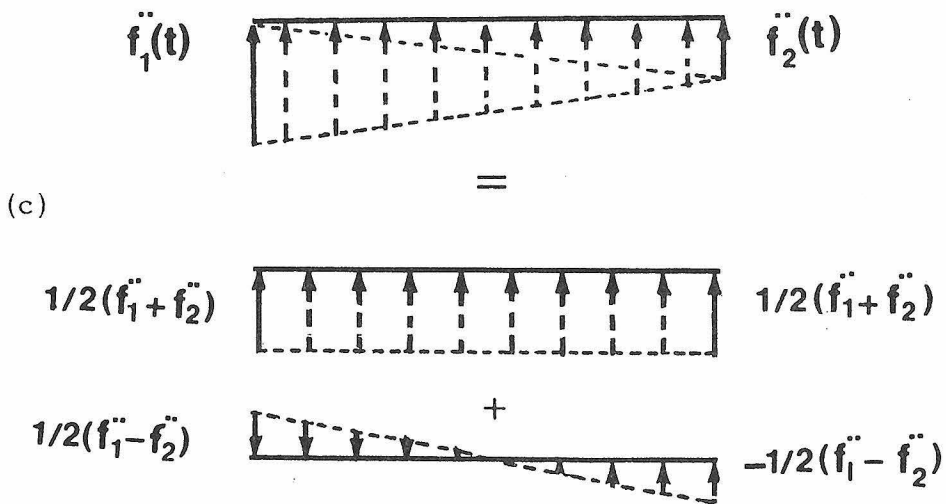
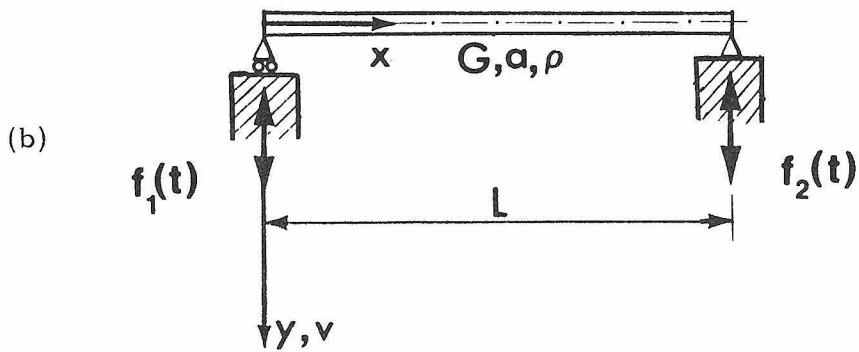
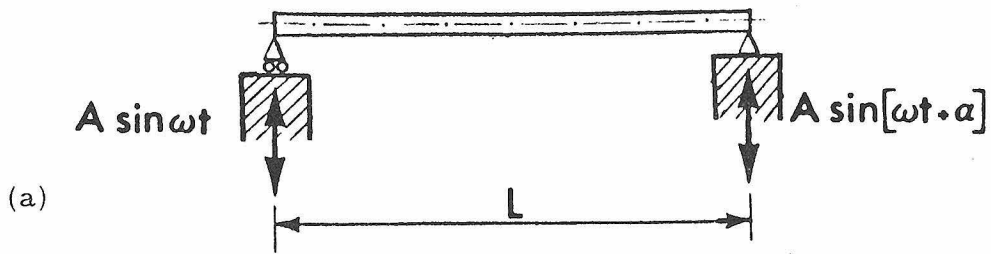


Fig. V-1. Bridge model subjected to motions at the support points.

In either case of random motion, the response of the beam structure has been calculated and plotted versus different cases of envelope functions for case (1) and different durations for case (2).

## V-2. Steady-State Vibration Analysis

In this section, a study is made of the shear beam excited by the motion of the two support points, as shown in Fig. V-1-a. The two harmonic excitations, evidenced in the form of displacements, are of the same frequency and amplitude, but differ in phase by  $\alpha$ . The steady-state vibration of the beam is studied, and the results are expressed in a nondimensional form that enables a concise graphical presentation of the dynamic characteristics of the system.

### V-2-1. Undamped natural frequencies and mode shapes

The free vibration of the undamped shear beam is described by the equation of motion

$$\rho a \frac{\partial^2 v}{\partial t^2} = k' a G \frac{\partial^2 v}{\partial x^2} \quad , \quad (5.1)$$

where  $\rho$  is the mass density,  $a$  is the cross-sectional area of the beam,  $k'$  is a numerical factor depending on the shape of the cross-section, and  $G$  is the shear modulus. From Eq. 5.1, the eigenfunctions or mode shapes for the simply supported beam are

$$\Phi_n(x) = \sin \frac{n\pi x}{L} \quad , \quad n = 1, 2, 3, 4, \dots \quad (5.2)$$

where  $L$  is the span length of the beam.

The natural frequencies are

$$\omega_n = \frac{n\pi}{L} \sqrt{\frac{k'G}{\rho}} \quad , \quad n = 1, 2, 3, \dots \quad (5.3)$$

Eqs. 5.2 and 5.3 are the  $n^{\text{th}}$  mode shape and the  $n^{\text{th}}$  natural frequency, with the understanding that these mode shapes and frequencies could be for fixed-end bridges as well as for hinged-end ones so long as they do not violate the boundary conditions of the displacement for such shear beams.

V-2-2. Equation of motion of damped shear beam

The differential equation of motion, in which a strain-rate type damping (relative damping) is assumed, can be written as

$$\rho \frac{\partial^2 v}{\partial t^2} = k' G \frac{\partial^2 v}{\partial x^2} + c \frac{\partial^3 v}{\partial t \partial x^2} \quad , \quad (5.4)$$

where  $c$  is the damping coefficient.

The initial and boundary conditions are

$$v(x, 0) = \dot{v}(x, 0) = 0 \quad , \quad (5.5)$$

$$v(0, t) = A \sin \omega t \quad , \quad (5.6-a)$$

$$v(L, t) = A \sin (\omega t + \alpha) \quad , \quad (5.6-b)$$

where  $A$  is the amplitude of the two harmonic excitations,  $\alpha$  is the phase difference, and  $\omega$  is the frequency of the excitations.

V-2-3. Steady-state solution

For the steady-state vibration, the solution of Eq. 5.4 may be written as

$$v(x, t) = X_1(x) \cos \omega t + X_2(x) \sin \omega t \quad , \quad (5.7)$$

where both  $X_1(x)$  and  $X_2(x)$  are functions of the spatial coordinate

x, only.

Substitution of Eq. 5.7 into Eq. 5.4 yields two simultaneous ordinary differential equations; putting these two equations in a matrix form containing the solutions and their derivatives, and then solving these four equations, one can obtain

$$X_1(x) = c_1 \cosh qx \cos px + c_2 \sinh qx \cos px + c_3 \sinh qx \sin px + c_4 \cosh qx \sin px, \quad (5.8)$$

and

$$X_2(x) = -c_1 \sinh qx \sin px - c_2 \cosh qx \sin px + c_3 \cosh qx \cos px + c_4 \sinh qx \cos px, \quad (5.9)$$

where  $c_1$ ,  $c_2$ ,  $c_3$  and  $c_4$  are arbitrary constants which can be determined from the boundary conditions (Eq. 5.6), and  $q$ ,  $p$  and  $\beta$  are given by

$$q = \omega \sqrt{\frac{\rho}{k'G}} \sqrt{\left[\frac{\beta-1}{2\beta^2}\right]}, \quad (5.10)$$

$$p = \omega \sqrt{\frac{\rho}{k'G}} \sqrt{\left[\frac{\beta+1}{2\beta^2}\right]}, \quad (5.11)$$

$$\beta = \sqrt{1 + \left(\frac{c\omega}{k'G}\right)^2}. \quad (5.12)$$

Upon using the boundary conditions (Eq. 5.6), the constants  $c_1$ ,  $c_2$ ,  $c_3$ , and  $c_4$  are found to be

$$c_1 = 0 \quad , \quad (5.13)$$

$$c_2 = A \left[ \frac{\sin\alpha \sinh qL \cos pL - \cos\alpha \cosh qL \sin pL + \cos pL \sin pL}{\sinh^2 qL \cos^2 pL + \cosh^2 qL \sin^2 pL} \right] \quad , \quad (5.14)$$

$$c_3 = A \quad , \quad (5.15)$$

$$c_4 = A \left[ \frac{\sin\alpha \cosh qL \sin pL + \cos\alpha \sinh qL \cos pL - \sinh qL \cosh qL}{\cosh^2 qL \sin^2 pL + \sinh^2 qL \cos^2 pL} \right] \quad , \quad (5.16)$$

Therefore, at any point  $\bar{x}$  on the beam, the displacement can be written as

$$v(\bar{x}, t) = X_1(\bar{x}) \cos \omega t + X_2(\bar{x}) \sin \omega t \quad , \quad (5.17-a)$$

or more conveniently as

$$v(\bar{x}, t) = V_0(\bar{x}) \sin(\omega t + \varphi) \quad , \quad (5.17-b)$$

where  $V_0(\bar{x})$  is the amplitude of the beam displacement at point  $\bar{x}$ ; it is expressed as

$$V_0(\bar{x}) = \sqrt{X_1^2(\bar{x}) + X_2^2(\bar{x})} \quad . \quad (5.18)$$

In Eq. 5.17-b,  $\varphi$  is the phase angle between the displacement at that particular point  $\bar{x}$  and the harmonic motion of the left support (where  $x = 0$  and  $\alpha = 0$ );  $\varphi$  is given by

$$\varphi(\bar{x}) = \tan^{-1} \left[ \frac{X_1(\bar{x})}{X_2(\bar{x})} \right] \quad . \quad (5.19)$$

To simplify the calculations, all the parameters involved in the steady-state solution are expressed in nondimensional form; for instance, define the dimensionless frequency  $\omega^*$  as

$$\omega^* = \frac{\omega}{\omega_1} \quad , \quad (5.20)$$

where  $\omega_1$  is the fundamental natural frequency of the beam which is given by

$$\omega_1 = \frac{\pi}{L} \sqrt{\frac{k'G}{\rho}} \quad . \quad (5.21)$$

Therefore, Eqs. 5.10 and 5.11 become

$$q = \frac{\pi}{L} \omega^* \sqrt{\left[ \frac{\beta-1}{2\beta^2} \right]} \quad , \quad (5.22)$$

and

$$p = \frac{\pi}{L} \omega^* \sqrt{\left[ \frac{\beta+1}{2\beta^2} \right]} \quad . \quad (5.23)$$

Now, the steady-state solution,  $v(x, t)$ , can be expressed in terms of the normal modes  $\Phi_n(x)$  as follows

$$v(x, t) = \sum_{n=1}^{\infty} \Phi_n(x) \eta_n(t) \quad (5.24)$$

where  $\eta_n(t)$  is the  $n^{\text{th}}$  normal or generalized coordinate and is a function of time only.

Substitution of Eq. 5.24 into Eq. 5.4 yields

$$\ddot{\eta}_n(t) + \frac{c}{Gk'} \omega_n^2 \dot{\eta}_n(t) + \omega_n^2 \eta_n(t) = 0 \quad , \quad n = 1, 2, 3, \dots \quad (5.25)$$

Let

$$\frac{c}{Gk'} \omega_n^2 = 2 \omega_n \xi_n \quad , \quad (5.26)$$

where  $\xi_n$  is the damping ratio which is given by

$$\xi_n = \frac{1}{2} \omega_n \frac{c}{Gk'} \quad ; \quad (5.27)$$

then, one can obtain

$$\frac{c\omega}{Gk'} = 2 \xi_n \frac{\omega}{\omega_n} = 2 \xi_1 \frac{\omega}{\omega_1} = 2 \xi_1 \dot{\omega}^* \quad (5.28)$$

where  $\xi_1$  is the damping ratio of the first mode. Therefore,

Eq. 5.12 becomes

$$\beta = \sqrt{1 + (2 \xi_1 \dot{\omega}^*)^2} \quad . \quad (5.29)$$

#### V-2-4. Dynamic response of the beam (numerical results)

With the aid of Eqs. 5.17, 5.18 and 5.19, the displacement  $v(x, t)$ , and the phase angle  $\varphi(x)$  were computed at three different points of the beam: at  $x = \frac{L}{2}$ ,  $\frac{L}{4}$  and  $\frac{3L}{4}$ . The damping for the first mode was assumed to be 2%, and  $\alpha$  was given several values:  $0^\circ$ ,  $45^\circ$ ,  $90^\circ$ ,  $135^\circ$  and  $180^\circ$ . Figures V-2, V-4 and V-6 show the displacement amplitudes  $V_0\left(\frac{L}{2}\right)$ ,  $V_0\left(\frac{L}{4}\right)$  and  $V_0\left(\frac{3L}{4}\right)$  as functions of the dimensionless frequency  $\dot{\omega}^*$ , with the excitation phase angle  $\alpha$  as a parameter. From these figures the following observations may be made.

1. In all cases, the amplitude curves for different values of the phase angle  $\alpha$ , all have the same value ( $|V_0| = 1.0$ ) when  $\omega^*$  approaches 0.
2. At the mid-point of the span ( $|V_0(\frac{L}{2})|$ , Fig. V-2), there is no contribution from the even modes (antisymmetric mode shapes), because that point ( $\frac{x^*}{L} = \frac{1}{2}$ ) is always a node point for these mode shapes.
3. In Fig. V-2, also, the maximum displacement is attained when  $\alpha = 0^\circ$ , i. e., when the two harmonic end-excitations are in phase, and this maximum (or peak value) decreases as  $\alpha$  increases in all the odd modes (symmetric mode shapes).  
Further understanding of this behavior of the system may be obtained by studying Fig. V-3 which corresponds to Fig. V-2. In Fig. V-3, when  $\alpha = 0^\circ$  to  $\alpha \simeq 60^\circ$  the rate of decrease is very slow, while from  $\alpha \simeq 60^\circ$  to  $\alpha = 180^\circ$ , the rate of decrease is very rapid.
4. Because of the type of damping assumed, the contribution from the third mode, in Figs. V-2 and V-3, is smaller than the contribution from the first mode (by about 80%).
5. At the points  $|V_0(\frac{L}{4})|$  and  $|V_0(\frac{3L}{4})|$ , the results are almost identical, as seen from Figs. V-4, V-5, V-6 and V-7. There is no contribution from the fourth mode where there are nodes at these points ( $\frac{x^*}{L} = \frac{1}{4}$  and  $\frac{3L}{4}$ ). For different values of the angle  $\alpha$ , the behavior of the system at the second mode is completely different from the behavior at the first mode.

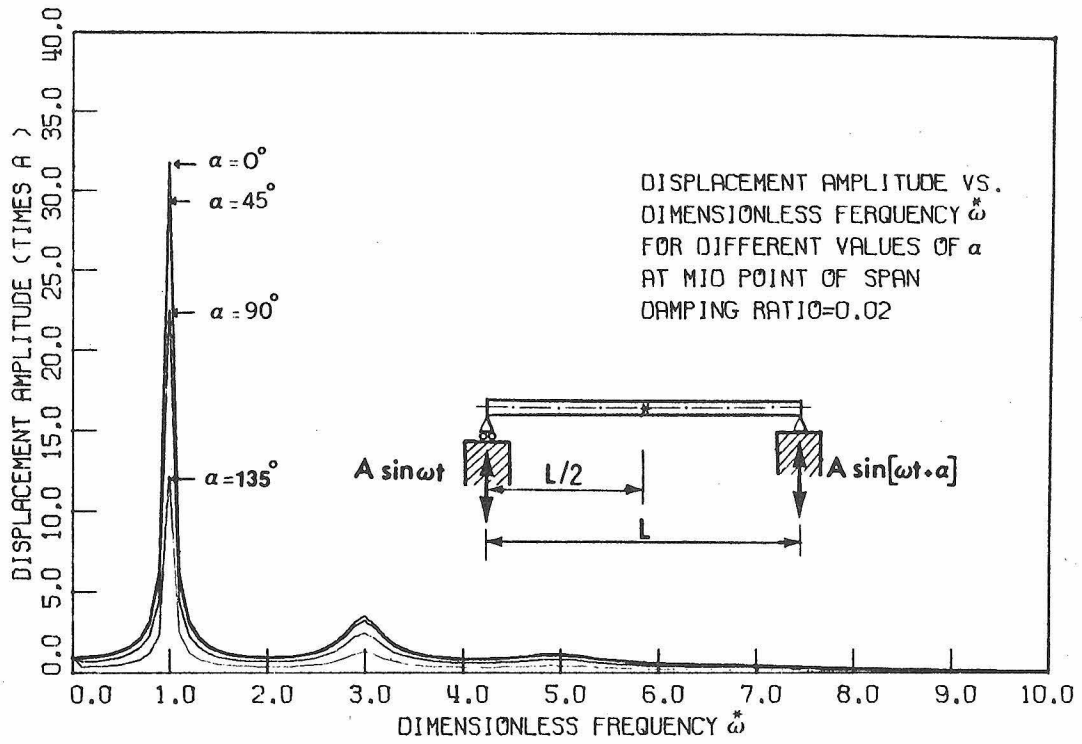


Fig. V-2

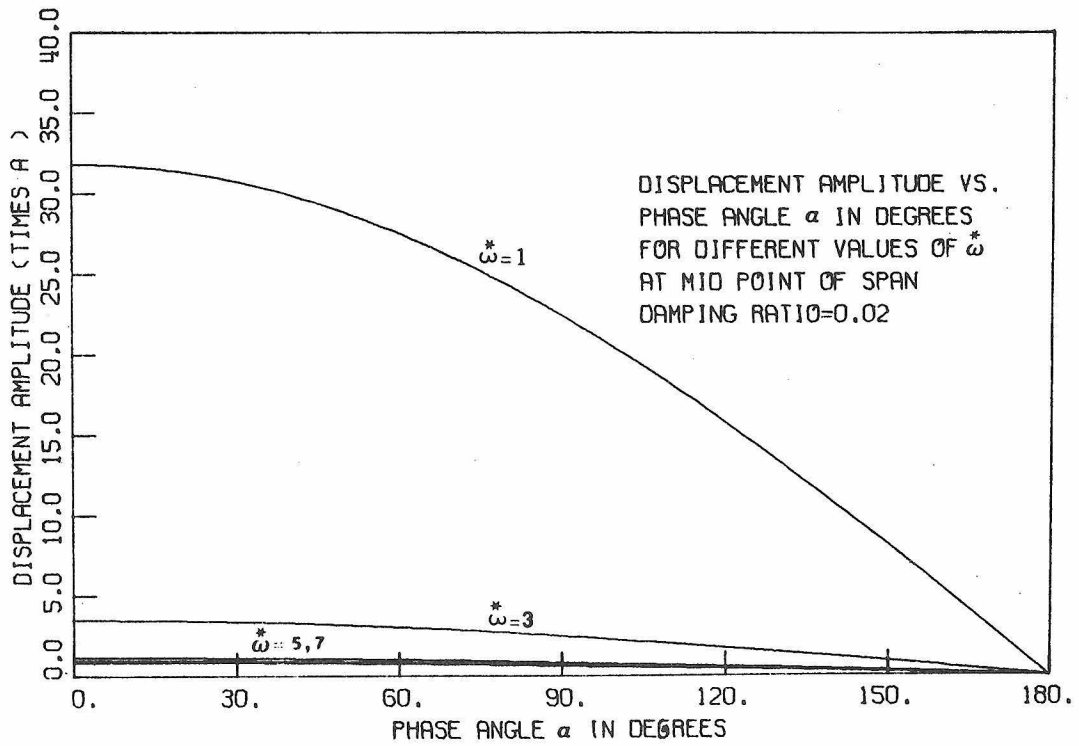


Fig. V-3

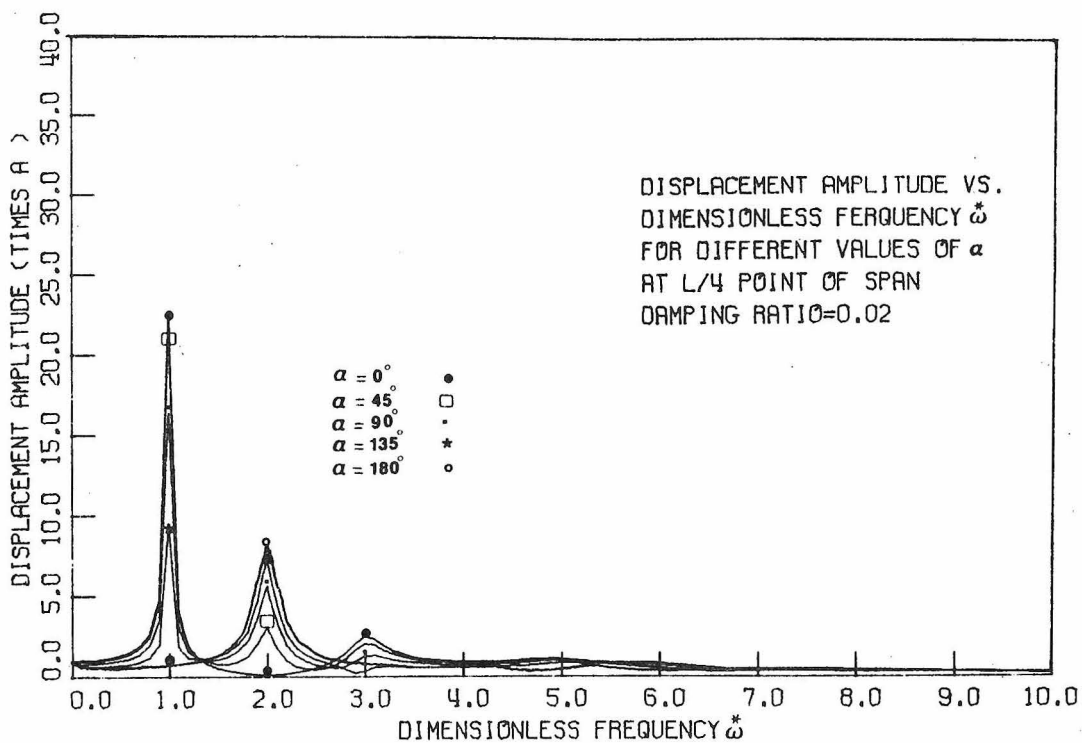


Fig. V-4

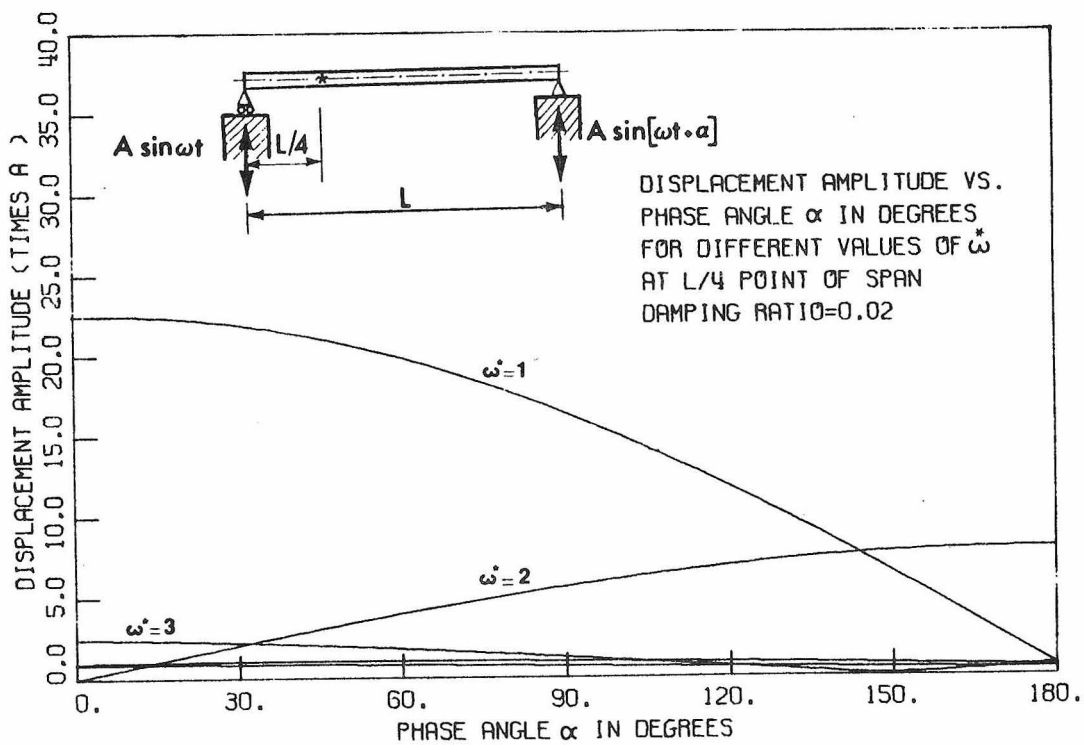


Fig. V-5

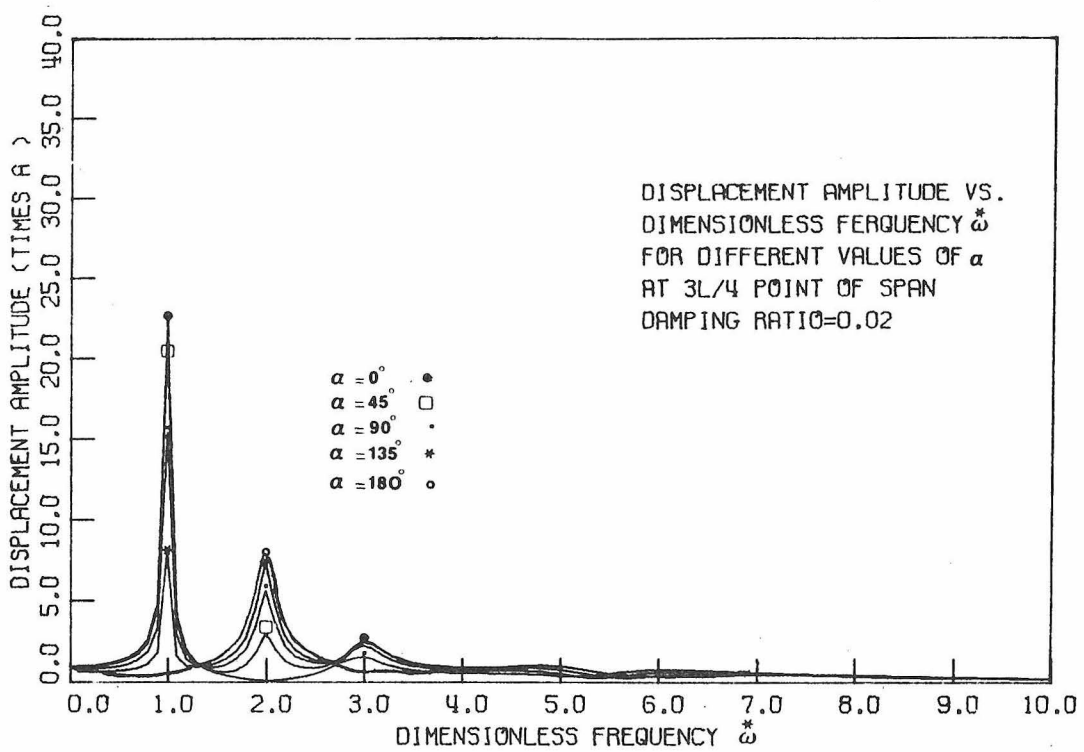


Fig. V-6

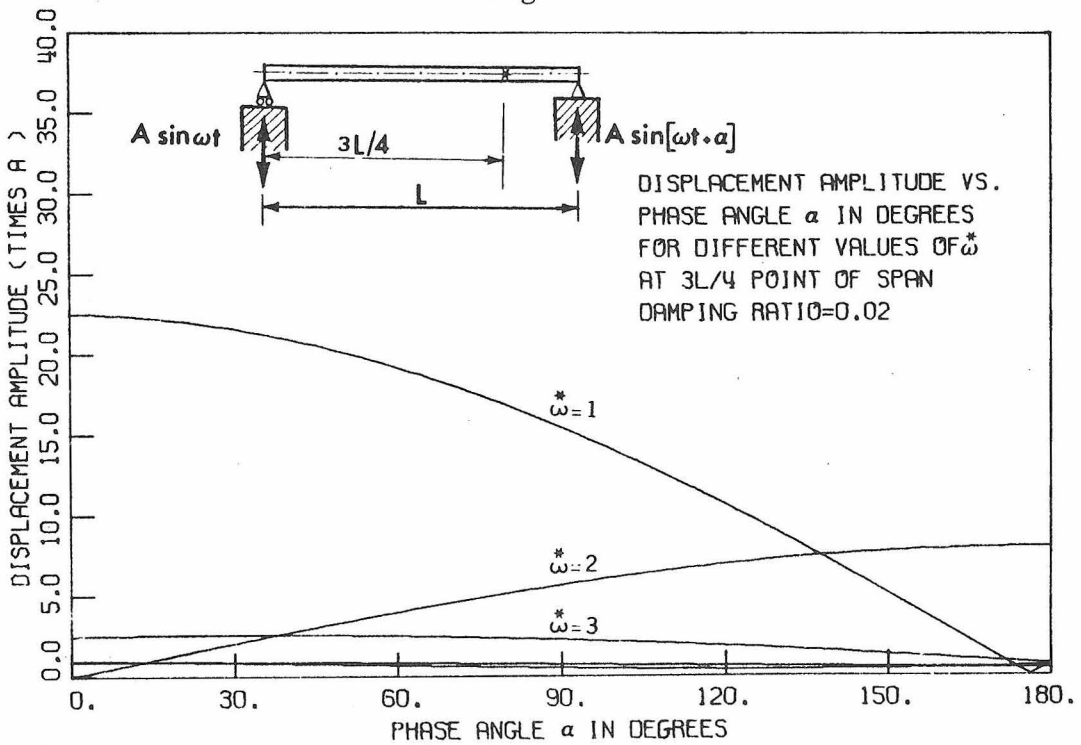


Fig. V-7

6. The phase difference  $\phi$  between the response and the left-support excitation (Eqs. 5.17-b and 5.19), has been plotted for these three points on the beam, as a function of the dimensionless frequency  $\omega^*$ , and with  $\alpha$  as a parameter. All three sets of curves in Figs. V-8, V-9 and V-10 indicated that during resonance of the first mode, the external forced displacement at the left support and the response have a phase difference of  $\frac{\pi}{2}$ .
7. By comparing Figs. V-9 and V-10, a considerable difference is seen in the phase characteristics of the two cases when  $\frac{x}{L} = \frac{L}{4}$  and  $\frac{3L}{4}$ , in contrast with the similarity of the amplitude characteristics (in the frequency domain) shown in Figs. V-4, V-5, V-6 and V-7.

V-2-5. Energy consideration

For an external force  $F(x, t)$ , the equation of motion (Eq. 5.4) can be written as

$$\rho \frac{\partial^2 v}{\partial t^2} = Gk' \frac{\partial^2 v}{\partial x^2} + c \frac{\partial^2 v}{\partial t \partial x^2} + F(x, t) \quad (5.30)$$

In terms of the inertia forces which result from the two end motions,  $F(x, t)$  can be described, as shown in Fig. V-1-c, as

$$F(x, t) = \rho \left[ \left(1 - \frac{x}{L}\right) \ddot{f}_1(t) + \frac{x}{L} \ddot{f}_2(t) \right] \quad (5.31)$$

Because  $f_1(t) = A \sin \omega t$  and  $f_2(t) = A \sin(\omega t + \alpha)$ , Eq. 5.31 becomes

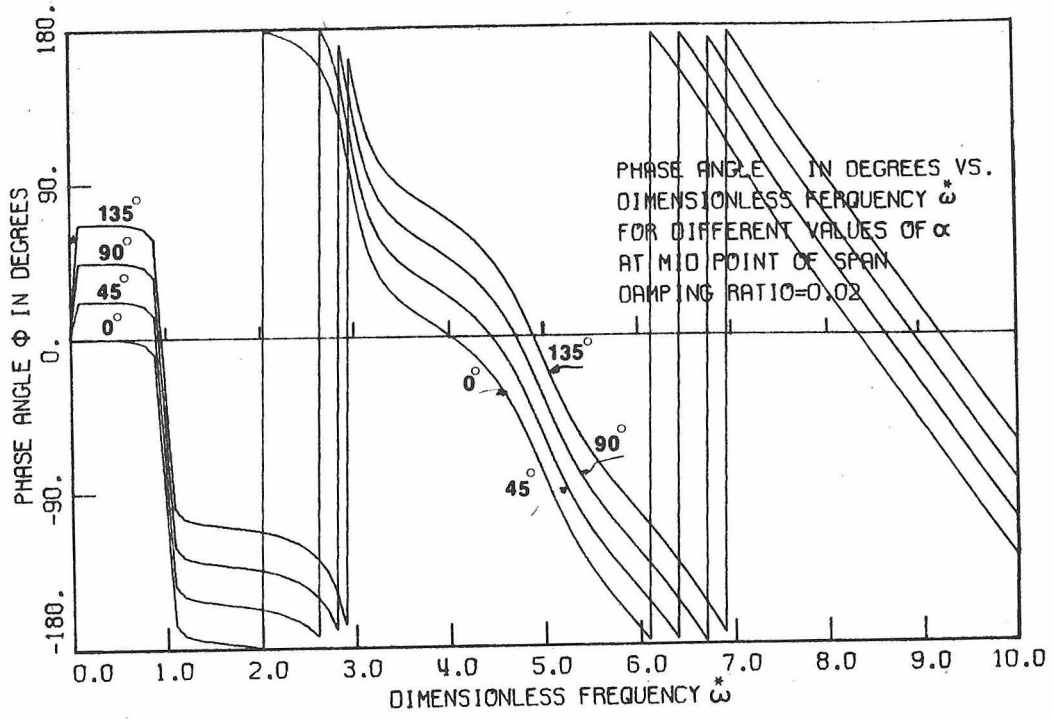


Fig. V-8

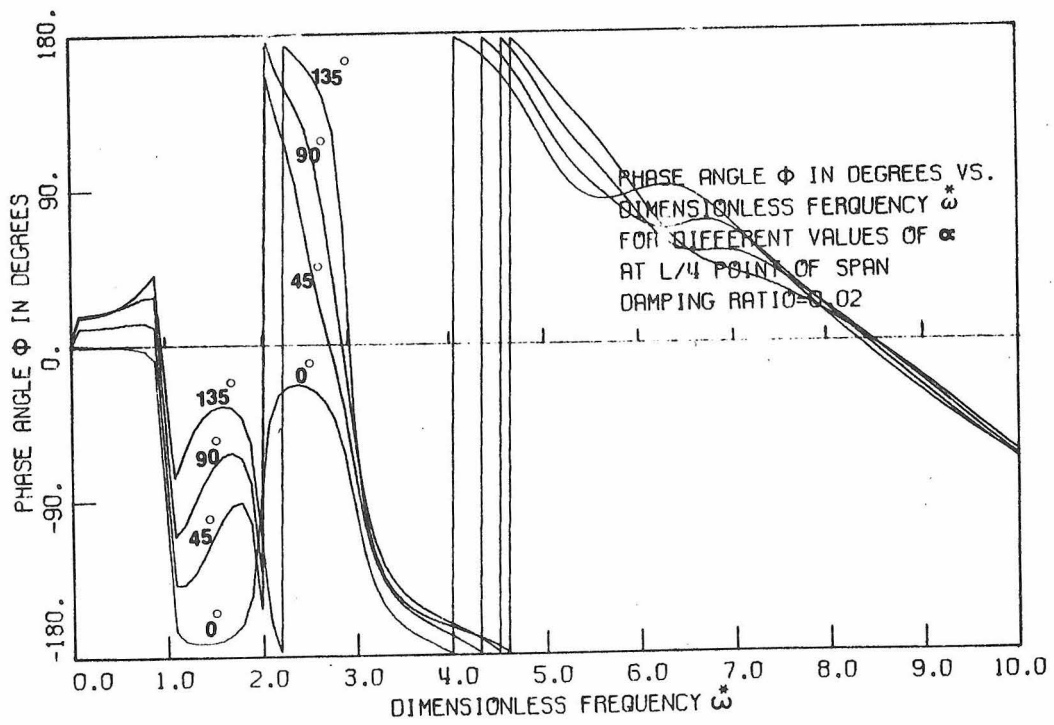


Fig. V-9

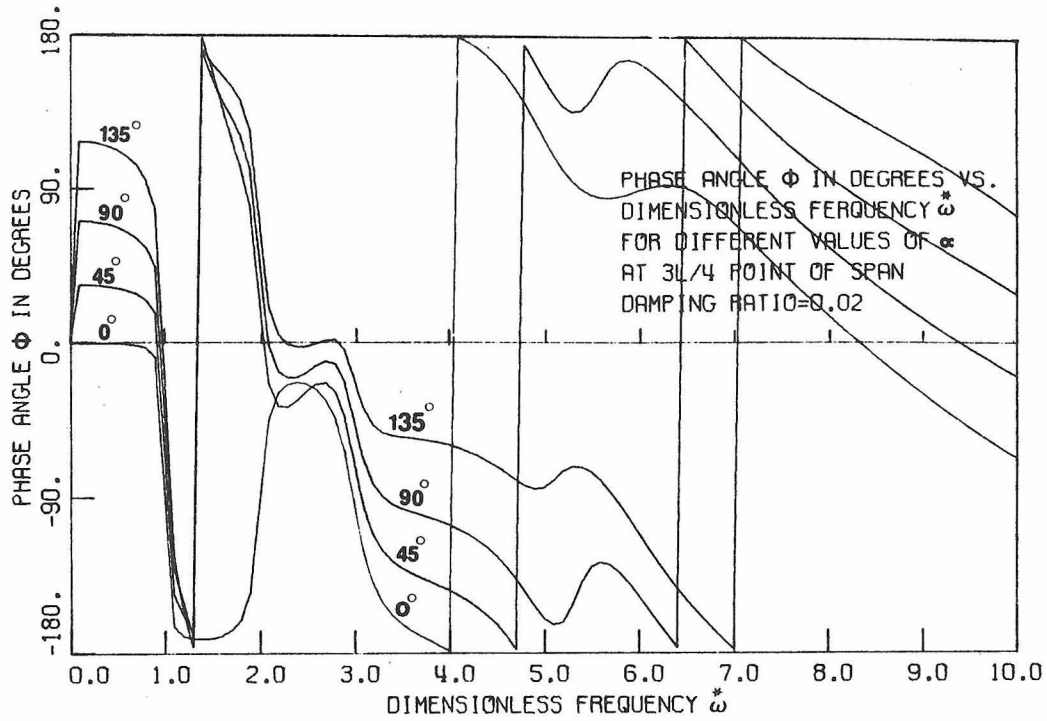


Fig. V-10

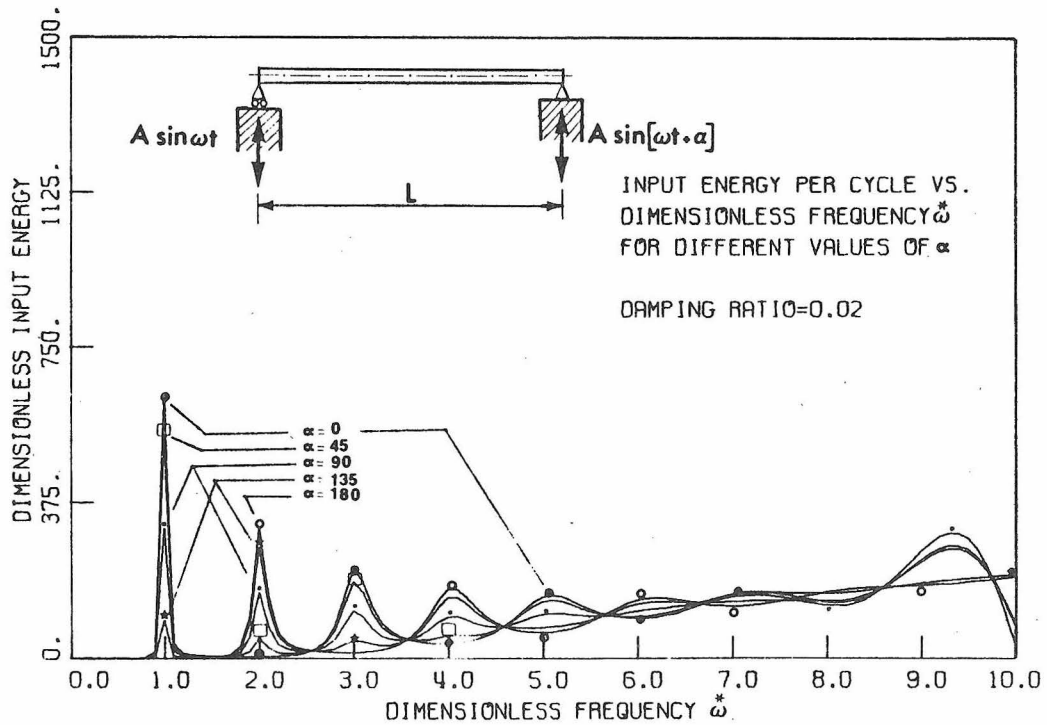


Fig. V-11

$$F(x, t) = \rho A \left[ -\omega^2 \sin \omega t - \omega^2 \frac{x}{L} (\sin \omega t \cos \alpha + \cos \omega t \sin \alpha - \sin \omega t) \right] . \quad (5.32)$$

Therefore, the amount of energy input into the system, which is supplied by the harmonically excited motions is

$$E_I(t) = \int_0^L F(x, t) \frac{\partial v}{\partial t} dt dx , \quad (5.33)$$

and the energy per cycle of the vibration is

$$E_I/\text{cycle} = \int_0^L \int_0^{2\pi/\omega} F(x, t) \frac{\partial v}{\partial t} dt dx . \quad (5.34)$$

This energy was calculated and plotted in dimensionless form  $E_I^*$ , as

$$E_I^* = \left( \frac{E_I/\text{cycle}}{\frac{ak'G}{L} \cdot A^2} \right) . \quad (5.35)$$

Fig. V-11 shows  $E_I^*$  versus  $\dot{\omega}^*$  with  $\alpha$  as a parameter. At resonance, this energy input is equal to the energy dissipated by the system due to damping. Fig. V-11 shows the increase of this energy in the higher modes. The contribution from the odd symmetric modes and the even antisymmetric modes are shown to be proportional with the phase angle  $\alpha$ . Finally, the energy of vibration as seen in Fig. V-11, is greatest in the normal modes of low order; this is to be expected because to excite the lower modes requires more energy.

A similar analysis was made for both the kinetic and strain energies of the system. The kinetic energy is

$$T(t) = \frac{1}{2} \int_0^L \rho a \left( \frac{\partial v}{\partial t} \right)^2 dx \quad , \quad (5.36)$$

and the mean value of this kinetic energy per cycle is

$$T_{\text{mean}}/\text{cycle} = \frac{1}{2} \frac{\omega}{2\pi} \int_0^L \int_0^{2\pi} \rho a \left( \frac{\partial v}{\partial t} \right)^2 dt dx \quad . \quad (5.37)$$

The strain energy of the system is

$$U(t) = \frac{1}{2} \int_0^L k' a G \left( \frac{\partial v}{\partial x} \right)^2 dx \quad , \quad (5.38)$$

and the mean value of this energy per cycle is

$$U_{\text{mean}}/\text{cycle} = \frac{1}{2} \frac{\omega}{2\pi} \int_0^L \int_0^{2\pi} k' a G \left( \frac{\partial v}{\partial x} \right)^2 dt dx \quad . \quad (5.39)$$

This strain energy is due to shear alone, because any element of the beam may undergo distortion but no rotation.

Expressing these energies in nondimensional form, one obtains

$$\overset{*}{T} = \left( \frac{T_{\text{mean}}/\text{cycle}}{\frac{k' a G}{L} \cdot A^2} \right) \quad , \quad (5.40)$$

and

$$\overset{*}{U} = \left( \frac{U_{\text{mean}}/\text{cycle}}{\frac{k' a G}{L} \cdot A^2} \right) \quad . \quad (5.41)$$

Figs. V-12 and V-13 show these two dimensionless energies as functions of  $\bar{\omega}^*$ ; they are almost equal at each normal mode.

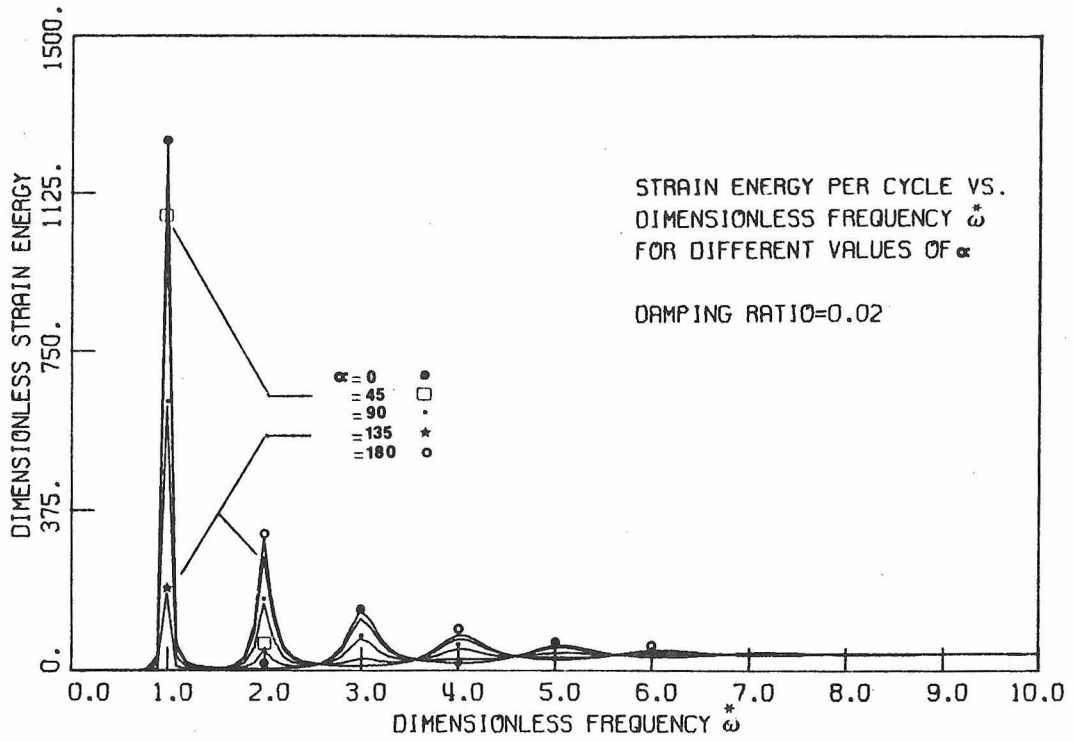


Fig. V-12

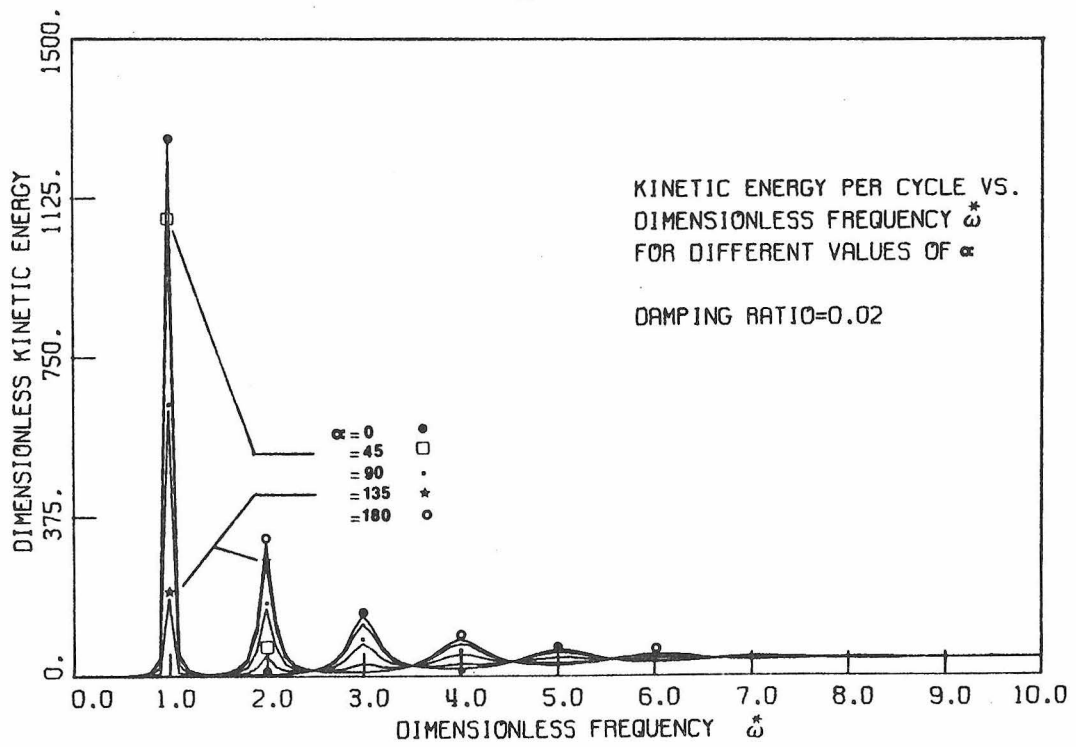


Fig. V-13

V-3. Random Vibration Analysis

This section contains a discussion of the transient response of the beam to random excitations applied at the support points. The analysis has been confined to the stationary aspects of the motion. Two types of input motion having various specific characteristics were considered, and the mean square displacement was calculated for both cases. The two end excitations were assumed to be identical in both cases.

V-3-1. Equation of motion

Substituting Eq. 5.24 into Eq. 5.30, with  $F(x,t)$  defined as in Eq. 5.31, one can obtain the following, after multiplying both sides of the resulting equation by  $\Phi_m(x)$ , integrating from 0 to  $L$  with respect to  $x$ , and making use of the orthogonality of the modes.

$$\ddot{\eta}_n(t) + 2\omega_n \xi_n \dot{\eta}_n(t) + \omega_n^2 \eta_n(t) = \frac{2}{n\pi} [\ddot{f}_1(t) - (-1)^n \ddot{f}_2(t)] , \quad n = 1, 2, 3, \dots \quad (5.42)$$

By considering Fig. V-1-c, one can decompose the two triangular inertia forces to the symmetric case where one has  $\frac{1}{2}(\ddot{f}_1(t) + \ddot{f}_2(t))$ , and the antisymmetric case where one has  $\frac{1}{2}(\ddot{f}_1(t) - \ddot{f}_2(t))$ ; using Eq. 5.42, these two cases can be written as

$$\ddot{\eta}_n(t) + 2\omega_n \xi_n \dot{\eta}_n(t) + \omega_n^2 \eta_n(t) = \frac{2}{n\pi} (\ddot{f}_1(t) + \ddot{f}_2(t)) , \quad n = 1, 3, 5, \dots \quad (5.43)$$

which includes the contributions from the odd modes (symmetric mode shapes), and

$$\ddot{\eta}_n(t) + 2\omega_n \xi_n \dot{\eta}_n(t) + \omega_n^2 \eta_n(t) = \frac{2}{n\pi} \left( \ddot{f}_1(t) - \ddot{f}_2(t) \right) , \quad n = 2, 4, 6, \dots \quad (5.44)$$

which includes the contributions from the even modes (antisymmetric mode shapes).

Because this analysis considers that  $f_1(t) = f_2(t) = f(t)$ , where  $f(t)$  is a random input motion, it shows only the contributions from the symmetric modes. Accordingly, Eqs. 5.43 and 5.44 reduce to

$$\ddot{\eta}_n(t) + 2\omega_n \xi_n \dot{\eta}_n(t) + \omega_n^2 \eta_n(t) = \frac{4}{n\pi} \ddot{f}(t) , \quad n = 1, 3, 5, \dots \quad (5.45)$$

If the initial conditions are assumed to be zero, a valid solution of Eq. 5.45 is obtained through the time domain using the convolution, or Duhamel, integral

$$\eta_n(t) = \frac{4}{n\pi} \int_0^t h(t-\tau) \ddot{f}(\tau) d\tau , \quad n = 1, 3, 5, \dots \quad (5.46)$$

in which  $\tau$  is a dummy time variable and  $h(t)$  is the unit-impulse-response function of the system; it is expressed by

$$\left. \begin{aligned} h(t) &= \frac{1}{\omega_{dn}} e^{-\xi_n \omega_n t} \sin \omega_{dn} t , & t \geq 0 \\ &= 0 & t < 0 \end{aligned} \right\} , \quad (5.47)$$

with  $\omega_{dn} = \sqrt{1 - \xi_n^2} \omega_n$  as the damped natural frequency.

The stochastic mean square of the normal coordinate of Eq. 5.46 can be written as

$$\langle \eta_n^2(t) \rangle = \left( \frac{4}{n\pi} \right)^2 \int_0^t \int_0^t h(t-\tau) h(t-\tau') \langle \ddot{f}(\tau) \ddot{f}(\tau') \rangle d\tau d\tau' , \quad n = 1, 3, 5, \dots \quad (5.48)$$

where  $\ddot{f}(t)$  is assumed to be mean square continuous. The quantity  $\langle \ddot{f}(\tau) \ddot{f}(\tau') \rangle$  is, by definition,  $R_{\ddot{f}}(\tau, \tau')$ , which is the autocorrelation function for  $\ddot{f}(\tau)$ . The autocorrelation function for a stationary process depends only on the time difference  $(\tau - \tau')$ , and not on  $\tau$  and  $\tau'$  individually.

The random excitation has been considered as either

- (1) Random input displacement  $f(t)$  with specific characteristics,

or

- (2) Random input acceleration  $\ddot{f}(t)$  with specific duration and other definite characteristics.

#### V-3-2. Dynamic response under random displacements

The particular form of random motion considered for the random function  $f(t)$  (case (1) above) might express ground motion resulting from earthquake acceleration as stated by Shinozuka and Henry [1]. Unfortunately, the amount of data on strong motion earthquakes is quite limited, so it has not been possible to obtain anything like a complete statistical description of earthquakes. However, there has been previous work concerning the statistical nature of ground motion; reference is made to studies by Bogdanoff, Goldberg and Bernard [3], Bolotin [4], Rosenblueth and Bustamante [5], Caughey and Stumpf [2], Sharpe, et al. [6], and Housner and Jennings [7].

The random displacement  $f(t)$  suggested by Shinozuka and Henry [1] was based on the evident condition that the ground velocity  $\dot{f}(t)$  must approach zero as time  $t$  approaches infinity. This ground displacement is in the form of the integral of the envelope deterministic time function times a random function having specific properties:

$$f(t) = \int_0^t G(\tau) g(\tau) d\tau, \quad (5.49)$$

where  $G(t)$  is the envelope function; it is expressed by

$$G(t) = (e^{-\alpha t} - e^{-\beta t}), \quad \beta > \alpha > 0; \quad (5.50)$$

$\alpha$  and  $\beta$  are constants.

The random function  $g(t)$  has the following properties:

1.  $g(t)$  is stationary
2.  $g(t)$  is Gaussian
3.  $g(t)$  has mean zero, i. e.,  $\langle g(t) \rangle = 0$
4.  $g(t)$  has power spectrum  $\Psi(\omega)$
5.  $\dot{g}(t)$  exists and is continuous in mean square; moreover,

because  $g(t)$  is stationary and Gaussian, so is  $\dot{g}(t)$ .

Hence,  $\dot{g}(t)$  and  $\ddot{g}(t)$  are Gaussian and continuous in mean square with mean  $\langle \dot{g}(t) \rangle = \langle \ddot{g}(t) \rangle = 0$ .

From Eq. 5.49, the expressions for the velocity and the acceleration are

$$\dot{f}(t) = (e^{-\alpha t} - e^{-\beta t}) \dot{g}(t), \quad (5.51)$$

and

$$\ddot{f}(t) = (-\alpha e^{-\alpha t} + \beta e^{-\beta t}) g(t) + (e^{-\alpha t} - e^{-\beta t}) \dot{g}(t) \quad (5.52)$$

The random function has a covariance given by

$$\langle g(t) g(s) \rangle = R_g(t-s) = \frac{1}{2\pi} \int_{-\infty}^{\infty} \Psi(\omega) e^{i\omega(t-s)} d\omega \quad (5.53)$$

where  $R_g(t-s)$  is the autocorrelation function for  $g(t)$ ; it depends only on the time difference  $(t-s)$ , and not on  $t$  and  $s$  individually.

The covariances of both the velocity (Eq. 5.51) and the acceleration (Eq. 5.52), are given by

$$\langle \dot{f}(t) \dot{f}(s) \rangle = (e^{-\alpha t} - e^{-\beta t}) (e^{-\alpha s} - e^{-\beta s}) \langle g(t) g(s) \rangle, \quad (5.54)$$

and

$$\begin{aligned} \langle \ddot{f}(t) \ddot{f}(s) \rangle &= (-\alpha e^{-\alpha t} + \beta e^{-\beta t}) (-\alpha e^{-\alpha s} + \beta e^{-\beta s}) \langle g(t) g(s) \rangle \\ &+ (-\alpha e^{-\alpha t} + \beta e^{-\beta t}) (e^{-\alpha s} - e^{-\beta s}) \langle g(t) \dot{g}(s) \rangle \\ &+ (e^{-\alpha t} - e^{-\beta t}) (-\alpha e^{-\alpha s} + \beta e^{-\beta s}) \langle \dot{g}(t) g(s) \rangle \\ &+ (e^{-\alpha t} - e^{-\beta t}) (e^{-\alpha s} - e^{-\beta s}) \langle \dot{g}(t) \dot{g}(s) \rangle \end{aligned} \quad (5.55)$$

in which

$$\langle \dot{g}(t) g(s) \rangle = -\langle g(t) \dot{g}(s) \rangle = \dot{R}_g(t-s) = \frac{i}{2\pi} \int_{-\infty}^{\infty} \omega \Psi(\omega) e^{i\omega(t-s)} d\omega \quad (5.56)$$

$$-\langle \dot{g}(t) \dot{g}(s) \rangle = \ddot{R}_g(t-s) = -\frac{1}{2\pi} \int_{-\infty}^{\infty} \omega^2 \Psi(\omega) e^{i\omega(t-s)} d\omega$$

Now, substitution of Eqs. 5.47, 5.53, 5.54, 5.55 and 5.56 into

Eq. 5.48, after lengthy algebra operations, yields

$$\begin{aligned} \langle \eta_n^2(t) \rangle = & \left( \frac{4}{n\pi} \right)^2 \frac{1}{2\pi} \int_{-\infty}^{\infty} \Psi(\omega) \left[ |J_n(\omega, t; \alpha, \beta)|^2 + \right. \\ & \left. + 2\omega \operatorname{Im}\{J_n(\omega, t; \alpha, \beta) \bar{J}_n(\omega, t; 1, 1)\} + \omega^2 |J_n(\omega, t; 1, 1)|^2 \right] d\omega, \end{aligned} \quad (5.57)$$

where  $\bar{J}_n$  denotes the complex conjugate of  $J_n$ . The expressions for  $J_n(\omega, t; 1, 1)$  are shown in Appendix V-a.

For the purpose of numerical computation, Shinozuka [1] suggested the following power spectrum

$$\Psi(\omega) = D e^{-B^2 \omega^2}, \quad (5.58)$$

where  $B$  and  $D$  are constants. Shinozuka admits that the applicability of this form of  $\Psi(\omega)$  to earthquake problems is open to question; however, due to the lack of statistical studies concerning earthquake ground displacement, a superior spectrum has not been discovered by this investigation. The autocorrelation function of Eq. 5.58 is

$$R_g(\tau) = \left( \frac{D}{2\sqrt{\pi} B} \right) e^{\left( \frac{-\tau^2}{4B^2} \right)}. \quad (5.59)$$

Expressing all the parameters in nondimensional form enables one to visualize some of the characteristics of the problem. By introducing  $\omega_1$  from Eq. 5.21, one can obtain the dimensionless quantities

$$\left. \begin{aligned} \bar{t}^* &= \omega_1 t, & \bar{\omega}^* &= \frac{\omega}{\omega_1}, & \bar{\omega}_n^* &= \frac{\omega_n}{\omega_1} = n, \\ \bar{\omega}_{dn}^* &= \frac{\omega_{dn}}{\omega_1} = n \sqrt{1 - \xi_n^2}, & \bar{\alpha}^* &= \frac{\alpha}{\omega_1} & \text{and} & \bar{\beta}^* = \frac{\beta}{\omega_1} \end{aligned} \right\}, \quad (5.60)$$

and

$$\bar{\Psi}^*(\bar{\omega}^*) = \frac{\Psi(\omega)}{D} = \frac{\Psi(\omega_1 \bar{\omega}^*)}{D} = e^{-B^2 \omega_1^2 \bar{\omega}^{*2}}. \quad (5.61)$$

Therefore, Eq. 5.57 becomes

$$\begin{aligned} \langle \eta_n^2(t) \rangle &= \left( \frac{4}{n\pi} \right)^2 \frac{D}{2\pi} \sqrt{\frac{\rho}{Gk'}} \frac{L}{\pi} \int_{-\infty}^{\infty} e^{-B^2 \omega_1^2 \bar{\omega}^{*2}} \left[ \left| J_n^*(\bar{\omega}^*, \bar{t}^*; \bar{\alpha}^*, \bar{\beta}^*) \right|^2 + \right. \\ &\quad \left. + 2\bar{\omega}^* \text{Im} \left\{ J_n^*(\bar{\omega}^*, \bar{t}^*; \bar{\alpha}^*, \bar{\beta}^*) \overline{J_n^*(\bar{\omega}^*, \bar{t}^*; 1, 1)} \right\} + \bar{\omega}^{*2} \left| J_n^*(\bar{\omega}^*, \bar{t}^*; 1, 1) \right|^2 \right] d\bar{\omega}^*. \end{aligned} \quad (5.62)$$

Upon using the modal solution  $v(x, t) = \sum_{n=1, 3, 5}^{\infty} \Phi_n(x) \eta_n(t)$ , one can obtain the mean square displacement as

$$\langle v^2(x, t) \rangle = \sum_{n=1, 3, 5}^{\infty} \sin^2 \frac{n\pi x}{L} \langle \eta_n^2(t) \rangle. \quad (5.63)$$

Evaluating the integral of Eq. 5.62 is very involved; so its value was obtained numerically by using the Hildebrand algorithm, which is based on the following relation

$$\int_{-\infty}^{\infty} e^{-\lambda^2 x^2} f(x) dx = \frac{\sqrt{\pi}}{6\lambda} \left[ f\left(-\frac{\sqrt{6}}{2\lambda}\right) + 4f(0) + f\left(\frac{\sqrt{6}}{2\lambda}\right) \right] \quad (5.64)$$

A numerical example is presented for the set of parameters  $\alpha^*$  and  $\beta^*$ , i. e., for different envelope functions as shown in Fig. V-14 where four types, designated by A, B, C and D, are as follows:

| Type | $\alpha^*$ | $\beta^*$ |
|------|------------|-----------|
| A    | 0.2        | 0.5       |
| B    | 0.5        | 1.0       |
| C    | 0.8        | 1.5       |
| D    | 2.0        | 4.0       |

The corresponding mean square displacement  $(\bar{v})^2$  was plotted in Fig. V-15, where

$$(\bar{v})^2 = \frac{\langle v^2(x, t) \rangle}{DL \sqrt{\frac{\rho}{k'G}}} \quad (5.65)$$

Only the first term of the series of Eq. 5.63 was considered because the series is rapidly convergent.

In the numerical example, the damping was taken to be 10%, which is quite high, and the quantity  $B^2 \omega_1^2$  in the power spectrum was taken equal to 0.5 .

It is important to note, also, that the contribution from the term  $\sin^2 \frac{n\pi x}{L}$  in Eq. 5.63 was taken to be equal to  $\frac{1}{2}$  indicating one of two possibilities

1.  $x = \frac{L}{4}$  or  $\frac{3L}{4}$  , or

2. the space average of the mean square displacement is in the form

$$\langle \overline{v^2(x, t)^*} \rangle = \sum_{n=1, 3, 5}^{\infty} \frac{1}{L} \int_0^L \sin^2 \frac{n\pi x}{L} dx \langle \eta_n^2(t)^* \rangle \quad (5.66)$$

Figs. V-14 and V-15 show the correlation between the shape of the envelope function  $G(t)$  and the corresponding mean square displacement  $(\overline{v})^2$ . In all curves of Fig. V-15, there is a rapid decaying of these response curves due to the high percentage of damping which has been assumed (10%).

### V-3-3. Dynamic response under random accelerations

Another example of random excitation is based on the random acceleration with specific duration, which is given as

$$F(t) = [H(t) - H(t - t_0)] \ddot{g}(t) \quad (5.67)$$

where  $H(t)$  is the unit step function (the Heaviside function), and  $t_0$  is the duration of this input excitation. The displacements both during and after the application of the random acceleration are presented.

The solution of Eq. 5.45, which is in the form of Eq. 5.48, may be reduced to the following form, after much algebra is performed

$$\langle \eta_n^2(t) \rangle = \frac{1}{2\pi} [H(t) - H(t - t_0)] \left( \frac{4}{n\pi} \right)^2 \int_{-\infty}^{\infty} \Psi(\omega) I(\omega, t) d\omega \quad ; \quad (5.68)$$

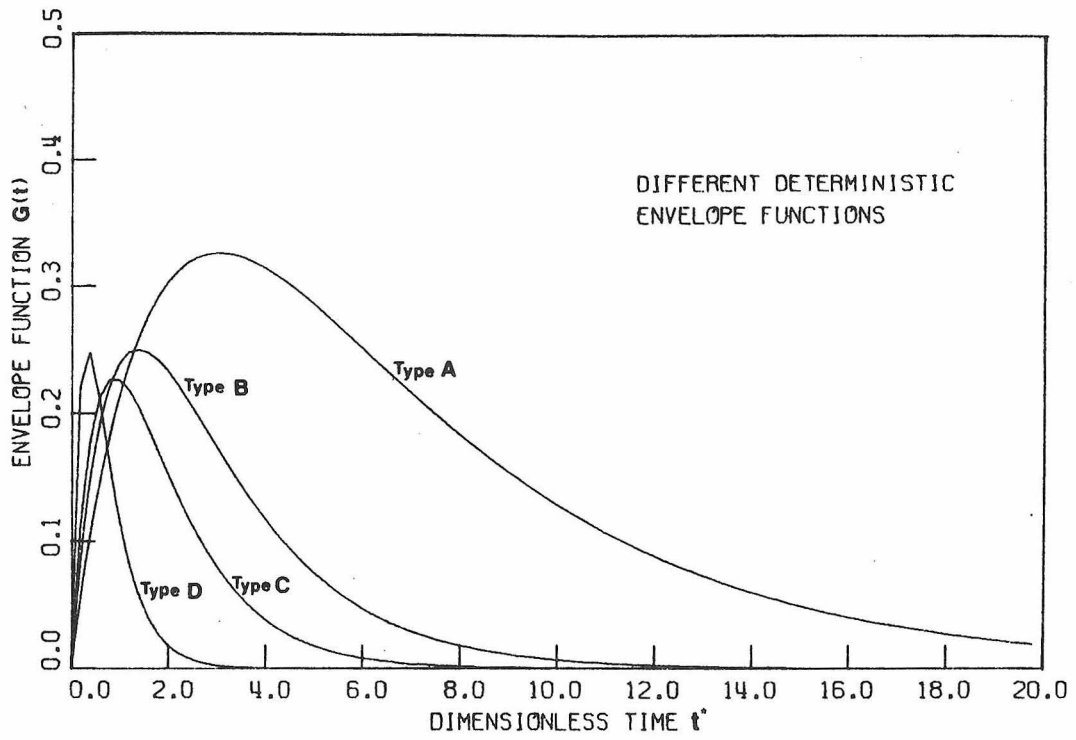


Fig. V-14

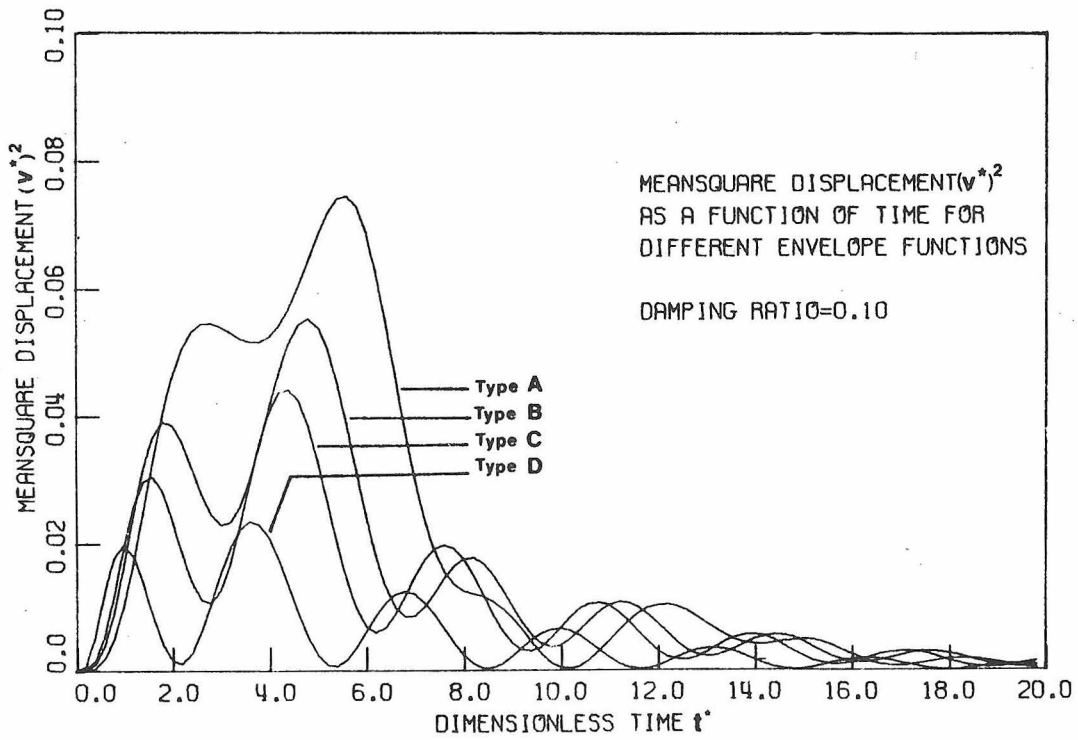


Fig. V-15

the expression for  $I(\omega, t)$  is given in Appendix V-b.

Another method to evaluate the integral of Eq. 5.68, is the one suggested by Caughey and Stumpf[2]; their method approximates the integral of Eq. 5.68 by

$$\langle \eta_n^2(t) \rangle \simeq \frac{\Psi(\omega_{dn})}{2\pi} [H(t) - H(t - t_0)] \left(\frac{4}{n\pi}\right)^2 \left[ \int_{-\infty}^{\infty} I(\omega, t) d\omega \right], \quad (5.69)$$

which, with the aid of Appendix V-b, becomes

$$\begin{aligned} \langle \eta_n^2(t) \rangle \simeq & \frac{\Psi(\omega_{dn})}{2\pi} [H(t) - H(t - t_0)] \left(\frac{4}{n\pi}\right)^2 \frac{1}{\xi_n} \left[ 1 - e^{-2\xi_n \omega_{nt}} \right. \\ & \left. + \xi_n^2 \left( e^{-2\xi_n \omega_{nt}} \cos 2\omega_{dn} t - \frac{\sqrt{1 - \xi_n^2}}{\xi_n} e^{-2\xi_n \omega_{nt}} \sin 2\omega_{dn} t - 1 \right) \right]. \end{aligned} \quad (5.70)$$

The power spectral density of strong motion earthquake acceleration suggested by Tajima[8] was used for the purpose of numerical computation. The power spectrum [7] is in the form

$$\Psi(\omega) = \frac{0.01238 \left(1 + \frac{\omega^2}{147.8}\right)}{\left(1 - \frac{\omega^2}{242}\right)^2 + \left(\frac{\omega^2}{147.8}\right)}. \quad (5.71)$$

The root mean square (rms) value of the displacement was computed for the random input, for different durations of the excitation ( $t_0 = 30, 20$  and  $10$  seconds). Also, the free vibrational displacement which followed the forced vibration was computed. The time history of the two displacements is shown in Figs. V-16 and V-17, where only two terms of the series of Eq. 5.63 were considered. In these figures,

$\omega_1$  (the fundamental frequency) was assumed to be 0.3 rad/sec.; i. e., the natural period was taken to be about 21 sec., which is the fundamental period of a long-span suspension bridge. The damping was taken to be 10% which is, again, a very high value. The figures show the displacement at the mid-point of the span; for the displacement at  $\frac{L}{4}$  and  $\frac{3L}{4}$ , or for the space average of the displacement, one has to multiply the ordinate by 0.707.

As is seen from Figs. V-16 and V-17, for the 30 seconds duration, the displacement at the mid-point of the beam reaches a value of 1.7 ft. at  $t \approx 33$  sec., while for 10 seconds duration, the displacement reduces to 1.2 ft. at about 13 seconds. One can notice, also, that the maximum displacement always occurs immediately after the excitation subsides.

Fig. V-18 shows the energy content of the system with both the strain and kinetic energies plotted for the example of 30 seconds duration. The figure demonstrates the gradual increase of the two energies during the input motion; subsequently, during free vibration, the kinetic energy is at its minimum when the strain energy is at its maximum. The sum of the two energies is the envelope of the two curves, and it is shown in the same figure.

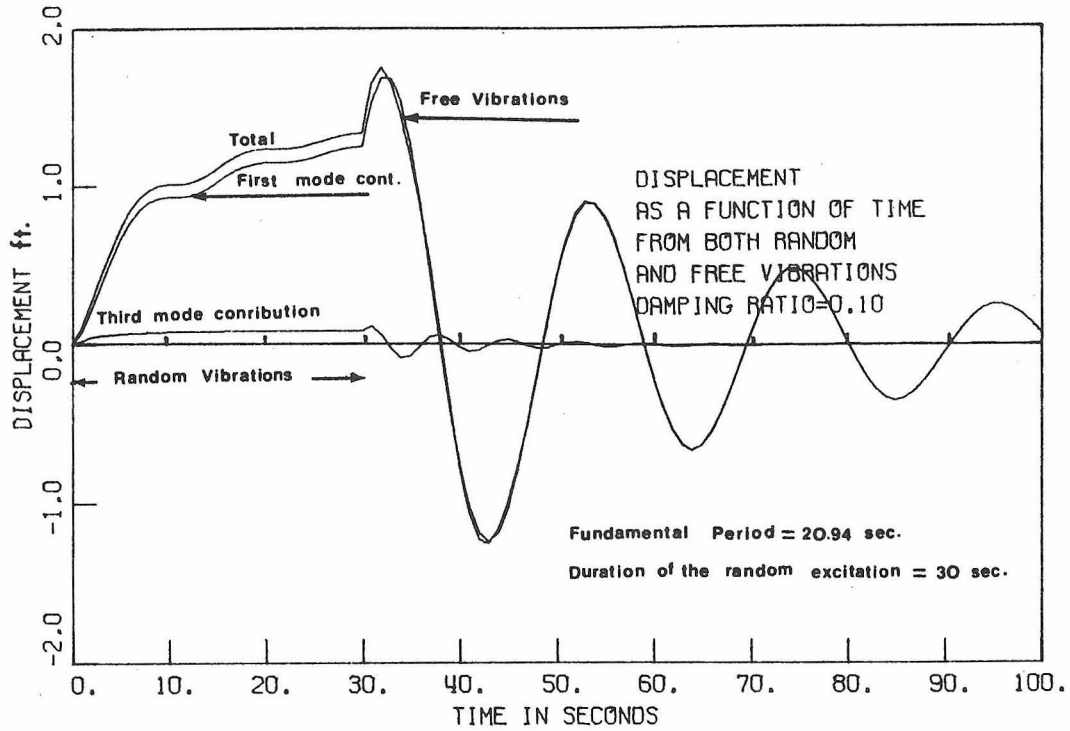


Fig. V-16

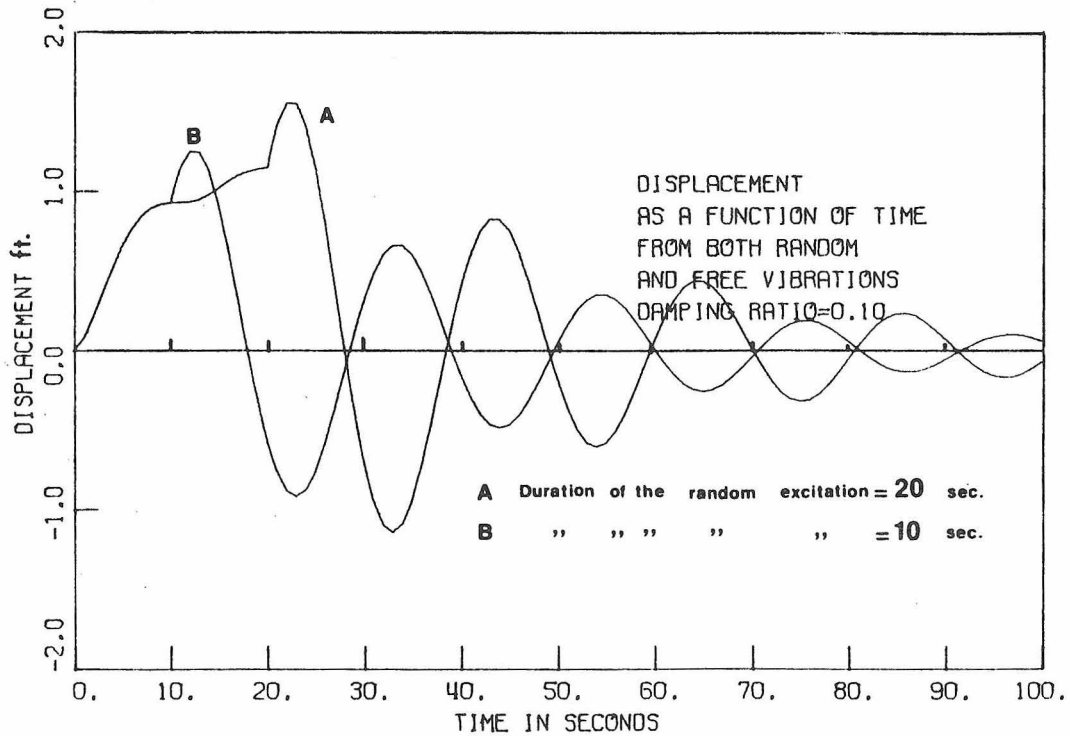


Fig. V-17

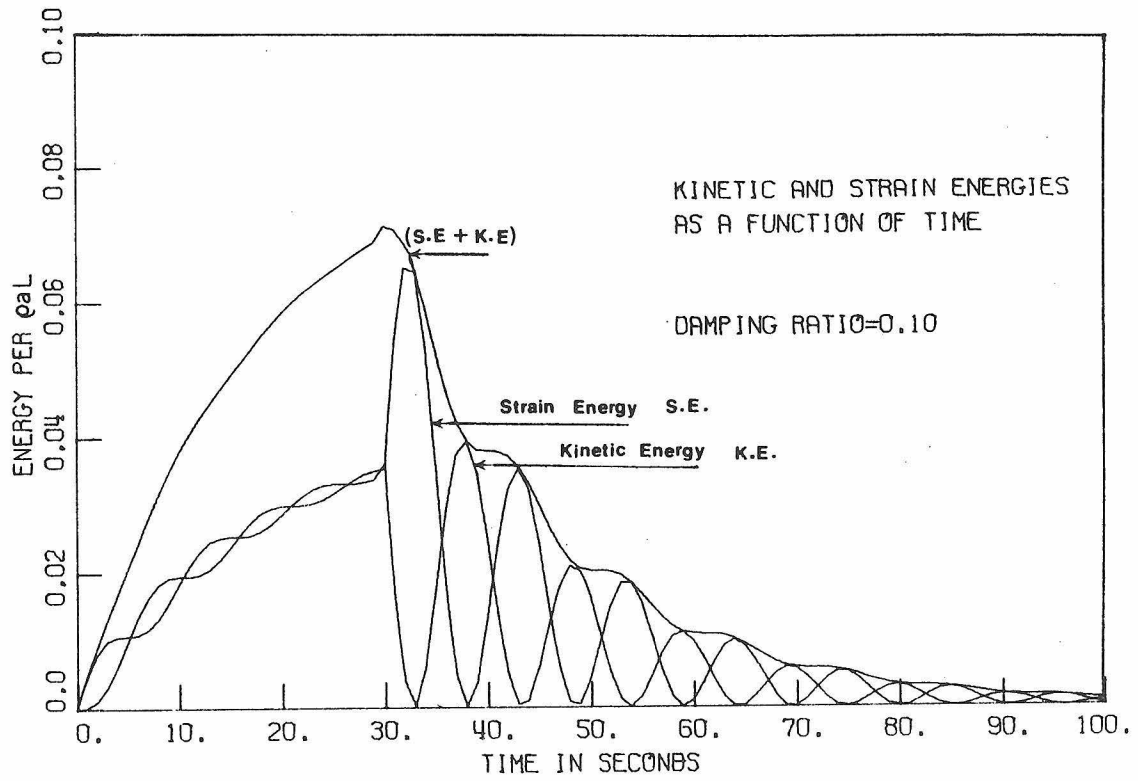


Fig. V-18

#### V-4. Conclusions

This study has examined the effect when the two end supports of a simply supported uniform bridge deck (assumed to be shear beam type) are shaken simultaneously by earthquake-type motion; this situation was analyzed in both the frequency and time domains, with harmonic and random excitations, respectively.

In the harmonic vibration analysis, the response of the beam as well as the correlation between the two support-point excitations have been investigated. The different modes of vibration are related to the nature of the support movement; in particular, they depend on the relative phase of the two support motions. When the two supports move in phase, symmetric modes of beam vibration can be excited, while when the end supports are moving  $180^\circ$  out of phase, the anti-symmetric modes are excited.

In the random vibration analysis, two methods are presented to determine the stochastic response of the beam when it is subjected to identical stationary Gaussian excitations acting simultaneously on both end supports. Both methods indicated that significant displacement amplitude occurs immediately subsequent to the end of the random excitations.

V-5. Appendices

Appendix V-a

Expressions for  $J_n(\omega, t; \alpha, \beta)$  and  $J_n(\omega, t; 1, 1)$

The complex quantities  $J_n(\omega, t; \alpha, \beta)$  and  $J_n(\omega, t; 1, 1)$  of Eq. 5.58 are given by

$$J_n(\omega, t; \alpha, \beta) = \int_G^t h(t - \tau)(\alpha e^{-\alpha\tau} - \beta e^{-\beta\tau}) e^{i\omega\tau} d\tau \quad ,$$

and

$$J_n(\omega, t; 1, 1) = \int_0^t h(t - \tau)(e^{-\alpha\tau} - e^{-\beta\tau}) e^{i\omega\tau} d\tau \quad .$$

Let  $G_n(\omega, t; \theta)$  and  $H_n(\omega, t; \theta)$  be defined as

$$G_n(\omega, t; \theta) = \operatorname{Re} \left\{ \int_0^t h(t - \tau) e^{(-\theta + i\omega)\tau} d\tau \right\}$$

and

$$H_n(\omega, t; \theta) = \operatorname{Im} \left\{ \int_0^t h(t - \tau) e^{(-\theta + i\omega)\tau} d\tau \right\}$$

where  $\theta$  stands for  $\alpha$  and  $\beta$  .

Then,  $J_n(\omega, t; \alpha, \beta)$  and  $J_n(\omega, t; 1, 1)$  can be written as

$$J_n(\omega, t; \alpha, \beta) = [\alpha G_n(\omega, t; \alpha) - \beta G_n(\omega, t; \beta)] + i[\alpha H_n(\omega, t; \alpha) - \beta H_n(\omega, t; \beta)]$$

and

$$J_n(\omega, t; 1, 1) = [G_n(\omega, t; \alpha) - G_n(\omega, t; \beta)] + i[H_n(\omega, t; \alpha) - H_n(\omega, t; \beta)]$$

$G_n(\omega, t; \theta)$  and  $H_n(\omega, t; \theta)$  are evaluated and given by

$$G_n(\omega, t; \theta) = \frac{1/\omega_{dn}}{\left[ (\xi_n \omega_n - \theta)^2 + \omega_{dn}^2 - \omega_n^2 \right]^2 + 4\omega^2 (\xi_n \omega_n - \theta)^2} \left\{ \left[ (\omega_n \xi_n - \theta)^2 + \omega_{dn}^2 - \omega^2 \right] \right. \\ \left. \left\{ \omega_{dn} e^{-\theta t} \cos \omega t - (\xi_n \omega_n - \theta) e^{-\xi_n \omega_n t} \sin \omega_{dn} t - \omega_{dn} e^{-\xi_n \omega_n t} \cos \omega_{dn} t \right\} \right. \\ \left. + 2\omega (\xi_n \omega_n - \theta) \left\{ \omega_{dn} e^{-\theta t} \sin \omega t - \omega e^{-\xi_n \omega_n t} \sin \omega_{dn} t \right\} \right]$$

and

$$H_n(\omega, t; \theta) = \frac{1/\omega_{dn}}{\left[ (\xi_n \omega_n - \theta)^2 + \omega_{dn}^2 - \omega^2 \right]^2 + 4\omega^2 (\xi_n \omega_n - \theta)^2} \left\{ \left[ (\omega_n \xi_n - \theta)^2 + \omega_{dn}^2 - \omega^2 \right] \right. \\ \left. \left\{ \omega_{dn} e^{-\theta t} \sin \omega t - \omega e^{-\xi_n \omega_n t} \sin \omega_{dn} t \right\} - 2\omega (\xi_n \omega_n - \theta) \left\{ \omega_{dn} e^{-\theta t} \cos \omega t \right. \right. \\ \left. \left. - (\xi_n \omega_n - \theta) e^{-\xi_n \omega_n t} \sin \omega_{dn} t - \omega_{dn} e^{-\xi_n \omega_n t} \cos \omega_{dn} t \right\} \right\} ;$$

again  $\omega_{dn} = \sqrt{1 - \xi_n^2} \omega_n$  is the damped frequency for the  $n^{\text{th}}$  mode.

Appendix V-b

Expression for  $I(\omega, t)$

$I(\omega, t)$  of Eq. 5.69 can be written, in terms of the unit-impulse-response function  $h(t)$  (Eq. 5.48), as

$$I(\omega, t) = \frac{1}{\omega_{dn}^2} e^{-2\xi_n \omega_n t} \int_0^t \int_0^t e^{(\xi_n \omega_n + i\omega)\tau} \sin \omega_{dn}(t-\tau) \cdot e^{(\xi_n \omega_n - i\omega)\tau'} \sin \omega_{dn}(t - \tau') d\tau d\tau'$$

or, more conveniently, as

$$I(\omega, t) = \frac{1}{\omega_{dn}^2} I_1 \cdot \bar{I}_1$$

where  $\bar{I}_1$  denotes the complex conjugate of  $I_1$  which is given by

$$I_1 = \frac{(\omega_n \xi_n)^2 + \omega_{dn}^2 - \omega^2 - 2i\omega \xi_n \omega_n}{\left[ (\xi_n \omega_n)^2 + \omega_{dn}^2 - \omega^2 \right]^2 + 4(\omega \xi_n \omega_n)^2} \left[ \left( \omega_{dn} \cos \omega t - \xi_n \omega_n e^{-\xi_n \omega_n t} \sin \omega_{dn} t - \omega_{dn} e^{-\xi_n \omega_n t} \cos \omega_{dn} t \right) + i \left( \omega_{dn} \sin \omega t - \omega e^{-\xi_n \omega_n t} \sin \omega_{dn} t \right) \right]$$

Therefore, the expression for  $I(\omega, t)$  is

$$\begin{aligned}
 I(\omega, t) = & \frac{1}{\left[ \left( \xi_n \omega_n \right)^2 + \omega_{dn}^2 - \omega^2 \right]^2 + 4 \left( \xi_n \omega_n \omega \right)^2} \left[ 1 + e^{-2\xi_n \omega_n t} \left( 1 + \frac{\left( \xi_n \omega_n \right)^2 - \omega_{dn}^2}{\omega_{dn}^2} \sin^2 \omega_{dn} t \right. \right. \\
 & + 2\xi_n \frac{\omega_n}{\omega_{dn}} \sin \omega_{dn} t \cos \omega_{dn} t \left. \left. \right) + e^{-2\xi_n \omega_n t} \frac{\omega^2}{\omega_{dn}^2} \sin^2 \omega_{dn} t \right. \\
 & + 2e^{-\xi_n \omega_n t} \left( -\cos \omega_{dn} t - \frac{\xi_n \omega_n}{\omega_{dn}} \sin \omega_{dn} t \right) \cos \omega t \\
 & \left. - 2e^{-\xi_n \omega_n t} \frac{\omega}{\omega_{dn}} \sin \omega_{dn} t \sin \omega t \right] .
 \end{aligned}$$

REFERENCES OF CHAPTER V

1. Shinozuka, M. and Henry, L., "Random Vibration of a Beam Column," Journal of Engineering Mechanics Division, Proceedings of the American Society of Civil Engineers, EM 5, October 1965, pp. 123-143.
2. Caughey, T.K. and Stumpf, H.J., "Transient Response of a Dynamic System under Random Excitation," Journal of Applied Mechanics, Transactions of the American Society of Mechanical Engineers, Vol. 28, December 1961, pp. 563-566.
3. Bogdanoff, J. L., Goldberg, J.E. and Bernard, M. C., "Response of a Simple Structure to a Random Earthquake-Type Disturbance," Bulletin of the Seismological Society of America, Vol. 91, 1961, pp. 293-310.
4. Bolotin, V. V., "Statistical Theory of the Aseismic Design of Structures," Proceedings of the Second World Conference on Earthquake Engineering, Japan, Vol. II, 1960, pp. 1365-1374.
5. Rosenblueth, E. and Bustamante, J. L., "Distribution of Structural Response to Earthquakes," Journal of Engineering Mechanics Division, Proceedings of the American Society of Civil Engineers, Vol. 88, EM 3, June 1962, pp. 75-106.
6. Goldberg, J. E., Bogdanoff, J. L. and Sharpe, D. R., "The Response of Simple Nonlinear Systems to a Random Disturbance of the Earthquake Type," Bulletin of the Seismological Society of America, Vol. 54, No. 1, February 1964, pp. 263-276.
7. Housner, G. W. and Jennings, P. C., "Generation of Artificial Earthquakes," Journal of Engineering Mechanics Division, Proceedings of the American Society of Civil Engineers, Vol. 90, EM 1, February 1964, pp. 113-150.
8. Tajima, H., "A Statistical Method of Determining the Maximum Response of a Building Structure During an Earthquake," Proceedings of the Second World Conference on Earthquake Engineering, Tokyo and Kyoto, Japan, Vol. II, July 1960.
9. Kanai, K., "Semi-Empirical Formula for the Seismic Characteristics of the Ground," Bulletin of the Earthquake Research Institute, University of Tokyo, Tokyo, Japan, Vol. 35, June 1957, pp. 309-325.

CHAPTER VI  
ANTIPLANE DYNAMIC SOIL-BRIDGE INTERACTION  
FOR INCIDENT PLANE SH-WAVES

VI-1. Introduction

The problem of the dynamic interaction between buildings and the soil during earthquake excitation has attracted considerable interest of many investigators [1, 2, 3, 4, 5]. However, such analyses have, so far, not been extended to more complicated structures, such as bridges or large industrial buildings, where differential motions of foundations might influence response in an important way, as seen in Chapter V.

There have been many cases reported in the literature in which bridges suffered damage during earthquakes [6, 7]. These examples clearly indicate the need for detailed investigations of the dynamic soil-bridge interaction to determine the significance of that interaction on the bridge response. The soil-bridge interaction effect is considered important, for example, when the motion of an abutment or foundation is significantly different from the motion of the ground in the absence of the bridge, the latter motion being usually referred to as the free-field ground motion.

The general dynamic soil-structure interaction problem can be broken down into three parts [8]. These are:

1. The determination of the input motion to the foundations (the contribution of the seismic waves) or equivalently the determination of the driving forces.
2. The evaluation of the force-displacement relationship (the impedance functions or their reciprocal, the compliance functions) for the foundations.
3. The solution of the equations of motion including both the foundations and the superstructure.

This approach has the advantage that once the solutions of the first two parts have been obtained for a class of foundations, the results can be used to calculate the interaction response of different structures. This is done by superimposing the results so that the equations of motion for the foundations are satisfied. This method, of course, is possible only if the problem is linear.

Luco and Contesse [5] have studied the dynamic interaction, through the soil for two parallel infinite shear walls placed on rigid foundations and for vertically incident SH-waves. In a similar study Wong and Trifunac [9] have determined the driving forces induced by harmonic plane SH-waves and the impedance functions for a class of embedded foundations with circular cross sections at different separation distances. These results will be used in the present analysis of a two-dimensional superstructure (the girder), the substructure (the two abutments) and the two foundations.

In the following study, the analysis of dynamic soil-bridge interaction has been performed in three steps. These are:

1. the analysis of input motions
2. the force-displacement relationships for the foundations
3. the dynamic analysis of the structure itself, i. e., the bridge.

Based on the exact solution of the first two steps, the dynamic interaction of a simple two-dimensional bridge model erected on the elastic half-space has been investigated for a single span case. The two-dimensional model under study consists of an elastic shear girder bridge supported by two rigid abutments and rigid foundations which have a circular cross section and are welded to the half-space. It has been shown that the dynamic interaction depends on:

1. the incidence angle of plane SH-waves,
2. the ratio of the rigidity of the girder and the soil,
3. the ratio of the girder mass to the mass of the rigid abutment-foundation system, and
4. the span of the bridge.

The dynamic response of the girder and the effect of the radiative damping in the half-space on the interaction of the girder have been studied.

Finally, the model considered in this study offers obvious analytical advantages and a simple and direct insight into a complicated wave propagation phenomenon. However, this model represents a highly simplified version of the actual three-dimensional problem, in which in-plane as well as anti-plane incident waves are present, and

where coupling between the horizontal, rocking, torsional and vertical motions of the structure and the foundations take place.

## VI-2. The Model, the Excitation and the Exact Solution

The two-dimensional model studied in this analysis is shown in Fig. VI-1-a. It consists of three structural elements: the superstructure (the girder), the substructure (the abutments) and the foundations. These elements are assumed to be infinitely extended in the z-direction. Furthermore, the following assumptions are made:

1. The soil, which is represented by the half-space, is elastic, isotropic and homogeneous. Its rigidity and the velocity of shear waves are  $\mu_s$  and  $\beta_s$ , respectively.
2. The two foundations are assumed to be rigid, semicircular in cross section, and welded to the half-space.
3. The abutments are also assumed to be rigid. They are welded to the foundations so they behave together as a rigid body partially embedded in the soil.
4. The model for the girder is a shear beam, of span  $L$  and depth  $d$ , supported at the ends by the rigid piers. The beam is isotropic and homogeneous; the rigidity and the velocity of the shear waves in the beam are given by  $\mu_b$  and  $\beta_b$ , respectively.

### VI-2-1. The coordinate systems

1. For the superstructure, i. e., the girder, the origin of  $x$  and  $y$  coordinates is located at the left support point as shown in Fig. VI-1-a. The  $x$ -axis is defined along the span of the bridge, while the  $y$ -axis is in the vertical direction.

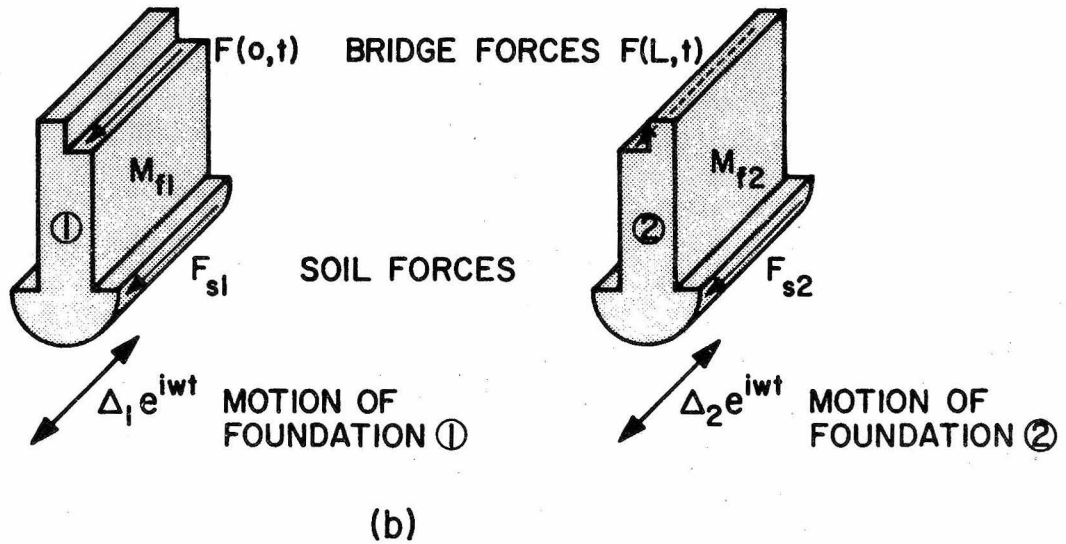
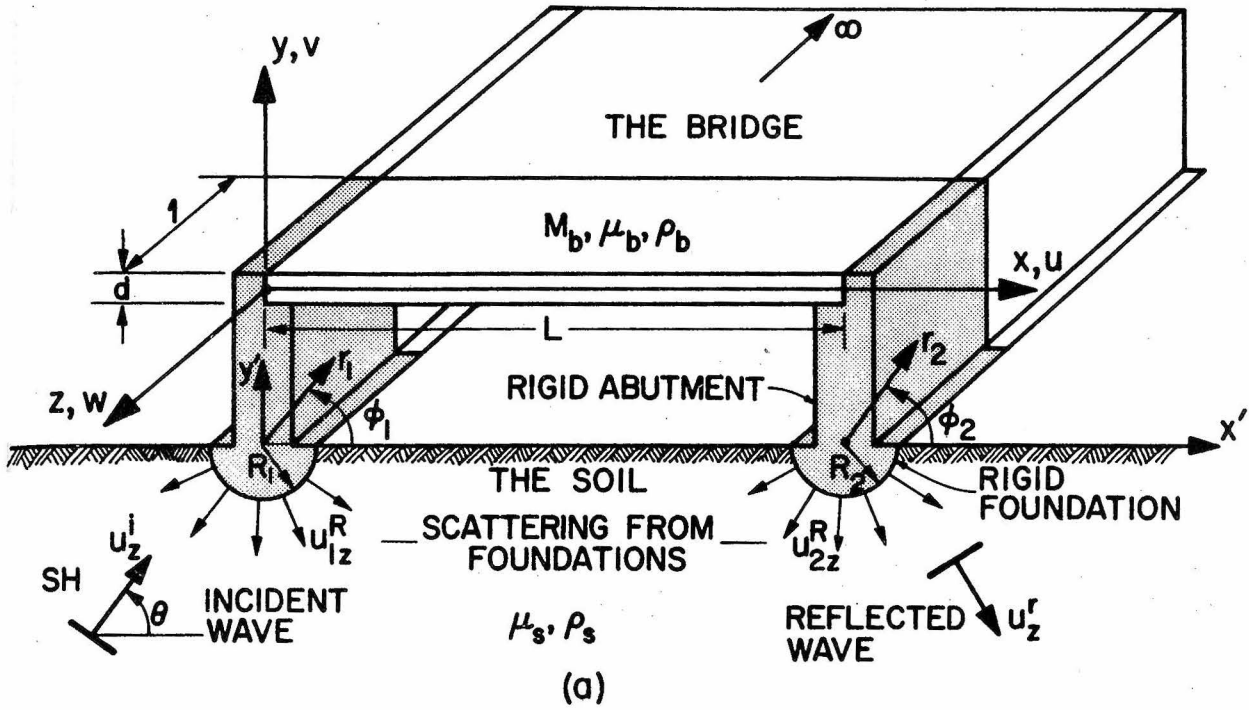


Fig. VI-1

2. For the two rigid abutment-foundation systems, the scattered waves from the two rigid foundations are best represented by polar coordinates  $(r_1, \phi_1)$  and  $(r_2, \phi_2)$ , which have their origins at the center of each foundation. The cartesian coordinates  $(x', y')$  are located at the left foundation such that

$$\begin{pmatrix} x_1 \\ x_2 \end{pmatrix} = \begin{pmatrix} x' \\ x' - L \end{pmatrix} = \begin{pmatrix} r_1 \cos \phi_1 \\ r_2 \cos \phi_2 \end{pmatrix}, \quad \begin{pmatrix} y_1 \\ y_2 \end{pmatrix} = \begin{pmatrix} r_1 \sin \phi_1 \\ r_2 \sin \phi_2 \end{pmatrix} . \quad (6.1)$$

This choice of the  $(r_1, \phi_1)$  and  $(r_2, \phi_2)$  coordinate systems is identical to that used by Wong and Trifunac [9].

As shown by several investigators [5, 9, 10], the interaction problem can be separated into three steps:

1. Input motion or "driving forces."
2. Impedance functions or "compliance functions."
3. Dynamic analysis of the structure (bridge).

The final results are then obtained by superposition. Some parts of these analyses are given in this study for the completeness of this presentation, as follows.

#### VI-2-2. Motion of the soil

It is assumed that the excitation is in a form of plane harmonic SH-waves with an amplitude equal to one and with the angle of incidence  $\theta$ , which is measured counterclockwise from the horizontal axis to the normal on the plane wave front (Fig. VI-1-a). This incident wave is given by

$$u_z^i(x', y', t) = e^{i\omega(t - x'/c_x - y'/c_y)} \quad , \quad (6.2)$$

where

$$c_x = \frac{\beta_s}{\cos\theta} \quad , \quad c_y = \frac{\beta_s}{\sin\theta} \quad , \quad (6.3)$$

and  $\beta_s = \sqrt{\frac{\mu_s}{\rho_s}}$  ... is the shear wave velocity in the soil;  $\mu_s$  is the shear modulus of the soil, and  $\rho_s$  is the density.

The resulting free-field motion, i. e., motion of the half-space in the absence of the bridge and its foundations, becomes

$$u_z^{i+r}(x', y', t) = 2 e^{i\omega t} \left[ e^{-i \frac{\omega}{\beta_s} x' \cos\theta} \right] \cos\left(\frac{\omega y'}{\beta_s} \sin\theta\right) \quad , \quad (6.4)$$

where  $u_z^{i+r}$  stands for the sum of incident,  $u_z^i$ , and reflected,  $u_z^r$ , waves from the half-space boundary  $y' = 0$ . This motion can be represented in terms of polar coordinates  $(r_1, \varphi_1)$  and  $(r_2, \varphi_2)$  [9].

The total displacement field  $u_z$ , in the half-space in the presence of the two rigid foundations is composed of the free-field motion  $u_z^{i+r}$  and the scattered waves,  $u_{1z}^R$  and  $u_{2z}^R$ , from the two foundations; i. e.,

$$u_z = u_z^{i+r} + u_{1z}^R + u_{2z}^R \quad . \quad (6.5)$$

This total displacement,  $u_z$ , must satisfy the Helmholtz equation in each of the  $(r_1, \varphi_1)$  and  $(r_2, \varphi_2)$  coordinate systems

$$\frac{\partial^2 u_z}{\partial r_j^2} + \frac{1}{r_j} \frac{\partial u_z}{\partial r_j} + \frac{1}{r_j^2} \frac{\partial^2 u_z}{\partial \varphi_j^2} + k_s^2 u_z = 0 \quad , \quad j = 1, 2 \quad , \quad (6.6)$$

in which  $k_s = \frac{\omega}{\beta_s}$  is the wave number, and the two boundary conditions:

1. Stress-free surface boundary condition

$$\sigma_{\varphi_j z} = \frac{\mu_s}{r_j} \frac{\partial u_z}{\partial \varphi_j} = 0 \text{ at } \varphi_j = -\pi, 0, \quad j = 1, 2, \quad r_j \geq R_j, \quad (6.7)$$

2. Harmonic displacement boundary condition

$$u_z(R_j, \varphi_j, t) = \Delta_j e^{i\omega t}, \quad -\pi \leq \varphi_j \leq 0, \quad j = 1, 2, \quad (6.8)$$

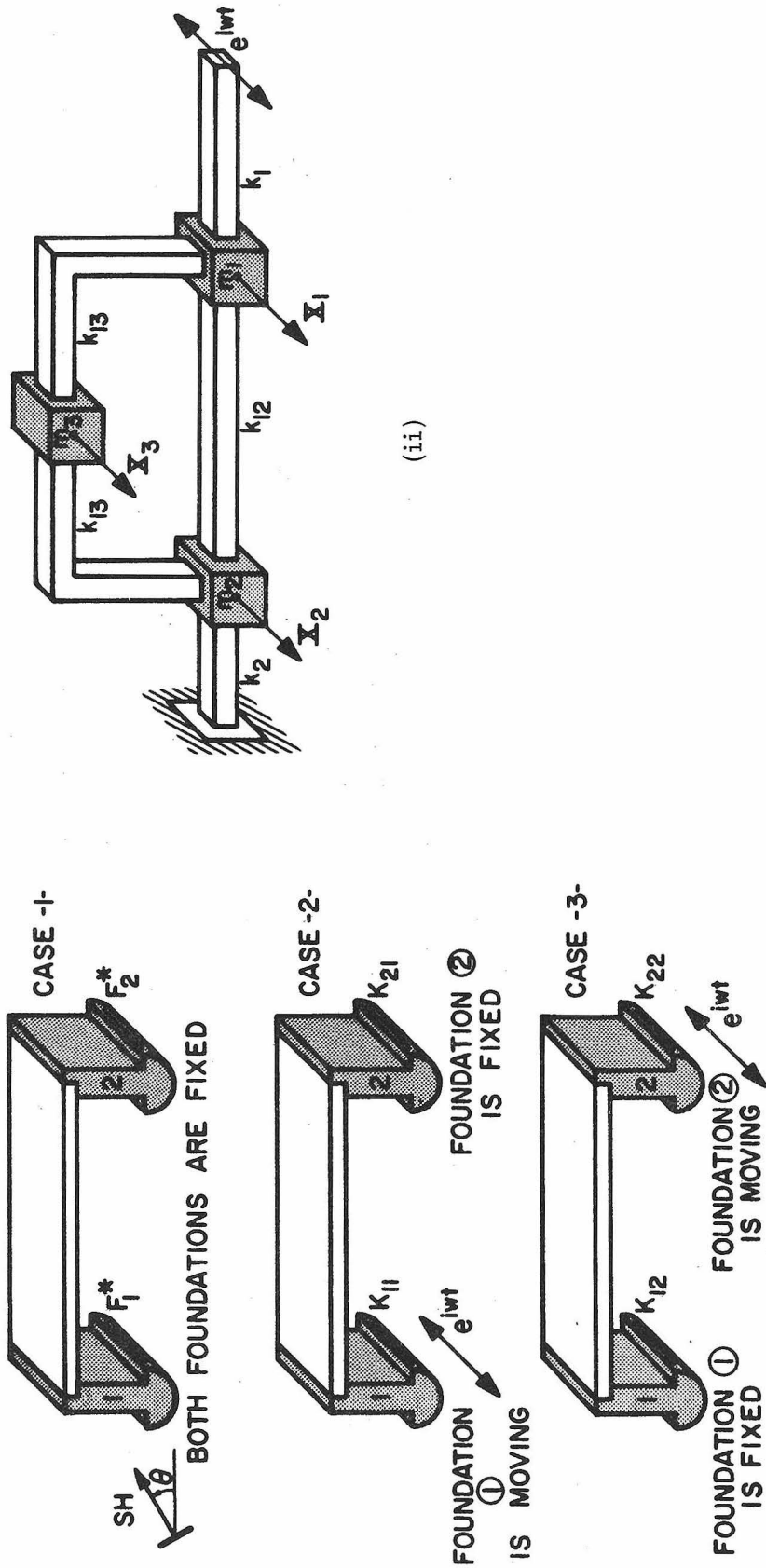
where  $\Delta_1$  and  $\Delta_2$  are the displacement amplitudes of the two foundations (Fig. VI-1-b).  $\Delta_1$  and  $\Delta_2$  are unknown and depend on the soil-structure interaction of both foundations and on the characteristics of the incoming waves.

This interaction problem can be analyzed in three parts which are illustrated in Fig. VI-2-i. This figure represents a generalization of the solution method presented by Wong and Trifunac [9] to the soil-bridge interaction problem studied in this analysis.

### VI-2-3. Forces generated by the soil and compliance functions

The forces exerted by the soil on the two foundations and caused by the incident waves and the motion of the neighboring foundations, as shown in Fig. VI-1-b, are given by

$$\begin{pmatrix} F_{s1} \\ F_{s2} \end{pmatrix} = - \begin{pmatrix} - \int_{-\pi}^0 \sigma_{rz}(R_1, \varphi_1) R_1 d\varphi_1 \\ - \int_{-\pi}^0 \sigma_{rz}(R_2, \varphi_2) R_2 d\varphi_2 \end{pmatrix}, \quad (6.9)$$



FORCES EXERTED BY THE SOIL  
 ON THE TWO FOUNDATIONS

(i)

Fig. VI-2

where

$$\sigma_{rz}(R_i, \varphi_i) = \mu_s \left. \frac{\partial u_z}{\partial r_i} \right|_{r_i=R_i}, \quad i = 1, 2. \quad (6.10)$$

Using the principle of superposition, the total soil forces can be expressed in terms of the "driving forces," and the unknown displacements  $\{\Delta\}$  premultiplied by the impedance matrix,

$$\begin{pmatrix} F_{s1} \\ F_{s2} \end{pmatrix} = \begin{pmatrix} -F_1^* \\ -F_2^* \end{pmatrix} + \begin{bmatrix} K_{11} & K_{12} \\ K_{21} & K_{22} \end{bmatrix} \begin{pmatrix} \Delta_1 \\ \Delta_2 \end{pmatrix}. \quad (6.11)$$

Here the driving forces  $F_1^*$  and  $F_2^*$  are the forces exerted by the soil on the two foundations which are held fixed during excitation by the incident waves  $u_z^i$ . The driving forces depend on the properties of the foundations and the soil and also on the nature of the seismic excitation. An element of the impedance matrix  $K_{ij}$  ( $i, j = 1, 2$ ) represents force acting on the motionless  $i^{\text{th}}$  foundation caused by the unit harmonic motion of the  $j^{\text{th}}$  foundation. The impedance matrix depends only on the characteristics of the foundations and soil and on the frequency of the motion. Fig. VI-2-i illustrates the physical meaning of these force coefficients.

VI-3. Dynamic Analysis of the Bridge

VI-3-1. Motion of the bridge

The displacements  $u$  and  $v$  of the two-dimensional bridge model are selected to be zero, while the displacement  $w$  depends only on the coordinate  $x$ . This displacement must satisfy the equation of motion of an undamped shear beam;

$$\frac{\partial^2 w(x, t)}{\partial x^2} = \frac{1}{\beta_b^2} \frac{\partial^2 w(x, t)}{\partial t^2} \quad , \quad 0 \leq x \leq L \quad , \quad (6.12)$$

in which  $\beta_b = \sqrt{\mu_b / \rho_b} \dots$  is the shear wave velocity in the beam;  $\mu_b$  is the shear modulus of the beam, and  $\rho_b$  is the density of the beam.

The boundary conditions for the beam are

$$\begin{pmatrix} w(0, t) \\ w(L, t) \end{pmatrix} = \begin{pmatrix} \Delta_1 \\ \Delta_2 \end{pmatrix} e^{i\omega t} \quad , \quad (6.13)$$

where  $\Delta_1$  and  $\Delta_2$  are the unknown complex displacements of the two foundations. The solution of Eq. 6.12, compatible with the boundary conditions given by Eq. 6.13, is

$$w(x, t) = \{ [\cos(k_b x) - \cot(k_b L) \sin(k_b x)], [\operatorname{cosec}(k_b L) \sin(k_b x)] \} \begin{pmatrix} \Delta_1 \\ \Delta_2 \end{pmatrix} e^{i\omega t} \quad (6.14)$$

in which  $k_b = \omega / \beta_b \dots$  is the wave number in the shear beam.

From Eq. 6.14, it is seen that the displacement  $w(x, t)$  depends on the instantaneous values of the harmonic boundary conditions.

VI-3-2. Forces exerted by the bridge

The end resisting forces, per unit length, acting on the two abutments (Fig. VI-1-b) are given by

$$\begin{pmatrix} F_1^b(t) \\ F_2^b(t) \end{pmatrix} = \begin{pmatrix} F(o, t) \\ F(L, t) \end{pmatrix} = \begin{pmatrix} d\sigma_{xz}^b(o, t) \\ -d\sigma_{xz}^b(L, t) \end{pmatrix} = \begin{pmatrix} -\mu_b d \frac{\partial w(o, t)}{\partial x} \\ -\mu_b d \frac{\partial w(L, t)}{\partial x} \end{pmatrix}, \quad (6.15)$$

where  $d$  is the depth of the shear beam and  $\sigma_{xz}^b$  is the shear stress in the  $z$ -direction.

By using Eqs. 6.14 and 6.15, and by introducing the expression

$$M_b = \rho_b d L, \quad (6.16)$$

which corresponds to the mass of the beam per unit length in the  $z$ -direction, these support forces can be written as:

$$\begin{pmatrix} F_1^b(t) \\ F_2^b(t) \end{pmatrix} = \begin{bmatrix} -\omega^2 M_b \frac{\cot(k_b L)}{(k_b L)} & \omega^2 M_b \frac{\operatorname{cosec}(k_b L)}{(k_b L)} \\ \omega^2 M_b \frac{\operatorname{cosec}(k_b L)}{(k_b L)} & -\omega^2 M_b \frac{\cot(k_b L)}{(k_b L)} \end{bmatrix} \begin{pmatrix} \Delta_1 \\ \Delta_2 \end{pmatrix} e^{i\omega t}. \quad (6.17)$$

It is convenient to recall here that the undamped natural frequencies of the simply supported shear beam are given by

$$\omega_n = \frac{n\pi}{L} \sqrt{\frac{\mu_b}{\rho_b}} = \frac{n\pi}{L} \beta_b, \quad n = 1, 2, 3, \dots \quad (6.18)$$

This corresponds to

$$k_b L = n\pi, \quad n = 1, 2, 3, \dots \quad (6.19)$$

The mode shapes are given by

$$W_n(x) = \sin \frac{n\pi x}{L}, \quad n = 1, 2, 3, \dots \quad (6.20)$$

VI-4. Dynamic Soil-Bridge-Soil Interaction

The unknown foundation displacement amplitudes  $\Delta_1$  and  $\Delta_2$  can now be determined from the balance of forces exerted on each foundation. These forces are:

1. Soil forces  $F_{s1}$  and  $F_{s2}$ , as given by Eq. 6.11.
2. Bridge end forces  $F_1^b(t)$  and  $F_2^b(t)$ , as given by Eq. 6.17.
3. Inertia forces of each rigid abutment-foundation system, with masses  $M_{f1}$  and  $M_{f2}$ , and accelerations  $-\omega^2 \Delta_1 e^{i\omega t}$  and  $-\omega^2 \Delta_2 e^{i\omega t}$ , as shown in Fig. VI-1-b.

The balance of the forces for the two abutment-foundation systems is then

$$\left. \begin{aligned} -\omega^2 \Delta_1 M_{f1} &= -[-F_1^* + K_{11} \Delta_1 + K_{12} \Delta_2 + F_1^b(t)] \\ -\omega^2 \Delta_2 M_{f2} &= -[-F_2^* + K_{21} \Delta_1 + K_{22} \Delta_2 + F_2^b(t)] \end{aligned} \right\} \quad (6.21)$$

Introducing

$$\begin{pmatrix} M_{s1} \\ M_{s2} \end{pmatrix} = \frac{\pi}{2} \rho_s \begin{pmatrix} R_1^2 \\ R_2^2 \end{pmatrix}, \quad (6.22)$$

which corresponds to the mass of the soil per unit length removed by the two foundations and by using Eqs. 6.17 and 6.21 there follows:

$$\begin{aligned} & \left[ \frac{k_s R_1}{2} \left( \frac{M_{f1}}{M_{s1}} + \frac{M_b \cot(k_b L)}{M_{s1} (k_b L)} \right) - \bar{K}_{11} \right] \left[ -\frac{k_s R_1}{2} \left( \frac{M_b \operatorname{cosec}(k_b L)}{M_{s1} (k_b L)} \right) - \bar{K}_{12} \right] \begin{pmatrix} \Delta_1 \\ \Delta_2 \end{pmatrix} \\ & \left[ -\frac{k_s R_2}{2} \left( \frac{M_b \operatorname{cosec}(k_b L)}{M_{s2} (k_b L)} \right) - \bar{K}_{21} \right] \left[ \frac{k_s R_2}{2} \left( \frac{M_{f2}}{M_{s2}} + \frac{M_b \cot(k_b L)}{M_{s2} (k_b L)} \right) - \bar{K}_{22} \right] \begin{pmatrix} \Delta_1 \\ \Delta_2 \end{pmatrix} \\ & = \begin{pmatrix} \bar{F}_1^* \\ \bar{F}_2^* \end{pmatrix}, \quad (6.23) \end{aligned}$$

where

$$\begin{pmatrix} K_{11} \\ K_{12} \end{pmatrix} = \mu_s \pi k_s R_1 \begin{pmatrix} \bar{K}_{11} \\ \bar{K}_{12} \end{pmatrix}, \quad \begin{pmatrix} K_{21} \\ K_{22} \end{pmatrix} = \mu_s \pi k_s R_2 \begin{pmatrix} \bar{K}_{21} \\ \bar{K}_{22} \end{pmatrix},$$

and

$$\begin{pmatrix} F_1^* \\ F_2^* \end{pmatrix} = \mu_s \pi k_s \begin{pmatrix} R_1 \bar{F}_1^* \\ R_2 \bar{F}_2^* \end{pmatrix}. \quad (6.24)$$

The foundation displacement amplitudes  $\Delta_1$  and  $\Delta_2$  are uniquely determined by solving the two simultaneous, complex, and non-homogeneous equations (Eq. 6.23).

Numerical examples presented in Figs. VI-3 through VI-12 depend mainly on the angle of incident waves  $\theta$  and five other dimensionless parameters:

1.  $\eta = \frac{\omega}{\beta_s} R_1 = k_s R_1 = \frac{2\pi}{\lambda_s} R_1$ , which is the dimensionless frequency which compares the wavelength  $\lambda_s$  of the incident wave to the width of the left foundation.
2.  $\frac{M_{f1}}{M_{s1}}$  and  $\frac{M_{f2}}{M_{s2}}$ , which are the ratios of the masses of the abutment-foundation systems to the masses of the soil replaced by the foundation only. They are set equal in the examples considered in this paper (i. e.,  $\frac{M_{f1}}{M_{s1}} = \frac{M_{f2}}{M_{s2}} = \frac{MF}{MS}$ ).
3.  $\frac{M_b}{M_{s1}}$  and  $\frac{M_b}{M_{s2}}$ , which are the ratios of the mass of the bridge girder to the masses of the soil replaced by its foundations. (In the figures these are denoted by  $\frac{MB}{MS}$  when  $R_1 = R_2$  and by  $\frac{MB}{MS1}$  and  $\frac{MB}{MS2}$  when  $R_1 \neq R_2$ .)

4.  $\epsilon = \frac{k_b L}{k_s R_2} = \frac{\beta_s}{\beta_b} \frac{L}{R_2} = \frac{\beta_s}{\beta_b} \frac{L}{R_1} \cdot \frac{R_1}{R_2}$  ; this ratio reflects the relative stiffness of the bridge and the soil; it also describes the ratio of the span to the radius of the foundation. Large values of  $\epsilon$  indicate a more flexible bridge with respect to the soil and/or a longer span, while  $\epsilon = 0$  implies a rigid structure composed of a rigid bridge girder, rigid abutments and rigid foundations. In that case  $\Delta_1 = \Delta_2$  .
5.  $\frac{R_1}{R_2}$  ; this geometric parameter which reflects the relative width of the two foundations is also needed unless  $R_1 = R_2$  . For different types of soil and a typical reinforced concrete structure "bridge" with  $\mu$  ,  $\gamma$  , and  $\beta$  as shown in Table VI-1 and for selected ratios of  $\frac{L}{R_2}$  and  $\frac{R_1}{R_2}$  , the range of values for  $\epsilon$  is as shown in Table VI-2.

Typical Values of  $\mu$ ,  $\gamma$  and  $\beta$  for Reinforced  
Concrete Girder Bridge and Different "Soils"

| Property                   | Superstructure<br>R.C. Girder Bridge | Different Soils |       |        |         |
|----------------------------|--------------------------------------|-----------------|-------|--------|---------|
|                            |                                      | I               | II    | III    | IV      |
| $\mu$ K/ft <sup>2</sup>    | 288,000                              | 1,400           | 5,130 | 15,530 | 388,200 |
| $\gamma$ K/ft <sup>3</sup> | 0.15                                 | 0.125           | 0.125 | 0.125  | 0.125   |
| $\beta$ ft/sec             | 7,000                                | 600             | 1,150 | 2,000  | 10,000  |
| $\beta_b/\beta_s$          |                                      | 13.17           | 6.87  | 3.95   | 0.79    |

$\mu$  = shear modulus  
 $\gamma$  = weight per unit volume  
 $\beta$  = shear wave speed,  $\beta_b$  for the bridge and  $\beta_s$  for the soil

TABLE VI-1

The Range of Values for  $\epsilon$

|  | Different Soils |      |      |       | L/R <sub>2</sub> | R <sub>1</sub> /R <sub>2</sub> |
|--|-----------------|------|------|-------|------------------|--------------------------------|
|  | I               | II   | III  | IV    |                  |                                |
| $\epsilon = \frac{k_b L}{k_s R_2} = \frac{\beta_s}{\beta_b} \frac{L}{R_2}$ | 0.39            | 0.73 | 1.27 | 6.33  | 5                | 1                              |
|  | 0.78            | 1.46 | 2.54 | 12.66 | 10               | 1                              |
|  | 1.17            | 2.19 | 3.81 | 18.99 | 15               | 1                              |
|  | 0.20            | 0.37 | 0.64 | 3.27  | 5                | 2                              |
|  | 0.39            | 0.73 | 1.27 | 6.33  | 10               | 2                              |
|  | 0.59            | 1.10 | 1.91 | 9.80  | 15               | 2                              |
|  | 0.13            | 0.24 | 0.42 | 2.11  | 5                | 3                              |
|  | 0.25            | 0.46 | 0.84 | 4.22  | 10               | 3                              |
|  | 0.38            | 0.73 | 1.26 | 6.33  | 15               | 3                              |

TABLE VI-2

### VI-5. Interpretation of the Interaction

The two displacement amplitudes  $\Delta_1$  and  $\Delta_2$  computed for the excitation corresponding to the incident plane harmonic SH-waves have been illustrated in Figs. VI-3 through VI-12. The displacement of the left foundation  $\Delta_1$  is represented by a dashed line, and the displacement of the right foundation  $\Delta_2$  by a solid line. These two displacement amplitudes have been plotted against the dimensionless frequency  $\eta$ .

Different cases have been considered which correspond to the following parameters:

1. The mass ratios have been considered in four cases:

a.  $\frac{MF}{MS} = 2$  ,  $\frac{MB}{MS} = 2$

b.  $\frac{MF}{MS} = 4$  ,  $\frac{MB}{MS} = 2$

c.  $\frac{MF}{MS} = 2$  ,  $\frac{MB}{MS} = 4$

d.  $\frac{MF}{MS} = 2$  ,  $\frac{MB}{MS2} = 2$  ,  $\frac{MB}{MS1} = 8$

2. The following geometric size ratios were examined:  $\frac{L}{R_2} = 5, 10$ ,  
for  $\frac{R_1}{R_2} = 1, 2$ , respectively.

3. The relative stiffness ratio of the bridge girder and the soil, which is represented by the parameter  $\epsilon$  (Note:  $\epsilon$  is written as EPS in these graphs), has been assumed to have the values 1, 2, 3, and 4.

4. The angle of incidence,  $\theta$ , of plane SH-waves has taken the values equal to  $0^\circ$ ,  $45^\circ$ ,  $90^\circ$ ,  $135^\circ$  and  $180^\circ$ . (Note: In the case of  $R_1 = R_2$ , only  $0^\circ$ ,  $45^\circ$ , and  $90^\circ$  have been shown because of symmetry.)

The figures have been arranged so that the influence of the angle of incidence and the relative stiffness ratio can be studied for the mass ratios and the geometric size ratios fixed in each figure. Each of these figures consists of parts a, b, c, and d which correspond to different values of  $\epsilon$ .

Some of the most important phenomena of the interaction of the bridge and the soil through the two rigid abutment-foundation systems and the dynamic characteristics of the bridge girder response are as follows:

1. As  $\epsilon \rightarrow 0$ ,  $\Delta_1 \rightarrow \Delta_2$  (from Eq. 6.23). In that case, one has a rigid structure composed of three elements (two foundations, two abutments and a girder) all acting as a rigid body. Fig. VI-3-a illustrates this case for  $\epsilon$  small. When  $\epsilon$  increases, the differences between  $\Delta_1$  and  $\Delta_2$  become more apparent. One notes, however, that in all cases these amplitudes approach the low frequency limit of  $|\Delta_1| = |\Delta_2| = 2$ , which corresponds to the displacement amplitude of the surface of the half-space for incident SH-waves with unit amplitude.

The amplitude  $\Delta_1$  may become larger than  $\Delta_2$  due to the amplification effect caused by the scattering from the right foundation. In the cases of  $\epsilon = 1.5$  in Fig. VI-3-d, for example, or for  $\epsilon = 2.0$  in Figs. VI-4-b and VI-5-b, the peaks of  $\Delta_1$  are considerably larger than 2 for small dimensionless frequencies.

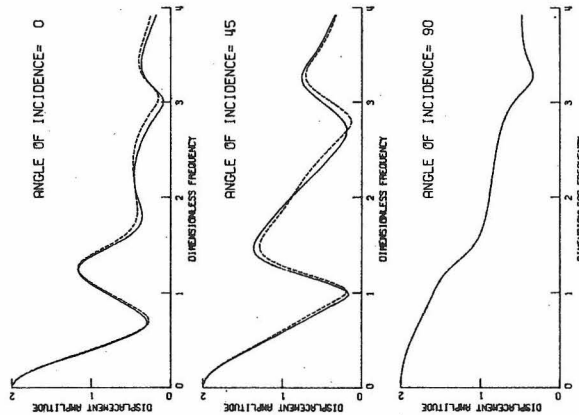
2. In the case of  $\theta = 90^\circ$ , when  $R_1 = R_2$ , the two foundations are in phase and have the same amplitude. These amplitudes

RIGID SUPPORTS  
DISPLACEMENT (1) -----  
DISPLACEMENT (2) -----  
R/R/MS= 2  
R/R/MS= 2  
(SPRM/RADIUS)= 5  
EPS = 0.25

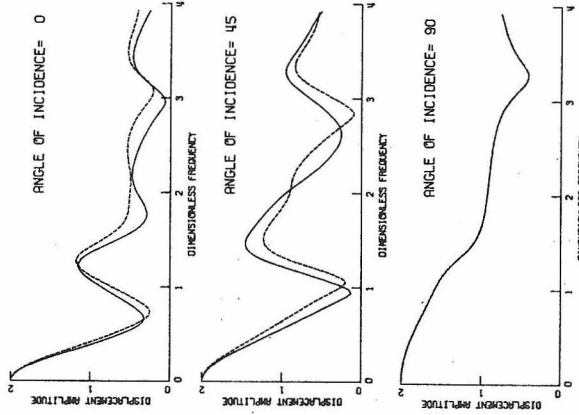
RIGID SUPPORTS  
DISPLACEMENT (1) -----  
DISPLACEMENT (2) -----  
R/R/MS= 2  
R/R/MS= 2  
(SPRM/RADIUS)= 5  
EPS = 0.5

RIGID SUPPORTS  
DISPLACEMENT (1) -----  
DISPLACEMENT (2) -----  
R/R/MS= 2  
R/R/MS= 2  
(SPRM/RADIUS)= 5  
EPS = 0.75

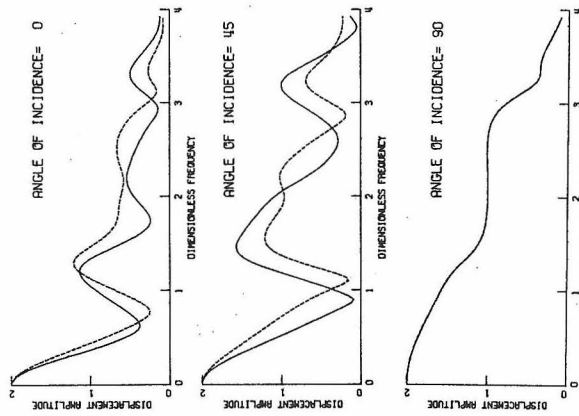
RIGID SUPPORTS  
DISPLACEMENT (1) -----  
DISPLACEMENT (2) -----  
R/R/MS= 2  
R/R/MS= 2  
(SPRM/RADIUS)= 5  
EPS = 1.50



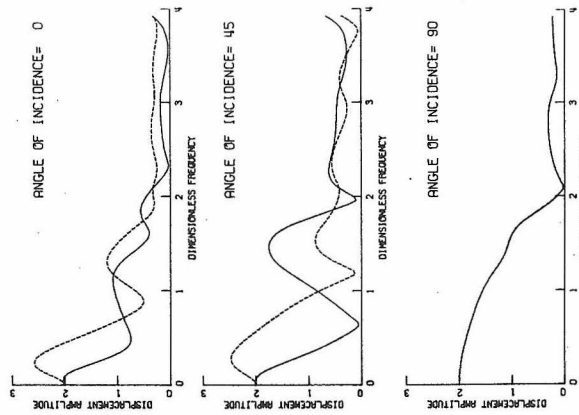
(a)



(b)



(c)



(d)

Fig. VI-3

become zero when the beam is excited at its odd frequencies, i. e., the symmetric mode-shapes. In that case

$$\eta = n\pi/\epsilon \quad , \quad n = 1, 3, 5 \dots \quad , \quad (6.25)$$

and the symmetric modes of the bridge are

$$W_n(x) = (\sin n\pi x)/L \quad , \quad n = 1, 3, 5, \dots \quad . \quad (6.26)$$

Thus, when  $\theta = 90^\circ$  and  $R_1 = R_2$ , the symmetry of vibration reduces mathematically to a single foundation problem [2, 3].

When incident waves have a frequency corresponding to a fixed base frequency of this structure, the foundation(s) is(are) located at a node of the standing wave pattern and the structure above and the soil below are moving  $180^\circ$  out of phase.

3. The dip of the displacement amplitude curve  $\Delta_2$ , which occurs for a shallow angle of incidence  $\theta = 0^\circ, 45^\circ$ , is displaced towards the lower values of the dimensionless frequency  $\eta$ , as the flexibility of the bridge increases (Figs. VI-4 and VI-7). If one compares Figs. VI-4 and VI-6 and VI-7 and VI-9, one notes that, for the same  $\epsilon$  and the same  $L/R_2$ , as the mass of the bridge increases, the dip moves again towards low values of  $\eta$ , i. e., the frequency decreases.

This behavior can be qualitatively explained by the simplified model consisting of three masses and several springs (shown in Fig. VI-2-ii) where the spring constants  $k_1$ ,  $k_2$ , and  $k_{12}$  depend upon the soil properties, while the spring constant  $k_{13}$  depends on the bridge stiffness. The displacements resulting from simple excitation, shown in Fig. VI-2-ii, can be deter-

mined from the following matrix equation

$$\begin{bmatrix} -\omega^2 m_1 + k_1 + k_{13} + k_{12} & -k_{12} & -k_{13} \\ -k_{12} & -\omega^2 m_2 + k_2 + k_{13} + k_2 & -k_{13} \\ -k_{13} & -k_{13} & -\omega^2 m_3 + 2k_{13} \end{bmatrix} \begin{pmatrix} X_1 \\ X_2 \\ X_3 \end{pmatrix} = \begin{pmatrix} k_1 \\ 0 \\ 0 \end{pmatrix}, \quad (6.27)$$

where  $X_1$ ,  $X_2$  and  $X_3$  are the displacement amplitudes of the three masses.  $X_2 = 0$  when  $k_{12}(-\omega^2 m_3 + 2k_{13}) + k_{13}^2 = 0$ ,  
i. e.,

$$\omega_* = \sqrt{\frac{k_{13} \left( 2 + \frac{k_{13}}{k_{12}} \right)}{m_3}} \quad (6.28)$$

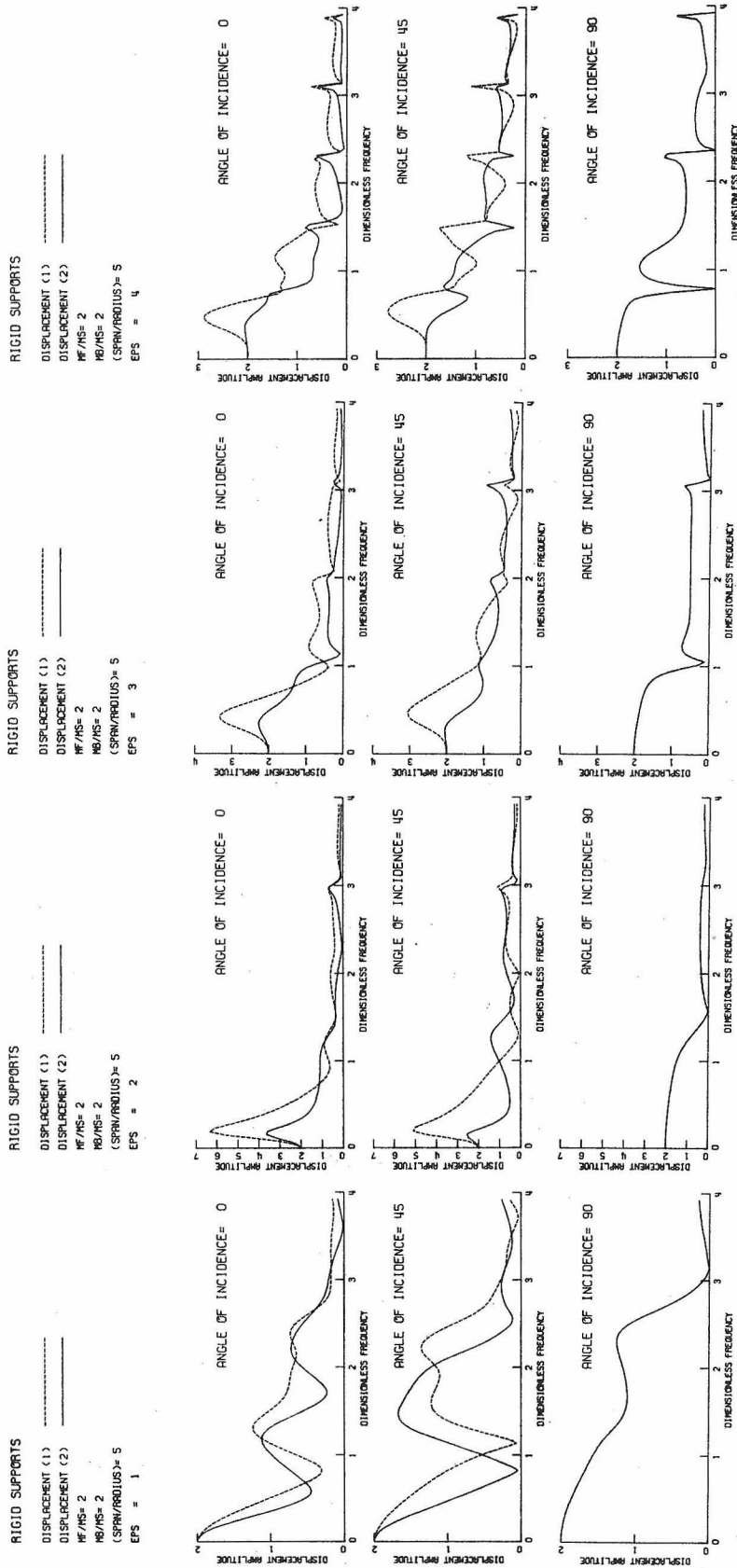
This frequency depends on the absolute stiffness of the bridge  $k_{13}$  and the ratio of stiffness of the bridge with respect to the soil underneath it  $k_{13}/k_{12}$ . As the stiffness of the bridge  $k_{13}$  or the stiffness ratio  $k_{13}/k_{12}$  decrease, the frequency for which the dip occurs decreases (e. g., Figs. VI-4, VI-6, VI-7 and VI-9). This frequency also decreases when the mass of the bridge increases. The above model is, of course, only a simple one-dimensional analogue, while the problem under consideration is a two-dimensional one involving propagation, reflection and scattering of waves from the rigid foundations in the soil and inside the beam. Nevertheless, in spite of its one-dimensional simplicity, the above model does allow one to obtain an approximate physical understanding of a more complicated wave propagation problem.

4. In all cases which have been shown in the figures for the non-vertical incidence of waves and when  $\eta = n\pi/\epsilon$ ,  $n = 1, 2, 3, \dots$ , (i. e., when the frequency of the incident waves corresponds to the natural frequencies of the girder), one finds that

$|\Delta_1| = |\Delta_2|$ . As was mentioned before,  $\Delta_1 = \Delta_2$  for  $n = 1, 3, 5, \dots$  and  $\Delta_1 = -\Delta_2$  for  $n = 2, 4, 6, \dots$ ; i. e., the two end displacements are  $180^\circ$  out of phase. This observation gives a better idea about the phase difference between the two amplitudes  $\Delta_1$  and  $\Delta_2$ , as shown, for example, in Fig. VI-10. In some cases,  $\Delta_1 = \Delta_2 \simeq 0$  at  $\eta = n\pi/\epsilon$ ,  $n = 1, 2, 3, 5$ , as in Figs. VI-5-b, VI-7, VI-8 and VI-9-c for the second mode, Fig. VI-7-c for the first mode, and Fig. VI-8-c for the third mode.

5. The peak amplitudes of the displacements  $\Delta_1$  and  $\Delta_2$  may be relatively high in some cases (e. g., Figs. VI-5 through VI-9). For the cases studied, these amplitudes are as much as four times greater than they would be if the foundations did not interact with the soil. These peaks occur at frequencies which increase as the parameter  $\epsilon$  increases for a constant span. Therefore, the more flexible the girder, the higher the frequency at which the peak occurs. Increasing the span while holding  $\epsilon$  constant decreases the frequencies of these peaks. This corresponds to increasing the rigidity of the bridge with respect to that of the soil since  $\epsilon = \frac{\beta_s}{\beta_b} \frac{L}{R_2}$ .

6. When the mass of the foundations increases with respect to that of the girder, the peak values of the  $\Delta_1$  and  $\Delta_2$  amplitudes increase moderately. This additional increase results from increasing the span, which also decreases the significance of the interaction (e. g., Figs. VI-5 and VI-8).
7. When the mass of the girder increases with respect to that of the foundation (e. g., Figs. VI-6 and VI-9), the peak amplitudes of  $\Delta_1$  and  $\Delta_2$  decrease appreciably. As the span increases, this effect becomes less pronounced.
8. In general, as the span  $L$  increases, there is a greater degree of fluctuation in both  $\Delta_1$  and  $\Delta_2$  amplitudes. For constant  $L$ , the fluctuations of  $\Delta_1$  and  $\Delta_2$  decrease as the angle of incidence  $\theta$  approaches  $90^\circ$ , since in that case the projected wavelength on the horizontal surface  $\lambda_s^* = \lambda_s / \cos \theta$  becomes infinite.
9. When the sizes of the two foundations differ, more complicated interaction phenomena occur (Figs. VI-11 and VI-12):
  - a. When the incident wave first hits the larger foundation (the left one), i. e., when  $\theta = 0^\circ$  or  $45^\circ$ , this foundation acts as a shield for the right foundation. This shielding effect is most evident in Figs. VI-11-a, b and VI-12-a, where the smaller foundation moves with nearly the same displacement as the larger one. The additional amplification effects caused by the smaller foundation are negligible in all these cases because of the massiveness of the larger foundation.



(d)

(c)

(b)

(a)

Fig. VI-4

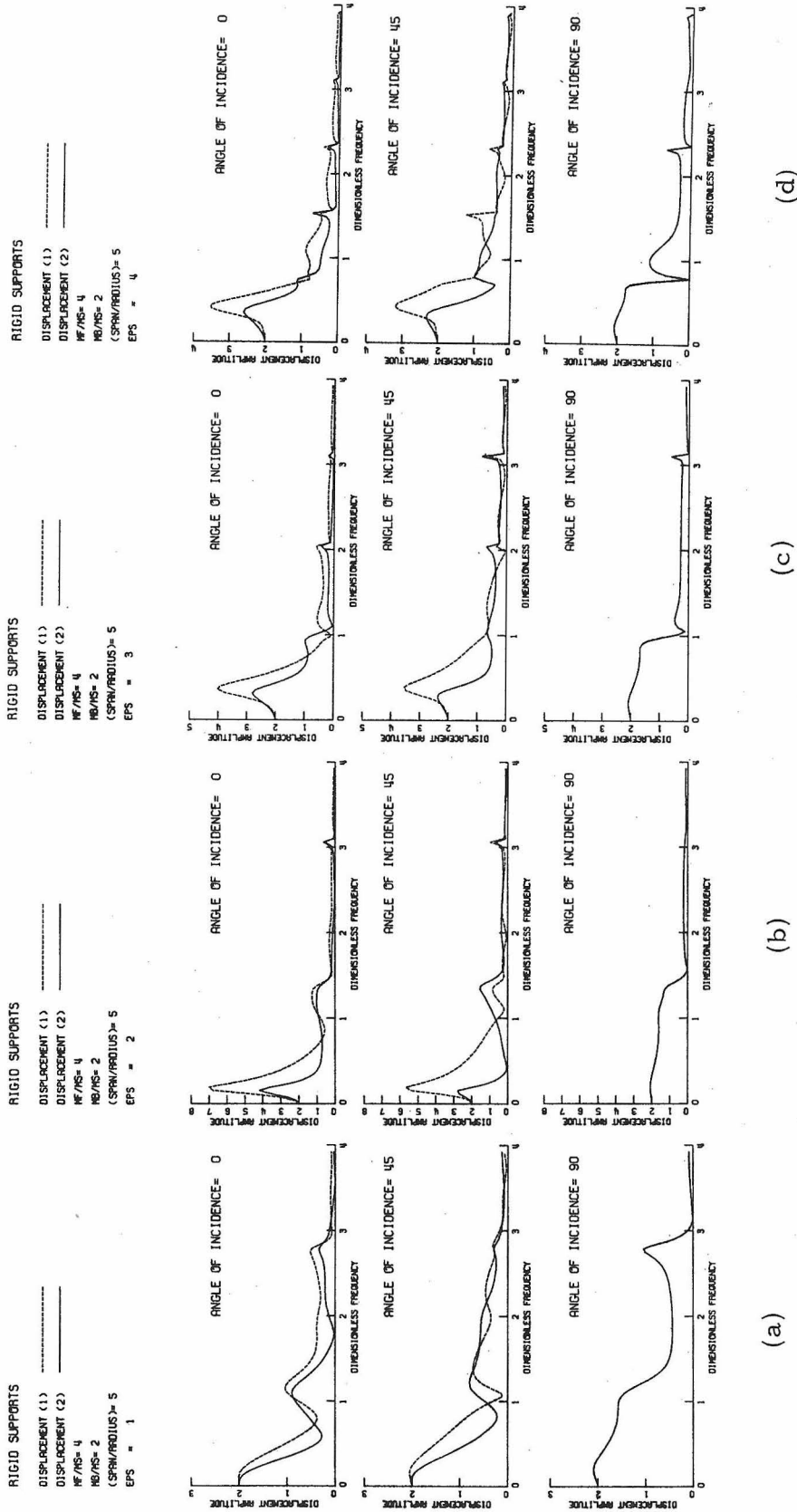


Fig. VI-5

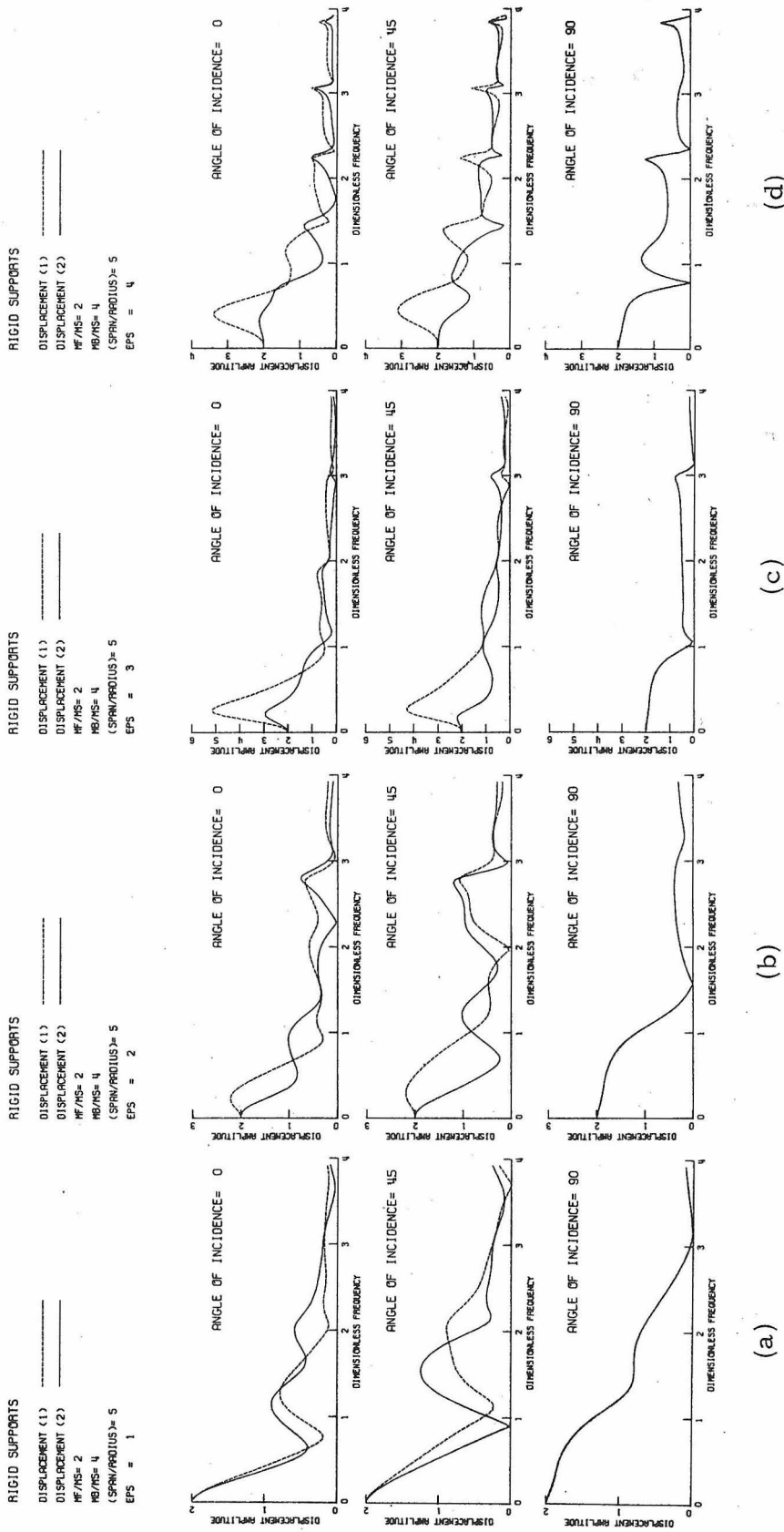


Fig. VI-6

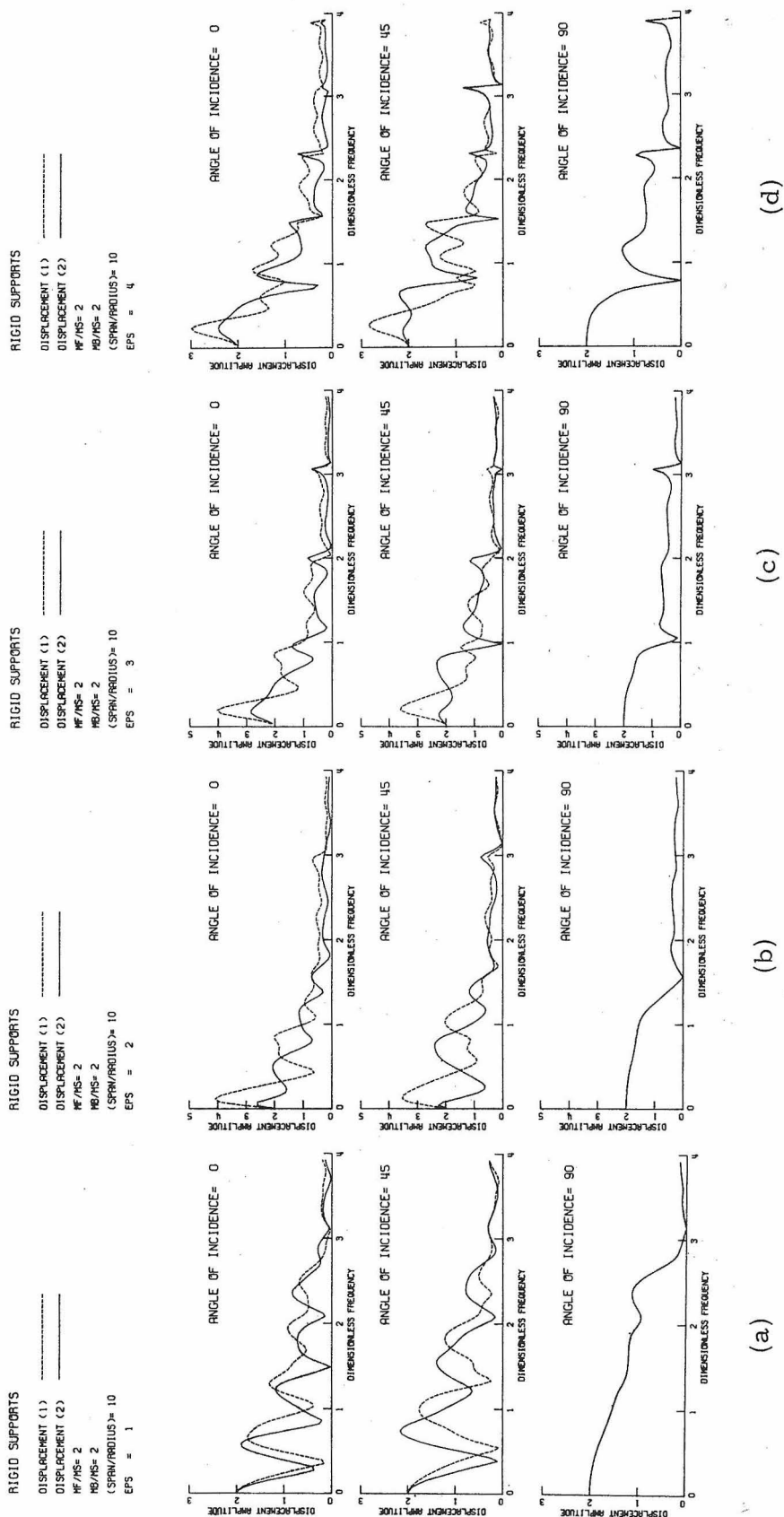
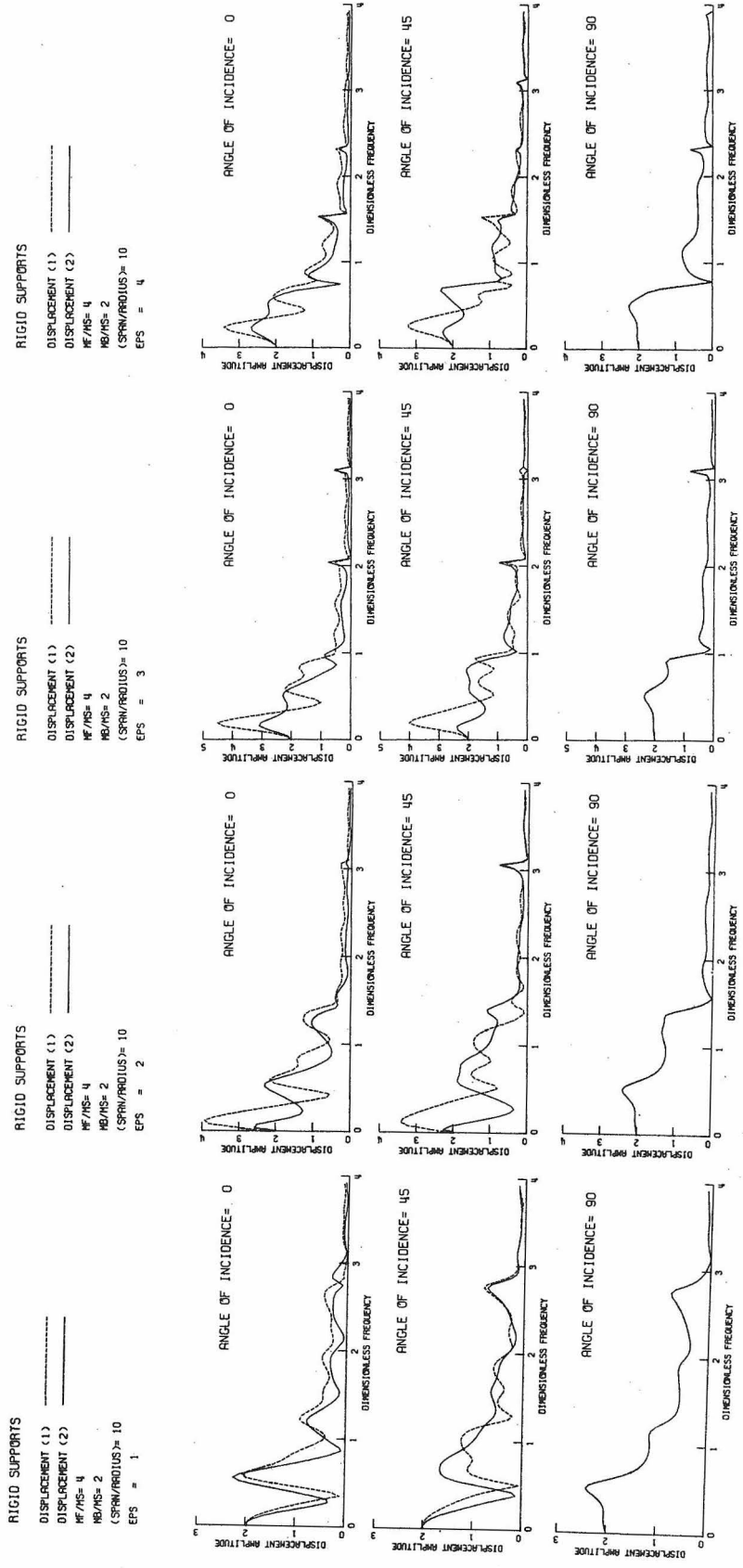


Fig. VI-7

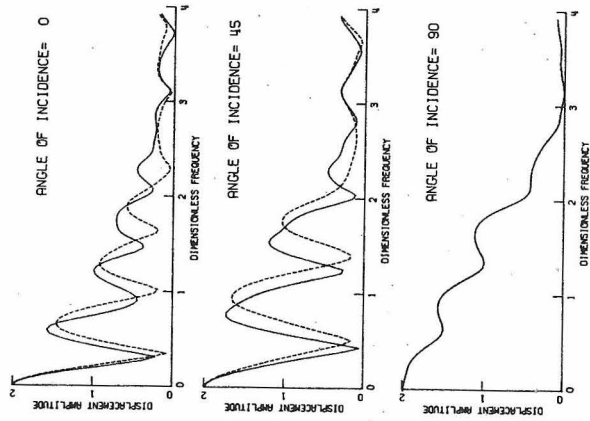


(a) (b) (c) (d)

Fig. VI-8

RIGID SUPPORTS

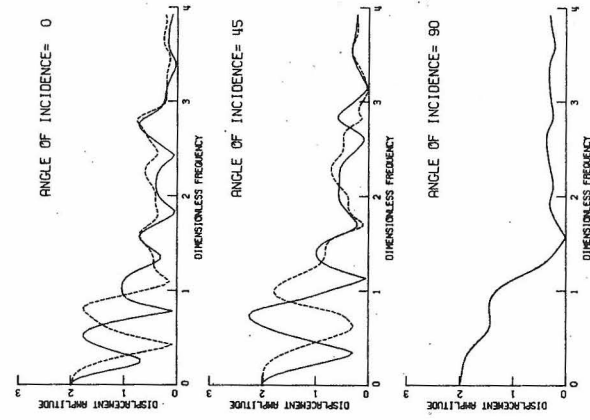
DISPLACEMENT (1) -----  
DISPLACEMENT (2) -----  
HF/MS= 2  
HB/MS= 4  
(SPRM/RADIUS)= 10  
EPS = 1



(a)

RIGID SUPPORTS

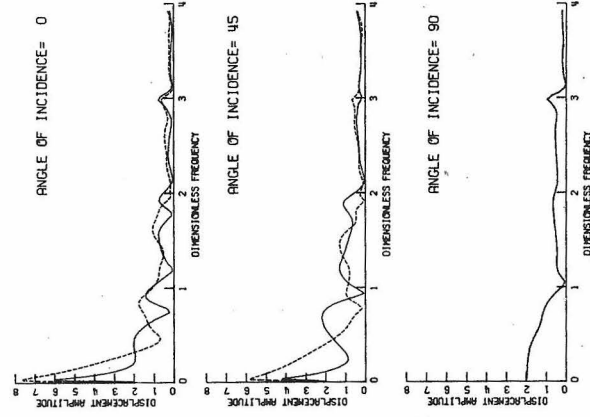
DISPLACEMENT (1) -----  
DISPLACEMENT (2) -----  
HF/MS= 2  
HB/MS= 4  
(SPRM/RADIUS)= 10  
EPS = 2



(b)

RIGID SUPPORTS

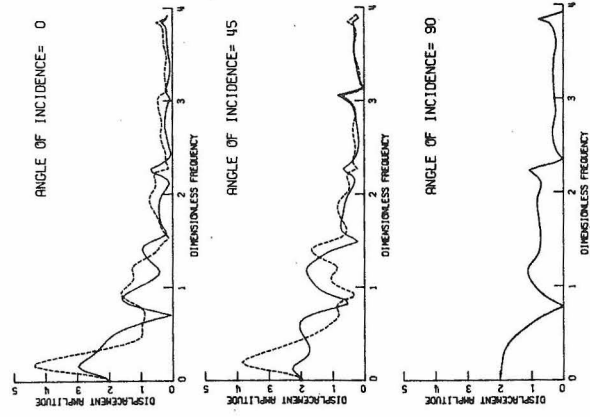
DISPLACEMENT (1) -----  
DISPLACEMENT (2) -----  
HF/MS= 2  
HB/MS= 4  
(SPRM/RADIUS)= 10  
EPS = 3



(c)

RIGID SUPPORTS

DISPLACEMENT (1) -----  
DISPLACEMENT (2) -----  
HF/MS= 2  
HB/MS= 4  
(SPRM/RADIUS)= 10  
EPS = 4



(d)

Fig. VI-9

RIGID SUPPORTS

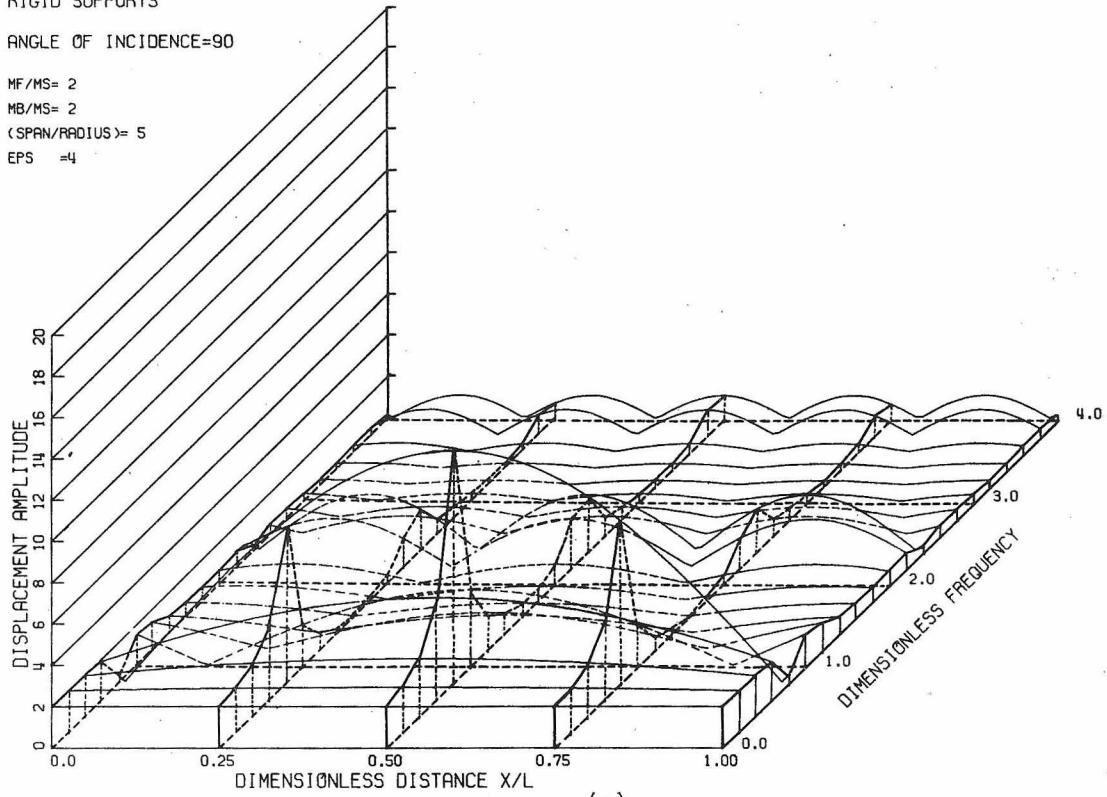
ANGLE OF INCIDENCE=90

MF/MS= 2

MB/MS= 2

(SPAN/RADIUS)= 5

EPS =4



RIGID SUPPORTS

ANGLE OF INCIDENCE=45

MF/MS= 2

MB/MS= 2

(SPAN/RADIUS)= 5

EPS =2

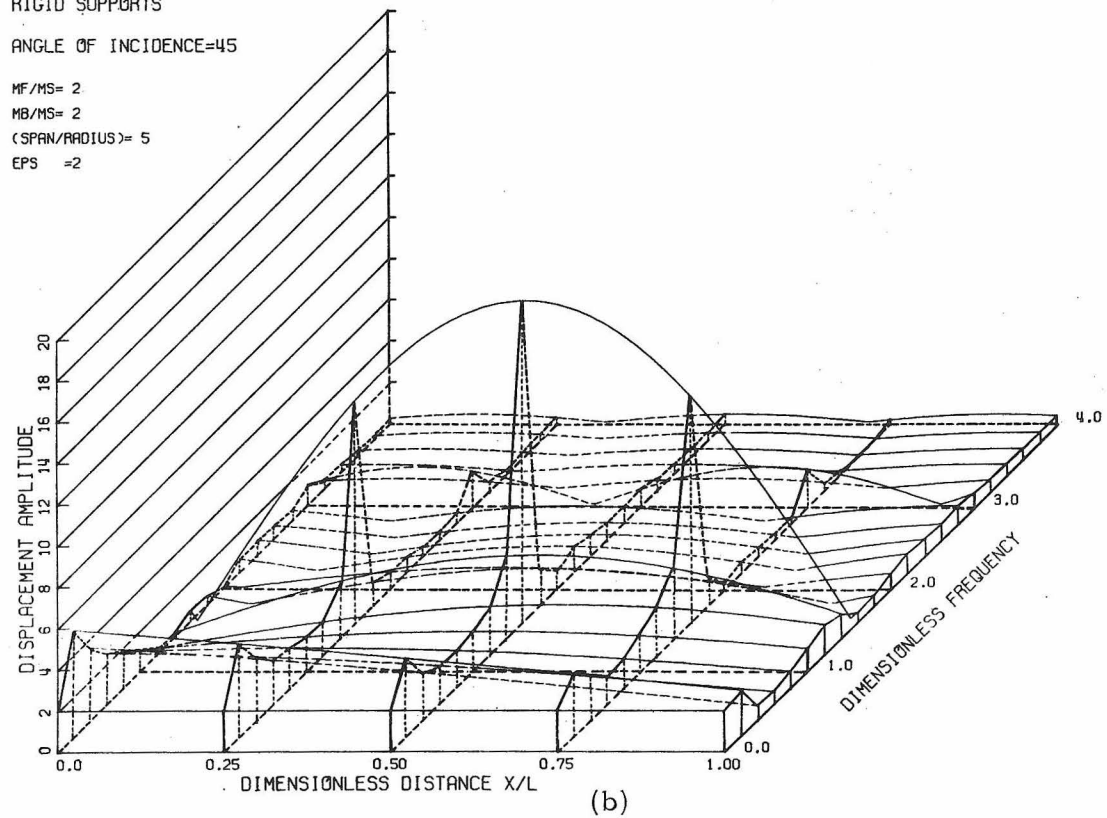


Fig. VI-10

The shielding effect decreases with an increase of the following parameters:

- (1) the flexibility of the girder
- (2) the span (Fig. VI-11)
- (3) the angle of incidence  $\theta$
- (4) the ratio  $R_2/R_1$  for the same span (Figs. VI-11 and VI-12).

- b. When the incident wave first hits the smaller foundation (the right one), i. e., when  $\theta = 135^\circ$  or  $180^\circ$ , the left foundation acts as a barrier which reflects significant wave energy back towards the small foundation while the shielding effect provided by the right foundation is negligible (Figs. VI-11-b and VI-12-b). The overall amplitudes of  $\Delta_1$  and  $\Delta_2$  are influenced by:
- (1) the flexibility of the girder;
  - (2) the span and the size of the foundations; and
  - (3) the angle of incidence  $\theta$ .
- c. The peak value of the displacement amplitudes  $\Delta_1$  and  $\Delta_2$  increases with the increase of flexibility of the superstructure and the increase of ratio  $R_1/R_2$  (Figs. VI-11-b and VI-12-a, b, c).
- d. For both vertical and nonvertical incident waves, small amplitudes of  $|\Delta_1|$  and  $|\Delta_2|$  occur at  $\eta = n\pi/\epsilon$ ,  $R_1/R_2 \neq 1$ ,  $n = 1, 3, 5, \dots$  as shown in Figs. VI-11 and VI-12. Since  $R_1 \neq R_2$ , the bridge system is not symmetric

now and, in general, one does not expect to find that

$$|\Delta_1| = |\Delta_2| \quad \text{for all } \theta \text{ and } \eta = \frac{n\pi}{\epsilon} \frac{R_1}{R_2} .$$

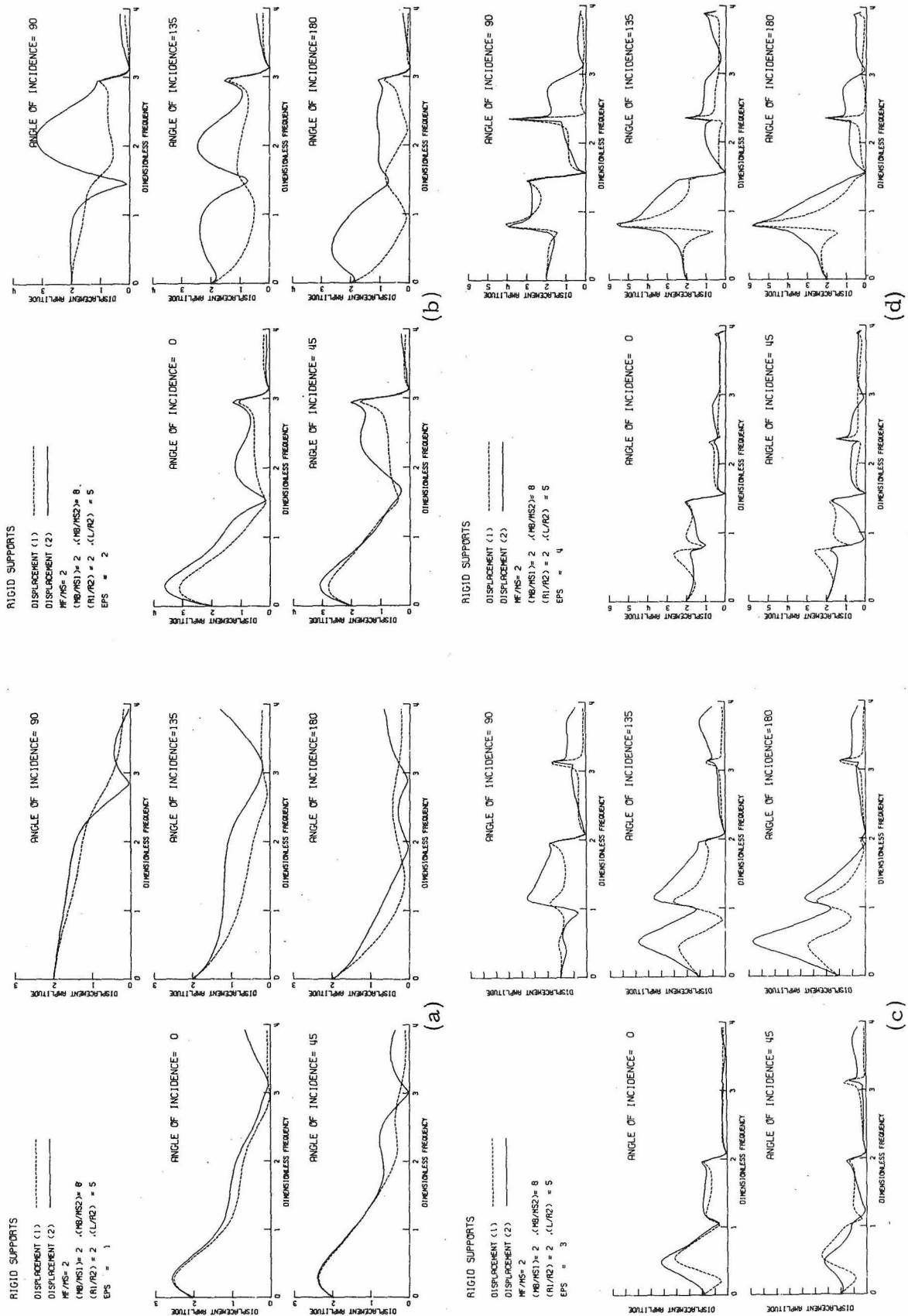


Fig. VI-11

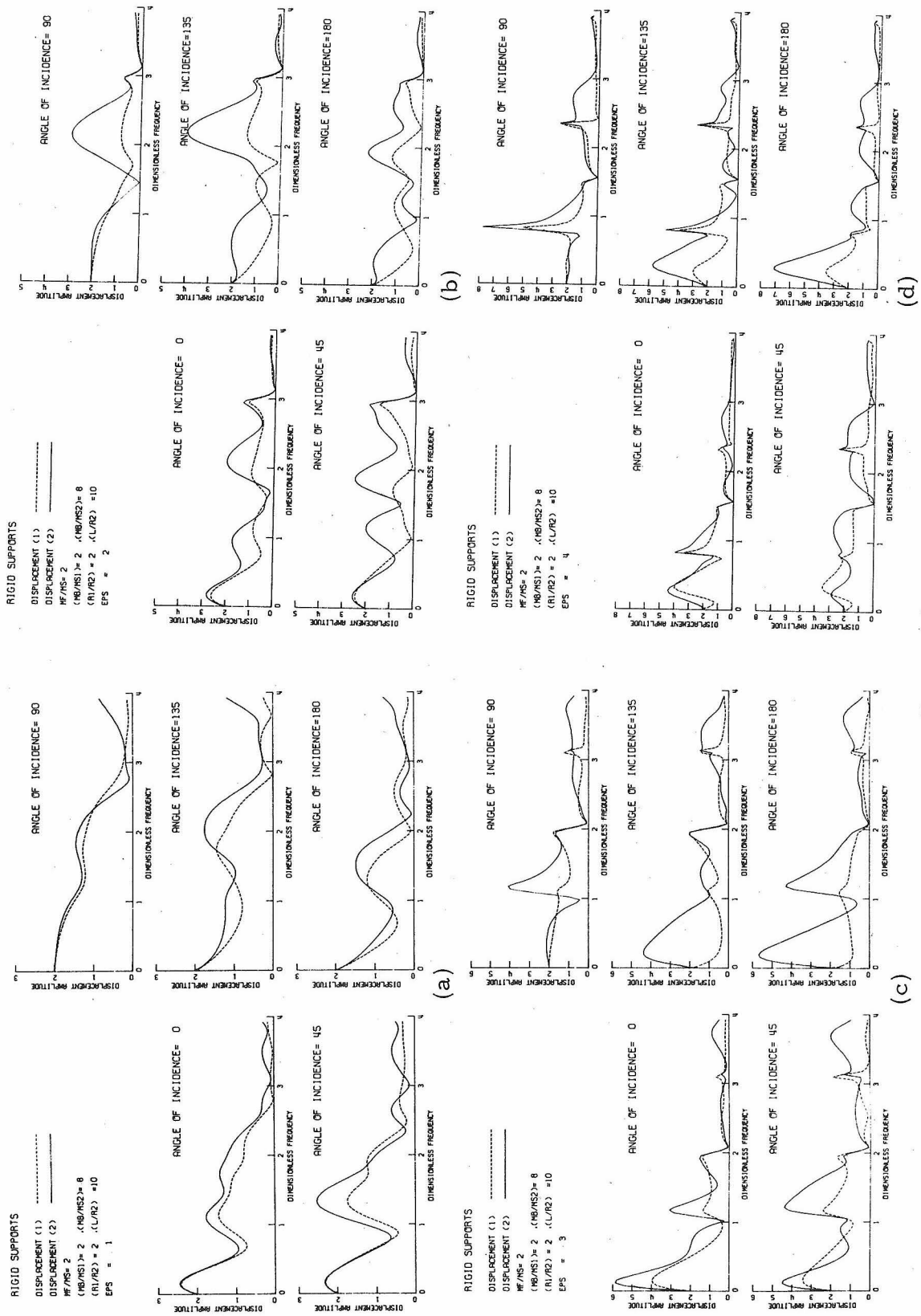


Fig. VI-12

### VI-6. Response of the Bridge

From the Earthquake Engineering and Structural Dynamics point of view, one of the more important problems is to find which are the critical sections of a structure and to estimate where the maximum displacements or the maximum stresses may occur. With this in mind, and to illustrate the effects of soil-bridge interaction on the girder of the single-span bridge studied in this analysis, the response of the midpoint and the two quarter points ( $x/L = 0.25, 0.75$ ), have been examined in some detail as shown in the three-dimensional Fig. VI-10.

Using Eq. 6.14 for  $x = L/2$ , the displacement amplitude  $|w(L/2, t)|$  is calculated at the midpoint of the span as:

$$w\left(\frac{L}{2}, t\right) = \left[ \cos\left(\frac{k_b L}{2}\right) - \cot(k_b L) \sin\left(\frac{k_b L}{2}\right) \right] \Delta_1 + \left[ \operatorname{cosec}(k_b L) \sin\left(\frac{k_b L}{2}\right) \right] \Delta_2 ,$$

which reduces to

$$\left| w\left(\frac{L}{2}, t\right) \right| = \left| \frac{(\Delta_1 + \Delta_2)}{2} \sec\left(\frac{k_b L}{2}\right) \right| . \quad (6.29)$$

When interaction is neglected, both  $\Delta_1$  and  $\Delta_2$  would become 1, and  $|w(L/2, t)|$  would become infinite at the natural frequencies of the shear beam, i. e., at  $k_b L = n\pi$ ,  $n = 1, 3, 5, \dots$  (since there is contribution only from the symmetric modes for the midpoint). However, if interaction is not neglected by using the results from the above analysis the following can be said about the beam response:

1. When  $\Delta_1 = \Delta_2 = 0$  at  $\eta = n\pi/\epsilon$ ;  $n = 1, 3, 5, \dots$ ;  $R_1 = R_2$ ; i. e., in the case of vertical SH-waves where  $\theta = 90^\circ$ , the response given by Eq. 6.29 remains finite and is characterized by relatively small peaks, as shown for example, in Fig. VI-13. It can also be seen in this figure that when  $\theta \neq 90^\circ$  the peaks, in general, are much larger and the effect of small  $\Delta_1$  and  $\Delta_2$  is less pronounced.
2. When  $\Delta_1$  and  $\Delta_2$  have considerable amplitudes at  $\eta = n\pi/\epsilon$ ,  $n = 1, 3, 5, \dots$ , and in the case of non-vertically incident SH-waves, the amplitude of the beam response is large at  $\eta = n\pi/\epsilon$ , i. e., at the fundamental resonant frequencies of the beam. It should be noted that the sharp peaks in Fig. VI-13 have been plotted only up to the amplitude equal to 40 to preserve the detail and resolution of the neighboring smaller amplitudes.

Other important characteristics of the results which can be shown in figures similar to Fig. VI-13 can be summarized as follows:

In general, the peak values of  $|w(L/2, t)|$  increase with  $\epsilon$ , when  $\theta = 90^\circ$ , i. e., for higher flexibility of the structure with respect to that of the soil and for the MB/MS fixed. The peak response amplitudes decrease for the higher modes and for the same  $\epsilon$ . Increasing the foundation mass [larger (MF/MS)] leads to more effective coupling of the bridge to the soil and thus less radiative damping, while increasing the mass of the girder [larger (MB/MS)] leads to higher radiative damping when  $L$  is constant. The increase of span  $L$  for a fixed value of  $\left(\frac{\beta_d}{\beta_s} = \frac{L}{\epsilon R_2}\right)$ , which is equivalent to

increasing the rigidity of the girder with respect to that of the soil, also leads to more radiative damping.

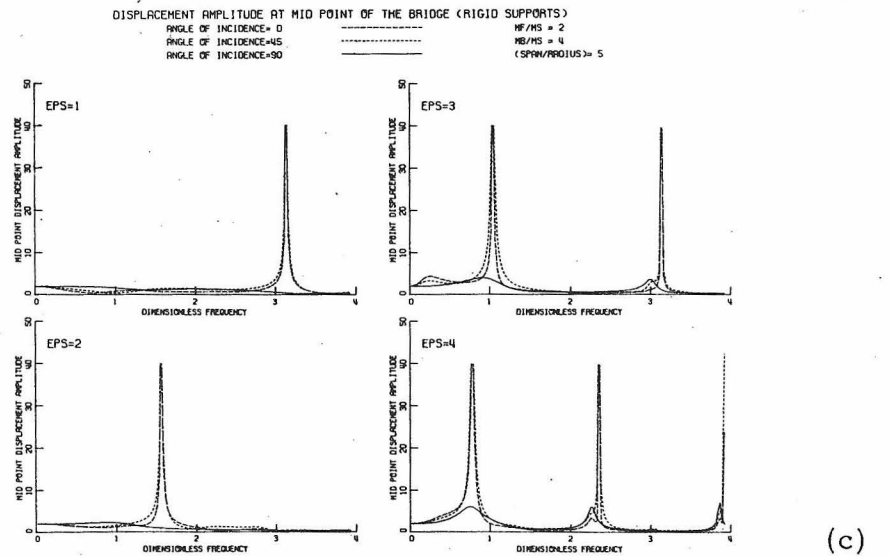
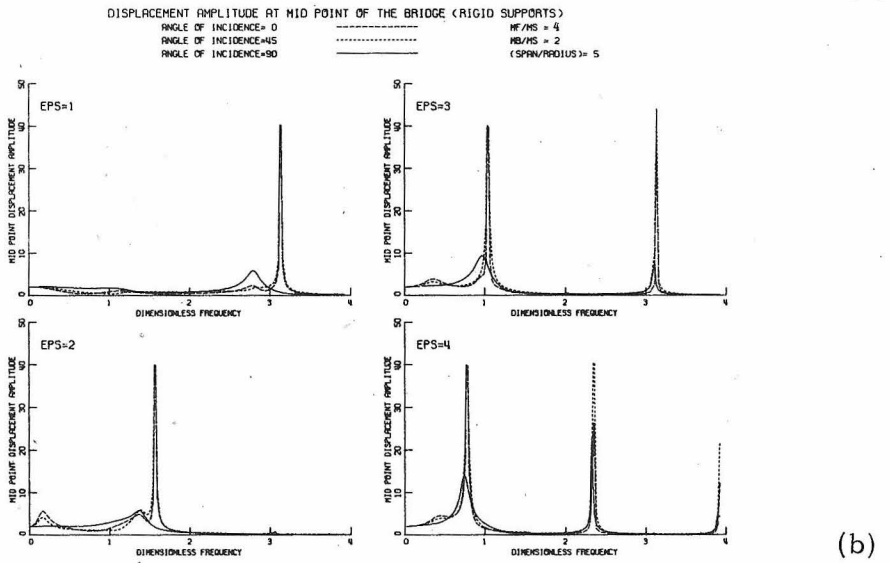
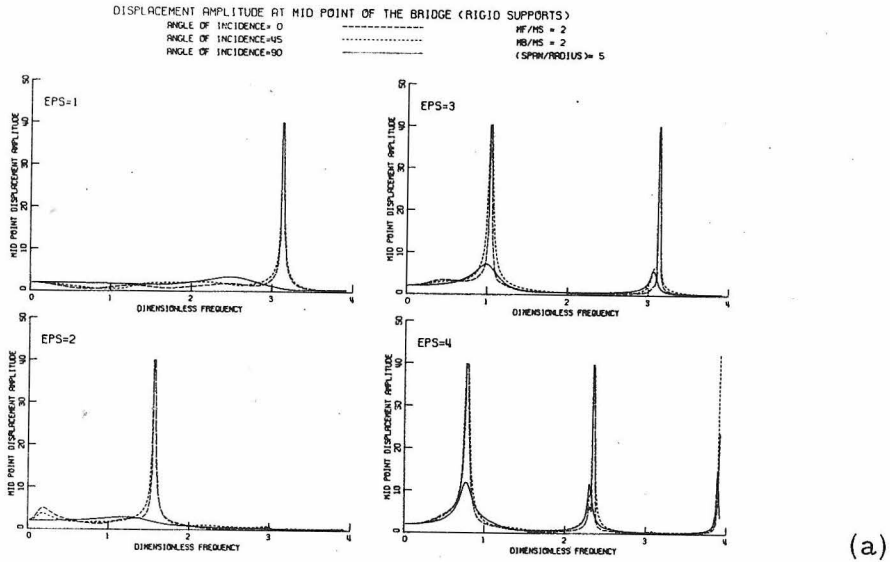


Fig. VI-13

### VI-7. Conclusions

A key step in the evaluation of the soil-structure interaction effects on the earthquake response of a structure is in the computation of the force-displacement relationships for the foundation. Several such relationships [2, 5, 8, 9], expressed in terms of impedance or compliance functions, are available in the literature.

Having obtained the impedance function for particular two-dimensional abutment conditions, represented by rigid foundations with semicircular cross sections, and having defined the input motion in terms of plane SH-waves, the calculation of the response of bridge girder depends on the stiffness, mass and damping characteristics of the bridge relative to that of the soil. For some input frequencies the amplitude of the foundation response has been found to be significantly larger than the free field surface displacement amplitude which could be obtained for the same excitation in the absence of a bridge or its abutments.

The excitation of different modes of vibration of the two-dimensional bridge girder is related to the nature of the foundation movement for different angles of incident SH-waves and, in particular, depends on the relative phase of motion for two bridge abutments. When two abutments move in phase, there is a tendency to excite symmetric modes of girder vibration; while when they are moving out of phase, the antisymmetric modes are excited more effectively. The simplest type of two-dimensional soil-bridge interaction occurs for the vertical incidence of SH-waves and for the symmetric bridge and its abutments. In that case, for the frequencies that

correspond to the symmetric modes of girder vibration, the two abutments do not move and the efficiency of radiation damping, which results from the wave scattering from the two foundations, is maximum. In all other cases, when the angle of incident waves is not vertical, or when the bridge girder is not symmetric and/or when the abutments are different, this simplicity is lost and the efficiency of radiative damping is significantly reduced. In general, when the angle of incident SH-waves is not vertical, large response of the bridge is obtained at the fixed base natural frequencies of the bridge.

When the bridge and its abutments are symmetric, the torsional motion of the whole bridge does not seem to be excited appreciably, at least not for the mass ratios and the geometries studied in this analysis. However, this tendency is completely reversed when the bridge abutments are not the same (i. e.,  $R_1 \neq R_2$  and/or  $MS_1 \neq MS_2$ ). Nonsymmetry of mass distributions enhances the overall torsional response, especially for horizontally incident SH-waves. Other related phenomena, such as shielding, amplification by the wave scattered from the other foundation, and the influence of the standing wave pattern on the excitation of two bridge abutments, are all accentuated and made more complex by the nonsymmetry of the two abutments.

REFERENCES OF CHAPTER VI

1. Housner, G. W., "Interaction of Building and Ground During an Earthquake," Bulletin of the Seismological Society of America, 47, no. 3, 1957, pp. 179-186.
2. Luco, J. E., "Dynamic Interaction of a Shear Wall with the Soil," J. Eng. Mech. Div., ASCE, EM2, 1969, pp. 333-345.
3. Trifunac, M. D., "Interaction of a Shear Wall with the Soil for Incident Plane SH-Waves," Bulletin of the Seismological Society of America, 62, no. 1, 1972, pp. 63-83.
4. Seed, H. B. and Idriss, I. M., "Soil-Structure Interaction of Massive Embedded Structures During Earthquakes," 5WCEE, Rome, Italy, 1973.
5. Luco, J. E. and Contesse, L. A., "Dynamic Structure-Soil-Structure Interaction," Bulletin of the Seismological Society of America, 63, no. 4, August 1973, pp. 1284-1303.
6. Okamoto, S., Introduction to Earthquake Engineering, John Wiley and Sons, New York-Toronto, 1973, Chapter 12, pp. 301-374.
7. Wiegel, R. L., Earthquake Engineering, Prentice-Hall, Inc. Englewood Cliffs, New Jersey, 1970.
8. Luco, J. E., Wong, H. L. and Trifunac, M. D., "A Note on the Dynamic Response of Rigid Embedded Foundations," Earthquake Engineering and Structural Dynamics, 1975.
9. Wong, H. L. and Trifunac, M. D., "Two-dimensional, Antiplane, Building-Soil-Building Interaction for Two or More Buildings and for Incident Plane SH-Waves," Bulletin of the Seismological Society of America, 65, 1975.
10. Thau, S. A., "Radiation and Scattering from a Rigid Inclusion in an Elastic Medium," Journal of Applied Mechanics, 34, 1967, pp. 509-511.